United States
Environmental Protection
Agency

Industrial Environmental Research
Laboratory
Research Triangle Park NC 27711

EPA-600/9-82-005c
July 1982

Research and Development

EPA

Third Symposium on the Transfer and Utilization of Particulate Control Technology:

Volume III. Particulate Control Devices

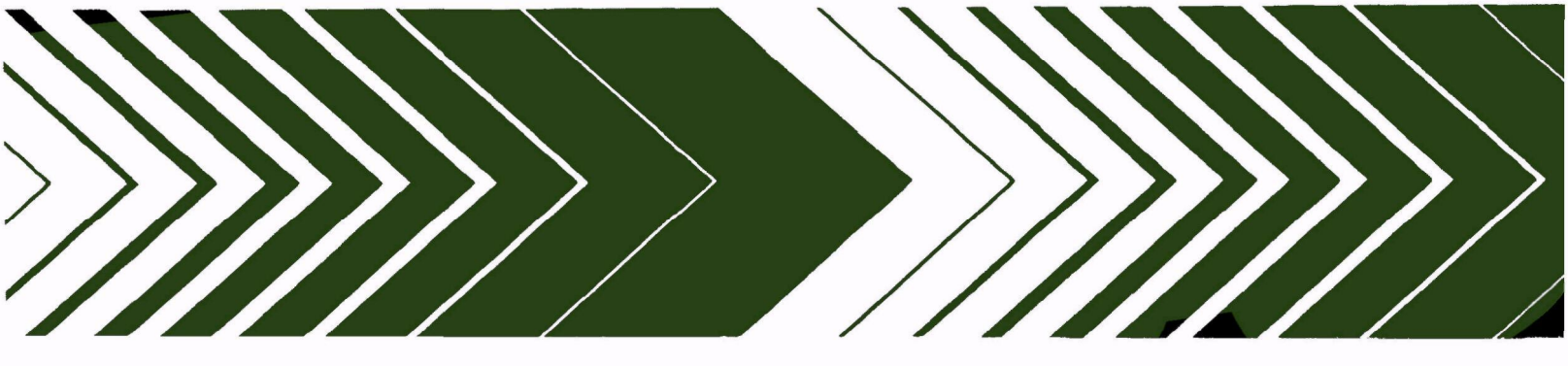

EPA-600/9-82-005c

THIRD SYMPOSIUM ON THE TRANSFER AND UTILIZATION OF PARTICULATE CONTROL TECHNOLOGY VOLUME III. PARTICULATE CONTROL DEVICES

Compiled by:

F.P. Venditti, J.A. Armstrong, and M. Durham

Denver Research Institute
P.O. Box 10127
Denver, Colorado 80208

Grant Number: R805725

Project Officer

Dale L. Harmon
Office of Environmental Engineering and Technology
Industrial Environmental Research Laboratory
Research Triangle Park, NC 27711

Prepared for:

INDUSTRIAL ENVIRONMENTAL RESEARCH LABORATORY
OFFICE OF RESEARCH AND DEVELOPMENT
U.S. ENVIRONMENTAL PROTECTION AGENCY
RESEARCH TRIANGLE PARK, NC 27711

DISCLAIMER

This report has been reviewed by the Industrial Environmental Research Laboratory-Research Triangle Park, North Carolina, Office of Research and Development, U.S. Environmental Protection Agency, and approved for publication. Approval does not signify that the contents necessarily reflect the views and policies of the U.S. Environmental Protection Agency, nor does mention of trade names or commercial products constitute endorsement or recommendation for use.

ABSTRACT

The papers in these four volumes of Proceedings were presented at the Third Symposium on the Transfer and Utilization of Particulate Control Technology held in Orlando, Florida during 9 March through 13 March 1981, sponsored by the Particulate Technology Branch of the Industrial Environmental Research Laboratory of the Environmental Protection Agency and coordinated by the Denver Research Institute of the University of Denver.

The purpose of the symposium was to bring together researchers, manufacturers, users, government agencies, educators and students to discuss new technology and to provide an effective means for the transfer of this technology out of the laboratories and into the hands of the users.

The three major categories of control technologies -- electrostatic precipitators, scrubbers, and fabric filters -- were the major concern of the symposium. These technologies were discussed from the perspectives of economics; new technical advancements in science and engineering; and applications. Several papers dealt with combinations of devices and technologies, leading to a concept of using a systems approach to particulate control rather than device control. Additional topic areas included novel control devices, high temperature/high pressure applications, fugitive emissions, and measurement techniques.

These proceedings are divided into four volumes, each volume containing a set of related session topics to provide easy access to a unified technology area.

VOLUME III

Page

VOLUME I. COAL FIRED BOILERS--CONTENTS x
VOLUME II. ELECTROSTATIC PRECIPITATORS--CONTENTS . . . xiv
VOLUME IV. ATYPICAL APPLICATIONS--CONTENTS. xviii

Section A - Scrubbers

THE CALVERT SCRUBBER 1
S. Calvert, R.G. Patterson and S. Yung

FLUX FORCE/CONDENSATION SCRUBBER SYSTEM FOR COLLECTION OF FINE PARTICULATE EMISSIONS FROM AN IRON MELTING CUPOLA 10
S. Calvert and D.L. Harmon

DEMONSTRATION OF HIGH-INTENSITY-IONIZER-ENHANCED VENTURI SCRUBBER ON A MAGNESIUM RECOVERY FURNACE FUME EMISSIONS 21
A. Prem, M.T. Kearns and D.L. Harmon

A NEW ENTRY IN THE HIGH EFFICIENCY SCRUBBER FIELD 33
L.C. Hardison and F. Ekman

PERFORMANCE OF PARTICULATE SCRUBBERS AS INFLUENCED BY GAS-LIQUID CONTACTOR DESIGN AND BY DUST FLOCCULATION 43
K.T. Semrau and R.J. Lunn

INVESTIGATION OF VENTURI SCRUBBER EFFICIENCY AND PRESSURE DROP 51
R. Parker, T. Le and S. Calvert

SCRUBBER TECHNOLOGY AND THE INTERACTION OF A UNIQUE STRUCTURE AS MIST ELIMINATOR 60
G.C. Pedersen

NOVEL ANNULAR VENTURI SCRUBBER DESIGN REDUCES WASTE DISCHARGE PROBLEMS 71
H.P. Beutner

CONSIDERATION OF THE PERTINENT DESIGN AND OPERATING CHARACTERISTICS ESSENTIAL FOR OPTIMIZATION OF VENTURI SCRUBBER PERFORMANCE 80
H.S. Oglesby

VOLUME III CONTENTS (cont.)

Page

APPLICATION OF SCRUBBERS FOR PARTICULATE CONTROL OF INDUSTRIAL BOILERS 90
M. Borenstein

APPLICATION OF HIGH ENERGY VENTURI SCRUBBERS TO SEWAGE INCINERATION 102
F.X. Reardon

AN INCINERATOR SCRUBBER THAT WORKS: A CASE STUDY 111
C. Menoher

EVALUATION OF ENTRAINED LIQUOR CONTRIBUTION TO TOTAL MASS EMISSIONS DOWNSTREAM OF A WET SCRUBBER . . . 119
W. David Balfour, L.O. Edwards and H.J. Williamson

Section B - Fabric Filters

A DUAL-BEAM BACKSCATTER BETA-PARTICLE GAUGE FOR MEASURING THE DUST CAKE THICKNESS ON OPERATING BAG FILTERS INDEPENDENT OF POSITION 128
R.P. Gardner, R.P. Donovan and L.S. Hovis

DIAGNOSING FILTER FABRIC CAPABILITIES WITH LIGHT SCATTERING AND NUCLEI DETECTING INSTRUMENTATION 140
R. Dennis, D.V. Bubenick and L.S. Hovis

ACID DEWPOINT CORROSION IN PARTICULATE CONTROL EQUIPMENT 150
T.E. Mappes, R.D. Tems and K.E. Foster

SECOND GENERATION OF EMISSIONS CONTROL SYSTEM FOR COKE OVENS 160
J.D. Patton

EFFECTS OF FLYASH SIZE DISTRIBUTION ON THE PERFORMANCE OF A FIBERGLASS FILTER 171
W.F. Frazier and W.T. Davis

FUNDAMENTAL STUDY OF A FABRIC FILTER WITH A CORONA PRECHARGER 181
K. Iinoya and Y. Mori

ECONOMIC EVALUATION FACTORS IN BID EVALUATIONS--A SENSITIVITY ANALYSIS 193
J.G. Musgrove and J.E. Shellabarger

VOLUME III CONTENTS (cont.)

Page

FLY ASH RE-ENTRAINMENT IN A BAGHOUSE--
WHAT DOES IT COST? 201
J.G. Musgrove

WHY PERFORM MODEL STUDY OF FABRIC FILTER
COLLECTOR? 211
W.T. Langan, N.Z. Shilling, W.A. Van Kleunen and O.F. Fortune

EXPERIENCES OF A SMALL INSULATION MANUFACTURER
IN MAINTAINING COMPLIANCE WITH AIR POLLUTION
CONTROL REGULATIONS 221
R.L. Hawks

ADVANCED FABRIC FILTER TECHNOLOGY FOR
DIFFICULT PARTICULATE EMISSIONS 228
H.P. Beutner

DEVELOPMENT OF GUIDELINES FOR OPTIMUM BAGHOUSE
FLUID DYNAMIC SYSTEM DESIGN 238
D. Eskinazi, G.B. Gilbert and R.C. Carr

THEORETICAL ASPECTS OF PRESSURE DROP REDUCTION
IN A FABRIC FILTER WITH CHARGED PARTICLES 250
T. Chiang, E.A. Samuel and K.E. Wolpert

EXPERIMENTAL CORRELATION OF DUST CAKE POROSITY,
AIR-TO-CLOTH RATIO AND PARTICLE-SIZE DISTRIBUTIONS 261
T. Chiang and R.L. Ostop

MODEL FOR DUST PENETRATION THROUGH A
PULSE-JET FABRIC FILTER 270
D. Leith and M.J. Ellenbecker

PERFORMANCES OF DUST LOADED AIR FILTERS 280
C. Kanaoka, H. Emi and M. Ohta

ELECTROSTATICALLY ENHANCED FABRIC
FILTRATION OF PARTICULATES 290
T. Ariman and S.T. McComas

A STAGGERED ARRAY MODEL OF A FIBROUS FILTER
WITH ELECTRICAL ENHANCEMENT 301
F. Henry and T. Ariman

VOLUME III CONTENTS (cont.)

Page

Section C - Granular Beds

AEROSOL FILTRATION BY A COCURRENT MOVING GRANULAR BED: PENETRATION THEORY 311
T.W. Kalinowski and D. Leith

FUNDAMENTAL EXPERIMENTS ON A GRANULAR BED FILTER 321
K. Iinoya and Y. Mori

DRY DUST COLLECTION OF BLAST FURNACE EXHAUST GAS BY MOVING GRANULAR BED FILTER 332
A. Wakabayashi, T. Sugawara and S. Watanabe

Section D - Novel Devices

IRON AND STEEL AIR POLLUTION CONTROL USING MAGNETIC SEPARATION 341
D.C. Drehmel, C.E. Ball and C.H. Gooding

TECHNICAL AND ECONOMIC EVALUATION OF TWO NOVEL PARTICULATE CONTROL DEVICES 353
R.R. Boericke, J.T. Kuo and K.R. Murphy

THE ELECTROSCRUBBER^{TM} FILTER--APPLICATIONS AND PARTICULATE COLLECTION PERFORMANCE 363
D. Parquet

HIGH EFFICIENCY PARTICULATE REMOVAL WITH SINTERED METAL FILTERS 373
B.E. Kirstein, W.J. Paplawsky, D.T. Pence and T.G. Hedahl

APPLICATION OF ELECTROSTATIC TECHNIQUES TO THE REMOVAL OF DUST AND FUME FROM THE INDUSTRIAL ENVIRONMENT 382
S.A. Hoenig

THE DRY VENTURI 393
A.J. Teller and D.R.J. Roy

FIBER BED FILTER SYSTEM CONTROL OF WELDING PARTICULATES 398
J.A. Bamberger and W.K. Winegardner

THE USE OF GLASS CAPILLARY FILTERS TO CLASSIFY ACTINOLITE FIBERS 406
J.W. Gentry, T.C. Chen, S.W. Lin and P.Y. Yu

VOLUME III CONTENTS (cont.)

Page

ULTRA-HIGH EFFICIENCY FILTRATION SYSTEMS (AIR RECIRCULATION) 417
R.W. Potokar

THE WET WALL ELECTROSTATIC PRECIPITATOR 428
J. Starke, J. Kautz and K-R. Hegemann

Section E - Mechanical Collectors

TROUBLESHOOTING MULTIPLE CYCLONES ON FUEL-OIL-FIRED BOILERS 438
F. Crowson and R.L. Gibbs

COLLECTION EFFICIENCIES OF CYCLONE SEPARATORS. 449
P.W. Dietz

ELECTROSTATICALLY AUGMENTED COLLECTION IN VORTICAL FLOWS 459
P.W. Dietz

HIGH PERFORMANCE CYCLONE DEVELOPMENT 468
W.G. Giles

AUTHOR INDEX 481

VOLUME I

COAL FIRED BOILERS

Section A - Fabric Filters

Page

COAL PROPERTIES AND FLY ASH FILTERABILITY 1
R. Dennis, J.A. Dirgo and L.S. Hovis

PULSE-JET FILTRATION WITH ELECTRICALLY CHARGED FLYASH 11
R.P. Donovan, L.S. Hovis, G.H. Ramsey and J.H. Abbott

ELECTRICALLY CHARGED FLYASH EXPERIMENTS IN A LABORATORY SHAKER BAGHOUSE 23
L.S. Hovis, J.H. Abbott, R.P. Donovan and C.A. Pareja

ELECTROSTATIC AUGMENTATION OF FABRIC FILTRATION 35
D.W. VanOsdell, G.P. Greiner, G.E.R. Lamb and L.S. Hovis

FABRIC WEAR STUDIES AT HARRINGTON STATION 45
R. Chambers, K. Ladd, S. Kunka and D. Harmon

SPS PILOT BAGHOUSE OPERATION 55
K. Ladd, W. Hooks, S. Kunka and D. Harmon

REVIEW OF SPS INVESTIGATION OF HARRINGTON STATION UNIT 2 FABRIC FILTER SYSTEM 65
K. Ladd, S. Kunka

A SUMMARY OF PERFORMANCE TESTING OF THE APITRON ELECTROSTATICALLY AUGMENTED FABRIC FILTER 75
D. Helfritch and L. Kirsten

FABRIC FILTER OPERATING EXPERIENCE FROM SEVERAL MAJOR UTILITY UNITS 82
O.F. Fortune, R.L. Miller and E.A. Samuel

EVALUATION OF THE 25 MW KRAMER STATION BAGHOUSE: TRACE ELEMENT EMISSION CONTROL 94
M.W. McElroy and R.C. Carr

CHARACTERIZATION OF A 10 MW FABRIC FILTER PILOT PLANT 96
W.B. Smith, K.M. Cushing and R.C. Carr

SPECIFYING A FABRIC FILTER SYSTEM 107
R.L. Ostop and D.A. Single

VOLUME I CONTENTS (cont.)

Page

EVALUATION OF THE 25 MW KRAMER STATION BAGHOUSE: OPERATIONAL FACTORS IN PARTICULATE MATTER EMISSION CONTROL 118
R.C. Carr and M.W. McElroy

PULSE-JET TYPE FABRIC FILTER EXPERIENCE AT AIR TO CLOTH RATIOS OF 5 TO 1 ON A BOILER FIRING PULVERIZED COAL 120
G.L. Pearson

SELECTION AND OPERATION OF BAGHOUSES AT R.D. NIXON STATION, UNIT #1 129
R.C. Hyde, J. Arello and D.J. Huber

POTENTIAL FOR IMPROVEMENT IN BAGHOUSE DESIGN 138
R.M. Jensen

REVIEW OF OPERATING AND MAINTENANCE EXPERIENCES WITH HIGH TEMPERATURE FILTER MEDIA ON COAL-FIRED BOILERS . . . 148
L.K. Crippen

Section B - Electrostatic Precipitators

PILOT DEMONSTRATION OF THE PRECHARGER-COLLECTOR SYSTEM. 157
P. Vann Bush, Duane H. Pontius

REMEDIAL TREATMENTS FOR DETERIORATED HOT SIDE PRECIPITATOR PERFORMANCE 165
R.E. Bickelhaupt

EVALUATION OF THE UNITED McGILL ELECTROSTATIC PRECIPITATOR 176
D.S. Ensor, P.A. Lawless, A.S. Damle

PREDICTING THE EFFECT OF PROPRIETARY CONDITIONING AGENTS ON FLY ASH RESISTIVITY. 185
R.J. Jaworowski and J.J. Lavin

SO_3 CONDITIONING TO ENABLE ELECTROSTATIC PRECIPITATORS TO MEET DESIGN EFFICIENCIES 197
J.J. Ferrigan, III

ENHANCED PRECIPITATOR COLLECTION EFFICIENCIES THROUGH RESISTIVITY MODIFICATION 206
D.F. Mahoney

VOLUME I CONTENTS (cont.)

Page

DEVELOPMENT OF A NEW SULFUR TYPE ASH CONDITIONING 216
R.H. Gaunt

OPERATING EXPERIENCE WITH FLUE GAS CONDITIONING SYSTEMS AT COMMONWEALTH EDISON COMPANY 226
L.L. Weyers and R.E. Cook

THE APPLICATION OF A TUBULAR WET ELECTROSTATIC PRECIPITATOR FOR FINE PARTICULATE CONTROL AND DEMISTING IN AN INTEGRATED FLY ASH AND SO_2 REMOVAL SYSTEM ON COAL-FIRED BOILERS 236
E. Bakke and H.P. Willett

FIELD EVALUATIONS OF AMMONIUM SULFATE CONDITIONING FOR IMPROVEMENT OF COLD SIDE ELECTROSTATIC PRECIPITATOR PERFORMANCE 237
E.C. Landham, Jr., G.H. Marchant, Jr., J.P. Gooch and R.F. Altman

EVALUATION OF PERFORMANCE ENHANCEMENT OBTAINED WITH PULSE ENERGIZATION SYSTEMS ON A HOT SIDE ELECTROSTATIC PRECIPITATOR 253
W. Piulle, L.E. Sparks, G.H. Marchant, Jr. and J.P. Gooch

A NEW MICROCOMPUTER AND STRATEGY FOR THE CONTROL OF ELECTROSTATIC PRECIPITATORS 265
K.J. McLean, T.S. Ng, Z. Herceg and Z. Rana

ASSESSMENT OF THE COMMERCIAL POTENTIAL FOR THE HIGH INTENSITY IONIZER IN THE ELECTRIC UTILITY INDUSTRY 272
J.S. Lagarias, J.R. McDonald and D.V. Giovanni

APPLICATION OF ENERGY CONSERVING PULSE ENERGIZATION FOR PRECIPITATORS--PRACTICAL AND ECONOMIC ASPECTS 291
H. H. Petersen and P. Lausen

Section C - Dry SO_2 Scrubbers

SO_2 REMOVAL BY DRY INJECTION AND SPRAY ABSORPTION TECHNIQUES 303
E.L. Parsons, Jr., V. Boscak, T.G. Brna and R.L. Ostop

DRY SCRUBBING SO_2 AND PARTICULATE CONTROL 313
N.J. Stevens, G.B. Manavizadeh, G.W. Taylor and M.J. Widico

FIBER AND FABRIC ASPECTS FOR SO_2 DRY SCRUBBING BAGHOUSE SYSTEMS 323
L. Bergmann

VOLUME I CONTENTS (cont.)

Page

TWO-STAGE DRY FLUE GAS CLEANING USING CALCIUM ALKALIS 333
D.C. Gehri, D.F. Dustin and S.J. Stachura

CONTROL OF SULFUR DIOXIDE, CHLORINE, AND TRACE ELEMENT EMISSIONS FROM COAL-FIRED BOILERS BY FABRIC FILTRATION 341
R.J. Demski, J.T. Yeh and J.I. Joubert

Section D - Scrubbers

FLYASH COLLECTION USING A VENTURI SCRUBBER--MINNESOTA POWER'S COMMERCIAL OPERATING EXPERIENCE 352
C.A. Johnson

AUTHOR INDEX 361

VOLUME II

ELECTROSTATIC PRECIPITATORS

Section A - Fundamentals

Page

MATHEMATICAL MODELING OF IONIC CONDUCTION IN FLY ASH LAYERS 1
R.B. Mosley, J.R. McDonald and L.E. Sparks

MEASUREMENTS OF ELECTRICAL PROPERTIES OF FLY ASH LAYERS 13
R.B. Mosley, P.R. Cavanaugh, J.R. McDonald and L.E. Sparks

LASER DOPPLER ANEMOMETER MEASUREMENTS OF PARTICLE VELOCITY IN A LABORATORY PRECIPITATOR 25
P.A. Lawless, A.S. Damle, A.S. Viner, E.J. Shaughnessy and L.E. Sparks

PROGRESS IN MODELING BACK CORONA 35
P.A. Lawless

A COMPUTER MODEL FOR ESP PERFORMANCE 44
P.A. Lawless, J.W. Dunn and L.E. Sparks

MEASUREMENT AND INTERPRETATION OF CURRENT DENSITY DISTRIBUTION AND CHARGE/MASS DATA 54
M. Durham, G. Rinard, D. Rugg and L.E. Sparks

THE RELATIONSHIP BETWEEN GAS STREAM TURBULENCE AND COLLECTION EFFICIENCY IN A LAB-SCALED ELECTROSTATIC PRECIPITATOR 66
B.E. Pyle, J.R. McDonald, W.B. Smith

PARTICLE DEPOSITION PROFILES AND REENTRAINMENT IN A WIRE-PLATE ELECTROSTATIC PRECIPITATOR 76
E. Arce-Medina and R.M. Felder

PARTICLE TRANSPORT IN THE EHD FIELD 87
T. Yamamoto

SURFACE REENTRAINMENT OF COLLECTED FLY ASH IN ELECTROSTATIC PRECIPITATORS 97
M. Mitchner, M.J. Fisher, D.S. Gere, R.N. Leach and S.A. Self

ELECTROMECHANICS OF PRECIPITATED ASH LAYERS 109
G.B. Moslehi and S.A. Self

VOLUME II CONTENTS (cont.)

Page

EXPERIMENTAL MEASUREMENTS OF THE EFFECT OF TURBULENT DIFFUSION ON PRECIPITATOR EFFICIENCY 120
G.L. Leonard, M. Mitchner and S.A. Self

CAN REENTRAINMENT BE EXPLAINED USING A NEW PRECIPITATOR FORMULA? 130
S. Maartmann

A LABORATORY FURNACE FOR THE PRODUCTION OF SYNTHETIC FLY ASH FROM SMALL COAL SAMPLES 141
K.M. Sullivan

COMPUTER SIMULATION OF THE WIDE PLATE SPACING EFFECT 149
E.A. Samuel

SIMULTANEOUS MEASUREMENTS OF AERODYNAMIC SIZE AND ELECTRIC CHARGE OF AEROSOL PARTICLES IN REAL TIME ON A SINGLE PARTICLE BASIS 160
M.K. Mazumder, R.G. Renninger, T.H. Chang, R.W. Raible, W.G. Hood, R.E. Ware and R.A. Sims

APPLICATION OF LASER DOPPLER INSTRUMENTATION TO PARTICLE TRANSPORT MEASUREMENTS IN AN ELECTROSTATIC PRECIPITATOR 169
M.K. Mazumder, W.T. Clark III, R.E. Ware, P.C. McLeod, W.G. Hood, J.E. Straub and S. Wanchoo

THE APPLICATION OF MEASUREMENTS OF AEROSOL CHARGE ACQUISITION BY BIPOLAR IONS TO THE PROBLEM OF BACK CORONA 179
R.A. Fjeld, R.O. Gauntt, G.J. Laughlin and A.R. McFarland

IDENTIFICATION OF BACK DISCHARGE SEVERITY 189
S. Masuda and Y. Nonogaki

Section B - Operations and Maintenance

MODELING OF ELECTROSTATIC PRECIPITATORS WITH RESPECT TO RAPPING REENTRAINMENT AND OUTLET OPACITY 199
M.G. Faulkner, W.E. Farthing, J.R. McDonald and L.E. Sparks

NEW PRECIPITATOR TECHNOLOGY FOR PARTICULATE CONTROL 208
J.R. Zarfoss

VOLUME II CONTENTS (cont.)

Page

AN APPLICATION SUMMARY OF HIGH ENERGY SONIC CLEANING APPLIED TO ELECTROSTATIC PRECIPITATORS 218
M.J. Berlant

THE IMPACT OF INTELLIGENT PRECIPITATOR CONTROLS 230
N.Z. Shilling, R.O. Reese and J.A. Fackler

AN ENERGY MANAGEMENT SYSTEM FOR ELECTROSTATIC PRECIPITATORS 242
R.R. Crynack and M.P. Downey

RELATIONSHIP BETWEEN ELECTROSTATIC PRECIPITATOR PERFORMANCE AND RECORDKEEPING PRACTICES 252
S.P. Schliesser

AN OPERATION AND MAINTENANCE PROGRAM FOR A PHOSPHATE ROCK ELECTROSTATIC PRECIPITATOR 262
D.B. Rimberg

Section C - Advanced Design

ELECTROSTATIC PRECIPITATOR PERFORMANCE WITH PULSE EXCITATION 273
D. Rugg, M. Durham, G. Rinard and L.E. Sparks

DEVELOPMENT OF A CHARGING DEVICE FOR HIGH-RESISTIVITY DUST USING HEATED AND COOLED ELECTRODES 283
G. Rinard, M. Durham, D. Rugg and L.E. Sparks

THE EVALUATION OF NOVEL ELECTROSTATIC PRECIPITATOR SYSTEMS USING A TRANSPORTABLE PROTOTYPE 295
G. Rinard, M. Durham, D. Rugg, J. Armstrong, L.E. Sparks and J.H. Abbott

ANALYSIS OF THE ELECTRICAL AND CHARGING CHARACTERISTICS OF A THREE ELECTRODE PRECHARGER 304
K.J. McLean

PARTICLE CHARGING IN AN ELECTROSTATIC PRECIPITATOR BY PULSE AND DC VOLTAGES 314
L.E. Sparks, G.H. Ramsey, R.E. Valentine and J.H. Abbott

PARTICLE COLLECTION IN A TWO STAGE ELECTROSTATIC PRECIPITATOR WITH VARIOUS COLLECTOR STAGES 326
L.E. Sparks, G.H. Ramsey, R.E. Valentine and J.H. Abbott

HIGH INTENSITY IONIZER DEVELOPMENT 334
M.H. Anderson, J.R. McDonald, J.P. Gooch and D.V. Giovanni

VOLUME II CONTENTS (cont.)

Page

DEMONSTRATION OF AIR POLLUTION SYSTEMS HIGH INTENSITY IONIZER/ELECTROSTATIC PRECIPITATOR ON AN OIL-FIRED BOILER 349
G.A. Raemhild, A. Prem and F. Weisz

PRIMARY AND SECONDARY IONIZATION IN AN ELECTRON BEAM PRECIPITATOR SYSTEM 358
W.C. Finney, L.C. Thanh, J.S. Clements and R.H. Davis

INFLUENCE ON PARTICLE CHARGING OF ELECTRICAL PARAMETERS AT DC AND PULSE VOLTAGES 370
H.J. Joergensen, J.T. Kristiansen and P. Lausen

BOXER-CHARGER MARK III AND ITS APPLICATION IN ESP'S 380
S. Masuda, H. Nakatani and A. Mizuno

THE PERFORMANCE OF AN EXPERIMENTAL PRECIPITATOR WITH AN ALL-PLATE ZONE 390
J. Dalmon

THE PHYSICS OF PULSE ENERGIZATION OF ELECTROSTATIC PRECIPITATORS 404
L. Menegozzi and P.L. Feldman

ADVANCED ELECTRODE DESIGN FOR ELECTROSTATIC PRECIPITATORS 405
S. Bernstein, K. Ushimaru and E.W. Geller

Section D - Industrial Applications

PROBLEMS IN APPLYING AN ELECTROSTATIC PRECIPITATOR TO A SALVAGE FUEL-FIRED BOILER. 415
C.R. Thompson

THE APPLICATION OF ELECTROSTATIC PRECIPITATORS TO BOILERS FIRING MULTIPLE FUELS 425
R.L. Bump

AUTHOR INDEX 435

VOLUME IV

ATYPICAL APPLICATIONS

Section A - Advanced Energy Applications

Page

HIGH TEMPERATURE PARTICLE COLLECTION WITH A.P.T. EPxP DRY SCRUBBER 1
S. Yung, T. Lee, R.C. Patterson, S. Calvert and D.C. Drehmel

PARTICLE COLLECTION IN CYCLONES AT HIGH TEMPERATURE AND HIGH PRESSURE 2
R. Parker, R. Jain, S. Calvert, D.C. Drehmel and J. Abbott

OPERATING RESULTS OF ELECTROSTATIC PRECIPITATORS AT HIGH TEMPERATURE AND HIGH PRESSURES 3
P.L. Feldman and K.S. Kumar

CONTROL OF PARTICULATES IN PROCESS AREA 12, SOLVENT REFINED COAL PROCESS 15
W.H. Wilks, P.D. Wilkinson and J.A. Schlosberg

NON-PLUGGING RETAINING STRUCTURE FOR GRANULAR BED FILTER FOR HTHP APPLICATION 26
A.M. Presser and J.C. Alexander

PARTICULATE EMISSIONS CONTROL FROM A COAL-FIRED OPEN-CYCLE MAGNETOHYDRODYNAMICS/STEAM POWER PLANT . . . 36
H.H. Wang and T.E. Dowdy

REAL TIME COARSE PARTICLE MASS MEASUREMENTS IN A HIGH TEMPERATURE AND PRESSURE COAL GASIFIER PROCESS TREATMENT 46
J. Wegrzyn, J. Saunders and W. Marlow

THE DESIGN, ENGINEERING, AND STARTUP OF A VENTURI SCRUBBER SYSTEM ON AN OIL SHALE OFF-GAS INCINERATOR . . . 55
P.A. Czuchra and J.S. Sterrett

FLUIDIZED-BED COMBUSTION HOT FLUE GAS CLEANUP PERSPECTIVE ON CYCLONES AND OTHER DEVICES 63
R.F. Henry and W.F. Podolski

PRESSURIZED AND NON-PRESSURIZED ACOUSTIC AGGLOMERATORS FOR HOT-GAS CLEANUP APPLICATIONS. 73
K.H. Chou and D.T. Shaw

VOLUME IV CONTENTS (cont.)

Page

ALKALIS AND THEIR CONTRIBUTIONS TO CORONA CURRENT AT HIGH TEMPERATURE AND HIGH PRESSURE 74
R.W.L. Snaddon

HOT GAS CLEANUP IN PRESSURIZED FLUIDIZED BED COMBUSTION 83
L.N. Rubow and M.G. Klett

VENTURI SCRUBBING FOR CONTROL OF PARTICULATE EMISSIONS FROM OIL SHALE RETORTING 95
G.M. Rinaldi and R.C. Thurnau

OVERVIEW OF THE DEPARTMENT OF ENERGY'S PRESSURIZED FLUIDIZED-BED COMBUSTOR CLEANUP TECHNOLOGY PROGRAM . . . 105
W.E. Moore

THE CYCLOCENTRIFUGE^{TM}--AN ADVANCED GAS/SOLIDS SEPARATOR FOR COAL CONVERSION PROCESSES 116
P.R. Albrecht, J.T. McCabe and W. Fedarko

Section B - Fugitive Emissions

DEMONSTRATION OF THE USE OF CHARGED FOG IN CONTROLLING FUGITIVE DUST FROM LARGE-SCALE INDUSTRIAL SOURCES 125
E.T. Brookman, R.C. McCrillis and D.C. Drehmel

THE CONTROL OF FUGITIVE EMISSIONS USING WINDSCREENS . . . 135
D. Carnes and D.C. Drehmel

THE INFLUENCE OF AGGREGATE PILE SHAPE AND ORIENTATION ON PARTICULATE FUGITIVE EMISSIONS 145
D. Martin

SPRAY CHARGING AND TRAPPING SCRUBBER FOR FUGITIVE PARTICLE EMISSION CONTROL 155
S. Yung, S. Calvert and D.C. Drehmel

IMPROVED STREET SWEEPER FOR CONTROLLING URBAN INHALABLE PARTICULATE MATTER 156
S. Calvert, H. Brattin, S. Bhutra, R. Parker and D.C. Drehmel

A WIND TUNNEL FOR DUST ENTRAINMENT STUDIES 168
A.S. Viner, M.B. Ranade, E.J. Shaughnessy, D.C. Drehmel and B.E. Daniels

VOLUME IV CONTENTS (cont.)

Page

TECHNIQUES AND EQUIPMENT FOR MEASURING INHALABLE PARTICULATE FUGITIVE EMISSIONS 179
H.J. Kolnsberg

BALLOON SAMPLING TO CHARACTERIZE PARTICLE EMISSIONS FROM FUGITIVE SOURCES. 188
J.A. Armstrong and D.C. Drehmel

AN ELECTROSTATICALLY CHARGED FOG GENERATOR FOR THE CONTROL OF INHALABLE PARTICLES 200
C.V. Mathai, L.A. Rathbun and D.C. Drehmel

RELATIVE EFFECTIVENESS OF CHEMICAL ADDITIVES AND WIND SCREENS FOR FUGITIVE DUST CONTROL. 210
D.C. Drehmel and B.E. Daniel

PARTICULATE IMPACT COMPARISON BETWEEN CONTROLLED STACK EMISSIONS FOR A 2000 MW ELECTRICAL GENERATING STATION 222
H.E. Hesketh and F.L. Cross

OPERATING EXPERIENCE AND THE TECHNIQUES IN THE CONTROL OF COAL DUST EMISSIONS FROM LARGE STORAGE PILE AT NANTICOKE TGS 232
N. Krishnamurthy, W. Whitman and Y.V. Nguyen

Section C - Opacity

MODELING SMOKE PLUME OPACITY FROM PARTICULATE CONTROL EQUIPMENT 242
D.S. Ensor, P.A. Lawless, S.J. Cowen

TETHERED BALLOON PLUME SAMPLING OF A PORTLAND CEMENT PLANT 252
J.A. Armstrong, P.A. Russell, M.N. Plooster

THE RELATIONSHIP OF FLY ASH LIGHT ABSORPTION TO SMOKE PLUME OPACITY 264
S.J. Cowen, D.S. Ensor

Section D - Measurements

A SPECIAL METHOD FOR THE ANALYSIS OF SULFURIC ACID MISTS 275
P. Urone, R.B. Mitchell, J.E. Rusnak, R.A. Lucas and J.F. Griffiths

VOLUME IV CONTENTS (cont.)

Page

A MICROCOMPUTER-BASED CASCADE-IMPACTOR DATA-REDUCTION SYSTEM 285
M. Durham, S. Tegtmeyer, K. Wasmundt and L.E. Sparks

DEVELOPMENT OF A SAMPLING TRAIN FOR STACK MEASUREMENT OF INHALABLE PARTICULATE 297
A.D. Williamson, W.B. Smith

INHALABLE PARTICULATE MATTER SAMPLING PROGRAM FOR IRON AND STEEL: AN OVERVIEW PROGRESS REPORT 306
R.C. McCrillis

DEVELOPMENT OF IP EMISSION FACTORS 317
D.L. Harmon

INHALABLE PARTICULATE EMISSION FACTOR PROGRAM PURPOSE AND DEVELOPMENT 326
F.M. Noonan and J.H. Southerland

INHALABLE PARTICULATE EMISSION FACTORS FOR BLAST FURNACE CASTHOUSES IN THE IRON AND STEEL INDUSTRY 335
P.D. Spawn, S. Piper and S. Gronberg

INHALABLE PARTICULATE EMISSIONS FROM VEHICLES TRAVELING ON PAVED ROADS 344
R. Bohn

QUALITY ASSURANCE FOR PARTICLE-SIZING MEASUREMENTS . . . 353
C.E. Tatsch

PARTICULATE EMISSIONS CHARACTERIZATION FOR OIL-FIRED BOILERS 363
D. Mormile, S. Hersh, B.F. Piper and M. McElroy

A CONTINUOUS REAL-TIME PARTICULATE MASS MONITOR FOR STACK EMISSION APPLICATIONS 373
J.C.F. Wang, H. Patashnick and G. Rupprecht

Section E - Mobile Sources

STUDIES OF PARTICULATE REMOVAL FROM DIESEL EXHAUSTS WITH ELECTROSTATIC AND ELECTROSTATICALLY-AUGMENTED TECHNIQUES 383
J.L. DuBard, M.G. Faulkner, J.R. McDonald, D.C. Drehmel and J.H. Abbott

VOLUME IV CONTENTS (cont.)

Page

STUDIES OF PARTICULATE REMOVAL FROM DIESEL EXHAUSTS WITH MECHANICAL TECHNIQUES 395
M.G. Faulkner, J.L. DuBard, J.R. McDonald, D.C. Drehmel and J.H. Abbott

UPDATE ON STATUS OF CONNECTICUT'S CONTROL PROGRAM FOR TRANSPORTATION-RELATED PARTICULATE EMISSIONS 406
H.L. Chamberlain and J.H. Gastler

AUTHOR INDEX 413

THE CALVERT SCRUBBER

BY: S. Calvert and R. G. Patterson
Calvert Environmental Equipment Co.
5191 Santa Fe St.
San Diego, CA 92109

S. Yung
Air Pollution Technology, Inc.
4901 Morena Blvd., Bldg. 400
San Diego, CA 92117

ABSTRACT

The Calvert Scrubber™ is a new and unique development in fine particle scrubbing. It is an advanced gas-atomized spray scrubber which can outperform the conventional Venturi scrubber for both particulate and gaseous pollutant removal.

The Calvert Scrubber is a very energy efficient fine particle scrubber and is especially well suited to utility applications because it can meet both particulate and sulfur dioxide removal requirements with a single control device. Other potential applications include metallurgical industries, chemical industries and any other industry where fine particle scrubbers are used.

Pilot scrubbers up to 3,000 CFM capacity have been built and tested. Experimental data for fine particle collection are presented. Collection efficiency data are presented as a function of particle aerodynamic diameter. The 50% cut diameter is presented as a function of pressure drop and energy input to the scrubber. Performance is compared to conventional Venturi scrubbers and other fine particle scrubbers.

INTRODUCTION

This paper presents the results of laboratory and pilot plant studies for a new type of scrubber, the Calvert Scrubber™, which has superior capability for particle collection and gas absorption. Particle collection efficiency as a function of particle size is presented for the Calvert Scrubber. Comparison of the Calvert Scrubber to a Venturi scrubber using the cut power method shows that the Calvert Scrubber can provide the same fine particle collection capability as a Venturi scrubber but with only 50% of the power required by a Venturi scrubber.

CALVERT SCRUBBER

The Calvert Scrubber is a gas atomized spray type scrubber whose patented design is a significant advancement over the Venturi and similar scrubbers. Its characteristics are as follows:

1. Its design is simple and rugged, comparable to the conventional Venturi and orifice type scrubbers.
2. It is capable of plug free operation, since it does not contain any small orifices or nozzles.
3. It has capability for high efficiency collection of fine particles.
4. It has a lower power requirement than a conventional Venturi or orifice type scrubber.
5. It has higher mass transfer efficiency than a conventional Venturi scrubber.

In a gas atomized scrubber the liquid is atomized by a high velocity gas stream. Particles are collected on the drops by impaction because of the high relative velocity between the gas and the drops in the throat section. Gas is also absorbed by the drops before they are separated from the gas stream in the entrainment separator.

Particle collection efficiency in the throat section increases as the relative velocity is increased or the drop size is decreased. As the drops accelerate in the throat section the relative velocity decreases and therefore the collection efficiency decreases.

The Calvert Scrubber has the following five zones:

1. Particle conditiong.
2. Primary atomization.
3. Secondary atomization, "Collision Zone".
4. Fog contact.
5. Entrainment separation.

The particle conditioning zone is designed to saturate the gas stream, remove large particles and provide some particle growth for easier fine particle collection. Primary atomization and particle collection take place in two Venturi throat sections as shown in Figure 1. In the primary atomization zone liquid is atomized by the high velocity gas stream, particles are collected and gas is absorbed the same as it would in the Venturi scrubber.

Then the Calvert Scrubber takes a step beyond the Venturi scrubber in the secondary atomization zone. The streams from the two throats are directed toward each other so that they collide at extremely high relative velocity. The head-on collision of the two streams at twice the individual throat velocity shreds the drops into finer drops and causes very intensive scrubbing. The Calvert Scrubber collision zone results in the following advantages over a Venturi scrubber:

1. High relative velocity causes small drops to be shredded away from some of the large drops.
2. Drops are also blown into half-bubbles which burst into small fragments.
3. Drops from one throat which collide with drops from the other throat shatter into small drops which are expelled outward.
4. In the secondary atomization zone, the drops are exposed to the gas stream at even higher relative velocity than in the primary (throat) zone. As a result, both the particle collection and gas absorption rates are abruptly increased to high levels.

5. The throats are subject to much less erosion than in a Venturi scrubber with equivalent efficiency, because the velocity in the throats is only half the relative velocity in the collision zone.
6. Pressure loss due to gas friction in the throats is reduced by lower velocity operation.

The gas in the fog zone is in contact with extremely small drops for an extended period of time so diffusional process such as gas absorption and diffusional deposition of particles are more effective. From the fog zone the gas passes through a high efficiency entrainment separator to separate the drops from the gas stream.

LABORATORY STUDIES

Many pilot plant tests have been completed in the course of developing the Calvert Scrubber and measuring its performance. Some previous data have been reported by Calvert, et al, (1) for particle collection and SO_2 absorption by Na_2CO_3 solution. The data reported in this paper are for particle collection only.

The experimental method used for determination of the particle collection efficiency of the laboratory scale Calvert Scrubber involved the use of two prototypes. One operated at air flow rates around 2.83 m^3/min (100 CFM). The other, larger unit, had a nominal 28.3 m^3/min (600-700 CFM) flowrate.

The following test aerosols were used to vary the size distribution and physical properties of the particles:

1. Fly ash.
2. TiO_2 pigment.
3. Cupola dust.
4. Hydrated lime dust.
5. Dibutylphthalate dispersed by evaporation/condensation.
6. Methylene blue dispersed by spray drying.
7. TiO_2 dispersed by spraying, evaporating and oxidizing tetra-isopropyl-titanate.
8. TiO_2 dispersed by spraying and combusting a suspension of tetra-isopropyl-titanate in alcohol.

The first four test aerosols were dispersed by means of a dust feeder with a screw feed. Deagglomeration was accomplished by means of a high pressure air jet ejector followed by a cyclone separator to remove any over sized material. The gas leaving the cyclone was then diluted with ionized air from a Polonium 210 source to neutralize any charged particles.

Particle size distribution and concentration at the scrubber inlet and outlet were determined by means of cascade impactors. The cascade impactors were operated with either greased aluminum or glass fiber substrates depending on the physical properties of the test aerosol. The experimental procedure used was essentially the same as that which has been used by A.P.T. in its field evaluations, Calvert, et al, (2) and in laboratory and power plant studies. The cascade impactors were calibrated in accordance with the "Cascade Impactor Calibration Guidelines", Calvert, et al, (3), developed by A.P.T. and adopted by EPA as their guideline method.

Air flow rates were measured by means of Venturi meters, which were calibrated with pitot tube traverses. Water flow rates were measured by means of calibrated rotometers and Venturi meters.

Particle Collection Results

Particle collection efficiency as a function of particle size was computed from the cascade impactor data by using three methods. All three, visual, spline fit, and finite difference, are based on the ratio of the slopes of the inlet and outlet cumulative mass concentrations as a function of aerodynamic particle diameter. These methods measure the slope of the inlet and outlet curves at the same particle diameter and then compute the penetration as the ratio of the slope of the outlet curve to the slope of the inlet curve. Aerodynamic particle diameter is defined as follows:

$$d_{pa} = d_p(p_p C')^{1/2} \qquad (1)$$

where d_{pa} = aerodynamic particle diameter, μmA

d_p = physical particle diameter, μm

ρ_p = particle density, g/cm^3

C' = Cunningham slip correction factor, dimensionless

Typical experimental particle collection data for the 28 m^3/min Calvert Scrubber prototype are shown in Figures 2 and 3. These figures show that the particle penetration increases with decreasing particle size until a maximum penetration is reached and then particle penetration decreases with further decrease in particle size. This is the result of the increased particle collection in the collision and fog zones of the Calvert Scrubber. These figures also show similar results for two different types of test dust when the scrubber is operating at a liquid to gas ratio of 1.33 l/m^3 (10 gal/MCF) and a gas phase pressure drop of 40 cm W.C. (16 in W.C.). Figure 3 shows the improved performance when the scrubber is operated at a liquid to gas ratio of 2 l/m^3 (15 gal/MCF) and gas phase pressure drop of 71 cm W.C. (28 in W.C.).

The particle collection performance of the Calvert Scrubber can be compared to a Venturi scrubber using the cut power method developed by A.P.T., Calvert, et al, (4). Since most runs resulted in particle penetrations less than 50% for all particle sizes, an equivalent cut diameter was determined from the overall penetration.

The equivalent cut diameter for the Calvert Scrubber is compared to that of a Venturi scrubber in Figure 4. This figure shows that the Calvert Scrubber requires less pressure drop for the same cut diameter as a Venturi scrubber. For a cut diameter of 0.3 μmA, the Calvert Scrubber requires a pressure drop of 76 cm W.C. (30 in. W.C.) compared to 140 cm W.C. (55 in W.C.) for a Venturi scrubber.

CALVERT SCRUBBER PILOT PLANT

The Calvert Scrubber pilot plant was designed to be entirely self-contained and requires only electrical and water connections. The scrubber system auxiliaries (pumps, tank, instrumentation and control systems) were installed on an 8' x 10' trailer which is easily transported from site to site. An exhaust fan is carried on the trailer and installed along with lightweight FRP or carbon steel ducting at the site. The Calvert scrubber pilot plant module was designed to be free standing to maintain flexibility

in locating the pilot plant at an industrial site. Typical set up times are 4-8 hours.

Gas flow rate through the pilot scrubber can be varied from 1000-2500 ACFM. Liquid circulation rates as high as 100 GPM can be achieved. The design of the scrubber allows maximum flexibility in terms of the particle conditioning, primary and secondary atomization zones. The ducting system, which can be transported on the trailer, contains sampling parts to allow measurement of the inlet and outlet particle mass concentration as well as particle size distributions.

The performance of the Calvert Scrubber pilot plant has been determined at an industrial site and in laboratory tests on the following types of particles:

1. Anhydrous borax.
2. Fly ash.
3. Hydrated lime dust.

Fractional particle penetration data for the Calvert Scrubber pilot plant was similar to that shown in Figures 2 and 3 for the laboratory scale Calvert Scrubber.

CONCLUSIONS

The Calvert Scrubber is well suited for scrubbing fine particles. Particle collection and gas absorption are greatly enhanced in the secondary atomization zone where the drops formed in the primary atomization zone are shredded into smaller drops. These smaller drops provide better mass transfer and additional fine particle collection because of the renewed high relative velocity. The power requirement for the Calvert Scrubber is lower than other scrubbers, such as the Venturi, packed and plate types.

REFERENCES

1. Calvert, S. and S. Yung. "Advanced Developments in Novel Particulate Control Technology". Paper No. 79-56.1. Paper presented at the 79th Annual Meeting of the Air Pollution Control Assoc., 1979.

2. Calvert, S., N. C. Jhaveri, and S. Yung. "Fine Particle Scrubber Performance Tests". EPA-650/2-74-093, October 1974.

3. Calvert, S., C. Lake, and R. Parker. "Cascade Impactor Calibration Guidelines". EPA-600/2-76-118, 1976.

4. Calvert, S. "Engineering Design of Fine Particle Scrubbers". J. Of Air Pollution Control Assoc. 24: 929-934 (1974).

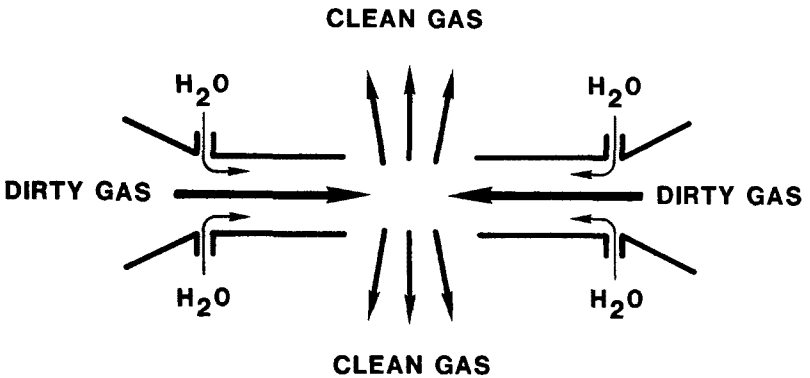

Fig. 1 CALVERT SCRUBBER COLLISION ZONE

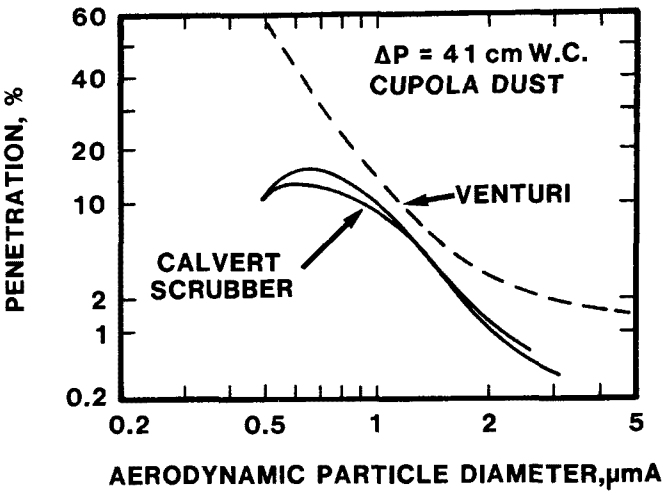

Fig. 2 CALVERT SCRUBBER PERFORMANCE COMPARED TO A VENTURI.

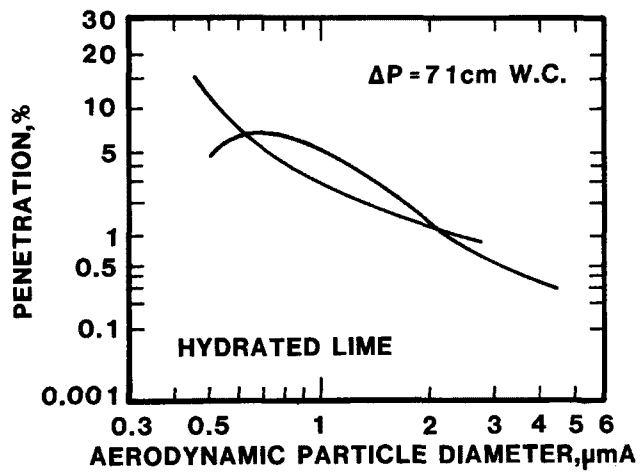

Fig. 3 LABORATORY SCALE CALVERT SCRUBBER DATA

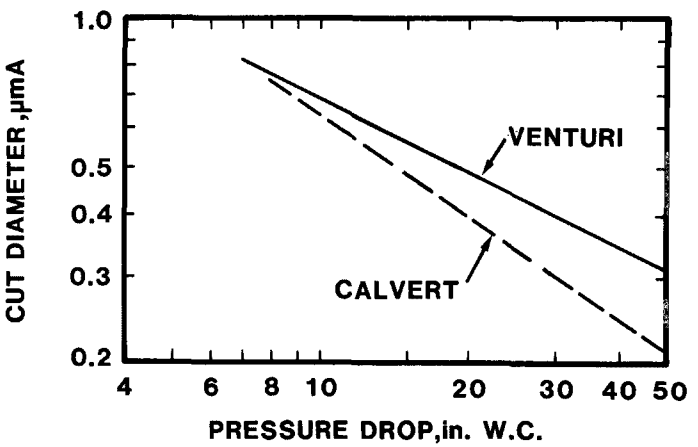

Fig. 4 CUT / POWER RELATIONSHIP

FLUX FORCE/CONDENSATION SCRUBBER SYSTEM FOR COLLECTION OF FINE PARTICULATE EMISSIONS FROM AN IRON MELTING CUPOLA

By: Seymour Calvert
Air Pollution Technology, Inc.
4901 Morena Blvd., Suite 402
San Diego, CA 92117

Dale L. Harmon
Particulate Technology Branch
Industrial Environmental Research Laboratory
U.S. Environmental Protection Agency
Research Triangle Park, NC 27711

ABSTRACT

A flux force/condensation (F/C) scrubbing system for the control of particulate emissions from an iron and steel melting cupola demonstrated its industrial feasibility during a 6-month test period.

A particle collection efficiency of 84% was required to meet the emission limit for a melting rate which ranged around 12,500 kg/hr. The demonstration plant was designed so as to enable experimental determination of operating characteristics when attaining efficiencies around the emission limit. Particle size distributions, flow rates, pressure drops, temperatures, and other parameters were measured and utilized for performance analysis and comparison with theoretical predictions.

After an initial period during which equipment and operating methods were refined, the system performed well and without significant difficulty. An optimized F/C scrubbing system for this application would require only about 65% of the predicted power requirement for a conventional high energy system.

INTRODUCTION

Flux force/condensation (F/C) scrubbing has been developed by Air Pollution Technology under EPA-sponsorship for the past several years. The object of F/C scrubbing is to reduce the power requirement for collection of fine particles as compared to conventional high energy scrubbers. The improvement in scrubber performance due to condensation effects is most apparent in the submicron size range where the mechanism of inertial impaction is difficult to apply economically. The condensation of water vapor from a hot saturated gas can be caused by contacting the gas with cold liquid.

Three condensation effects are utilized in F/C scrubbing. The suspended particles in the gas act as condensation nuclei, resulting in growth of particle mass due to the condensation of water vapor. The transfer of water vapor toward the cold liquid results in diffusiophoresis, causing particles to collect by movement of the condensing vapor toward the cold surface. Simultaneously, the temperature gradient established in the condenser causes a thermal force which leads to collection by thermophoresis. The three effects enhance the particle collection efficiency of the F/C scrubber system.

Flux force effects on particles have been known for many years and the background has been reviewed and discussed in depth by many authors. The research and development work supported by the EPA had the objectives of first assessing the potential of F/C scrubbing, then developing rational means for exploiting it, and then demonstrating the technology.

This report presents the results of a demonstration project to test further the design methods and economics of F/C scrubbing on a large scale in an industrial environment. An F/C system for the total exhaust gas stream from a 12,500 kg/hr iron melting cupola was designed, built, and tested. The operating experience included summer, fall, and winter in a demanding environment and resulted in a good test of the equipment design and materials selection.

SYSTEM DESIGN

As a replacement system in an operating plant, the F/C scrubber had to be designed to fit in the space around the existing scrubber system. Once the new apparatus was in place it had to be connected and the old system disconnected with the minimum loss of productive operation of the cupola. This and the space constraints imposed by the foundry operations had the major influence on F/C system layout.

Conservation of project cost required that the maximum amount of existing auxiliary equipment be used. Thus, the old afterburner, scrubber pump and sump, fan, and stack were used.

The F/C system was built to operate in two basic configurations, induced draft (I.D.) and forced draft (F.D.). The F.D. mode has the potential advantage of reducing the fan power requirement by about 6%, with the possible disadvantage of entrained liquid entering the fan.

The system flow diagram is shown in Figure 1 for the I.D. configuration. Only the ducting was modified to switch from forced to induced draft; the remaining components remained unchanged.

Process Description

The cupola melts scrap iron and steel using heat generated by the combustion of coke. Raw materials when the program started were scrap structural steel, engine blocks, metal stampings and turnings, cast iron piping and fittings, and other miscellaneous metal parts. During the

construction period the cupola was converted to water cooled operation and the metal charge was changed to small steel scrap.

The scrap and coke are charged together in 1,800 kg batches with an iron-to-coke-mass ratio of 6. Small amounts of limestone, 20-30 kg, are also charged to form slag. The nominal rate is 12,500 kg/hr and the normal tuyere air flow rate is 3.5 DNm^3/s.

The exhaust gas from the bed of material in the cupola is composed typically of 14% CO, 13% CO_2, and 73% N_2. Additional combustion air which enters the charging door at a rate of 2.3 DNm^3/s allows for complete conversion of CO to CO_2. An ignition burner ensures that a flame source is available for combustion of the CO to CO_2. (It was not needed or used during initial tests.)

Combustion is completed in a brick lined afterburner. The exhaust gases should leave the afterburner tank at a temperature ranging from 800 to 1,000°C. The exhaust gas flow rate at this point is about 6.6 DNm^3/s. After the cupola modification and the change to steel scrap charge, the cupola gas would not burn consistently so the gas temperature was lower and more variable than in preliminary tests.

The hot gas leaves the afterburner and is cooled in the saturator by water sprays and the temperature approaches the adiabatic saturation temperature. Typically, the saturation temperature achieved ranges from 71°C to 77°C. The maximum water spray rate in the saturator is 4.5 l/s (75 gpm).

The condenser and cooling tower system has a design heat rejection rate of 9.6×10^6 J/s (33×10^6 Btu/hr). The water flow rate can be varied up to 69 l/s (1,100 gpm). The cold gas temperature leaving the counter-current packed-bed condenser is about 55°C at design flow rates.

The exhaust gases leave the condenser and enter either the exhaust fan or the scrubber, depending on the ducting configuration. The primary particle collection device in the system is a gas-atomized scrubber with a variable area throat, an integral water sump, and an entrainment separator.

The fan used in the demonstration plant was re-built from that used in the previous system and is a straight radial blade design. The flow rate of the fan is approximately 14 Am^3/s (30,000 cfm) at -96 cm W.C. (-38 in. W.C.).

The condenser water comes from the cooling tower which is designed to cool 69 l/s (1,100 gpm) of water from 66°C to 38°C with ambient air. This is accomplished by evaporative cooling.

The settler was designed to remove particles collected by the scrubbing liquid. A 1.3 l/s (20 gpm) stream of sump water is clarified by the settler. The thickened sludge (10-30% by wt) is disposed of as land fill. The clarified water (100 ppm solids) is returned to the sump.

PERFORMANCE TESTING

In the course of system start-up, a significant problem with the original exhaust fan caused excessive power consumption and tripping of the electrical overload device. This condition continued until a new fan wheel, which A.P.T. designed, was installed. Some problems due to foaming and entrainment carry-over had to be resolved, but system operation was otherwise quite good during the test period. No lost production time was experienced by the foundry due to problems associated with the operation of the F/C scrubber system.

The major test program variables were the condenser liquid flow rate and scrubber pressure drop. The condenser liquid flow rate affected the amount of cooling in the condenser and, hence, the condensation ratio. The scrubber pressure drop could be varied by changing the scrubber throat flow area and the scrubber liquid-to-gas ratio.

Samples were usually taken at the inlet to the condenser and at the scrubber outlet. For some runs samples were also taken at the scrubber inlet. Sampling at three locations allowed the condenser performance and scrubber performance to be evaluated separately.

The particle size distribution and mass concentration were measured with University of Washington cascade impactors equipped with precutters. Several modified EPA Method 5 total filter runs were made to determine total mass concentration for compliance tests and to confirm impactor mass loadings.

From measurements of cumulative mass concentration as a function of particle size, particle penetration was computed as a function of particle size. The data was analyzed using a computer program which calculated impactor cut points and cumulative mass concentrations based on weight gain per stage, impactor flow rate, and impactor calibration data.

Performance Model

The system performance model can be used to predict the emission from a F/C scrubber system installed on a pollutant source with a known particle concentration and size distribution. The model allows independent variation of condensation ratio and scrubber pressure drop.

Without going into the details of the mathematical model, the basic concepts and outline of the approach will be discussed. The gas leaving the source is hot and has a water vapor content which depends on the source process. The first step is to saturate the gas by quenching it with water.

In the condenser there is diffusiophoretic and thermophoretic deposition as well as some inertial impaction (and, perhaps, Brownian diffusion). The particles in the gas leaving the condenser will have grown in mass due to the layer of water they carry.

Subsequent scrubbing of the gas will result in more particle

collection by inertial impaction. There may be additional condensation, depending on water and gas temperatures, and its effects can be accounted for.

The mathematical model for the F/C demonstration plant accounts for the mechanisms and assumptions outlined below:

Saturator
1. Gas is humidified and cooled to adiabatic saturation temperature.
2. No condensation occurs.
3. Particle collection in the saturator is negligible.

Condenser
1. Particles are collected by impaction in packed column.
2. Condensation occurs, causing growth of particles.
3. Collection occurs in condenser due to diffusiophoresis.

Scrubber
1. Grown particles are collected by impaction in scrubber.
2. Negligible condensation occurs.

EXPERIMENTAL RESULTS

Experimental performance measurements which were made during the last 2 months of the test period represent the best level attained after system adjustment was nearly completed. The "36 series" of runs were in the I.D. mode.

Runs 36/12 and following were made after the foaming problem was resolved and the scrubber liquid piping revised to give better purging of the internal sump. The "37 series" of runs were made in the F.D. mode with the exception of 37/21 and following, which were in the I.D. mode.

The hot gas temperature leaving the afterburner was for most of the runs significantly lower than anticipated. The design-basis hot gas temperature was 1,000°C, as measured in preliminary tests. The maximum temperature measured was about 850°C. The low gas temperature resulted in a reduction in the attainable condensation ratio and the maximum was about 0.2 g H_2O/g D.G. (dry gas). It had been anticipated that a condensation ratio of 0.30 g H_2O/g D.G. could be achieved with the higher gas temperature.

Particle Mass and Size

The average particle mass concentration at the inlet to the condenser was 2.4 g/DNm^3, which is 33% higher than the design basis mass concentration of 1.8 g/DNm^3.

Condenser inlet mass concentration measurements varied significantly from run to run, which reflects the problem of having to sample during various periods in the charging cycle. Inlet sampling times had to be much shorter than outlets because the inlet concentrations were so high. Consequently, one inlet sample would not be representative of the period

over which the outlet sample was taken. When scrubber penetrations were computed on the basis of the inlet and outlet samples for each run, there was great and random variation in the results.To cope with this difficulty an average condenser inlet size distribution was used in determining the grade penetration curves.

The average cumulative mass inlet concentration distribution was used in combination with the cumulative mass outlet concentration distribution for each run to compute the grade penetration relationship for that run. Figures 2 through 5 present experimental and predicted grade penetration curves for runs 36/10 through 36/13.

The grade penetration curves show that predictions and experiment compare well in some cases but not in others. Experimental penetrations at around 1 μmA tend to be higher than predictions, and this is true for both F/C and non-F/C conditions.

The performance in the F.D. mode was erratic and not improved as much by condensation as it was in the I.D. mode. Some of the condensed water may have evaporated in the fan so that the particles entering the scrubber were smaller than those entering the fan. It was not possible to resolve this question during the test period.

The variation of computed penetrations appears to be caused by the uncertainty of the inlet size distribution. The agreement between predictions and experiment for many of the series 36 runs is considered good for field experimental conditions, where the equipment is being modified and the source process is cyclic.

ECONOMIC ANALYSIS

An optimum F/C scrubber system design for this application would not be significantly different from the demonstration plant and the process design would remain substantially unchanged. The major modifications recommended for an optimum system involve equipment redesign and specifications to reduce capital expense and to ensure that the gas temperature would be high.

Significant cost savings can be achieved by using a single combined condenser/scrubber vessel. Experiments with the demonstration plant showed that the vessel diameter and the packing depth can be smaller than used.

Because of space requirements, the cooling tower had to be elevated on a platform above the saturator and sump. Consequently the most compact tower was chosen, not the most economical or energy efficient. A wood-filled cooling tower would have been the best choice if space were not at a premium. Such a tower would require only 22 kW (30 HP), compared to 44 kW for the tower used on the demonstration plant. The wood packing may have some advantage over epoxy coat steel for corrosion resistance. A second circulating water pump would be required for the system but the total cost would be less because an expensive structural steel platform would not be needed.

The saturator, which was designed to fit into the available space at the foundry, would be smaller in an optimum system. The settler used on the demonstration system provided acceptable performance, however the condenser, scrubber and sump all were subject to deposition of sandy material which required removal at frequent intervals. Sloped bottoms should be used in all of these vessels.

It is also recommended that a moving belt filter be used instead of the gravity settler to remove this sandy material. These can be purchased at a lower cost than the settler which was used on the demonstration plant.

In order to evaluate the potential benefits of an F/C scrubber system as compared to a conventional one, the costs for a venturi scrubber system were estimated. The process conditions and emission criteria were the same for both systems.

Capital Cost Estimates

The capital cost of an optimum F/C system would consist of direct costs for delivered major equipment and other items such as installation, piping, and electrical, along with indirect costs such as engineering, construction overhead, and contingencies. Table 1 shows the estimated direct and indirect costs for the F/C system and the high energy scrubber. All costs were adjusted to December 1979 by means of the Marshall and Stevens cost index.

TABLE 1. DIRECT AND INDIRECT COSTS

	F/C SYSTEM		CONVENTIONAL SCRUBBER	
Direct	Ratio	Cost, $	Ratio	Cost, $
Equipment	1.00	$102,380	1.00	$ 73,765
Installation	0.40	40,952	0.40	29,506
Instruments	0.10	10,238	0.10	7,377
Piping and Ducting	0.40	40,952	0.40	29,506
Electrical	0.05	10,238	0.10	7,377
Site Preparation	0.05	5,119	0.05	3,687
Total Direct Costs	2.00	$209,879	2.05	$151,218
Indirect				
Engineering	0.40	40,952	0.40	29,506
Construction Overhead	0.45	46,071	0.45	33,193
Contractor's Fee	0.10	10,238	0.10	7,377
Contingency	0.40	40,952	0.40	29,506
Total Indirect Costs	1.35	$138,213	1.35	$99,582
Fixed Capital Investment	3.40	$348,092	3.40	$250,800

OPERATING COSTS

The operating costs for the air pollution control system consist of the annual cost of the utilities (power and water), raw material, and maintenance. Table 2 shows the power requirement for both the F/C scrubber system and a conventional scrubber. The F/C scrubber system would require only 65% of the power of the conventional scrubber. The exhaust fan for the conventional scrubber would require more than twice the power of the F/C system.

TABLE 2. SUMMARY OF POWER REQUIREMENTS

	Power, kW (HP)	
	F/C Scrubber	Conventional Scrubber
Exhaust Fan	156 (210)	332 (445)
Saturator Pump	10 (13)	10 (13)
Scrubber Pump	2 (2)	3 (4)
Cooling Water Pumps	33 (44)	--
Cooling Tower Fan	22 (30)	--
Total Power Required	223 (299)	345 (462)

The estimated total operating costs are summarized in Table 3. The total operating cost for the F/C scrubber system was found to be $131,230 compared to $150,300 for the conventional scrubber. The annual operating cost of the F/C scrubber system would be about $19,100 less than the cost for a conventional scrubber for the conditions stated. If the operating time were reduced below 4,000 hr/yr the F/C system would be less favorable, but longer operating time would make it more favorable. Power cost will also have an obvious effect on the economics.

TABLE 3. SUMMARY OF ESTIMATED ANNUAL OPERATING COSTS

Item	Unit Cost	F/C Scrubber System	Conventional Scrubber
Capital Cost	@ 10% of F.C.I.	$ 34,810	$ 25,080
Maintenance	Materials @ 3% of F.C.I.	10,440	7,520
Labor	@ 8 hr/wk shift, $9/hr	7,200	7,200
Operating Labor	@ 12 hr/wk shift, $9/hr	10,800	10,800
Power Cost*	$0.065/kWhr	57,980	89,700
Water Use	$0.035/1,000 liters	2,000	2,000
Raw Materials	Soda ash $0.265/kg flocculant $1.15/liter	8,000	8,000
TOTAL OPERATING COST		$131,230	$150,300

*Power cost estimated for 4,000 hr/yr.

CONCLUSIONS

The following conclusions can be drawn from the results of this study:

1. The performance data were in general accord with predictions based on design methods developed by A.P.T. on previous EPA contracts.
2. The F/C scrubber system was capable of complying with all applicable air pollution regulations for the site.
3. The F/C scrubber system needs only about 65% of the predicted power requirement of a conventional high energy scrubber to achieve the same performance.
4. The particle mass concentration and size distribution emitted during the cupola charging cycle varied greatly. Continuous or semi-continuous cupola charging with a conveyor system would probably reduce the variation in emissions and gas temperature.
5. The solid/liquid separation presented some maintenance problems. Additional attention should be given to equipment design, both to prevent settling in the scrubber equipment and to improve solids separation in the water treatment system.
6. Corrosion of the cooling tower packing was severe. Acids must be neutralized in order to prevent significant deterioration of steel components in the system. Maintenance of the proper circulating water pH is also important if stainless steel materials are used because of the chloride content present.
7. Operation over a 6-month period showed that the F/C system is capable of performing well and without significant difficulty in the demanding conditions of a ferrous foundry. During the entire test period there were no production stoppages due to the F/C scrubbing system.
8. F/C scrubbing becomes more economically advantageous than conventional scrubbing as either power cost or plant operating time increases.

RECOMMENDATIONS

Experience with the demonstration plant has led to several recommendations about equipment changes; most of them are discussed above under "Economic Analysis." The essential aims of the recommendations are:

1. Minimize the costs of the equipment required to obtain F/C effects.
2. Maximize the cupola flue gas temperature.
3. Provide adequate solids removal capacity for the scrubbing liquid recycle stream.

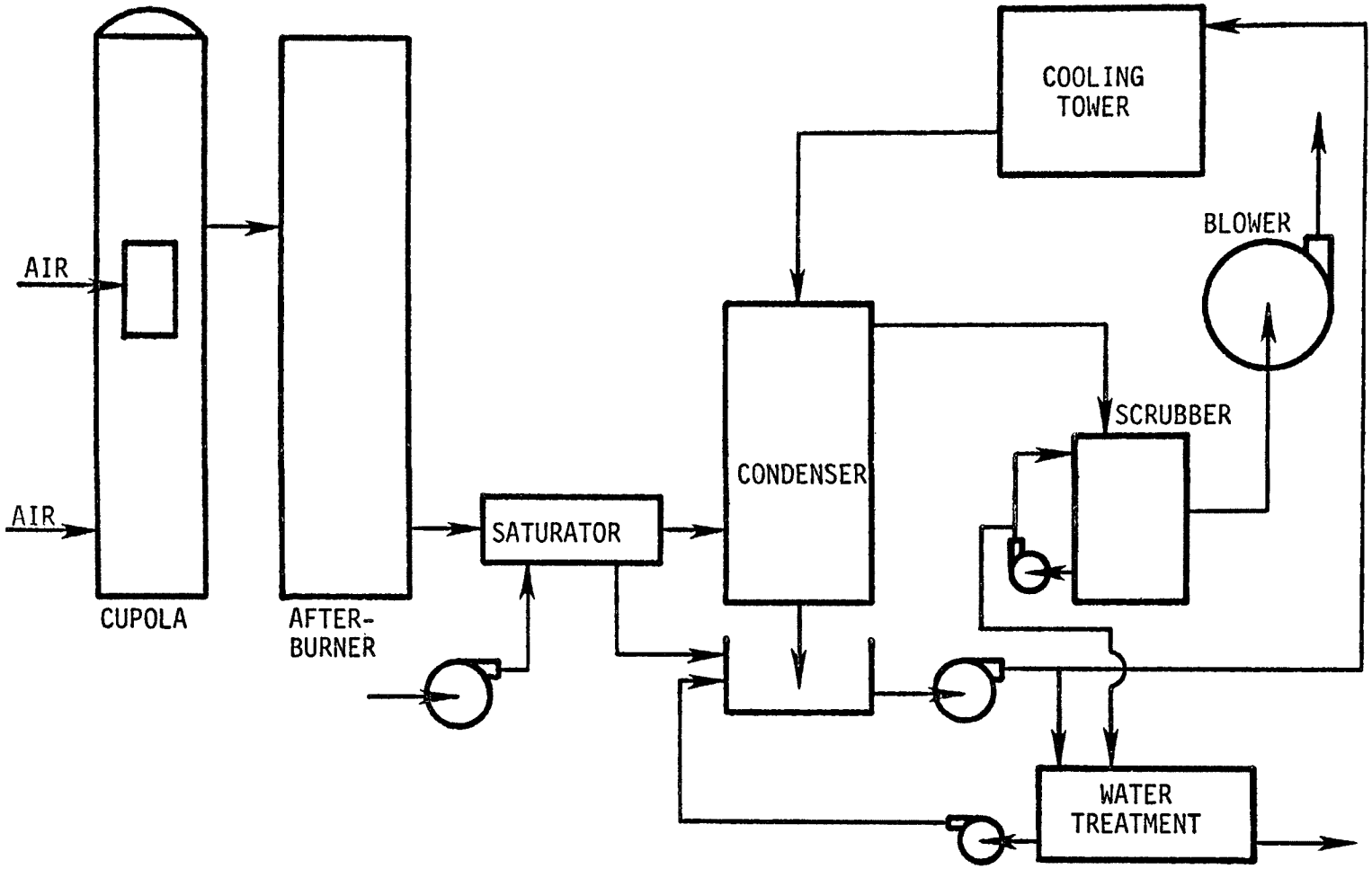

Figure 1. F/C demonstration plant flow diagram, induced draft.

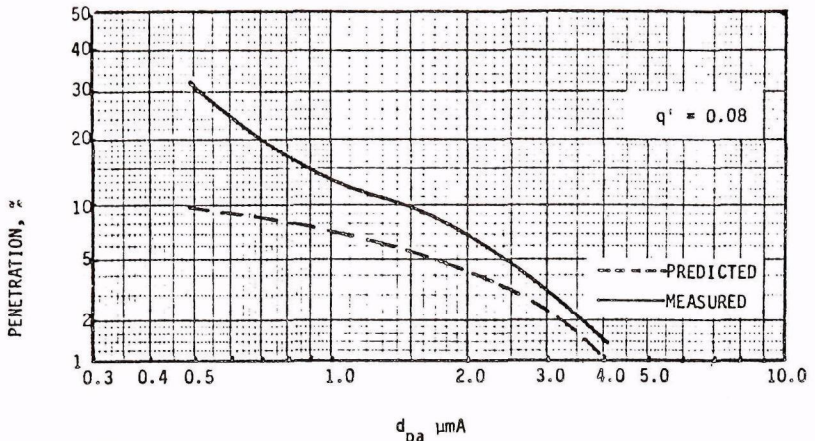

Figure 2. Particle penetration, Run 36/10

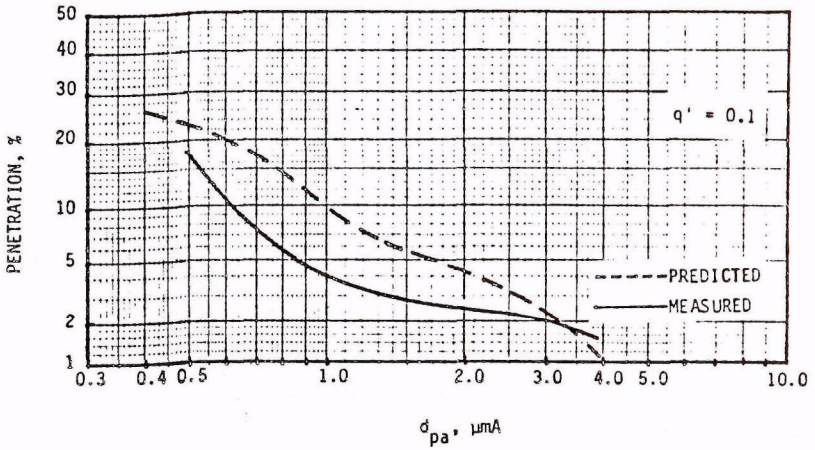

Figure 3. Particle penetration, Run 36/11

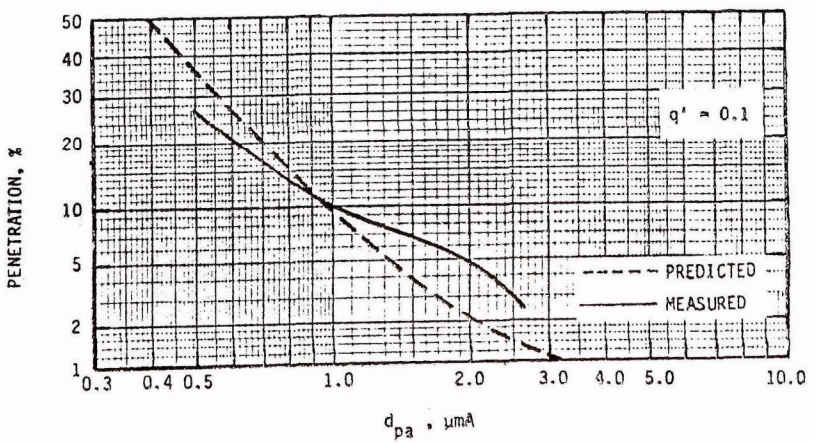

Figure 4. Particle penetration, Run 36/12

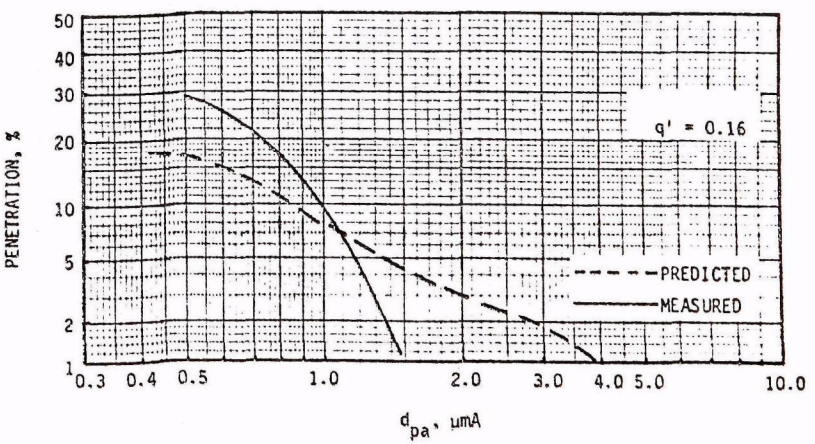

Figure 5. Particle penetration, Run 36/13

DEMONSTRATION OF HIGH-INTENSITY-IONIZER-ENHANCED VENTURI SCRUBBER ON A MAGNESIUM RECOVERY FURNACE FUME EMISSIONS

By: Anil Prem, M. T. Kearns
Air Pollution Systems, Inc.
18642 - 68th Avenue South
Kent, Washington 98031

Dale L. Harmon
Environmental Protection Agency
Industrial Environmental Research Laboratory
Research Triangle Park, N. C. 27711

ABSTRACT

A 33,960 Am^3/hr (20,000 acfm) permanent demonstration system, consisting of the Air Pollution Systems' High Intensity Ionizer (HII) and a variable throat venturi scrubber, has been installed on a magnesium recovery furnace at Teledyne Wah Chang Albany, Albany, Oregon. The particulate emission from this source is predominantly submicron in nature. Fairly high stable electric fields of 10-12 kV/cm have been successfully maintained in the HII. Comparing the measured charge/mass, and the calculated charge/mass based on the measured particulate size distribution at the outlet of the scrubber, the HII appears to be imparting fairly high charge to the incoming particulate. Preliminary performance test results indicate higher performance of the venturi scrubber when the HII is energized for all the venturi pressure drops tested. The penetration reduction due to HII increased as the venturi pressure drop was increased, and as the particle size decreased.

INTRODUCTION

Particulate emissions from industrial stack gases are usually collected by one or more types of three conventional devices--electrostatic precipitators, scrubbers, and fabric filters--the design of which has virtually remained unchanged since the turn of the century. However, with the increased need for fine particulate control, the cost of these particulate collection devices is also substantially increasing. This has resulted in a flurry of research and development activity to produce more cost effective pollution control systems.

The objective of the novel device program of EPA/IERL-RTP's Particulate Technology Branch was to identify and evaluate new technology or new combinations of well studied mechanisms that are cost effective in controlling fine particle emissions. Air Pollution Systems's (APS) High Intensity Ionizer (HII) falls in this category. Due to its unique geometry, HII can maintain very high electric fields, resulting in a significant improvement in the particle charging capability compared to a conventional particle charger.

Using an HII, APS has developed an electrostatically enhanced venturi scrubber (Scrub-E) that is capable of high fine particle collection at a reduced pressure drop compared to a conventional venturi scrubber. Based on results of an EPA sponsored test of a laboratory scale unit (1), APS won a contract from EPA to demonstrate the Scrub-E on an industrial application. A magnesium recovery furnace which predominantly emits fine particulate was selected as the demonstration site. A 33,960 Am^3/hr (20,000 acfm) demonstration Scrub-E system was designed, fabricated, and installed. This paper describes the APS Scrub-E, the system setup at the demonstration site, and the preliminary test results.

APS Scrub-E

Conventional scrubbers usually have low particle efficiencies in the 0.01 to 2.0 μm diameter range. This low particle collection efficiency in the fine particle size range is caused by conventional wet scrubbers' primary use of inertial impaction. In order to increase the fine particle collection efficiency of conventional scrubbers, it is necessary to increase the energy input substantially. For high efficiency collection of fine particles at a moderate energy consumption, one must apply some particle collection force that is not dependent on increasing the relative velocity between the drops and gas stream. Electrostatics is one such promising particle collection force.

APS Scrub-E utilizes electrostatics to improve the performance of a conventional venturi scrubber. The APS HII is utilized to highly charge the particulate in the flue gas. The negatively charged particle sees an induced positive charge on the neutral droplet (charged particle image force) in the venturi scrubber and is attracted to it. This results in increased collection efficiency. The higher the particle charge, the higher the improvement in collection efficiency.

The APS HII, due to its unique electrode geometry, is successful in maintaining a highly stable intense corona discharge. The cathode is a solid metal disc supported by a structurally reliable tube section centered in a cylindrical anode arrangement. The electrode configuration produces a substantially uniform three dimensional field which is a principal factor in the greater electrical stability. Typical operating field strengths of 10-13 kV/cm have been obtained compared to 3.5 kV/cm for wire electrode geometry in an industrial flue gas.

In addition to the very high electric fields, the HII electrode geometry produces a concentrated field with ion densities of $10^9 - 10^{10}$ $ions/cm^3$, many times that obtained in the wire electrode geometry. As a result of higher fields and ion densities, both the level of charge acquired by the particles and the rate of charging are significantly higher. For example, even with the significantly lower residence time in an HII compared to an electrostatic precipitator, the level of charge obtained by the particles exiting an HII are two to three times higher compared to the particles exiting an ESP. This means that particles can be charged to a high level in a very small volume resulting in a

very compact system that can be retrofitted to existing scrubbers.

Demonstration Project

The site selected for the demonstration project was a magnesium recovery furnace at Teledyne Wah Chang Albany (TWCA), Albany, Oregon. TWCA is a large production facility for zirconium and hafnium metals, and columbium and tantalum alloys.

The particulate gas stream to the demonstration unit originates in four emission sources. Two of these are the magnesium recovery furnaces where the spent magnesium, as $MgCl_2$, is reduced to magnesium metal for recycle. $MgCl_2$, along with the flux, is loaded into crucibles which are placed in a gas fired furnace. Once the reduction is completed, first the magnesium metal and then the slag are manually ladled from the furnace. The third emission source is the $MgCl_2$ furnace which is essentially a concentrator operation to recover whatever magnesium is left in the crucibles. The fourth emission source is the smokehouse, where the $MgCl_2$ crucibles are heated in a burnout operation.

All the furnaces primarily emit MgO fume. The majority of the MgO fume emission is attributed to the magnesium recovery furnaces during the ladling process. Significant emissions occur during the slag ladling from the magnesium recovery furnace. The magnesium reduction process is a batch operation. Each furnace is tapped four or five times a day.

Prior to designing the demonstration unit, the magnesium recovery furnace emissions were sampled to characterize the particulate. Scanning electron microscope (SEM) photographs indicated that the greatest proportion of the particulate were less than 1.0 μm in diameter. The size distribution of the particulate was also measured using a University of Washington Mark III cascade impactor. The mass mean diameter of the particulate was found to be 1.48 μm and the average mass concentration 0.19 g/DNm^3. The above measurements indicated that the emissions are predominantly ultrafine particulate. Brief resistivity measurements of the particulate in the APS laboratory indicated fairly low resistance (3×10^8 to 1×10^9 Ω-cm).

Figure 1 is a flow diagram of the EPA demonstration system at Teledyne Wah Chang Albany, Albany, Oregon. Flue gas from the four emission sources enters the demonstration system at the top of the HII module. The HII module consists of seven anode cylinders each with a concentric probe with three discharge electrodes. The flue gas stream is distributed amongst these cylinders to charge the particulate prior to entering the venturi scrubber.

The venturi scrubber is a variable throat design utilizing a Bombay type damper to vary the throat opening. A 90° elbow is directly below the venturi. The gas stream leaving the venturi enters a conventional separator and exits to the atmosphere through two in-line induced draft fans, operated individually or in series.

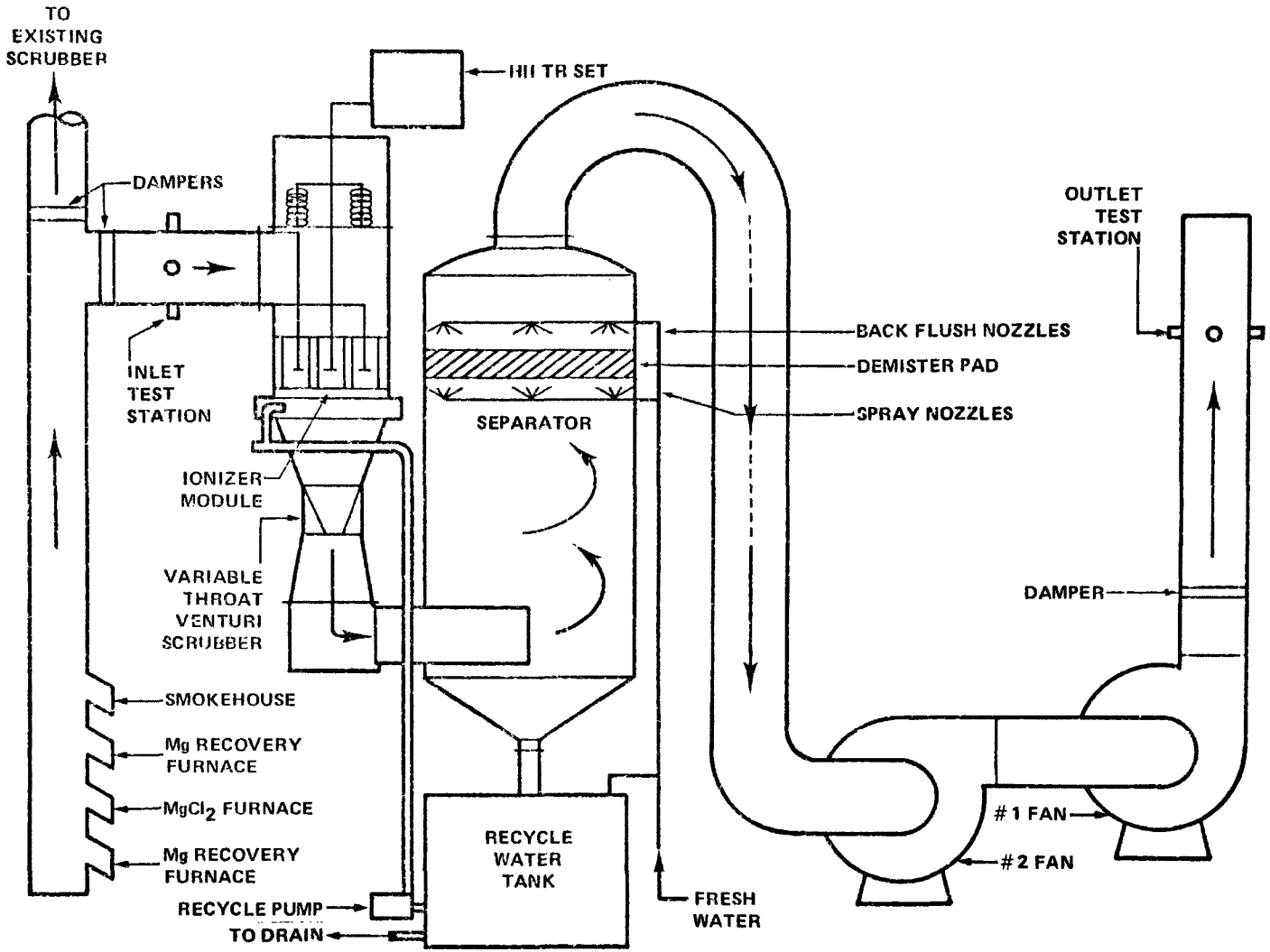

Figure 1. EPA demonstration system flow diagram.

The pressure drop across the venturi is controlled by the Bombay damper and the gas flow rate through the system can be controlled by both the inlet and outlet dampers. The liquid flow rate to the venturi can be controlled by the valves in the liquid flow lines. Liquid to the venturi is supplied from the recycle tank. Kimre demister pads, retrofitted into the separator to eliminate droplet carryover, are wetted with 100 percent fresh water.

Inlet sampling ports to the system are upstream of the Scrub-E inlet damper. Outlet sampling ports are approximately four duct diameters upstream of the stack outlet.

Results

The first preliminary performance tests on the APS Scrub-E at TWCA used EPA Method 5 and University of Washington Mark III impactors. The main gas flow rate was maintained at 25,500 Am^3/hr and the liquid flow rate at 52 m^3/hr. The venturi pressure drop (ΔP) was maintained at 51 cm H_2O. Both HII "on" and "off" cases were evaluated.

As the tests progressed, a significant droplet carryover from the separator became apparent. This droplet carryover made it almost impossible to accurately determine system performance. The liquid flow rate was arbitrarily reduced to 45 m^3/hr and, in the final two tests, 22 m^3/hr. Neither reduction alleviated the droplet carryover problem.

In another effort to alleviate the droplet carryover problem, APS installed demister pads in the outlet section of the separator. A few spray nozzles were installed upstream and downstream of the demister pad to irrigate them. This alleviated the droplet carryover problem.

System performance was next evaluated, as a function of venturi ΔP for both HII "on" and "off" cases. The main gas flow was maintained at 25,500 Am^3/hr and the liquid flow rate 30 m^3/hr. University of Washington Mark III cascade impactors were used for the performance evaluation. For the HII "on" tests, the HII was left in the automatic mode.

Inlet mass concentration during the above tests varied from 0.025 to 0.16 g/DNm^3. Outlet mass concentration varied from 0.005 to 0.053 g/DNm^3. Inlet mass mean diameter ranged from 0.52 to 0.79 μm. Outlet mass mean diameter ranged from 0.36 to 0.47 μm. Figure 2 illustrates overall collection efficiency as a function of venturi ΔP for both the HII "on" and "off" cases. Overall, the collection efficiency for the HII "on" cases was higher compared to the HII "off" cases. For both the HII "on" and "off" cases, collection efficiency increased as venturi ΔP was increased.

Figures 3 and 4 illustrate collection efficiency as a function of ΔP across the venturi scrubber for particles ≤ 3 m and ≤ 1 μm diameter, respectively. As with overall collection efficiency, the collection efficiency was higher for the HII "on" case than for the HII "off."

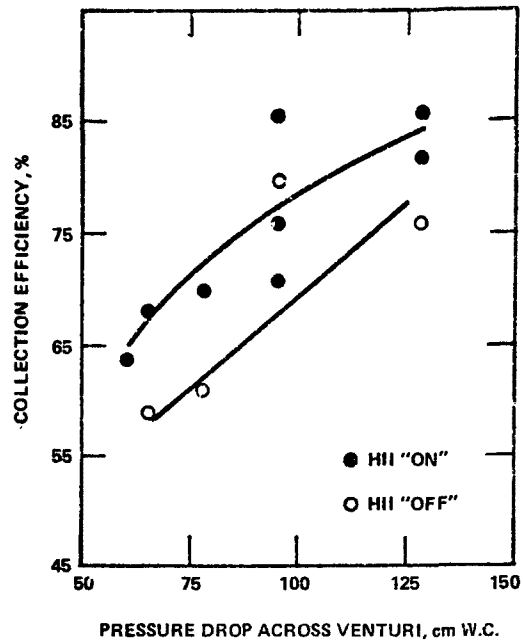

Figure 2. Overall collection efficiency as a function of pressure drop across the venturi scrubber.

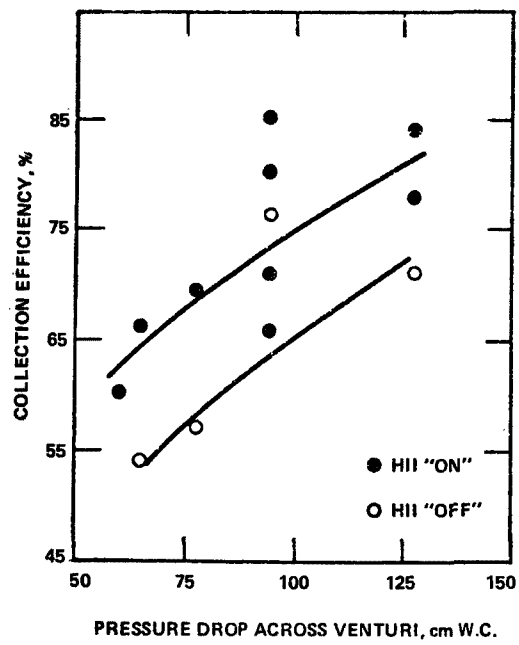

Figure 3. Collection efficiency of particles ~ 3 μm as a function of pressure drop across the venturi scrubber.

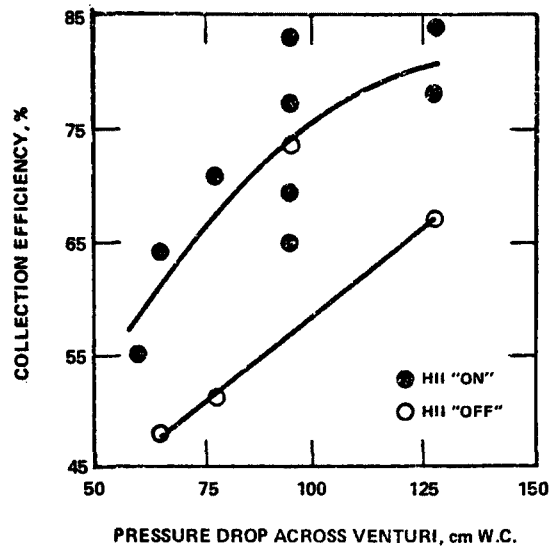

Figure 4. Collection efficiency of particles ≤ 1 μm as a function of pressure drop across the venturi scrubber.

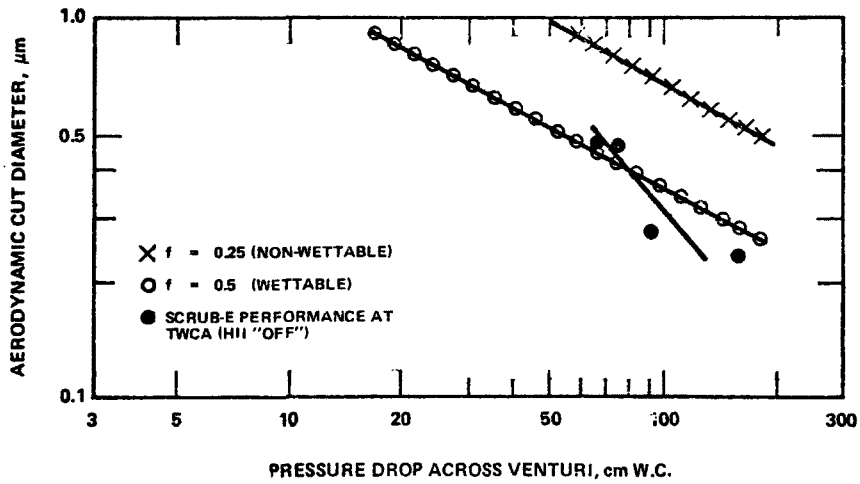

Figure 5. Representative cut diameters as a function of pressure drop for venturi scrubbers (3).

Also, for both the HII "on" and "off" cases, collection efficiency increased as venturi ΔP was increased.

Though the preliminary test results were encouraging, based on the past data, APS felt that the electrostatic charge on the particulate was not being fully utilized. At this point, APS reviewed all the data to date and attempted to arrive at a brief test program that would help optimize system operation.

An effort was made to determine how well the venturi scrubber performance at TWCA agreed with the general correlation between cut diameter and pressure drop. The aerodynamic cut diameter was calculated using simultaneous inlet and outlet particle size distribution for the Scrub-E with the HII "off." Figure 5 illustrates the aerodynamic cut diameters for various ΔP's across the venturi scrubber at TWCA along with the representative cut diameters as a function of ΔP for a venturi scrubber (2). The data shows that, with the HII "off," the venturi scrubber performance at TWCA agrees fairly well with the general correlation of cut diameter with ΔP for venturi scrubbers used to collect wettable particulate.

During the optimization tests, it was noted that the sparkover voltage in the HII was lowered significantly during the slag tap. Once the tap was completed, the HII voltage would go back up to 100 kV. This lower sparkover voltage was probably related to significant current suppression created due to high concentration of small particles and the presence of three discharge electrodes in the HII.

In an attempt to decrease the sparking, the gas flow through the system was increased to 37,400 Am^3/hr. No effect was noted on the sparkover voltage; however, the water from the separator started re-entraining. This water droplet carryover was alleviated by reducing the gas flow through the system to approximately 34,000 Am^3/hr.

Due to the fairly low HII sparkover voltage during the slag tap, the unit was turned "off" for visual inspection. The HII and the scrubber appeared to be in fairly normal condition and the sparking appeared to be in the anode section. The seven discharge electrode probes were dismantled and two out of three electrodes on each probe were removed to decrease sparking. The probes were put back into the unit with only the last electrode. On restarting the unit, for the no-tap case, the HII was operating at 110 kV - 15 mA (higher voltage and current/electrode). During the slag tap, the HII was sparking between 80 and 100 kV, compared to around 60 kV earlier, indicating significant improvement.

Using EPA Method 17, brief mass tests were conducted to determine system performance. The outlet was sampled using an APS charge/mass probe which gave both the mass loading and charge/mass at the outlet of the Scrub-E. To accurately determine the performance of the Scrub-E for the two distinct taps (magnesium and slag), tests were conducted so as to bracket each phase individually. The main gas flow rate was maintained at 34,000 Am^3/hr, the liquid flow rate to the venturi at 42 m^3/hr,

venturi ΔP at 51 cm H_2O, and the water flow rate to the demister at 4.5 m^3/hr.

Inlet mass concentration during the magnesium tap ranged from 0.0087 to 0.044 g/DNm^3 (average 0.021 g/DNm^3); for the slag tap, inlet mass concentration ranged from 0.061 to 0.16 g/DNm^3 (average 0.090 g/DNm^3). The charge/mass measured at the Scrub-E outlet ranged from 85 to 655 $\mu C/g$. On the average, the values were higher for the magnesium tap than for the slag tap. The Scrub-E performance improved when the HII was "on." The collection efficiency on the average was of the same magnitude (72.5 percent) for both the magnesium and slag taps when the HII was "on." For the HII "off" case, the collection efficiency for the slag tap was higher than the magnesium tap (61 percent vs. 42 percent).

Table 1 summarizes preliminary test results to date. Bearing in mind that the quantitity of data obtained is very limited, and that no definite conclusions can be drawn from it, a few general trends can be seen. The Scrub-E collection efficiency is increased when the HII is "on."

The penetration reduction with the HII "on" appears to increase both as the particle size decreases and the venturi ΔP increases. Since the inertial forces decrease as a function of particle size, the relative effect of electrostatics should increase as the particle size decreases (3). Increase of venturi ΔP should increase the atomization of the liquid resulting in smaller droplet size. The relative effect of electrostatics increases with the decrease in the droplet size (3).

The baseline efficiency, for a given venturi ΔP and approximately the same liquid/gas flow ratio, decreased as the gas flow rate was increased, possibly due to the lower residence time in the scrubber. However, the penetration reduction with the HII "on" increased, probably due to higher sparkover voltage in the HII during the tap.

Throughout the preliminary tests, the number of furnace taps during a day was around three, compared to nine taps when the site was selected. This is related to the lower demand of the zirconium metal. Due to the manual nature of the process, the emissions are very erratic and no two taps are alike. This is reflected in the scatter of the mass emission and charge/mass data. The reduced number of taps a day appears to have changed the particle characteristics. Both the grain loading and the mass mean diameter of the particulate appear to have decreased.

Conclusions

A 33,960 Am^3/hr (20,000 acfm) demonstration system, consisting of an Air Pollution Systems' High Intensity Ionizer and a variable throat venturi scrubber, has been installed on a magnesium recovery furnace at Teledyne Wah Change Albany, Albany, Oregon. Preliminary tests were conducted by APS to evaluate the performance of the system. Tests were conducted to study the effect of pressure drop across the venturi

TABLE 1

SUMMARY OF PRELIMINARY TEST RESULTS

GAS FLOW (Am^3/hr)	LIQUID FLOW (m^3/hr)	VENTURI ΔP (cm H_2O)	TYPE OF MEASUREMENT	BASE EFFICIENCY (%)	PENETRATION REDUCTION (%)
25,500	30	64	C.I.-Overall η	57	21
"	"	95	"	67.5	29
"	"	127	"	76	33
"	"	64	C.I.-Part $\leq$3 μm	52.5	23
"	"	95	"	62.5	30
"	"	127	"	71	34
"	"	64	C.I.-Part $\leq$1 μm	47	26
"	"	95	"	57.5	40
"	"	127	"	67	41
34,000	42	74	EPA Method 17	51.5	43

scrubber for both the HII "on" and "off" cases. Problems were encountered during the testing which resulted in some modifications to the system.

Conclusions drawn from the preliminary test results to date are:

1. The APS Scrub-E installation has been fully functional for all aspects of operation.

2. Most of the particulate emissions occur during the magnesium recovery furnace tap. There are two distinct phases within a single tap: ladling of magnesium and slag.

3. For the whole tap, the average mass mean diameter at the scrubber inlet was 0.64 μm, and 0.41 μm at the outlet.

4. Emissions are generated over a very short time span and are very sporadic, which makes testing difficult.

5. The retrofitted Kimre packing in the separator eliminated the earlier carryover problems.

6. The initial HII configuration with three discharge electrodes gave a lower sparkover voltage and current during the tap. Increasing the main gas flow rate from 25,500 Am^3/hr to 37,400 Am^3/hr did not improve the HII electrical characteristics.

7. Removing two of the three discharge electrodes from the probe in the HII significantly improved the electrical characteristics.

8. High charge/mass values were obtained at the outlet of the scrubber for both the magnesium and slag taps.

9. For the HII "off" tests, the venturi scrubber performance data is in fairly good agreement with the general correlation of cut diameter with pressure drop for venturi scrubbers.

10. The collection efficiency for both the HII "on" and "off" cases increased as the pressure drop across the venturi increased.

11. The collection efficiency with the HII "on" was higher than with the HII "off."

12. The penetration reduction due to HII increased as the venturi pressure drop was increased, and as the particle size decreased.

ENDNOTES

Acknowledgements

The demonstration projected has been supported by Industrial Environmental Research Laboratory, U. S. Environmental Protection Agency, RTP, N. C.,

under Contract No. 68-02-2666, Dale L. Harmon, Project Officer. Special appreciation is noted to Gerald Sing of Teledyne Wah Chang Albany, for his support and cooperation on this project.

References

1. Calvert, S., et al. (1976), "APS Electrostatic Scrubber Evaluation," EPA-600/2-76-154a (NTIS No. PB 256335).

2. Calvert, S., (1976), "Engineering Design of Fine Particle Scrubbers," JAPCA, 24, No. 10, p. 929.

3. Prem, A. and M. J. Pilat (1978), "Calculated Particle Collection Efficiencies by Single Droplets Considering Inertial Impaction, Brownian Diffusion and Electrostatics." Atmospheric Environment, Vol. 12, pp. 1981-1990.

A NEW ENTRY IN THE HIGH EFFICIENCY SCRUBBER FIELD

By: L.C. Hardison, President
Air Resources, Inc.
600 N. First Bank Drive
Palatine, Illinois 60067

Frank Ekman, Ph.D., P.E.
US Environmental Protection Agency
(Current Affiliation)
R.R. 5
Barrington, Illinois 60010

ABSTRACT

The use of Venturi, flooded-disk and various orifice-type scrubbers for wet collection of fine particles at high energy levels and high levels of particulate collection efficiency is well known. In general, these scrubbers may be characterized as roughly equivalent in performance level and various models are competitive only with respect to price and mechanical considerations and ease of maintenance or operation.

The MVS (Modular Venturi Scrubber) invented by Frank Ekman and being marketed by Air Resources, Inc. is the latest entry into this competitive field, and has several advantages in size, cost and simplicity over more conventional designs. This paper describes the development, design and operation of the MVS units.

INTRODUCTION

The ARI MVS(TM) Modular Venturi Scrubber represents a significant improvement in the art of wet particulate collection. While it involves no essentially new principles of collection of particulates by impaction, it does represent the embodiment of proven techniques into a modular system which has distinct performance advantages, which can be manufactured at lower cost and which can be adapted to larger gas volumes than existing techniques.

This paper reviews the evolution of Venturi scrubbers and the derivation of the MVS(TM) design. It describes a unique application concept made possible by the modular construction, and develops application criteria for accommodation of the modular design to industrial processes.

VENTURI SCRUBBER DEVELOPMENT

The development of the ARI MVS(TM)(1) does not represent a scientific breakthrough, in which new or startling different physical principles are invoked to accomplish particulate collection at previously unobtainable low levels of energy consumption. Rather, it is the culmination of many years of gradual development of the Venturi scrubbing principle originally embodied in the Pease-Anthony scrubber.

During World War II, a method was needed to disperse the newly discovered DDT over the Pacific islands, by air, to kill mosquitos. Dr. E.D. Comings and others at the University of Illinois adopted the dry venturi meter to this use. A few years later, Dr. H.F. Johnstone of the University of Illinois, was consulting on a Pease-Anthony spray tower that was not performing properly. Johnstone, remembering the success of the venturi in creating droplets in an airplane slip-stream, inserted a venturi with nozzles into the duct ahead of the spray tower. The purpose of the venturi was strictly to supply fine droplets so the spray tower would work more efficiently. The combination worked well and everyone was delighted. Later, someone turned off the nozzles in the spray tower and scrubbing efficiently was not diminished at all. The Venturi Scrubber was born!

The typical configuration of the first scrubber, as shown in Figure 1, was not changed appreciably for many years. Converging and diverging angles were held at 25° and 7°, just as they were on the existing dry Venturi. At first, throats were round as in a conventional Venturi, and nozzles were placed upstream of the throat in elaborate patterns to distribute the water evenly across the throat. Unfortunately, particulate built up on the nozzles and their support structure so that the design was modified to remove the spray nozzles from the gas stream. This was done by making the Venturi throat rectangular, up to 14 inches in width by whatever length was required for the capacity. Nozzles were positioned on the long side of the Venturi, flush with the gas stream. However, the traditional 25° and 7° angles were maintained, with the result that 20 feet of length, or more, were needed for the Venturi to contract from duct diameter down to throat width and back again for large ducts. The mist eliminator continued for many years to be designed to spray-tower dimensions.

The result was a new design of scrubber that was much more efficient than anything that had gone before, but one that took up a great deal of room, and one that had to be individually designed for each installation. In later years, after the first patents expired, competition entered the field and a variety of changes were made in the design. However, the changes were mostly minor and cosmetic, and not much progress was made to ward evolution of a truly functional design.

With this historical background, the development of the MVS Modular Venturi Scrubber design and application concept follow logically, and are described in the subsequent sections of this paper.

DEVELOPMENT CONCEPT

A principal disadvantage of Venturi scurbber is that the size of the system had a marked influence on the design of the enturi approach section, throat and diffuser. Circular Venturis have long suffered from the size limitation imposed by the inability to wet the gas stream uniformly when wetter wall designs such as that incorporated into the Pease-Anthony scrubber are used. In very large sizes, the throat length required for uniformly mixing the water droplets from the outer wall into the center of the throat section is sufficiently long that all of the droplet acceleration has taken

place before all of the gas has been wetted. This imposed a nearly immutable upper limit on the size of simple Venturis. Various devices have been used to minimize this problem, such as the elongated rectangular slot Venturi and the flooded disk. These approaches are illustrated in Figures 2 and 3.

Unfortunately, the problem can be mitigated, but not eliminated completely, for large installation. Therefore, the possibility exists that in any given application, a large unit will not function as well as small prototypes or test units.

The MVS(TM) design, as illustrated in Figure 4, seeks to bring a new approach to the field. First of all, the throat of the Venturi, including both converging and diverging sections, is now the space between two round parallel bars spaced about 1 inch apart. If 3/4 inch I.P.S. pipe is used for the bars, as it usually is, the length of the Venturi in the direction of flow is just over 1 inch. Now a series of bars placed side by side having a depth of only 1 inch in the direction of flow, displace a whole Venturi that can easily be more than 20 feet long.

The MVS(TM) modular design concept assures that no upper size limit is imposed on the scrubber design. Each element of gas flow is treated identically, and there is substantially no variation in performance from the smallest units to those of extremely large size. None of the elements incorporated into the design have inherently decreasing efficiency levels with increasing size, nor to any of them have features which are inherently more costly for scrubbers of extremely large or extremely small size. Rather, all of the elements can be treated as identical "building blocks" and assembled to match the requirements of any particular scrubbing job. The next step was to miniaturize the spray-tower collection, which was done by using Z-vanes. These steps were accomplished by an earlier patent(1) issued to one of the authors.

The new patent, assigned to ARI, carried simplification one step further by modularizing construction. Further, problems in the design of high energy scrubbers relate to the difficulty in achieving de-entrainment of the scrubbing liquid from the gas stream after the throat of the Venturi. The Pease-Anthony scrubber illustrated in Figure 1 often incorporates a cyclonic separator in which the efficiency of de-entrainment varies inversely with the diameter of the cyclonic section. Whereas small units incorporating this design are highly effective, larger units are both cumbersome to design and inherently less efficient in the separation of scrubbing liquid. Compound entrainment separator designs which use the cyclonic action only for a "rough cut" followed by a chevron or mesh mist eliminator have been used successfully, but inherently require compromise between the optimum design of the cyclonic section and the design of the chevron or mesh containment vessel. Also, when such separators are located in a vertical gas stream, the mechanism for draining collected water back into the scrubber becomes cumbersome and, at very large sizes, it is nearly impossible to provide sufficient slope to the streams to assure adequate drainage of liquid to the side walls. This means that the entrainment separators must be operated at a velocity low enough that the liquid droplets can fall downward against the rising gas velocity without being re-entrained.

With modular organization of the Venturi, all elements of gas in the scrubber are treated exactly the same for the first time, so that all portions of gas can be treated to maximum efficiency. It also means that scrubbers can be prefabricated to reduce cost. Prefabrication means that customers can be given almost instant delivery instead of the several months required in many instances. For very large units that are difficult to ship, shipping of prefabricated elements is indicated. These can be quickly and easily assembled on site. Lastly, a considerable number of scrubbers have to be situated in extremely crowded plants. With standard scrubbers such expensive tactics as tearing out walls on roofs are required, and, even then, the scrubber sometimes has to be constructed on site. With the MVS(TM) design, flat prefabricated sections can be brought in through existing passageways and can then be assembled in the field. The small size of the MVS reduces the space and money required for installation substantially.

THEORY

When a sphere of diameter D_d (in Venturi scrubbers the sphere is usually a water droplet) sweeps through a gas, the flow lines part to let it through, as shown in Figure 5.

Small particulates suspended in the gas do not follow the flow lines because of inertia. As shown, some impinge upon the droplet while others that are further away from the center line of the sphere escape. If the distance between symmetrical flow lines that carry particles that just barely impinge is "X", an efficiency of collection can be as the ratio of areas perpendicular to the gas stream, or X^2/D_b^2. Other properties of the gas stream and of the particle must be taken into consideration, and these are all assembled together in the correlation shown in Figure 6. Here target efficiency, η, is correlated against a Separation Number which can be expressed as:

$$N_S = \frac{d^2 \rho_p V_o}{18 \mu D_d}$$

Where:

N_S = Separation Number, Dimensionless
d = Particle Diameter
D_d = Diameter of Droplet
ρ_p = Particle Density
V_o = Relative Velocity Between Droplet and the Gas Stream
μ = Gas Viscosity

Several things can be seen be examining the Separation Number. First, collection efficiency varies as the square of the particle diameter, directly as the relative velocity, and inversely as the diameter of the water droplet. Particle density and gas viscosity cannot be changed, and in industrial gases, particles vary in diameter over an enormous range. Nevertheless, as efficiency varies as the square of particle diameter, it is very obvious that efficiency falls off sharply for the smaller particles, and they are much more difficult to collect.

Design can influence the two remaining properties, V_o and D_d. In a gas stream, a small particle reaches the velocity of its carrier gas almost instantly. A water droplet, typically having a diameter of from 100 to 200μ, takes a little longer, but very quickly travels at substantially the same velocity as its carrier gas. For V_o, the relative velocity, to have an appreciable value then, there must be acceleration in deceleration of the gas.

Droplet size can also be changed within limits. Nukijama and Tanasawa(2) have developed a dimensional equation which can be used to estimate the mass-mean diameter created in a enturi throat. For average conditions it can be written:

$$D_d = \frac{16,500}{V_o} + 1.5\ L^{1.5}$$

Where:
D_d = Droplet Diameter, Microns
V_o = Differential Velocity, Ft/Sec
L = Liquid-Gas Ratio, Gallons per 1000 ACF of Gas

Even though the equation does not estimate D_d precisely, it does show that D_d varies inversely as V_o. A high value of V_o then raises the Separation Number directly by inversely affecting D_d which is the denominator.

As V_o is the relative velocity, the function of a Venturi scrubber is to provide acceleration and the deceleration of the gas stream to obtain this relative velocity. In conventional Venturis this occurs over a length of many feet. In the MVS(TM), however, acceleration and the deceleration occurs over the length of the throat which is now only about 1 inch. Consequently, both acceleration and deceleration are much greater than before and efficiency improves.

MVS(TM) SYSTEM DESCRIPTION

Implicit in the modular design concept is the ability to apply the MVS(TM) scrubber to scrubbing jobs with substantially no special design considerations relating to the size of the flowing gas stream or the physical configuration needed to accommodate the scrubber.

For many years, it has been the practice in the scrubber industry to find a limited number of scrubber sizes which can be applied on the basis of past experience, and to custom design intermediate sizes, to tailor the physical design of the scrubber to the required geometry of the process, or, more frequently, to tailor the physical design of the process to match the required geometry of the scrubber. With the MVS(TM) Modular Venturi Scrubber approach, it is possible for the system designer to select the Venturi scrubbing components by a simple two-step procedure:

1. Select the pressure drop requirement to provide sufficient collection efficiency for the application in question.

2. Calculate the gas flow rate on a saturated basis and select the

number of modules required.

The design engineer can, at this point, elect to purchase a scrubbing unit tailored to hold the desired number of modules, or he can design an enclosure to purchase throat and the entrainment modules to use within it. A few very simple principles apply to the orientation of the elements.

The venturi throat element can be operated in any orientation whatever. Gas flow is ordinarily horizontal, but can be vertical, upwards or downwards or at an angle.

The mist eliminator consists of two sections as shown in Figure 7. These sections are designed for operation with horizontal gas flow, and with collected liquid draining downward at a slight angle tc vertical to the bottom of the scrubber. If these elements are piled one upon another in configuration more than two elements high, it is necessary to provide a "gutter" at the bottom of each two-section layer to drain the collected water to a side wall, thereby preventing re-entrainment in the high velocity gas leaving the separator elements. Elements designed for vertical gas flow with an angle of approximately 30° to the horizontal plane can be obtained for configurations which accommodate vertical gas flow.

There is no requirement that the Venturi section and mist eliminator sections operate with gas flow in the same general direction. For example, a vertical down flow of gases through the Venturi scrubber can be matched with horizontal gas flow through the entrainment separators as shown in Figure 7 if this mechanical arrangement fits better into the process scheme.

Because it is economical to select standard module sizes for mass production, the gas flow required may not match precisely the combination of a convenient combination of elements. For example, 5000 saturated ACFM fits conveniently in the smallest standard module. A flow rate of 50,000 ACFM would, consequently, require ten standard modules. This fits conveniently in an arrangement five modules wide by two high, but it may not be convenient to accommodate a scrubber with this width to height ratio.

How can the size be modified so as to provide a nearly square cross-section? Two ways of handling this problem are suggested. One approach is to select nine modules, and to operate with a slightly higher pressure drop than the category specified, or a combination of slightly higher pressure drop at slightly lower liquid flow rate. An alternative approach is to use a configuration four modules wide by three high, wich would normally have a capacity of 60,000 saturated ACFM. The oversized arrangement can be modified by the insertion of a few clip-on covers between the rods, so as to reduce the cross-section area available for gas flow in the desired ratio of five to six. This is accomplished by simply blanking off every sixth opening.

Problems of turndown are handled similarily. Venturi scrubbers are basically constant flow devices. For application where substantial variation in gas flow rate is expected, the system should be designed to allow the induction of ambient air or recycle of clean gas to the scrubber inlet to

keep the gas flow volume approximately constant.

However, some circumstances will be encountered under which variation gas flow rate must be accommodated. These can be handled on a continuous basis by varying the liquid flow rate above and below the design flow rate to accommodate variations of gas flow below and above than for which the system was designed. In order to obtain substantial turndown, it is necessary to resort to banks of spray nozzles which can be turned on as the flow decreases so as to provide a uniform spray pattern.

The design criteria for the MVS(TM) Modular Venturi Scrubber system are summarized in the table presented as Figure 8, and in the performance characteristics in Figures 9 and 10.

CONCLUSION AND SUMMARY

The MVS(TM) Modular Venturi Scrubber design represents a substantial improvement in the mechanics of application of the mature Venturi scrubbing principle to particulate collection problems. The modular Venturi scrubber approach provides for scrubbers varying in size from very small to very large without any variation in performance due to geometry of the system.

The modular scrubber permits the design engineer to fashion a venturi scrubber from standardized low-cost elements and arrange them to suit the geometry of his application. Conversely, he may select from among standard housing designs prefabricated units covering the size range to 500,000 ACFM.

ENDNOTES

1. U.S. Patent Number 3,488,039.

2. Nukiyama, S. and Tanasawa, Y. Transactions of the Society of Mechanical Engineers (Japan) 4, No. 14, 86 (1938).

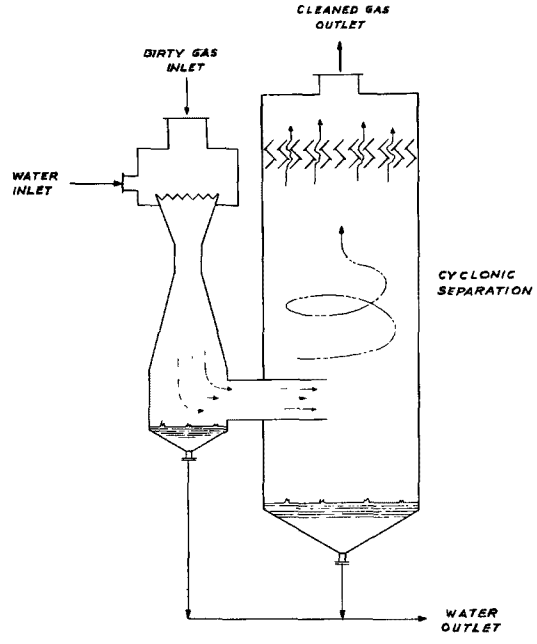

FIGURE 1
TYPICAL
PEASE-ANTHONY SCRUBBER
CONFIGURATION

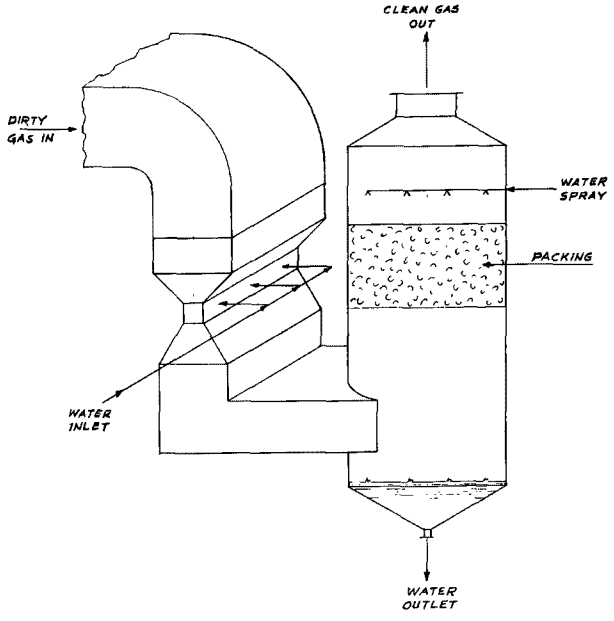

FIGURE 2
RECTANGULAR THROAT VENTURI

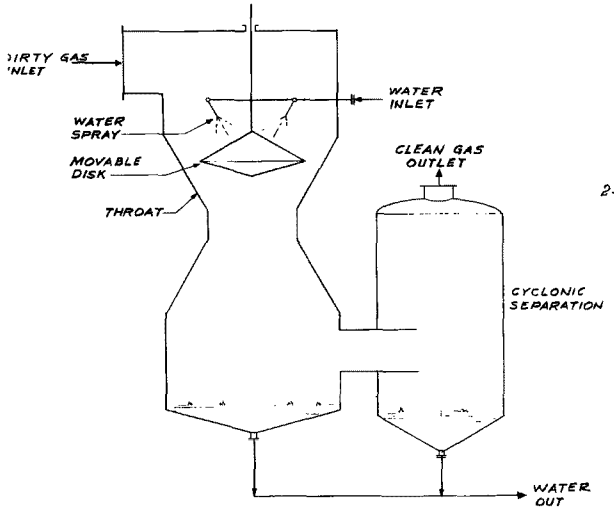

FIGURE 3
FLOODED DISK SCRUBBER

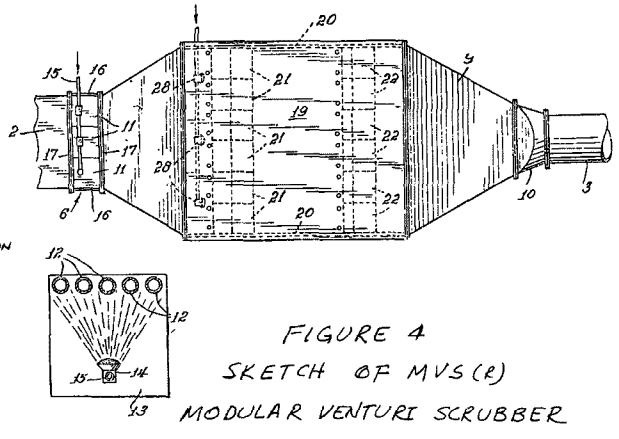

FIGURE 4
SKETCH OF MVS(R)
MODULAR VENTURI SCRUBBER

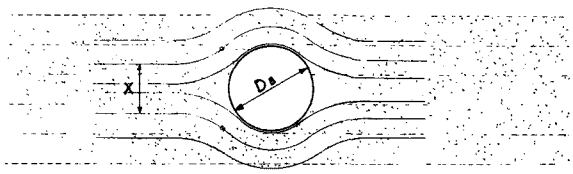

FIGURE 5
PARTICULATE MATTER IMPACTION
AT WATER DROPLET

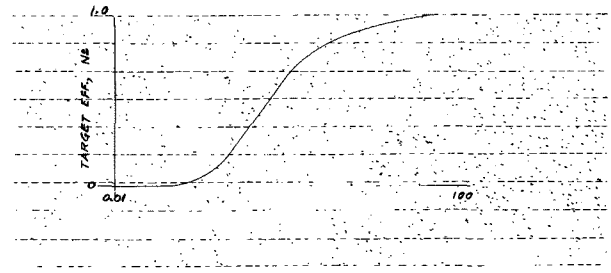

SEPARATION Nº = $\psi_t V_0 / g_L D_B = \frac{d^2 \rho_p V_0}{18 \mu D_B}$

FIGURE 6
EFFICIENCY AS A FUNCTION OF
SEPARATION NUMBER

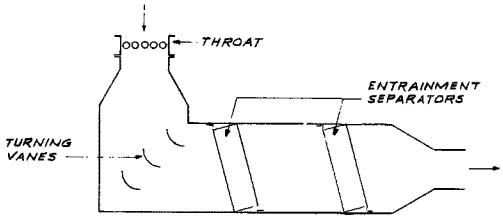

FIGURE 7
LINE DRAWING OF A MVS™ SCRUBBER WITH VERTICAL
THROAT AND HORIZONTAL ENTRAINMENT SEPARATORS

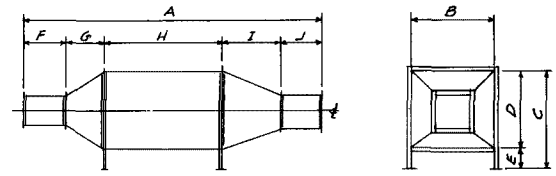

FIGURE 8
TYPICAL DIMENSIONS OF
MVS™
MODULAR VENTURI SCRUBBER

APPROXIMATE DIMENSIONS

SCFM	A	B	C	D	E	F	G	H	I	J
5000	13'-11"	3'-0"	3'-2"	1'-8"	1'-6"	2'-0"	1'-2"	7'-6"	1'-5"	2'-0"
10,000	13'-11"	3'-0"	4'-8"	3'-4"	1'-4"	2'-0"	1'-2"	7'-6"	1'-5"	2'-0"
20,000	15'-8"	6'-0"	5'-10"	3'-4"	2'-6"	2'-0"	2'-0"	7'-6"	2'-2"	2'-0"
30,000	15'-8"	6'-0"	7'-4"	5'-0"	2'-0"	2'-0"	2'-0"	7'-6"	2'-2"	2'-0"
45,000	15'-8"	9'-0"	8'-0"	5'-0"	3'-0"	2'-0"	2'-0"	7'-6"	2'-2"	2'-0"
60,000	15'-8"	9'-0"	9'-5"	6'-8"	2'-8"	2'-0"	2'-0"	7'-6"	2'-2"	2'-0"

LARGER SIZES ON REQUEST

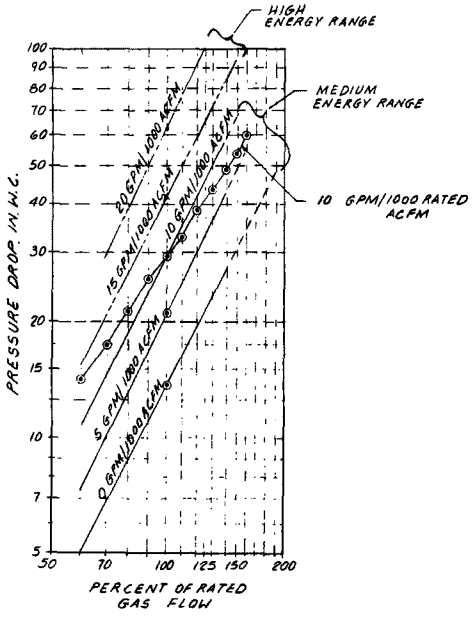

FIGURE 9
PRESSURE DROP VS FLOW RATE
FOR AIR AND WATER
FOR MVS™ MODULAR VENTURI SCRUBBER

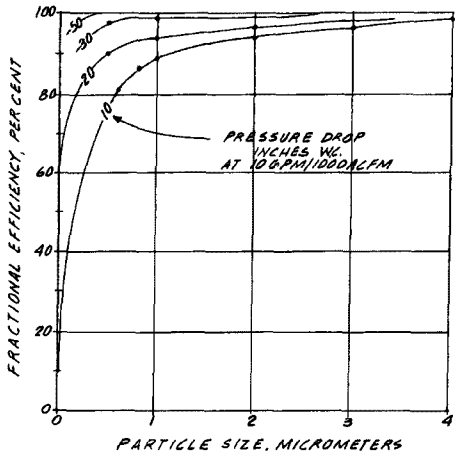

FIGURE 10
APPROXIMATE FRACTIONAL EFFICIENCY
CURVES FOR MVS™
MODULAR VENTURI SCRUBBER

PERFORMANCE OF PARTICULATE SCRUBBERS AS INFLUENCED BY GAS-LIQUID CONTACTOR DESIGN AND BY DUST FLOCCULATION

By: Konrad T. Semrau
SRI International
Menlo Park, CA 94025

Robert J. Lunn
Donaldson Company, Inc.
Minneapolis, MN 55440

ABSTRACT

Several types of gas-liquid contactors were compared experimentally, using both flocculated and deflocculated test dusts. Performances were compared on the basis of the effective friction loss across the contactors. The various devices generally gave very similar or identical performances except over some limited ranges of operating variables in which inferior performance was encountered. A fiber-bed contactor gave superior performance, apparently by superimposing filtration upon scrubbing. Dust flocculation afforded increased collection efficiencies, but with some collectors partial deflocculation occurred before contact of the dust with liquid was effective.

INTRODUCTION

A recent paper (1) summarized the conclusions from various investigations of the relationship of particulate scrubber efficiency to the energy expended in gas-liquid contacting (the contacting power). The present paper presents a summary of the results of tests made under a common set of conditions with a variety of gas-liquid contactors. The tests were made under laboratory conditions using standardized test dust in both dispersed and flocculated conditions.

EXPERIMENTAL METHODS AND EQUIPMENT

The primary investigation was made with the DP scrubber, which had a maximum air flow capacity of about 180 ft^3/min and is shown schematically in Figure 1. The DP scrubber was actually a test assembly in which the gas-liquid contactor and the entrainment separator could be changed as desired. Atmospheric air carrying dust entered the scrubber through the sparger tube, the lower end of which was immersed in water in the contactor pot. The air and entrained water then passed through the contactor (orifice, venturi, or fiber bed) located at the gas exit of the contactor pot and flowed upward to the entrainment separator. Two different entrainment separators were used. The first was a simple cyclone. The second was a combination of an inertial separator followed by a wire-mesh separator, shown schematically in Figure 1. The inertial separator embodied a simple 90^0 change of direction for the air stream. The wire-mesh separator consisted of the upper part of a Donaldson

A-8073 engine-intake air cleaner.

The DP scrubber effectively incorporated multiple stages of gas-liquid contacting, including the sparger, the designated contactor, the duct to the entrainment separator, and the entrainment separator itself. In one arrangement, termed the impinger, a nozzle was fitted to the immersed lower end of the sparger tube.

The contactor pot also served as the reservoir for the scrubbing water, which was neither added nor withdrawn during a test run. There was no provision for measuring the circulation rate of the water. The gas pressure drop through the scrubber could be changed by varying the air flow rate, the water depth in the contactor pot, or the contactor.

Tests were also made with a Donaldson A-8073 engine-intake air cleaner, using both water and lubricating oil as scrubbing liquids.

Additional tests were made with a venturi scrubber (Figure 2) made from glass and provided with several alternative water-fed arrangements. A metered flow of water was fed once through to the scrubber. The cyclone was used as the entrainment separator.

The general test procedure used was that prescribed in the SAE Air Cleaner Test Code (2). Weighed charges of dust were fed to the scrubber, and the entire exit air stream was filtered to determine the penetration. The principal test dust used was the standardized Air Cleaner Fine (ACF) test dust, 39% of which is in the size range 0 to 5 μm. Some tests were also made with the 0 to 5 μm fraction of dust classified from the ACF dust.

The dust charges were fed from a vertical elutriator, which delivered the dust in a flocculated state. To obtain a dispersion of deflocculated dust, the stream from the elutriator was drawn through and discharged from a compressed-air ejector.

RESULTS AND DISCUSSION

The initial tests, which provided a baseline for the remainder of the investigation, were made with the DP scrubber, using the sparger alone and in combination with the orifice and venturi contactors (Figure 3). Performance curves were established for both flocculated and deflocculated ACF dust, and these curves from Figure 3 are repeated for reference in the following Figures 4-7. All three contactor arrangements gave essentially the same results for given levels of the effective friction loss. The sparger/orifice combination alone was used to establish a performance curve for deflocculated 0-5 μm dust (Figure 3).

In the initial tests, the cyclone was used as the entrainment separator. Later tests were made with the combination inertial and wire-mesh separator. When compared, the two sets of results agreed if the gas pressure drop across the wire-mesh separator unit was subtracted from the total measured pressure drop. Evidently, insufficient water reached the mesh section to produce

significant gas-liquid contacting there. Hence, the energy loss across the mesh section did not contribute to scrubbing efficiency.

The A-8073 air cleaner had a contacting scheme somewhat similar to that of the DP scrubber. The air entered the cylindrical air cleaner through a concentric sparger tube that dipped into an oil bath in the bottom of the cleaner body, then flowed upward through a thick pack of screens that formed the principal gas-liquid contactor. The scrubber air then flowed upward through the wire-mesh separator for removal of the residual droplets of entrained oil. Apparently, the quantity of oil reaching the wire-mesh separator was small. The only method for changing the pressure drop across the A-8073 unit was by varying the air flow. At high air flow rates, the velocities of air entering the oil bath were probably high enough to sweep the inner cup in the oil bath free of oil at the surface where the air stream turned upward.

The A-8073 unit was tested with both flocculated and deflocculated ACF dust. No difference could be distinguished between the results obtained with oil and with water as the scrubbing liquid. As the other studies had suggested, the pressure drop across the wire-mesh separator section was subtracted from the total pressure drop to give the effective friction loss, which reached only 9 inches of water at the maximum practical air flow rate. The efficiencies obtained significantly exceeded those obtained in the baseline studies with the sparger/orifice contactor in the same range of effective friction loss (Figure 4). To simulate the same scrubbing action, the DP scurbber was fitted with a fiber-bed contactor composed of steel wool, and with this unit it was feasible to operate in a higher range of effective friction loss without using inconveniently high air flow rates. The data points obtained with the DP/fiber-bed scrubber on deflocculated ACF dust clearly fell along the same performance curve as did the data points for the A-8073 (Figure 4). With the flocculated ACF dust, the efficiency of the A-8073 unit actually decreased at effective friction losses exceeding about 4 inches of water, which correspond to increasing velocities of the entering air. Comparison of these results with those for deflocculated dust clearly indicate that deflocculation of the initially flocculated dust was taking place in the A-8073 before effective contacting with liquid was achieved. Further confirmation was obtained by tests with the DP/fiber-bed arrangement at higher levels of effective friction loss; the resulting data points fell along a rising performance curve consistent with that for the A-8073 when operated in the range of effective friction loss under 4 inches of water (Figure 4).

The use of a fiber-bed as a contactor gave definitely superior performance, suggesting that filtration (particle deposition on fibers) was being added to scrubbing (particle deposition on droplets). However, extrapolation of the performance curve for fiber-bed scrubbing of deflocculated ACF dust suggests that the superiority of performance might disappear in the effective friction loss range of 30-35 inches of water. In that range, the residual dust would be in the lower submicrometer range at which the coarse steel wool fibers would give only very low collection efficiencies. Extrapolation of the performance curve for flocculated dust indicates relatively superior performance continuing into a much higher range of effective friction loss, which

would be consistent with the larger effective particle size of the flocculated dust.

With the impinger contactor, the energy for gas-liquid contacting was derived from the jet of air entering the contactor pot. The performance curves with both flocculated and deflocculated ACD dust showed flatter slopes than the corresponding baseline curves obtained with the DP/orifice configuration, with a trend to relatively poorer performance with increasing effective friction loss derived from increasing air jet velocities (Figure 5). A study of the jet velocity-pressure drop relationship indicated that the higher jet velocities may have coincided with increasing channeling of the air jet through the liquid in the contactor pot, which could account for the relatively poor performance.

The first tests with the venturi scrubber (Figure 6) were made with water injection at the four throat taps. The venturi was placed in a horizontal orientation. Visual inspection indicated that most of the contacting and energy dissipation took place in the diffuser. A marked transition in the flow pattern took place at a liquid-to-gas ratio of about 11.5 gal/1000 ft^3. At ratios below this value much of the water appeared to be held in a thick boundary layer, or eddy, in the diffuser. Some channeling of dust-laden air through the contacting zone may have taken place under that condition. At liquid-to-gas ratios above the critical value, the water broke up into a dense spray that appeared to fill the diffuser uniformly.

In tests made with liquid-to-gas ratios under the critical value for the flow transition, both deflocculated and flocculated dusts were collected with efficiencies far below those obtained in the corresponding baseline tests (Figure 6). Nevertheless, with liquid-to-gas ratios above the critical value, the data points for collection of deflocculated ACF dust are in excellent agreement with the baseline performance curve. In corresponding tests with flocculated ACF dust, the three data points for tests with venturi throat velocities of 235 to 260 ft/sec also gave excellent agreement with the baseline performance curve. On the other hand, the three data points for tests at throat velocities of 280 to 320 ft/sec fall substantially below the baseline curve, probably indicating partial deflocculation of the dust in the throat upstream of the water injection points.

A few additional tests were made with water injection at various other locations (Figure 7). With feed at the four forward throat taps, virtually the entire length of the venturi throat was used in gas-liquid contacting. With all the water injection configurations, the data points were generally in reasonably good agreement with the baseline performance curve. Upstream water feed with a liquid-to-gas ratio of 51 gal/1000 ft^3 and a throat velocity of 155 ft/sec gave a data point falling along the established performance curve. On the other hand, the same configuration with a liquid-to-gas ratio of only 1.3 gal/1000 ft^3 and a throat velocity of 400 ft/sec gave an efficiency far below the baseline value, despite the visual appearance of a good distribution of spray entering the venturi throat.

CONCLUSIONS

With the exception of the A-8073 air cleaner and the DP/fiber bed scrubber, all the scrubber configurations gave essentially the same performance when operating in their best modes. Nevertheless, at least three of the contactors displayed performances that were less than optimum over some part of their ranges of possible operating conditions. With the DP/impinger scrubber and the venturi scrubber with throat feed taps, the inferior performance may have been associated with channeling of the air flow. On the other hand, the experiments with the venturi scrubber with upstream water feed appeared to indicate that low water rates as such tended to give inferior performance, even in the absence of a flow pattern that could properly be termed "channeling." In general, there were at least indications that low or very low liquid-to-gas ratios may coincide with inferior performance.

Well-established performance curves such as those of Figure 3 appear to represent the maximum performance that can be obtained from a scrubber on a given dust or aerosol. Deviations such as those observed in this investigation have been in the direction of inferior performance and appear to be characteristic of some range of operating conditions rather than of the particular device. The fiber-bed contactor was the only device that showed a positive deviation from the performance curve, and this was apparently associated with the introduction of a particle deposition mechanism not normally operative in conventional scrubbers.

ACKNOWLEDGMENT

This investigation on which this paper is based was supported by the Donaldson Company, Inc., Minneapolis, Minnesota.

ENDNOTES

1. Semrau, K. T. Practical Process Design of Particulate Scrubbers. Chem. Eng. 84: 87-91, September 26, 1977.

2. Society of Automotive Engineers. Air Cleaner Test Code, SAE J726b. SAE Handbook, Part 2. Warrendale, PA, Soc. Auto. Engrs., 1979.

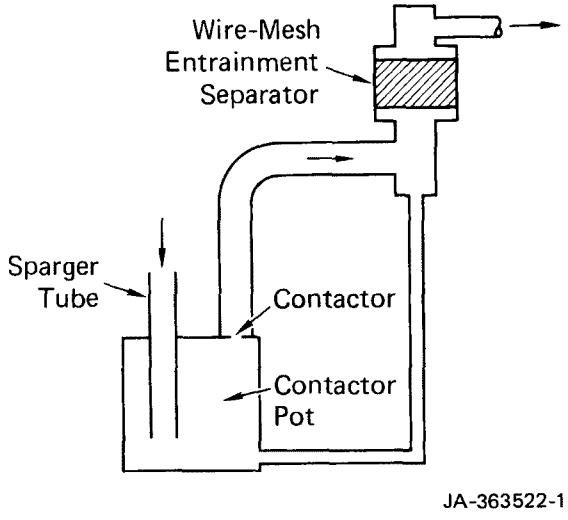

FIGURE 1 DP SCRUBBER WITH WIRE-MESH ENTRAINMENT SEPARATOR

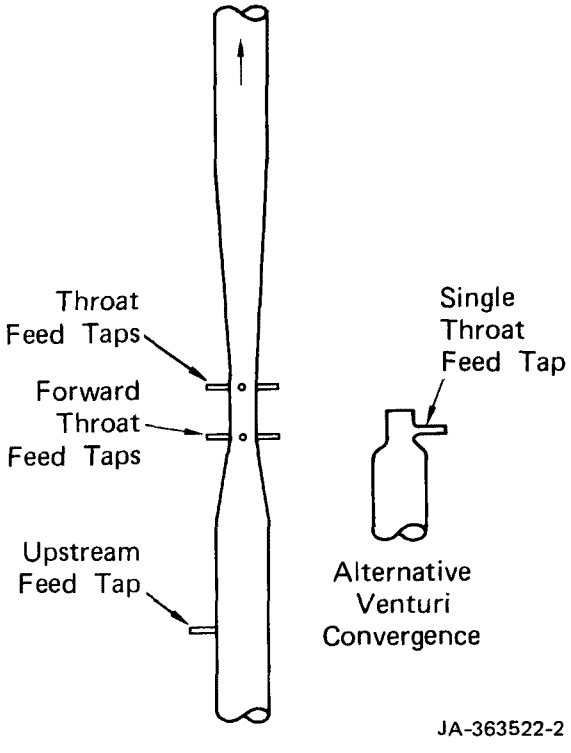

FIGURE 2 VENTURI GAS-LIQUID CONTACTOR

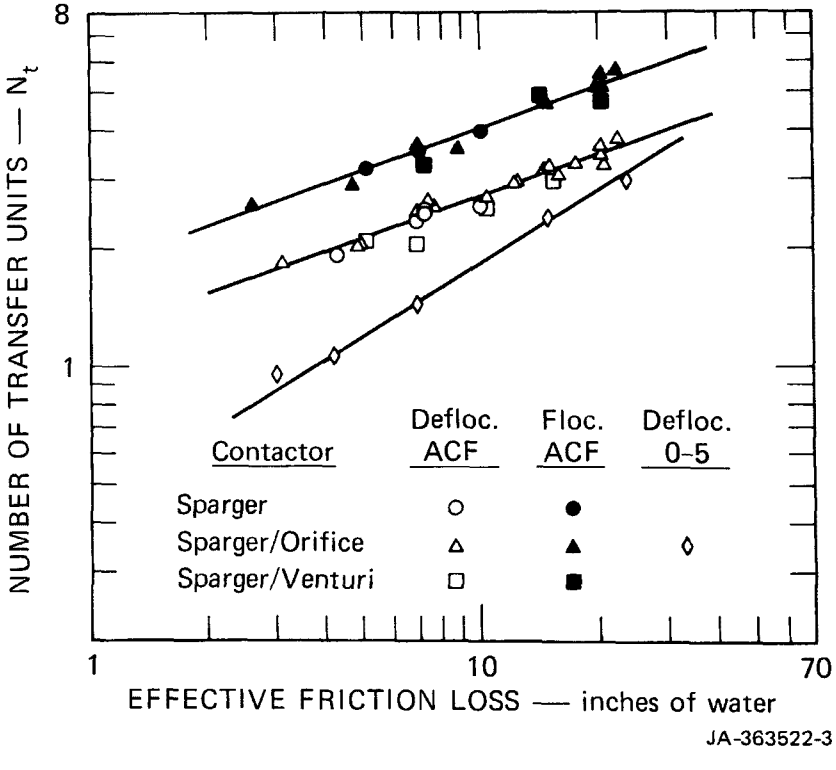

FIGURE 3 PERFORMANCE CURVES FOR DP SCRUBBER

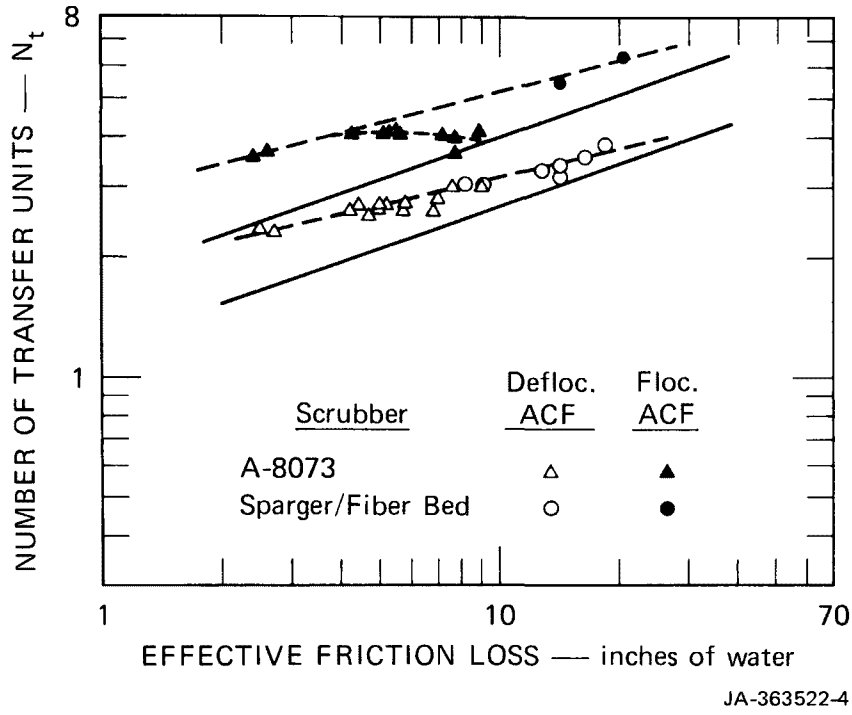

FIGURE 4 PERFORMANCE CURVES FOR A-8073 AND DP/FIBER BED SCRUBBERS

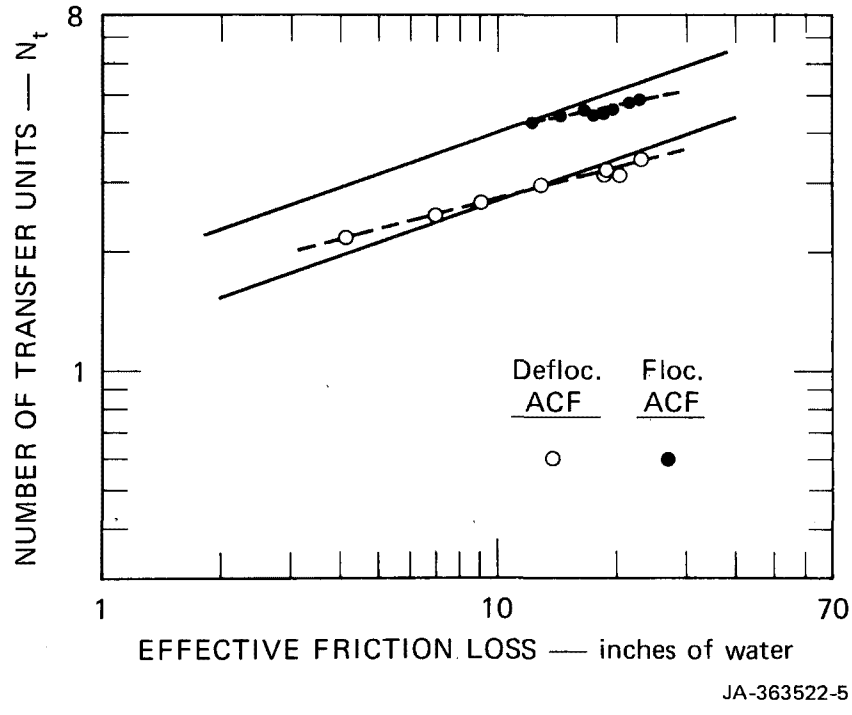

FIGURE 5 PERFORMANCE CURVES FOR DP/IMPINGER SCRUBBER

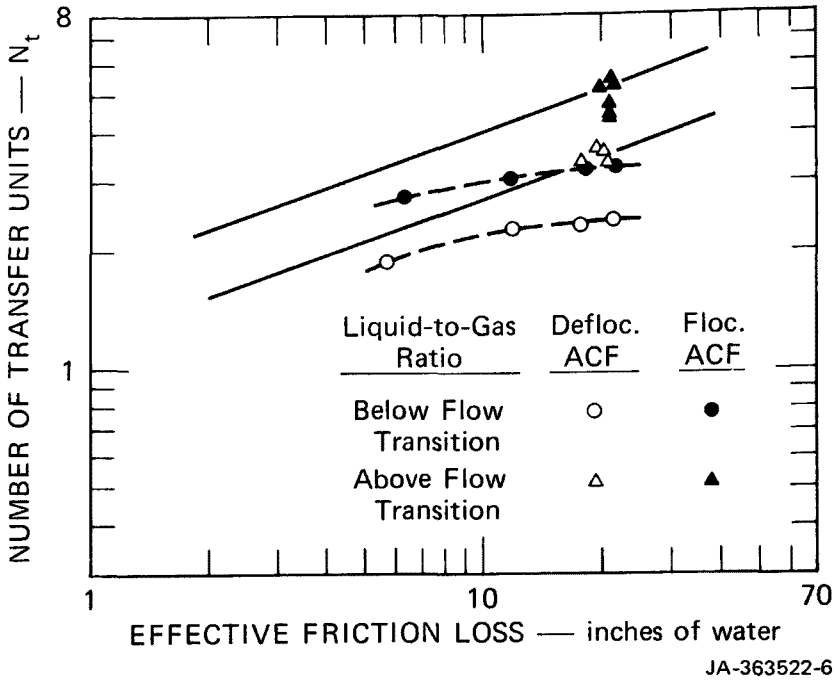

FIGURE 6 PERFORMANCE CURVES FOR VENTURI SCRUBBER WITH THROAT WATER-FEED TAPS

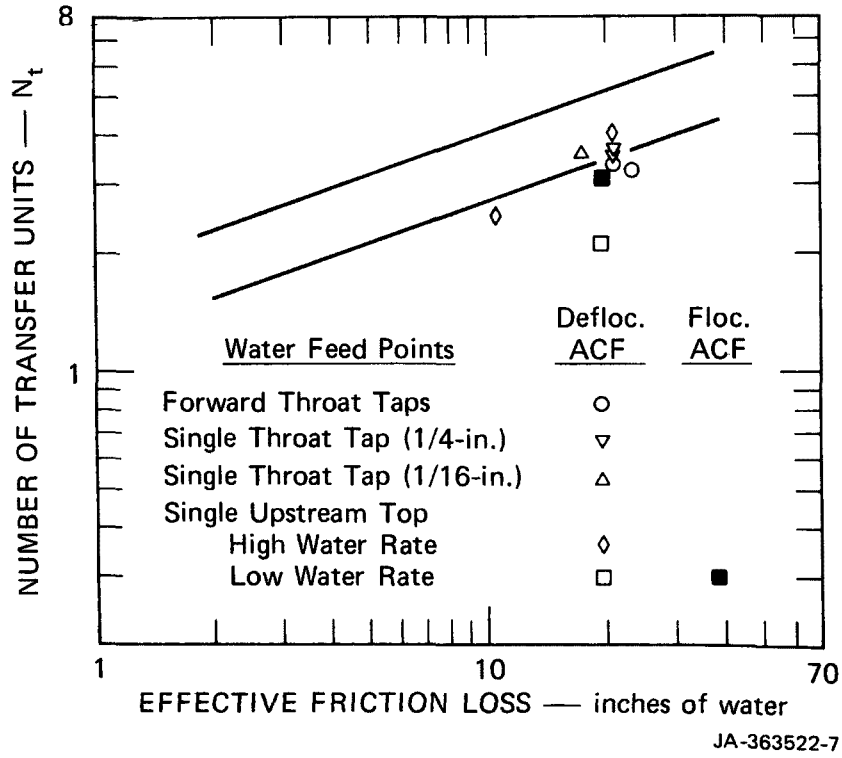

FIGURE 7 PERFORMANCE OF VENTURI SCRUBBER WITH VARIOUS WATER FEED POINTS

INVESTIGATION OF VENTURI SCRUBBER EFFICIENCY AND PRESSURE DROP

By: R. Parker, T. Le, and S. Calvert
Air Pollution Technology, Inc.
4901 Morena Blvd., Suite 402
San Diego, CA 92117

ABSTRACT

The Venturi scrubber performance model (EPA-600/2-77-172) gives good results when used to predict the performance of industrial scrubbers. However, insufficient data have been available to make a detailed parametric evaluation of this model. A parametric study is needed in order to properly predict Venturi scrubber performance in nonconventional environments such as high pressure gas streams.

Pilot plant data on a 7.6cm (3 in.) throat diameter Venturi scrubber are presented. Flow rates from 10 to 20m^3/min (350-700 CFM) and liquid-to-gas ratios from 1 to 3ℓ/m^3 (7.5 - 22.4 gal/MCF) were used. Throat length and diffuser length were also varied.

These parameters resulted in throat velocities from 30 to 70m/s and pressure drops from 10 to 50 cm W.C. Experimental data showed higher penetrations than predicted, especially for particles larger than 1 or 2 μmA aerodynamic diameter.

INTRODUCTION

The Venturi scrubber performance model (1) gives generally good results when used to predict the performance of industrial scrubbers. However, field tests do not allow sufficient control over operating parameters, and field test data are not sufficiently accurate to enable an adequate evaluation of the model. On the other hand, available laboratory data are scarce and are generally for too small a scale to be representative of industrial scrubbers. Experimental performance data for a pilot scale Venturi scrubber are needed in order to evaluate the available mathematical models and to provide a more adequate basis for further refinement of models.

The purpose of this project was to evaluate the Venturi scrubber model on a pilot scale and obtain scrubber performance data which could be used as a baseline for evaluating Venturi scrubbers operating at high gas pressure. High pressure Venturi scrubbers are important components in many advanced coal conversion processes currently being developed. This work has been funded under a contract with the U. S. Department of Energy.

THEORY

Yung, et al (1) developed a revised model for Venturi scrubber performance from the basic equations governing particle collection and pressure drop derived by Calvert (2, 3) and Boll (4). Several assumptions were made:

1. The flow is one-dimensional, incompressible and isothermal.

2. Liquid drops are uniformly spread across the duct and the drop diameter is invariant with axial distance.

3. Drops are of uniform diameter.

4. There is no wall loss of liquid drops.

5. At any cross section of the scrubber, liquid fraction is small. Therefore, at any location gas velocity can be calculated by the following equation:

$$u_G = \frac{m_G}{\rho_G A} \tag{1}$$

Pressure Drop

Yung found that pressure drop predictions by a modified Calvert's equation and by Boll's equation agree with experimental data. The modified Calvert's equation has the following form:

$$\Delta P = 1 \times 10^{-3} F u_{Gt}^2 \left(\frac{Q_L}{4Q_G} \right) \tag{2}$$

where:

ΔP = pressure, cm W.C.

u_{Gt} = gas velocity in the throat, cm/s

F = fraction of the gas velocity which is attained by the liquid drops, dimensionless

Particle collection by inertial impaction depends on the relative velocity and the drop holdup, and both of these decrease as the drops approach the gas velocity ($F \rightarrow 1$).

Yung defines a dimensionless throat length, L, by the following:

$$L = \frac{3 \ell_t C_{Do} \rho_G}{2 d_d \rho_L} \tag{3}$$

where:

ℓ_t = throat length or distance between liquid injection point and the exit of throat, cm

C_{Do} = drag coefficient at the liquid injection point

ρ_G = gas density, g/cm^3

d_d = Sauter mean drop diameter given by the empirical correlation of Nukiyama and Tanasawa (5), cm

ρ_L = liquid density, g/cm^3

Yung shows that L = 2 or 3 is the optimum throat length and a value of F = 0.82 accurately predicts pressure drop.

Particle Penetration

Most industrial Venturi scrubbers have dimensionless throat lengths

between 2 and 3, and the infinite throat length model may be used to predict their penetration. The Venturi scrubber penetration for an infinite throat length is given by:

$$Pt_d = \exp\left[- B \frac{4K_{po} + 4.2 - 5.02\ K_{po}^{0.5} \left(1+ \frac{0.7}{K_{po}}\right) \tan^{-1}\left(\frac{K_{po}}{0.7}\right)^{0.5}}{K_{po} + 0.7} \right] \quad (4)$$

where:

Pt_d = penetration for particles with diameter d_p, fraction

B = dimensionless liquid-to-gas ratio parameter

$$B = \left(\frac{Q_L}{Q_G}\right) \left(\frac{\rho_L}{\rho_G}\right) \frac{1}{C_{Do}} \quad (5)$$

Q_L = liquid flow rate, m^3/s

Q_G = gas flow rate, m^3/s

K_{po} = inertial parameter = $\dfrac{d_{pa}^2\ u_{Gt}\ 10^{-8}}{9\ \mu_G\ d_d}$ (6)

d_{pa} = particle aerodynamic diameter, μmA

u_{Gt} = velocity of the gas in the throat, cm

μ_G = gas viscosity, g/cm-s

EXPERIMENT

Approach

The experimental setup is shown in Figure 1. The Venturi throat was 7.8 cm in diameter and 12, 27, 43, or 58 cm in length. The diffuser section was 50 cm long with an exclusive expansion angle of 7°. The entrainment separator consisted of four rows of chevron baffles arranged in a zigzag pattern.

Fly ash was redispersed, then injected directly into the blower inlet to promote good mixing. The flow rate was varied from 10 to 20 m^3/min (350 to 700 CFM) and the liquid-to-gas ratio was set at 1, 2, or 3 ℓ/m^3 (7.5, 15, 22.5 gal/MCF). The throat velocity varied from about 30 to 70 m/s with most runs falling between 40 and 50 m/s. The scrubber pressure drop (Venturi only) varied from 10 to 50 cm W.C.

Cascade impactors were used at the scrubber inlet and outlet to measure particle mass concentration and size distribution. These data were used to compute grade penetration curves, which were used to determine the scrubber cut diameters.

Because our data are most consistent between about 0.8 and 3.0 μmA, we used an extrapolation technique to obtain cut diameters below 1 μmA. This technique assumes the general relationship:

$$Pt_d = \exp\ (-A\ d_{pa}^2) \qquad (7)$$

where "A" is a constant. We used the measured penetration at 1 μmA to predict the effective cut diameter. Scrubber performance was evaluated in terms of the cut diameter as a function of pressure drop.

Results

The pressure drop data are plotted against predictions in Figure 2. The agreement between theory and data is excellent even for the short throat lengths.

Scrubber cut diameters are plotted as a function of pressure drop in Figures 3, 4 and 5 for liquid-to-gas ratios of 1.2, 2.2, and 3.0 ℓ/m^3 respectively. The solid lines are theoretical predictions from Yung's model.

Discussion and Conclusions

For all conditions studied, the experimental cut diameters are larger than predicted by theory. This implies that the theory over-predicts the Venturi scrubber collection efficiency. For a liquid-to-gas ratio of 1 to 2 ℓ/m^3 (the most common range for industrial scrubbers) the predicted cut diameters are approximately 20% smaller than those measured. The pressure drop theory does a good job of predicting the experimental data.

ENDNOTES

1. Yung, S.C. et al., "Venturi Scrubber Performance Model", EPA 600/2-77-172, August 1977. Also J.A.P.C.A., 27, 4, 1977 and E.S.&T., 12, 456, 1978.

2. Calvert, S., "Scrubbing," Chapt. 6 in "Air Pollution," A. Stern, Vol. IV, 1977.

3. Calvert, S. et al., "Scrubber Performance for Particle Collection, " AIChe Symposium Series, Volume 70, No. 137, 1970.

4. Boll, R.H., "Particle Collection and Pressure Drop in Venturi Scribber, " Ind. Eng. Chem. Fund 12, 40, 1973.

5. Nukiyama, S., and Tanasawa, Y. Transactions of the Society of Mechanical Engineers (Japan). Vol. 4, 86, 1938.

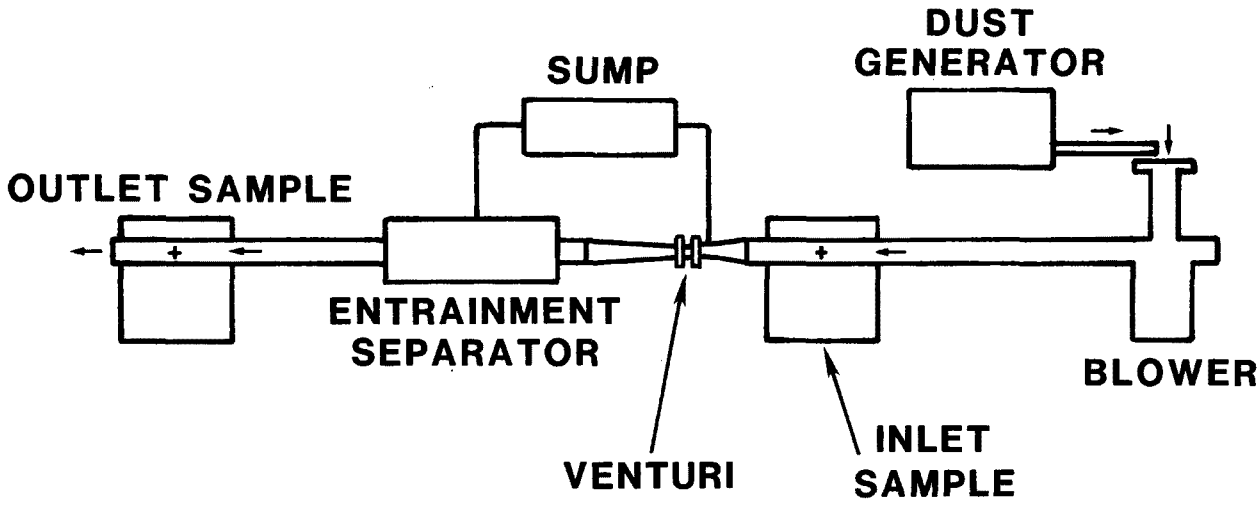

FIGURE 1. EXPERIMENTAL SETUP

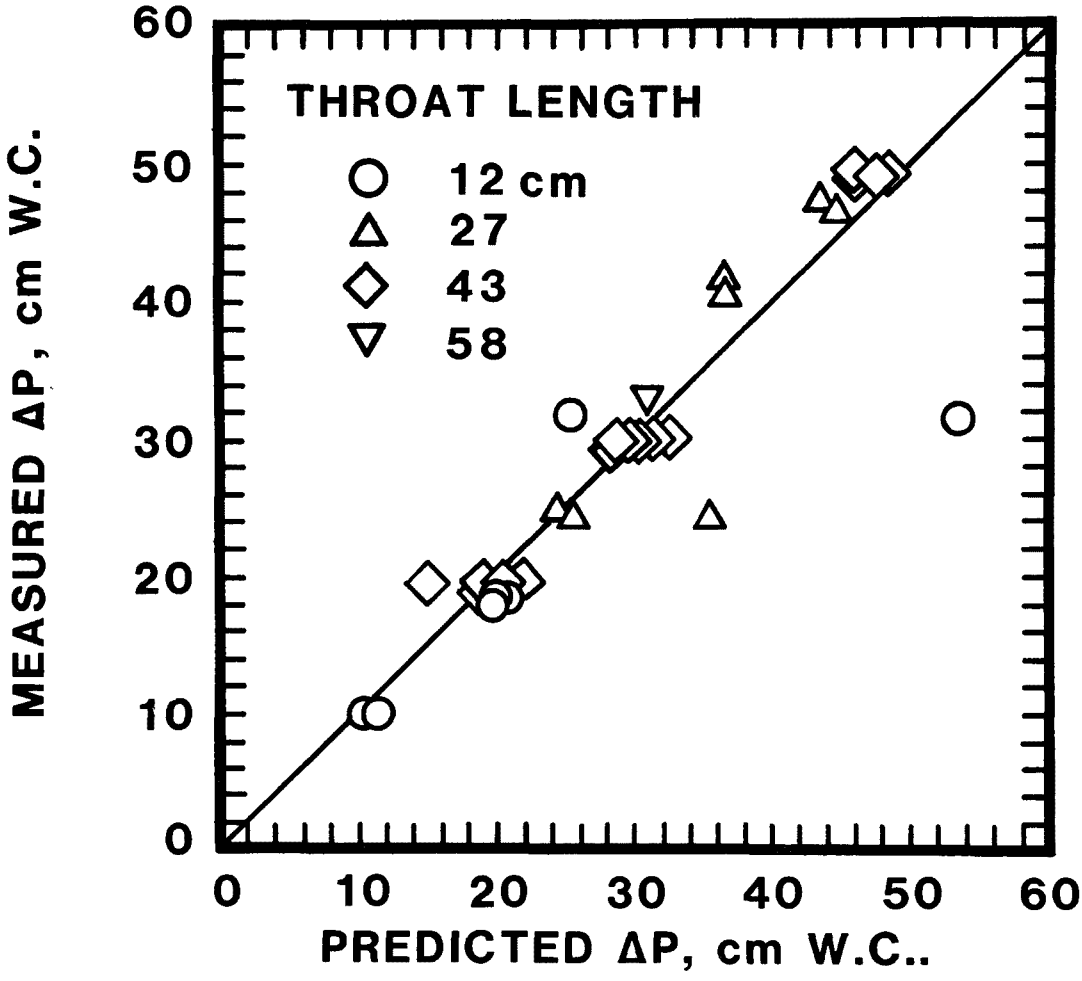

FIGURE 2. PRESSURE DROP DATA

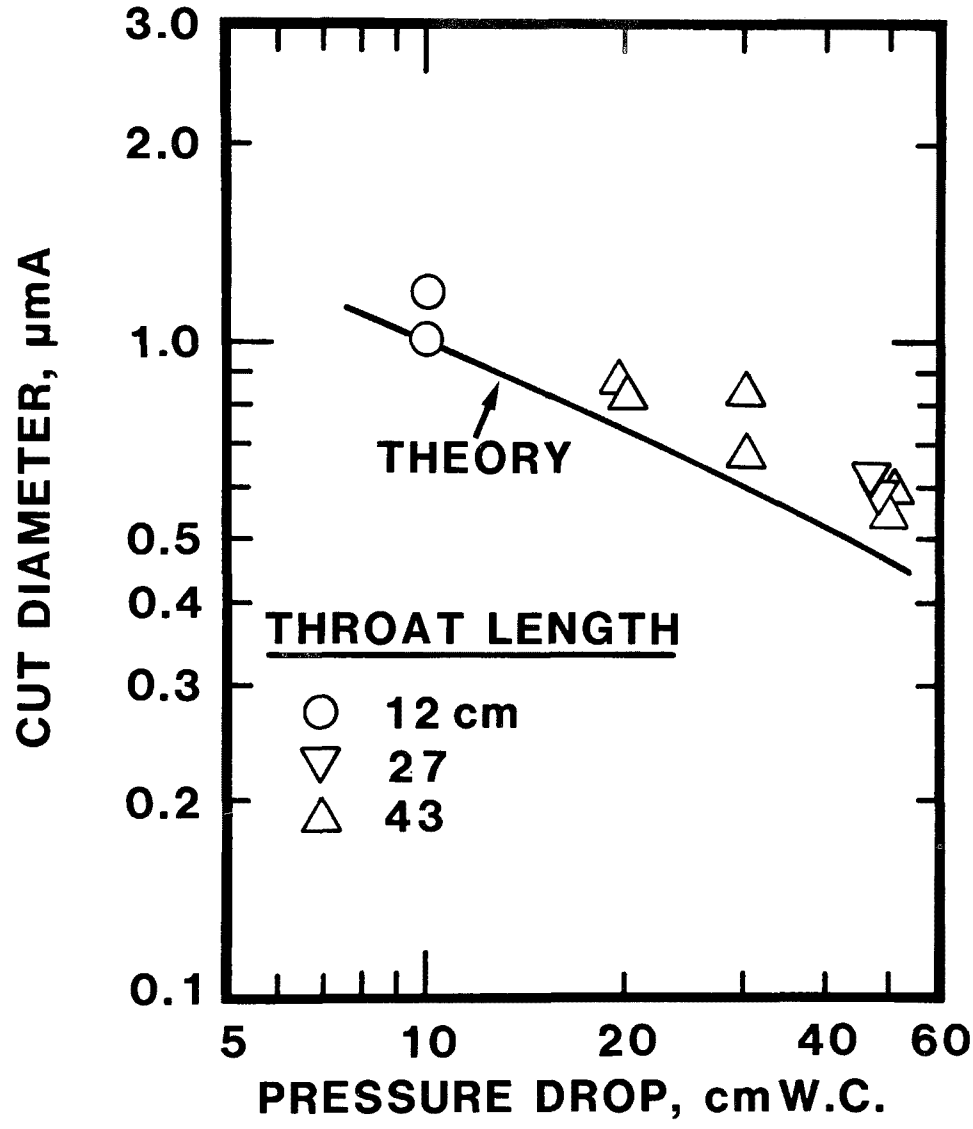

FIGURE 3. CUT-POWER PLOT FOR L/G=1l/m^3

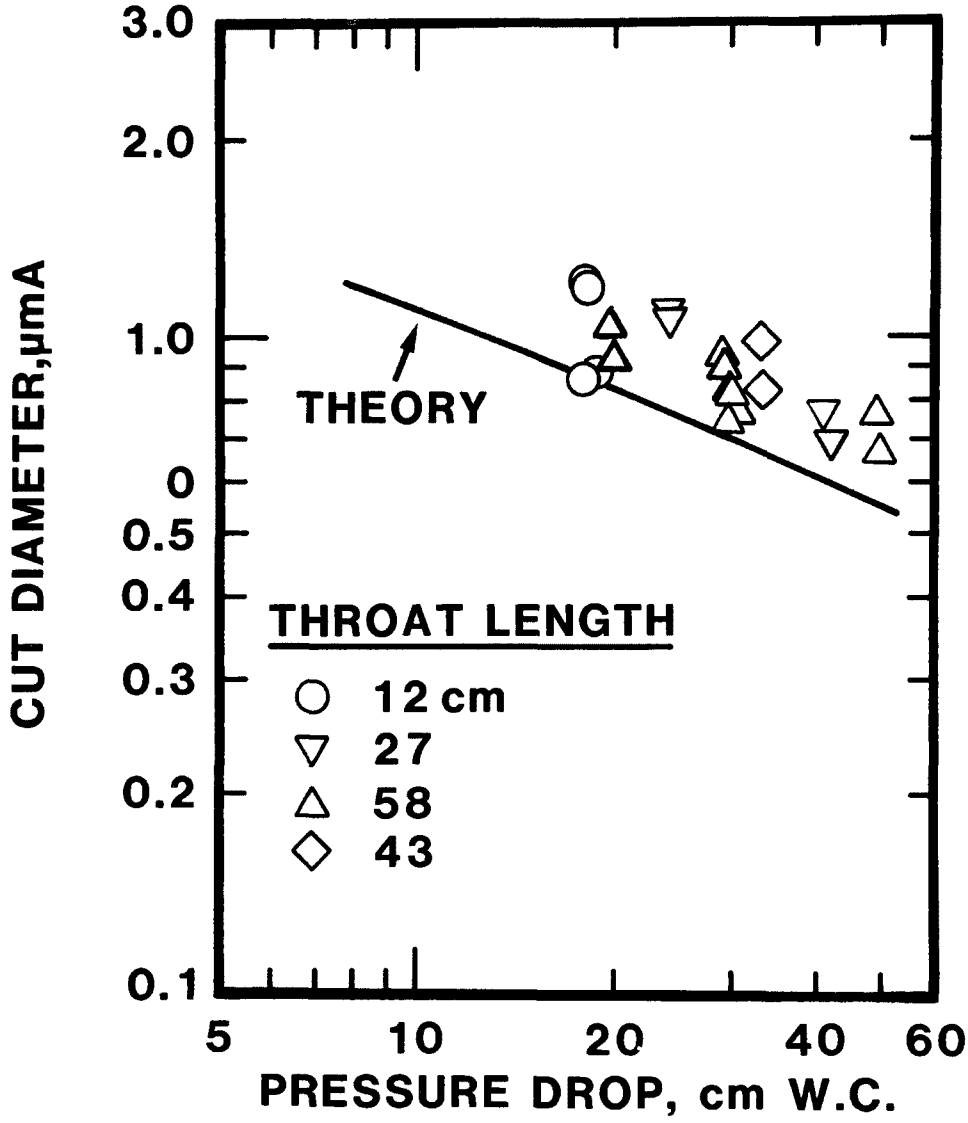

FIGURE 4. CUT-POWER PLOT FOR $L/G=2l/m^3$

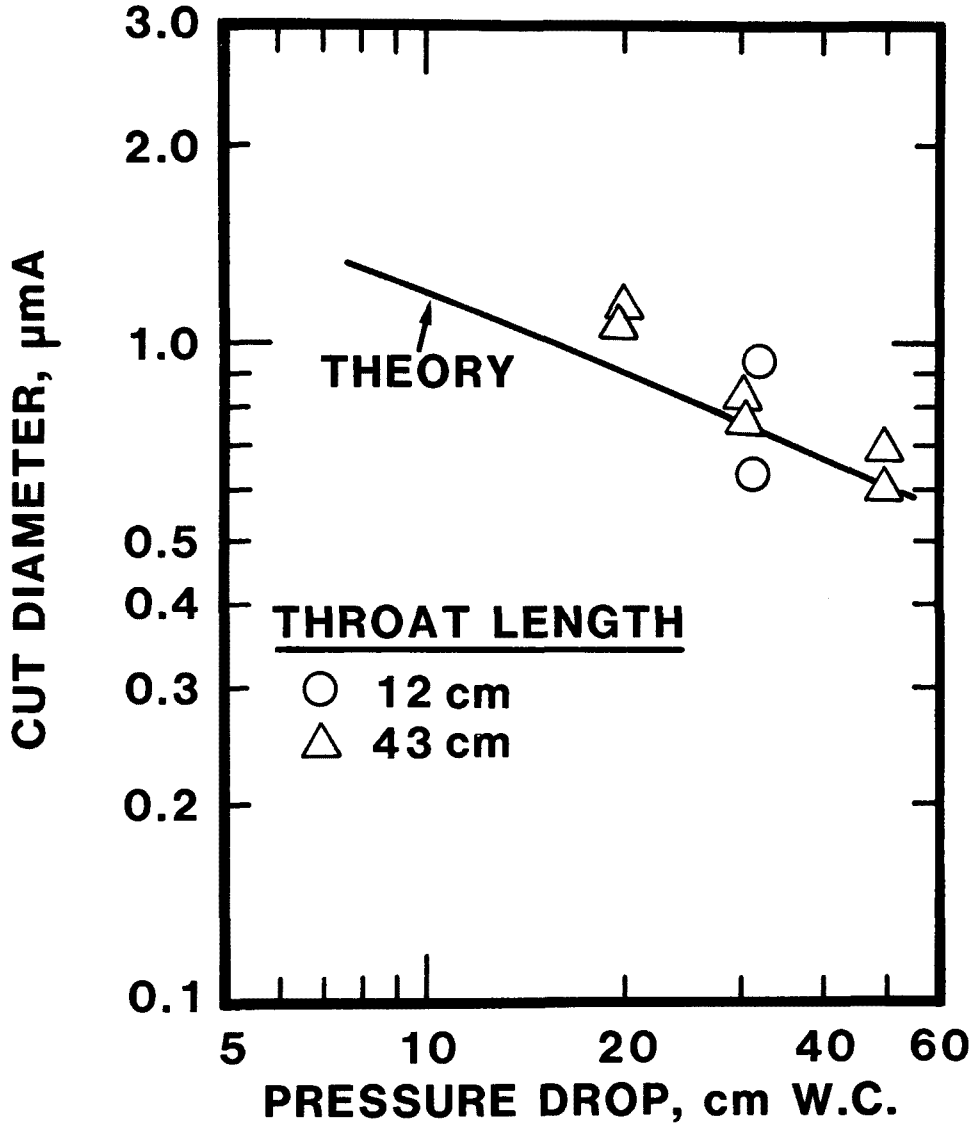

FIGURE 5. CUT-POWER PLOT FOR L/G=3l/m^3

SCRUBBER TECHNOLOGY AND THE INTERACTION OF A UNIQUE STRUCTURE AS MIST ELIMINATOR

BY: GEORGE C. PEDERSEN, P.E.
KIMRE, INCORPORATED
P.O. BOX 570846
PERRINE, FL 33157 USA

ABSTRACT

Mist eliminators should not be an afterthought addition to a scrubbing system. As the last line of defense, they should be an integral part of the control technology. The role of Kimre's unique patented structure as a mist eliminator for use with other scrubbing devices is considered.

The wider range of physical properties now available yields new capabilities in systems design. This media is being used successfully on four continents and is a standard for many United States scrubber manufacturers.

INTRODUCTION

We show how the scrubber situation and the scrubber technology used interact on the selection of a mist eliminator. Emphasis will be placed on the B-GON™ patented mist eliminator structure. In order to explore this interaction, first of all we will consider just what this structure is, familiarize the reader with the material; and then also familiarize him with the use of this material. Basic considerations in the selection of mist eliminator structure, as it relates to the scrubbing technology will be emphasized by case history analysis. Conclusions regarding these considerations are made.

There is a considerable overlap between scrubbing technology and mist eliminator technology. We are attempting to consider only the mist eliminator aspects, but it is impossible to completely differentiate functions. The case histories given are examples drawn from Kimre's extensive experience as consultant and supplier to the industry over the last six and a half years.

BACKGROUND

In the beginning -- which in this case was quite some time ago -- there was only an idea: If it were possible to produce a structure made of monofilaments, wherein all the monofilaments were perpendicular to the flow of the gas, then this should be an efficient mist eliminator. The technical and commercial development of this concept led to the evolution of a wide range of structures. These structures can be made to vary in void fraction up to 97%; they are available in fiber diameters from 31 microns (just slightly more than 1 mil) up to 62 mils -- a range of 60 to 1 in fiber diameter (Figure 1).

KIMRE B-GON™ FIBERS

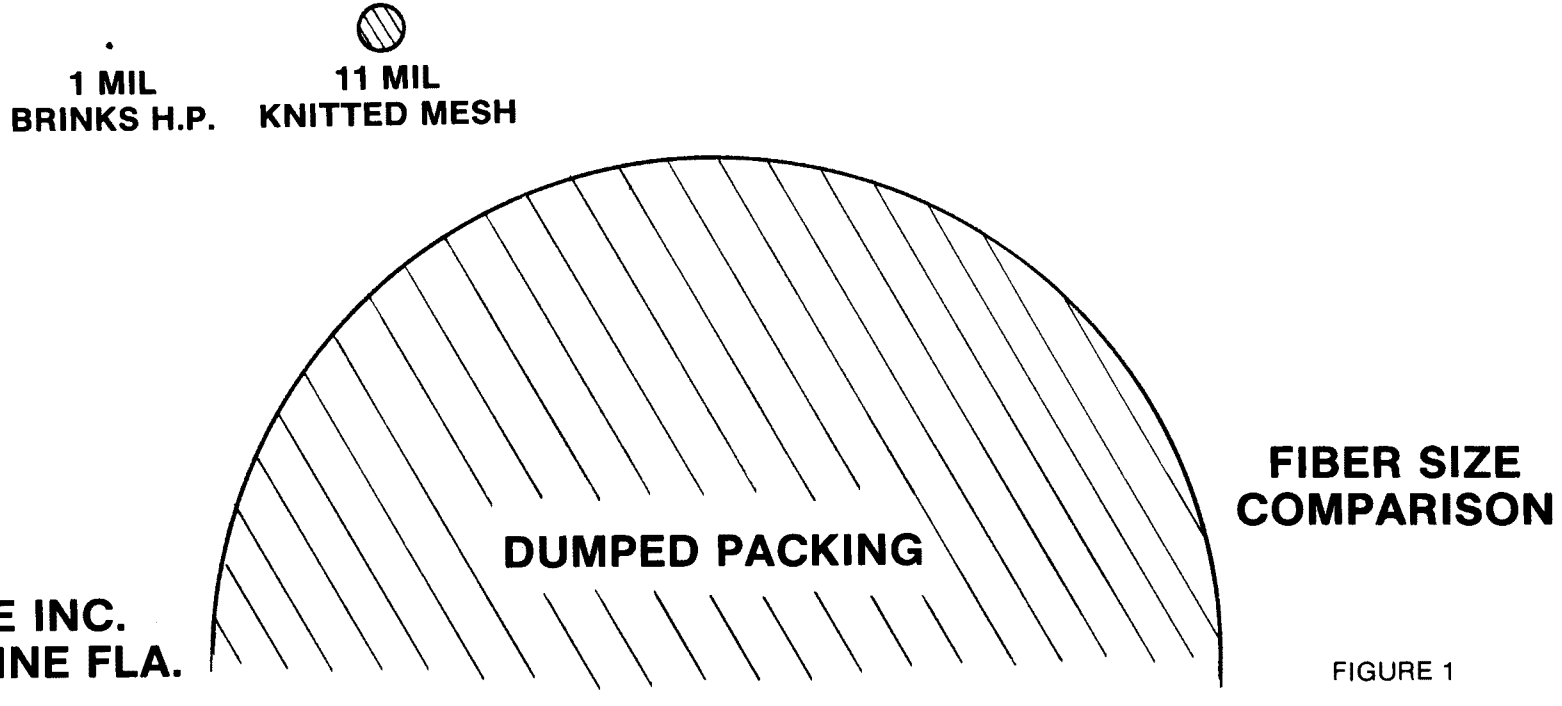

FIBER SIZE COMPARISON

TI-32

KIMRE INC.
PERRINE FLA.

FIGURE 1

The commercial evolution of the structure's use led to the formation of Kimre, Incorporated, with its own manufacturing facilities South of Miami, Florida.

Technical Development

The structure used in the B-GON™ Mist Eliminator and the KON-TANE™ patented Tower Packing products are based on a unique means of interlocking fibers so that they maintain a specific geometric orientation. The simplest form of this structure is diagrammed in Figure 2. The methodology of producing these structures from a wide range of fiber diameters was developed, but at that time there wasn't any proof that the structure actually functioned. Commercial tests were run in the Spring of 1974 by Calspan Corporation, and the performance parameters were verified.

It was demonstrated that this structure was amenable to analysis, based on single-fiber studies by others for collection of mist and particulates. There is a curious exception when predictions are compared to actual results. For relatively "small" drops for which the effectiveness is expected to drop off in a pronounced fashion, the decrease in performance is nowhere near as rapid as is anticipated. We have theories for why this occurs, but no bona fide answers. The specific surface areas and fiber diameters range over far too wide a scale to describe velocity units by the conventional "Souder-Brown" Equation. A method was developed to predict pressure drop, flooding, and efficiency for the different configurations for almost any range of physical conditions.

It was also found that the structure could be made at high void fractions with smaller fiber diameters than were available with other manufacturing methods. The manufacturing methods developed also led to the ability to make the product in large pieces, which has technical advantages during installation, and to prevent problems of bypassing around the edge of sectioned pads. Other technical advantages are its strength and stability. The breaking strength of some of the coarser materials exceeds 1,000 pounds per inch of width. In some cases, the materials can take enormous loads, and this led to a supplementary business in the support of beds of other materials.

Commercial Development

Kimre, Incorporated was founded to commercialize these structures starting with the basic structure and personal financing (with no government assistance), manufacturing equipment was developed, a manufacturing plant was put into operation, and an international sales force was developed. Through our contacts with almost every part of the air pollution control and chemical processing industries, Kimre's technology and products are well-proven. Today, the products are specified extensively by many scrubber manufacturers,engineering/constructor firms, consultants, and a variety of other buying influences.

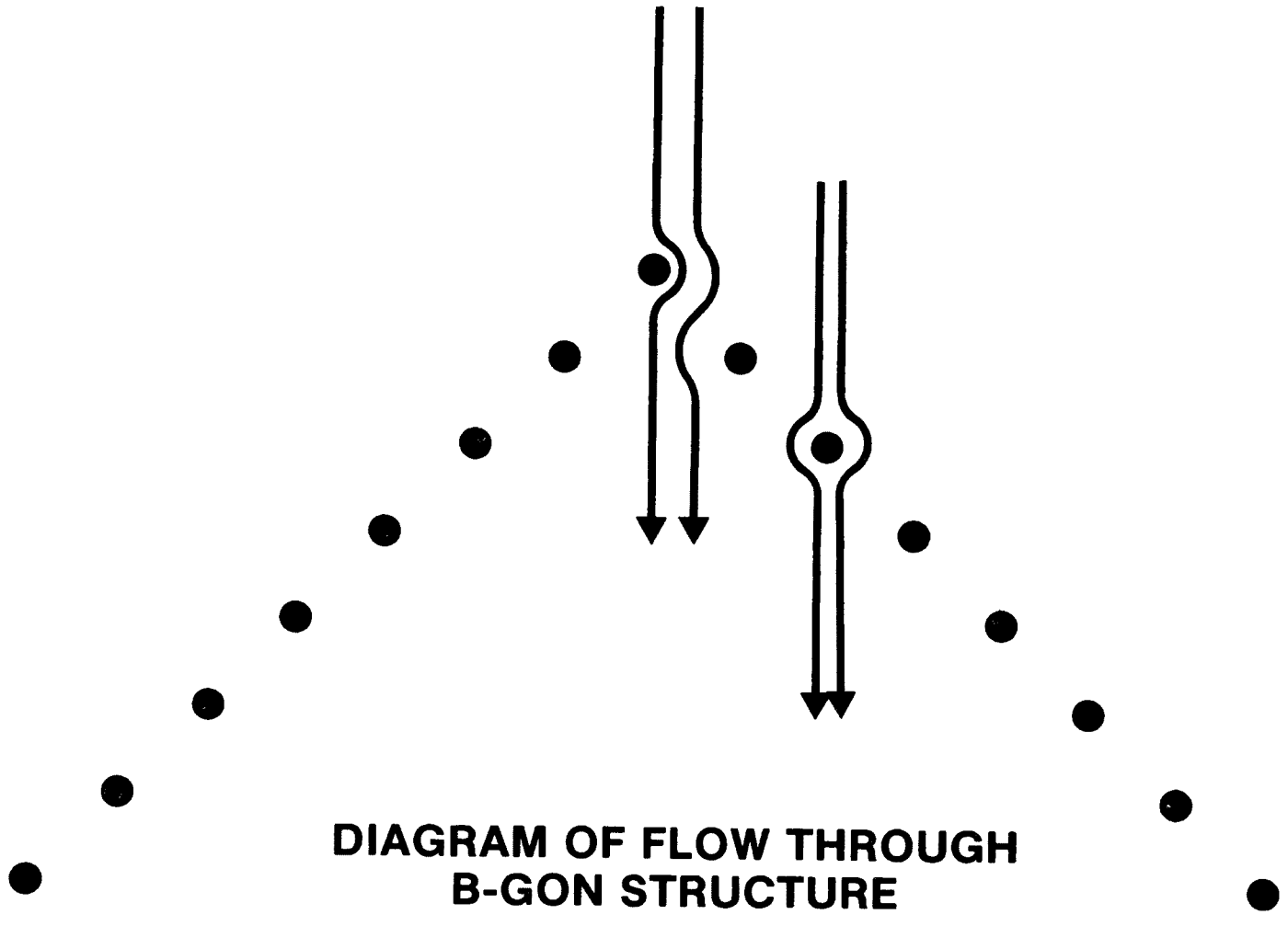

DIAGRAM OF FLOW THROUGH B-GON STRUCTURE

FIGURE 2

Kimre is not a scrubber manufacturer. We supply control concepts and internals applicable to air pollution control and chemical processing operations. The control concepts utilizing our products and technology are wider-ranging than other basic approaches. Literally, the products have been used from the extreme of keeping out birds to removing half-micron-size particulate or mist, to the removal of "rain", or the removal of reacting glue; from one millimeter of mercury to 2500 psi; from 100 degrees below zero to 300 degrees above zero; from less than 1 cfm to over half a million cfm. Chemical resistance requirements have varied from removal of pure water to removal of aqua regia, including radioactive operations.

Physically, the B-GON™ Mist Eliminators span a wider range of physical configurations and usability than is available from any other single source. In cases where we didn't already produce something that would satisfy a need, custom-designed and custom-made products have been used.

DISCUSSION

For the purposes of this paper, we define a mist eliminator to be a device primarily intended for the removal of relatively non-viscous (less than 10,000 cp) mist from a gas stream. Such mist might include entrainment, fine mist intentionally allowed to pass through other parts of the control device, or condensation mist. While it is recognized that mist may include particulates collected in the rest of the scrubber, the mist eliminator's function is not to remove otherwise uncaptured material from the gas -- i.e., it's not an absorber or particulate scrubber in its own right. It should be recognized of course, that in many cases it's hard to differentiate between the mist eliminator and the scrubbing section.

Based on this interpretation of a mist eliminator, and considering situations where the particulates are being collected, then:

It must be anticipated that the mist eliminator should never be a more efficient scrubbing device than the scrubber.

To ignore this rule invites a disastrous installation. We have noted many times in conversations that otherwise knowledgeable people will install a mist eliminator that's going to be so efficient in collecting remaining particulates that it will plug in short order.

As secondary considerations we offer:

1. Consider everything.
2. Don't overdo efficiency.

There are a lot of considerations that go into the selection of a mist eliminator; all of these must be considered, even though the answers to the consideration in many cases is routine. However, in others the decision becomes surprisingly complex.

1. Flooding.
   Easy to say, but what's it mean?
2. Pluggage resistance.
3. Accessibility.
4. Spatial and temporal distribution of the gas flow.
5. Corrosion.
6. Temperature.
7. Bypassing.
8. Supports.

A great deal of "black art" has materialized over the selection of mist eliminators. It usually isn't necessary, and should be avoided wherever possible. In almost all cases, it's possible to at least make a narrow selection of possibilities. When based on thorough analysis, it's surprising how often the final decision bears no resemblance to the original idea for the mist eliminator.

Perhaps the best way to consider these interactions is to look at specific examples:

A. Fertilizer Plant

In 1975, Kimre bid on a mist eliminator for a 22-foot-diameter scrubbing tower and lost the job for less than $200. The mist eliminator was specified only as "6-inch-thick polypropylene".

In early 1977, the unit started up; and in about 7 weeks the mist eliminator plugged up so solidly that the pressure drop caused the support beams to bend upward, and it tore the mist eliminator sections loose, causing significant damage to the inside of the vessel and duct. This was on top of 20 feet of packing. The original knitted mesh mist eliminators could not be cleaned and had to be discarded.

Those familiar with fertilizer plant operations recognize a classic case of difficult service. The incoming gases contain soluble fluorides which react in the liquid to give a silica-containing deposit. Incoming gases also contain dust, and the scrubbing liquid itself contains the same compound, and others besides, which cause substantial problems. However, one does not expect to find tar-like materials.

At the request of the owner, Kimre personnel visited the site and made a number of recommendations:

1. A man-supporting bottom grid be installed, and that a B-GON™ Mist Eliminator in very large sections, each approximately 6 feet wide, be used. The use of the bottom grid allows the mist eliminator to be installed in large sections, and merely rolled out piece by piece. It also provides structural integrity for the entire assembly. The large pieces of B-GON Mist Eliminator can be removed through the manway very readily. The ultimate objective of all this is to minimize the impact of an upset situation, and so the changeover of mist eliminators could be made as rapidly as possible.

2. They obtain 2 mist eliminators, with one as a standby, each comprised of 4 layers of style 37/97 and 4 layers of style 16/97.

3. A lightweight top hold-down grid, to hold the entire assembly in place.

4. Pressure taps be added to provide a means to monitor the pressure drop increase.

The mist eliminator was obviously a better scrubber that the scrubber (reaction products were detected in the mist eliminator). By putting the 37/97 on the downstream -- i.e., bottom -- side of the mist eliminator, it was anticipated this would remove the great majority of the water drops prior to collection on the finer 16/97 material. Also, since the 37/97 material drains liquid at a very high rate, the total amount of water held in the pad at any time would be greatly reduced, decreasing the rate of the deposition from liquid phase reactions. The combination provided the ability to make a changeover at a very rapid rate, and would allow the mist eliminator sections to be cleaned of almost anything that could get on them.

Immediately after start-up, the mist eliminators worked fine, but after 8 weeks' service, excessive pressure drops occurred across the mist eliminator, and the change-out was made. The changeover to the spare mist eliminator went very smoothly, but when we examined the mist eliminator there was a great surprise.

The bottom material, the 37/97, contained a small amount of a light red scale removable by flexing the pads and washing them. However, the 16/97 on the top side of the mist eliminator was completely plugged up with a tarry black material. The user developed a way to clean these by soaking them in a commercial cleaning solution, so that this tarry material was completely dispersed. The pads were exchanged on an approximate 8-week cycle.

After about a year the customer decided to purchase additional 37/97 and discontinue the use of 16/97 material. Our customer continued along very happily with the installation. I was notified in 1980 that they had found the source of the original pluggage problem. They were using an oil-based de-foamer in the recycled scrubbing liquor. It worked well as a de-foamer, but reaction products plugged the 16/97 part of the mist eliminator. A change of de-foamer eliminated the original problem.

It is interesting that the tarry material did not collect on the coarser material -- it only occurred on the finer material, style 16/97, thus emphasizing in a negative way the selectivity due to fiber diameter.

We think it's obvious that the original specification calling for only 6 inches of a polypropylene mist eliminator was inappropriate. Considering the technology that was available, or at least well known to most people, it was, however, understandable.

B. Condensation Mist

It frequently occurs that relatively hot, moisture-laden gas is cooled in a scrubber. I wonder how often anyone ever thinks about the condensation mist that can occur in such situations. One can get condensation mist where cooling a gas with liquid, when heating a cool gas with hot liquid, or just by mixing 2 saturated gas streams. Such condensation situations can by mystifying.

One of our customers came to us with an emission problem which they had been attempting to solve for over 2 years. They had added more packing to a crossflow scrubber and had provided additional cooling, to no avail. Kimre personnel found this perplexing, and suggested a series of tests to derive the cause of the actual problem. After three false starts, it was finally determined that mist was going into the mist eliminator at a drop size too small for the mist eliminator to catch. This mist was then going into the blower, where it was warmed up slightly, and water evaporated. The contaminants ended up in the stack as a combination of gaseous and particulate components.

The solution to that problem was very simple: We merely added a mist eliminator section efficient enough to catch that size droplet. The cost was completely insignificant, and the results very dramatic -- a factor of 5 reduction in emissions.

Consider Everything

In this case, many different alternatives had been considered in the original analysis, but one crucial alternative was missed. The original mist eliminator would never have removed the sub 4-5 microns which actually caused the emissions.

In the example given above, the first material we installed was too fine and plugged up quickly. We had to back off to a coarser material adequate to give the required performance. The most common error that we see is overdoing the efficiency by specifying too fine a material.

Analagous problems are commonplace on hydrochloric acid scrubbers, which are usually complicated by the presence of large amounts of entrainment.

Recently, one of our accounts in West Germany, ordered -- without specification for use -- a mist eliminator comprised of many layers of our style 4/96. After testing it, he complained bitterly that it didn't work, and then provided us with the process information. We had to report back to them that it would have been impossible for the unit he ordered to ever have removed any mist. Given the conditions and the vessel size, this very fine mist eliminator was always flooded. It would take the mist that was there and make it from very small drops into large drops, but would not remove anything. We suggested that he throw that one away, and replace it with a composition of our design which included allowance for flooding.

The curious part of all that was that the unit which would work cost less than one-fifth as much as the original design specified by the user.

C. Flux-Force Condensation

This is one of those operations in which it is not obvious whether the mist eliminator is a scrubber or a mist eliminator. What do you call it when you take aerosols, use thermodynamic driving forces to cause those aerosols to"grow" into much larger aerosols, and then collect them in a mist eliminator? Is the mist eliminator a scrubber, or is the section where you grow the particles the scrubber?

For the purposes of this paper, we're not concerned about how the growth can be accomplished; it can. The drops containing the contaminants have been increased in size, but they still aren't very large, and they still have to be collected. In these situations the coarser materials have been removed prior to beginning the flux-force condensation techniques. Only fine particulate and soluble materials are present, which helps relieve the pluggage problem, but it doesn't necessarily prevent plugging since the materials may be reactive. It takes considerable judgment and complete information to arrive at a suitable decision.

A customer of ours has what we believe to be the world's largest installation at around 100,000 cfm. In this case there was an existing vessel, so we were constrained to relatively high velocities of well over 10 feet per second. It took us several changes to reach a suitable balance between efficiency, pressure drop, and pluggage resistance. We eventually ended up with a composite involving 4 different styles: Our 4/96, 8/96, 16/96, and 37/94 materials.

The savings to the user were in the seven-figure range. Other technologies that might have been used were: Venturi, followed by a routine mist elimination device; a candle-type mist eliminator; or an electrostatic precipitator.

In this particular case, the primary consideration was very high efficiency (at about 1-1/2 microns), flooding resistance, and pluggage resistance.

This is a commercial contract incinerator owned by a well-known company.

D. Flooding: Localized and Otherwise

One of our customers, located in Missouri, operates an incinerator for the destruction of chlorinated hydrocarbons. This facility had been on-stream for some time, and operated marginally satisfactorily at design conditions of around 13 feet per second in the mist eliminator. They did have one problem, and that was in the winter there was condensation occurring in the stack, which was blowing out the top of the stack and causing local problems.

When the throughput of the unit was increased a very small amount -- feasible from the incinerator and collection standpoint -- the mist eliminator overloaded and substantial emission problems resulted. A substantial problem developed because their total demand exceeded their capacity. Our customer related to us that he did a continent-wide search

for a mist eliminator that would handle his very high flow rate and very high liguid-load conditions.

Although we considered the application routine, there were no other responses to his inquiries. An order was placed with Kimre for one of our very high-flow-capacity units, comprised of style 37/97. This order was placed on an emergency basis. The unit was manufactured, shipped, installed and in service in 5 days. The result: elimination of the problem -- and a good many happier employees. Even the receptionist commented on what an improvement this change had made.

In our opinion, the original design velocity was higher tha it should have been. Of course, that does keep down the capital cost. The alternative to B-GON™ would have been expensive. The customer elected to add a second entire eliminator at the top of the stack. This B-GON loads directly down on the top of a stack enlargement.

In a similar situation, another of our customers operates a rock-dryer kiln fired with oil. This produces some sulfuric acid, and of course a heavy load of particulate, as well as some decomposition products from the rock. The particulate is intended to be collected in a circular enturi of Lurgi-type design. The gas discharges in a radial direction inside of the vessel, the gas load turns upward, passes through a mist eliminator, and through an overhead stack located directly over the mist eliminator.

How does 100 gallons a minute of entrainment from a 90,000 cfm system seem to you? We diagnosed the problem as one of too high a velocity, particularly in view of the highly irregular flow distribution inherent in that type of design.

The solution: Drop a high-capacity B-GON™ Mist Eliminator right on top of the existing chevrons, add a few hold-down grids on top, tie it all in place -- and the problem disappeared. Total cost: Less than $5,000. Alternative cost -- well, nobody ever added all the figures up, but it certainly would have been over $150,000. Subsequently, we've converted 2 or 3 similar units for the same reason.

The combination of relatively high velocities and flow non-uniformity with a high liquid load is a common problem. Most of the situations that we've run into can be handled by a simple B-GON™ Mist Eliminator of high-capacity design. However, in some cases it has been necessary to go to a more radical solution: A variable-resistance mist eliminator. In this situation, the mist eliminator is put together so the flow resistance is higher in the areas where the flow is the greatest, causing a correction of the flow distribution, and therefore lower peak velocities.

One last example of this type of problem How would you like to have a scrubber for which the emissions are higher than the inlet? One of the clients of a consultant knowledgeable about our products has that problem.

They have a Venturi system with chevron mist eliminators, using a

contaminated scrubbing liquid. The mist carryover from the mist eliminator is contributing higher emissions than the incoming gas. Re-design of this system to accommodate a B-GON™ Mist Eliminator of appropriate design is currently under way; installation is anticipated within a few months.

E. Electrostatically-Enhanced Scrubbers

There is a great deal of interest in electrostatically-enhanced scrubbing for the collection of fine particulates. The best scrubbing appears to be with the finest droplets, which requires an efficient mist eliminator. This situation is essentially analagous to that of flux-force condensation, and Kimre has been working with other parties -- one of whom, Dr. Stuart A. Hoenig, will be reporting at this Symposium on his work.

SUMMARY

There's more to the selection of a mist eliminator than plugging some numbers into the Souder-Brown equation. Tremendous strides have been made in the science of predicting mist eliminator performance, but there's still some art.

Faced with a mist elimination situation, consider all the aspects. Consider the cost; consider the downside risk due to uncertainty in the process. Consider scenarios of what might happen under particular conditions -- you could save somebody a lot of trouble.

Don't be like the fellow who ordered a mist eliminator that cannot conceivably work at 5 times the cost of one that will. And most assuredly, don't be the other fellow, who in an attempt to save 2% on the price of a mist eliminator, selects one that is marginal.

NOVEL ANNULAR VENTURI SCRUBBER DESIGN REDUCES WASTE DISCHARGE PROBLEMS

By: Heinz P. Beutner, Ph.D., President
Interel Corporation
7108 South Alton Way, Bldg. M
Englewood, Colorado 80112

ABSTRACT

Characteristics of a new type annular venturi scrubber system, developed by Leisegang Umwelttechnik of West Germany, are presented.

The scrubber has internal circulation of the scrubbing liquid and allows solids buildup in the liquid to 20% or more. The liquid spray is generated without use of nozzles by contact of the gas with the liquid surface. Solids are discharged either as concentrated slurry or as sludge by means of a scraper.

The annular venturi scrubber achieves highest energy efficiency at any pressure drop from 1 to 80 inches WG. It can be operated as variable flow venturi by regulating the water level. Fractional particle removal efficiencies as a function of pressure drop are presented. Examples of installations on product dryers, incinerators, and in foundry and steel mill operations are described.

INTRODUCTION

The venturi effect in particulate scrubbing is based on the rapid growth of water droplets by condensation and coalescense during the high velocity flow of the saturated gas through the venturi zone. In the process, dust particles are collected by collision with water droplets (Fig. 1).

The basic principle has been applied in the Leisegang Annular Venturi Scrubber combined with internal generation of the water spray. The system offers the advantage that liquid with a high solids content is recirculated internally without need for external piping, pump, settling tank, and spray nozzles.

The system achieves the highest possible energy efficiency for any pressure drop from 1 to 80 inches WG. Because of the very low amount of waste water generated, the low scrubbing energy required and the low maintenance needs (no recirculation pump or sensitive spray nozzles), this advanced design offers the user substantial operating cost savings compared with other types of scrubber systems.

The Leisegang Annular Venturi Scrubber is protected under U.S. patent No. 3,876,398 issued April 8, 1975, and patents in all major countries.

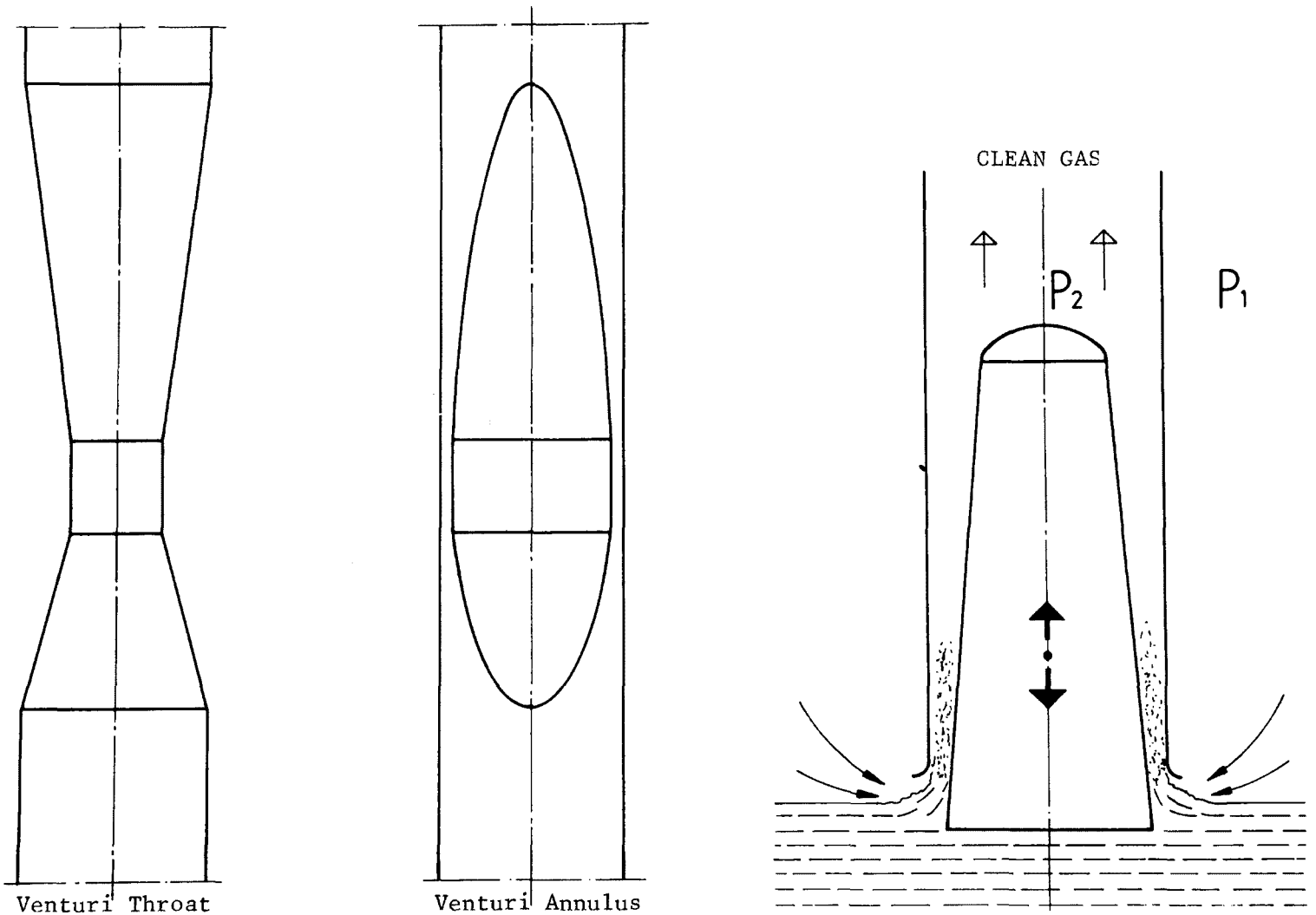

FIGURE 1.
PRINCIPLE OF ANNULAR VENTURI SCRUBBER

Principle of Design

The basic scrubber design is shown in Fig. 2. The venturi annulus is formed by a cone positioned in a vertical tube inside the scrubber vessel. The gas to be cleaned enters the scrubber vessel and impacts on the liquid surface before entering the narrow annulus between the tube and the cone. The strong acceleration of the gas to high velocity in the annulus and change of direction breaks droplets from the liquid surface and carries them into the gas stream.

The opening of the annulus can be adjusted mechanically to change the pressure drop through the scrubber. The position of the liquid level can be regulated either by a simple mechanical overflow weir or by control of the liquid inflow and outflow based on the set point of a liquid level sensor or a pressure differential transmitter. The latter approach maintains a constant pressure drop across the scrubber with variable gasflow conditions.

The gas leaving the venturi orifice decelerates and regains static pressure as the annulus increases in size. A deflector plate knocks down large droplets before the gas enters a demister section. The demister typically consists of S-shaped, parallel arranged lamella plates of polypropylene or metal. Liquid drains off on collection edges while the gas passes through the spaces between the plates at a minimum of pressure loss. Solids in the liquid are easily flushed down with the liquid.

The liquid collected in the upper housing section returns by gravity flow to the tank section of the scrubber. The liquid tank can be designed for turbulence to maintain solids in suspension for removal by a slurry pump or as a settling tank to promote sedimentation of solids for removal by a built-in sludge scraper. Standard scrubber sizes from 600 to 60,000 cfm are available. The larger sizes include multiple venturi tubes.

When compared with other scrubber systems, the Leisegang venturi achieves maximum possible energy utilization for particulate removal, i.e., for any required removal efficiency for a given dust problem, the overall power requirements for the Leisegang annular venturi are always equal to or better than those of other scrubber designs (Ref. 1, 2). This statement applies over the complete range of pressure drops used in practice, from very low energy scrubbing to very high energy scrubbing. It should be noted that the Leisegang Annular Venturi system produces water spray from the energy supplied to the system fan for gas movement. Other venturi systems require a separate pump to produce high pressure atomized water. In this case, the pump power must be added to the fan power requirements when comparing power requirements.

The Leisegang Annular Venturi Scrubber can be operated at any selected pressure drop from as low as 1 inch WG (25mm WG, or 250 Pascals) to 80 inches WG (2,000mm WG, or 20,000 Pascals).

The efficiency of particulate removal in a venturi scrubber is a function of the pressure drop and particle size. The fractional removal efficiency for quartz dust (specific density 2.6g/cm^3 or 162.2 lbs/ft^3), shown in Fig. 3, is based on actual test results.

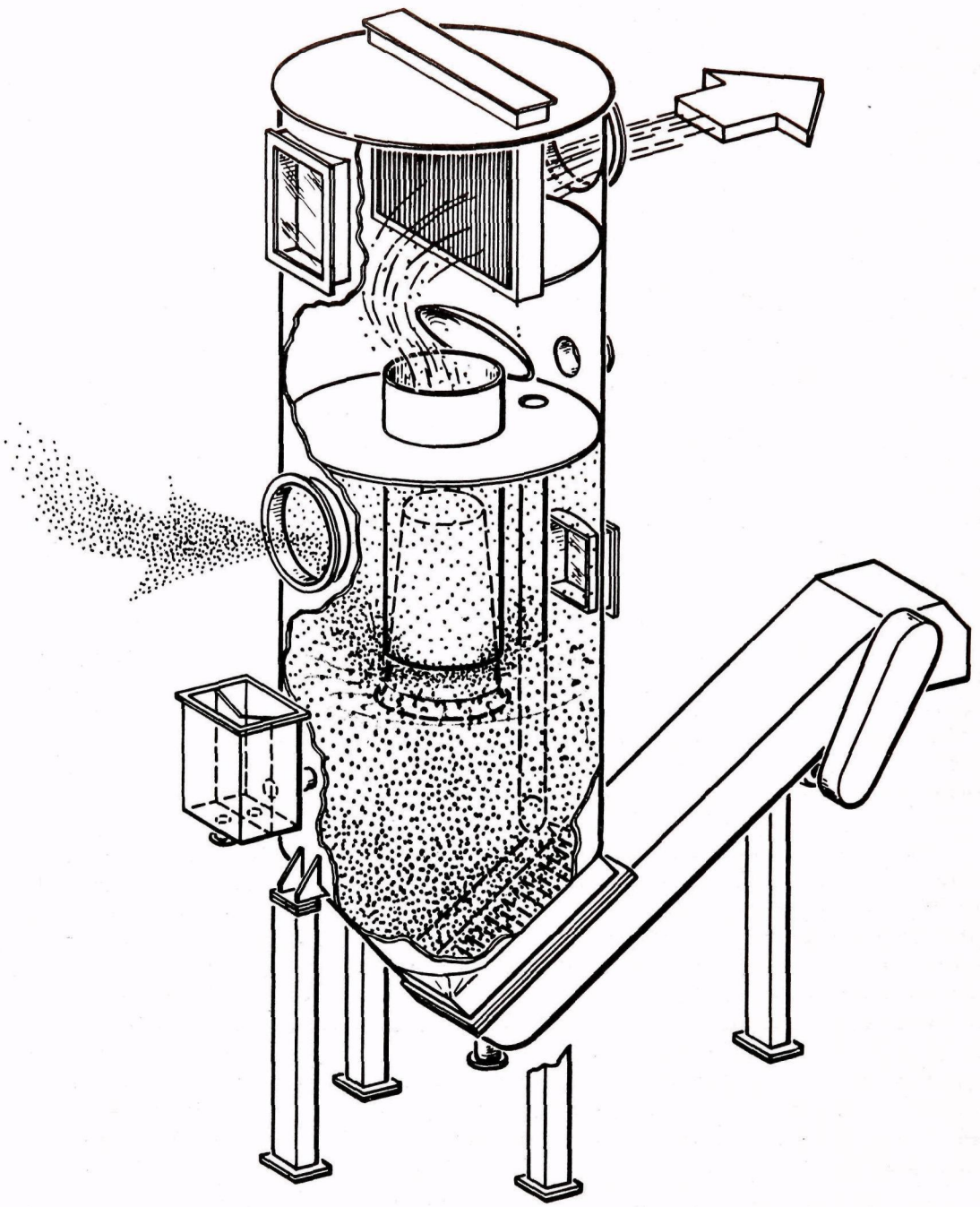

FIGURE 2
LEISEGANG ANNULAR VENTURI SCRUBBER
INCLUDING SLUDGE SCRAPER FOR SOLIDS DISCHARGE

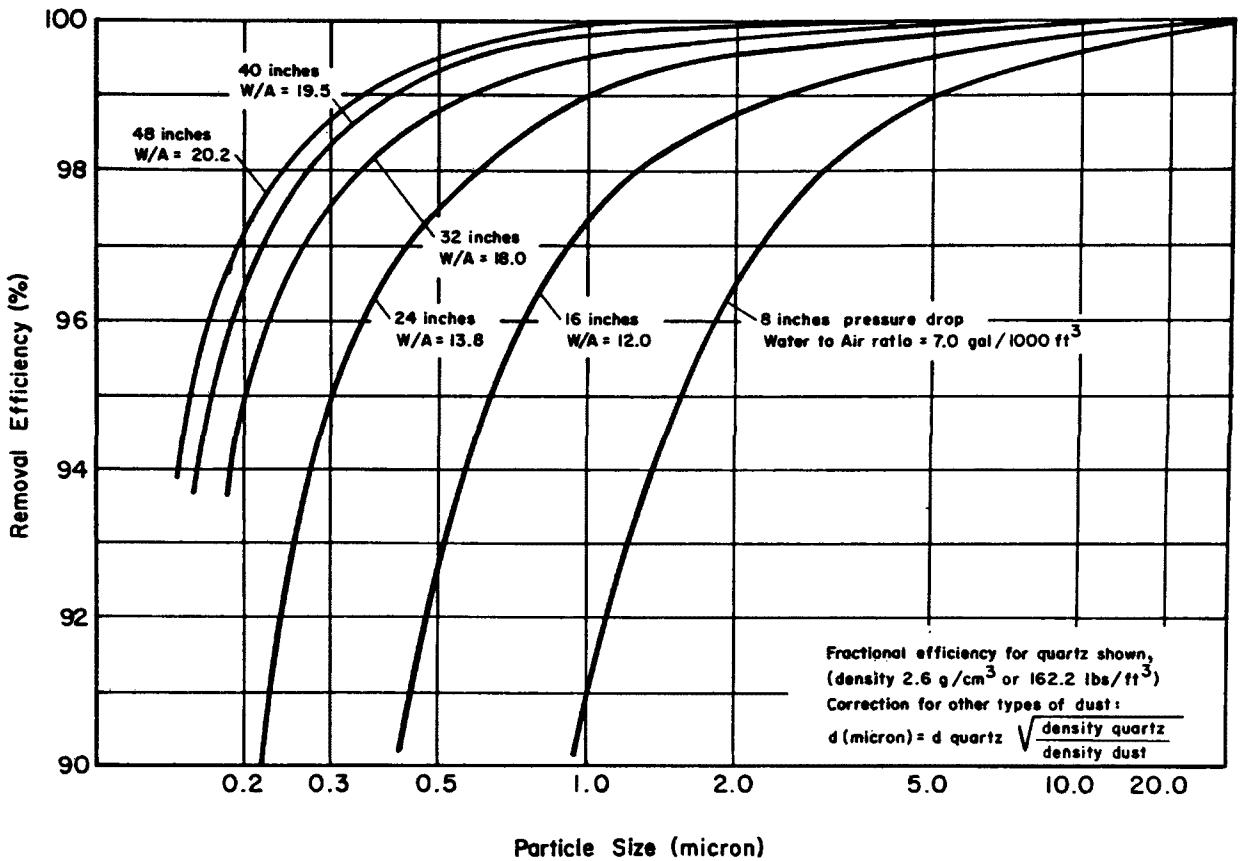

FIGURE 3
FRACTIONAL PARTICULATE REMOVAL EFFICIENCY
FOR LEISEGANG VENTURI SCRUBBER

Variable Venturi Operation

A simple approach to variable venturi operation is a continuous control of the water level in the scrubber relative to the annulus opening. This is best accomplished by a differential pressure controller that automatically turns on and off the flow of fresh water at a constant rate of slurry discharge from the scrubber. Alternatively, the slurry discharge rate can be varied at constant water feed rate. A typical schematic for variable venturi operation is shown in Fig. 4.

The variable venturi operation by control of the liquid level allows the turn-down of the gasflow rate to 30% of design without loss in scrubbing efficiency.

Installation Experience

Typical uses of the Leisegang Annular Venturi Scrubber to date are in the foundry industry, on product dryers of various types, and on incinerator emissions.

A large installation of five identical scrubber units, each for 36,000 cfm gasflow, controls all emission sources from the Autocast Foundry near Johannesburg, S. Africa (Fig. 5). The foundry makes parts for Toyota cars. Except for a small amount of overflow liquid, there is no requirement for liquid waste processing, since all solids are discharged as a sludge. The scrubber meets the required outlet dust level of 50 mg/Nm^3 (0.023 gr/scf) at a pressure differential of 14 inches WG.

A typical installation of a high energy type scrubber (60 inches pressure differential) is a small installation processing only 280 cfm from a dissolver for nuclear reactor elements. Because of the radioactivity of the collected solids and liquid aerosols, the Leisegang scrubber was selected to avoid any external pumping loop. The stainless steel scrubber includes a pressure differential sensor and controller to maintain the required liquid overflow (Fig. 6).

An installation in the U.S. in FRP construction on incinerator exhaust includes a packed bed section above the venturi section for absorption of hydrochloric acid. The venturi scrubber removes gases only partially because of the very short contact time between gas and liquid. The packed bed contactor, using caustic reagent, allows gas absorption to very low outlet levels.

A major installation on a foundry cupola was started up in 1979 at Klockner Werke in Manstaed, W. Germany. The venturi scrubber, operating at a pressure differential of 40 inches WG, follows a spray dryer installation with cyclone. The spray dryer system was required to remove sulfur dioxide. The sludge from the scrubber is recirculated into the spray dryer and the only waste discharge is solid product from the cyclone.

ENDNOTES: 1. Wicke, M. Fortschrittsberichte der VDI Zeitschriften, R.3, Vr 33, VDI Verlag, 1970
2. Leisegang, L. Swiss Chem 1, Nr. 12, 1979

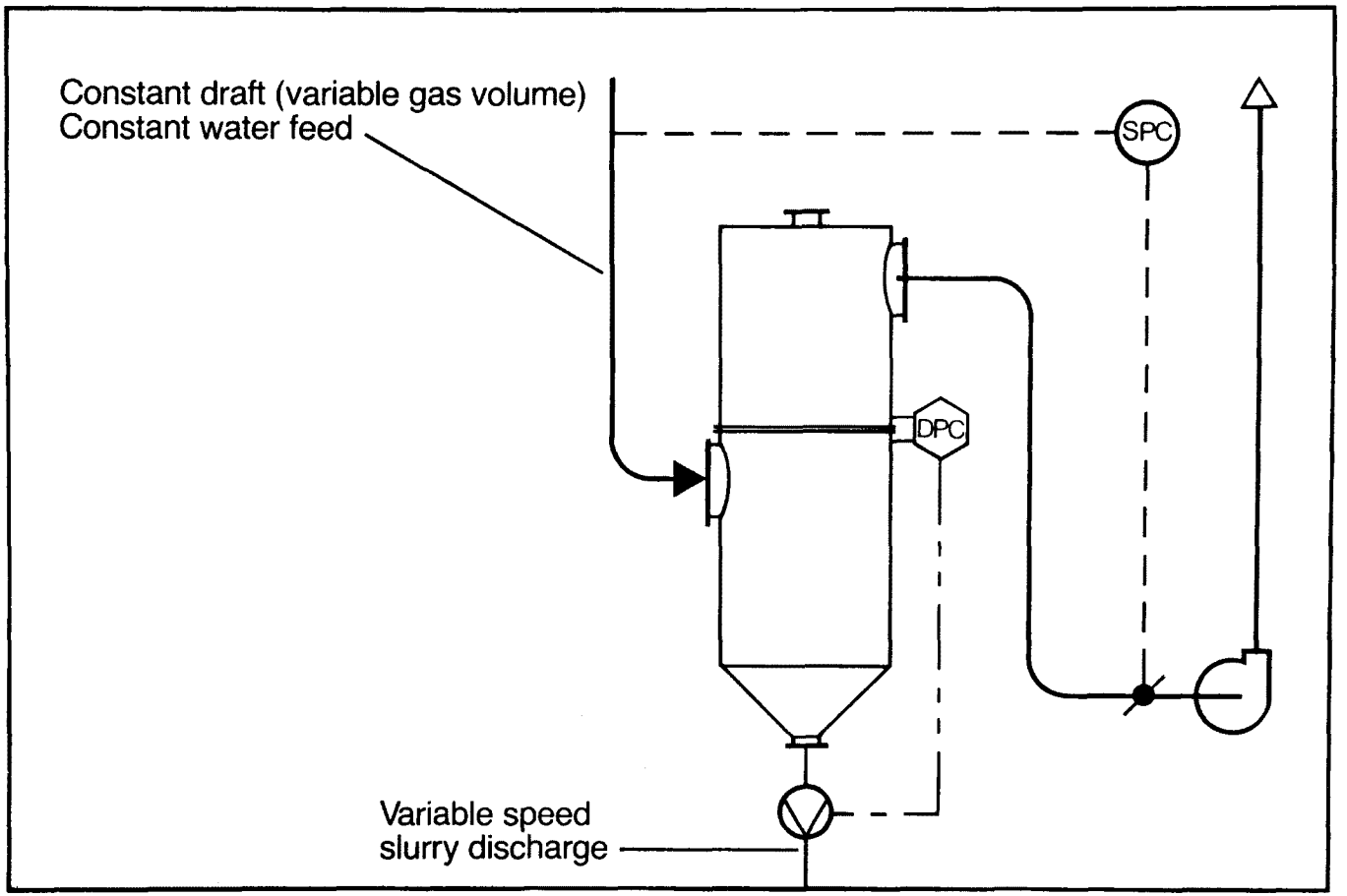

FIGURE 4
TYPICAL CONTROL DIAGRAM FOR VARIABLE VENTURI OPERATIONS AT CONSTAT DELTA P

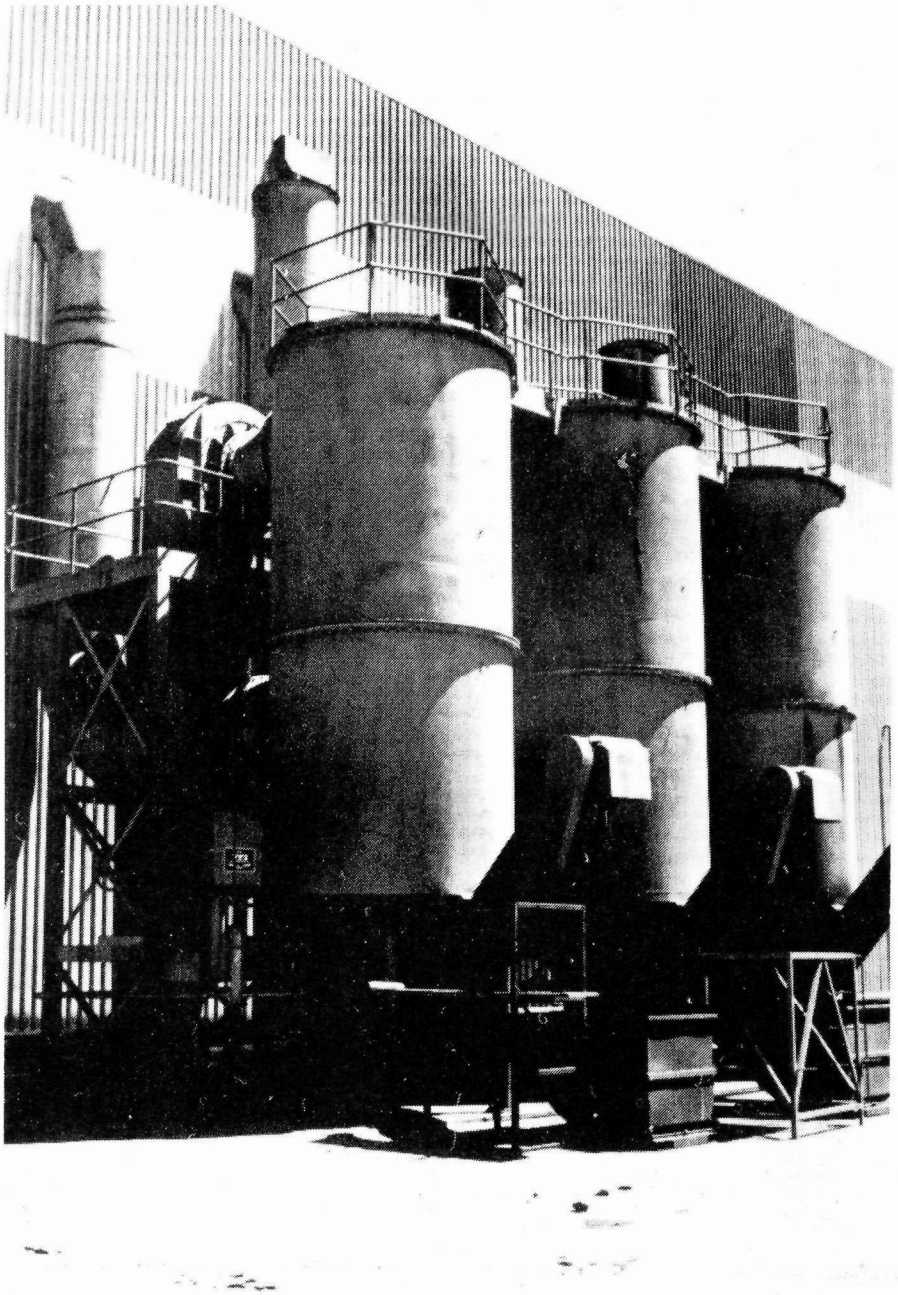

FIGURE 5
VENTURI SCRUBBER INSTALLATION ON FOUNDRY OPERATIONS
AT AUTOCAST PTY NEAR JOHANNESBURG, S. AFRICA

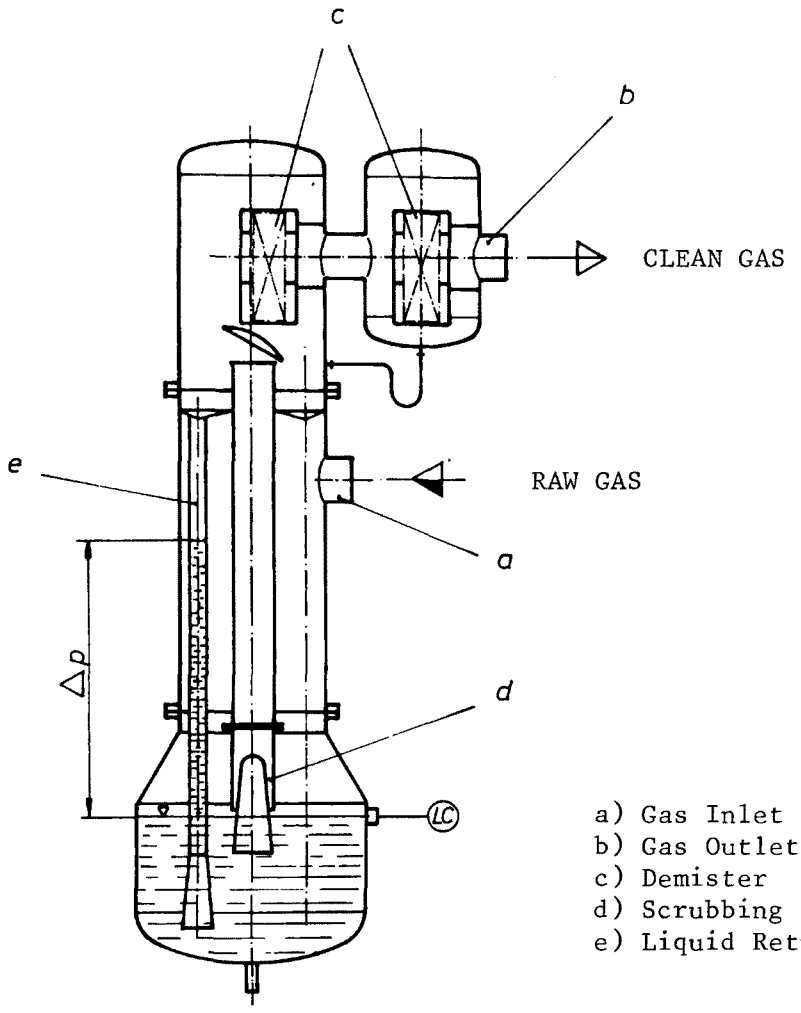

FIGURE 6
HIGH ENERGY SCRUBBER
FOR RADIOACTIVE AEROSOLS
(DELTA P = 60 INCHES WG)

CONSIDERATION OF THE PERTINENT DESIGN AND OPERATING CHARACTERISTICS ESSENTIAL FOR OPTIMIZATION OF VENTURI SCRUBBER PERFORMANCE

By: H. Scott Oglesby
National Council of the Paper Industry
for Air and Stream Improvement, Inc.
Southern Regional Center
P.O. Box 14483
Gainesville, Florida 32604

ABSTRACT

The use of medium to high energy venturi scrubbers in the pulp and paper industry has increased substantially over the past eight to ten years. Accompanying this increased use is a wider spectrum of applications, and a demand for a sustained higher level of performance to meet the current and emerging regulatory requirements. Accordingly, there is a need to review the critical factors affecting performance relative to optimization, process compatibility and energy requirement minimization. In this respect, it is essential that considerations be given to the pertinent design and operation parameters in assessing performance. This paper addresses these issues and develops a methodology for troubleshooting scrubber performance.

INTRODUCTION

For many years the application of venturi scrubbers was almost exclusively confined to controlling submicron particulate emissions from the lime kiln, but more recently these devices are being applied to combination fuel-fired boilers, recovery furnaces, smelt dissolving tank vents, and on causticizer vents, for the same purpose. Also, with the emerging requirements for flue gas desulfurization on new coal-fired power boilers, it is anticipated that the application of wet scrubbers will grow at an accelerated pace.

DESIGN FUNDAMENTALS

Venturi scrubbers have been used in a variety of applications for many years. Experience has been vast, and yet a condensation of this experience in terms of a reliable design equation has been lacking. Perhaps the earliest published work relating design and performance parameters empirically, was that of Stairmand (1), which appeared in 1965. Also, a very useful relationship was developed by Hesketh (2) in 1974, which related the pertinent scrubber operating variables. More recently, results of a number of highly comprehensive studies have been published (3) relative to optimizing the design and performance of venturi scrubbers.

Since the performance of a venturi scrubbing system is achieved at the expense of a high pressure drop in the gas stream, accompanied by high fan operating cost, designs of system which for a given gas flow rate and particulate removal efficiency, have minimum pressure drop, may be considered optimal.

Gas-Liquid Relationship

It has been shown to be generally true that scrubber efficiency increases with increased energy consumption, whether this is achieved by employing high gas velocities in the throat, or using a high water/gas ratio. It has also been shown (1), however, that at any particular throat velocity there is an optimum pressure drop at which the scrubber should be operated. This is shown clearly in Figure 1, in which the interrelation between efficiency, water/gas ratio, and pressure drop is given. The points of maximum efficiency for a given pressure drop are joined to produce the economic design curve shown, which indicates that there is a particular combination of operating parameters which gives maximum efficiency for minimum pressure drop.

It is known that the target efficiency of a droplet increases by decreasing the diameter and increasing the relative velocity between the gas and the droplet. Figure 2 was developed from published data (1) to show that the optimum droplet size and the induced droplet size are equal for only a particular throat velocity for any given dust size. Thus, there is an optimum throat velocity for any given set of conditions.

Throat Geometry

Fundamental to scrubber design is the throat area which is specified based upon the saturated gas volume and pressure drop requirements. A more recent analysis (4) of performance suggest that other aspects of throat geometry may be important in optimizing performance. For instance, it has been shown (5) that increasing venturi length will increase the collection efficiency of particles greater than approximately 0.5 μm in size without a commensurate increase in pressure drop. Further it has been demonstrated (4) that the pressure recovery is strongly influenced by the throat length.

Other important aspects of throat geometry are those which relate to throat coverage. Regardless of the concepts which are utilized in designing a scrubber, it is imperative that these provide for maximum throat coverage over the full operating range.

Elbow and Entrainment Separator

The diffuser and regain section of the venturi scrubber discharges into the elbow which turns the gases and liquid into the entrainment separator. A "flooded" elbow, which provides for a pad of liquid in the horizontal section, has become standard design in recent years. This liquid pad provides a surface for turning the gases, thus reducing wear on the elbow, and serves as an additional impaction zone for collecting particulates remaining in the gases.

The design criteria for venturi scrubber entrainment separators, which is straightforward, involves cyclonic separation design principles for collecting liquid droplets as small as 15 μm in diameter. From the foregoing, it is obvious that inlet volumes to the separator must be limited to fluctuations of ±15 percent, if high separating efficiencies are to be maintained.

If the separator is not properly designed and/or operated, carryover or reentrainment of liquid droplets will occur resulting in increased dust lost to the atmosphere. Also, a poorly designed separator can cause excessive pressure drop across the system, thus reducing overall capability.

System Ancillaries

Equally important to the venturi scrubber and its major components, relative to optimizing performance, are the pertinent ancillaries which comprise the total system. These items, and the vital role they play, are addressed in the sections which follow.

OPERATING PRINCIPLES

Once the scrubbing system is placed in operation, it is essential that the actual conditions be compatible with that on which the design was based, if optimal performance is to be achieved. Because the venturi scrubber is extremely flexible, it is relatively easy to operate the system beyond the range intended, at a sacrifice in performance and/or energy consumption.

Relationship Between Operating Design Parameters

Those responsible for operation and maintenance of venturi scrubber systems should be provided with the appropriate operating and performance curves such as the one shown in Figure 3. If the curves or the data for plotting such are not available, then the relationship developed by Hesketh (2) as summarized in Table 1, may be utilized for this purpose. Performance curves such as these are essential in employment of diagnostic routines for optimization.

TABLE 1. VENTURI SCRUBBER PRESSURE DROP RELATIONSHIP (2)

$$\Delta P = \frac{Vt^2 \rho\varepsilon \, A^{0.133} L^{0.78}}{1270}$$

Where:

ΔP = Venturi Pressure Drop, inches W.G.
L = Liquid to Gas Ratio, Gal/1000 ACF
$\rho\varepsilon$ = Gas Density Downstream from Venturi, lb/ft^3
Vt = Throat Velocity of Gas, ft/sec
A = Throat Cross-section Area, ft^2

Control Options

Continuous measurement of throat pressure differential is the most direct way to monitor scrubber performance. However, in order to optimize performance a comprehensive instrumentation package is required as indicated in Figure 4. Control options include a liquid control valve, variable speed pump drive, an adjustable throat, or various combinations of these devices coupled with feed-back control. More complex control systems may include variable speed I.D. fan drive, or fan damper controls as well.

Separator Limitations

Since the separator is so important to the overall performance of the scrubber system, and its operation range is more limited than the scrubber, set-points should be utilized to activate an alarm (and record) when the scrubber is operating outside the capability range of the separator. Although this is a passive control approach, at least the operator would be aware that the system was not operating under optimal conditions.

CONSIDERATIONS FOR OPTIMIZING PERFORMANCE AND MINIMIZING ENERGY REQUIREMENTS

This section will briefly address those innovations which may be utilized to improve scrubber performance or reduce energy requirements at the same level of performance. The choice for optimization, of course, will depend upon the specific application and the degree of system modification which can be justified.

Preconditioning of Gases

It has been stated (6) and demonstrated that the key to low power scrubbing involves the judicious use of sufficient gas retention after quenching to effect conditioning, thus enabling agglomeration and absorbtion of particulate fume and gases. The impact on particle size distribution due to particle growth resulting from water vapor condensation is shown in Figure 5. A recent, modern version of this concept (7), called flux force/condensation scrubbing, claims to use only 70 percent as much power as a conventional scrubber system would. While the theory surrounding this concept is somewhat complex, applications using simple spray nozzels to quench gases prior to the scrubber and resulting in improved performance have been reported (8).

Multiple Throat Arrangement

Recent experimental work (5) has demonstrated that two venturi throats in series can improve scrubber performance by as much as 30 percent over a single throat at the same pressure drop. It may perhaps be too early to judge whether this same level of performance can be achieved by the more simple preconditioning approach, and if in fact the multiple throat approach does provide an additional advantage.

Separator and Duct Configuration

System energy consumption to a greater extent and performance to a lesser degree can be affected by inlet duct configuration and separator design. Good ductwork design procedures are well documented (9) and should be reviewed if this part of the system is suspect. As previously mentioned, the importance of the separator cannot be over emphasized, hence good separator design, operation and maintenance are essential for optimizing performance and energy consumption.

I.D. Fan Location and Design

Since performance of a venturi scrubber depends on development of the

required static pressure, the induced draft (I.D.) fan is a vital component of the system. A well designed fan will be an asset in the quest for optimizing performance and energy consumption (10,11).

The power required to drive wet scrubber I.D. fan can vary in a given situation depending on whether the fan is before (scrubber under pressure) or after (scrubber under vacuum) the scrubber. When the I.D. fan is operated in the "cold" (after) position, the brake horsepower (BHP) reduction can be 20-35 percent compared to a fan located in the "hot" (before) position. This reduction is achievable due to the lower saturated gas volume and lower equivalent static pressure (ESP) prevailing at saturated temperature, therefore reducing the fan capacity and power requirements. In lieu of the energy savings, the system static capability (and efficiency) may be increased by placing an existing I.D. fan after the scrubber.

TROUBLESHOOTING VENTURI SCRUBBERS

In the interest of maintaining continuity of high performance it is essential to develop a troubleshooting procedure with routine followup. A lot more can be said about this aspect than time will allow, but a brief summary if provided. The most important tool in diagnosing poor performance is the use of the operating and performance curves, to determine how close actual operating conditions relate to design. Usually, this will allow one to zero in on the area of suspect.

Static Pressure

Development of a system static pressure profile is another useful tool in troubleshooting a system. This is not overly time consuming and will allow an immediate assessment of the pressure drop distribution relative to design.

Separator Velocity

Perhaps the most common reason for poor scrubber performance is poor entrainment separation. Reentrainment may be described by a number of mechanisms, but is primarily due to either too high or too low of a vertical velocity in the separator, as depicted in Figure 6. Knowing the separator dimensions and gas volume being processed, it is a simple matter to determine this velocity. The separator may also be the source of excessive pressure drop.

Throat Area

For fixed throats the throat area selected for a given application should be in the mid-range, so that the liquid flow rate required to maintain the pressure differential is neither too high nor too low. High liquid flowrates, in addition to consuming excessive energy, tend to aggravate reentrainment conditions in the separator. On the other hand, low liquid rates usually result in reduced efficiencies and poor throat coverage.

Recently, we have seen increased use of the adjustable (variable) throat,

and this provides an excellent mechanism for optimizing performance. The intent of this concept is to maintain the throat velocity which achives highest efficiency at lowest pressure drop. Unfortunately, the flexibility afforded by this concept also allows operation to drift outside the optimal range.

Pump and Scrubbing Fluid Control

The scrubbing fluid pump, piping, valves, sump tank and controls must be designed and operated to respond to the scrubber demands. Quite often the scrubber operating range will exceed the pump capacity, which results in reduced efficiency. Also, where systems operate with high fluid recirculation rates it is essential that adequate attention be given to the sump tank, piping and liquid level control arrangements.

Fan Characteristics

Generally, the system's static pressure requirements are stipulated, and it is readily obvious as to whether the I.D. fan will meet this demand. However, there may develop, due to a combination of physical conditions, a situation where a fan "falls off its curve" and will not perform as specified (11). Therefore, it is essential to have the fan performance curves and "test block" specifications available during performance analysis. This information is also useful in determining if the fan may be upgraded to develop more static or volume capacity.

CONCLUSIONS

The pertinent aspects of optimizing venturi scrubber performance relative to maximizing efficiency and minimizing energy consumption have been reviewed. Reliable design equations and relationships have been developed, and recent studies have extended their use toward optimizing performance. Also, today there are available excellent relationships for developing operating and performance curves to assist in achieving and maintaining continuity of high performance.

Mechanisms are now being advanced which offer the opportunity to boost venturi scrubber system efficiencies, or reduce energy requirements for the same level of performance. Some of these concepts are new in principal while others have been utilized in the past, but were not fully quantified until recently.

The importance of the cyclone entrainment separator, and the part it plays in overall system optimization cannot be overemphasized. The entrainment separator is much more susceptible to volume swings than the scrubbers and the failure to recognize this aspect is one of the major reasons for poor performance. Optimal performance may indeed be difficult to achieve without devoting proper attention to the major ancillaries which comprise the complete system.

With the development of appropriate operating and performance curves for a specific system, a troubleshooting routine may readily be performed in the

interest of optimization. In troubleshooting a system, the major components to be considered in the analysis are the I.D. fan, throat, entrainment separator, and liquid flow control equipment.

REFERENCES

1. Stairmand, C. J., Removal of Grit, Dust, and Fume from Exhaust Gases from Chemical Engineering Processes, The (British) Chemical Engineer, Dec. 1965, pp. CE310-326.

2. Hesketh, Howard E., Fine Particle Collection Efficiency Related to Pressure Drop, Scrubbant and Particle Properties, and Contact Mechanism, JAPCA, Vol. 24, No. 10, Oct. 1974, pp 939-42.

3. Goel, K. C. and K. G. T. Hollands, Optimum Design of Venturi Scrubbers, Atmospheric Environment, Vol. 11, pp. 837-845, Pergamon Press 1977.

4. Overcamp, Thomas J. and Steven R. Bowen, Effect of Throat Length on Pressure Loss in a Venturi Scrubber, Presented at the 73rd Annual Meeting of the APCA, Montreal, Quebec, June 22-27, 1980.

5. Muir, D. M. and Y. Miheisi, Comparison of the Performance of a Single and Two-Stage Variable-Throat Venturi Scrubber, Atmospheric Environment, Vol. 13, pp. 1187-1196, Pergamon Press 1979.

6. Taeler, David H., Gas Scrubbing Pays Double Dividend, Minerals Processing, Jan. 1964, Jan. 1964, pp. 24-27.

7. Anon., Science/Technology Concentrates, Chemical and Engineering News, Dec. 3, 1979.

8. Oglesby, H. S. and A. V. Barron, Economic Considerations for Selection of Pollution Control Systems, Presented at TAPPI 22nd Engineering Conference, Sept. 19-21, 1967, Atlanta, Ga.

9. Jorgensen, Robert, Editor, Fan Engineering, Sixth Ed., Chap. 3, Buffalo Forge Co., Buffalo, N.Y.

10. Perry, Robert E., Power Conservation through Proper Fan Operation, Southern Pulp and Paper Manufacture, June 1977, pp. 29-36.

11. Barron, Alvah V., Fan Application for High Energy Scrubbers, Presented at the TAPPI 26th Engineering Conference, November 18, 1971, pp. 609-622.

12. Oglesby, H. Scott, Design and Operating Characteristics of Venturi Scrubbing Systems which contribute to Excessive Reentrainment, Proceedings of the 1977 NCASI Southern Regional Meeting, Special Report No. 77-07, Oct. 1977, pp. 109-121.

13. Calvert, Seymour, Get Better Performance from Particulate Scrubbers, Chemical Engineering, Oct. 24, 1977, pp. 133-140.

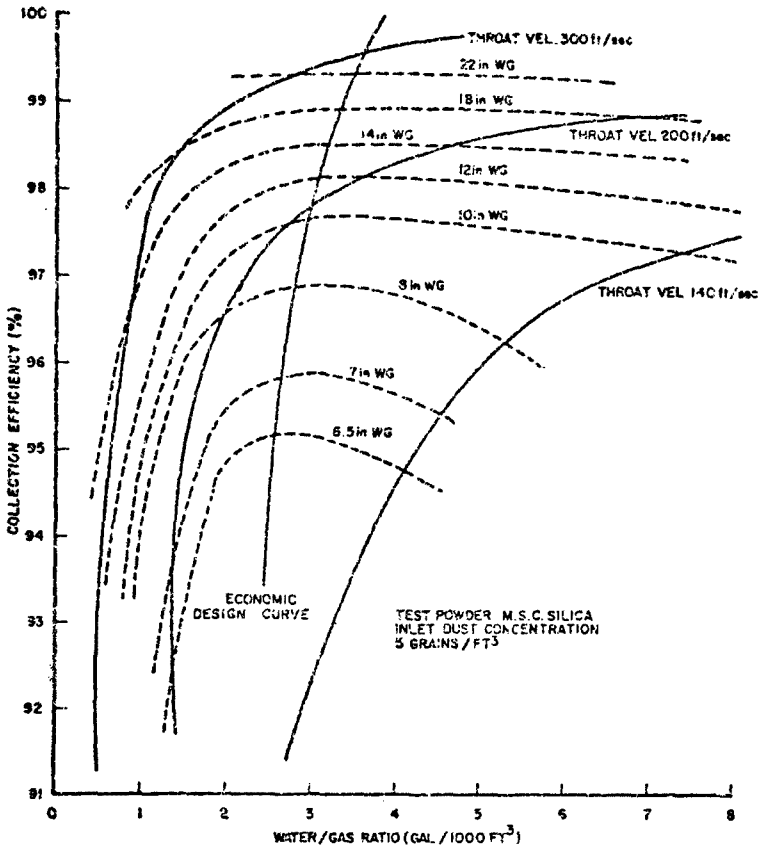

FIGURE 1. OPTIMUM OPERATING CONDITIONS FOR VENTURI SCRUBBER

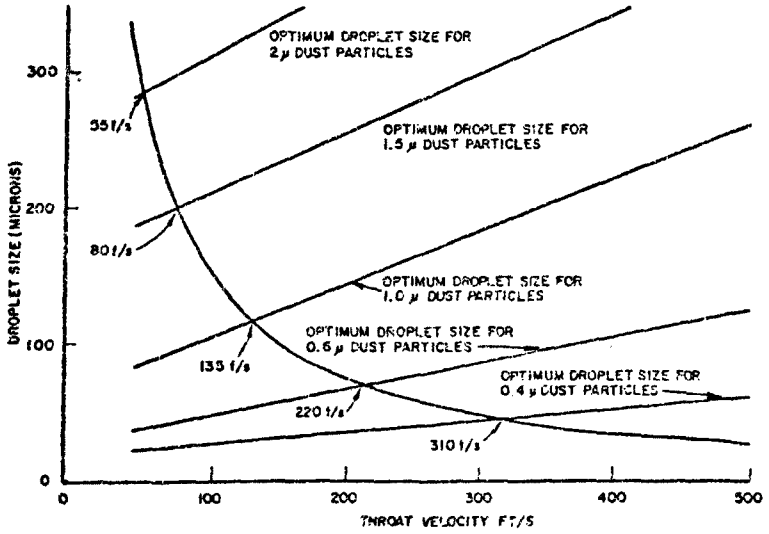

FIGURE 2. OPTIMUM VELOCITY FOR OPERATION OF VENTURI SCRUBBER

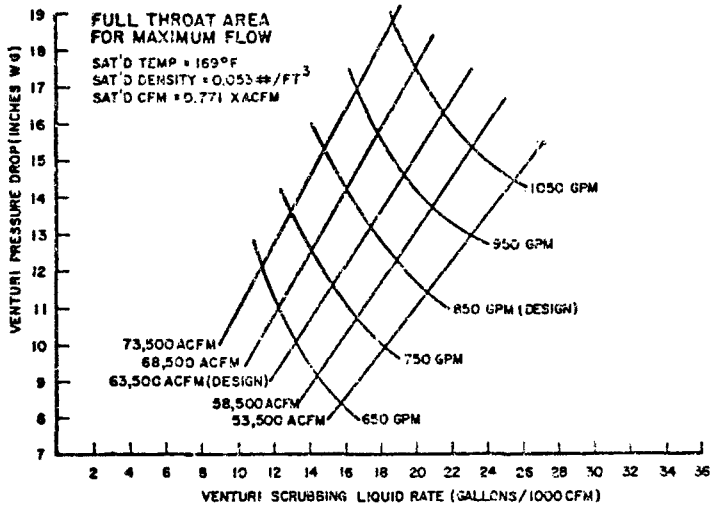

FIGURE 3. SCRUBBER OPERATING VARIABLES (12)

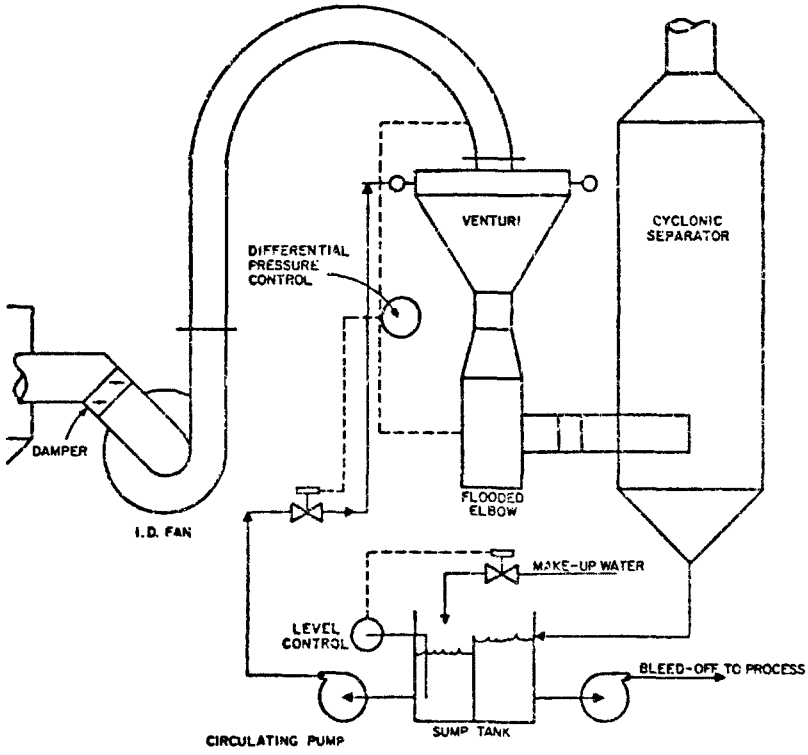

FIGURE 4. VENTURI SCRUBBING SYSTEM COMPONENTS AND INSTRUMENTATION

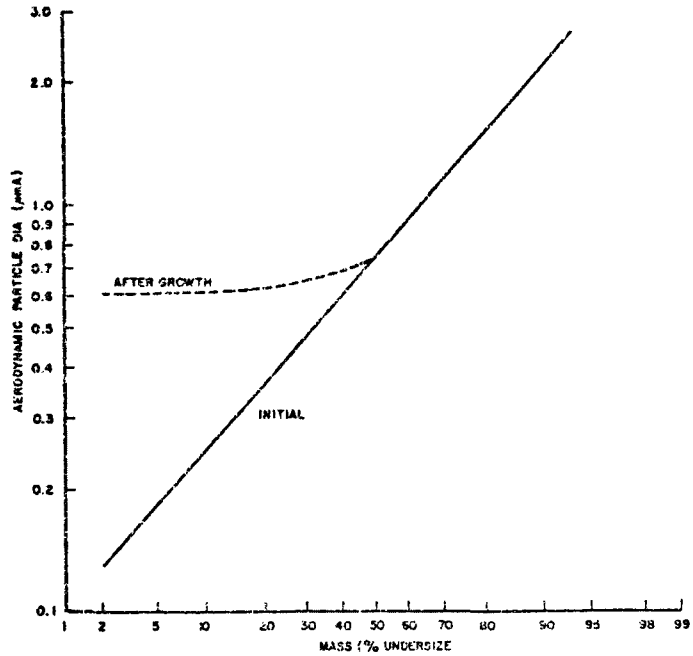

FIGURE 5. PARTICLE GROWTH RESULTING FROM WATER-VAPOR CONDENSATION REDUCES POWER DEMAND (13)

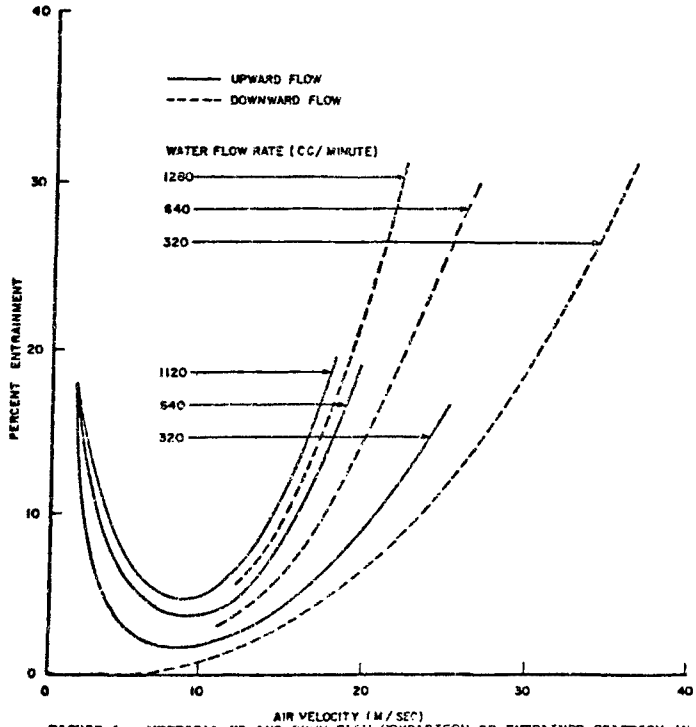

FIGURE 6. VERTICAL UP AND DOWN FLOW COMPARISON OF ENTRAINED FRACTION IN UPWARD AND DOWNWARD COCURRENT ANNULAR FLOW IN 1.25 cm I.D. TUBE

APPLICATION OF SCRUBBERS FOR PARTICULATE CONTROL OF INDUSTRIAL BOILERS

By: Murray Borenstein
Neptune AirPol Inc.
Sub. of Wheelabrator-Frye Inc.
Englewood, NJ 07631

ABSTRACT

Cyclone dust collectors were formerly used as the means of dust control on bark boilers, but are no longer adequate. More stringent requirements call for higher efficiency collection, and scrubbers have been successful in meeting the codes. This paper will explore the operating parameters, operating experience, and test results of scrubbers on wood and coal fired boilers, particularly in the pulp and paper industry. It will also review the power requirements, materials of construction, scrubber design and mechanical collectors.

Background

Prior to the 1970's mechanical dust collectors were almost the exclusive method of pollution control on industrial wood and coal fired boilers. These were principally the multiple cyclone type with cast iron tubes ranging in diameter from 6" to 12". Gas enters the cyclones axially, being given its rotation spin by vanes. The smaller the diameter, the greater the centrifugal force, and the higher the efficiency. Fly ash is highly abrasive, and the cyclones must be constructed of iron of relatively high Brinell hardness.

Efficiency falls off rapidly as particle size falls below 10 microns. Typical efficiency for a multiple cyclone collector handling flue gas containing fly ash from a pulverized coal fired boiler is about 80%. Thus, with an inlet loading of 3 gr/scf, it is obvious that an outlet loading of .6 gr/scf would not suffice for today's standards.

For wood fired boilers, the bark char is particularly light, specific gravity of .2 to .5 so that the efficiency would be even less. It has been demonstrated that a second stage mechanical type collector in series with the first may increase overall efficiency by 2 - 5%. This percentage varies depending on the ability to design a proper system for primary hopper evacuation or out-tube shave off which contains the finer material. Even with the most efficient two-stage type units which are reported capable of providing a total of 90-95% efficiency, they will still not meet federal and state standards of about .1#/m BTU input.

It should be noted that particle size distribution of dust at outlet of primary dust collectors have over 50% of the material less than 5m. The particles smaller than 5m have a very low terminal velocity and are relatively unaffected by inertial or gravitational force so that the probability of collection of these size particles is poor for any second stage mechanical cyclone device.

Further, particles of less than 5m range also are the major contributors to stack opacity and substantial removal is necessary in order to meet low Ringleman member requirements.

In some installations where dust emission is very marginal, a shave off arrangement in which a portion of the dust rich gas of about (10-50%) of the volume can be scrubbed and then recombined with main gas stream. Reports on few installations of this type have not been successful in meeting current stringent codes.

With the advent of the more stringent state codes of the 1970's and the Federal Clean Air Act of 1977, it was apparent that secondary air cleaning for industrial boilers would be required. In 1979, the EPA promalgated the NEW SOURCE PERFORMANCE STANDARDS (NSPS) for boilers generating electricity greater than 73 MW (250 MM BTU/hr) which limits the emission to .03 lbs/MM BTU. Boilers less than 73 MW are handled by state codes which generally require emissions ranging from .1 to .8 lbs/MM BTU. Some of the larger industrial boilers exceed this capacity and would come under the federal standards. The standards also call for maximum emissions of 1.2 lbs. SO_2/MM BTU plus a 70-90% reduction of SO_2, depending upon the sulfur content of the fuel. In almost all cases of coal burning boilers, the user is faced with SO_2 removal as well as particulate.

The user has a choice between 4 alternate methods of secondary control:

1. Wet Scrubber
2. Fabric Filter
3. Electrostatic Precipitator
4. Dry Scrubber

Each method has its pros and cons, but this paper will deal with Wet Scrubbers only.

Advantages of Wet Scrubbers

1. Have the capability to collect both particulate and absorb gases.
2. Function in wet corrosive and/or explosive gas mixtures.
3. Not sensitive to high temperatures.
4. Occupy less space than fabric filter or electrostatic precipitator.

Disadvantages of Wet Scrubbers

1. Higher power consumption.
2. Water and sludge disposal problems.
3. Highly visible steam plume.
4. Possible corrosion problems if material of construction not properly selected.

Types of Scrubbers

All scrubbers operate on the principal of inertial impaction between a droplet of liquid and a solid particle, or impingement of a high velocity particle on a wetted surface. To achieve the desired impaction, water is finely divided into droplets and accelerated to achieve its impact velocity. This may be accomplished by injecting jets of water into a high velocity gas stream (such as is done in the Venturi Scrubber) or generating a fine spray in high pressure spray nozzles. The types of scrubbers that have been used on industrial boilers are:

1. Venturi
2. Flooded Disc
3. Impingement Tray
4. Dynamic Scrubber

This paper will deal primarily with Venturi Scrubbers since they are the type most commonly used for particulate collection, although they also have the capability for gas absorption.

See Figs. 1, 2, 3, 4

Fuels

In determining the design parameters for scrubbers for industrial boilers, the design engineer must review several factors, such as:

1. What type of fuel?
   a. Coal
   b. Bark and Wood
   c. Oil
   d. Combinations of the Above
2. In coal fired boilers, what is the method of firing?
   a. Pulverized
   b. Spreader Stoker
   c. Chain Grate Stoker
   d. Under Feed Stoker
3. What is the excess air rate?

Coal fired boilers have heavier dust loadings and finer particulate sizes than wood fired; and, therefore, require higher pressure drops in the range of 12-18" w.g. water gauge to achieve emissions of 0.1 lb/MM BTU. Bark or wood, when efficiently burned, has relatively light loadings and requires pressure drop in the range of 8-10" w.g. Combinations of wood and coal would need pressure drop somewhere in between.

See Fig. 5

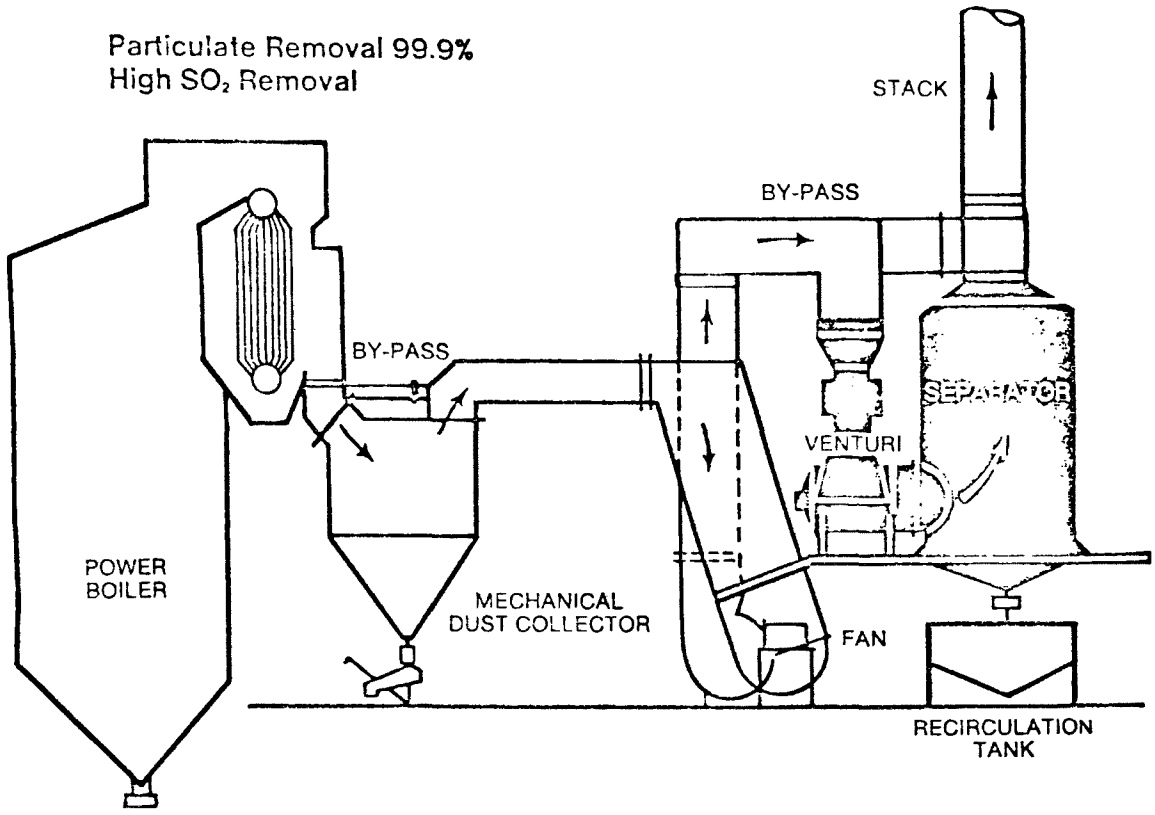

Fig. #1

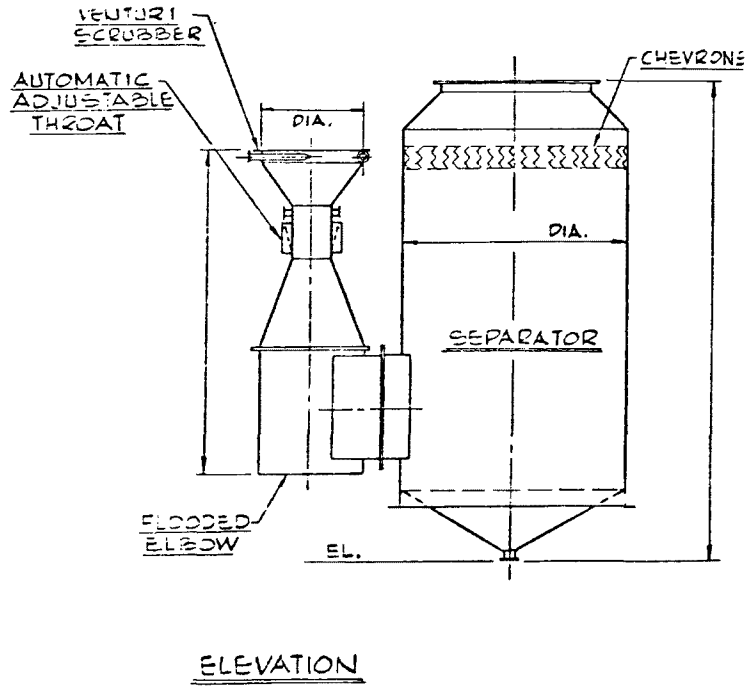

ELEVATION

FIGURE 2. AIRPOL BARK BOILER SCRUBBER SYSTEM

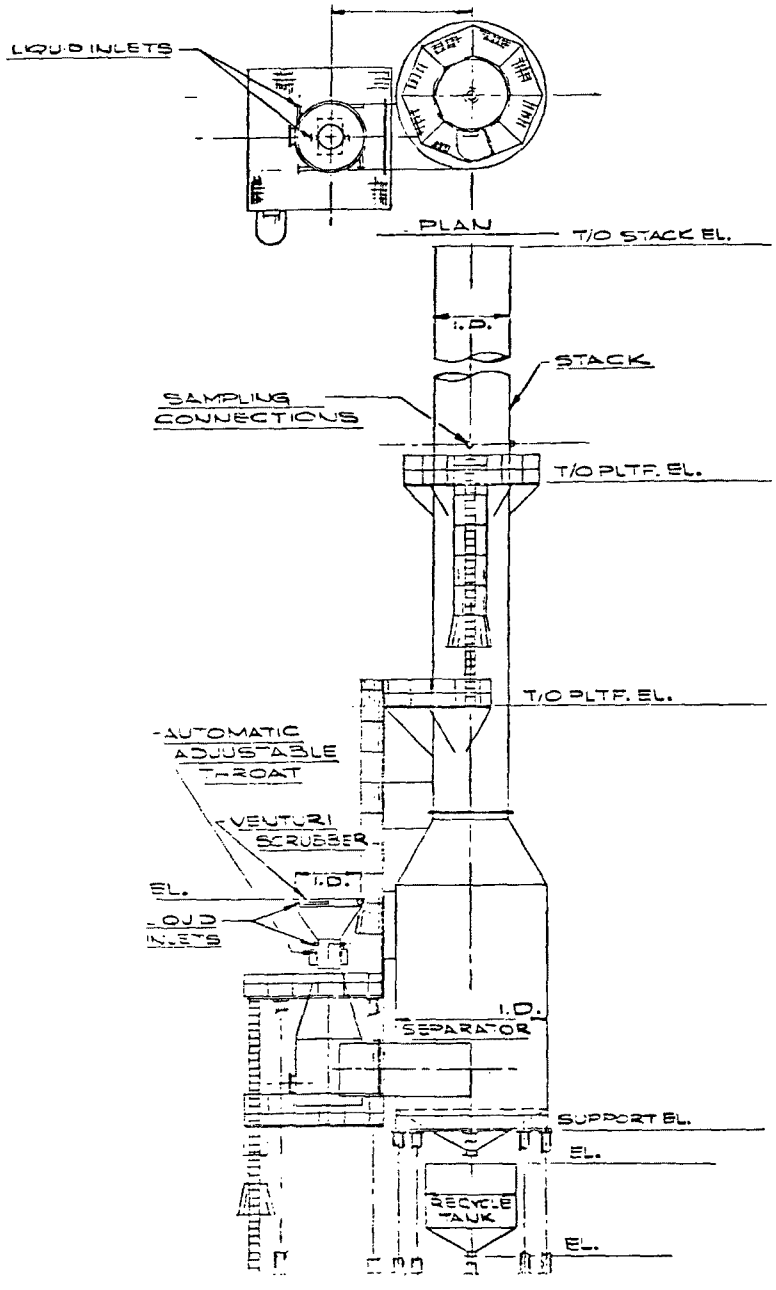

FIGURE 3. AIRPOL VENTURI SCRUBBER AND SEPARATOR GENERAL ARRANGEMENT

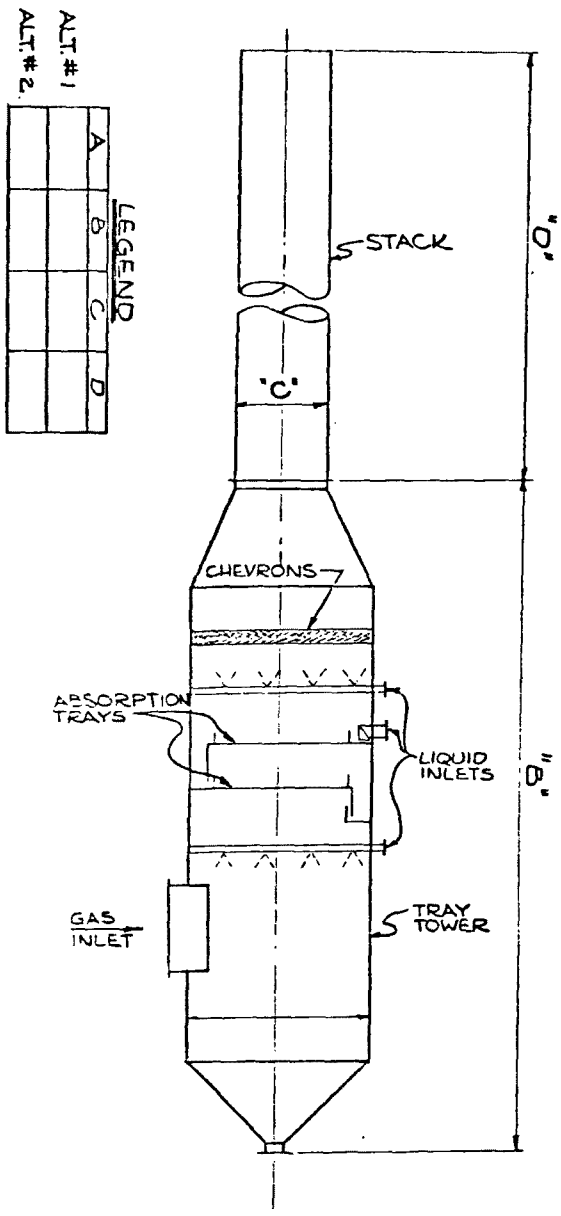

FIGURE 4. AIRPOL SO_2 ABSORPTION TOWER

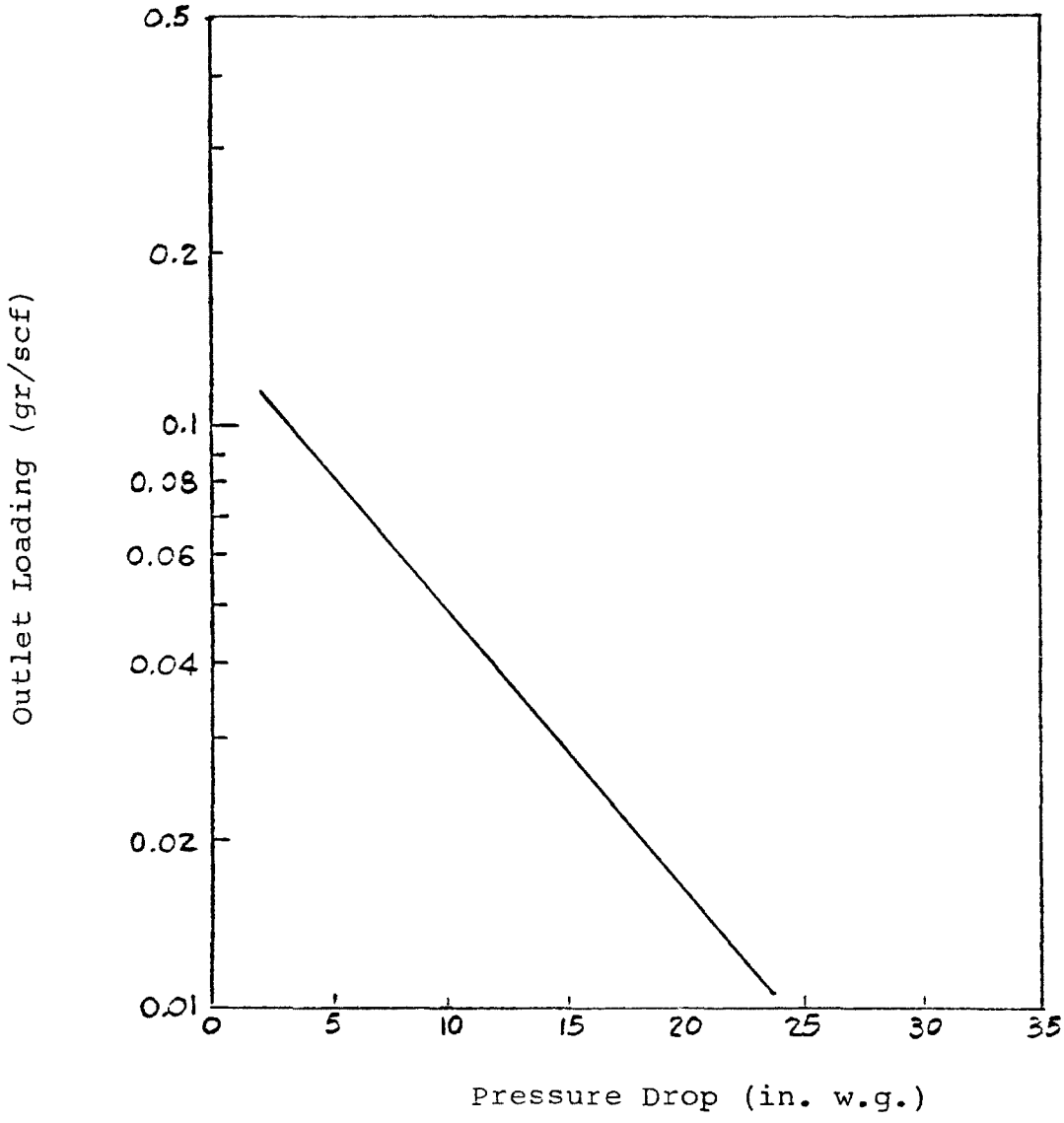

SCRUBBER PERFORMANCE ON COAL FIRED BOILERS

Fig. #5

Oil fired boilers, although having very light loadings, have extremely fine, submicron particles which would require a relatively high pressure drop for efficient removal. Scrubbers are not usually designed for particulate alone on oil fired boilers, but only when SO_2 collection is also required.

Studies done by the Mid-West Research Institute have shown that there is a substantial difference in the particulate size of the fly ash in the flue gas, depending upon which firing method is used. For example: The mass median diameter of the particles for these four methods is as follows:

Method of Firing	Median Particle Diameter (microns)
Pulverized	20
Spreader Stoker	48
Chain Grate Stoker	75
Underfeed Stoker	16
Oil	2

Since the particle size determines the pressure drop required, the method of coal firing must be taken into consideration by the design engineer.

Our experience has shown that the rate of excess air to the boiler is an important factor in the particle size formation. When the excess air rate starts to exceed 40%, we have noticed that efficiency of fly ash collection begins to decrease.

Venturi Scrubber Design

Since boilers operate at various loads, gas volume to the scrubber will vary as much as 30 to 100% of capacity. At the reduced gas volume, the pressure drop will tend to decrease because of lower velocity in the Venturi throat, resulting in lower efficiency.

It is necessary to compensate for this condition by restricting the throat area, maintaining the design throat velocity which in turn will maintain the efficiency. This is done by means of an adjustable venturi throat which may consist of either side dampers, movable plug type cone, or flooded disc. For automatic adjustable throat operation, controls can be installed to maintain constant pressure drop or constant furnace draft. Today, most Venturi Scrubber manufacturers inject water at the top of the Venturi, maintaining a falling film of water down the convergent section to prevent any dust build-up at the junction line of dry gas and water. This prevents the formation of wet/dry line deposits. In addition, our company also directs jets of water directly into the throat to insure good water coverage at the throat.

After the gas is scrubbed in the Venturi, the liquid must be separated. Separators most commonly used today are either centrifugal or impingement type.

With the centrifugal separator, gas enters tangentially and spirals upward through a cylindrical tank throwing the water against the walls by centrifugal force which then drains down by gravity. However, as the gas volume gets large; and, consequently, the diameter of the separator gets very large, the centrifugal force decreases inversely proportionately to the diameter, decreasing the efficiency of droplet separation. It then becomes necessary to use an impingement type separator, such as a chevron mist eliminator. Our company uses a diameter of about 14 ft. as the border between a cyclonic and an impingement type separator. With chevron mist eliminators, it is necessary to have spray headers for an intermittent wash.

Materials of Construction

For boilers burning 100% bark or wood, carbon steel is a satisfactory material of construction. However, most boilers that burn primarily wood also burn one of the fossil fuels in combination, or at least have it on stand-by. Therefore, practically all scrubbers today are designed for corrosion resistance. Type 316L stainless steel is the preferred material of construction. When sulfur bearing fuels are burned and scrubbing is done with water which is recirculated, the water will quickly build up to a saturated soltuion of sulfurous acid, with a pH down to about 2. This is low enough to attack the 316L stainless steel so that the scrubbing water must be raised to a pH of at least 4 by means of a caustic liquor.

An alternate material for corrosion resistance is carbon steel lined with polyester fiberglass. While this is satisfactory for ductwork and stacks, it should not be used in the high abrasion areas of the scrubber, such as the Venturi, or the tangential inlet of the separator. Experience has shown that these coatings do not stand up over the long run in these areas. Also, if organic coatings are used, provision must be made against high temperature attack in case of loss of water. One of the advantages of stainless steel is that temperature is not a factor.

Occasionally, there may be a high chloride content of the scrubbing medium which ultimately would attack the 316L stainless steel. In such cases, the stainless steel with a higher molybdenum content, such as 317L stainless steel has been used. Alternately, polyester fiberglass may also be used if proper temperature controls are installed.

Outlook for Industrial Boilers

Present regulations of the DOE require that new industrial boilers of greater than 100 MM BTU must use coal rather than oil or gas, unless this proves to be impractical. The DOE also has the power to require existing boilers over 100 MM BTU to switch from oil or gas to coal.

It is fortunate that the United States has an abundance of coal but, ironically, this is the dirtiest of the fuels. This means that air pollution equipment manufacturers should be kept busy over the next several years.

Market projections by McIlvaine show the projected sales of various air pollution devices over the next several years.

See Figs. 6, 7

Acknowledgments

1. "Technology Assessment Report for Industrial Boiler Applications: Particulate Control"
Industrial Environmental Research Lab.
U. S. Environmental Protection Agency
Research Triangle Park, NC 27711

2. "Air Pollution Control Market for Industrial Boilers"
The McIlvaine Co.
2970 Maria Ave.
Northbrook, Ill. 60062

3. "Controlling Bark Boiler Fuel Gas Emissions"
Louis A. Mason
Neptune AirPol Inc.
Sub. of Wheelabrator-Frye Inc.
Englewood, NJ 07631

GROWTH OF INDUSTRIAL BOILER AIR POLLUTION CONTROL EQUIPMENT SEGMENTS

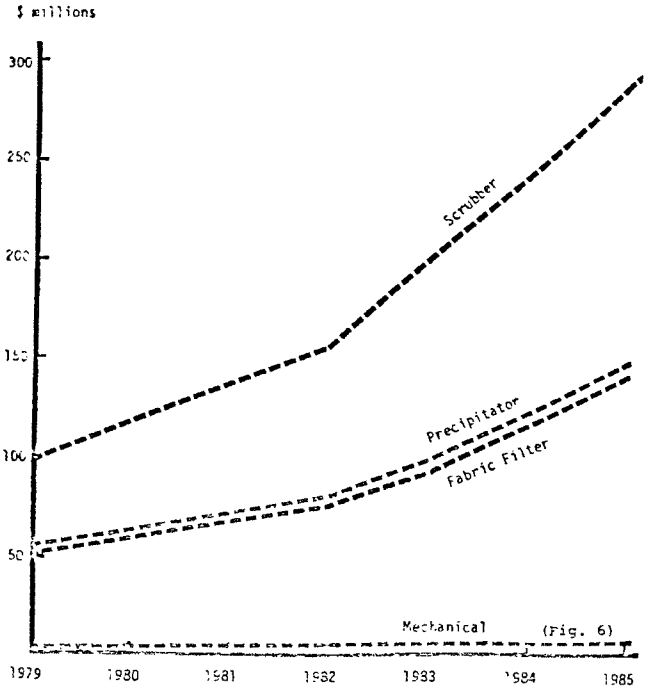

(Fig. 6)

EB-57

GROWTH OF TOTAL INDUSTRIAL BOILER POLLUTION CONTROL EQUIPMENT

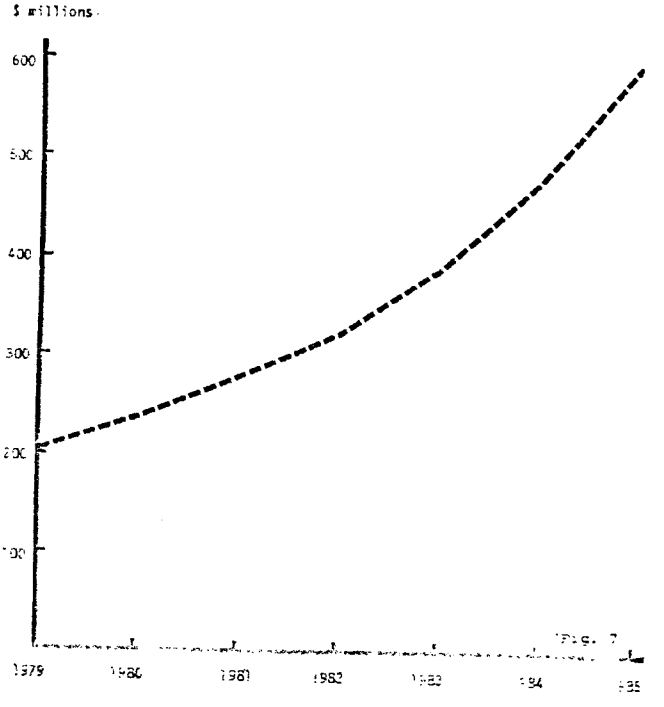

(Fig. 7

EB-58

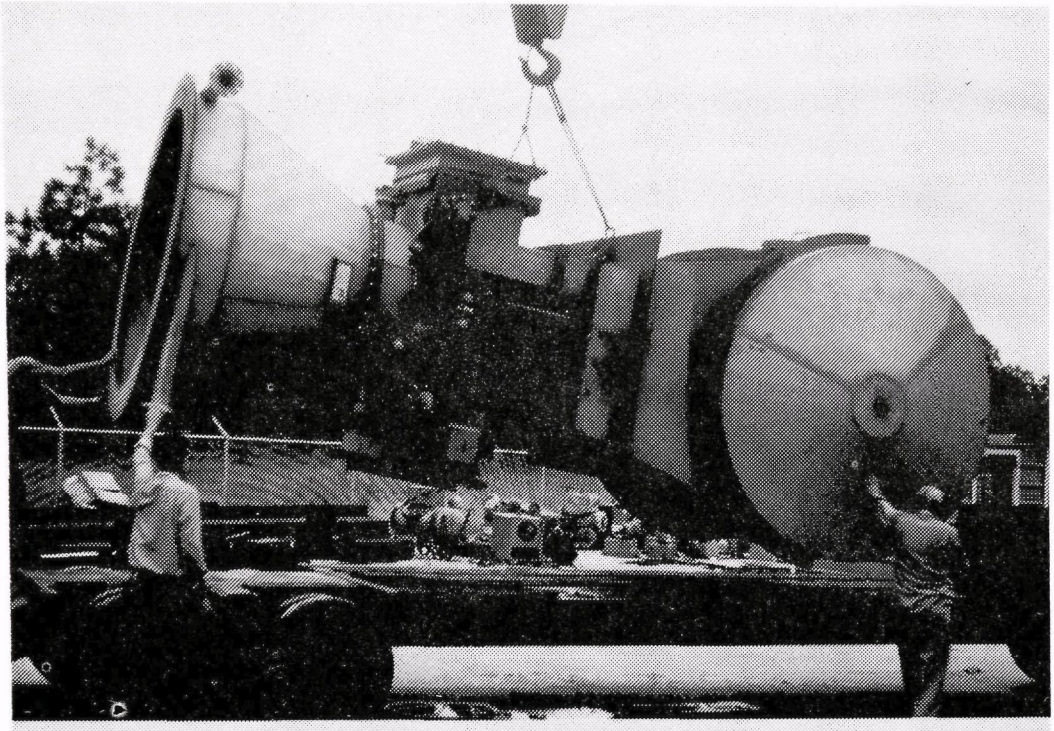

Great Northern Paper - Power Boiler Adjustable Throat Venturi

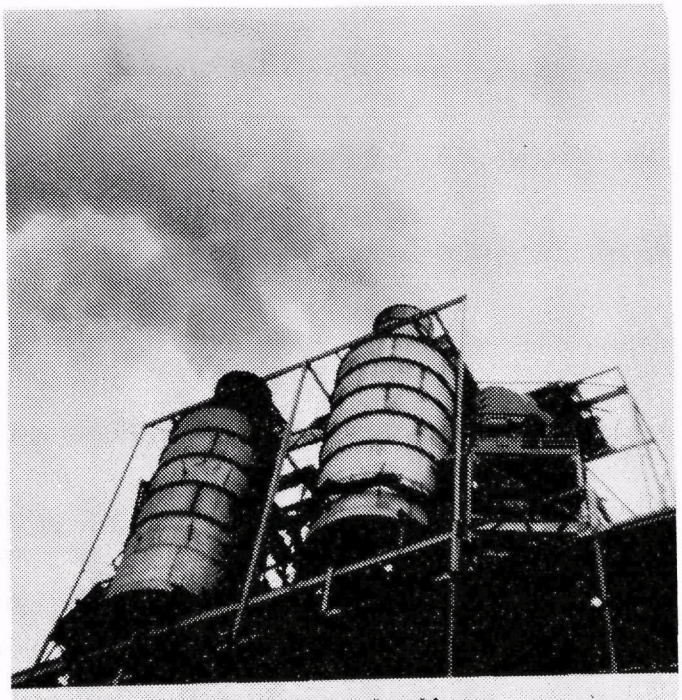

Power Boiler Scrubber
GREAT SOUTHERN PAPER

APPLICATION OF HIGH ENERGY VENTURI SCRUBBERS TO SEWAGE INCINERATION

By: Francis X. Reardon
Metcalf & Eddy, Inc.
Boston, Massachusetts

ABSTRACT

Wet scrubbers were installed on the flash drying sludge incinerator furnaces at the Allegheny County Sanitary Authority plant as part of a program to upgrade the furnaces, thereby removing mechanical dust collectors which were not capable of complying with the emission code under formulation in 1969 by the Allegheny County Health Department.

Features of the engineering application of the flooded disc scrubber to the furnaces, the anticipated performance of the scrubbing system, the actual test results and operation of the units which continue to perform successfully today are explained and discussed. It is our purpose to adhere as closely as possible to the engineering aspects of the intended and continuing furnace rehabilitation program.

INTRODUCTION

The Allegheny County Sanitary Authority has been engaged in a program of incinerator improvements for many years. In 1969, incinerator modifications included a major program in which pulverized coal facilities and all ancillary equipment for coal-firing in the incinerator furnaces were demolished and removed. Natural gas burners were installed to fulfill the auxiliary fuel requirements for sludge burning and have resulted in greatly improved environmental and operational conditions within the plant. Venturi scrubbers were installed. Modifications to vapor recycling ductwork and to the air and gas systems for each furnace to reduce and limit air infiltration and auxiliary fuel costs were completed. The furnaces continue to require a consistently high level of operator attention and maintenance.

Basic engineering problems requiring a solution prior to the scrubber selection are noted as follows:

1. The selection of the required capacity or flow rating of the scrubbers consistent with the expected excess air levels achievable in the flash drying furnaces. It was apparent that there were many potential sources of infiltration of ambient or furnace room air into the furnace systems. An intensive maintenance program was imminent because of forthcoming repairs and rehabilitation to the heat exchanger sections of the furnaces, new auxiliary fuel burners, vapor return ductwork, cage mill repairs, and dryer cyclones. The proposed new sludge conveyor system providing vacuum filter cake to sludge mixers would require modification to effect sealing against room air.

2. An assessment of venturi scrubbers operating at a medium pressure drop, say in the 15- to 25-inch range, to meet the proposed EPA New Source Performance Standards for sludge incinerators. A proposed emission of 0.031 gr. per dscf (grains per dry, standard cubic foot) eventually became 1.30 pounds of particulates per ton of dry sludge input. The Allegheny County Health Department, Rules and Regulations, Article XVII, Smoke and Air, was being discussed at hearings and was to be adopted while contracts for scrubbers and other equipment were out for bids.

3. A reliable estimate of the expected dust load from the flash drying furnace, considering the use of natural gas burners for auxiliary fuel in lieu of pulverized coal burners.

4. The physical and chemical characteristics of the anticipated fly ash.

5. The selection of an alloy steel for the scrubber which would withstand the corrosive and erosive attack of particulate-laden flue gases.

DESIGN CONSIDERATIONS

Factors which were to affect furnace operation and subsequently scrubber operation were the result of both furnace modifications and the installation of a new vacuum filter facility. It is proper and truthful to say that not all of the effects of the furnace modification and rehabilitation were or could have been foreseen in planning the scrubber installation.

At this point in time, the furnaces were to operate with filter cake, and during the scrubber emission testing the vacuum filters and the newly installed sludge conveyors were put into initial operation. Prior to this time, a liquid sludge had been pumped to the furnaces. The run-in period for the new sludge conveyors and the feed to mixers and cage mills required much attention before a steady sludge feed, necessary for the emission testing, was realized.

Prior to the writing of specifications for the scrubber system, it was noted that excess air levels of gases from the furnaces were on the order of 180 to 190 percent. These measurements

were made with exit gases at 600 deg F to 700 deg F during operation with mechanical collectors. Combustion Engineering Company heat balances are customarily based on 40 percent excess air for sludge burning in flash drying furnaces. Thus it is seen that the data available to the designers spanned a broad range of conditions.

It was decided that the scrubber exhaust gases at saturation could be approximately 200,000 pounds of wet gas per hour and that the excess air level resulting from excessive infiltration might reach 200 percent before system adjustments and furnace modifications could achieve a reduction. The maximum test run conducted on Furnace No. 4 indicated a gas flow of 189,200 pounds of gas per hour at 160 deg F or 49,456 acfm.

The specified scrubber duty required each unit to handle 85,000 acfm of gases leaving the furnace preheater at approximately 1,000 deg F. The dust loading entering the scrubber was specified as four (4) grains per scfm. The emission rate was specified not to exceed 0.05 pounds particulates per 1,000 pounds of flue gas. Testing was to be based on 60 to 100 percent of maximum rated furnace capacity.

The physical constraints involving the location of scrubbers, induced draft fans, breechings, and integration with a new sludge conveyor system, and the existing flash drying furnaces required a specific arrangement of venturi scrubber and separator vessels. Figures 1 and 2 are provided which give plan views and sectional elevations of the installed equipment in the incinerator building. Scrubbers were specified to have a flanged, vertical gas inlet to the venturi section, a cyclonic separator with a tangential inlet and a bottom, vertical outlet, a hopper bottom with a flanged outlet, water connections and structural support brackets. The flooded disc scrubber selected suited the structural and geometric requirements.

The scrubbers and the downstream breeching were constructed of Incoloy Alloy 825. The inlet duct from the air preheater hood of the furnace to the scrubber is constructed of annealed carbon steel plate conforming to ASTM Designation A-283-67. Expansion joints in the Incoloy breechings were constructed of Incoloy Alloy 825. All of the breechings from each scrubber were constructed as individual breechings from the fan to the stack.

Scrubber water is provided from the plant secondary treatment effluent discharge. The adjustable disc is perpendicular to the gas flow and forms an open annulus of varying size as it travels in the tapered throat section of the scrubber. Gases flowing through the opening have a high degree of disturbance and at the same time, water is introduced through the large diameter disc support pipe and is ejected across the face of the disc. The principle, as described by the manufacturer, is based on high velocity gas striking the disc face, shearing water particles at the edge of the disc, and transforming the water into a fine mist, which is thoroughly mixed with the gas. The specified pressure drop for the system was not to exceed 20 inches w.g. The recommended pressure drop for the scrubbers conforms to the specifications, that is, 20 inches w.g.

An ash slurry system consists of a slurry tank designed to receive a continuous ash slurry discharge from each pair of scrubbers. Fly ash pumps convey the slurry by force main to the plant ash pits.

SUMMARY OF TEST RESULTS

Data from the stack emission test report prepared by The Rust Engineering Company and issued in February 1973 is presented which indicates that all test runs resulted in values below the allowable emission rate of 0.05 pounds per 1,000 pounds of flue gas in accordance with the contract documents. Tests were made in the incinerator breechings downstream of the scrubbers and the induced draft fans, before the breechings leave the incinerator building to enter the stack. Four (4) test runs were made on unit No. 2 and three (3) runs were made on unit No. 4. Highlights of the test results are tabulated below:

Run	*Flue gas flow*		*Particulate emission*		*% excess*
No.	*ACFM*	*lb/hr*	*lb/hr*	*lb/1000 lb gas*	*air*
2SO-1A	43,733	158,200	6.53	.0413	157.23
2SO-2	47,121	169,200	3,18	.0188	157.23
2SO-3	34,885	133,600	1.00	.0075	174.72
2SO-4	43,362	157,500	6.08	.0386	174.72
4SO-1	44,027	158,500	2.85	.0180	165.64
4SO-2	50,643	175,200	6.66	.0380	203.11
4SO-3	49,456	189,200	8.32	.0440	136.42

The first digit of the Run No. designates the incinerator unit, SO designates "scrubber outlet" and the last digit designates the sequence of the run on that incinerator. Test 2SO-1 was not completed, so its successive test was designated 2SO-1A. During all of these runs, a pressure drop of 20 inches was maintained at the scrubber.

OPERATION

The mechanical functioning and the response of the flooded disc scrubbers to changing furnace conditions resulting from sludge feed variations, sludge moisture variations, and furnace off-

gases for any reason was immediately perceived to be excellent. The rugged construction of the disc actuator, the hydraulic system and the basic venturi section has assured reliable service. It is apparent that the equipment has been designed to serve well in many applications demanding durability such as foundry and blast furnace service.

A review of the history of the scrubber systems starting with scrubber No. 3 in August 1971, No. 1 in November 1971, No. 2 in February 1972, and No. 4 in May 1972 revealed a severe wearing or "thinning out" in the tapered side wall, just below each disc. Each worn area spanned the center line of the long arc of the inlet duct from the furnace to the scrubber. The area of "thinning out" or reduction in metal thickness was estimated to be approximately 24 inches long by 6 to 8 inches high. None of the remainder of the scrubber shell or the disc itself exhibited any wear. One scrubber had exhibited wear in 352 hours of operation. Others had required patching by welding carbon steel plate to the outside of the shell in 1,500 to 2,000 hours.

A laboratory analysis of the fly ash deposited in the disc area revealed that the silica content of the ash was over 55 percent on a dry basis. Subsequently, the contractor and the scrubber manufacturer proposed and installed a refractory-lined throat area. A 3/16-inch thick, carbon steel plate section was used to replace the Incoloy 825 material in the sloped throat of the scrubber. Applied to the steel plate are 4 inches of fiberfrax insulation, a bed of Pennwalt HB mortar and 2 inches of Norton Company CN163 silicon carbide shapes. This type of lining has been applied in blast furnace applications. From present reports, it is still resisting wear well and is expected to have long life. Subsequent to the rapid erosion of scrubber throats experienced at the Alcosan plant, our specifications have required that venturi throat sections have an allowance for refractory linings. It has not been necessary to line any of the scrubbers used on sludge furnaces for municipal sewage treatment that we have designed since Alcosan.

From an analysis of the volumes of flue gas flow through the scrubbers during the test runs conducted during January 1973, particularly noting the maximum scrubber outlet gas flow of 189,200 pounds per hour during run 4SO-3, the scrubbers have performed at the intended design point. During an analysis of furnace operations in 1974 and 1975, heat balances were prepared utilizing the Combustion Engineering Company computer program. Data from these illustrate the volume, temperature and moisture of the furnace off gases to the scrubber.

YR 1974	Feed	21,000 lbs	
	Dry solids	4,670 lbs	
	Furnace - off gas temperature, deg F		800
	Furnace - off gas volume, cfm		75,921
	Moisture in off gas, gr/lb d.a.		1,409
	Excess air, percent		172
	Gross heat input, Btuh		53,647,485

YR 1975	Feed	20,000 lbs	
	Dry solids	4,000 lbs	
	Furnace - off gas temperature, deg F		760
	Furnace - off gas volume, cfm		76,989
	Moisture in off gas, gr/lb d.a.		1,255
	Excess air, percent		200
	Gross heat input, Btuh		52,024,090
	Feed	20,000 lbs	
	Dry solids	4,000 lbs	
	Furnace - off gas temperature, deg F		760
	Furnace - off gas volume, cfm		69,985
	Moisture in off-gas, gr/lb d.a.		1,394
	Excess air, percent		180
	Gross heat input, Btuh		49,408,301
	Feed	20,000 lbs	
	Dry solids	4,000 lbs	
	Furnace - off gas temperature, deg F		760
	Furnace - off gas volume, cfm		66,741
	Moisture in off gas, gr/lb d.a.		1,471
	Excess air, percent		170
	Gross heat input, Btuh		48,196,630

Noting the specified scrubber duty requiring it to handle 85,000 acfm at approximately 1,000 degrees F. and comparing the furnace off-gas volumes displayed in the heat balance calculations, one observes that the specified volume exceeds the computed volumes, even at such high excess air levels. It is also significant that the dry solids loading to the furnaces during the emission testing exceeded the feed values utilized in the computer program examples.

SUMMARY AND CONCLUSIONS

The discussion of the suitability of the flooded-disc scrubber for the intended service and its performance at Alcosan cannot terminate without a well considered attempt to describe, in simple terms, the sensitive furnace system in which the unit functions. As we have noted, efforts to reduce infiltration air and to conserve auxiliary fuel have continued since the onset of the furnace modifications and the construction of the sludge preparation and filter facilities.

Improvements have been ongoing in the roof mounted sludge burners and in the gas burners. Gas burner flames have been shaped to avoid impingement and the resultant slagging on the walls and roof arches of the furnaces. A furnace cooling air ductwork system was devised utilizing sludge

combustion air which flows through the furnace preheater to cool specific areas of the roof arches and walls. A parallel benefit of restoring the preheater air flow circuit would be to depress the gas outlet temperature to the scrubber, thereby improving furnace efficiency and reducing the input of auxiliary fuel.

The reduction of slagging had been a plant priority for many years under operation with the mechanical collectors and the slag burden continued as the rehabilitated furnaces continued to operate utilizing wet scrubbers. The slag problem had caused the destruction of furnace target walls at times and had become so severe that, even if target walls were not burdened sufficiently to cause a furnace shutdown, other slag-burdened areas would necessitate a halt to furnace operation.

The need to air cool specific areas of the furnace to prevent slagging was in direct contradiction to the requirement to greatly reduce excess air to an amount only necessary for completing combustion of the sludge solids.

This discussion, noted in the opening remarks as intending to limit itself to the engineering application and performance of the flooded disc scrubber for this plant, might expand into many undertakings which were of major concern to the plant modifications and operation. Nevertheless, we trust that the system in which the scrubber was applied is more readily understood. The writer gained a sincere respect for the Authority and it's people due to the willingness they applied to the solution of many difficult operational problems.

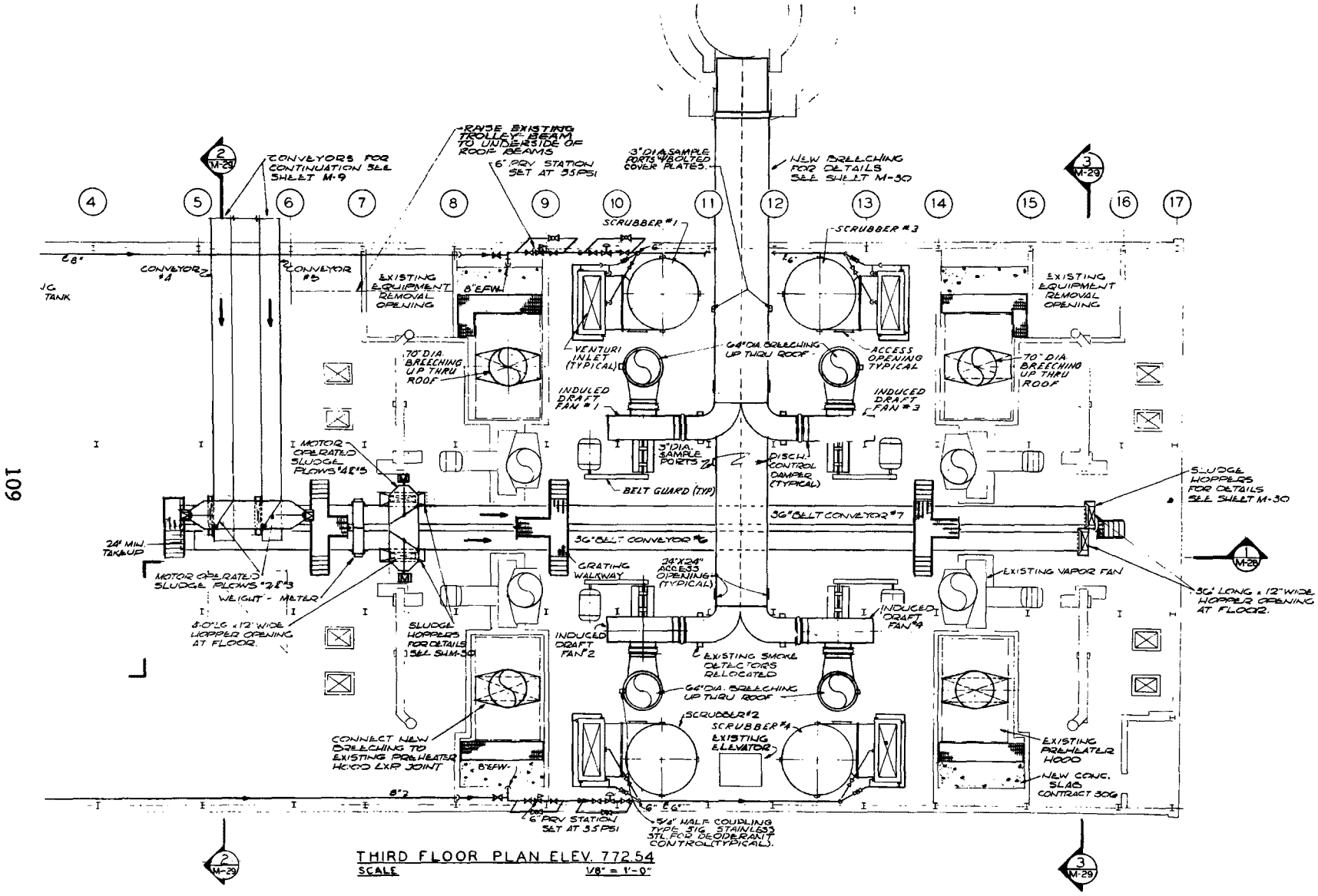

FIG. 1 THIRD FLOOR PLAN

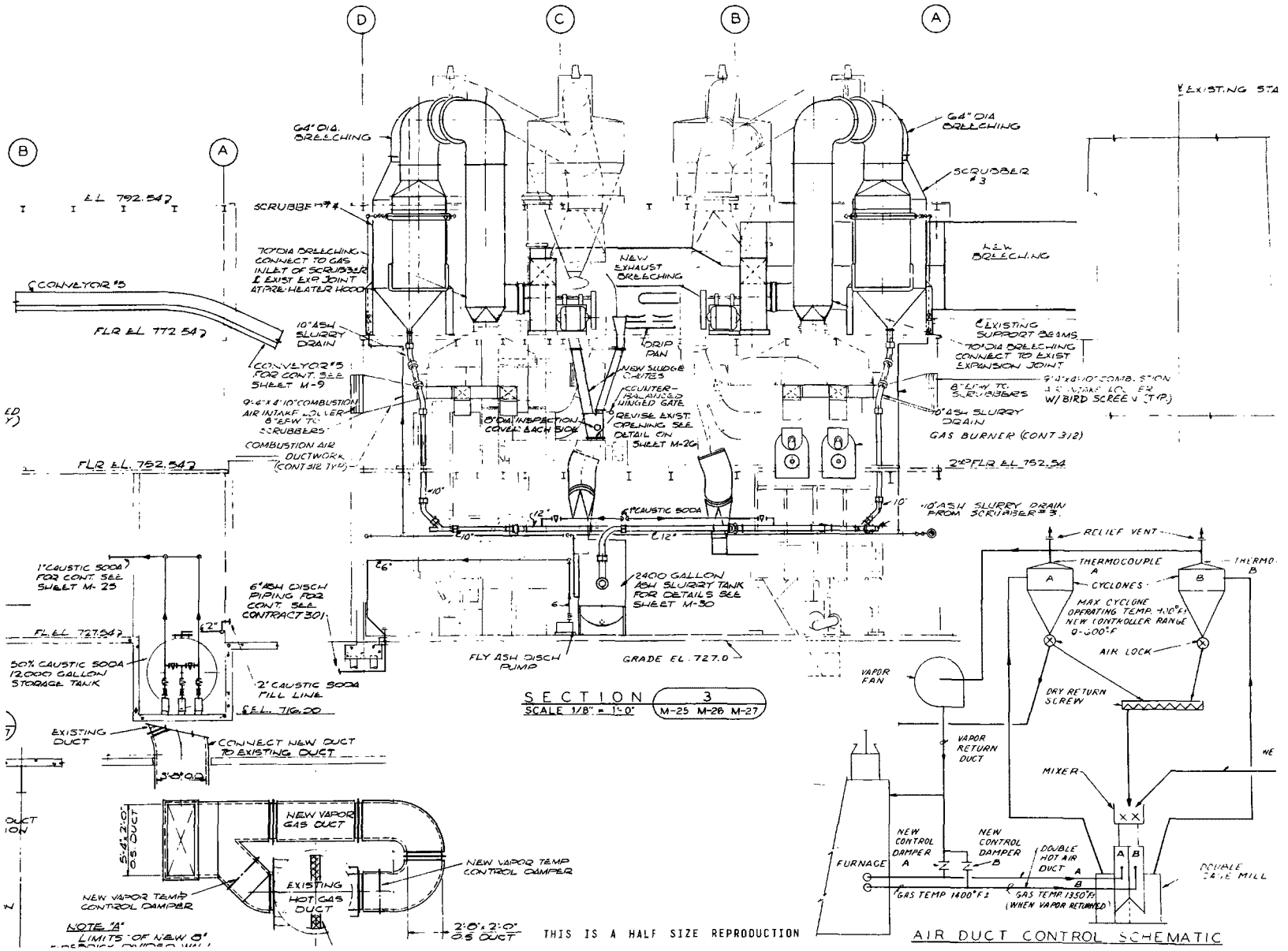

FIG. 2 SECTION

AN INCINERATOR SCRUBBER THAT WORKS: A CASE STUDY

By: Charles Menoher, Product Manager
Zurn Industries, Inc.
Air Systems Div.
245 North Center Street
Birmingham, AL 35204

ABSTRACT

A midwestern chemical company has recently started up a medium energy scrubber on an industrial trash burning incinerator. Compliance testing verified an outlet particulate loading of less than the guaranteed 0.15 #/1,000 pounds of dry gas. This level of performance was achieved with 30" W.C. of venturi pressure drop, with final subcooling to remove volatiles and condensibles. This system was purchased because of the horsepower savings when compared to the "convential" scrubbing approach that requires 60" W.C. or more of pressure drop. The savings will pay for the scrubber system in four years.

"TEXT"

In January of 1980, Zurn Air Systems was contacted by a midwest chemical company to provide a quotation for a high energy scrubber to clean the off-gases from one of their several in-plant incinerators. The subject incinerator had an existing low energy scrubber on it, following the customer's quenching chamber. In this chamber, the 1,600°F off-gas temperature is quenched to adiabatic saturation at 170°F.

The type of trash being incinerated included all of the normal range of refuse one would expect to find being fed into an incinerator of this service but did not, however, include organics, solvents, or heavy metals. The Bartlett Snow incinerator operation generates an average particulate loading of approximately 1.0 Gr/SCFD, with periodic excursions up to 2.3 Gr/SCFD, for which the dynamic type scrubber was able to achieve an outlet average loading of only 0.3 Gr/SCFD. The Bartlett Snow unit, Model 12, uses a batch feed, and operates 24 hours per day, seven days a week. The incinerator is rated for an input of 3,000 pounds per hour.

Since the customer's other incinerator scrubber systems were of a conventional design using a high pressure drop venturi and cyclonic separator, the request for quotation called for a similar concept. After all, those scrubbers were keeping their incinerators in compliance. Thus, their expectation was that a venturi pressure drop of 60" W.C. or more would also be required for this incinerator. With the exception of Zurn, the other bidders did not disagree with the specification.

Zurn took the position that with nearly three-quarters of the dust specified as being less than 0.5 microns by weight, high pressure drop alone was not going to do the job in getting down to the state requirement

of 0.15 pounds/1,000 pounds dry gas (nearly equal to 0.08 Gr/SCFD). The creation of this much sub-micron dust is caused by the intermittent burning of pharmaceutical powders in the incinerator.

We felt the solution to the problem lay in using a medium energy venturi followed by a direct contact gas cooling tower. The rationale was that at 30" W.C. of venturi drop, we would do 80 to 85% efficiency, and that the remaining ten to 15% could be predictably removed only by condensation scrubbing. A secondary, but very important, benefit was the savings in fan horsepower.

Credit for the concept of condensation scrubbing belongs, not to Zurn, but to Dr. Seymour Calvert of Air Pollution Technology, from whose articles in Chemical Engineering Magazine the concept was taken. Dr. Calvert gives the phenomenum the esoteric name of diffusiophoresis; more frequently referred to as condensation or mass transfer scrubbing. Associated with mass transfer scrubbing is "particle growth", which is caused by the condensation of water vapor around a particle, thus enlarging the particle mass, and making it more susceptible to collection by impaction in the packed bed.

Diffusiophoresis occurs during condensation of water vapor into the cooling water mass. This condensation exerts a force on the particles that causes them also to deposit on the cooling water surface. The percentage of particles removed in this manner is approximately equal to the percentage of the gas stream condensed out.

The easiest way to visualize this phenomenum is to imagine that the gas stream is pure steam, or water vapor. Obviously, if one condensed the entire gas stream to water, there would be no air pollution left, because there would be no gas stream left . . . . . .

Now some specifics. The gas volume from the quencher to the Zurn venturi was designed for 23,000 ACFM at 170°F and -12" W.C. static pressure. After subcooling, the volume to the I.D. fan was 13,200 ACFM at 100°F and -47" W.C. static pressure.

The cooling water supply rate of 650 GPM at 80°F condensed nearly 43 GPM of water vapor from the gas stream, which amounted to 7,500 SCFM. This reduced the gas volume by more than 40%, and by all accounts, lowered the particulate loading from the venturi by about 60%. Of this 60%, it is assumed that 40% was due directly to diffusiophoretic or mass transfer scrubbing, with the remaining 20% being removed by impaction after particle growth. As stated, this can only be assumed since there is no way it can be readily verified.

The 150 GPM scrubbing water used at the venturi is taken from the customer's quencher sump, and thus is already contaminated. Given the configuration of the scrubber/cooling tower, there is no suitable intermediate location between the venturi and packed bed to take samples.

For the astute among you who might observe that an approximation could be made by measuring the percent solids in both the supply and return lines of both the scrubbing water and the cooling water, this is perhaps true. However, it would pre-suppose that the cyclonic separator portion of the vessel is nearly 100% efficient in removing the scrubbing water entrainment before the gas stream gets to the cooling section. Since no reliable separator is that efficient, lets look at the reality of how difficult it would be to verify how effective the cooling section is as a particulate removing device.

Based on the performance requirement for the scrubbing system, the allowable amount of dust to the stack is approximately 0.12 pounds/minute. If only one GPM of the 150 GPM scrubbing water gets to the cooling section and that gallon per minute contains only one-half percent solids, this converts to a loading of 0.04 pounds/minute of particulate. This represents fully one-third of the allowable dust out! It is therefore reasonable to argue that the cooling section and subsequent mesh pad demister perform a necessary service in lowering the entrainment to the final stack. Even so, it is a certainty that even without entrainment to worry about, it would take a significantly higher venturi pressure drop to meet the guarantee if no subcooling was used.

When measured last week according to the procedures in the EPA Title 40, Chapter 1, Subchapter C, Part 60, the outlet dust loading was 0.12 pounds/1,000 pounds dry gas (against the requirement of 0.15 pounds/1,000 pounds) and the stack opacity was 10%.

Since we were hopeful that even our specified 30" W.C. of venturi pressure drop was going to be more than adequate because of the subcooling that followed, the throat was intentionally sized large enough to permit a pressure drop as low as 20" W.C. Since the test results were well under the code, there is no reason why the customer should not back off from the 30" pressure drop design number and operate at a lower horsepower.

As alluded to previously, the much lower power consumption of the Zurn system was extremely important to the customer. They are very happy with the horsepower savings the system is providing compared to what they had originally expected.

If, for the sake of discussion, they had bought a scrubbing system that called for a 60" W.C. drop on the venturi and with no subcooling, the I.D. fan would had to have been sized for approximately 28,000 ACFM at 75" W.C. static pressure. Assuming a brake horsepower efficiency of 72%, the operating horsepower would be approximately 472. The fan actually used on this installation operated at a brake horsepower of about 145. The savings on the fan power, then, is 327 horsepower. From this must be subtracted the horsepower of the cooling water supply pump. Assuming a 55% efficient pump rated at 650 GPM and 40 PSIG TDH, the operating horsepower would be 27. The total net savings in horsepower, therefore, of the installed system versus the conventional approach, is approximately 300 HP. At $250/HP/Year, the annual savings at that rate is $75,000. The power savings will pay for entire installation in less than four years.

The materials of construction used in the system are what one would expect for this application, given the concern for chlorides. The duct work from the quencher to the venturi if FRP; the venturi is rubberlined carbon steel with a Hastelloy C adjustable throat; the cooling tower, duct work to the I.D. fan, and final stack are FRP, and the I.D. fan has a rubberlined carbon steel housing and Hastelloy G. wheel.

The hook-up to the customer's existing quench chamber was made by removing the dynamic scrubber and installing a "plenum box" in its place. The duct work was then run from the top of the box over to the venturi inlet.

The venturi design is conventional. Given several types of venturi to offer, we chose the one with open pipe water feed. Since the scrubbing water is the re-used quenching water from the customer's existing sump, it was felt that the use of spray nozzles ran the risk of pluggage. At the very least, spray nozzles would require periodic replacement simply due to erosion. With open pipes at low pressure, it is hoped the venturi selected will give the customer many years of maintenance free service.

The separator/cooling tower is also of a conventional design. The lower cyclonic separator section is isolated from the cooling section with a ring and cone arrangement. This, of course, is to keep the dirtier, lower pH scrubbing water from mixing with the cooling water.

The necessary cooling is achieved throug a 9' deep bed of polypropylene packing supported on an FRP grid. The cooling water is applied to the bed through a PVC water distributor, using no nozzles, at low pressure. Here again, the intent was to provide the customer with a design that would require no spare parts, and thus minimize maintenance.

Finally, the cleaned and cooled gas stream passes through a polypropylene mesh pad to strip out all entrainment before going to the I.D fan and stack.

The pH of the scrubbing water is controlled by a continuous small addition of caustic from the customer's effuent stream from one of these processes. He monitors the pH continuously, and sets the caustic flow rate to keep the pH of the scrubbing water above four.

Other than some minor problems with instrument calibration, the start-up went smoothly. The system has been on line for about three weeks now, with no indication of any operational problems. The customer is pleased with the system.

In an era of high energy costs, the scrubber industry can no longer continue to advocate the same scrubbing techniques that were popular, or at least acceptable, less than ten years ago. Frankly, there is little in the Zurn scrubber system on this job that is terribly innovative. We like to feel that the system is simply the solid application of proven scrubber techniques.

Endnotes

1. Chemical Engineering; August 29, 1977 and October 24, 1977.

Author Background

Charles Menoher is Product Manager of Wet Scrubber Products at Zurn Air Systems, having been an Application Engineer in wet scrubbers at American Air Filter, Koch Engineering, Sheldons Engineering (Canad) and Chemico. He has authored articles for 33 Metal Producing, and Iron and Steel Engineer.

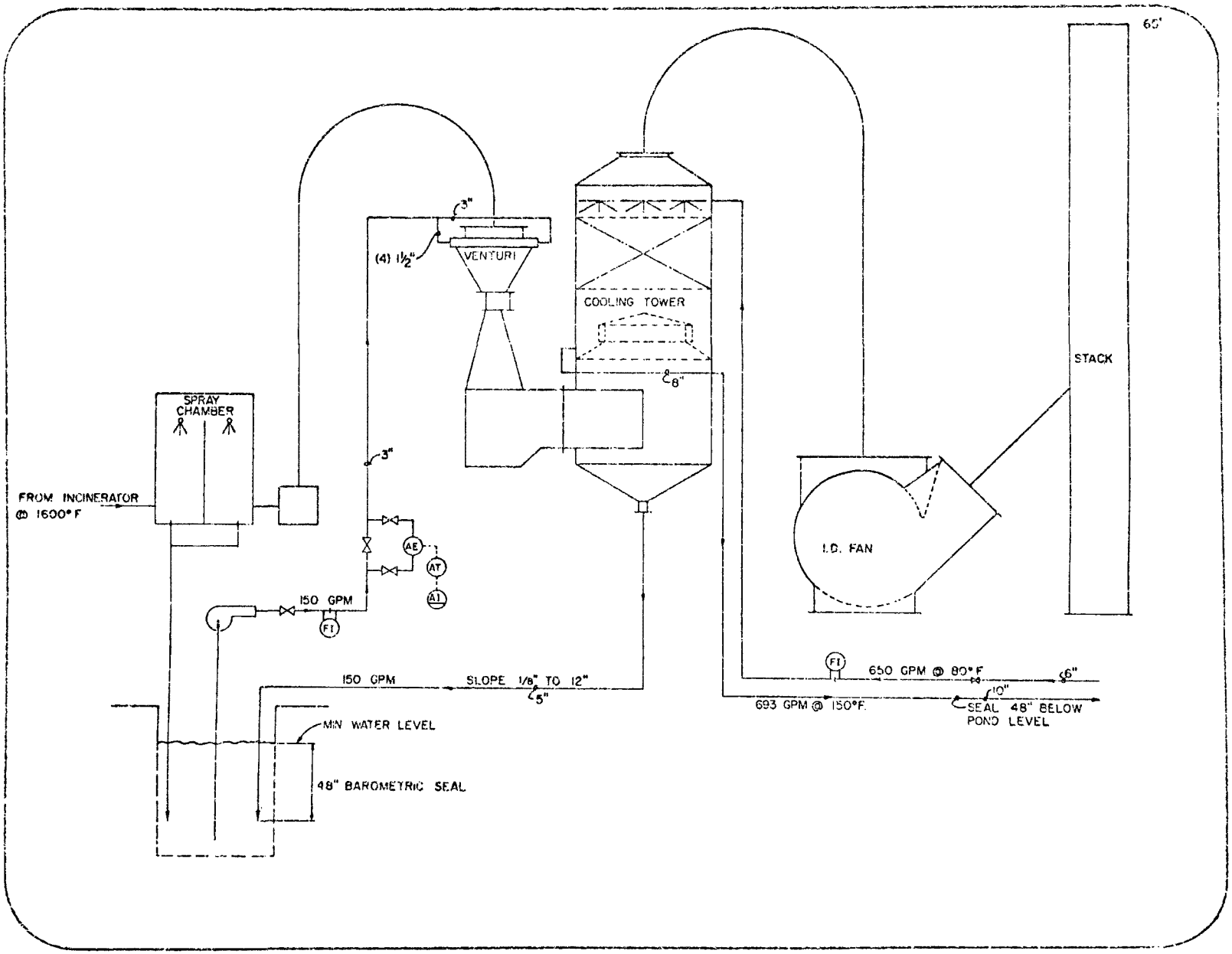
65'
3"
(4) 1½"
VENTURI
COOLING TOWER
STACK
8"
SPRAY CHAMBER
3"
FROM INCINERATOR @ 1600°F
AE
AT
AI
150 GPM
FI
I.D. FAN
FI
650 GPM @ 80°F
6"
150 GPM
SLOPE 1/8" TO 12"
5"
10"
693 GPM @ 150°F
SEAL 48" BELOW POND LEVEL
MIN WATER LEVEL
48" BAROMETRIC SEAL

RACETRACK VENTURI

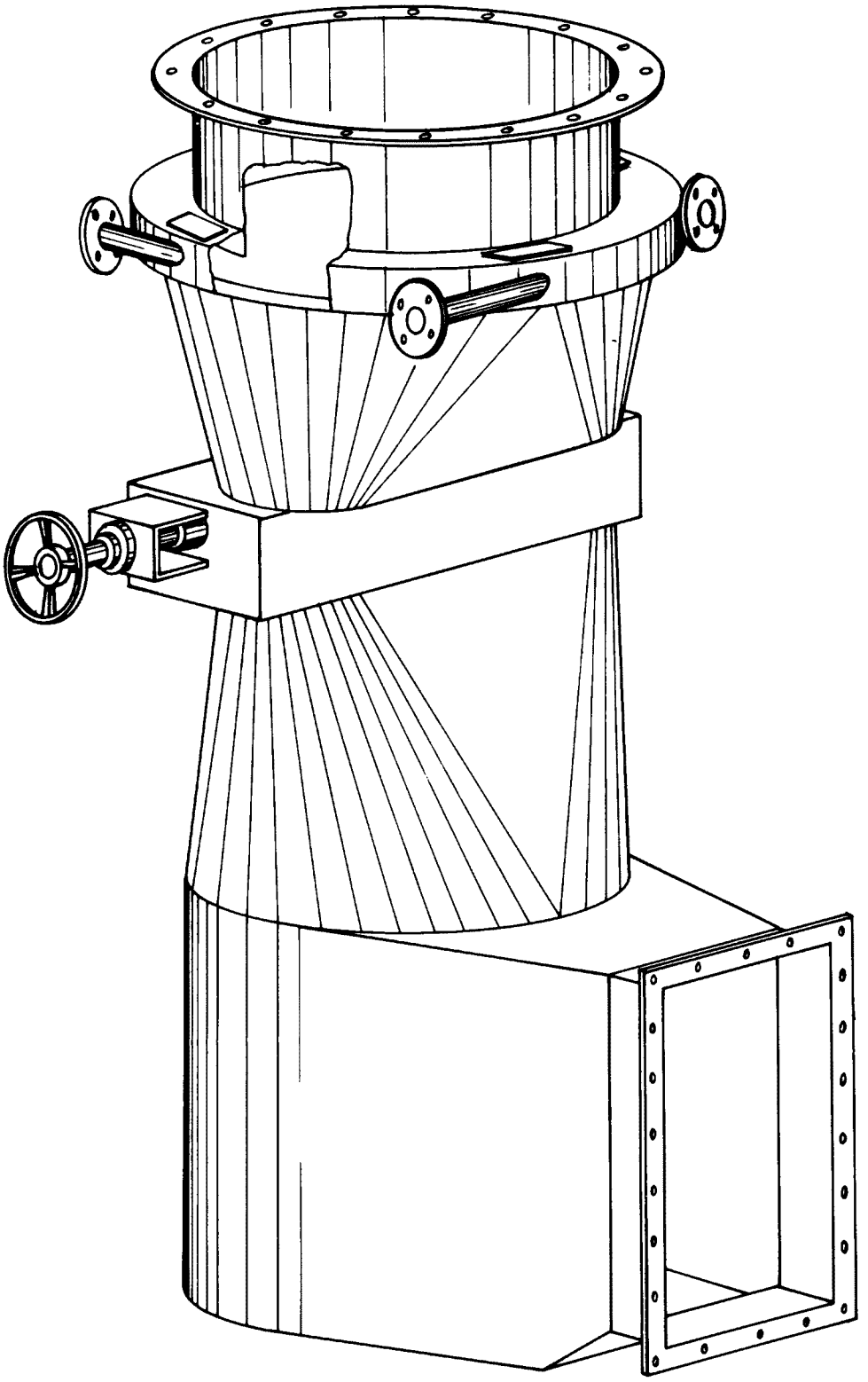

SEPARATOR - COOLING TOWER

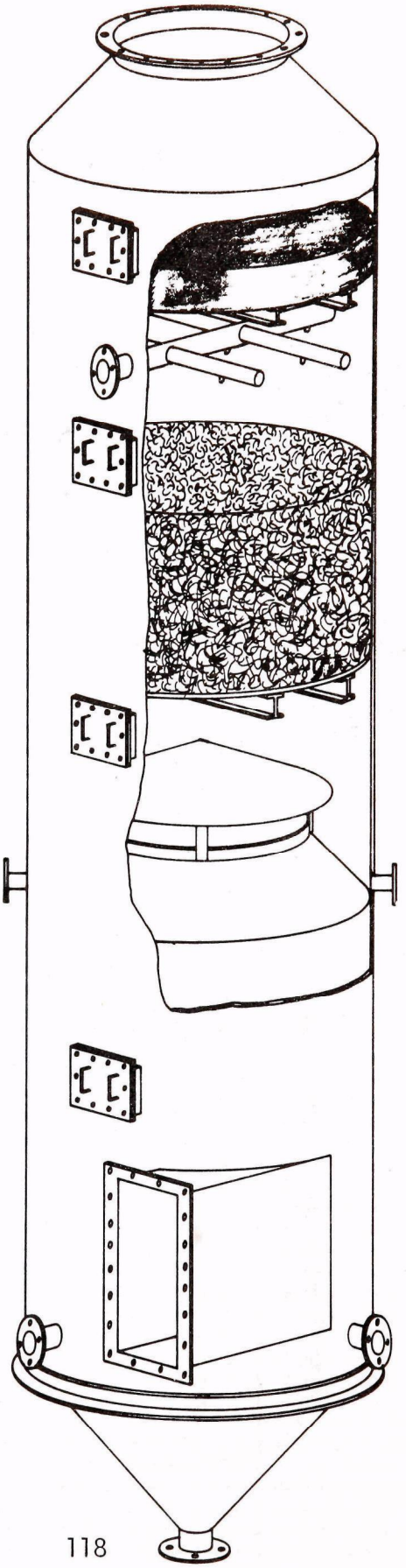

EVALUATION OF ENTRAINED LIQUOR CONTRIBUTION TO TOTAL MASS EMISSIONS DOWNSTREAM OF A WET SCRUBBER

By: W. David Balfour, Larry O. Edwards, Hugh J. Williamson
Radian Corporation
8501 Mo-Pac Boulevard
Austin, Texas 78766

ABSTRACT

As flue gas passes through a wet scrubber, both SO_2 and particulate matter can be removed. The scrubber can, however, contribute mass through entrainment of scrubber liquor high in suspended and/or dissolved solids. The contribution of mass by a variety of scrubbing systems has been calculated using the concept of a chemical element balance, as:

$$\phi_j^{out} = P\ \phi_j^{in} + C_j\ V$$

where:

ϕ_j^{out} ≡ mass flow rate of species j out of scrubber

P ≡ penetration fraction of fly ash through scrubber

ϕ_j^{in} ≡ mass flow rate of species j into scrubber

C_j ≡ concentration of species j in scrubber liquor

V ≡ volume rate of entrained scrubber liquor

Particulate compositions into and out of the scrubber were obtained from chemical analyses (ion chromatography and inductively coupled argon plasma emission spectroscopy) of total particulate catches. Scrubber liquor composition was obtained by similar analyses of liquor samples collected during the particulate sampling. A weighted regression analysis was performed on the set of equations (for each chemical species).

Results for a variety of combustion and scrubber processes show that entrained liquor can contribute from 1 to 80 percent of the total mass emissions from the wet scrubber.

The Clean Air Act and subsequent New Source Performance Standards (NSPS) require that sulfur dioxide (SO_2) emissions be controlled. The flue gas desulfurization (FGD) technology most commonly used in controlling SO_2 emission is the wet scrubber. A variety of reagents can be used as a scrubbing liquor including soda ash, caustic, lime or limestone. Similarly, a variety of contactors are used to provide the necessary liquor surface area required for the gas-to-liquid transfer. The dissolved solids content of the scrubber liquor can be quite high due to recycling of the liquor, with addition of reagents and make-up water as needed (Figure 1). The solids content is kept at an acceptable level by blowing down the liquor as necessary. Any entrained

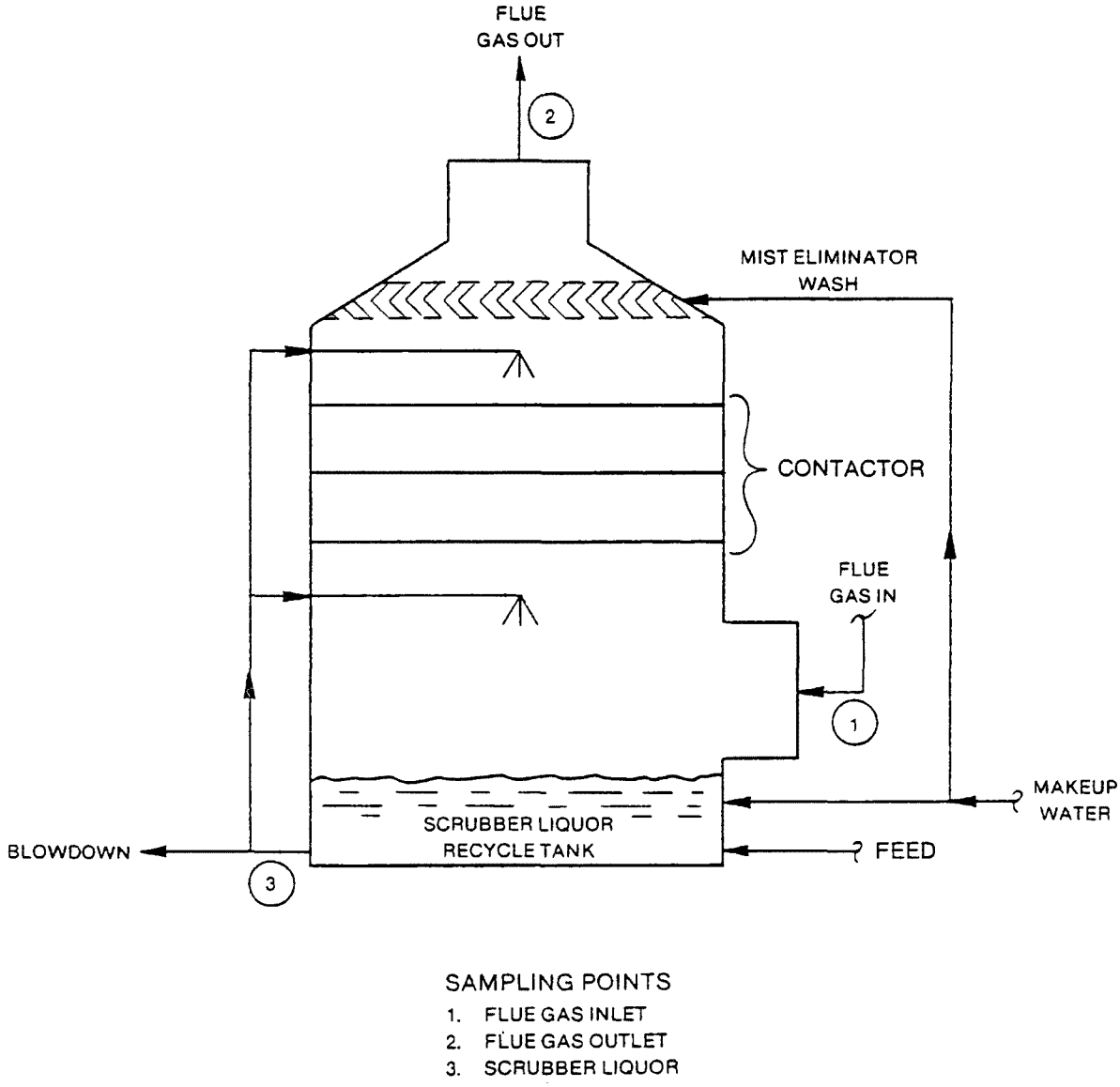

Figure 1. Schematic of a Wet Scrubber

liquor droplets which penetrate the mist eliminator can contribute to the overall particulate mass emission as a result of these dissolved solids in the liquor droplets. This mechanism is commonly used to generate test aerosols in the laboratory.

This paper describes an approach for determining the contribution of entrained liquor to the total mass emission downstream of a wet scrubber. The information can be used to evaluate mist eliminator performance and define actual versus apparent particulate penetration through the control device. With increased concern over fine particle emissions, particularly sulfate particles, such an evaluation can be helpful in determining the source of such emissions.

Approach

The contribution of mass by entrained liquor to the total mass penetrating the scrubber can be calculated using the concept of a chemical element balance. If one assumes that the mass flow of species j out of the scrubber is made up of contributions from the fly ash and entrained liquor, then the mass balance equation may be written:

$$\phi_j^{out} = P\ \phi_j^{in} + C_j\ V \qquad [1]$$

where:

ϕ_j^{out} is the mass flow rate (g/min) of species j out of the scrubber,

P is the penetration fraction of the fly ash particles,

ϕ_j^{in} is the mass flow rate (g/min) of species j into the scrubber,

C_j is the concentration (g/mℓ) of species j in the scrubber liquor, and

V is the volume rate (mℓ/min) of entrained scrubber liquor.

The mass flows into and out of the scrubber can be measured directly. Similarly, the solids content of the scrubber liquor can be measured. The penetration fraction and volume rate of entrained liquor can then be calculated indirectly. By solving the chemical element balance for multiple species, greater confidence can be gained in the solution, and an indication of the error for the solution obtained.

Several assumptions are necessary, however, to use this approach. First, the fly ash penetration fraction must be constant for all species. This is to say that the species selected for the chemical element balance must not exhibit appreciable particle size dependence in the fly ash. Previous studies (1,2) have shown that Ca, Mg, Ti, K, Mn, Na and Fe all show minimal size dependence in fly ash. Elements such as Ba, Zn, V, Cr, Co, As, Br, Se, Hg and Ni can show large particle size dependence, and as such may not be suited to this chemical element balance approach. Similarly, highly soluble species such as sulfate, chloride and fluoride may not be suited, as discussed later in this paper.

The final assumption requires that the scrubber liquor be homogeneous. This assumption should be good, since most scrubbers are well mixed systems. Notice that the volume rate calculated is for entrained liquor only and does not include evaporated liquor. While the scrubber liquor can contain both suspended and dissolved solids, the suspended solids are assumed not to be a significant source of mass. Justification of this assumption is provided later in the paper.

A variety of statistical methods may be used in the solution of this chemical element balance. The equation used in the statistical model development is

$$\phi_j^{out} = P\ \phi_j^{in} + C_j\ V + I + e_j \qquad [2]$$

where an intercept term I has been added, e_j represents a random error term, and the other terms are as defined above (see Equation [1]). Weighted regression analysis can then be used to determine the values of P, V, and I. In weighted regression, the fact that the different measured values have different error variances is taken into account; that is, P, V, and I are chosen so as to minimize the following sum of squares:

$$\sum_{j=1}^{n} (\phi_j^{out} - \hat{\phi}_j^{out})^2 / s_j^2 \qquad [3]$$

where:

$\hat{\phi}_j^{out}$ is the j^{th} predicted value of mass flow rate out of the scrubber,

s_j^2 is the error variance of the corresponding observed value ϕ_j^{out}, and

n is the number of species included.

In standard regression analysis, the term s_j^2 would be left out, giving all observations the same weight; in the above, the data points with the smallest error variances are weighted more heavily. This weighted regression procedure also prevents one or two points far away from a cluster from exerting a dominant influence in determining the slope.

The intercept term I in Equation [2] represents the mass flow rate out of the scrubber for a hypothetical species with $\phi_j^{in} = 0$ (zero mass flow rate into the scrubber) and $C_j = 0$ (zero concentration in the scrubber liquor). Clearly, such a species should have zero mass flow rate out of the scrubber, within random error, unless there is a source which is not accounted for by the model. Thus, the intercept term together with its standard error serves to provide a check on the closure of the chemical element balance.

One additional statistical point should be mentioned briefly. Near linear dependencies (multicollinearities) among the predictor variables,

(ϕ_j^{in} and C_j) is present, can cause spurious results in regression analyses. This problem and its effects have been discussed widely in the statistical literature (3). An investigation of selected scrubber cases with larger-than-average standard errors in the regression coefficients has revealed that the results presented here have not been affected significantly by multi-collinearity. This conclusion is based on several statistical measures (variance inflation factors in weighted ridge regression, etc.).

Sampling and Analysis

Particulate mass and chemical composition into and out of the scrubbers were obtained from analysis of EPA Method 5 (4) and/or 17 (5) particulate catches. Scrubber liquor composition was obtained from similar analyses of scrubber liquor samples collected during the particulate sampling.

Collection of particulate samples into the scrubber were usually obtained using an EPA Method 17 type sampling train. The instack filtration system eliminates the possible losses in a probe during extraction of the sample out of the stack. However, collection of particulate samples out of the scrubber typically must be obtained using the extractive EPA Method 5 type sampling train. This requirement is necessary due to the high moisture content of the flue gas and frequent presence of entrained droplets in the flue gas (in the case of no reheat). The heated probe and filter holder elevates the gas temperature sufficiently to evaporate any droplets and prevent condensation of moisture on the filter which may result in blinding.

In both the EPA Method 5 and 17 sampling trains, filters with low chemical backgrounds must be used. Gelman Micro Quartz filters have been used with success due to the compatibility with the required digestion procedures for the chemical analysis. Sampling times must be chosen to ensure adequate sample for the species detection limits.

The sampling point for the scrubber liquor sample must be chosen to ensure that the sample is representative of the liquor being exposed to the flue gas. The liquor sample should be filtered immediately as it is being obtained. A high capacity Millipore filtration system is suitable. The filtration is necessary to prevent any equilibrium interaction between the solid and liquid phases. Temperature and pH measurements can be obtained to further characterize the scrubber process (and serve to help check the chemical analyses results). The dissolved solids in the filtrate and the filtered solids are both determined gravimetrically and held for chemical analysis.

Prior to analysis, samples were digested using a mixed acid technique (6). Elemental analysis was performed on the digested particulate and scrubber solids samples using inductively coupled argon plasma emission spectroscopy (ICAPES) (7). The emitted spectral bands specific for each element are detected by separate photomultiplier tubes. The system (Applied Research Laboratories 34000) is computer controlled which allows for simultaneous multi-element determination. Filter background and matrix interferences are automatically adjusted.

Soluble species analysis ($SO_4^{=}$, Cl^-, F^-) was obtained using ion chromatography (IC) (8). Separate aliquots of sample were leached using a carbonate solution. This leachate was then injected directly into the IC (Dionex Model 10) for qualitative and quantitative analysis.

The expected errors in these analyses are less than 15 percent for the particulate samples and less than 10 percent for the scrubber liquor samples. This information is used in the chemical element balance model, as previously described.

Results and Discussion

The chemical element balance approach to determining the contribution of entrained liquor to the total mass emissions from three individual wet scrubber systems was investigated. Table 1 summarizes the combustion and scrubber processes for each of these systems. All scrubbers included mist eliminators of either a chevron or wire mesh design. Contactors included a variety of configurations. Scrubbing reagents included limestone and caustic.

TABLE 1. SUMMARY OF COMBUSTION AND SCRUBBER PROCESSES

System Number	Fuel Type	Scrubber Type	Boiler Load	Special Conditions
1	coal	limestone - venturi + spray	550 Mw	hot air injection reheat
2	oil	radial flow venturi for particulate control	650 Mw	no reheat
3	oil	radial flow venturi for particulate control	650 Mw	caustic addition, no reheat

Table 2 presents the results of the weighted least squares analysis for each of the systems investigated. The number of species available for inclusion in the chemical element balance are listed for each system. The square of the multiple correlation coefficient (r^2) for the analyses range from 0.81 to 0.99, indicating valid relationships in all cases. The intercept values (I) represent less than one percent of the mass rate out of the scrubber, indicating good closure of the chemical element balance. Comparison of the penetration fraction (P) and the volume rate of entrained liquor (V) with their respective standard errors indicate that the calculated values of P and V are usually statistically significant.

TABLE 2. RESULTS OF CHEMICAL ELEMENT BALANCE - WEIGHTED LEAST SQUARES

System Number	Number of Species	Penetration Fraction (P)	Standard Error in P	Volume Entrained (V) (ℓ/min)	Standard Error in V (ℓ/min)	Intercept (I) (g/min)	Standard Error in I (g/min)	Correlation Squared (r^2)
1	5	0.001	0.0004	6.9	5.	0.033	0.029	0.87
2	7	0.76	0.12	10.	13.	-4.44	15.4	0.93
3	7	0.76	0.16	5.5	12.	-12.1	15.8	0.89

Table 3 presents these results of the chemical element balance for total mass emissions. Results are expressed as a percentage of the total mass emission due to either 1) penetration of incident fly ash or 2) entrainment of scrubber liquor. From these results, it can be seen that entrained scrubber liquor can contribute from 1 to 40 percent of the total mass emissions measured downstream of a scrubber. The value for system number 1 was not calculated directly, because the total dissolved solid concentration was not available. However, a value of 30 percent was calculated indirectly based upon the total predicted concentrations of species entrained from the scrubber.

TABLE 3. CALCULATED CONTRIBUTION OF SCRUBBER LIQUOR TO TOTAL MASS EMISSIONS

System Number	Percent Total Mass Due to Penetration	Percent Total Mass Due to Entrainment
1	63	*
2	98	1
3	99	1

*TDS value not available.

The solutions to this chemical element balance model consistently underestimate the measured value of sulfate emissions. Several explanations are offered. Sulfate does show particle size dependence, with a large fraction of the total sulfate concentration found in fine particles. As a result, the calculated penetration fraction may not be applicable for sulfate due to the poorer removal of fine particles by a wet scrubber. Additionally, gaseous SO_2 may be transferred directly to entrained droplets. Once in solution, the SO_2 may be readily oxidized to sulfite and/or sulfate. Finally, sulfuric acid mist may contribute to the sulfate emissions from the scrubber. However, the sulfuric acid mist concentrations measured at these systems cannot by themselves account for the underprediction of sulfate. Undoubtedly, the difference between the predicted and observed values for sulfate are due to a combination of mechanisms.

Similar discrepancies have been found for chloride and fluoride. Like sulfate, sources of chloride and fluoride can be found in the gas phase, and are highly soluble in the scrubber liquor. This fact may explain the observed low predicted values for these species.

Conclusions

A chemical element balance approach has been described which determines the contribution of entrained scrubber liquor to the total mass emissions from a wet scrubber. A weighted regression analysis of the data is used.

Results from a variety of combustion and scrubber processes show that the approach provides statistically significant results with good closure of the mass balance. Contributions from entrained liquor to the total mass emissions were observed to range from 1 to 80 percent of the total mass. As such, wet scrubbers can be a significant source of mass emissions.

ENDNOTES

Acknowledgments

The authors thank Ms. Judy Tobias for her help in the statistical analysis of the data.

References

1. Meserole, F. B. et al. Trace Element Emissions from Coal-Fired Power Plants. Journal of Engineering for Power, 101:620-624, 1979.

2. Ondov, J. M. et al. Emissions and Particle-Size Distributions of Minor and Trace Elements at Two Western Coal-Fired Power Plants Equipped with Cold-Side Electrostatic Precipitators. Environ. Sci. Technol., 13:946-961, 1979.

3. Hoere, A. E. and R. W. Kennard. Ridge Regression: Biased Estimation for Monothogonal Problems. Technometrics, Vol. 12, 1979.

4. EPA Method 5: Determination of Particulate Emissions from Stationary Sources. Environmental Reporter, October 21, 1977.

5. EPA Method 17: Determination of Particulate Emissions from Stationary Sources (In-Stack Filtration Method). Federal Register, Vol. 41, No. 187. September 24, 1976.

6. McQuaker, N. R. et al. Digestion of Environmental Materials for Analysis by Inductively Coupled Plasma Atomic Emission Spectroscopy. Anal. Chem., 51:1082-1084, 1979.

7. McQuaker, N. R. et al. Calibration of an Inductively Coupled Plasma Atomic Emission Spectrometer for the Analysis of Environmental Materials. Anal. Chem., 51:888-895, 1979.

8. Mulik, J. D. and E. Sarviki. Ion Chromatographic Analysis of Environmental Pollutants, Vol. 2, Ann Arbor Sci., Ann Arbor, MI, 1979.

A DUAL-BEAM BACKSCATTER BETA-PARTICLE GAUGE FOR MEASURING THE DUST CAKE THICKNESS ON OPERATING BAG FILTERS INDEPENDENT OF POSITION

By: Robin P. Gardner
Center for Engineering Applications of Radioisotopes
North Carolina State University
Box 5636
Raleigh, NC 27650

R. P. Donovan
Process and Chemical Engineering Division
Research Triangle Institute
Post Office Box 12194
Research Triangle Park, NC 27709

L. S. Hovis
Utilities and Industrial Processes Division
Industrial Environmental Research Laboratory
U.S. Environmental Protection Agency
Research Triangle Park, NC 27711

ABSTRACT

A prototype, dual-beam, backscatter beta-particle gauge for measuring the dust cake thickness on operating bag filters has been designed, constructed, and tested. The device uses the two beta-particle sources Kr-85 and Sr-90 with an end-window GM counter so that the measurement of dust cake thickness is essentially independent of the position of the bag in relation to the gauge. A plastic rotating-shutter shield operated by a small electric motor is used to provide signals alternately from each source. The shutter position is sensed by an infrared detector and the response to each source is appropriately routed to separate counters. The low-energy Kr-85 source provides a backscatter response that depends only on filter position while the high-energy Sr-90 source provides a backscatter response that depends on both filter position and dust cake thickness. The real-time simultaneous solution of appropriate models for the two responses with a microcomputer gives the dust cake thickness, an estimate of the standard error of dust cake thickness due to statistical counting rate fluctuations, and the filter position for each set of responses. Laboratory and pilot plant results indicate that the gauge is accurate and will be useful for research purposes.

INTRODUCTION

The usual operation of bag filters for removing particulates from gas streams is cyclic. The cycle consists of a normal filtration period followed by a period in which the dust cake is removed, usually by shaking or reversing the gas flow. The efficient operation of bag filters involves the consideration of a number of operating variables for a given system of particulates in a gas. One of the most important of these is the dust cake thickness. While this thickness can be inferred from pressure

drop measurements across the bag filter or by other indirect methods, it would be very advantageous to have a direct, continuous, in situ measurement of it. Such a measurement would be important both in research applications in the laboratory or pilot plant and in the normal control of an industrial facility.

This paper describes the development and preliminary testing of a dual-beam backscatter beta-particle gauge for making the desired measurement. Others (1-3) have investigated the use of transmission beta-particle gauges for this application. While the transmission approach has merit, it suffers from the disadvantages that: (1) the in-situ response depends on sample position in an unknown way, (2) access is required to both sides of the bag filter, and (3) the measurement obtained represents the average of both sides of the bag filter at a particular position. The development of the back-scatter approach described here was undertaken to avoid these disadvantages.

Although the response of a backscatter type beta-particle gauge also depends on sample position, the effect is easier to specify than that for a transmission type gauge. Therefore, in principle, the effect of variable sample position can be eliminated by using a dual-beam approach with two sources of different beta-particle energies. It is assumed in this approach: that the backscatter responses for two beta-particle sources of different characteristic energies will depend on sample position and thickness differently, that the two responses can be modeled, and that the two models can be solved simultaneously to give a measurement of thickness independent of position. The parameter that is directly measured by such a device is the combined density thickness or areal density of the cloth filter and the dust cake layer. Therefore, to derive either the dust cake porosity or thickness from this measurement requires an independent knowledge of the other.

BETA-PARTICLE BACKSCATTER MODELS

The final beta-particle backscatter response models are modifications of previous models (4). The basic beta-particle backscatter response is taken to be an exponential function that yields saturation values. The models are:

$$R_A = \{R_{S1A}[1-\exp(-k_1x)]+R_{S2A}[1-\exp(-k_2x)]\}\ G\ \exp(-k_Gd)+R_{B1A}+R_{B2A}+R_{BA} \quad (1)$$

$$R_B = \{R_{S1B}[1-\exp(-k_1x)]+R_{S2B}[1-\exp(-k_2x)]\}\ G\ \exp(-k_Gd)+R_{B1B}+R_{B2B}+R_{BB} \quad (2)$$

where R_A and R_B are the total gauge responses in channels A and B in counts per second; the R_{SXY}(R_{S1A}, R_{S2A}, R_{S1B}, and R_{S2B}) are the net saturation responses due to backscatter from source X(1 or 2) to channel Y(A or B) in counts per second; the R_{BXY}(R_{B1A}, R_{B2A}, R_{B1B}, and R_{B2B}) are the source generated background responses from source X(1 or 2) to channel Y(A or B) in counts per second; R_{BA} and R_{BB} are the constant background responses in channels A and B in counts per second; k_1 and k_2 are the backscatter coefficients for sources 1 and 2 in cm^2/g; G is a constant in the geometry factor; k_G is a constant in the geometry factor in cm^{-1}; d is the sample distance from the gauge in cm, and x is the sample density thickness or areal density in g/second.

When all the model parameters and the model responses in Eqs. 1 and 2 are known, sample density thickness x can be solved for independently of sample distance d by using a simple trial-and-error method. The authors used the iterative Newton-Raphson method in which a root of the function f(x) is found from an initial estimate x_0 from the relationship:

$$x_i = x_{i-1} - f(x_{i-1})/f'(x_{i-1}) \tag{3}$$

where x_i is the ith estimate of the root and f'(x) is the derivative of the function f(x). In this case, f(x) is obtained by solving Eqs. 1 and 2 for G exp($-k_G d$) and setting the results equal to each other. The resulting f(x) is given by:

$$f(x) = (R_A - R_{B1A} - R_{B2A} - R_{BA}) / \{ R_{S1A}[1-\exp(-k_1 x)] + R_{S2A}[1-\exp(-k_2 x)]\} -$$

$$(R_B - R_{B1B} - R_{B2B} - R_{BB}) / \{ R_{S1B}[1-\exp(-k_1 x)] + R_{S2B}[1-\exp(-k_2 x)]\} = 0 \tag{4}$$

After the value of x has been obtained, Eq. 1 or 2 can be solved directly for d. An analytical estimate of the standard deviation of x can be obtained by using the standard approach of expanding the explicit x function in a Taylor Series and using only the first-order terms. The resulting relationship is:

$$s(x) = [A^2 R_A/t + B^2 R_B/t]^{1/2} \tag{5}$$

where t is the counting time for each channel in seconds and the A and B are given by

$$A = [k_1 R_{S1A} \exp(-k_1 x) + k_2 R_{S2A} \exp(-k_2 x)] G \exp(-k_G d) \tag{6}$$

$$B = [k_1 R_{S1B} \exp(-k_1 x) + k_2 R_{S2B} \exp(-k_2 x)] G \exp(-k_G d) \tag{7}$$

This relationship for s(x) assumes that the standard deviations of the dual-beam responses are independent and equal to that due to counting rate fluctuations only. These assumptions are not strictly valid and a more exact method has also been employed to evaluate the s(x). This method consists of randomly choosing sets of R_A and R_B values that have Gaussian distributions about their true values with arbitrarily chosen standard deviations. The resulting measured values of x and d are calculated for each set of R_A and R_B and are then used with the known values of x and d in the general estimator for standard deviations to obtain accurate estimates of the standard deviations.

SOURCE OPTIMIZATION STUDY

A study was performed to determine the optimum two beta-particle sources for the dual-beam backscatter gauge. This was accomplished by using modifications of the models given in the previous section to evaluate a design objective function consisting of the sum of the squares of the standard deviations in measured filter cake thickness due to: (1) statistical counting rate fluctuations and (2) variations in beta-particle attenuation in the

backscatter path. This objective function was minimized by an appropriate nonlinear search program called OPTCON (5) to obtain the optimum values of source backscatter coefficients k_1 and k_2. The objective function was taken as:

$$s_T^2(x) = s_S^2(x) + s_A^2(x) \tag{8}$$

where $s_T^2(x)$ is the objective function or the total variance in the measured value of sample density thickness, $s_S^2(x)$ is the variance of x due to statistical counting rate fluctuations, and $s_A^2(x)$ is the variance due to variable attenuation of the beta particles in their backscatter path. The variance of x due to statistical counting rate fluctuations is equal to the sum of the variances due to each of the two dual-beam responses:

$$s_S^2(x) = s_{AS}^2(x) + s_{BS}^2(x) \tag{9}$$

To account for detection system stability as well as statistical counting rate fluctuations, the standard deviations of the two dual-beam responses were assumed to be 1 percent of the response values. Then standard deviations $s_{AS}(x)$ and $s_{BS}(x)$ are determined by separately solving the modified versions of Eqs. 1 and 2 simultaneously for values of R_A and R_B equal to 1.01 times their actual values, respectively. The differences between the values of x obtained for 1.01 R_A and R_A and 1.01 R_B and R_B are taken to be the standard deviations $s_{AS}(x)$ and $s_{BS}(x)$, respectively.

The measurement variance due to variations in beta-particle attenuation is introduced by first including additional attenuation factors in Eqs. 1 and 2. Since the values of R_{S2A} and R_{S1B} are small compared to the values of R_{S1A} and R_{S2B}, the latter two values are neglected in the present analysis. For the optimization study, the two dual-beam responses previously given in Eqs. 1 and 2 become:

$$R_A = R_{S1A}[1-\exp(-k_1x)]G\exp(-k_Gd)\exp(-2u_1dr_G)+R_{B1A}+R_{B2A}+R_{BA} \tag{10}$$

$$R_B = R_{S2B}[1-\exp(-k_2x)]G\exp(-k_Gd)\exp(-2u_2dr_G)+R_{B1B}+R_{B2B}+R_{BB} \tag{11}$$

where u_1 and u_2 are the attenuation coefficients in cm^2/g for sources 1 and 2, respectively, and r_G is the atmospheric density along the backscatter path in g/cm^3. Various values of $s_A(x)$ are obtained by solving Eqs. 10 and 11 simultaneously for x for specified variations in the atmospheric density r_G and subtracting the values obtained for x with the base value of r_G. Although the standard deviation $s_A(x)$ is actually based on variations in atmospheric density, it can be thought of as representing a class of attenuation type errors; e.g., the presence of dust particles in the gas or dust layers on the source or detector.

The fixed parameters in the present problem include: (1) the dust cake thickness and density, (2) the filter thickness and density, (3) the atmospheric density r_G, (4) the gauge background responses R_{BA} and R_{BB}, (5) the measurement time interval, and (6) the gauge-to-sample distance d. The first two of these parameters are given by the sum of their density thicknesses: each is taken as 0.1 g/cm^2 to give a sum of 0.2 g/cm^2 for the design value of

x. Atmospheric density r_G is taken as 1.3×10^{-3} g/cm^3. The gauge background responses R_{BA} and R_{BB} are both taken to be 20 counts per second. The measurement time interval is fixed by the desired response time and is taken as 10 seconds. The gauge-to-sample distance should be as small as practical, so a value of d of 2 cm is taken. The remaining fixed parameters required in Eqs. 10 and 11 are related to source intensities. The values of R_{S1A} and R_{S2B} are taken to be 1.0×10^3 counts per second, the value of G is taken to be 1.5×10^3, the value of k_G is taken to be 0.171 cm^{-1}, and the values of R_{B1A}, R_{B2A}, R_{B1B}, and R_{B2B} are taken as zero.

The remaining design parameters to be optimized are u_1, u_2, k_1, and k_2, which are the attenuation and backscatter coefficients for the two sources chosen. According to Knoll (6) there is a power law dependence of characteristic maximum beta-particle energy and the attenuation coefficient. That relationship is:

$$E_{max} = (u/14.23)^{-0.722} \quad \text{(MeV)} \tag{12}$$

where u is in cm^2/g units. One can also identify a relationship between the attenuation and backscatter coefficients (4). It is taken to be approximately linear and is given by:

$$k = 3.27u \tag{13}$$

This relationship can be used to eliminate two of the four design parameters to be optimized.

The results of the design optimization for various levels of the attenuation error are given in Table 1. The results indicate that the maximum

TABLE 1. SOURCE OPTIMIZATION RESULTS

Attenuation Error, Δr_G (g/cm^3)	Standard Errors ($\times 10^3$)		Source Maximum Energies	
	$s_A(x)$ (g/cm^2)	$s_S(x)$ (g/cm^2)	Source 1, E_{max} (MeV)	Source 2, E_{max} (MeV)
2.6×10^{-5}	1.99	7.22	3.500*	0.245
1.3×10^{-4}	2.20	9.51	3.500*	1.086
2.6×10^{-4}	3.14	9.96	3.500*	1.351
5.2×10^{-4}	5.22	10.37	3.500*	1.503

*The maximum value allowed.

energy for one of the sources is always the maximum allowed. The maximum energy for the second source varies with the amount of attenuation error chosen. For low values of the attenuation error, small second-source maximum energies are obtained.

The commonly available beta-particle radioisotope sources are given in Table 2 with their pertinent characteristics. The radioisotope Ru-106 emits useful high-energy beta particles but has an impractical half-life of only

1.0 year. Consideration of the half-lives and beta-particle energies leads to the selection of Sr-90(Y-90) and Kr-85 as the most likely combination of sources.

TABLE 2. CHARACTERISTICS OF COMMON BETA-PARTICLE RADIOISOTOPE SOURCES

Source	Maximum Energy, E_{max} (MeV)	Half-Life (years)	Attenuation Coefficient (cm^2/g)
Ru-106	3.53	1.0	2.5
Sr-90(Y-90)	2.26	28	4.6
Tl-204	0.764	3.6	20.7
Kr-85	0.672	10.3	24.7
Pm-147	0.225	2.6	112.
C-14	0.156	5730	187.

PROTOTYPE DESIGN

A prototype gauge was designed and constructed. It consisted of a plastic base plate 0.63 cm thick, 10 cm long, and 10 cm wide. A thin end-window GM tube with a 2.5 cm diameter was mounted in a hole in the center of the plastic base. Holes were drilled on opposite sides of the GM tube for mounting beta-particle sources. A circular 180-degree sector of plastic was mounted on an axle so as to rotate and alternately shield each source. A small electric motor was attached to this rotating shield with a pulley arrangement to drive it. Finally an infrared source and detector were mounted in line with one of the sources to detect the position of the rotating shield. This infrared detector was used in an electronic circuit to switch the GM tube signal from one counter (A) to another (B). The resulting device records the response of source 1 in counter A and source 2 in counter B. A schematic diagram of the device is shown in Fig. 1.

Three different beta-particle sources have been purchased for use in the prototype device. These include 1 millicurie (mCi) sources of Ru-106 and Sr-90(Y-90) encapsulated in steel, a 0.1 mCi source of Sr-90(Y-90) encapsulated in aluminum, and two 10 mCi sources of Kr-85 encapsulated in aluminum. All sources are encapsulated in right circular cylinders 2.22 cm long. The first three sources have diameters of 0.32 cm; the last two, 0.64 cm. The windows of all sources were originally 0.025 cm thick, but the windows on the two Kr-85 sources were subsequently milled down to about 0.008 cm or less.

The ancillary electronics used with the device are a standard high voltage supply (ORTEC Model 456), a Timer Counter (ORTEC Model 773), a Dual Counter/Timer (ORTEC Model 715), a Print-Out Control (ORTEC Model 432A), and a Printer-Paper Tape Punch (Teletype). The rotational speed of the shield was adjusted so that a complete revolution is obtained in exactly 3.00 seconds. Therefore, the timer can be adjusted to any integer multiple of 3 seconds (3, 6, 9, 30, 60, etc.) to ensure an equal amount of time for the counts accumulated in each channel. In addition to this, a standard pulse

inverter was used to invert the GM tube pulses and an electronic circuit to route the pulses according to the condition of the infrared detector was designed and built. In the future an Apple II Microcomputer will be connected to the system so that real time calculations can be made to obtain the filter cake thickness directly from the present dual-beam responses.

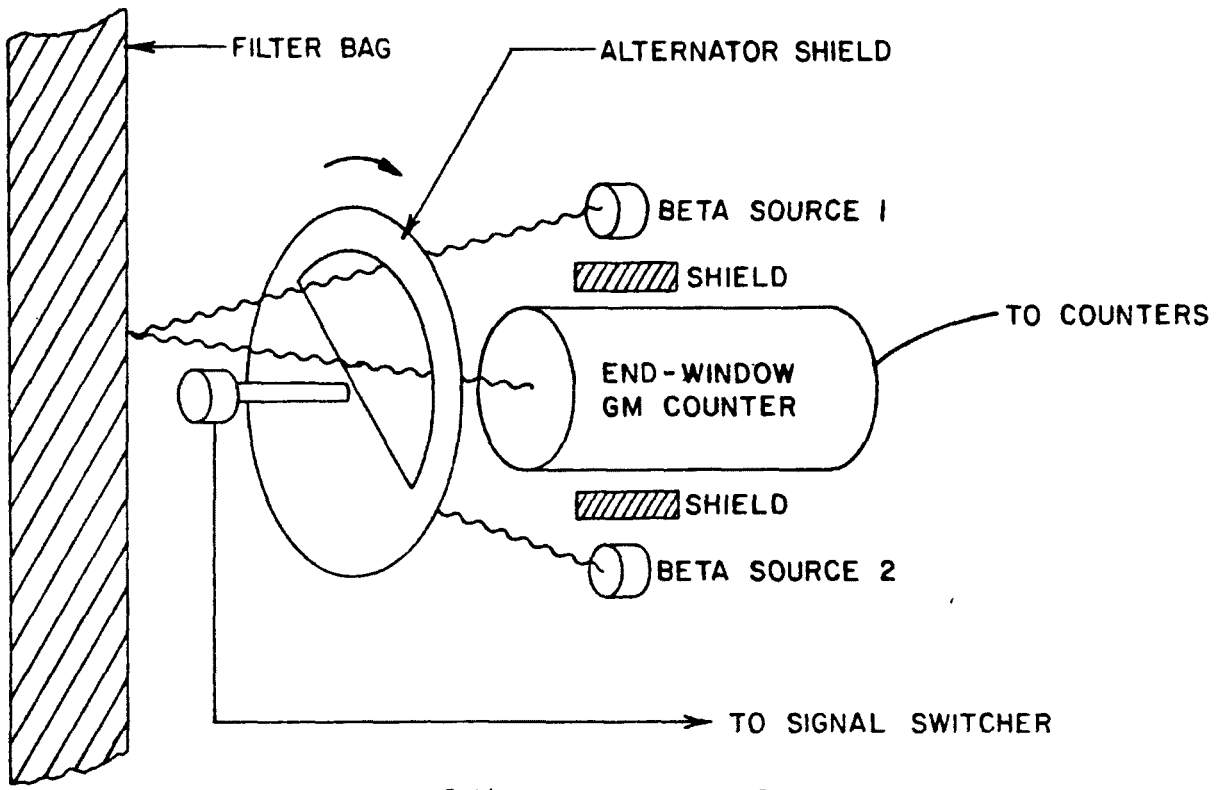

Fig. 1. Schematic diagram of the prototype, dual-beam, backscatter beta-particle gauge.

DETERMINATION OF CALIBRATION MODEL PARAMETERS

When initial responses were taken with the dual-beam gauge it was found that counting rates were high enough with the existing sources to cause significant dead time losses and corresponding low observed counting rates in the GM tube. Rather than decrease the counting rates by several possible methods, it was decided to correct for the dead time losses mathematically. This approach has the advantage that the device will have the fastest possible response times for a particular desired accuracy level.

For GM tubes, the observed counting rate R_0 is related to the true counting rate R_T and the dead time r by:

$$R_0 = R_T \exp(-R_T r) \tag{14}$$

where R_0 and R_T are the observed and true counting rates in counts per second, respectively, and r is the dead time in seconds. This is the relationship for parallyzable (4) detectors where the total dead time in the detector is a function of the true counting rate. The dead time r can be measured when

the true and observed counting rates are known. One method for determining the true counting rate is the decaying source method. In this method a radioisotope of known half-life and sufficient initial intensity to cause significant counting losses is placed next to the detector and the observed counting rate is recorded as a function of time. At sufficiently long decay times, negligible counting losses occur and the exponential decay curve with the decay constant appropriate to the half-life of the radioisotope used can be established. This permits extrapolating the true counting rate back to the short decay times and determining dead time r as a function of true counting rate.

This experiment was performed with the radioisotope Si-31 with a half-life of 2.62 hours. The dead time r was found to fit the following relationship with true counting rate:

$$r = D_1 \exp(-D_2 R_T) - D_3 \exp(-D_4 R_T) \quad \text{seconds} \tag{15}$$

where D_1, D_2, D_3, and D_4 are constants with the values 1.20×10^{-4}s, 2.69×10^{-5}s, 2.69×10^{-4}s, and 9.71×10^{-4}s. Substituting Eq. 15 for r into Eq. 14 gives a transcendental relationship that must be solved for the true counting rate in terms of the observed counting rate.

The counting rate as a function of sample distance from the gauge was found to be exponential for a wide range of distances. The resulting relationship for backscatter response as a function of sample distance for all sources is:

$$R_d = R_o G \exp(-k_G d) \qquad d \geq 2 \text{ cm} \tag{16}$$

where G is a constant, d is the distance to the sample in cm, k_G is a constant (found to be 0.397), and R_d and R_o are the counting rates at distances d and zero, respectively.

The remaining model parameters in Eqs. 1 and 2 were found by first obtaining data on paper and pasteboard samples of known density thickness at known distances from the dual-beam gauge for each radioisotope source separately. Then a nonlinear least-squares method was used to evaluate the parameters for the data obtained. The model parameters so obtained for each radioisotope source are given in Table 3.

TABLE 3. MODEL PARAMETERS OBTAINED FOR VARIOUS SOURCES AT A SAMPLE DISTANCE OF 3.9 cm

Source	R_{S1A} (c/s)	R_{B1A} (c/s)	R_{S1B} (c/s)	R_{B1B} (c/s)	k_1 (cm^2/g)
Ru-106	39.08	139.6	1.729	48.69	10.36
Sr-90(steel)	1006.	1945	---	---	11.42
Sr-90(Al)	244.5	796.6	4.250	35.59	11.42
Kr-85(No. 1)	16.62	93.48	0.0	52.58	46.25
Kr-85(No. 2)	20.88	105.7	0.0	50.15	52.33

A typical set of data for obtaining the model parameters is shown plotted versus the model values in Fig. 2.

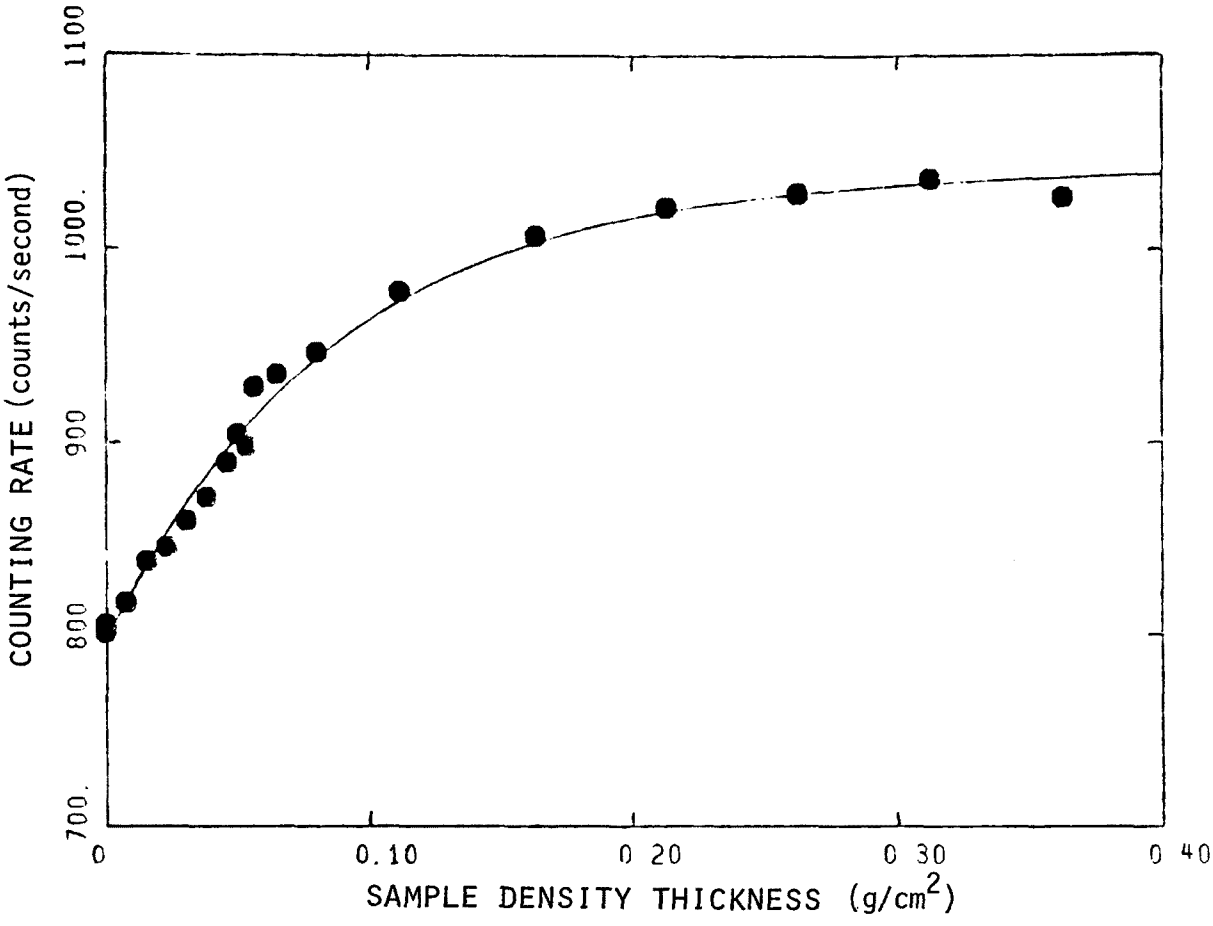

Fig. 2. Experimental data and calibration model for the Sr-90(Al) source.

A MICROCOMPUTER PROGRAM FOR OBTAINING REAL TIME MEASUREMENTS

A computer program has been written and tested to process the response data from the dual-beam gauge to give a measurement of the filter and dust cake density thickness, the distance to the filter, and the estimated standard deviation of the density thickness. The program was written in BASIC for the Apple II Microcomputer. The program includes a decay correction for each of the two radioisotope sources used, a correction for dead time losses, and a trial-and-error solution of the two models for the density thickness, the estimated standard deviation of the density thickness, and the distance to the sample.

RESULTS

Prior to calibration of the prototype device, an opportunity arose to obtain data using the in-house shaker baghouse at EPA. The Ru-106 and Sr-90 sources were available at that time. The filter bag used was a silicone-graphite finished fiberglass one and the test dust was Southwestern Public

Service fly ash as described by Hovis et al. (7). This baghouse is a top-fed inside collector. The dual-beam backscatter beta-particle gauge was mounted on the outside of the bag about 4 cm from the bag surface. A typical result is shown in Fig. 3 for one complete filtration and cleaning cycle. Note that although most of the dust cake removal occurs in less than 20 seconds, the shaking cycle lasts 120 seconds.

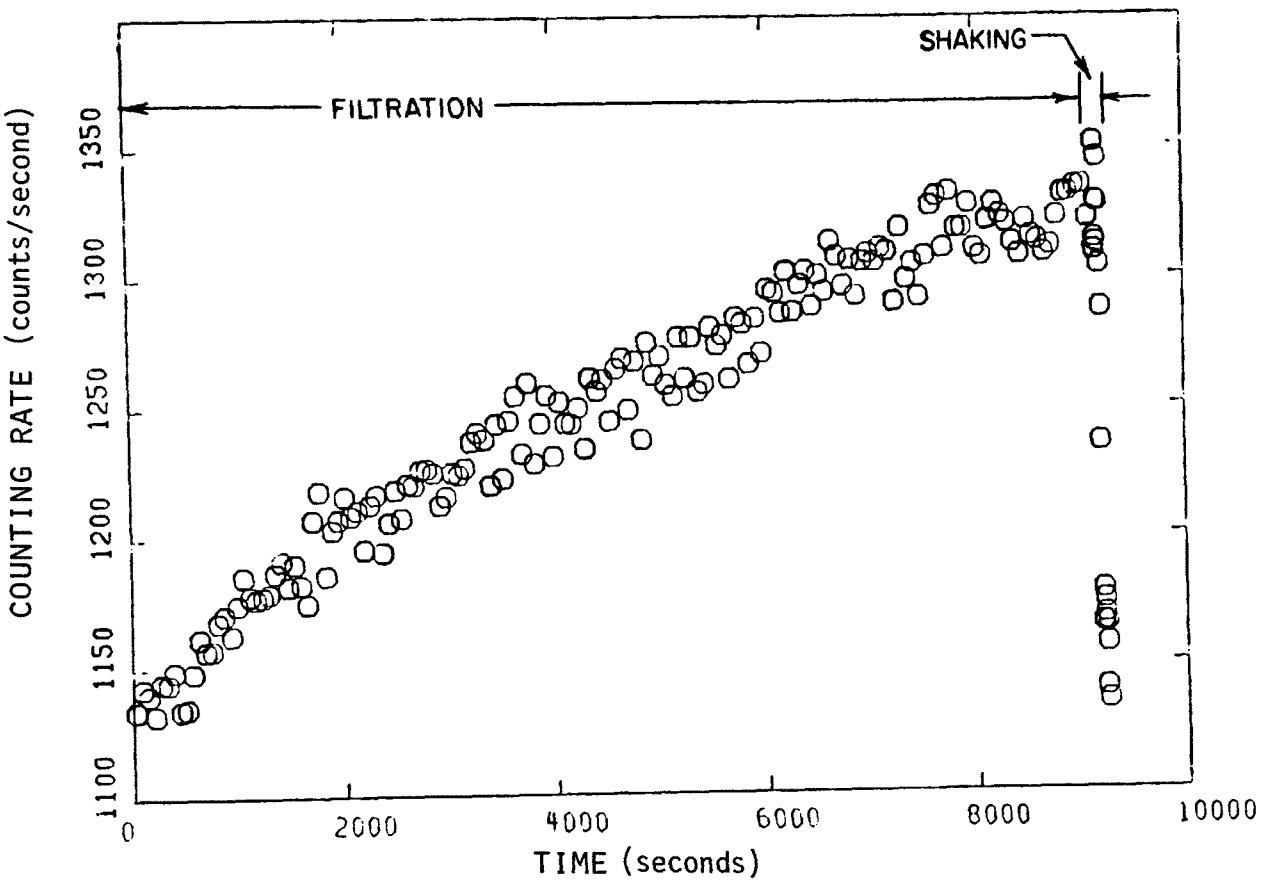

Fig. 3. Response data for Ru-106 source signal channel for one complete cycle of filtration. Time increments per point are six seconds.

Some laboratory results have also been taken at the Center for Engineering Applications of Radioisotopes, using the dual-beam gauge and known density thicknesses of paper at known distances from the gauge. The experimental and model responses are shown in Fig. 4. These results were obtained for the Kr-85 (No. 2) source and the Sr-90 (Al) source combination. By using model parameters approximately the same as those listed in Table 3 in the computer program previously described for obtaining sample density thickness, measured values for sample density thickness and sample distance were obtained for all experimental responses. The standard deviations of the measured from the actual values were found to be 0.068 g/cm^2 and 0.54 cm, respectively.

DISCUSSION AND CONCLUSIONS

The accuracy of the laboratory results was somewhat disappointing. This was primarily due to the high background counting from both

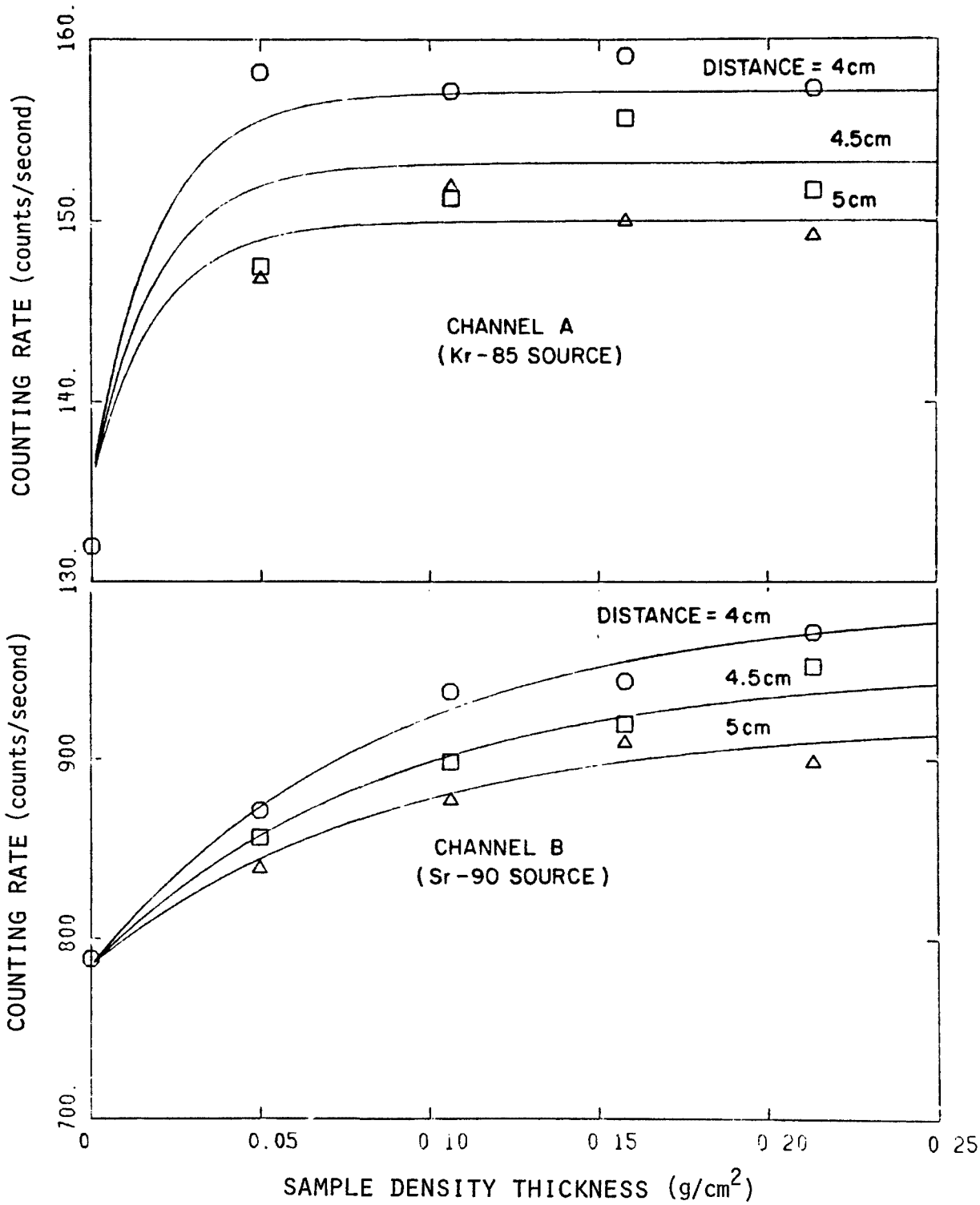

Fig. 4. Experimental and model responses for laboratory measurements of various paper density thicknesses at various distances.

sources and the much higher response of the Sr-90 source (about a factor of seven). Subsequently the prototype has been modified by placing lead cylindrical shields (20 mm diameter) around both sources. The background response to the Sr-90 source was decreased by a factor of about six in this manner. The resulting measurement standard deviation of the gauge was reduced to half the original value.

Additional improvements, such as increasing the Kr-85 source intensity, decreasing the amount of material in the superstructure for the rotating shield, decreasing the variations in the rotation shield speed, and increasing the accuracy of placing samples in the calibration procedure, would probably decrease the measurement standard deviation by another factor of one-half. The resulting dual-beam gauge should prove to be sufficiently accurate for both research and control purposes. However, the present device can only be used in environments of moderate temperature and pressure. In addition the prototype must be removed and cleaned after about 8 hours of operation. The rubber pulleys should probably be changed after 40 hours of operation. These characteristics of the gauge indicate that the present device will probably only be useful in laboratory or pilot plant research applications.

If possible, mechanical movement in a device for measuring dust cake thickness should be avoided. For this reason, investigation of a dual-beam device is anticipated based on responses to different beta-particle energies -- a device which does not require a rotating shield. A detector capable of beta-particle spectroscopy will be required as well as either single- or multi-channel analyzer pulse processing capability. Such a device should be capable of operation in much higher temperatures and pressures without frequent maintenance.

ENDNOTES

1. Stephan, D. G., P. T. Bohnslav, R. A. Herrick, G. W. Walsh, and A. H. Rose, Jr. A New Technique for Fabric Filter Evaluation. Amer. Ind. Hyg. Assoc. Journal. 19:276-284, August 1958.
2. Mazur, M., J. Mejer, and S. Waratowicz, Radioisotopic Measurement of the Surface Mass Density of a Dust Layer Deposited on Bag Filter Cloth, translated from Ochrona Powierza. 10(5): 130-134, 1976.
3. Ellenbecker, Michael J. and David Leith. Dust Deposit Profiles in a High Velocity Pulse-Jet Fabric Filter. Journal of the Air Pollution Control Association. 29(12): 1236-1241, December 1979.
4. Gardner, R. P. and R. L. Ely, Jr. Radioisotope Measurement Methods in Engineering. New York, The Reinhold Publishing Corporation, 1967.
5. Gardner, R. P. and K. Verghese. Analysis and Design of Radioisotope Gauges. To be published by Plenum Publishing Company.
6. Knoll, G. F. Radiation Detection and Measurement. New York, John Wiley and Sons, 1979.
7. Hovis, L. S., J. H. Abbott, and R. P. Donovan. Electrically Charged Fly Ash Experiments in a Laboratory Shaker Baghouse. These proceedings.

DIAGNOSING FILTER FABRIC CAPABILITIES WITH LIGHT SCATTERING AND NUCLEI DETECTING INSTRUMENTATION

Richard Dennis

David V. Bubenick

GCA/Technology Division
213 Burlington Road
Bedford, MA 01730

Louis S. Hovis

Industrial Environmental Research Laboratory
U.S. Environmental Protection Agency
Research Triangle Park, NC 27711

ABSTRACT

Fabric penetration measurements based upon long term averaging periods, ~hours, do not reveal the probable range of outlet concentrations and size properties, nor short term effects that play important roles in the selection of fabric and collector design and operating parameters. Bench scale and pilot tests at ambient temperatures using a single particle, light scattering device and a condensation nuclei counter to augment mass and size determinations by filter and cascade impactor measurements, respectively, permitted short term resolution, ~seconds, of changes in effluent properties. Data are presented relating particulate emissions to variations in inlet concentration, fabric structure, degree of cleaning, and filtration velocity. The effect of fabric defects and mechanical disturbances of the dust cake are traced over typical filtration cycles for fly ash aerosols with woven glass, cotton, and Dacron fabrics.

BACKGROUND

Concurrent mass sampling of inlet and outlet gas streams provides good estimates of average fabric filter efficiency for the precise aerosol and operating conditions prevailing during the test. Unfortunately, EPA Method 5 sampling may require several hours to collect weighable amounts of effluent dust. Additionally, such tests do not delineate transient, ~minutes, changes in effluent properties related to variations in fabric cleaning action, the state of the fabric before and after cleaning, the fabric dust loading, filtration velocity, and certain unique relationships between the type of dust being filtered and the properties of the filter fabric.

Although field applications of fast response sensing devices such as whole-cloud or single-particle light scattering detectors may signal rapid changes in effluent properties (particularly those caused by accidents such as bag ruptures), they seldom provide quantitative data because of gas stratification and mixing problems.[1] Insofar as upstream sampling is concerned, current applications of single particle detectors present serious

measurement difficulties, not only because of the sample representativeness factor, but also because of inability to satisfy the extreme dilution requirement (3 to 4 orders of magnitude), sampling line losses, and potential instrument malfunction due to temperature, pressure, corrosion, and condensation difficulties.[1]

On the other hand, the same instrumentation can provide invaluable support in appraising filter fabric capabilities under controlled laboratory or pilot plant conditions.[2,3] The only constraints to such testing are that (a) the concentrations of the filter effluents fall within the normal working range (no dilution required) of the sensing device, (b) the aerosol properties at the sampling point be representative of average conditions, and (c) the particle losses in the sampling lines be minimal.

Extensive use of a light-scattering, single-particle counter* and a condensation nuclei counter+ in prior filtration studies demonstrated a diagnostic potential far exceeding that anticipated for these highly sensitive instruments.[2,3] The fact that such measurements could be translated to both mass and particle number concentrations provided heretofore unavailable information on the rapid changes taking place in filter effluent properties over a broad range of simulated field operating conditions at bench and pilot (single bag) scales. This paper describes experimental systems, calibration procedures, and specific test results that demonstrate how well the particulate removal characteristics for various fabrics can be related to fabric structure, fabric state (new, used, partially cleaned), and basic filtration parameters such as filtration velocity, inlet concentration, and dust properties.

EXPERIMENTAL PROCEDURES

Fabric Test Assembly and Particle Sampling Instrumentation

Fabric test panels, 15 cm x 23 cm, were mounted without backing support in the filter assembly shown in Figure 1.[3] The system geometry simulated insofar as practical the typical approach velocity conditions encountered in the field. Fly ash aerosols, generated by an NBS† dust feeder,[3] were injected into the aerosol loop from which the desired quantity was extracted for filtration at air-to-cloth ratios varying from 0.3 to 2 m/min. The inlet dust concentrations, ~2 to 8 g/m^3, were determined by all-glass filter or cascade impactor sampling immediately before the fabric panel as well as by weighing the dust accumulation on the fabric panel. Outlet dust concentrations were sampled as far downstream as possible to attain optimum mixing of the effluent. Total gas volumes handled by the system, which ranged from roughly 0.01 to 0.07 m^3/min, were filtered through all-glass (Method 5)

---

*Model 40-1 Dust Counter manufactured by Bausch & Lomb (B&L), Rochester, New York.

+Model Rich 100 Condensation Nuclei Counter (CNC) manufactured by Environment One Corporation, Schenectady, New York.

†National Bureau of Standards (NBS).

filter media except for that fraction required for CNC and B&L analyses. Limited fly ash filtration tests with single, woven glass bags (Menardi), 3 m x 16 cm, were also performed to confirm the test panel results.[3]

The manufacturers and code designations for the commonly used fabrics discussed in this paper are: Menardi Southern, Woven Glass 601T (Tuflex); W.W. Criswell, Woven Glass No. 640048; Albany International, Cotton Sateen No. 960 (Napped); and Dacron, No. 865B (Crowfoot).

Comments on Instrumental Methods

Sampling the filter effluent with all-glass (Method 5) filters provides an accurate measure of average exit concentrations, but fails to reveal short term variations regardless of the cause. Use of an in-stack type Andersen impactor upstream furnished the usual degree of accuracy attributable to this device under similar field loading conditions. Use of a short, 12 cm extension, probe did not appear to affect impactor collection.

Although the accuracy of the B&L single-particle light-scattering counter depends strongly on its application, this instrument can provide time resolutions down to 0.1 minute insofar as reflecting changes in number concentration for particle diameters in the 0.3 to 5 μm range. Prior GCA studies have indicated that mass concentrations derived from B&L data are usually lower than those determined by parallel gravimetric sampling whenever a significant fraction of the particles exceeds 5 μm diameter.[2] The latter problem is believed to result mainly from particle settling losses in the sampling lines and not to defects in the electro-optical system. The CNC is claimed to detect number (nuclei) concentrations in the 0.0025 to 0.5 μm diameter range. Although it may not provide an absolute nuclei count, the fact that the CNC can, with calibration, provide reasonable estimates of mass concentration, makes it invaluable for tracking rapid changes in effluent properties. Similarly, the good linear correlation indicated between CNC and B&L measurements, Figure 2, also suggests that generally parallel concentration versus fabric loading (or time) curves should be expected in the micrometer or lower size range.

Special Calibration Procedures

CNC Versus B&L Measurements with Atmospheric Dust--

Background nuclei concentrations in the laboratory area varied from 3×10^{10} to 5×10^{10} n/m^3 for the mass concentration range of 25 to 40 μg/m upon concurrent B&L measurements and an assumed average particle density of 2 g/cm^3. For those measurements wherein the mass, but not the particle size spectrum, underwent changes, a linear correlation was shown between the nuclei concentrations and those derived from B&L measurements, Figure 2. Thus, rapid changes in ambient mass concentrations could be estimated from CNC counts provided that the particle size distribution underwent no significant change. Since long term (24 hour) high-volume filter sampling in the building area indicated ambient mass concentrations in the 20 to 100 μg/m^3 range, it was concluded that insofar as atmospheric dust was concerned, B&L and filter measurements could be equated when greater than 98 to 99 percent of the aerosolized particles were less than 5 μm diameter. One gram of ambient dust in the testing area was equivalent to a nuclei concentration of 10^{15} n/m^3.

CNC Counts Versus Mass Concentrations Determined by Gravimetric Procedures--

The test aerosol used in this study consisted of a resuspended coal fly ash with an aerodynamic mass median diameter (aMMD) of 5.8 μm and a geometric standard deviation (σ_g) of 2.5. Concurrent effluent sampling with all-glass filters and a nuclei counter (CNC) also showed a strong linear correlation between CNC counts and mass concentration for a coal fly ash aerosol, Figure 2. Note, however, that the condensation nuclei in the coal fly ash represent a much smaller fraction of the total particulate material than that observed for atmospheric dust; viz., 5×10^{11} versus 1.45×10^{15} n/g dust, respectively. Nuclei and mass measurements were compared on the basis of the average nuclei concentration, the latter obtained by integrating over the time interval required to collect the mass sample. Both bench scale and single bag measurements also demonstrate a linear relationship over the outlet concentration range, 5×10^{-3} g/m^3 through 10^{-1} g/m^3. The calibration curve for fly ash, Figure 2, was extended beyond the actual data points to outlet loadings exceeding 1 g/m^3 for those special situations where no significant changes in size distribution were noted between up- and downstream fly ash aerosols.[3]

Concurrent Filter Drag Measurements

Although the analytical potential of the CNC and B&L devices is the main theme of this paper, it is emphasized that the application of these instruments, in conjunction with parallel filter drag determinations for the dust-fabric combinations of interest, enhances the CNC and B&L diagnostic capabilities. Several characteristic forms for filter drag versus fabric loading curves based upon filtration at constant inlet dust concentration and face velocity are presented in Figure 3. Sketches showing the appearance of axial yarns (horizontal) and fill yarns (seen on end) demonstrate that fabric surface depressions are greatest when no free fibers are available to partially fill the pore regions (Sketch 4) and smallest when a combination of heavy napping and all-staple yarns provides a relatively even surface (Sketch 2). An initial concave-down form reflects the early pore filling phase during which the pressure loss increase per unit mass of dust deposit commences at high levels followed by a gradual reduction to a nearly constant level once the depressions are filled (Curve 1, Figure 3). The linearity will persist for some time provided that the surface dust layer itself undergoes no compression as the fabric loading increases. The readily discernible free or loose fiber content of napped sateen weave cotton creates a partially penetrable, spring-like layer that gradually compresses as the surface dust layer accumulates. Such behavior is therefore reflected by a concave-upward form for the drag curves due to the progressively higher resistance to gas flow presented by the underlying fabric (Curves 2 and 3, Figure 3). When continuous, multifilament yarns alone constitute the fabric weave (Sketch 4, Figure 3), the initial pore filling or concave-down phase appears to continue over the complete fabric loading process. However, subsequent decreases in slope, once the linear level shown in Sketch 1 has been reached, are due to a progressive collapse of the early pore bridging under the influence of increasing aerodynamic drag. Consequently, filter penetration approaches the 100 percent level as more and more aerosol "detours" through the pores.

DIAGNOSTIC APPLICATIONS, FACTORS AFFECTING FLY ASH COLLECTION

New (Unused) Glass - Fabric Loading and Mechanical Perturbation Effects

A good example of the CNC and B&L diagnostic potential is given by the concentration measurements shown in Figures 4 and 5. Mass concentrations are seen to decrease rapidly from an initial value of $\sim$0.1 g/m^3 to 0.0013 g/m^3 as fabric loadings increase from zero to approximately 120 g/m^2, Figure 4. Subsequent interruptions of filtration, because of removal of the filter sandwich for weighing, caused transient increases in emissions that became progressively smaller until no discernible effect was noted at the end of the D filtration interval. These perturbations arose from the checking and puncturing of the essentially homogeneous dust surface due to filter handling. Over filtration intervals B through E, the dust cake revealed a capability to mend itself such that no permanent damage resulted. The time required to develop the dust deposits for inlet concentrations of 1 to 3 g/m^3 at a filtration velocity of 0.61 m/min varied from about 2.5 hours for the A interval to 5.5 hours for the E interval.

Similar concentration spikes (and related drag perturbations) should also be expected during the operation of large, multi-compartment baghouses due to shocks and vibrations caused by rapid damper closings, fan imbalance, mechanical shaking of adjacent off-line compartments, or the emergency hammering of a plugged hopper to restore dust removal. The intensity of the disturbance, the mass of the baghouse (light- or heavy-weight construction), and presumably the unique adhesion properties for the specific dust-fabric combination will determine the impact of such mechanical effects on dust penetration. In the event of minor disruptions, dust emissions will probably return to the "unperturbed" levels, and no net changes will be indicated in the form and slope of the drag curves. Conversely, if a heavily-laden fabric is severely shocked, its dust retention capacity may be seriously impaired. Figure 4 indicates that the final perturbation, after the fabric loading had increased to about 950 g/m^2 (Region F), caused emissions to rise to levels characterizing the clean fabric. More importantly, the fabric dust layer no longer was able to repair itself as indicated for Regions A through D. Actual effluent concentration fell slightly to a nearly constant level approximately 60 times greater than that observed during the <950 g/m^2 loading range. Although failure to mend itself may have been partially attributable to the intensity of the mechanical shock, the behavior indicated on Figure 4 also signifies that dust cake defects are more amenable to repair at low to moderate surface dust loadings where proportionately lower gas velocities occur in the pinhole zones. Once the gas velocity through a pore becomes large enough to prevent any further pore bridging, emission levels tend to remain constant for a fixed inlet dust concentration. Upon cleaning, however, former defects will be eradicated in most cases by the freshly deposited dust layer.

Analyses of concurrent B&L and CNC measurements over the E filtration interval, Figure 5, show that all B&L size categories over the range >0.3 μm to >2.0 μm generated parallel curves whose paths were closely traced by the

concurrent nuclei measurements. These findings appear to demonstrate that,at the initiation of the E filtration phase, a maximum in pore closure or bridging had been achieved for the prevailing inlet concentration and velocity conditions. The parallel up and down paths displayed by the B&L traces reflect variations in the mass inlet concentration where, for a constant gas flow volume through the unblocked pores, the emissions are directly proportional to the inlet concentrations. Because roughly 50 percent of the fly ash effluent is composed of particles >5 μm diameter, one cannot translate directly the B&L data to equivalent mass loadings. However, for those sizes that appear to reach the B&L sensing zone without significant loss of <5 μm diameter particles, reasonable estimates of mass concentration appear possible as discussed earlier in this paper.

Multifilament Dacron - Effect of Minimal Free Fibers on Emissions

The results of CNC and B&L measurements on several new and unused Dacron test panels showed very high fly ash penetrations for both nuclei and B&L particles over the complete fabric loading range, Figure 6. In each case, the initial effluent concentrations not only exceeded by an order of magnitude their glass and cotton fabric counterparts, but also remained nearly constant over the ~70 minute filtration interval. Although both CNC and B&L counts were internally consistent, they were considered suspect until the final gravimetric efficiencies, ~76 to 81 percent as determined by concurrent sampling with all-glass filters, were analyzed. The unexpectedly poor performance of these test panels was attributed to the multifilament character of the weave whose lack of free fibers allowed for comparatively easy pore penetration (see Sketch 4, Figure 3). The predicted efficiencies for this fabric, 83 to 85 percent based upon pinhole concentrations ranging from ~5000 to 9000 openings/m^2, confirmed the poor collection determined by gravimetric sampling.

New (Unused) Sateen Weave Cotton - Fabric Loading and Napping Effect

It has been emphasized that particle size distributions determined immediately before and after the filter face are nearly identical when coal fly ash is filtered with woven glass fabrics.[3,4] This behavior has been attributed to the fact that there is negligible removal of particles less than 15 to 20 μm diameter from the flue gas fraction that passes through pinhole openings during the early minutes of filtration. Since 95 to 99 percent of the total emissions are contributed by the early penetration phase, the size properties for the effluent dust are closely described by those of the inlet dust.

The penetration characteristics change appreciably, however, when a more efficient fabric (such as a napped, sateen weave cotton) is used, Figure 7. An increased free fiber population within the pore structure and upon the fabric surface results in far fewer and usually smaller pinhole-type openings in the filtering surface. At the initiation of filtration, dust deposits mainly upon the napped surface with minimal penentration in the direction of the yarn substrate. Thus, as shown previously by Curve 2, Figure 3, the pore-filling phase characterized by woven glass fabrics is practically non-existent.

Furthermore, the increasing pressure gradient across the accumulating dust layer and its supporting nap also leads to a gradual compression of the napped region. The net result is an increase in the rate of change in drag with fabric loading as shown by the concave-up form of Curve 2, Figure 3.

According to B&L measurements, particle concentrations in the >1 μm size class underwent four orders of magnitude decay before the fabric loading had reached 150 g/m^2, while similar, but less rapid reductions in the >0.5 μm particle category were still occurring at the 400 g/m^2 load level. In contrast, however, nuclei concentrations (constituting the particle class <0.5 μm) and the B&L particles in the >0.3 μm category underwent a general levelling off at the 200 g/m^2 fabric loading level while displaying the previously noted tendency to parallel each other. It was concluded, therefore, that fiber proximity in the cotton filter permitted much more effective pore bridging than that attainable with woven glass media. The fact that a low-level penetration persisted for the very small, <0.5 μm, particles suggested either incomplete pore bridging or cake defects in the form of minute cracks or perforations. Concurrent mass emission rates for the cotton fabric, however, were still approximately 15 times lower than those observed for the woven glass media because of the absence of >1.0 μm diameter particles.[3]

Filtration of atmospheric dust through a uniformly distributed fly ash layer (>200 g/m^2) would be expected to show no reduction in particle size because the parent dust contains few particles, usually <1 to 2 percent, greater than 1 μm. Figure 7 suggests that most particles in the <1.0 μm category should penetrate any residual pores with negligible particle capture. This penetration concept also applies to fly ash filtration with glass fabrics where, except for the fact that the pores and particles are larger, the penetration through the pores for the fly ash particles is nearly 100 percent.

Well-Used Glass - Partial Cleaning, Fabric Loading, and Velocity Effects

Figure 8 shows that particulate emissions are strongly dependent upon the uniformity of the fabric dust layer. Effluent concentrations decreased rapidly, Test 71,[3] when fly ash was filtered with a completely cleaned Menardi test panel excised from a well-used bag. At all times during this test, up to a fabric loading of 530 g/m^2, the dust was uniformly distributed on the fabric surface. After cleaning, however, wherein the dust characteristically separated at the interface region between the surface layer and the fabric,[3] approximately 35 percent of the fabric surface was reduced to its formerly completely cleaned state. At this point, the only dust remaining in the cleaned region was that irreversibly retained within the fiber interstices. When filtration was resumed, the emissions rose to a level about 200 times greater than that previously noted for a uniformly distributed layer of 350 g/m^2 because a disproportionate fraction of the gas flow was diverted through the less efficient but much lower resistance filtration path. The higher gas velocities prevailing at the initiation of Test 72[3] explained the excessive penetration while the preferential deposition of fly ash on the cleaned zone accounted for the gradual improvement in

performance. A tabulation of equilibrium emission levels associated with selected filtration velocities (based on CNC tests with uniformly loaded filters, Figure 8) suggested that a gradual velocity reduction over the cleaned region should lead to decreased penetration. However, since filtration is always initiated at high velocities on a cleaned surface, it also appeared that the early pore bridging process might not be as effective. The final concentration excursions noted for Test 72 were attributed to two factors: possible variations in inlet concentration and/or an enlargement in pore size caused by some unidentified mechanical disturbance.

CONCLUSIONS

Experimental data presented in this paper demonstrate the capabilities of nuclei counters and single-particle light-scattering counting and sizing instruments when used under pilot testing conditions where problems pertaining to high temperatures, corrosion, and pressure variations can be minimized. Procedures described in this report enable the researcher and filter manufacturer to examine fabric potential on the basis of small panel tests or single bag pilot tests.

The capability to identify unexpected performance characteristics and to determine, in conjunction with drag measurements and visual (microscope) observations of the fabric, how fabric design or selection may be improved, can eliminate unnecessary trial and error procedures in the field. Considerable data evolving from test procedures discussed in this paper were used to develop the predictive model for fly ash filtration described in the filtration literature.[3,4]

ACKNOWLEDGMENTS

This project has been funded at least in part with Federal funds from the U.S. Environmental Protection Agency under Contract No. 68-02-1438, Task No. 5. This paper does not necessarily reflect the views or policies of the U.S. Environmental Protection Agency, nor does mention of trade names, commercial products, or organizations imply endorsement by the U.S. Government.

REFERENCES

1. Dennis, R., and D. V. Bubenick. Apparent Fractional Efficiencies of Available Control Techniques. In: APCA Spring Specialty Conference Proceedings, The Technical Basis for a Size Specific Particulate Standard, Parts I and II. pp. 129-155. March and April 1980.

2. Dennis, R., and J. E. Wilder. Fabric Filter Cleaning Studies. GCA/Technology Division. EPA-650/2-75-009 (NTIS PB 240372). January 1975.

3. Dennis, R., et al. Filtration Model for Coal Fly Ash with Glass Fabrics. GCA/Technology Division. EPA-600/7-77-084 (NTIS PB 276489). August 1977.

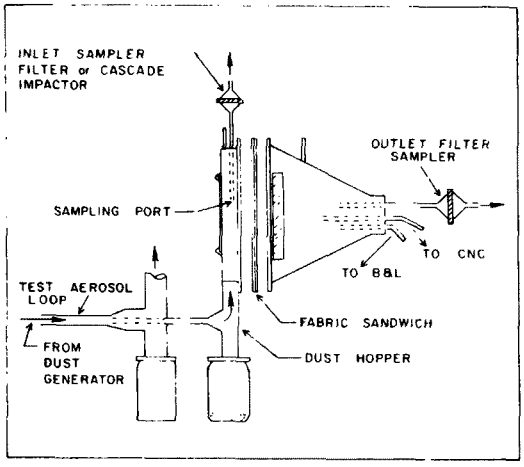

Figure 1. Exploded view of filter test assembly.

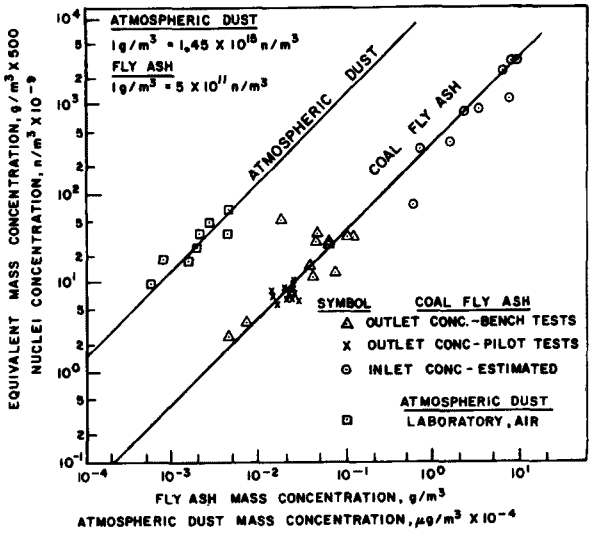

Figure 2. Calibration curve - Average nuclei and related mass concentrations for GCA fly ash and atmospheric dust.

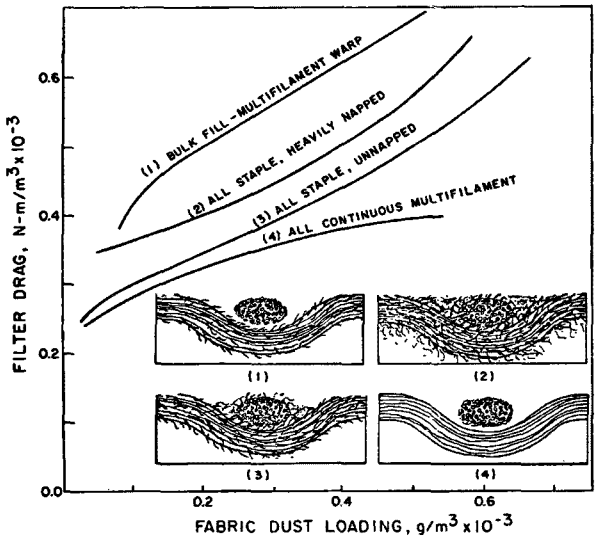

Figure 3. Characteristic drag-loading curves, dust filtration with common fabric weave and yarn combinations.

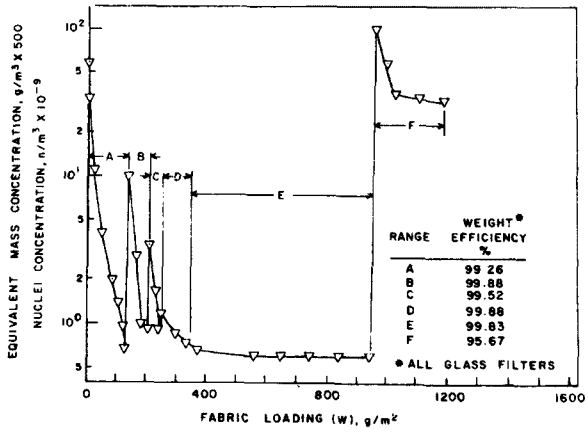

Figure 4. Effluent nuclei concentration versus fabric loading with coal fly ash filtration at 0.61 m/min on unused Menardi glass fabric. Test 65.[3]

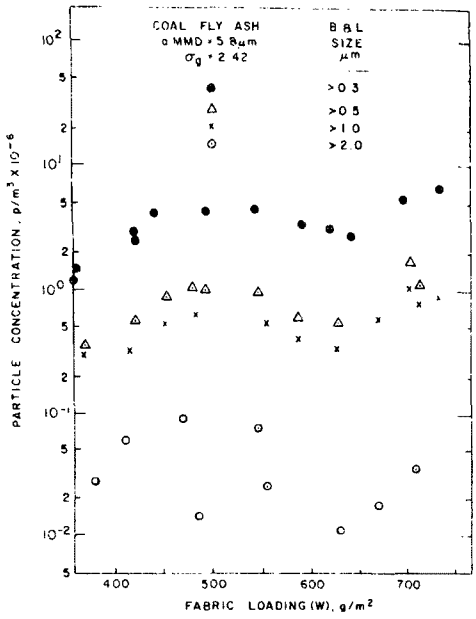

Figure 5. Effluent particle concentration versus fabric loading with coal fly ash filtration at 0.61 m/min on new Menardi glass fabric. Test 65.[3]

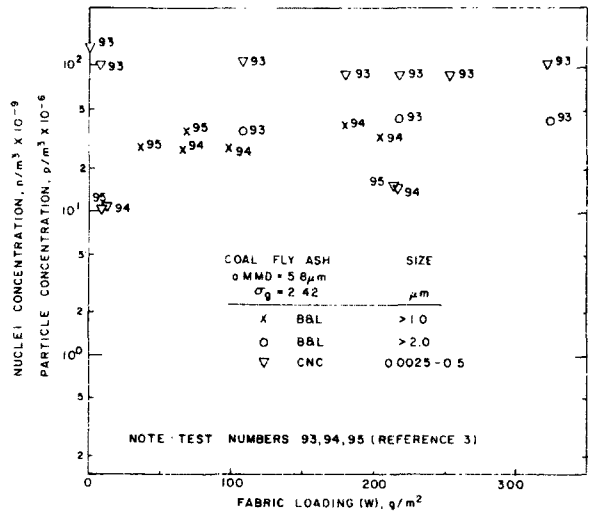

Figure 6. Effluent concentrations versus fabric loading for coal fly ash filtration with Dacron (crowfoot weave) test panels, face velocity = 0.61 m/min, inlet loading = ~7.5 g/m³.

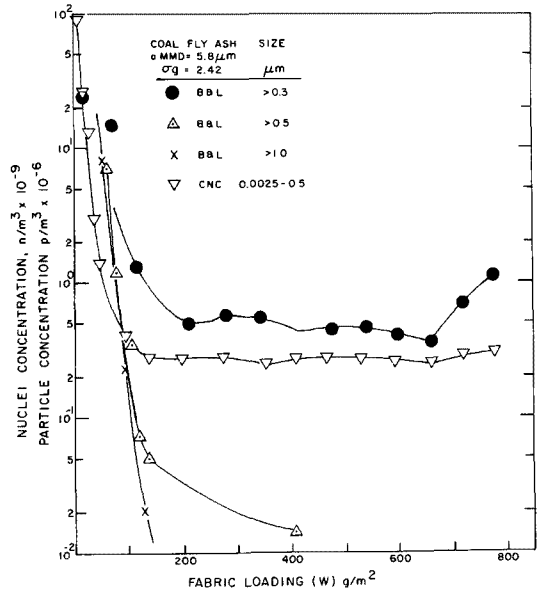

Figure 7. Effluent concentrations versus fabric loading for coal fly ash filtration with napped cotton sateen test panel, face velocity = 0.61 m/min, inlet loading = 7.1 g/m³.

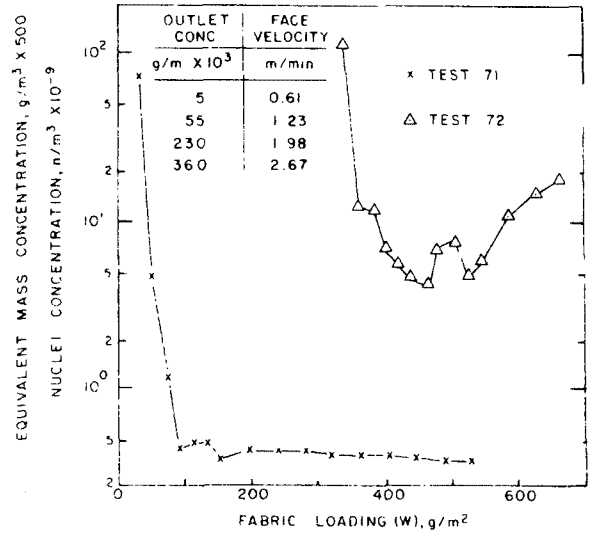

Figure 8. Effluent concentration versus fabric loading for Menardi fabric and coal fly ash with uniform and non-uniform surface dust loading.[3]

ACID DEWPOINT CORROSION IN PARTICULATE CONTROL EQUIPMENT

By: T.E. Mappes and R.D. Tems, Ph.D*
PEDCo Environmental, Inc.
505 S. Duke St., Suite 503
Durham, North Carolina 27701

K.E. Foster
Technical Support Branch
Division of Stationary Source Enforcement (MD-7)
U.S. Environmental Protection Agency
Research Triangle Park, North Carolina 27711

ABSTRACT

A large portion of the corrosion problems observed in particulate control equipment results from flue gas temperatures falling below the sulfuric acid dewpoint. A study for the U.S. Environmental Protection Agency (EPA) included an investigation of 11 fabric filters and 1 electrostatic precipitator (ESP) that had been affected by acid dewpoint corrosion. The study also included comments of design engineers at seven particulate control equipment manufacturers on the subject of acid dewpoint corrosion. Results of this study indicate that acid dewpoint corrosion is a serious problem that can destroy expensive particulate control equipment after only a few years of service or reduce particulate control efficiency and equipment availability. This paper discusses how many corrosion problems can be prevented or ameliorated by the use of thermal insulation, hopper heaters, sealing of entry hatches, control of process gas temperatures, and preheating during process startup.

INTRODUCTION

In 1978 the President's Council on Environmental Quality conducted a survey to identify the causes of excess emissions from controlled stationary sources that had initially been in compliance with emissions regulations. Inspection of 20 such sources showed that corrosion-related malfunctions in the control equipment were the primary cause of excess emissions at three sources and contributing causes at six others(1). Subsequent source inspections conducted for the Division of Stationary Source Enforcement (DSSE) confirmed that acid dewpoint corrosion is a common cause of malfunction in particulate control equipment(2). These inspections also revealed that many sources do not devote sufficient attention to acid dewpoint corrosion control when they select particulate control systems. In many cases proper corrosion control measures have been determined by trial and error, at great expense.

Based on these results, DSSE saw a need to assist particulate control equipment users and State Enforcement Agency personnel in coping with corrosion problems. They commissioned a study to characterize the effects that

*Presently with Mobil Research and Development Corp., Field Services Laboratory, P. O. Box 900, Dallas, Texas 75221

corrosion can have on the performance and operating life of particulate control equipment and to assemble guidelines to help reduce the frequency and severity of excess emissions incidents due to corrosion. The study included four phases--a review of the technical literature, the identification of emissions sources where control equipment corrosion was a problem, the inspection of a sampling of 18 of the identified sources, and a series of interviews with several particulate control equipment manufacturers. The 18 sources inspected included 11 fabric filters and 1 electrostatic precipitator (ESP) that had been affected by acid dewpoint corrosion.

The acid dewpoint generally refers to the temperature at which sulfur trioxide vapor (SO_3) will combine with water vapor to form sulfuric acid (H_2SO_4). SO_3 is found most frequently in flue gases produced by processes using sulfur-bearing fuels such as coal, coke, and oil. SO_3 can also be formed in primary metals-refining processes (e.g., copper smelting) because the ores typically contain large quantities of sulfur.

Combustion of sulfur-bearing fuel results first in the formation of sulfur dioxide (SO_2), some of this which is further oxidized to SO_3 The amount of SO_2 converted to SO_3 depends on many variables, including gas temperatures in the combustion zone, the configuration of the combustion chamber, and the availability of oxygen in the flame(3).

Sulfur trioxide and water have a tremendous affinity for each other; when temperatures are lowered to the dewpoint the two combine rapidly to form sulfuric acid molecules. The sulfuric acid molecules, in turn, have a high affinity for water; as they condense they draw additional water molecules from the gas stream forming a concentrated acid solution. Therefore, when flue gases containing relatively small concentrations of SO_3 reach the dewpoint temperature, droplets of concentrated sulfuric acid can condense on the cooler surfaces. For example, an 82.5 percent sulfuric acid solution (by weight) will condense at 148°C from flue gases containing as little as 40 ppm (by volume) SO_3 and 10 percent (by volume) water vapor(4).

Verhoff and Banchero developed an empirical relationship from which the dewpoint temperature can be calculated when the percentages of water vapor and sulfur trioxide are known(5).

$$T_{DP} = \frac{1{,}000}{1.7842+0.0269\log P_{H_2O}-0.1029\log P_{SO_3}+0.0329\log P_{H_2O}\log P_{SO_3}}$$

where

T_{DP} = dewpoint temperature in degrees kelvin

P_{H_2O} = vapor pressure of water in atmospheres

P_{SO_3} = vapor pressure of sulfur trioxide in atmospheres.

This equation has agreed with most experimental results to within about 7 degrees kelvin. In cases where measurement or estimation of SO_3 and water vapor concentrations is not practical, gross estimates of the dewpoint can be

based on sulfur content of the fuels(6). In either case it is advisable to add a factor of safety to the estimated dewpoint temperature to allow for variations in flue gas composition and to compensate for nonuniform flue gas temperature throughout the system.

FACTORS THAT CONTRIBUTE TO ACID DEWPOINT CORROSION

The following factors influence the tendency for acid dewpoint corrosion to occur: types of raw materials and fuels used in a process, temperature and moisture content of the flue gases, process operating cycles, and operation and maintenance practices.

Raw Materials and Fuels

Process raw materials are a primary source of sulfur and water in particulate-laden gases entering control devices. Ores, aggregates, recycled scrap metals, slags, and other raw materials may contain a variety of unwanted corrosive materials in addition to their primary economically valued components. For example, iron and copper ores contain high percentages of sulfur, some of which can be oxidized to SO_3 during refining processes. Aggregates used in the production of asphalt concrete typically contribute significant amounts of water vapor to the flue gases exiting the rotary dryer. Feedstocks for secondary lead blast furnaces consist primarily of lead-acid batteries, which contain sulfuric acid. Metallurgical slags, which are sometimes used as raw materials for rock wool insulation cupolas, can contain large quantities of sulfur that can oxidize to SO_3. Fossil fuels, especially coal, metallurgical coke, and residual fuel oils, also contain significant quantities of sulfur that can oxidize to SO_3 during combustion.

Flue Gas Temperatures and Moisture Content

High temperatures can damage fabric filter bags, protective coatings and linings, and fiberglass-reinforced plastic components. Gas temperatures can be reduced by dilution air dampers, quench chambers, or heat exchangers. Reducing gas temperatures, however, can set the stage for acid condensation. Therefore, when hot flue gases are to be cooled, it is important to determine their moisture and SO_3 contents so that the sulfuric acid dewpoint can be estimated. An inventory should be taken of all possible sources of flue gas water vapor including the water vapor added with dilution air or evaporative cooling and that which forms as a byproduct of fossil fuel combustion. If analysis indicates that flue gas temperatures will be close to the acid dewpoint, it is advisable to reduce the amounts of water vapor and/or SO_3 in the flue gases or to select an alternative particulate control strategy.

Process Operating Cycles

The operating cycles of a controlled process can sometimes influence the corrosion activity in a particulate control device. Operating cycles can affect dewpoint corrosion because of the close relationship between process variations and variations in flue gas temperatures. In general, the more frequently a hot process starts up and shuts down or varies between full production and partial production, the more frequently the flue gases in the control device will pass through the acid dewpoint.

Several operating cycles are possible in industrial processes, and each produces different flue gas temperature cycles. At one extreme is the characteristic cycle of a cast iron cupola, which typically operates for melts lasting less than 24 hours between startup and shutdown. While a cupola melt is in progress, there are frequent charges of fuel, scrap iron, and fluxing; periodic blasts of combustion air through the tuyeres; and frequent iron and slag taps. Each of these operations affects the temperature of the cupola flue gases. Wide fluctuations in cupola flue gas temperatures can be tempered by gas cooling devices such as dilution air dampers, quench chambers, and heat exchangers. It is often difficult, however, to simultaneously protect particulate control equipment from high-temperature stresses and acid dewpoint corrosion. At most fabric filter installations, high temperature protection has priority over dewpoint control because a single high-temperature excursion can do immediate damage, whereas dewpoint corrosion is a cumulative problem.

The other extreme in operating cycles is represented by the base-loaded utility boiler, which runs for months at a time near the maximum firing rate. Industrial boilers fall somewhere between the two extremes in operation. These usually operate for periods lasting 5 to 6 days, and their firing rates vary slowly during this period.

The significance of the operating cycle of a process must be considered when developing a corrosion control strategy for particulate control equipment. Variability in flue gas temperatures and chemical constituents may be a determining factor in the selection of a cooling device or a particulate control device.

Operation and Maintenance Practices

Operation and maintenance practices often affect corrosion activity in fabric filters and ESP's. Some process parameters affecting dewpoint corrosion can be controlled or partially controlled by plant operators. Maintenance practices such as the frequency of equipment inspections and the speed of repair of deteriorating parts are also important.

In attempting to control the sulfuric acid dewpoint, it is often advisable to preheat a cold fabric filter or ESP before introducing moist, sulfur-bearing flue gases(7). For processes having wide fluctuations in temperatures, it is advisable to vary the amount of dilution air or quench spray to match the changing temperatures, rather than presetting the amount of cooling for the highest expected temperature. Automatic cooling controls are preferable to manual controls. In processes such as cement kilns or hot-mix asphalt dryers, operators must avoid the temptation to lower process exhaust temperatures to save fuel without considering the effects the lower temperatures may have on dewpoint corrosion.

Changes in raw materials sometimes alter corrosion activity in a particulate control device. For example, a change in fuel from distillate oil to residual oil can increase the sulfur levels in the gases. A change in the source of coal can also change the amounts of sulfur introduced into the

system. Finally, the moisture content of raw materials and fuels that come from open storage can vary as rainfall varies.

Maintenance practices that can affect corrosion activity in particulate control equipment include the frequency of inspection of the various components and the speed at which malfunctioning components are repaired. Items that should be inspected frequently include temperature control instrumentation, hatches, hoppers, fans and fan vibration sleeves, insulation, fabric filter enclosures, and ESP enclosures.

CONTROLLING ACID DEWPOINT CORROSION

Most of the manufacturers interviewed during this study agreed that acid dewpoint corrosion can be adequately controlled in nearly all fabric filter and ESP applications. The principal means available for this control are reduction of SO_3 and moisture levels in the flue gases, control of exhaust gas temperatures, use of proper thermal insulation, and prevention of cool air inleakage into the control device. In some cases the use of protective coatings and special alloys can be helpful; however, the cost of the latter is usually prohibitive for the major structural components of fabric filters and ESP's.

Acid dewpoint corrosion is most likely to occur in locations where flue gas temperatures are the coolest or where steel surfaces are the coolest. Temperatures in dust hoppers are often cooler because gas detention is longer than at other locations (which allows more time for cooling) and because the hoppers have a large surface-to-volume ratio (which increases the rate of radiant heat loss to ambient air). Thus, hoppers without properly designed heaters or insulation are frequently affected by acid dewpoint corrosion. Outer walls (especially corners) of a filter or an ESP are often cooler and therefore subject to acid dewpoint corrosion (Figure 1). Entry hatches and hatch frames are also more likely to corrode because of cool air inleakage and because the hatches are often not as well insulated as the rest of the structure (Figure 3).

In the 11 fabric filters studied; dust hoppers, sidewalls, corners, entry hatches, filter compartment isolation dampers, and "top end" components such as bag support hardware and bag cleaning mechanisms were affected by acid dewpoint corrosion. Five fabric filter manufacturers reported that dust hoppers, top-end components, and bag hardware are the components most frequently affected.

ESP enclosures are subject to cooling effects similar to those in fabric filter enclosures; therefore, many corrosion problems reported in fabric filters also occur in ESP's. As in fabric filters, acid dewpoint corrosion often attacks dust hoppers, corners of the enclosures, access hatches, hatch frames, and the undersides of roof plates. It can also occur in penthouses that contain support insulators. At installations where flue gas temperatures are very low, acid dewpoint corrosion can attack structures within the ESP, such as discharge plates and discharge wires.

Reduction of Sulfur Trioxide and Moisture Levels

If there is no moisture inleakage into a control device, the levels of SO_3 and moisture in the flue gases depend on the levels of sulfur and water introduced with the process raw materials, fuels, combustion air, and gas cooling. The best ways to keep the sulfuric acid dewpoint temperature as low as possible is to select fuels and raw materials with as low a sulfur content as possible and to select dry-type flue gas cooling systems whenever possible.

It should be noted, however, that the use of low-sulfur fuels is no panacea for acid dewpoint corrosion. Low-sulfur coals and oils generate sufficient sulfur oxides when burned to cause acid dewpoint corrosion; the use of these fuels merely lowers the dewpoint temperature, which makes acid condensation easier to prevent. Economics usually governs the ultimate decision on the type of fuel to be used. Any cost analysis of available fuel options should consider the possible costs of corrosion damage to the particulate control equipment and lost production following corrosion failures as well as the relative costs of the fuels.

Control of Flue Gas Temperatures

Flue gas temperatures are a function of the process characteristics and of the flue gas cooling systems. Processes such as cast iron production are not amenable to flue gas temperature control at the process. Sources such as these require the use of flue gas cooling devices. Primitive systems such as a manually operated dilution air damper are usually not sufficient to insure that flue gases remain above the dewpoint. Control devices with temperature sensors that automatically control dilution air are preferable. Evaporative cooling is not recommended for cast iron cupolas using fabric filters, but recuperative heat exchangers have been used successfully.

In processes where operating conditions are relatively stable (e.g., cement kilns) it is sometimes possible to control exhaust temperatures by adjusting the firing rates and the amounts of excess combustion air. In such processes, it is helpful to have temperature sensors in the control device that can automatically control the process firing rates or sound alarms in the plant's control room whenever temperatures in the control device fall below a safe level. The increase in fuel consumption required to maintain high kiln exhaust temperatures must be weighed against the savings attributable to reduced corrosion in the particulate control system.

Another important means of controlling acid dewpoint corrosion is to preheat the control device prior to the introduction of corrosive flue gases(7). For example, a rotary dryer can be preheated by firing the burner at a reduced rate for a limited time before introducing the wet aggregate. A cupola can be preheated by firing natural gas afterburners for a limited time before lighting the sulfur-bearing coke charge. The advantage of preheating is that the hot corrosive flue gases will not contact cold steel surfaces in the control device during startup as would occur without preheating. As in the case of other flue gas temperature control measures, the advantages of preheating must be weighed against the additional fuel expenses.

Thermal Insulation

Thermal insulation is another means of maintaining flue gas temperatures above the acid dewpoint. The ultimate purpose of insulation is to reduce the amount of flue gas cooling that takes place between the time the gases enter the ducting to the control device and the time they exit the stack. At some installations insulation alone will solve acid dewpoint corrosion problems; in others it is only a supplementary measure.

Insulation will be most effective if a few simple guidelines are followed(8). Any insulation must be thick enough to impede sufficiently the flow of heat through the external surfaces of the control device. The insulation also must cover all exposed surfaces including the dust hoppers, access doors, and the ductwork. It must be installed in such a manner that it will remain intact over the life of the equipment. Most types of insulation should have a protective sheath (usually sheet metal) on the outside to repel rainwater and to prevent mechanical damage. An insulation blanket must be sealed at the top and bottom to prevent a "chimney effect" circulation of air underneath the blanket. Windbreaks can also be helpful in insulating a fabric filter or an ESP. An example of a properly insulated ESP is shown in Figure 2.

Among the common errors made in insulating control equipment are the failure to insulate all exposed ductwork (including reverse air ductwork in fabric filters), the failure to insulate hatches, and the failure to attach the insulation securely. Another common error (Figure 4) is to allow structural members to protrude through the blanket of insulation; these members radiate heat away from interior surfaces of the control device and foster condensation at these locations.

Air Inleakage

Unexpected air inleakage can spoil a well-designed acid dewpoint control program in a fabric filter or an ESP. Inleakage not only allows moisture from the ambient air to enter the control system, but also causes severe localized cooling at the point of entry. Both phenomena can contribute to acid dewpoint corrosion. Inleakage is a self-feeding process--the metal adjacent to the initial penetration tends to corrode at an accelerated rate, which promotes enlargement of the penetration. Inleakage is common in poorly fitting hatches, hatches with worn seal gaskets, rotary air locks with worn seals, cracked vibration sleeves, and incomplete welds. It can also occur in ductwork or at the process. Inleakage should be repaired promptly to avoid further damage.

Special Alloys and Protective Coatings

The relatively large size of most fabric filters and ESP's makes it uneconomical to use higher priced stainless steels or nickel alloys as the principal materials of construction. Most structural components of these devices are constructed of carbon steel or, in some cases, Corten or cement block. Special alloys are used, however, for some of the smaller components within these devices, such as filter bag hardware and ESP discharge wires.

Nearly all exterior surfaces of fabric filter and ESP enclosures receive a protective coating; however, the interior surfaces of these devices are not always coated. One fabric filter manufacturer reported that only 10 percent of its filters receive internal coatings. The reason that interior coatings are not always used is that few seem to be very effective on hot sources. Despite claims of some coatings manufacturers, long-term performance of most available coatings systems is not good in hot corrosive flue gases. All control device manufacturers interviewed reported that most coatings fail when exposed for prolonged periods to acid-bearing flue gases with temperatures above 300 to 400°F. In cases where a coating is appropriate, it is important that the coating be applied in the proper manner to a properly prepared surface. In most cases this requires that the coating be applied in the shop rather than in the field.

ENDNOTES

1. Booz, Allen, and Hamilton, Inc. Final Evaluation of North Carolina's Program to Regulate Air Pollution From Stationary Sources. Prepared under President's Council on Environmental Quality, Contract No. EQ8AC015, Bethesda, Maryland, July 1, 1979.

2. PEDCo Environmental, Inc. Unpublished data obtained during SIP audit inspections under contract to the U.S. EPA, Division of Stationary Source Enforcement, Contract No. 68-01-4147, Tasks 110, 131, and 137, 1979-80.

3. Balasic, P. J. Electrostatic Precipitator Corrosion Problems on Recovery Boiler Applications. Paper No. 185, presented at the National Association of Corrosion Engineers, Corrosion/79, Atlanta, Georgia, March 12-16, 1979.

4. Pierce, R. P. Estimating Acid Dewpoints in Stack Gases. Chemical Engineering 84(4): 125-28, 1977.

5. Verhoff, F. H., and Banchero, J. T. Chemical Engineering Progress, Vol. 70, p. 71, 1974.

6. Katz, J. The Art of Electrostatic Precipitation, Chapter 7. Precipitator Technology, Inc., Pittsburgh, Pennsylvania, 1979.

7. Beggs, T. W., and U. M. Patankar. Accelerated Baghouse Corrosion in a Waste Oil Burning Asphalt Concrete Plant. Presented at the 72nd annual meeting of the Air Pollution Control Association, Cincinnati, Ohio, June 24-29, 1979.

8. Landrum, R. J. Equipment. Chemical Engineering 77(22): 75-82, October 12, 1970.

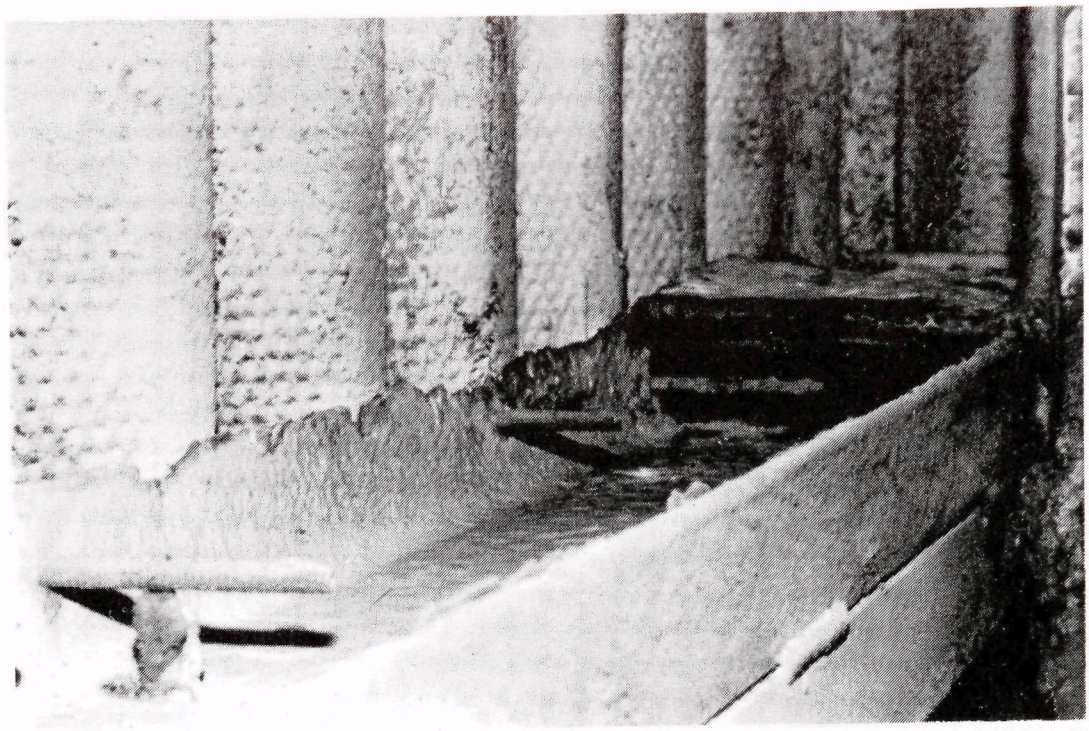

Figure 1. Closeup of a cupola fabric filter cross member showing that dewpoint corrosion is more severe along surfaces nearest the cooler outer wall (the outer wall is constructed of corrugated transite).

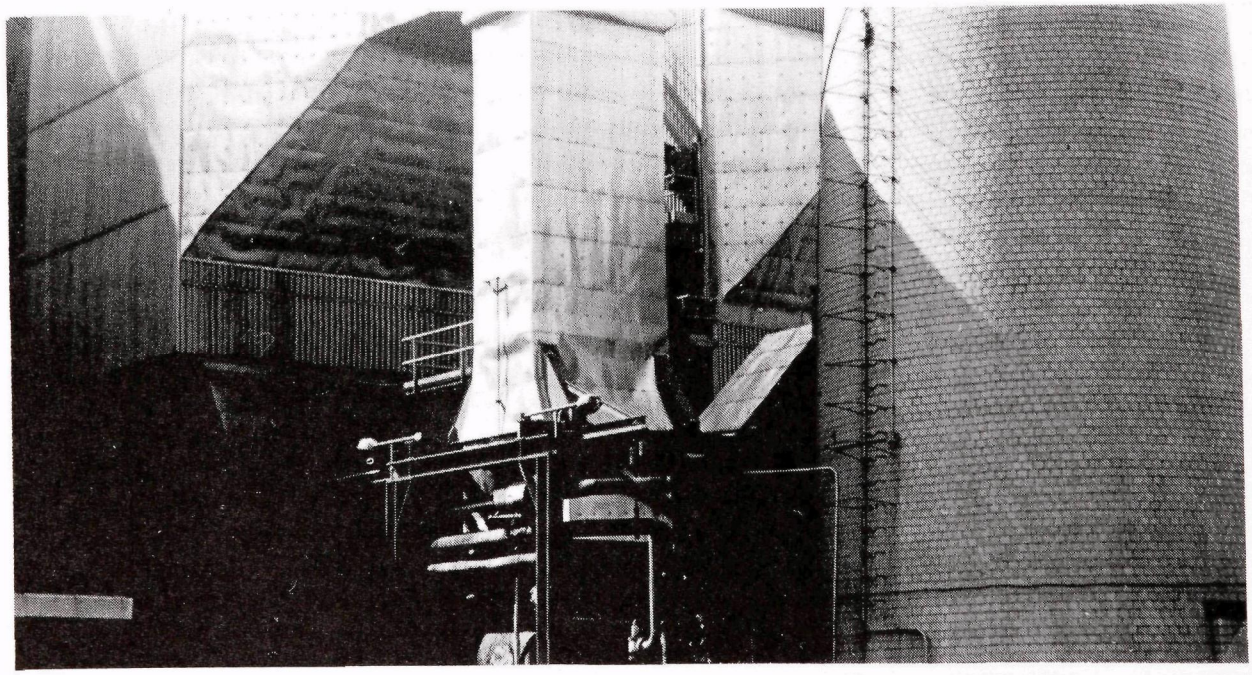

Figure 2. Electrostatic precipitator with a complete blanket of insulation covering the chambers, hoppers and ductwork.

Figure 3. Corrosion of fabric filter access door and door frame. Opening permits inleakage of cool ambient air, accelerating condensation and further corrosion.

Figure 4. Insulated fabric filter with structural steel protruding through the insulation blanket. The exposed steel radiates heat away from the filter, promoting cold spots along the interior of the filter.

SECOND GENERATION OF EMISSIONS CONTROL SYSTEM FOR COKE OVENS

By
James D. Patton
Consultant on Coke Side Shed Systems
MikroPul Corporation
Summit, New Jersey U.S.A.

ABSTRACT

The body of information in this paper is directed to coke oven operators and their management, to the Environmental Control and Protection Agencies, and labor organizations interested in further protection of their members.

There are a number of areas of concern in pollution control for coke ovens. We are directing our efforts to properly control all the emissions on the coke side of the ovens.

In the past four to five years the interest in Coke Side Sheds has been set aside in favor of a number of concepts relating to "land base systems", traveling hooded hot cars, etc. Each of these systems looked favorable, but some have not proven out for a variety of reasons, others have worked well. Some were not as dependable as expected and for others the maintenance costs were high. Lately, many of these companies are looking for a system that meets the required standards, is more dependable and requires a minimum of maintenance.

The author of this paper is co-inventor of the "Roe-Patton" Coke Side Shed, U.S. Patent 3,844,901, offered through Great Lakes Carbon Corporation and promoted by the MikroPul Corporation. This has been the most successful shed system to date.

The author is also the inventor of the "Patton" Emission Control System, U.S. Patent 3,972,782, acquired by MikroPul as the latest in shed technology. Its unique design overcomes the two major objections to the original G.L.C. shed: fallout of the large particulate during the push and fume escaping the hood during periods of adverse wind conditions. With the improved air flow, it proposes to be the cleanest and most efficient "Coke Side Shed" to date.

MikroPul's newest adaptation to the "Patton" system has incorporated the baghouse filtering system within the coke side shed structure, requiring no ductwork, reduced energy requirements, and many other cost reducing factors.

The author believes this to be a major breakthrough in new technology and is worthy of consideration where adaptable.

INTRODUCTION

A coke side shed is a special designed structure that is erected on the coke delivery side of a battery of coke ovens. Its purpose is to capture all the emissions developed on that side of the ovens. There can be emissions on the coke side from the following sources:

1. Removal of the coke oven doors.

2. The actual pushing of the incandescent coke from the oven slot through the coke guide and falling into a waiting quench car.

3. At times there is slight spillage on the bench area that is hand-shoveled back into the open oven causing emissions.

4. In some cases there could be emissions at the door seals after replacing the oven doors or around the door frames if the ovens are older and in need of repairs.

In fact, we believe the coke side shed control system is the only type system that can completely control this many emission points with one approach. In order to talk about the second generation of coke side sheds, I must mention the basic principals of the original shed system. Being the co-inventor of this system, I would like to compare this original system with my later developments.

Since MikroPul Corporation has been marketing this first shed system through Great Lakes Carbon Corporation, it shall be referred to as the MikroPul-G.L.C. shed system. Great Lakes Carbon owns the patent and MikroPul has the exclusive sales rights.

For illustrative purposes, we are using the following symbols to aid in the following slides.

Figure 1

(A) Thermal wall panel.

(B) Thermal heat deflector.

(C) Throat or structure orifice.

(D) Capture and expansion zone.

(E) Evacuation duct.

(F) Filter or cleaning device.

(G) Fallout capture area.

(H) End walls.

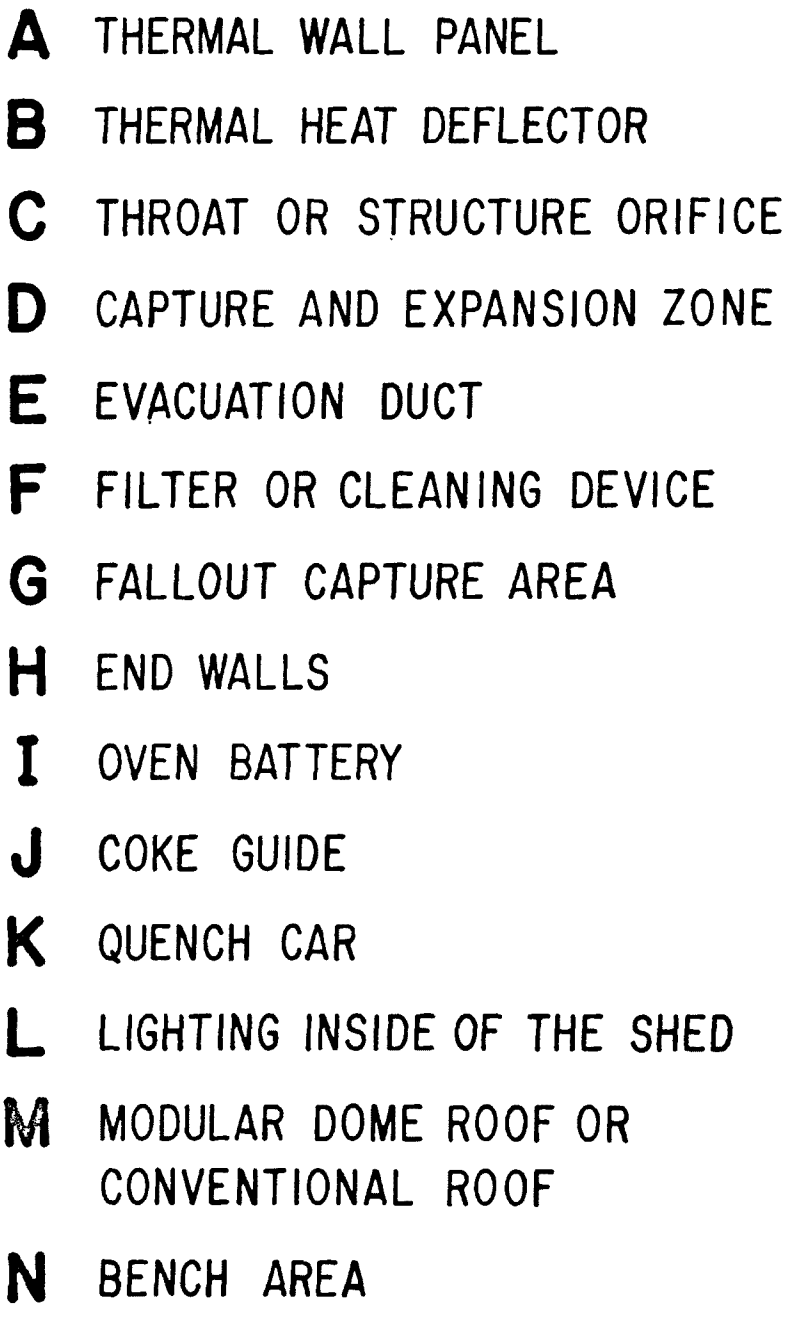
A THERMAL WALL PANEL
B THERMAL HEAT DEFLECTOR
C THROAT OR STRUCTURE ORIFICE
D CAPTURE AND EXPANSION ZONE
E EVACUATION DUCT
F FILTER OR CLEANING DEVICE
G FALLOUT CAPTURE AREA
H END WALLS
I OVEN BATTERY
J COKE GUIDE
K QUENCH CAR
L LIGHTING INSIDE OF THE SHED
M MODULAR DOME ROOF OR CONVENTIONAL ROOF
N BENCH AREA

Fig. 1

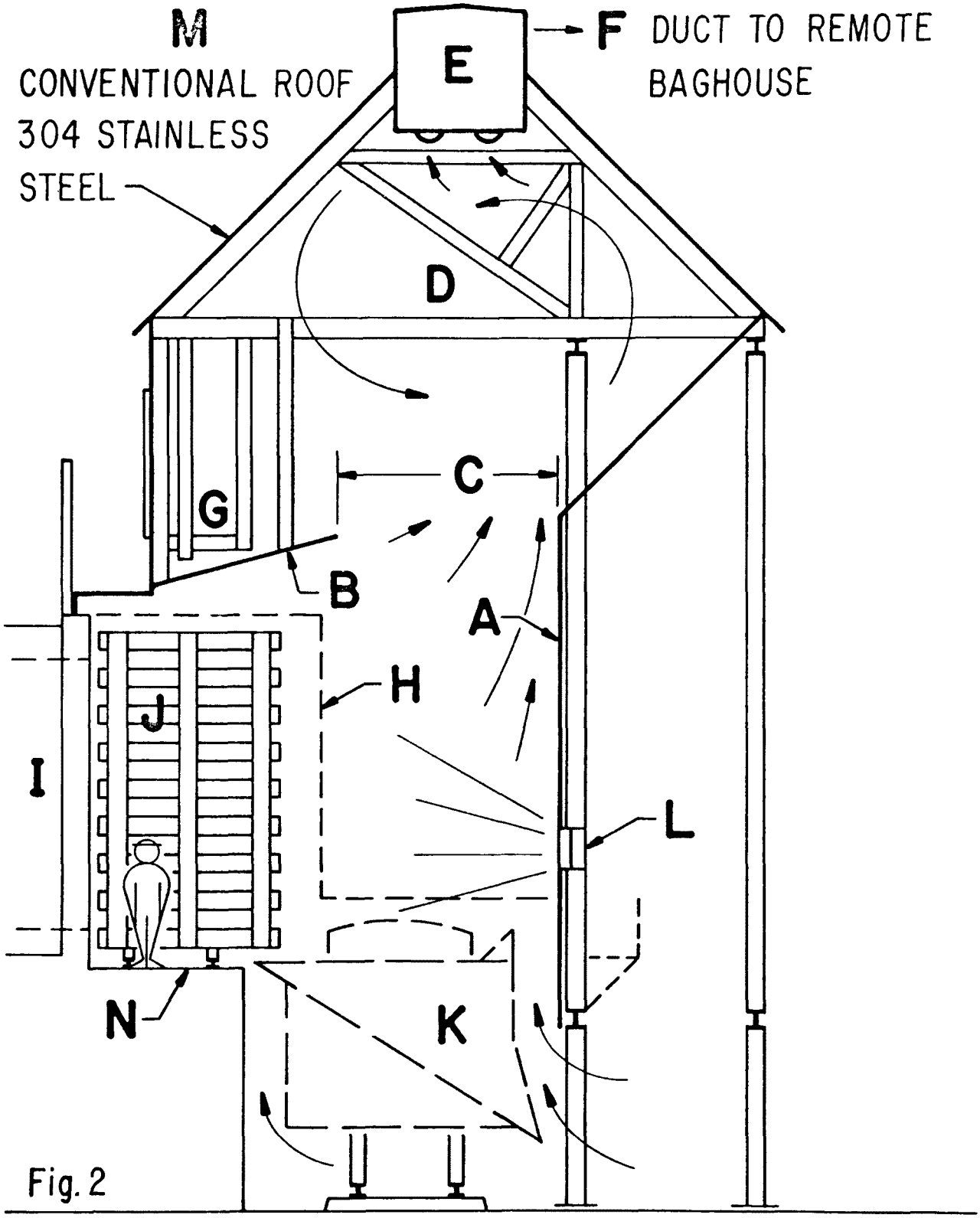

Fig. 2

MIKROPUL – G.L.C. COKE SIDE SHED

(I) Oven battery.

(J) Coke guide.

(K) Quench car.

(L) Lighting inside of the shed.

(M) Modular dome roof or conventional roof.

(N) Bench area.

Figure 2

This is a cross section of the MikroPul-G.L.C. shed system. This is the system that has operated successfully at four major steel plants since 1975 and is presently being installed on ten additional coke ovens.

(I) is the area where the pulverized coal is heated to 1800^{o}F to 2200^{o}F for a period of 16 to 24 hours, depending upon the type of coke produced. (J) is the coke guide used to direct the incandescent coke across the bench area (N) and into the waiting quench car (K). When this movement occurs, there is a great thermal mass released. This thermal discharge is confined by the thermal wall panel (A) which confines the mass and causes it to be driven upwards toward the throat or orifice (C). Any heat release coming from the face of the ovens is directed up to the heat deflector (B) which also directs the thermal mass into the throat (C). This area (C) is critically sized to cause the gas velocity to be increased and directed up and over back toward the oven area. The flow is directed downward and back up in a swirling action. By a constant controlled air flow through the orifice (C), the mass is contained in area (D) known as the capture and expansion zone. As the thermal mass is driven up into this zone, it expands the length of the structure. During this time the smaller airborne particulate is being evacuated through the evacuation duct (E) to an offsite filter or cleaning device.

At the same time all this movement is taking place, the natural forces of gravity are taking place. As the contaminated air is cooled, the heavier particles fall out. In this design, MikroPul-G.L.C., there is only one area that actually captures the fallout, that is area (G) on top of the heat shield. This is good, as it does not fall right back on the people working on the bench (N). But this only collects about 1/3 of the fallout generated. The balance falls back through the throat (C) and onto the inclined siding and down the thermal wall panel (A). By this fallout getting back into the working area and the normal flow of incoming air going up toward the orifice, it causes a slight disturbance. This one factor has caused some controversy. Being that this fallout coming back down is of such size that it's too large to be inhaled by the workers, but becomes a slight annoyance when it gets into their collars, etc. In spite of this condition, the men who have worked under a shed prefer it over no shed at all. It is cooler in the hot weather and they are protected during the inclement weather. The ends of the structure are extended down as close to the coke guide (J) and quench car (K) and engine as possible. This helps keep the emissions confined so they can be directed upwards to the evacu-

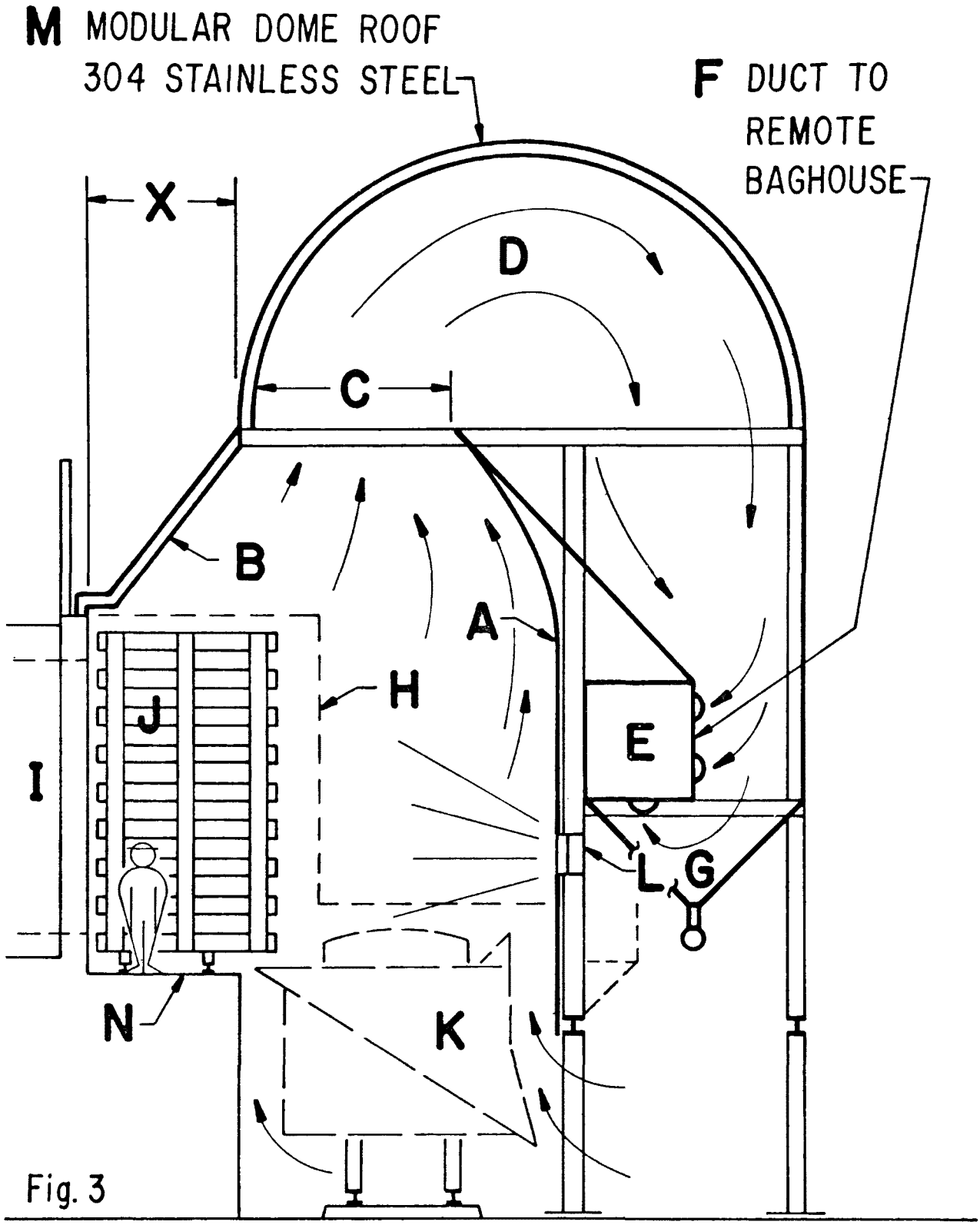

Fig. 3

MIKROPUL-PATTON COKE SIDE SHED

ation duct for proper processing. On an extremely windy day there can be some end blow out.

One area of attention on the MikroPul-G.L.C. shed system is the fallout that is collected up on top of the thermal heat deflector (B). The accumulation of material in this area must be cleaned out on the average of every three to six months. This can be done manually or by vacuuming. Aside from this, the maintenance on this system is almost nil, mainly because it has no moving parts and the outside siding is of 304 stainless.

The earlier coke side shed systems used MikroPul "Elektrofil" wet electrostatic precipitators as the air cleaning device. In terms of pollution control, this was a relatively new application with no prior history from which to draw. The selection of the wet electrostatic precipitator was made primarily due to its ability to tolerate the hydrocarbons in the gas stream and collect the particulate at acceptable efficiencies. While in every case these systems performed successfully, the main objections to the use of the WEP were the initial high cost and the cost of maintenance due to corrosion, plus an expensive water treatment plant.

An extensive testing program was conducted with pilot Mikro-Pulsaire baghouses on existing coke side shed. The results showed that the use of a dry additive pre-coat, such as limestone, to act as an absorber, would prevent the bags from blinding. While the principle of dry additive injection has been well known for many years, its application has been limited primarily to low-ratio type baghouses. In recent years MikroPul has been successful in applying it to huge installations in the aluminum industry. The Mikro-Pulsaire reverse jet type baghouse is now used exclusively on our coke side shed systems and is widely specified in the competitive land-based system concept.

Figure 3

This is the cross section of the "second generation" of coke side shed emissions control system. This is to be known as MikroPul-Patton shed design. MikroPul has acquired complete patent rights of this concept.

This concept is very similar to the original but offers some very important improvements that have corrected the problems that exist in original shed concept. The distance (x) is closer to the oven face (I) permits the flow of air to pass closer to the oven doors. This gives improved ventilation in the bench area (N) where the men work. The thermal wall panel (A) is in the same position to the quench car (K) as in the original, but as the thermal mass is forced upward, it turns into the throat or orifice area (C) and the thermal heat deflector (B) comes together closer to the oven. The throat or orifice (C) is narrow causing the velocity of the thermal mass to increase. It comes in contact with the modular dome roof, which due to its configuration, quickly directs the air flow mass over into a true capture and expansion zone (D). Since the distance across the dome area (D) is twice the orifice (C) distance, this slows the air flow down by half and the air mass expanding and traveling the length of the expansion zone (D) is greatly slowed down. Cooling is taking place during this period and the natural forces (gravity) are causing the heavier particles to fall out of the air stream. Different from the original

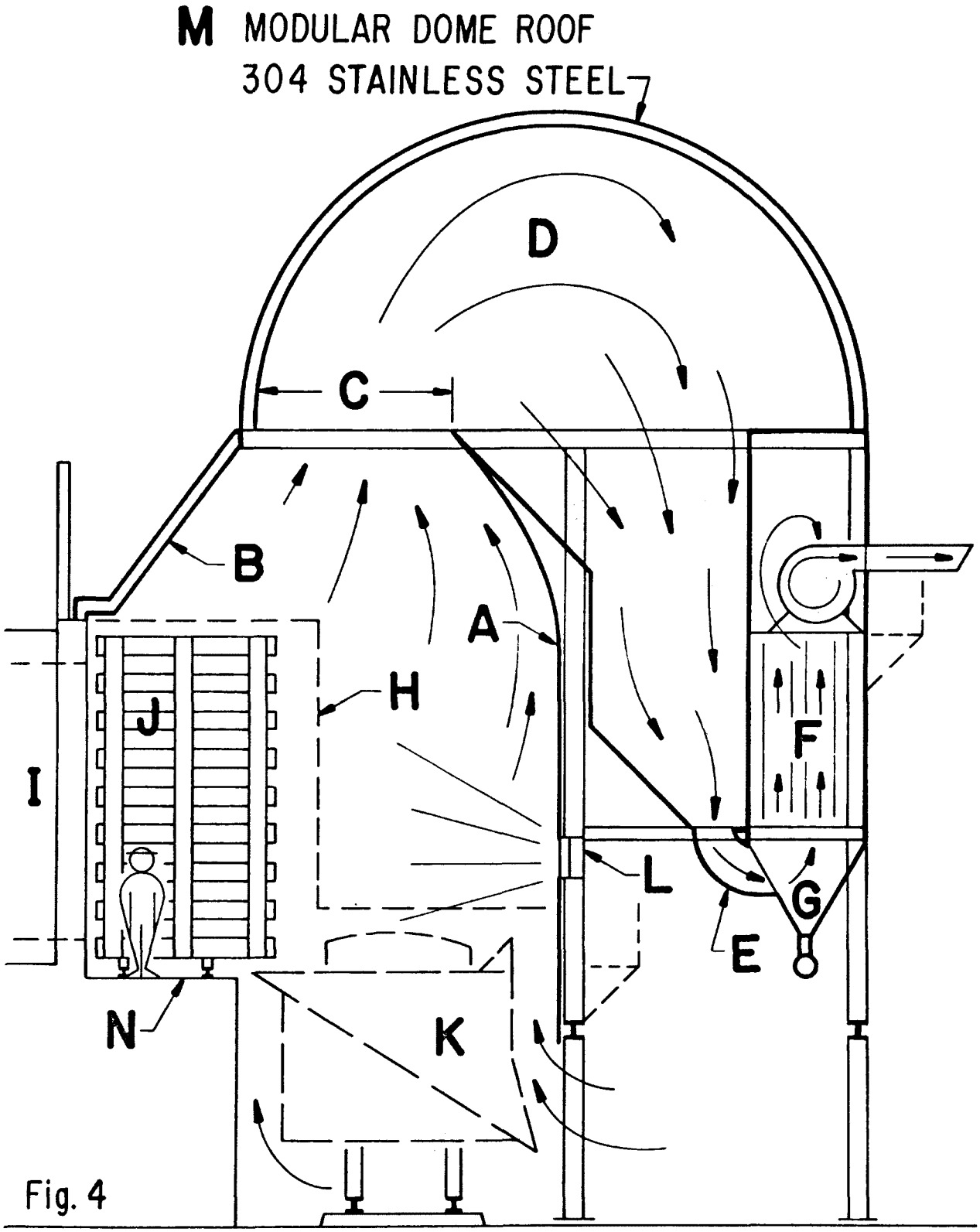

Fig. 4

MIKROPUL-PATTON COKE SIDE SHED

concept, here the completely captured volume is directed downward and the smaller particles are sucked into the evacuation duct (E) which is connected to an offsite baghouse cleaning device.

As another improvement, the complete volume taken in the structure along with the emissions has to pass through zone (D) to the cleaning system. Once the thermal mass is beyond the peak of the thermal wall panel (A) the particulate laden air flow is in complete entrapment and under positive control. The fallout captured in this system falls down into a hopper for controlled removal by mechanical or vacuum conveyance.

By comparison with the original concept, it is easy to see the more positive control we have in this second generation concept. The dome (M) is of modular design and type 304 stainless. The structure has basically no weight on the oven buckstays. Doors and buckstays can be serviced with proper equipment. The ends (H) are very similar to the original shed concept but the end blow through is under better control as the mass of emissions are completely locked in area (D) and not affected by windy days.

The MikroPul-Patton shed design offers a good positive lighting system (L) with proper means to service it. This system is adaptable to most oven installations and offers a more desirable working area for the workers on the bench (N). The maintenance on this system is almost nil and the reliability approaching 100% for continuous operations, tops all known systems.

Figure 4

This is a cross section of the latest in technology, the MikroPul-Patton coke side shed with a series of modular baghouses incorporated within the structure. As you will notice the air flow is the same as shown in Figure 3, only the capture and expansion zone (D) comes down lower and connects with the evacuation opening (E). This is connected through a controlled opening and enters into the bottom of the modular baghouses (F). This opening (E) is where the precoat system is attached to precoat the filter bags. The air volume travels up through the bags and up through a chamber before going through the exhaust fans to the atmosphere. These modular baghouses are constructed so any one can be serviced without a noticeable difference in performance. Say the structure had 20 bays and 20 baghouses. If one unit had to be shut down for service, it would increase the evacuation time by approximately six to eight seconds. This system is the same as Figure 3 where the complete air volume drawn into the structure has to pass through the filtering devices before exhausted to the atmosphere. At this point we meet all existing requirements for allowable emissions.

This concept needs a slight more width than the Figure 3 concept, but the savings on real estate required and long ductwork to an offsite cleaning device is considerable. The power demand is almost one-half of the other two systems. This integral filtering concept is adaptable to many installations, but not all, as if there is too much in-plant interference it is not practical. For any new installation, this system should be given much consideration in the early planning stages.

METHOD OF CONSTRUCTION TO AID IN MINIMUM INTERFERENCE WITH NORMAL OPERATIONS

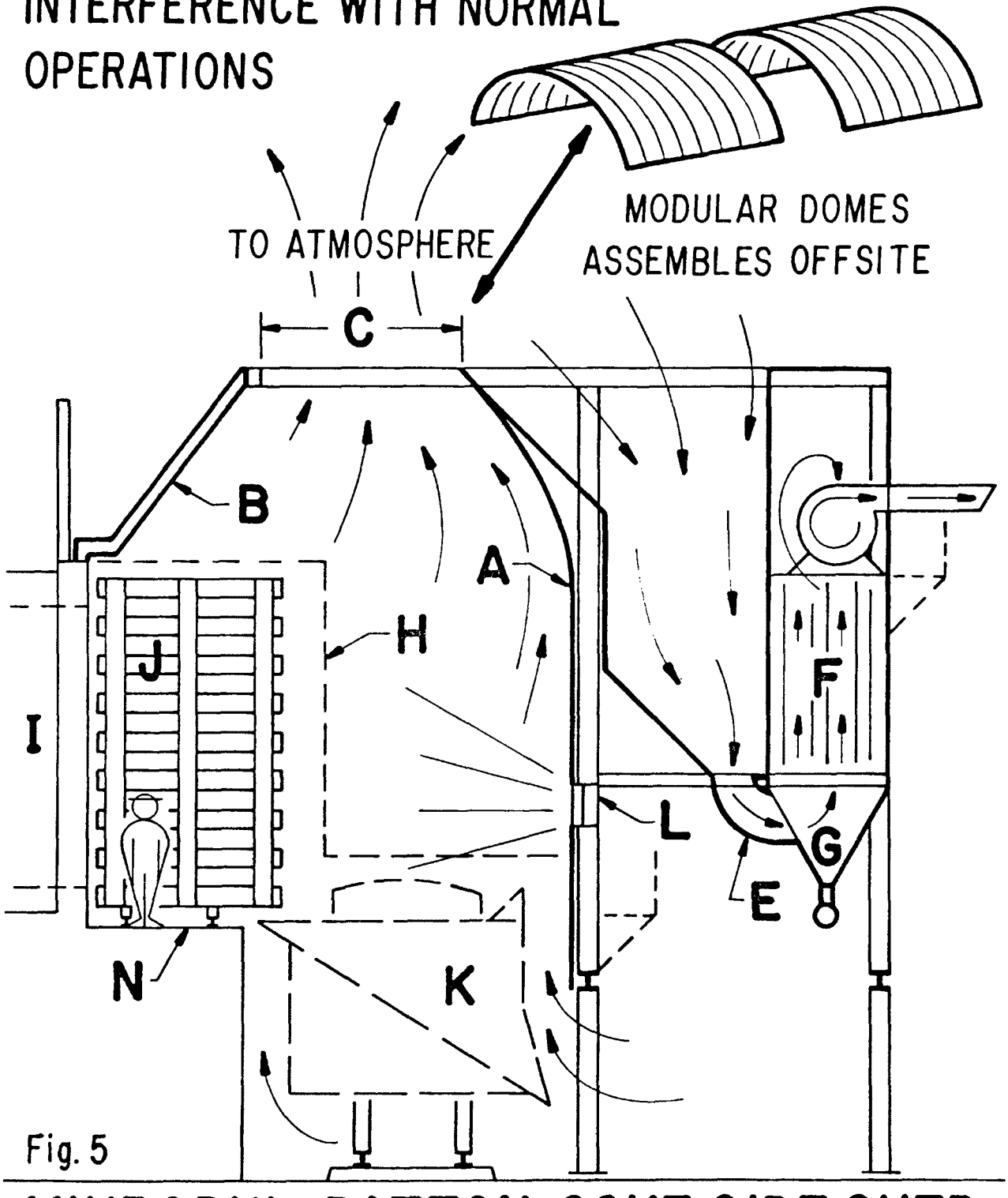

Fig. 5

MIKROPUL-PATTON COKE SIDE SHED

Figure 5

This is a cross section showing how the MikroPul-Patton shed concept is erected in a simple fashion so as to interfere with normal operations as little as possible.

As you see in this figure, the basic structural is erected with thermal wall panel (A) and thermal heat deflector (B) leaving opening (C) open to the atmosphere during construction. The hoppers as part of (D) and (E) and the end walls (H) are installed. Then the filtering devices (F), baghouses of modular design, are fit in place in each bay of the structure. All of this is to be completed and started up before the final capping of the dome. The dome is type 304 stainless and is pre-assembled offsite in approximately 30 foot sections. These sections, being very light but extremely strong, are hoisted into place. When the last section is fitted in place, the shed concept is totally operational.

CONCLUSION

The coke side shed emission control concept is only one of a number of concepts in this area of control. MikroPul, being the forerunner in the shed concepts, has a number of successful operating installations and many new orders are in engineering and fabrication stages. The latest association with the patented "Patton" shed concept provides us with new and improved technology, enabling us to offer a coke side shed for almost any existing or new coke oven facility. This is a part of MikroPul's continuing effort to reduce costs and offer reliable emission control systems to the coking industry. We refer to these latest developments as "The Second Generation of Coke Side Sheds".

EFFECTS OF FLYASH SIZE DISTRIBUTION ON THE PERFORMANCE OF A FIBERGLASS FILTER

By
William F. Frazier
Wayne T. Davis

The Department of Civil Engineering
The University of Tennessee
Knoxville, Tennessee 37916

ABSTRACT

This study was undertaken to quantify the effects of flyash size characteristics on the pressure drop and efficiency of a conditioned fiberglass fabric filter typical of the fabrics being utilized in fabric filter particulate collectors on coal-fired boilers. These effects were determined by conducting a series of filtration tests in which six flyash dusts, each with a different size distribution, were used to determine the performance. The range of mass mean diameters was 3.5-13 μm.

Graphs are included showing the experimentally measured relationships between particle penetration, residual pressure drop and coefficient of resistivity for the six flyash size distributions on the conditioned fiberglass fabrics.

INTRODUCTION

The fabric filter is one type of high efficiency dust collector whose performance, as measured by its pressure drop and dust penetration is affected by the size characteristics of the dust being collected. Collection of smaller size flyash particles creates the potential for a higher fabric pressure drop due to the formation of a dust cake of more finely divided particles as well as decreased collection efficiency (or increased penetration) of the particles. This study was undertaken to quantify the effects of flyash size characteristics on the pressure drop and efficiency of a conditioned fiberglass fabric filter typical of the fabrics being utilized in fabric filter particulate collectors on coal-fired boilers.

Experimental Facility

To accomplish the above objective, a pilot plant fabric filter collector containing a single 30' x 11½" diameter filter bag was used. The system (shown in Figure 1) provided for operation at a constant temperature, humid-

ity, and filtration velocity. During the filtration cycle, the test filter compartment was in a closed loop with an environmental control room which was utilized to maintain system temperature and humidity. Compartment flow was maintained by a damper which was controlled by a Dwyer Photohelic on/off controller. The controller was activated by the pressure differential across an orifice plate located in the ductwork on the downstream side of the filter bag.

At the initiation of the cleaning cycle the test filter compartment was placed in a closed loop with the reverse-air conditioning compartment. This latter compartment supplied a source of cleaned air to reverse-air clean the test fabric. The reverse-air conditioning compartment was required to prevent carry-over of dust from the test filter compartment into the control room or laboratory during the reverse-air cleaning cycle. The reverse-air flow was determined by the pressure differential across an orifice plate calibrated with a standard type pitot tube and inclined water manometer, and was controlled by a manually adjusted damper.

During each filtration cycle, flyash test dust was injected from a Vibrascrew dust feeder (located in the environmental control room) into the duct leading to the filter compartment. The flyash utilized in this study had a mass median diameter of 13.0-14.0 μm and was obtained from the hoppers of an electrostatic precipitator installed at a nearby pulverized coal-fired boiler (Kingston Steam Plant, Tennessee Valley Authority). In order to produce six different size distributions, it was necessary to pass the particle-laden air leaving the environmental room through various configurations of precleaners. By controlling the inlet loading with the Vibrascrew feeder and the particle size distribution with the precleaners, it was possible to produce six size distributions of flyash as shown in Table 1. Also included in the table is the equivalent surface mean diameter, $\bar{d}_{32}$, for each dust. The $\bar{d}_{32}$ was employed in this study since it has been found to be related to the resistance through packed beds of granular material (1).

The same style of fabric material was used throughout the test program. The fabric was a 14.5 ounce/square yard fiberglass woven fabric with a 3 x 1 twill and an air permeability of 30-45 CFM/ft^2 at 0.5" H_2O. A new filter bag was installed in the filter test compartment prior to testing each different flyash size distribution to eliminate any conditioning effects caused by interaction of the different dusts.

The two performance parameters which were used as direct measures of the performance were (1) the pressure drop across the fabric and (2) the particle penetration, Pn, defined as

$$Pn = 1 - (\text{Efficiency}/100\%)$$

The fabric penetration was monitored by extracting (1) an isokinetic sample through a filter followed by gravimetric determination of the weight gain on the filter, (2) and an isokinetic sample into a Climet Model 208/210 optical particle counter (OPC) and multichannel analyzer (MCA) (0.3-10.0 μm range). Measurements using the gravimetric technique were conducted to determine the overall average efficiency of the filter for an entire filtration

TABLE 1. PARTICLE SIZE DISTRIBUTION OF FLYASH

Test	Mass Median Diameter	Geometric Standard Deviation	$\bar{d}_{32}$
1	13.0 μm	2.2	9.5 μm
2	9.5 μm	2.1	7.2 μm
3	7.7 μm	2.1	5.8 μm
4	7.1 μm	2.0	5.6 μm
5	4.0 μm	1.8	3.4 μm
6	3.5 μm	1.9	2.8 μm

cycle. The optical particle counter was used to obtain the temporal resolution needed to measure changes in the filter penetration during each filtration cycle (updated every 24 seconds).

The operating conditions for all of the tests were as follows: a filtration velocity, V, of 0.64 m/min (2.1 feet/minute); reverse-air cleaning ratio, R/A, of 0.49 m/min (1.6 feet/minute); a temperature, of 38°C ± 5°C; a relative humidity, of 40% ± 5%; and a mass loading, C_i of 6.9 grams/m^3 (nominal).

Analysis of Data

The performance data were analyzed in this study in a manner similar to the EPA Filtration Model for Coal Flyash with Glass Fabrics (1). Normalized performance curves were constructed from the data obtained after each filter had reached a conditioned state by transforming the fabric pressure loss data to normalized filter drag, $\Delta P/V$, and time to areal cake density, $C_i Vt$. Figure 2 is a schematic of a drag performance curve. The slope of the linear portion of each performance curve, referred to as the specific resistance coefficient, K_2, was determined for each test. The intercept of the linear portion of the curve with the ordinate was defined as the effective residual drag, S_E, for the conditioned fabric. The residual fabric drag, S_R, was the value of initial drag after the fabric had been cycled through sufficient filtration and cleaning cycles to reach a conditioned state. The initial slope of the fabric drag performance curve, defined as the conditioned residual specific resistance coefficient (K_r), was also determined for each test. The equation describing the filter drag performance curve was as follows:

$$S = S_R + K_2 W + (S_E - S_R) \left[1 - \exp \left(\frac{-W(K_r - K_2)}{S_E - S_R} \right) \right] \qquad \text{(eq. 2)}$$

where $W = C_i Vt$ and represented the dust cake added to the fabric during each filtration cycle.

Fabric penetration, Pn, versus time, t, was also recorded for each fabric after it had reached a conditioned state. Figure 2 also shows a schematic of a fabric penetration performance curve. The relationship between penetration and areal cake density, $C_i Vt$, was described by the following equation:

$$Pn = Pn_s + (Pn_o - Pn_s) \exp(-aW) \qquad \text{(eq. 3)}$$

where Pn = penetration at time, t
Pn_s = steady state penetration
Pn_o = initial penetration
W_o = actual fabric loading above residual ($C_i Vt$)
a = concentration decay function

In this study, the initial penetration, Pn_o, was measured at one minute into the filtration cycle. The steady-state penetration, Pn_s, was measured near the end of the filtration cycle. The decay constant "a" was determined for each penetration performance curve.

Results

The above equations 2 and 3 described fabric drag and penetration using the performance parameters S_E, S_R, K_2, K_r, Pn_o, Pn_s and a. In this study, the average value of each performance parameter was determined for each of the six size distributions that were tested. The results of the filtration tests have been summarized graphically to illustrate the basic relationships between the surface mean diameter, $\bar{d}_{32}$, and each of the above performance parameters.

The effects of $\bar{d}_{32}$ on the effective residual drag S_E, the residual drag S_R, and the residual resistance coefficient, K_r, are shown in Figure 3. A least squares fit was determined for the data obtained on each performance parameter. The relationships illustrated in Figure 3 showed that the parameters S_R, S_E, and K_r were relatively independent of the surface mean diameter, d_{32}, for distributions for which d_{32}, was greater than 6 μm. For values of d_{32} less than 6 μm, however, large changes in the fabric drag parameters were observed. For example, the residual fabric drag, S_R, doubled when d_{32} was reduced from 4 to 3 μm.

Figure 4 illustrates the relationship between K_2 and $\bar{d}_{32}$. A least square fit was performed on this data to illustrate the relationship between $\ln K_2$ and $\ln \bar{d}_{32}$. The following equation was the result of the least square fit:

$$K_2 = 10.94\ \bar{d}_{32}^{\,-1.28}$$

where the units on $\bar{d}_{32}$ and K_2 were micrometers and newton-minutes/gram-meter, respectively. This relationship is in qualitative agreement with other re-

searchers who have found K_2 to be proportional to $\bar{d}_{32}^{-1}$(1,2,3).

Figure 5 illustrates the relationship between the parameters Pn_o and Pn_s and the surface mean diameter $\bar{d}_{32}$; the values of Pn_o and Pn_s were found to increase as $\bar{d}_{32}$ was decreased. These data are in agreement with other research efforts which have shown fabric penetration to increase as the particle diameter was decreased (1,4,5). It is significant to note that the reproducibility of the penetration measurements was found to be approximately one half an order of magnitude due to real variations in the penetration between successive cycles. The decay constant, a, presented in Equation 2 was not found to be significantly dependent on $\bar{d}_{32}$. The mean value of a for the six different size flyashes tested was 0.04 m^3/gram. Best fit equations were calculated for the relationships between each of the fabric performance parameters and the surface mean diameter, $\bar{d}_{32}$ (See Table 2.)

Figures 6 and 7 illustrate the effect of $\bar{d}_{32}$ on the performance curves of filter drag and penetration, respectively for the data in this study. The solid lines superimposed on the data represent the curves obtained by applying the equations summarized in Table 2.

Discussion

The data obtained in this study were obtained on a specific style of fabric using six different flyash distributions. The effects of particle size on fabric performance may be different for other dust/fabric combinations. However, the effects of particle size on fabric drag and penetration for the fabric and dust used in this study demonstrate the need to quantitatively evaluate the effect of particle size on fabric performance for various dust/fabric combinations.

The results of this study indicate that the best fabric performance was obtained for the flyashes with $\bar{d}_{32}$ greater than 6 μm. Caution should be used when designing fabric filter systems for flyashes with $\bar{d}_{32}$ less than 6 μm, however. A comparison of the flyash with a $\bar{d}_{32}$ of 2.8 μm to that of a flyash with a $\bar{d}_{32}$ of 5.8 μm showed that the penetration increased by approximately two and one half orders of magnitude and the pressure drop increased by a factor of five.

The relationships developed in this study were developed at an air-to-cloth ratio of 2.1 CFM/ft^2 (0.64 m/min.) and reverse-air cleaning ratio of 1.6 CFM/ft^2 (0.48 m/min.). It has been shown previously that both the air-to-cloth ratio and reverse-air ratio also affect fabric performance for a single dust (1,3), thus the relationships developed in this study are only applicable at the operating conditions used during the testing. Additional research is needed to investigate the combined effects of particle size, air-to-cloth ratio and reverse-air ratio on fabric filter performance.

Conclusions

This research study has shown the effect of the flyash particle size distribution on the basic performance of a conditioned fiberglass filter.

Although the data are for only one specific fabric, and a specific set of operating conditions, the fabric is typical of those being applied to full scale fabric filter collectors on coal-fired boilers in the United States.

The following conclusions were reached in the study:

1. A decrease in the median diameter of the particle size distribution (as measured either by the mass median diameter or the surface mean diameter) resulted in significant increases in both the residual and effective fabric drag, and the residual specific resistance coefficients of the filter for MMD $\leq$ 8 m ($\bar{d}_{32} \leq 6$ µm). A change in MMD from 7.7 µm to 3.5 µm resulted in a 5-fold increase in the values of these parameters. For MMD $\geq$ 8 µm, the values were found to be relatively constant indicating only a minor dependence on the particle size distribution.

2. The specific resistance coefficient, K_2 was found to be proportional to $\bar{d}_{32}$ to the negative power of 1.28. This is in support of previous research where K_2 was found to be approximately proportional to d_{32}^{-1}(2).

3. A decrease in the median diameter of the particle size distribution resulted in significant increases in the flyash penetration for all particle size distributions studied (MMD = 3.5-13.0 µm). A change in MMD from 13.0 µm to 3.5 µm resulted in greater than a three order of magnitude increase in flyash penetration. (The efficiency of the fabric decreased from 99.99+% to less than 95%.)

4. Within the limits of the study, the relationships developed can be used to predict changes in fabric filter performance resulting from different inlet size distributions.

Acknowledgement

The research conducted in this study was funded under a contract with the Tennessee Valley Authority. The contents do not necessarily reflect the views of TVA, nor does the mention of trade names or commercial products constitute endorsement or recommendation for use.

ENDNOTES

1. Dennis, Richard, R.W. Cass, D.W. Cooper, R.R. Hall, Vladimir Hampl, H.A. Klemm, J.E. Langley, and R.W. Stern, Filtration Model for Coal Flyash with Glass Fabrics, EPA-600/7-77-084, August 1977.

2. Davis, W.T. and R.F. Kurzynske, "The Effect of Cyclonic Precleaners on the Pressure Drop of Fabric Filters," Filtration and Separation, January 20, 1979.

3. Strangert, S. and S. Flaktfabriken, "Predicting Performance of Bag Filters," Filtration and Separation, January/February 1978.

4. McKenna, J.D. and R. Weisburg, "A Pilot Scale Investigation of Fabric Filtration as Applied to Coal-Fired Industrial Boilers," Enviro-Systems and Research, Inc., P.O. Box 658, Roanoke, Virginia, 24004, USA.

5. Dennis, Richard and John Wilder, Fabric Filter Cleaning Studies, National Technical Information Service #EPA-650-2-75-009, Springfield, Virginia, 22161, USA.

TABLE 2. RELATIONSHIP BETWEEN FABRIC PERFORMANCE PARAMETERS

Fabric Drag

$$S = S_R + K_2 W + (S_E - S_R)\left[1 - \exp\left(\frac{-W\,(K_r - K_2)}{S_E - S_R}\right)\right] \quad \text{(eq. 2)}$$

$$K_2 + 10.9\ \bar{d}_{32}^{\,-1.28}\ \frac{\text{N-min}}{\text{g-m}} \quad \text{(eq. 4)}$$

$$K_r = 3.6 + 645 \exp(-1.12\ \bar{d}_{32})\ \frac{\text{N-min}}{\text{g-m}} \quad \text{(eq. 5)}$$

$$S_E = 269 + 3.95 \times 10^4 \exp(-1.23\ \bar{d}_{32})\ \frac{\text{N-min}}{\text{m}^3} \quad \text{(eq. 6)}$$

$$S_R = 216 + 2.09 \times 10^4 \exp(-1.11\ \bar{d}_{32})\ \frac{\text{N-min}}{\text{m}^3} \quad \text{(eq. 7)}$$

where $\bar{d}_{32}$ = surface mean diameter (micrometers)

Fabric Penetration

$$Pn = Pn_s + (Pn_o - Pn_s) \exp(-aW) \quad \text{(eq. 3)}$$

$$Pn_o = 0.42 \exp(-0.81\ \bar{d}_{32}) \quad \text{(eq. 8)}$$

$$Pn_s = 0.77 \exp(-1.09\ \bar{d}_{32}) \quad \text{(eq. 9)}$$

$$a = 0.04\ \text{m}^3/\text{gram}$$

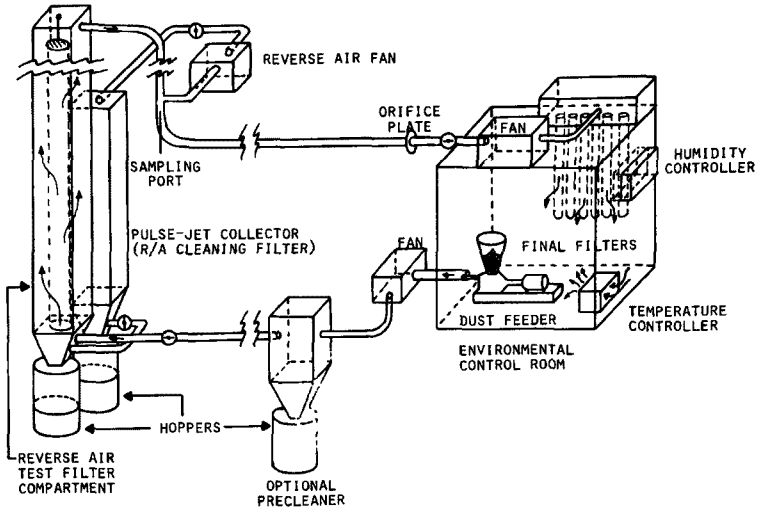

FIGURE 1. SCHEMATIC DIAGRAM OF THE FABRIC FILTER TEST FACILITY.

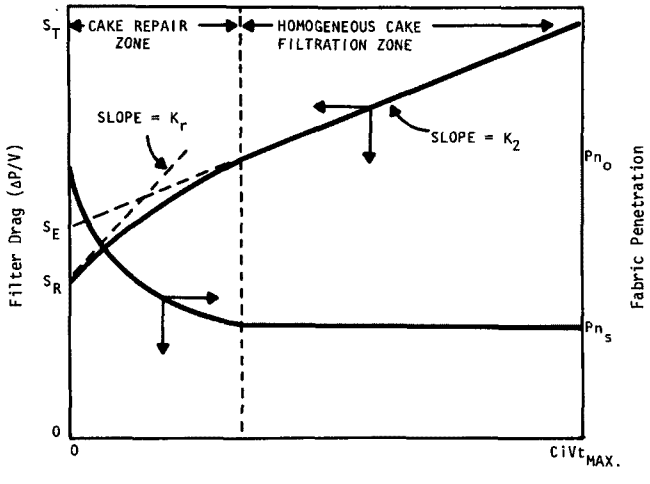

Figure 2. Graphs of Filter Drag and Fabric Penetration versus Areal Cake Density Added During the Filtration Cycle for a Conditioned Filter.

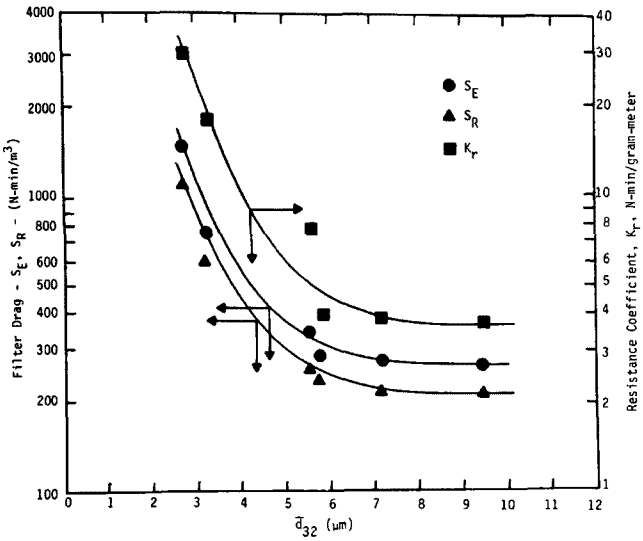

Figure 3. K_r, S_E, and S_R as a Function of Surface Mean Diameter ($\bar{d}_{32}$).

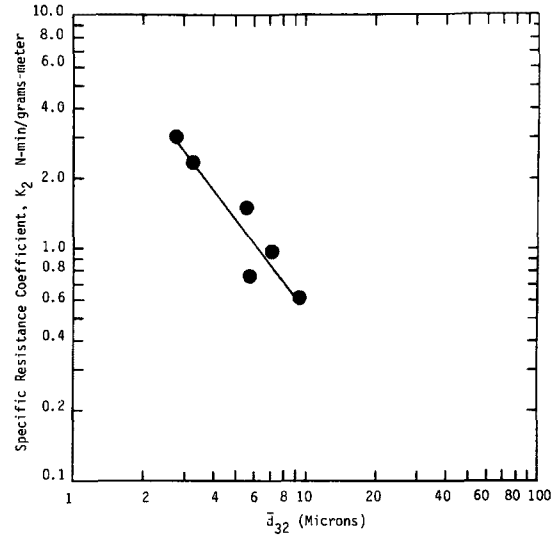

Figure 4. Specific Resistance Coefficient (K_2) as a Function of Surface Mean Diameter ($\bar{d}_{32}$)

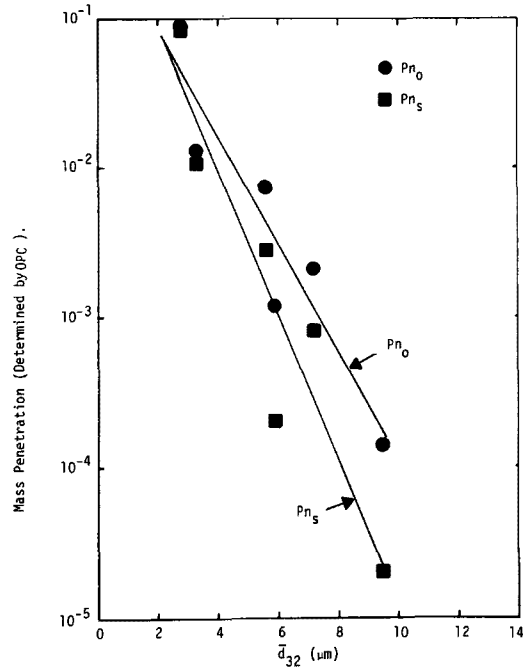

Figure 5. Pn_o and Pn_s as Functions of Surface Mean Diameter ($\bar{d}_{32}$).

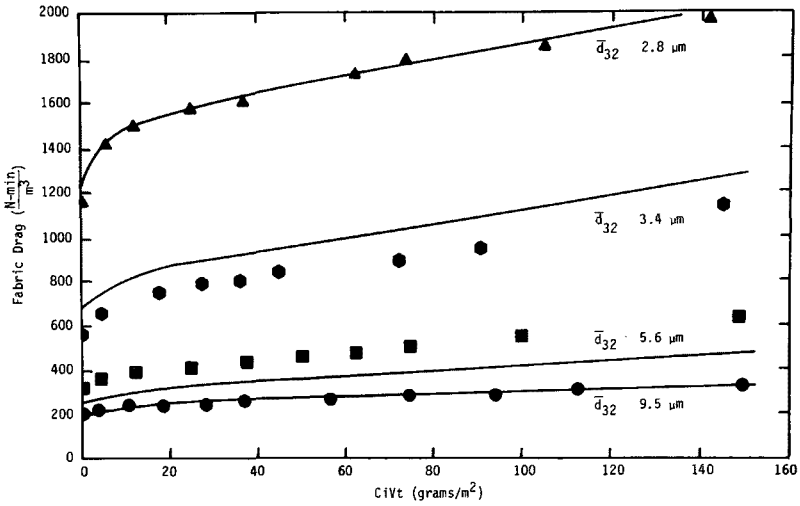

Figure 6. Fabric Drag as a Function of Areal Cake Density for Four Bags Conditioned with Different Sizes of Flyash.

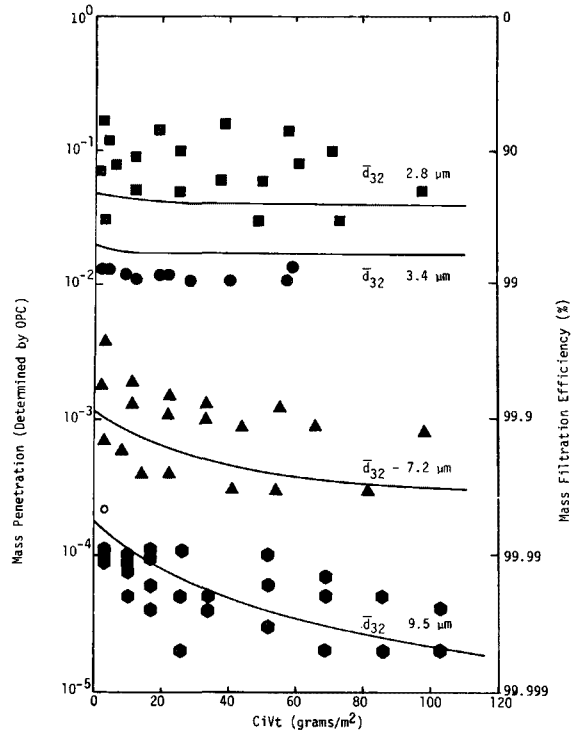

Figure 7. Mass Penetration as a Function of Areal Cake Density for Different Sizes of Flyash.

FUNDAMENTAL STUDY OF A FABRIC FILTER WITH A CORONA PRECHARGER

By: K. Iinoya and Y. Mori
Department of Chemical Engineering
Kyoto University, Kyoto 606, JAPAN

ABSTRACT

The effects of a corona precharger on the performance of a fabric filter have been studied experimentally in air with controlled humidity. The test dust, that is fly ash, is precharged and then ducted to a test fabric.

For a small bench scale apparatus, charged dust reduces the pressure loss across the filter at lower filtration velocity and lower relative humidity. The collection efficiency of a fabric filter can usually be improved by using a corona precharger.

Using a larger bench scale apparatus, by which continuous filtering and cleaning operations can be performed, the electrostatic effects on the pressure loss across a filter and on the collection efficiency are the same as for that of a small bench scale. The dust dislodged from a fabric filter with a corona precharger in a cleaning operation is larger than that that dislodged without a precharger. However, the residual dust fraction for charged dust is the same as or larger than that without a corona precharger.

INTRODUCTION

Dust collectors with the highest efficiency, such as an electrostatic precipitator or a fabric filter, must be used to meet the requirements of the particulate emission regulation. However, every collector has both advantages and disadvantages. Therefore, efforts to develop a combination type having the advantages of both collectors are necessary. One such example is the Apitron collector developed in the United States. The Apitron incorporates a pulse jet fabric filter, preceded by a wire-in-cylinder type of electrostatic precipitator. However, fundamental studies have been little concerning with its performance and economy [1-6].

This report, first, describes the preliminary and experimental results of the filtration performance of the hybrid filter obtained by the use of a small bench scale test facility, which is called the "small device". This paper also presents the results of the dust filtration and dislodging performances using another type of continuously operated hybrid filter called the "large device".

EXPERIMENTAL APPARATUS AND PROCEDURE

Figure 1 shows a flow diagram of the small experimental device for the investigation of the effects of a corona precharger on filtration performances at various relative humidities and filtration velocities. Test dust is uniformly fed into a mixer-type disperser by a Micro Feeder (Sankyo Dengyo Co.), and is ducted to the test filter through both a positive corona

precharger and a settling (or mixing) chamber. The dust collection area of a test fabric is about 50 cm^2, and the fabric is polyester (Tetron) felt, the surface of which is treated in order to dislodge the collected dust easily. Dust, which penetrates through the test fabric, is completely collected by a high efficiency glass fiber filter (AP20, Millipore Co.). The electrostatic charge of dispersed test dust is also measured just in front of the test fabric by use of a Faraday cage with the high efficiency glass fiber filter.

Fly ash (JIS No.5) is used as the test dust for the small device. The size distributions of charged dusts, which are measured by a cascade impactor (226 type, Sierra Co.) just in front of the test fabric, are almost the same as those of uncharged dusts, and are expressed approximately as log-normal distributions with a mass median diameter of 5 μm and a geometric standard deviation of 2.1.

Figure 2 shows a schematic diagram of the large experimental device, which can be operated continuously. A test filter consists of one bag which is about 12 cm diameter and 20 cm long. The collection area of a test bag is about 754 cm^2, and the fabric is wool felt. The dust laden gas flows from the outside to the inside of the test bag, and the filtration velocity through the test fabric is automatically controlled at 3.0m/min. In order to sample the inlet dust, a probe is located between the corona precharger and the test fabric. The concentration and the electrostatic charge of the inlet dust are measured by the Faraday cage and nearly isokinetic sampling. The size distribution of the inlet dust is also measured by a cascade impactor (226 type, Sierra Co.) using the same sampling probe. The dust concentration of the outlet dust is measured continuously by use of a aerosol mass monitor (model 51-1111, Piezo balance, Kanomax, Osaka) and a high efficiency glass fiber filter (GB 100R, Toyo Roshi Co., Tokyo). The mean concentration of outlet dusts measured by the mass monitor agrees well with that by a glass fiber filter. The cleaning operation is activated whenever the pressure loss across the test fabric reaches the predetermined value of 1.96 kPa. Therefore, the filtration period is variable. The dust collected on the test fabric is dislodged by using pulse jets. Cleaning jet pressure is about 390 kPa, and the electromagnetic valve for cleaning is opened for about 60 ms.

The test dust for the large device is also fly ash collected by an electrostatic precipitator at a coal-fired power station in Japan. It has a mass median diameter of 3.6 μm and a geometric standard deviation of 2.7, measured by a cascade impactor just in front of the test fabric.

CHARACTERISTICS OF A CORONA PRECHARGER

The corona precharger for the "small device" is a kind of a short electrostatic precipitator, which is constructed with 8 discharge electrodes of tungsten wire (0.2 mm x 100 mm) and 9 plate electrodes (11 mm x 100 mm). The distance between the above two electrodes is 10 mm. The velocity of the air loaded with test dusts is about 17 cm/s in the precharger, and the resident time is about 0.06 seconds. The field strength is about 4 kV/cm

and the corona current per unit length of the wire electrode is 0.35 to 0.75 μA/cm. Test dusts are charged by positive corona. The precharger for the "large device" is composed of a discharge electrode of tungsten wire of 0.2mm diameter and a cylindrical electrode of 2.8 cm inner diameter. The length of the corona precharger is 11 cm. Flyash dust is charged by the negative corona in the "large device". The field strength is about 5 kV/cm, and the corona current per unit length of the wire electrode is 5.5 to 9.1 μA/cm.

EXPERIMENTAL RESULTS OF THE "SMALL DEVICE"

Surface Characteristics of the Dust Layer Collected on the Test Fabric

Figure 3 is a photograph of the rugged surface of the charged dust layer collected on the test fabric. Figure 4 is the smooth surface of the uncharged dust on the same fabric. The pressure loss of the loaded test fabric in the case of Figure 3 is lower than that in the case shown in Figure 4.

Pressure Loss

Figures 5 to 8 show the comparisons of the drags of charged and uncharged flyash for various relative humidity ranges. Except at a high relative humidity of 85 to 95 %, the charged dust reduces the pressure loss.

Figures 6 and 8 also show the effects of filtration velocities on the drags. For a relative humidity of 45 to 55 %, the drags without the corona precharger at higher filtration velocity are lower than those at lower filtration velocity, as shown in Figure 6, because of pinhole formations in the dust layer. The rugged surface of the charged dust layer collected on a test fabric becomes smoother at higher filtration velocity than at lower filtration velocity. Figure 8 shows a relationship between the drags and dust loads at a relative humidity of 85 to 95 %. The drags at a filtration velocity of 6.4 m/min are almost the same as those at 2.55 m/min. This means that there is no pinhole formation at high relative humidity. Furthermore, the corona precharger does not reduce the pressure loss, regardless of the filtration velocity.

Collection Efficiency

Figure 9 shows the cumulative penetrations for the same conditions as those in the pressure loss experiments. The penetration seems to decrease with lower relative humidity for uncharged dust, but shows no definite change for charged dusts.

Figure 10 shows the effect of the filtration velocity on the efficiencies. Unlike the results of the pressure loss, the corona precharger improves cumulative collection efficiencies even at higher filtration velocity. The cumulative penetration is higher at a filtration velocity of 6.4 m/min than at 2.55 m/min, because of pinhole formation in the dust layer.

The gradients of the straight lines in a log-log chart of cumulative penetration vs. dust load are mostly minus unity, which means 100 % collection efficiency. Therefore, in Figures 9 and 10, the collection efficiencies of

higher dust load collected at lower filtration velocity are 100 %, and are independent of the electrostatic charges of the test dusts. The effect of electrostatic charge of test dust on the cumulative penetrations becomes conspicuous at lower dust loads.

Figure 11 shows a relationship between the cumulative penetrations at $100g/m^2$ dust load and the electrostatic charges per unit dust weight. The collection efficiency becomes higher as the electrostatic charge per unit dust weight increases.

Electrostatic Charge of Test Dust

Figure 12 shows the electrostatic charge of flyash dust caused by the corona precharger. The charge is not always consistent, though the applied voltage is constant. One of the reasons for this phenomena may be the change of field strength which is reduced by the amount of dust deposited on the electrodes. The relationship between the charges and the relative humidity is shown as a solid line obtained by the least squares method. The charges decrease as the relative humidity increases. Therefore, this result indicates that the formation of the rugged surface depends on not only the electrostatic charge but also on other factors.

Figure 13 shows the electrostatic charge of flyash dust without the corona precharger, i.e. a natural charge. The charge depends on the relative humidity. The reason for this may be the leakage of charges.

EXPERIMENTAL RESULTS OF THE "LARGE DEVICE"

Filtration Performance

Figure 14 shows the comparison of pressure losses across a fabric filter with and without a corona precharger after a start-up. The filtration period with a corona precharger is about 1.5 times longer than that without a precharger, at the same operating condition.

Figure 15 shows the cumulative penetrations for every filtration period. They decrease at the beginning and then remain nearly constant. The penetrations with a corona precharger are almost one fifth of that without a precharger, during the first several filtration cycles of a new fabric. However, the ratio decreases about 2.5 times after 10 filtration cycles. Figure 16 shows the cumulative dust emission from the test fabric for several filtration periods. The solid lines indicate the dust weight penetrated with the precharger. The broken lines are also the dust weight without the precharger. The dust emission at the first filtration cycle is larger than that at other filtration cycles in both operating conditions. Most of the dust emission takes place during the first few minutes in both operating conditions. The dust emissions with the corona precharger are lower and decrease faster than those without the precharger.

Cleaning Performance

Figure 17 shows the comparison of dust loads dislodged from a fabric

filter with and without the precharger. The dislodged dust loads decrease at the beginning and remain constant after about ten cycles. The dust load dislodged from the fabric with the precharger is larger than that without the precharger. However, it can't be concluded that the residual dust fraction for the former case is less than that of the latter case, because the dust load of each filtration period for the former is larger than that for the latter.

Figure 18 shows the relationship between the residual dust fraction and the filtration cycle. At the beginning, the residual fraction of the new fabric with the precharger is slightly larger than that without the precharger. However, both residual dust fractions become equal and remain constant over ten filtration cycles after the start-up.

CONCLUSION

The effects of a corona precharger on the performance of a fabric filter have been studied experimentally, and the following conclusions are obtained:
1) When the charged fly ash dust is collected on a test fabric at below 75 % humidity, the rugged surface of the charged dust layer takes place, and reduces the pressure loss across the loaded test fabric.
2) At the filtration velocity of 6.4 m/min, which is about twice as high as usual, the rugged surface of the charged dust layer is smoother than that at the usual velocity, and the pressure loss is not reduced. Furthermore, pinholes emerge in the dust layer at lower relative humidity.
3) The collection efficiency of a fabric filter is improved by the corona precharger for wide ranges of relative humidity and filtration velocity. The collection efficiency gets higher as the electrostatic charge per unit dust weight increases. It is improved especially at lower dust load by using a corona precharger.
4) The electrostatic charges of dusts decrease as the relative humidity increases, because of leakage caused by moisture in the air. The reduced pressure loss by use of the corona precharger depends not only on the amount of electrostatic charge of the test dust, but also on other factors.

Furthermore, A bench scale experiments of continuous filtration and cleaning cycles have been conducted. The following conclusions are obtained:
5) The filtration period of the fabric with the precharger is longer than that without the precharger at the constant maximum pressure loss across the fabric.
6) The cumulative penetration of every filtration period with the precharger is lower than that without the precharger. And the penetrations decrease at the beginning and remain constant after a few filtration cycles for both cases.
7) The dust weight dislodged from the fabric with the precharger is larger than that without the precharger in every cleaning operation. The residual dust fractions in both cases are nearly the same sand remain constant after a few filtration cycles.

NOMENCLATURE

c_i = inlet dust concentration [g/m^3]

E	= cumulative collection efficiency	[-]
m	= dust load collected on a fabric	[g/m^2]
m_d	= dust load dislodged from a fabric	[g/m^2]
n_f	= number of the filtration cycle	[-]
p	= pulse pressure for cleaning in gauge	[kPa]
Δp	= pressure loss across a fabric filter	[kPa]
Δp_{max}	= pressure loss just before cleaning operation	[kPa]
u	= filtration velocity	[m/min]
w_o	= dust weight penetrated through a fabric	[g]
Λ	= residual dust fraction on a fabric by weight	[-]
ϕ	= relative humidity	[%]

ENDNOTES

1. Helfritch, D.J. Performance of an Electrostatically Aided Fabric Filter. Chem. Eng. Prog. 73: 54-57, August 1977.
2. Lamb, G.E.R. and P.A. Costanza. Improving Performance of Fabric Filters. Chem. Eng. Prog. 73: 51-53, January 1977.
3. Lamb, G.E.R. and P.A. Costanza. Electrical Stimulation of Fabric Filtration. Textile Res. J. 47: 372-380, May 1977.
4. Penney, G.W. Using Electrostatic Forces to Reduce Pressure Drop in Fabric Filters. Powder Tech. 18: 111-116, 1977.
5. Penney, G.W. Electrostatic Effects in Fabric Filtration: I. Fields, Fabrics, and Particles. EPA600/7-78-142a, September 1978
6. Costanza, P.A., G.E.R. Lamb, and J.B. Dunbar. Electrical Stimulation of Fabric Filtration (ESFF) for Cotton Dust Control. J. Eng. Ind. Trans. ASME. 101:65-68, February 1979.

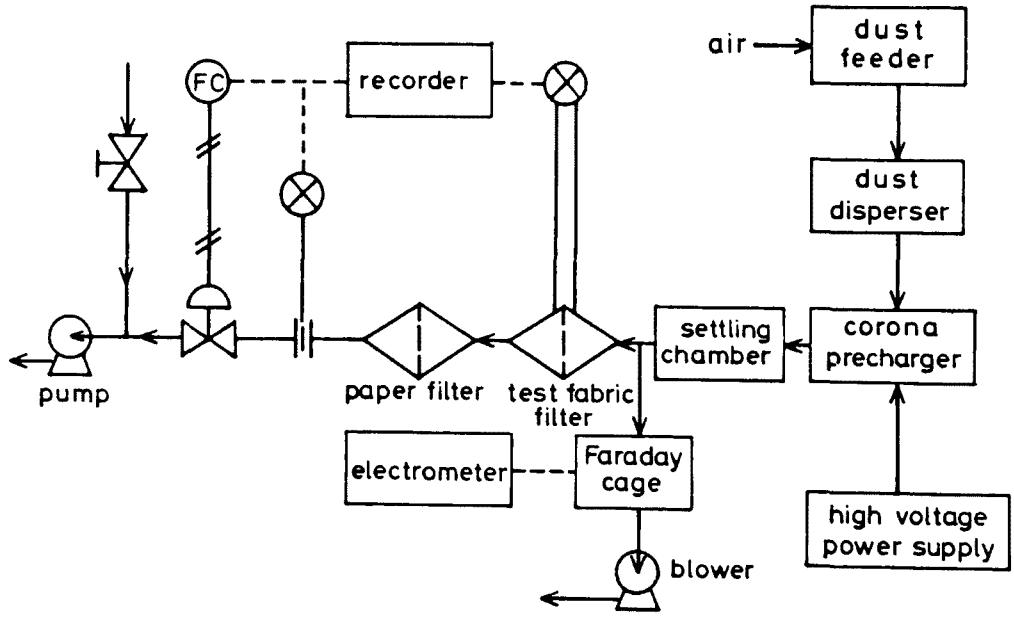

Figure 1. Experimental apparatus for electrostatic effects in fabric filtration ("small device").

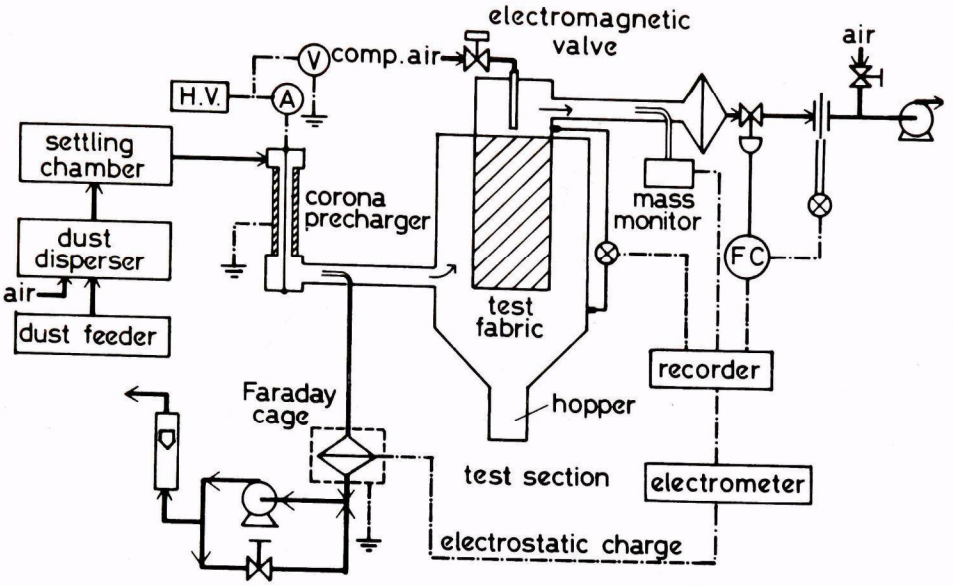

Figure 2. Pulse jet type bench scale apparatus for electrostatic effects in fabric filtration ("large device").

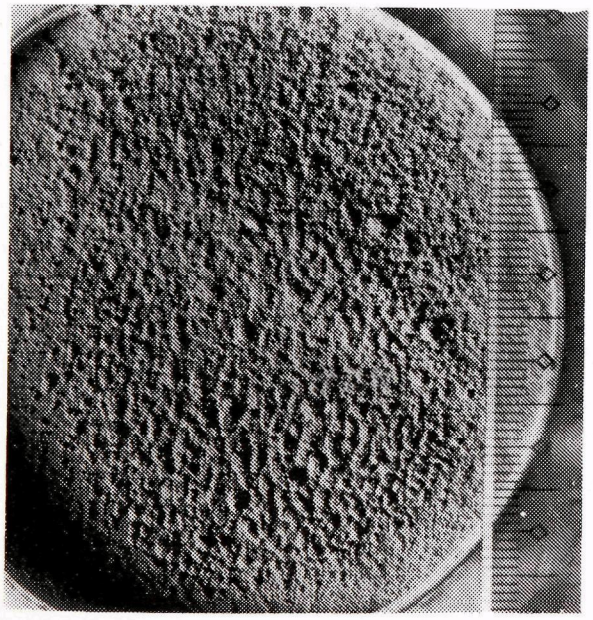

Figure 3. Photograph of rugged surface of deposited dust with corona precharger, m=304 g/m^2,R.H.=50%.

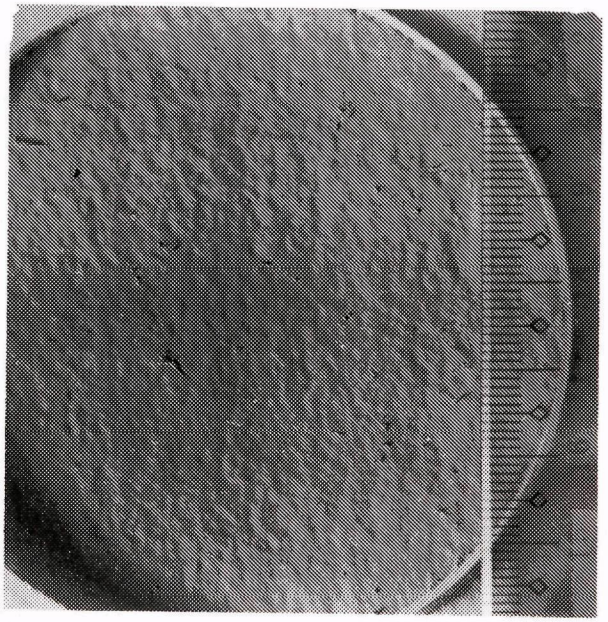

Figure 4. Photograph of smooth surface of deposited dust without corona precharger, m=329 g/m^2, R.H.=52%.

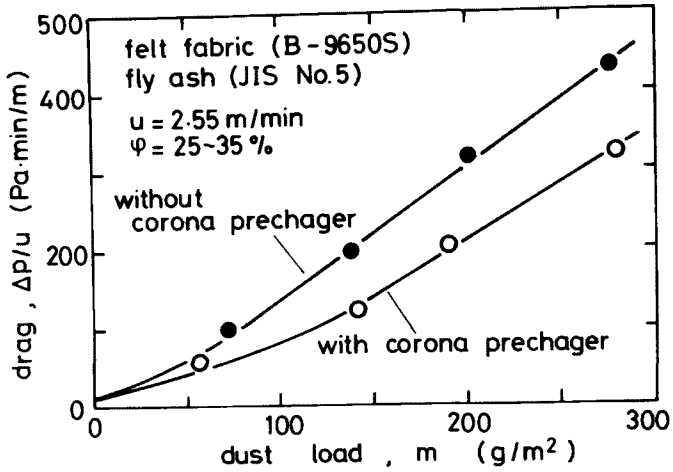

Figure 5. Relationship between drags and dust loads on a filter, R.H.=25-35%.

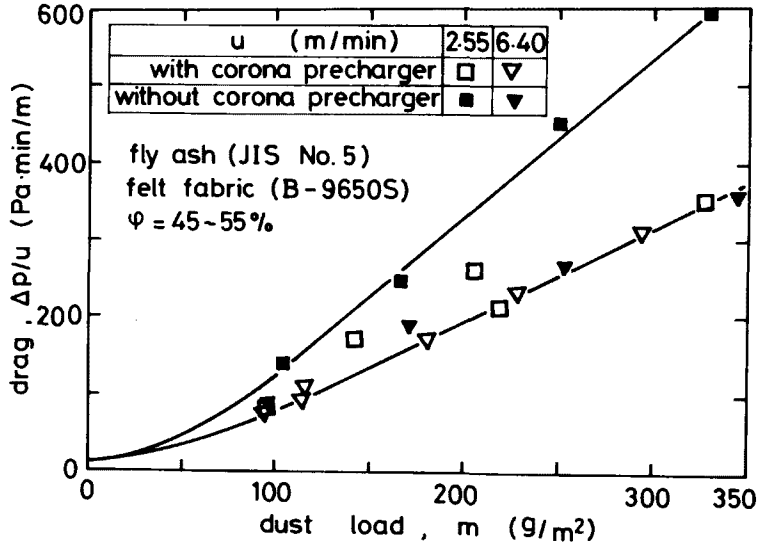

Figure 6. Relationship between drags and dust loads on a filter, R.H.=45-55%.

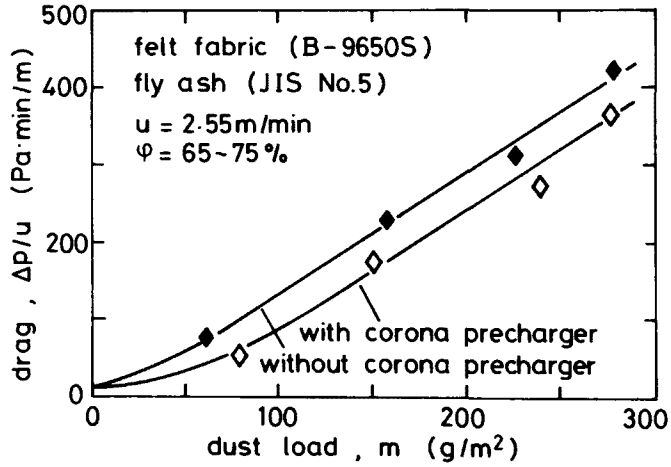

Figure 7. Relationship between drags and dust loads on a filter, R.H.=65-75%.

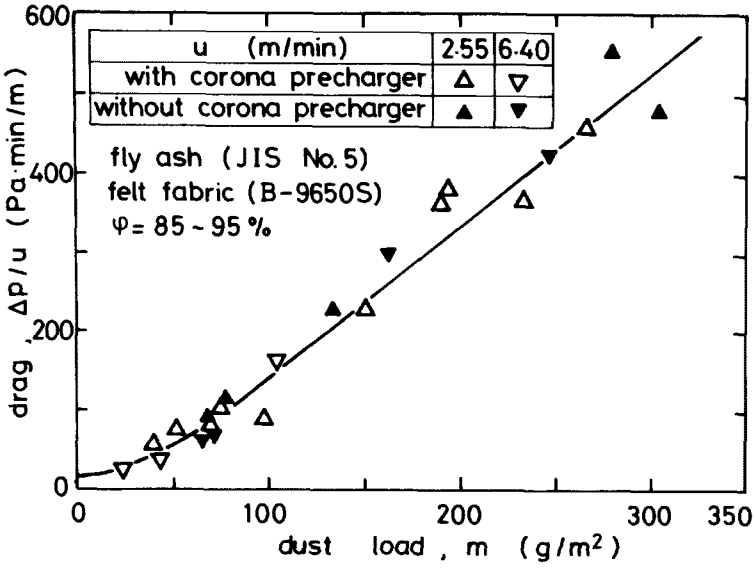

Figure 8. Relationship between drags and dust loads on a filter, R.H.=85-95%.

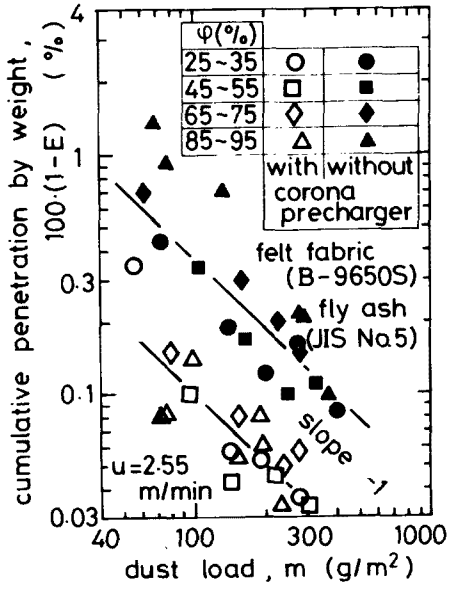

Figure 9. Relationship between cumulative penetrations and dust loads on a filter

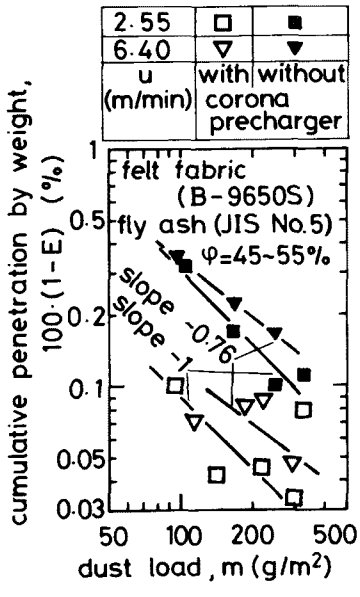

Figure 10. Effect of filtration velocity on cumulative penetrations, R.H.=45-55%.

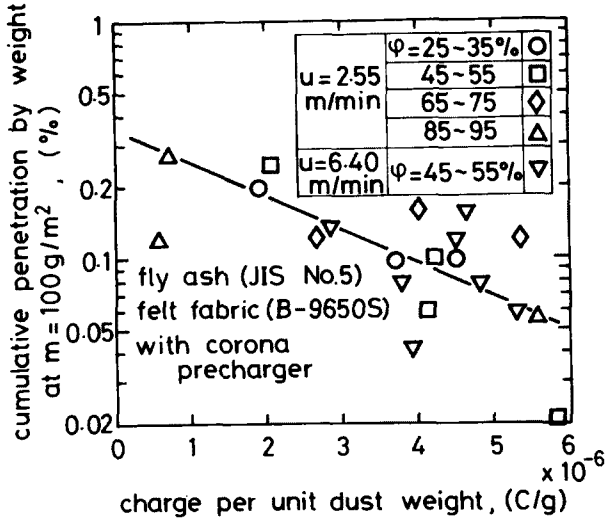

Figure 11. Effect of electrostatic charges on cumulative penetrations.

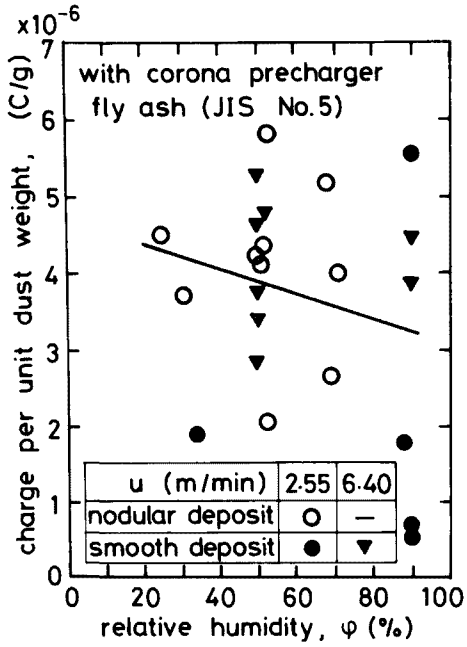

Figure 12. Effect of relative humidity on electrostatic charge by corona precharger.

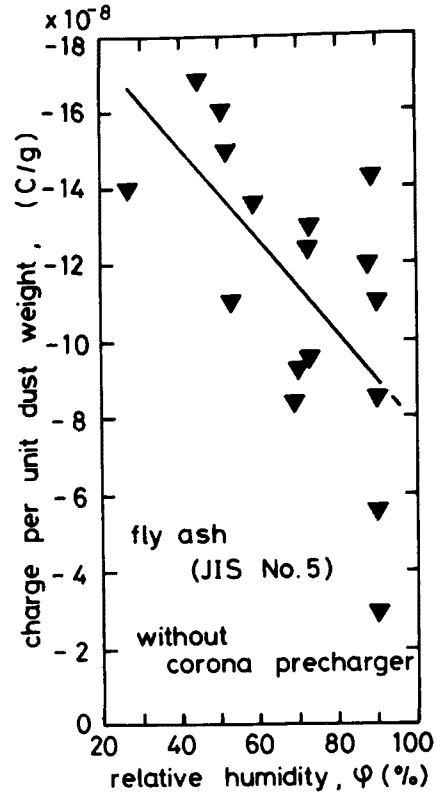

Figure 13. Effect of relative humidity on natural charge of fly ash dust

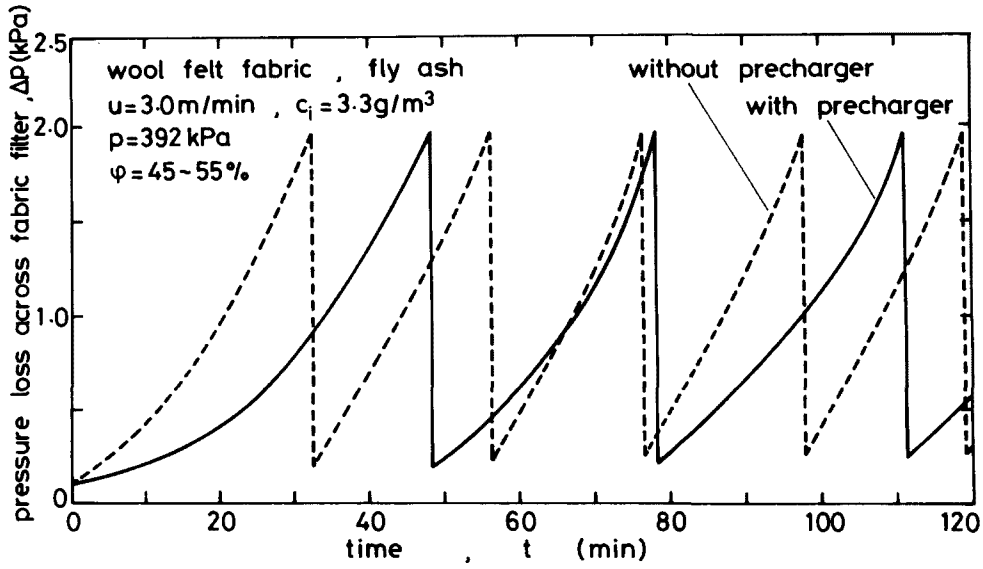

Figure 14. Comparison of pressure loss across test fabric with and without corona precharger after start-up

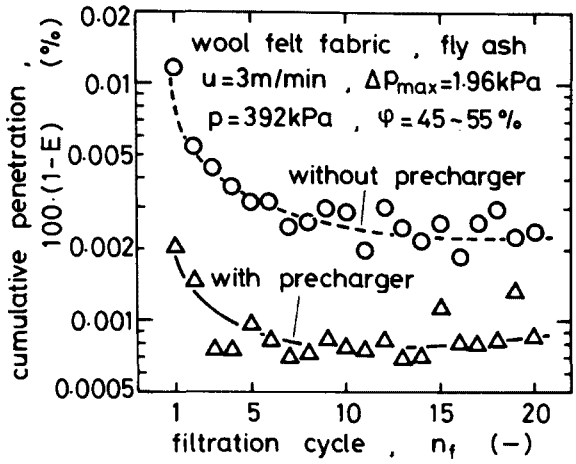

Figure 15. Comparison of cumulative penetrations through test fabric with and without corona precharger for every filtration period.

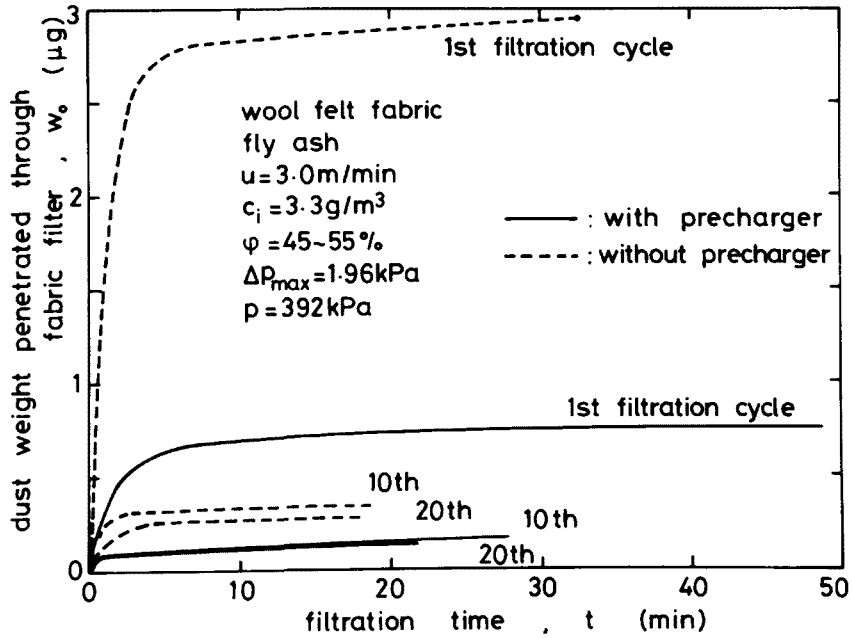

Figure 16. Cumulative dust emissions from test fabric for several filtration periods.

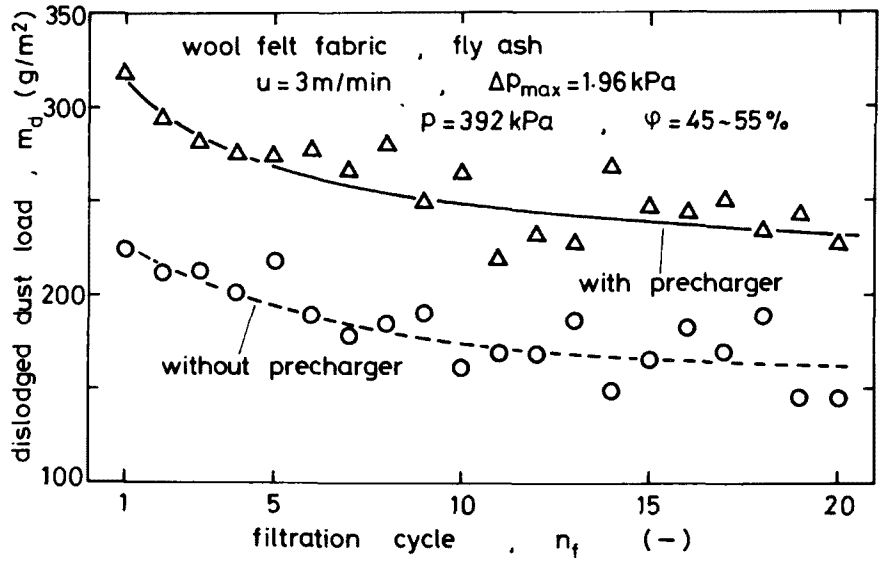

Figure 17. Comparison of dust load dislodged from test fabric with and without corona precharger.

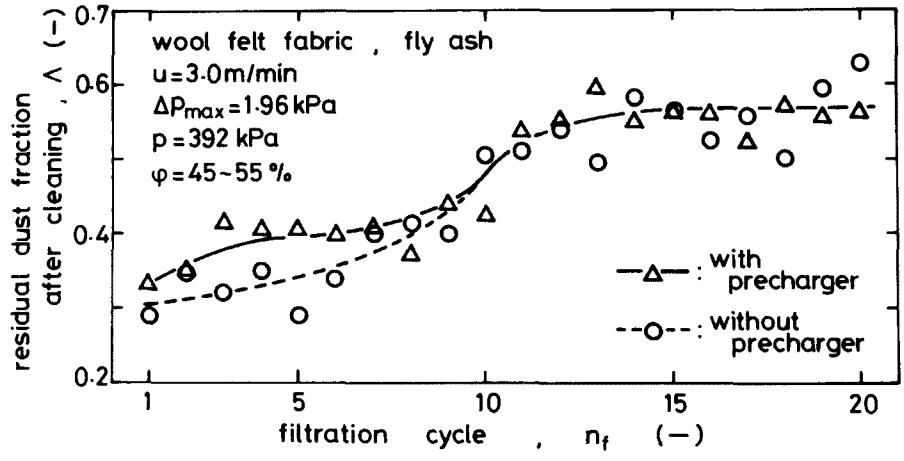

Figure 18. Comparison of residual dust fraction of test fabric with and without corona precharger.

ECONOMIC EVAULATION FACTORS IN BID EVALUATIONS
A SENSITIVITY ANALYSIS

By: John G. Musgrove, J. E. Shellabarger
Bechtel Power Corporation
P. O. Box 2166
Houston, TX 77001

ABSTRACT

The trend to evaluate major utility equipment bids on life cycle costs rather than just on first capital costs has increased due to a greater awareness of the costs of equipment maintenance and of borrowing money. The rapidly changing economic climate and changes in interest rates impact the establishment of a utility's economic evaluation factors.

An analysis has been conducted to determine the extent to which changes in the basic economic factors (interest rates, demand charge, fuel charge, escalation rates and plant life) alter the economic evaulation factors used in competitive bid evaluations. This analysis was made to determine to what extent these changes might alter the outcome of equipment selection for major air pollution control systems. In particular, recent budgetary studies comparing baghouses and cold-side electrostatic precipitators have been analyzed to determine the sensitivity of the equipment selection to the economic factors employed.

INTRODUCTION

The trend to evaluate major utility equipment bids by considering life cycle costs rather than just first capital costs has increased. This trend is due to a greater awareness of the costs of equipment operation and maintenance. In order to better understand the consequences of this trend on equipment evaluations a parametric analysis was conducted to determine the sensitivity of the total evaluated cost of air pollution control equipment to several economic factors provided by utility clients.

FACTORS OF ANALYSIS

Recently, equipment evaluation studies have been conducted comparing the use of fabric filter baghouses and cold-side electrostatic precipitators for particulate collection on coal-fired utility boilers (1)(2). The equipment capital costs and operating parameters were obtained from budgetary proposals of equipment suppliers. Engineering estimates were made for Purchaser-supplied related equipment and services.

Equipment costs used in the analysis included:

- Collector capital costs, fully erected.
- Other equipment capital costs.
- Annual maintenance costs.
- Surface area requiring insulation.
- Average electrical load.
- Maximum electrical load.
- Flue gas draft loss.

The economic factors considered in the analysis included:

o	Incremental cost of induced draft fan	$60,000/in. w.g.
o	Fan power cost	300 KW/in. w.g.
o	Heat conductivity	31 Btu/hr/ft^2
o	Plant life	20 to 40 years
o	Net station heat rate	9000 to 13000 Btu/KWhr
o	Average capacity factor	60 to 80 percent
o	Fuel charge rate	$1.80 to $2.60/10^6 Btu
o	Demand charge	$800 to $1200/KW
o	Fixed charge	8 to 20 percent
o	Discount rate	7 to 15 percent
o	Escalation rate, goods and services	6 to 14 percent
o	Escalation rate, fuel	6 to 14 percent

Each of the nine variables was analyzed independently with all other variables held constant at the midpoint of their ranges. For the variable being analyzed, five values equally spaced within its range were selected. Thus, a total of 45 cases were computed. Calculations for each case were made of the total evaluated present worth of each supplier's offering (3)(4). Study one contained capital and operating cost data from eight suppliers each of baghouses and precipitators. Study two contained data from ten

suppliers each of baghouses and precipitators. The resulting comparisons were based on the average values of computed present worth for the two types of equipment in each study.

RESULTS

Figures 1 through 3 present the results of the calculations of average total present worth of baghouses and average total present worth of precipitators for each study. The calculations were repeated for each variable at each of the five points within its range. The costs are presented as differential present worth for rising values of the economic factor analyzed. The following conclusions from these analyses appear reasonable:

Factors Favoring a Baghouse

Figure 1 presents the results of the sensitivity analysis for the factors of demand charge ($/KW), discount rate (percent) and fixed charge rate (percent). Increasing values of discount rate clearly favor selection of a baghouse, at the rate of $200,000 to $2,000,000 per percent. Increasing values of demand charge and fixed charge only slightly favor a baghouse, at the rate of $100 to $1450 per kilowatt and $41,000 to $77,000 per percent, respectively.

That these factors tend to favor selection of a baghouse is reasonable when one considers that for collectors of comparable first cost, the baghouse is more labor intensive, particularly in operation (material and labor for bag changes) whereas the precipitator is more capital intensive. It is then logical that increasing values of discount rate (cost of capital) and fixed charge (on capital) would more heavily penalize the precipitator and therefore favor the selection of a baghouse. Similarly, since demand charge is applied against maximum possible electrical consumption and the precipitator is the higher consumer of electrical power it is reasonable that increasing values of demand charge would favor a baghouse.

Factors Favoring a Precipitator

Figure 2 presents the results of the sensitivity analysis for the factors of plant life (years) and for escalation rate for goods and services (percent). Increasing values of the assumed escalation rate of goods and services and of the plant life clearly favor selection of a precipitator, at the rate of $54,000 to $400,000 per year and $54,000 to $2,500,000 per percent, respectively.

That these factors tend to favor selection of a precipitator is also reasonable. As previously discussed, a precipitator has a lower operating expense than does a labor intensive baghouse. Since increasing values of the escalation rate for goods and services impact maintenance costs for future years, and since increasing values for plant life extend the time for which there must be maintenance expenditures, the baghouse is impacted more highly than is the precipitator.

Factors Reinforcing Design Selection

Figure 3 presents the results of the sensitivity analysis for the factors of fuel charge ($/10^6 Btu), net station heat rate (1000 Btu/KWhr), plant capacity factor (percent) and fuel escalation rate (percent). Fuel escalation rate has the greatest impact on total evaluated present worth, $100,000 to $300,000 per percent. The factor of next greatest impact is net station heat rate, $100 to $125 per Btu/KWhr. Of lesser impact are fuel charge and plant capacity factor, $500,000 to $1,500,000 per 10^6 Btu and $16,500 to $19,500 per percent.

As can be seen from Figure 3, rising values of these four factors have opposite impacts for the two studies considered. The explanation for the phenomenon that increasing values for the four economic factors tends to reinforce the existing economic selection lies in the portions of the total present worth cost that are influenced by these four factors. Inspection of the method of evaluation (4) reveals that all four factors influence only the present worth penalties for thermal losses, average power consumption and draft loss. Capital costs and annual maintenance costs are not influenced by these factors. Close inspection of the data from suppliers indicates that only surface area, average electric load and draft loss are influenced by these variable factors.

Additional analysis, not presented in Figure 3, further substantiates that increasing values for these four economic factors tends to reinforce an existing economic selection. If the supplier-provided data for surface area, draft loss and electrical load in both studies are doubled, the differential total present worth based on rising values of the four economic factors favors the existing design, baghouse or precipitator, by greater amounts (graphs move outward on Figure 3). Similarly, if the supplier-provided data are halved, the differential total present worth based on rising values of the four economic factors continues to favor the existing design selection but by smaller amounts (graphs move inward on Figure 3).

CONCLUSIONS

- Comparatively high values of demand charge, discount rate and fixed charge rate cause present worth economic evaluations to favor selection of equipment having relatively low capital cost and relatively high operating and annual maintenance costs.

- Comparatively high values of plant life and escalation rate for goods and services cause present worth economic evaluations to favor selection of equipment having relatively high capital cost and relatively low operating and annual maintenance costs.

- Comparatively high values of fuel charge, net station heat rate, plant capacity factor and fuel escalation rate do not seem to bias present worth economic evaluations toward equipment of low or high capital

cost. Instead, they seem to exaggerate differences in evaluated cost that exist for comparatively low values of the economic factors.

- Use of the above conclusions may reduce the need for budgeting equipment comparisons because inspection of the economic factors to be used will permit forecasting any biases that will be inherent in such a comparison.

ENDNOTES

1. Musgrove, J. G. A Survey of Particulate Collection Devices for Coal-Fired Boilers. In: Proceedings of the International Coal Utilization Convention, Houston, Texas, October 17-19, 1978.

2. Particulate Removal Equipment Selection Study for Gulf States Utilities Company, Roy S. Nelson Power Station - Unit 5, Westlake, Louisiana. Bechtel Power Corporation, Houston, Texas, November, 1980.

3. Hickman, R. S. Methods and Terms Used in Engineering and Economic Studies. Interoffice Memorandum, Bechtel Power Corporation, Houston, Texas, February 3, 1976.

4. Musgrove, J. G. Present Worth Calculation Program. Bechtel Power Corporation, Houston, Texas, February, 1981.

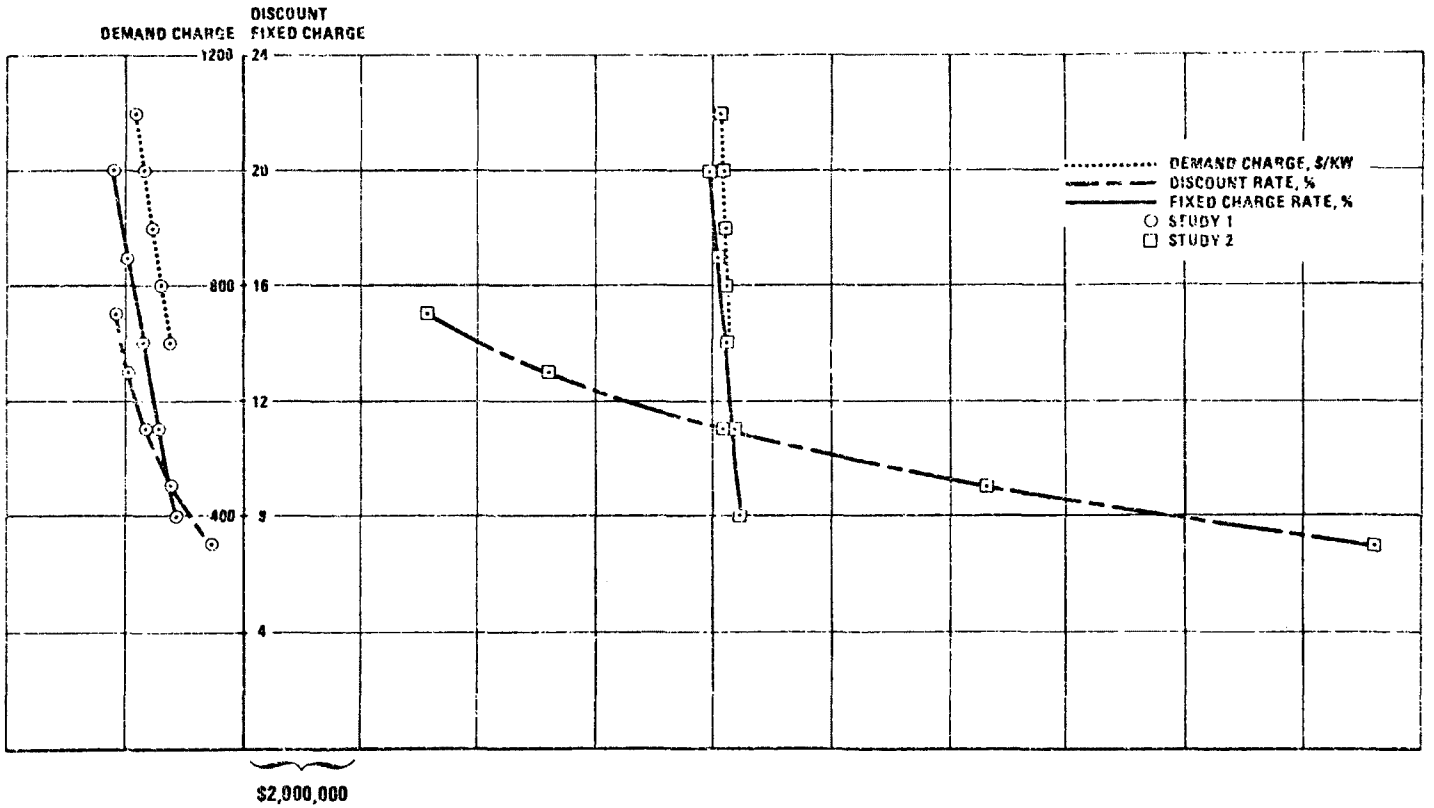

FIGURE 1 – FACTORS WHOSE RISING VALUES FAVOR A BAGHOUSE

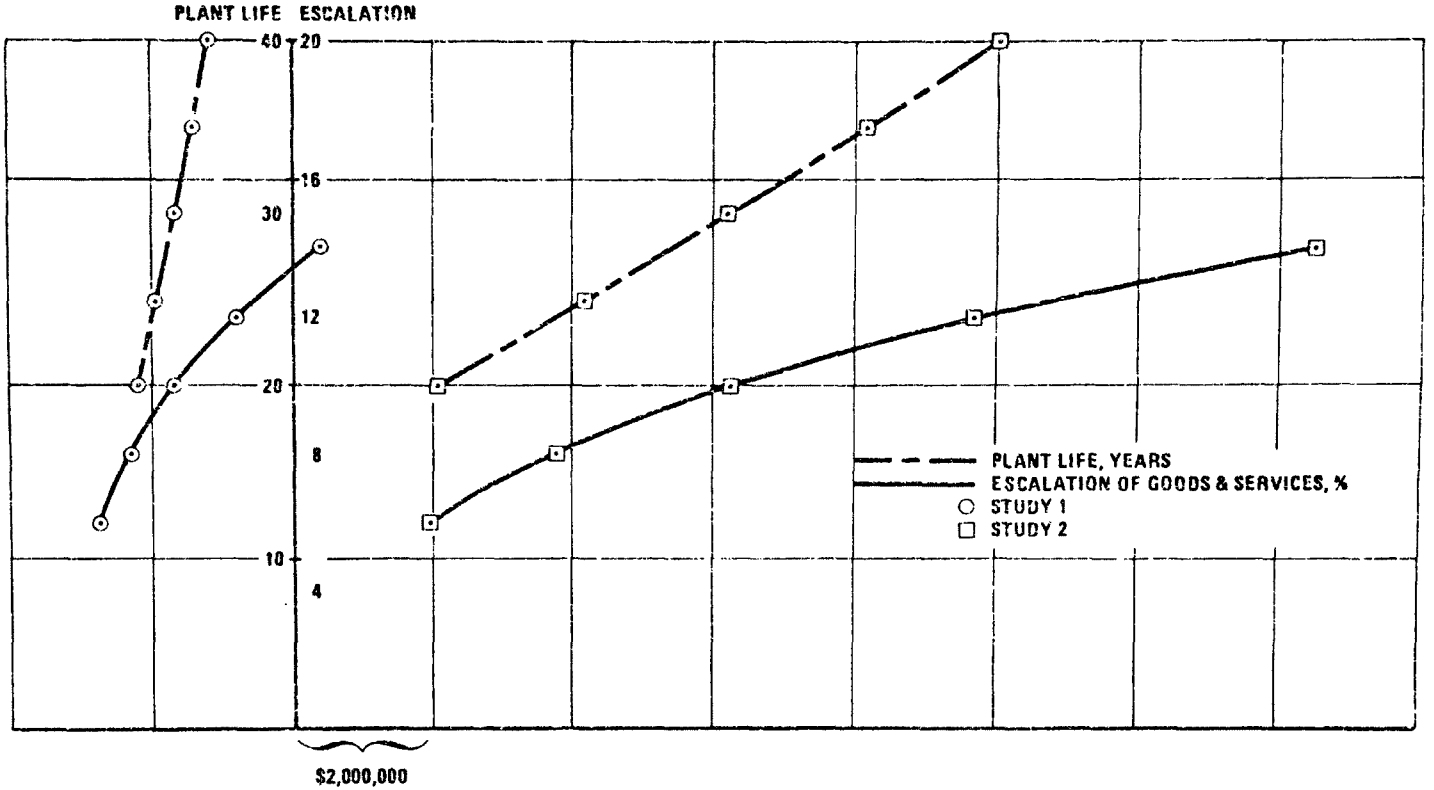

FIGURE 2 – FACTORS WHOSE RISING VALUES FAVOR A PRECIPITATOR

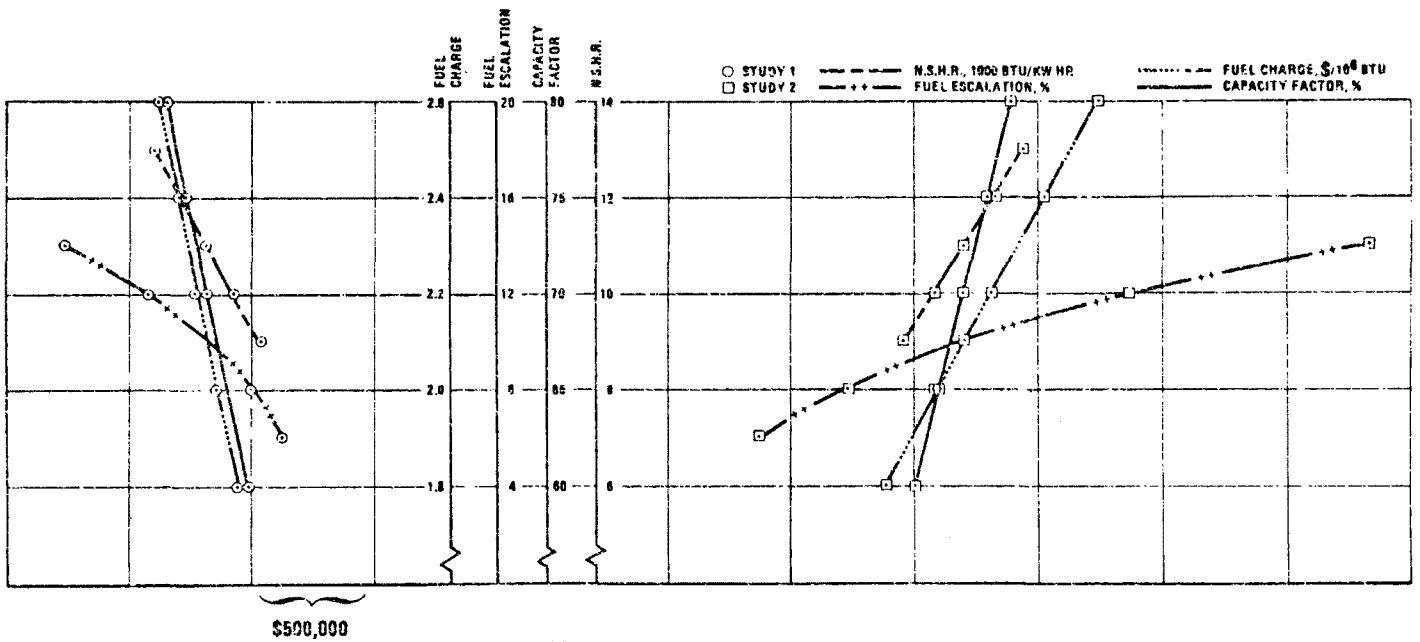

FIGURE 3 – FACTORS WHOSE RISING VALUES REINFORCE THE DESIGN SELECTION

FLY ASH RE-ENTRAINMENT IN A BAGHOUSE
WHAT DOES IT COST?

By: J. G. Musgrove
Bechtel Power Corporation
P. O. Box 2166
Houston, TX 77001

ABSTRACT

The re-entrainment of fly ash from the hoppers of utility baghouses is acknowledged by baghouse suppliers but is considered by them to be inconsequential. A continuing concern about the extent and cost of re-entrainment in a baghouse designed for a 550 MW utility generating station led to an analysis of its costs.

The analysis hypothesizes the impact on baghouse operation that would be caused by re-entrainment and estimates its present worth cost as a function of increased draft loss across the baghouse compartments. An estimate is also made for the cost of conducting a scale model test program to determine the actual degree of re-entrainment to establish a break-even point for cost of re-entrainment versus costs of conducting the model tests. The analysis then suggests a method of determining the component costs of implementing corrections to reduce re-entrainment. From the costs of correcting re-entrainment, curves of equal cost are presented to suggest when re-entrainment should be determined and corrected and when it should be ignored.

INTRODUCTION

A presentation of baghouse air flow model testing at the 4th International Fabric Alternatives Forum (1) demonstrated the clear potential for chaotic gas flow in the hoppers of bottom inlet baghouses. This chaotic flow could easily lead to re-entrainment into the flue gas of ash stored in the hopper and its subsequent redeposition onto the bag.

Bechtel had selected a bottom inlet baghouse for particulate collection on a large utility boiler and was concerned about the potential for re-entrainment in its design. Subsequent testing of the gas flow model for the project indicated similar chaotic gas flow in the hoppers and therefore a potential for significant re-entrainment problems. The baghouse supplier repeatedly stated that re-entrainment would not be a problem but failed either to provide convincing evidence or to perform, at no cost to our client, additional testing to obtain convincing evidence.

Bechtel, therefore, proceeded to analyze the factors in re-entrainment and to estimate the cost of re-entrainment to determine if client participation in further model testing was warranted.

RE-ENTRAINMENT - DEFINITION, IMPACT AND DERIVATION OF COST

Bechtel's analysis of the cost of re-entrainment began with defining re-entrainment as that portion of particulate material stored in the hopper at the start of a filtering cycle which again enters the flue gas stream and is recollected by being deposited on the bag surface. Therefore, 10% re-entrainment means that 10% of the material stored in a hopper at the start of the filtering cycle will be deposited on the bag and add to the filter cake. It was also defined that a 10% increase in material on the bag produced a 10% greater pressure drop across the bag surface. These definitions permitted the analysis to calculate the cost of re-entrainment as a function of draft loss, a characteristic for which a dollar value had already been obtained (2).

Table I, Parameters of Baghouse Re-entrainment for R=10%, presents the values for selected baghouse parameters (ash in the hopper, ash on the bag, compartment ΔP) assuming the recommended maximum ΔP prior to bag cleaning is 5 in. w.g. and that the amount of re-entrainment is 10%. Table II, Percent Draft Loss from Re-entrainment, R=10%, presents, for 10% re-entrainment, the percentage of compartment draft loss during a cleaning cycle that is due to re-entrained ash from the hopper.

In all cases, it is assumed one unit of ash enters the compartment during each cycle, and the Cycle Number is the number of reverse air bag cleaning cycles since the latest hopper evacuation cycle.

From Table II it can be extrapolated that for any cycle, n, of bag filtering and cleaning and for an assumed value of re-entrainment, R (%, expressed decimally), the draft loss in that cycle, W, due to the re-entrained material may be expressed as:

$$W = (n-1)R/4 \qquad (1)$$

Similarly, for a design with maximum recommended compartment draft loss, P_M (in. w.g.), and a penalty for draft loss, V ($/in. w.g.), the cost of re-entrainment, C_R ($), may be expressed as:

$$C_R = P_M V(n-1)R/4 \qquad (2)$$

Figure 1, Cost of Re-entrainment, C_R, presents a family of curves for C_R based on the number of bag cleaning cycles between hopper evacuation cycles, the assumed percent re-entrainment and the product of the draft loss penalty and design maximum compartment draft loss. From this Figure any customer which has a draft penalty value, V, and a proposed baghouse design ΔP, P_M, can determine the cost of re-entrainment for various numbers of bag cleaning cycles between hopper evacuation cycles.

FACTORS IN THE COST OF CORRECTING RE-ENTRAINMENT

Once the cost of uncorrected re-entrainment has been established it follows that one should determine the cost of correcting the re-entrainment to determine if correction is economically justified. The costs of correcting re-entrainment are divided into three categories:

- The cost of a scale model test to determine the extent of re-entrainment and the selection of a design modification that reduces re-entrainment.
- The cost of implementation of that modification in full scale.
- The additional draft loss such a modification may itself create.

The cost of building and testing a scale model, C_M ($), has a fixed cost based on building the model and a variable cost based on the number of test configurations examined. For a quarter scale model the fixed cost would be $50,000 and the variable cost would be $10,000 per configuration (3). Figure 2, Cost of Model Testing, presents the cost of model testing versus the number of test configurations examined. The superposition of percent re-entrainment on number of test configurations follows from the hypothesis that if one test indicated less than 5% re-entrainment, no further tests would be conducted, if 10% were indicated a second configuration would be examined to attempt to reduce re-entrainment to less than 5%, and so on. Therefore, model test costs as a function of re-entrainment, R, are:

$$C_M = \$50,000 + \$200,000R \quad (3)$$

The additional costs of correcting re-entrainment, the implementation, installation and draft loss of a correction have been estimated as follows:

The cost of fabricating and installing a design modification, C_{IM} ($), was the product of the cost to modify each hopper, C_H ($), and the number of hoppers to be modified, H. C_{IM} was presumed to range from $1,000 per percent re-entrainment to $16,000 per percent re-entrainment. These costs were subsequently substantiated by a supplier (4) as reasonable for the design modifications considered.

$$C_H \times H = C_{IM} = \$100,000R \text{ to } \$1,600,000R \quad (4)$$

The cost of draft loss associated with a design modification, C_D ($), was assumed to be 0.5 in. w.g. to correct 25% re-entrainment.

$$C_D = \$2VR \quad (5)$$

This, too, was confirmed as reasonable by one supplier (4). In order to assure that all costs are in constant dollars, the capital costs, C_M and C_{IM}, must be multiplied by a present worth factor for capital, here assumed to be 1.6, to obtain all dollars evaluated in present worth.

$$C_M = \$80,000 + \$320,000R \tag{6}$$

$$C_{IM} = \$160,000R \text{ to } \$2,560,000R \tag{7}$$

Therefore, the total cost of determining and implementing a design modification to correct re-entrainment, C_{CR} ($), is the sum of C_M, C_{IM}, and C_D:

$$C_{CR} = \$80,000 + \$320,000R + \$160,000R + \$2VR \tag{8}$$

to

$$C_{CR} = \$80,000 + \$320,000R + \$2,560,000R + \$2VR \tag{9}$$

DECISION CURVES FOR CORRECTING RE-ENTRAINMENT

While it is beneficial to know the cost of re-entrainment for a given baghouse design and set of economic evaluation factors and the cost of correcting that re-entrainment, it would be most beneficial to develop curves of equal cost, $C_R = C_{CR}$, such that one could readily determine if testing and correction were warranted.

$$C_R = C_{CR} \tag{10}$$

$$P_M V(n-1)R/4 = 80,000 + 2VR + 320,000R + C_{IM} \tag{11}$$

$$R = \frac{320,000}{((n-1)P_M - 8)V - 1,280,000 - C_{IM}} \tag{12}$$

or

$$n = \frac{320,000 + R(V(8+P_M) + 1,280,000 + C_{IM})}{P_M VR} \tag{13}$$

Figure 3, Re-entrainment Decision Curve, $C_{IM}=C_H=\$160,000R$, through Figure 8, Re-entrainment Decision Curve, $C_{IM}=C_H=\$2,560,000R$, present the curves of equalization for varying values of P_M, for values of V of \$250,000/in., \$500,000/in., \$750,000/in., and \$1,000,000/in., respectively, for values of C_{IM} of \$160,000R to \$2,560,000R.

CONCLUSION

From the family of curves, presented in Figures 3 through 8, a decision regarding whether or not to pursue model testing and corrective modifications to decrease re-entrainment can readily be made. This decision will be based on accurate estimates of the cost of re-entrainment and reasonable estimates of the costs of determining and implementing corrective modifications. Determination of the optimum duration of time between hopper evacuation cycles may be made by calculating the time per cycle, t (min.), to reach P_M, according to the equation (5).

$$P_M = \frac{k\ C_i\ t\ v^{1.8}}{7000} \tag{14}$$

or

$$t = \frac{P_M\ 7000}{C_i\ k\ v^{1.8}} \tag{15}$$

ENDNOTES

1. Bowen, P. The Modeling of A Baghouse. In: Proceedings of the 4th International Fabric Alternatives Forum, Phoenix, Arizona, December 5-6, 1979.

2. Musgrove, J. G. A Survey of Particulate Collection Divices for Coal-Fired Boilers. In: Proceedings of the International Coal Utilization Convention, Houston, Texas, October 17-19, 1978.

3. Musgrove, J. G. In: Conference Notes Number 13051-133, Bechtel Power Corporation, April 23, 1980.

4. Zierak, S. Modified Hopper for Re-entrainment Study. In: Letter to John Musgrove, September 4, 1980.

5. Jensen, R. M. Baghouse Bid Evaluation. In: Proceedings of the 2nd International Fabric Alternatives Forum, Denver, Colorado, July 27-28, 1977.

TABLE I - PARAMETERS OF BAGHOUSE RE-ENTRAINMENT FOR R = 10%

Cycle Number	Ash in Hopper at Start of Cycle	Ash in Hopper at End of Cycle	Ash in Hopper After Bag Cleaning	Ash on Bag from In Flow	Ash on Bag from Hopper	Total Ash on Bag	Maximum ΔP This Cycle	Max. ΔP Due to Ash from Hopper This Cycle	Avg. ΔP Due to Ash from Hopper, This Cycle	Avg. ΔP Due to Ash from Hopper, All Cycles
1	0.0	0.0	1.0	1.0	0.0	1.0	5.0	0.0	0.0	0.0
2	1.0	0.9	2.0	1.0	0.1	1.1	5.5	0.5	0.25	0.125
3	2.0	1.8	3.0	1.0	0.2	1.2	6.0	1.0	0.5	0.25
4	3.0	2.7	4.0	1.0	0.3	1.3	6.5	1.5	0.75	0.375
5	4.0	3.6	5.0	1.0	0.4	1.4	7.0	2.0	1.0	0.5
6	5.0	4.5	6.0	1.0	0.5	1.5	7.5	2.5	1.25	0.625
7	6.0	5.4	7.0	1.0	0.6	1.6	8.0	3.0	1.5	0.75
8	7.0	6.3	8.0	1.0	0.7	1.7	8.5	3.5	1.75	0.875
9	8.0	7.2	9.0	1.0	0.8	1.8	9.0	4.0	2.0	1.0
10	9.0	8.1	10.0	1.0	0.9	1.9	9.5	4.5	2.25	1.125
11	10.0	9.0	11.0	1.0	1.0	2.0	10.0	5.0	2.5	1.25
12	11.0	9.9	12.0	1.0	1.1	2.1	10.5	5.5	2.75	1.375
13	12.0	10.8	13.0	1.0	1.2	2.2	11.0	6.0	3.0	1.5
14	13.0	11.7	14.0	1.0	1.3	2.3	11.5	6.5	3.25	1.625
15	14.0	12.6	15.0	1.0	1.4	2.4	12.0	7.0	3.5	1.75

TABLE II - PERCENT DRAFT LOSS FROM RE-ENTRAINMENT, R = 10%

Cycle Number	1	2	3	4	5	6	7	8	9	10	11	12	13	14	15
ΔP due to Re-entrainment	0	.5	1.0	1.5	2.0	2.5	3.0	3.5	4.0	4.5	5.0	5.5	6.0	6.5	7.0
ΔP/5.0 in.w.g.	0	0.1	0.2	0.3	0.4	0.5	0.6	0.7	0.8	0.9	1.0	1.1	1.2	1.3	1.4
Avg. ΔP_R for All Cycles	0	.125	.25	.375	.5	.625	.75	.875	1.0	1.125	1.25	1.375	1.5	1.625	1.75
Avg. ΔP_R/5.0 iwg	0	.025	.05	.075	.10	.125	.15	.175	.20	.225	.250	.275	.30	.325	.35
Percent ΔP due to R	0	2.5	5.0	7.5	10.0	12.5	15.0	17.5	20.0	22.5	25.0	27.5	30.0	32.5	35.0

FIGURE 1
COST OF RE-ENTRAINMENT, C_R

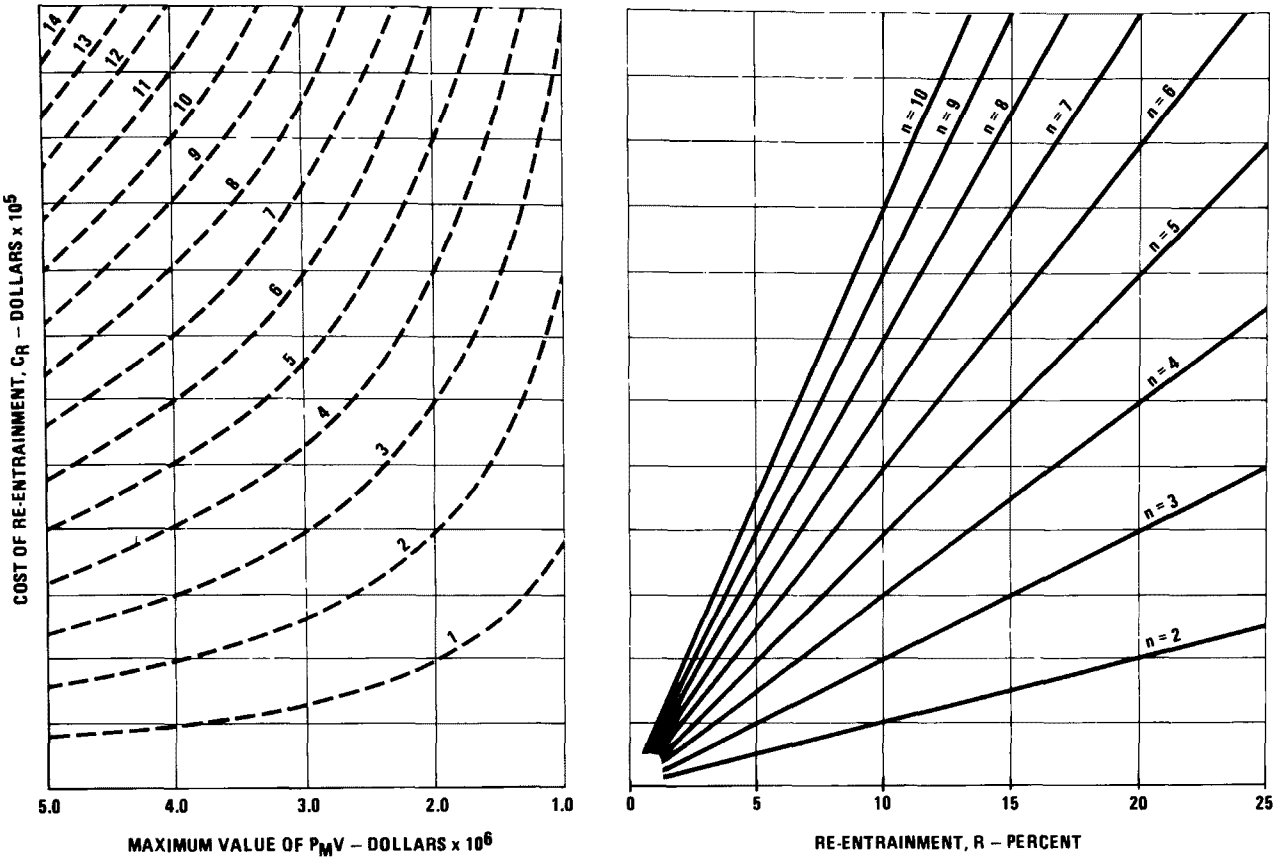

FIGURE 2
COST OF MODEL TESTING

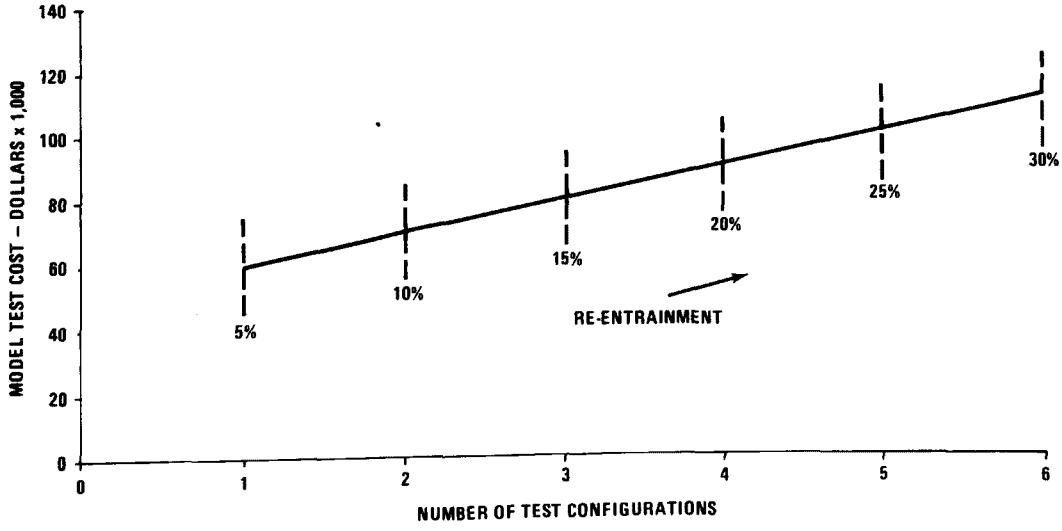

FIGURE 3
RE-ENTRAINMENT DECISION CURVE
$C_{IM} = C_H H = \$160{,}000R$

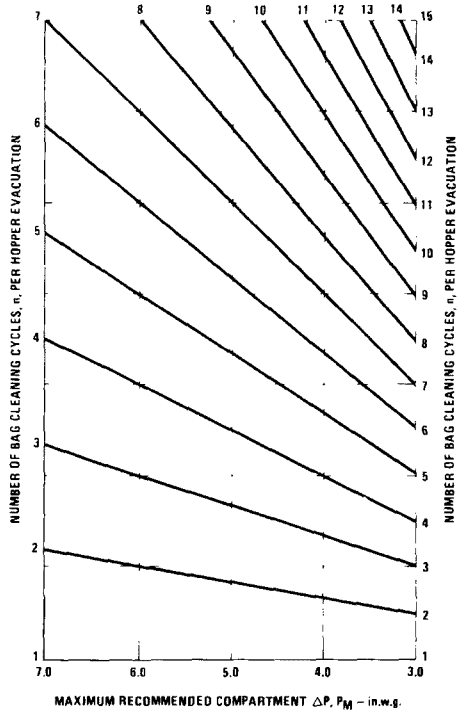

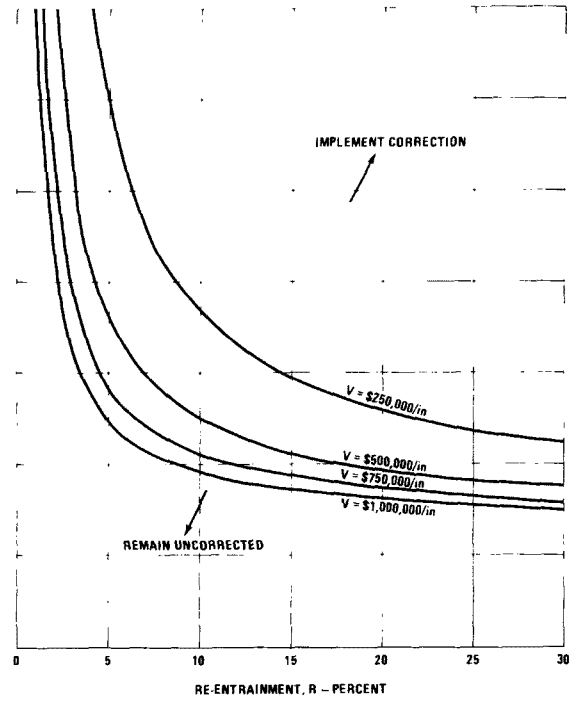

FIGURE 4
RE-ENTRAINMENT DECISION CURVE
$C_{IM} = C_H H = \$320{,}000R$

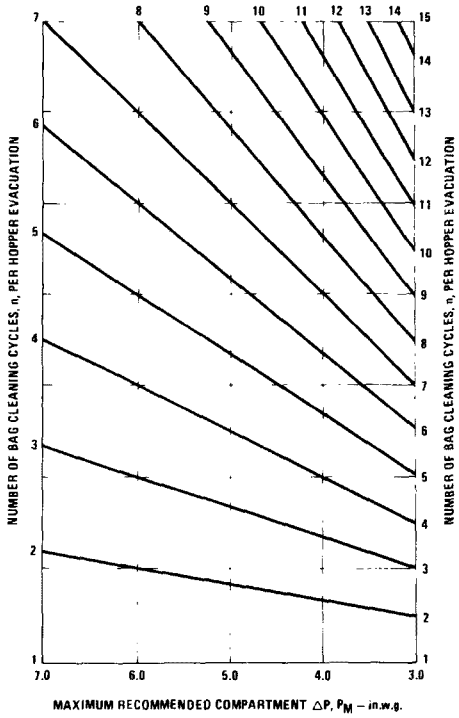

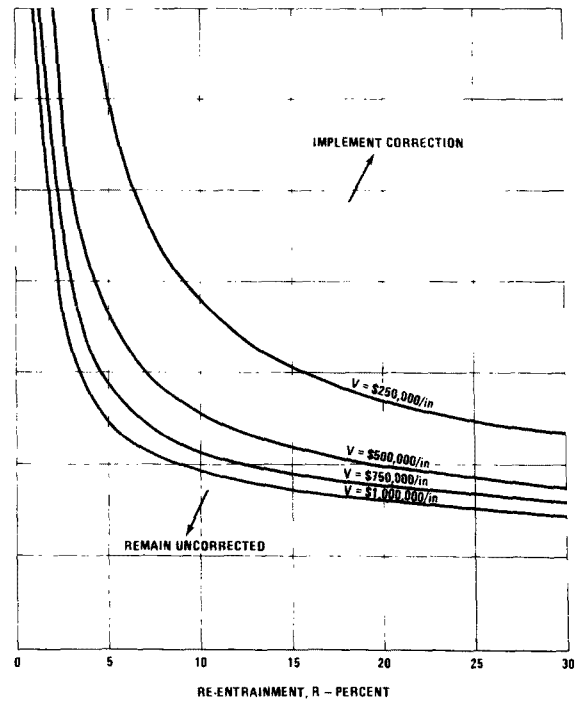

FIGURE 5
RE-ENTRAINMENT DECISION CURVE
$C_{IM} = C_H H = \$640{,}000R$

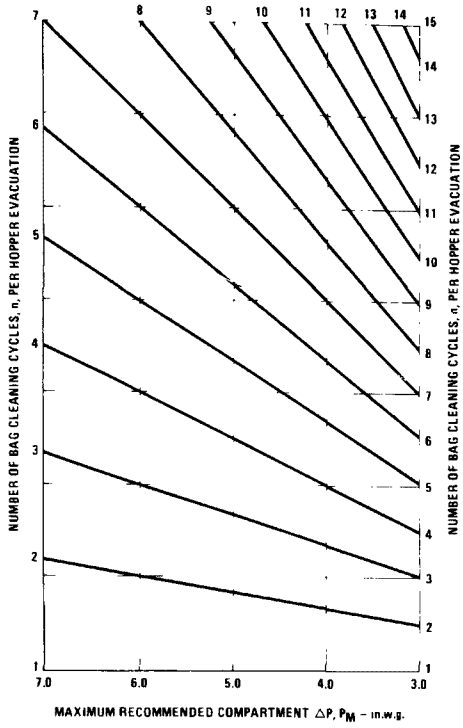

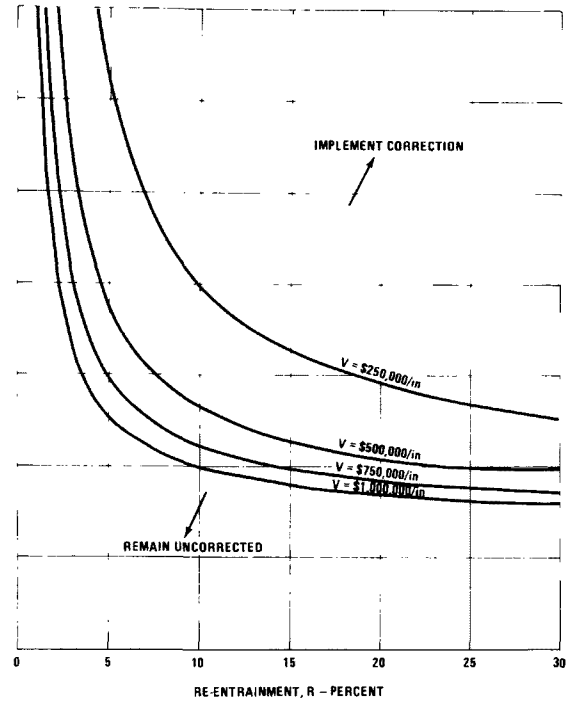

FIGURE 6
RE-ENTRAINMENT DECISION CURVE
$C_{IM} = C_H H = \$1{,}280{,}000R$

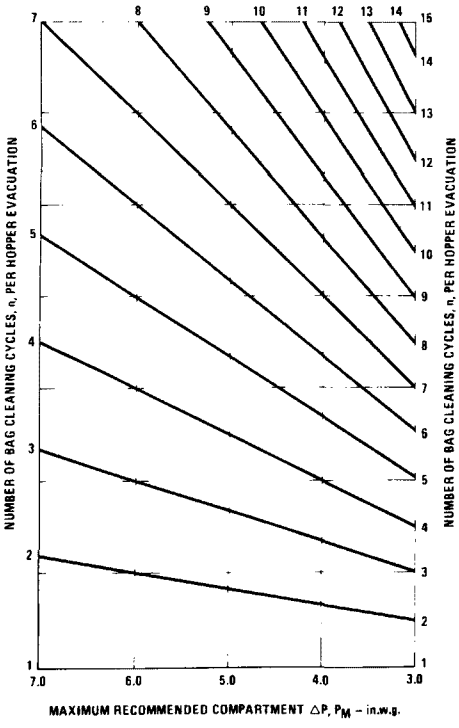

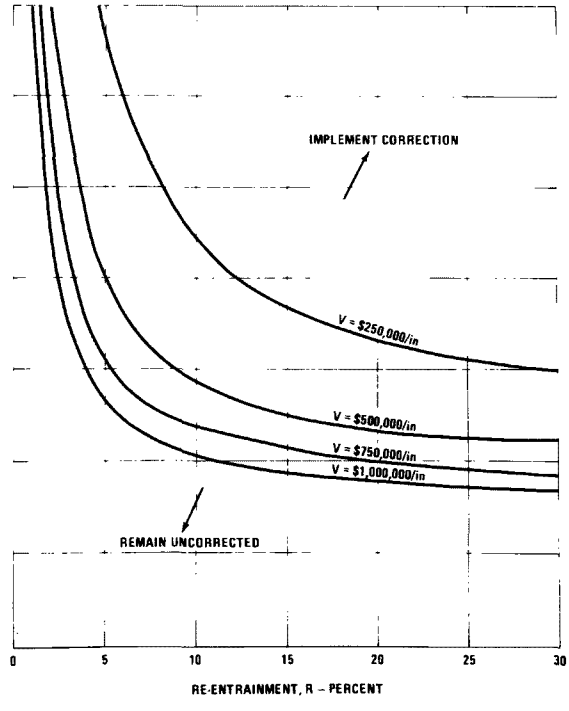

FIGURE 7
RE-ENTRAINMENT DECISION CURVE
$C_{IM} = C_H H = \$1{,}920{,}000R$

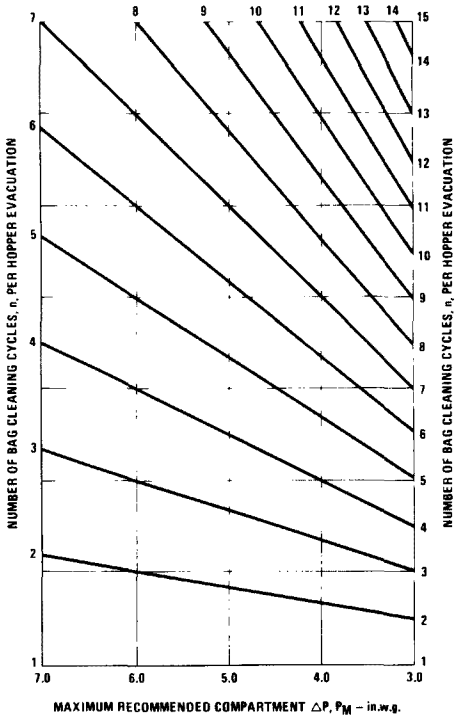

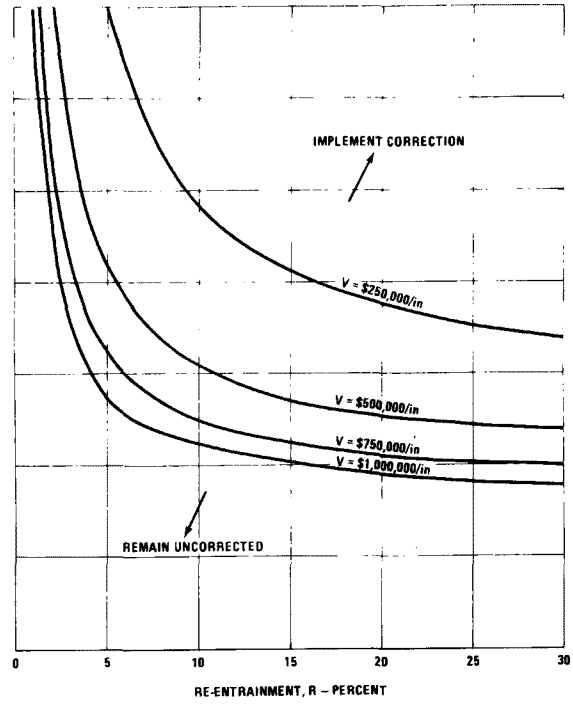

FIGURE 8
RE-ENTRAINMENT DECISION CURVE
$C_{IM} = C_H H = \$2{,}560{,}000R$

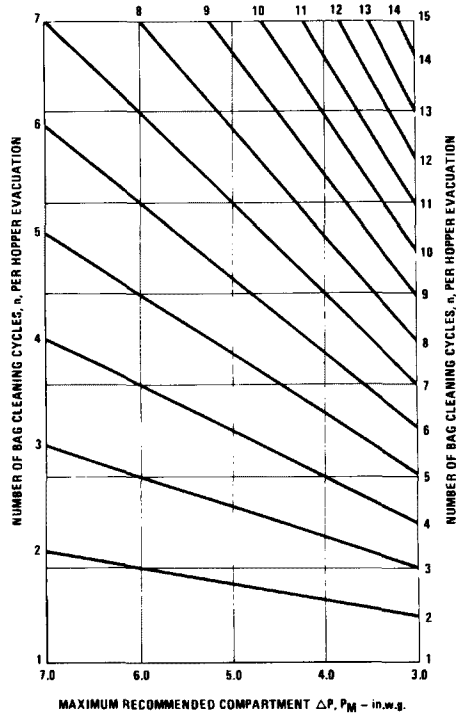

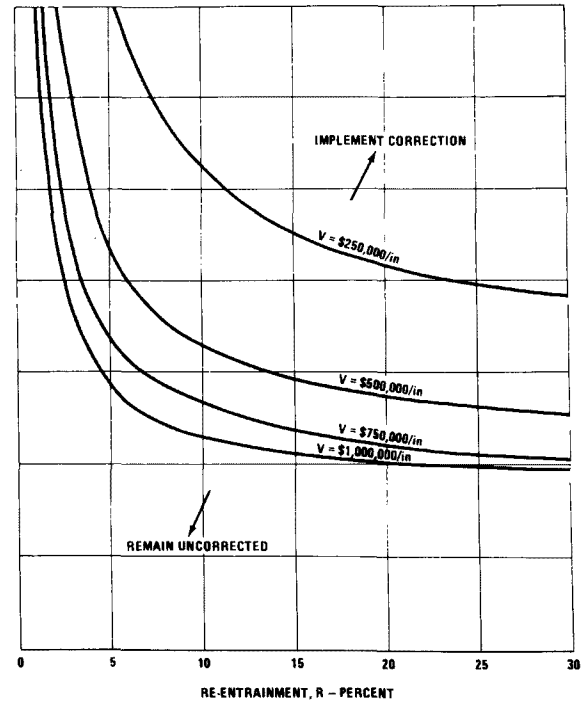

WHY PERFORM MODEL STUDY OF FABRIC FILTER COLLECTOR?

By: William T. Langan
Buell Emission Control Division
Envirotech Corporation
Lebanon, Pennsylvania 17042

Dr. Norman Z. Shilling
Buell Emission Control Division
Envirotech Corporation
Lebanon, Pennsylvania 17042

William A. Van Kleunen
Buell Emission Control Division
Envirotech Corporation
Lebanon, Pennsylvania 17042

Owen F. Fortune
Buell Emission Control Division
Envirotech Corporation
Lebanon, Pennsylvania 17042

ABSTRACT

The industry historically has performed model studies of electrostatic precipitators to achieve good gas distribution in the field unit. Standards for electrostatic precipitators are well developed, and field experience has proven such modeling is important to achieve high collection efficiency for these particulate collecting equipment. Differences in model study evaluation of fabric filters and precipitators are contrasted in light of the fundamental differences between the two types of particulate control devices.

The performance criteria required for satisfactory fabric filter operation are presented. These criteria are translated into goals to be met through a model study effort.

Specific results from model studies of several major utility facilities are reviewed. The impact of the model study results upon the design features of fabric filter collectors are described. Field data verification of good particle size distribution within compartments of operational units are presented to demonstrate the results of proper design for gas flow/particulate distribution.

INTRODUCTION

Precipitator model studies are performed to obtain the high quality gas flow distribution required to achieve low outlet emissions. The model construction is typically one-sixteenth scale of the field unit to ensure turbulent flow. The ductwork design and gas flow devices are selected to achieve field gas flow distribution of I.G.C.I. quality. These requirements are: (1) no velocity measurement is to deviate more than $\pm$40% from the average velocity, and (2) 85% of the velocity measurements are to be within $\pm$25%

of the average velocity. The predicted influence of gas flow distribution upon precipitator collection efficiency is presented in Figure 1. As this figure illustrates, significant performance improvements can be achieved by reducing high RMS gas flow distributions to I.G.C.I. gas distribution quality. The cost effectiveness of attempting to obtain even lower RMS gas flow distribution values must be seriously questioned through the evaluation of the amount of steel for the required gas flow devices, the scale-up correlation between the field and the model, and the estimated performance enhancement. Gas flow distribution must be uniform and gas treatment velocity must be low (typically less than 4.5 ft/sec., depending upon the flyash conductivity) to minimize re-entrainment of captured flyash.

The precipitator model study is typically conducted for a steady state condition. The only transient conditions investigated in a precipitator model study are dust desposition and sweepage studies. This is fundamentally different than the fabric filter collector which normally operates in transient conditions due to the cleaning modes.

To establish criteria that should be utilized for a fabric filter model study, an overview of potential field problems and their causes are presented in Table 1. To ensure successful field operation of the fabric filter, the model study effort should evaluate pressure losses in the ductwork, distribution of gas flow and/or particulate to baghouse compartments, distribution of gas flow and/or particulate within baghouse compartments, and distribution of reverse air within baghouse compartments.

MODEL STUDY APPROACH

The fabric filter collector should be designed for good flow distribution to ensure high reliability and performance. The design guidelines for good flow distribution are:

- Relatively constant transport velocity (3000 to 4500 feet per minute).
- Flow impedance at compartment inlet, to compensate for various operating modes.
- Low hopper entrance velocity.
- Reverse air distribution over the entire compartment.

These fabric filter designs are based upon extensive fabric filter field experience and several fabric filter model studies, including: Tennessee Valley Authority, Shawnee Steam Plant, Units No. 1 through 10; Public Service of Colorado, Cherokee Units No. 2 and 3; Baltimore Gas & Electric Company, Crane Units No. 1 and 2; Arizona Public Service Company, Four Corners Units No. 4 and 5; Plains Electric Generating and Transmission Coop, Inc., Escalante Generating Station, Unit 1, and Board of Light and Power, Marquette, Michigan, Shiras Unit No. 3.

The model study investigates the transient conditions associated with

the fabric filter operation. Typically, the following four conditions are investigated:

A. "Pressure Limit" or "Time" mode cleaning cycle, at a point in time when all compartments have just been cleaned. At this time, all compartments will evidence essentially identical Pressure drop characteristics corresponding to a 2-3 in. W.G. filter media/residual filter cake pressure drop characteristic.

B. "Pressure Limit" or "Time" mode cleaning cycle, at a point in time when all compartments are about to be cleaned. At this time, all compartments will evidence an essentially identical filter media/filter cake pressure drop characteristic of 3-5 in. W.G.

C. Also in "Pressure Limit" or "Time" mode cleaning cycle, but at a point in time when the first compartment has just been cleaned. In this short duration situation, one compartment will demonstrate a minimum pressure drop characteristic, while all other operating compartments demonstrate the maximum pressure drop characteristic. This one compartment will then experience a maximum gas flow rate excursion.

D. In "Integrated" mode of cleaning cycle. At each repetitive situation when a compartment is being cleaned, there will be one compartment (the next compartment to be cleaned) which will evidence a maximum pressure drop characteristic, while one compartment (the most recent compartment cleaned) will evidence a minimum pressure drop characteristic.

Model test operating Mode "C" represents an instantaneous situation, before any equalization of filter cake deposition has occurred. This is also an exaggerated situation because it includes the maximum amount of filter cake deposition in all other compartments. Although this situation is of very short duration during baghouse operation, it does demonstrate excursions of gas flow rate which are approached. The magnitude of the gas flow rate excursions illustrate why attention must be given to this parameter of baghouse operation.

Model test operating Modes "A" and "B" represent operating situations which reflect the natural occurring equalization of filter cake deposition. Model study test experience shows that there is minimal difference of the division of gas flow to operating baghouse compartments for either just cleaned filter bags, or bags with maximum filter cake deposition. The model program investigates identical simulated pressure drop in all baghouse compartments so that the effect of the baghouse design configuration may be investigated, apart from the effect of the filter bag/filter cake pressure drop.

The "Integrated" mode bag cleaning cycle, as illustrated by model test operating Mode "D", illustrates reduced gas flow rate excursion in the just

cleaned compartment. However, this is again a short duration situation, before any natural equalization of filter cake deposition.

The operation of the 1:16 scale model at scaled flow rates of ambient temperature air allows the model to be operated in fully-developed turbulent flow regime (as defined by a Reynolds number >4000), at all pertinent model locations, and at all load gas flow conditions. This is a necessary requirement to insure dynamic similitude between the model and prototype installation operating conditions.

The division of volumetric flow rate between baghouse compartments is determined by measuring the pressure drop created by perforated plate, which simulates the filter media/filter cake pressure drop, and for which the pressure drop vs. volumetric flow rate characteristic is known.

Investigations of gas flow distribution within baghouse compartments are performed utilizing flow visualization techniques. This procedure permits optimization of such parameters as: Baghouse compartment isolation valve size and location, internal baffles and gas flow directing vanes within the baghouse compartment hoppers, and the configuration of baghouse inlet and outlet gas flow manifolds. A superior procedure for performing flow visualization investigations is the Neutrally-Buoyant Helium Bubble technique.

Gas flow distribution tests are performed in the high-velocity transport ductwork systems. Typical locations in the model for these investigations are: Air heater outlet ductwork, air heater outlet crossover duct, entrance to baghouse, discharge from baghouse, baghouse bypass ductwork system, and inlets to I.D. fan.

Incremental pressure drop surveys are performed in the model for pertinent model configurations of simulated filter media/filter cake pressure drop, number and arrangement of operating baghouse compartments and operating load flue gas flow rates. Model data consists of static pressure measurements and the contributing effect of the computed velocity pressure at the model test volumetric flow rate. Model test results are projected to the full-scale installation operating conditions. Typical locations for incremental model measurements are: Discharge from air heaters, baghouse system inlet performance test port location or baghouse inlet, within baghouse compartment hoppers (entrance to baghouse compartments), discharge from baghouse compartments (downstream of simulated filter media/filter cake pressure drop), baghouse outlet or baghouse system outlet test port location, and inlets to I.D. fan.

These measurements are performed at both normal baghouse operation and baghouse bypass system operation.

Particulate deposition and distribution tests are performed in the model for pertinent baghouse configurations and expected flue gas flow rates. In assessing these parameters, the testing procedure employs a test particulate of appropriate density and particle size distribution characteristics, to simulate the dynamics of particulate at prototype operating conditions. Model tests include observations of dust deposition within the transport duct and within the baghouse

for the full range of expected flue gas flow rates. Model investigations are also performed to survey particulate deposition within the baghouse inlet manifold and in the operating baghouse compartment hoppers.

RESULTS

The design areas modified, based upon model study results, include: hopper baffling, outlet poppet valves, inlet poppet valves, bypass poppet valves, and bypass ductwork.

The impact of proper hopper baffling is illustrated by a comparison of Figures 2 and 3. Clearly, proper hopper baffling, as shown by Figure 3, minimizes the probability of detrimental dust re-entrainment.

The impact of proper poppet sizing is illustrated by a comparison of the compartment gas flow distribution shown by Tables 2 and 3. By modification of the outlet poppet dimensions, the gas flow distribution RMS was improved significantly.

Particulate particle size distribution measurements have been performed for filter cake obtained from an operating baghouse. Filter cake samples were extracted from various operating baghouse compartments, as well as from various locations within an operating compartment. The purpose of these determinations was to verify that the distribution of particulate is uniform in a properly designed baghouse. Table 4 illustrates particulate particle size distribution for various compartments. Table 5 illustrates the particle size distribution of particulate within a compartment. These data verify that excellent particulate distribution was achieved in the operating baghouse.

SUMMARY

Early model studies have been important in impacting the fabric filter design to ensure high performance levels. The need to perform model studies for future plants decreases since the results of past model studies and field experience are incorporated in Engineering design standards. The focus of future fabric filter model studies will be more cost-effective designs, as well as even lower maintenance designs.

ILLUSTRATIONS

Figure 1 - Precipitator efficiency vs. % RMS
Figure 2 - Hopper without baffles
Figure 3 - Hopper with baffles
Table 1 - Potential fabric filter field problems and associated causes
Table 2 - Division of gas flow between compartments - not optimized
Table 3 - Division of gas flow between compartments - optimized
Table 4 - Particle size distribution - between operating baghouse compartments
Table 5 - Particle size distribution - within operating baghouse compartment.

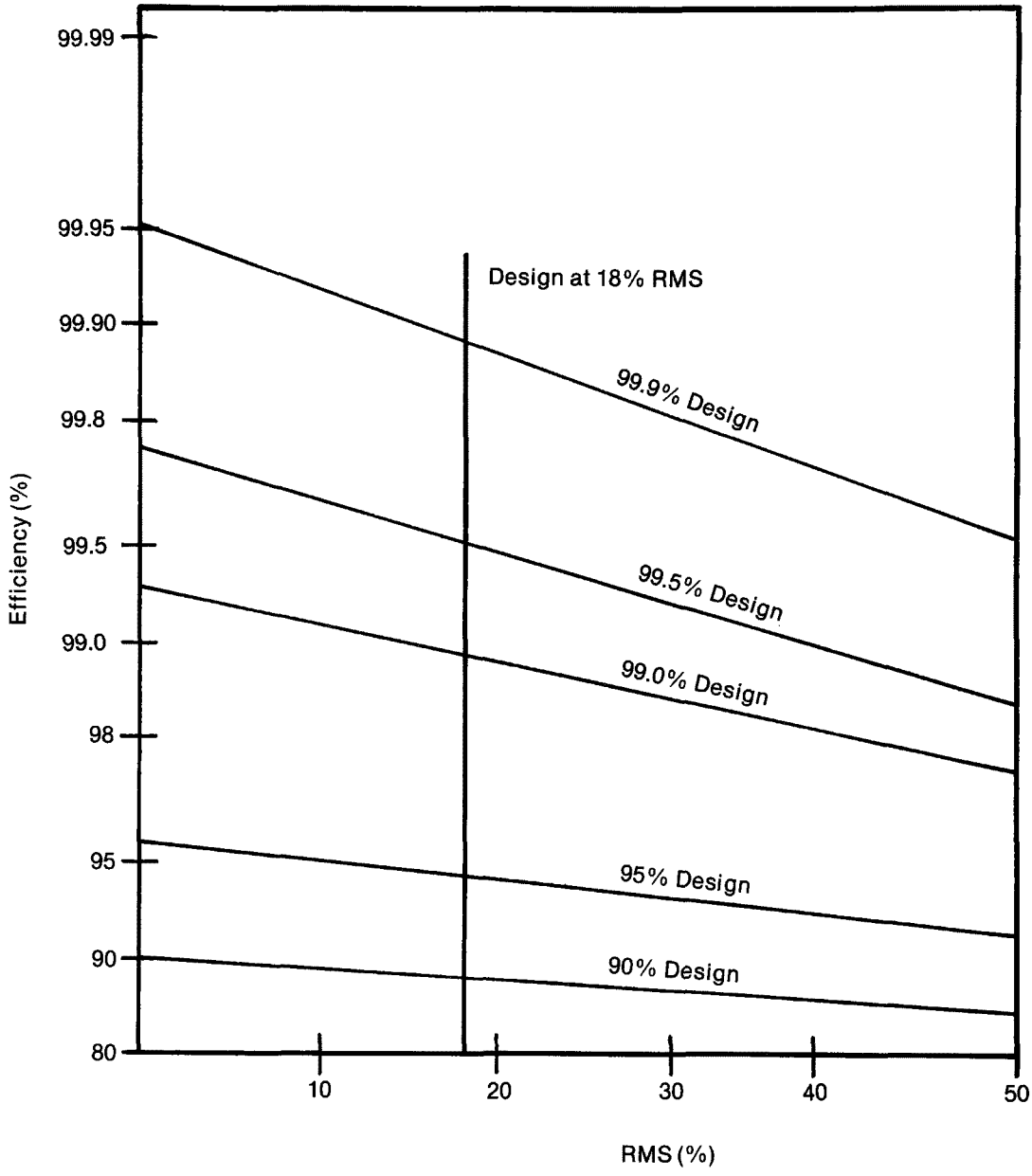

Prediction Of Effect Of Flow
Uniformity On Precipitator Efficiency

Figure 1

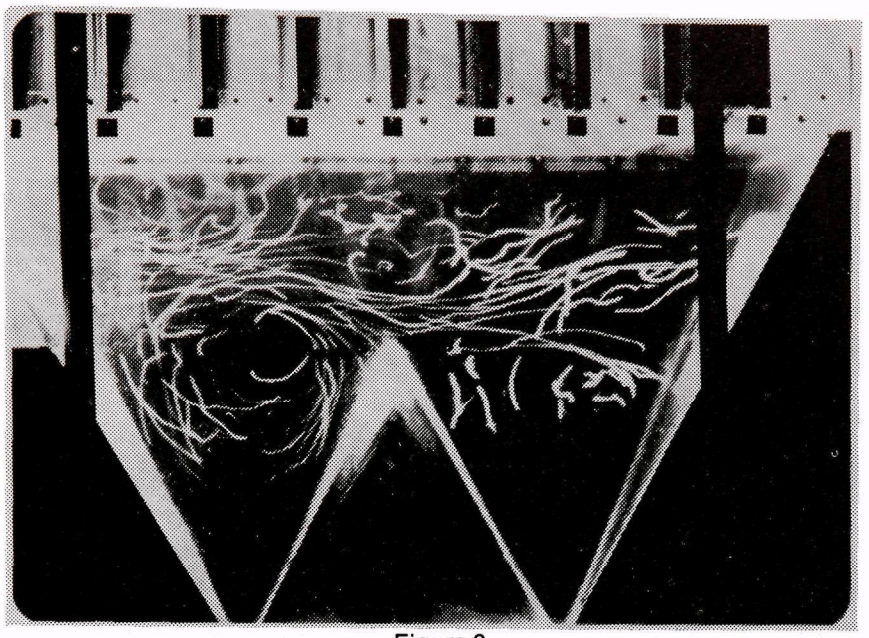

Figure 2

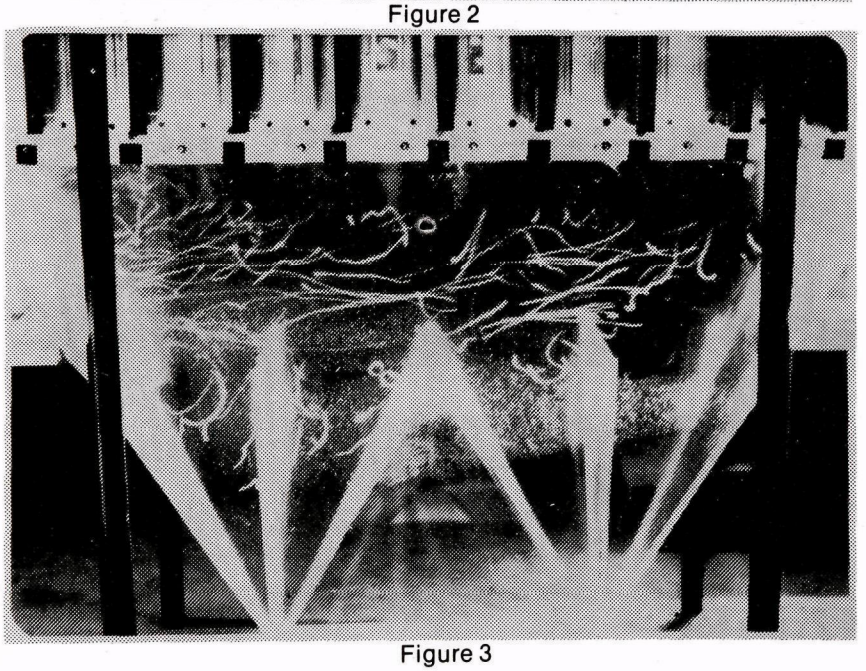

Figure 3

Flow Distribution Within Baghouse Hopper Illustrated By Flow Visualization

Fabric Filter

Problem	Potential Cause
Excessive Pressure Drop	• Pressure Losses In Ductwork • Maldistribution Of Gas Flow And/Or Particulate To Baghouse Compartment • Maldistribution Of Gas Flow And/Or Particulate Within Baghouse Compartment • Maldistribution Of Reverse Air Within Baghouse Compartment • Excessive Sub-Dewpoint Operation Of Unit (Normal Operation/Reverse Air Cleaning)
Short Bag Life	• Abrasion Due To Improper Inlet Conditions • Excessive Sub-Dewpoint Operation Of Unit (Normal Operation/Reverse Air Cleaning) • Maldistribution Of Gas Flow And/Or Particulate To/Within Baghouse Compartment
Excessive Emissions	• Ineffective Utilization Of Available Cloth Area Due To Flow/Particulate Maldistribution To/Within Baghouse Compartment • Damaged Bags Resulting From Mechanical Or Operational Problem

Table 1

All Outlet Poppets At 5'-6" Diameter
Simulated Bag Δ TP = 2.0 IN. W.G.
8 Of 10 Compartments In Operation With Clean Bags

	Compartment	Test No. 1	Test No. 2	Test No. 3	Test No. 4	Test No. 5
% Deviation From Average	1	Off	Off	+8.48	+5.76	+6.48
	2	Off	+19.04	+11.36	+7.68	+10.40
	3	+8.80	Off	+3.44	−0.32	+1.44
	4	+7.84	+9.60	+4.48	+1.76	+1.44
	5	+3.68	−0.56	Off	−0.32	+1.44
	6	+2.64	−1.76	Off	−2.24	+0.40
	7	−4.00	−1.76	−5.20	Off	−4.96
	8	−5.12	−5.04	−6.32	−5.60	−16.64
	9	−7.52	−9.76	−8.72	Off	Off
	10	−6.32	−9.76	−7.52	−6.72	Off
	RMS	6.10%	9.42%	7.35%	4.70%	7.51%

Table 2

Outlet Poppets In Compartment 1 & 2 - 4'-0"
Outlet Poppets In Compartment 3 & 4 - 4'-6"
Outlet Poppets In Compartments 5-10 - Unchanged 5'-6"
Simulated Bag ΔTP = 2.0 IN. W.G.
8 Of 10 Compartments In Operation With Clean Bags

	Compartment	Test No. 6	Test No. 7	Test No. 8	Test No. 9	Test No. 10
% Deviation From Average	1	Off	Off	−1.52	−2.48	−3.20
	2	Off	+7.28	+2.88	−0.40	−1.04
	3	+4.96	Off	+2.88	+0.72	+1.12
	4	+4.96	+5.28	+4.00	+0.72	−1.04
	5	+4.96	+3.12	Off	+3.76	+5.20
	6	+2.80	+3.12	Off	+2.72	+3.20
	7	−3.84	−1.28	−0.32	Off	−1.04
	8	−3.84	−5.84	−1.52	−1.44	−3.20
	9	−6.16	−7.04	−3.76	Off	Off
	10	−3.84	−4.64	−2.64	−3.60	Off
	RMS	4.52%	5.09%	2.70%	2.34%	2.79%

Table 3

Fly Ash Samples From Filter Bags In Various Operating Baghouse Compartments

Baghouse Compartment/ Sample I. D.	Mean Particle Diameter, D, Microns
1/1	5.7
1/2	5.7
1/3	5.8
2/1	6.0
2/2	5.8
2/3	5.9
3/1	6.8
3/2	6.1
3/3	5.8
4/1	5.9
4/2	5.9
4/3	5.7
5/1	6.2
5/2	6.2
5/3	5.5
6/1	5.8
6/2	6.2
6/3	5.7
7/1	6.2
7/2	6.6
7/3	6.4
8/1	6.1
8/2	5.9
8/3	6.1
9/1	6.1
9/2	6.0
9/3	6.6
10/1	6.5
10/2	6.3
10/3	5.9

Table 4

Fly Ash Samples From Filter Bags In Operating Baghouse Compartment

Baghouse Compartment/ Sample I. D.	Mean Particle Diameter, D, Microns
7/1	6.4
7/2	6.7
7/3	6.9
7/4	6.6
7/5	6.6
7/6	6.4
7/7	6.6
7/8	6.3
7/9	6.5
7/10	8.0
7/11	7.0
7/12	6.3
7/13	6.3
7/14	7.0
7/15	6.1

Table 5

EXPERIENCES OF A SMALL INSULATION MANUFACTURER IN MAINTAINING COMPLIANCE WITH AIR POLLUTION CONTROL REGULATIONS

By: R. L. Hawks
PEDCo Environmental, Inc.
505 South Duke Street, Suite 503
Durham, North Carolina 27701

ABSTRACT

The implementation of stringent regulations has created a hardship on small businesses who have little technical expertise in the area of environmental control. This paper presents the experiences of a small blown-insulation producer that has been in operation in Southeast United States since 1976. Numerous difficulties with air pollution control equipment have hindered this plant from achieving full production capacity and have led to a tiring series of sparring exercises with local regulatory officials. Many of the problems could have been avoided had the equipment been designed better and had the supplier given better instructions to company management responsible for its operation. The author contends that the equipment suppliers have a special obligation to educate small companies regarding important design factors and operation and maintenance procedures. The author further believes that regulatory agencies should provide a thorough permit review of smaller pollution sources and assist them in developing technical expertise in air pollution control.

INTRODUCTION

The enactment of the Clean Air Act in 1970 has resulted in major economic and technical impacts on American business. The setting and implementation of emission limits has created a particular hardship for small business.

Most small businesses do not initially have the technical ability to design, operate, or maintain air pollution control equipment. Nor do most of these small sources have technical staffs versed in the disciplines of industrial ventilation or control equipment design. Therefore, they must rely on local regulatory agencies, control equipment manufacturers, and vendors to provide them with knowledge regarding air pollution control requirements.

Historically, the regulatory agencies have not provided technical assistance in design, operation, or maintenance, either because of legal restraints or their own limited manpower and experience. Thus, the design of abatement equipment at small sources has been based on limited experience, recommendations of vendors, or in some cases, guesswork. Unfortunately, the equipment installed in this manner has been susceptible to operation and maintenance problems, and most importantly, the small firms have frequently been subjected to compliance penalties due to excess emissions.

This paper describes the experiences of one small business in its attempt to maintain compliance with emission limits with improperly designed air pollution control equipment and process variables that were not fully appreciated.

PLANT DESCRIPTION

The plant, a conventional mineral wool manufacturer, uses a cupola and blow chamber to produce blowing wool for insulation. There are two 32-in.-diameter water-cooled cupolas. These cupolas are charged with coke, trap rock, copper and steel slags, and limestone. The flue gases from the cupolas are diluted with ambient air and exhausted by an induced-draft fan through a reverse-air/shaker-type fabric filter.

This privately owned plant employs approximately 100 persons and operates on a 24-h schedule for periods up to 60 days without cupola outages for major maintenance. Staffing consists of production personnel, maintenance crews, and management. The plant does not have sufficient operating funds to employ a staff engineer.

CUPOLA PARTICULATE CONTROL EXPERIENCES

Construction of the plant was completed in August 1976, and the firm filed a construction permit application with the local air pollution agency to operate two cupolas and two blow chambers. Because the uncontrolled particulate emissions from these sources would not comply with emission limitations set by the agency, the plant specified low-energy scrubbers to control blow chamber emissions and fabric filter systems to control cupola emissions.

The fabric filter specified for each cupola was a reverse-air/shaker design with a total cloth area of 16,000 ft^2 in four isolatable compartments. The filter was designed to operate at an air volume of 20,000 acfm and at an air-to-cloth ratio of 1.25 acfm/ft (gross). The system was equipped with dilution air cooling to reduce gas temperatures to below 500°F and with silicon/graphite-finished fiberglass bags. The plant installed a limestone precoat system to increase collection efficiency and remove sulfur dioxide (SO_2) emissions from the gas stream, which later proved to be an unnecessary and costly investment.

The local regulatory agency reviewed the filter design and issued an operating permit. The agency's review was superficial and considered only the air-to-cloth ratio and the compatibility of the fabric with the expected gas temperature range. Also, it was assumed that emissions would be less than 1.0 lb/h, based on an expected collection efficiency of 99.5 percent. The agency did not evaluate the variability of the cupola operation, composition of charge materials, or potential for filter failure due to process influences. The regulatory agency included a stack test stipulation in the permit, which required an EPA Method 5 test 30 days after plant startup.

A local contractor installed the filter under the direction of the filter manufacturer's field representative. The erection period was

lengthy and plagued by bad weather and inexperienced installation personnel.

After a shakedown period the plant conducted the required particulate stack test. Emissions were determined to be 9.85 lb/h, which complied with the regulatory limit of 13.0 lb/h. However, the efficiency of the fabric filter on line 1 was only 91 percent, much less than the expected 99.5 percent.

Shortly after the initial particulate stack test, the filter static pressure drop began to increase sharply. At the direction of the manufacturer, the plant increased the intensity and frequency of cleaning. This vigorous cleaning soon caused failure of the fiberglass bags and increased filter maintenance, which resulted in periods of excess emissions. The reason for the abnormally high static pressure drop was not determined, only the symptom was treated.

A review of the particulate stack test showed that the average exit gas temperature was lower than expected (136°F) and below the gas stream moisture dewpoint of 160°F. A check of the inlet gas stream temperature confirmed the low temperature and suggested that this was a typical operating pattern for the cupola. The cupola exhaust is diluted with ambient air and quenched from approximately 1200°F. The amount of dilution air was not measured, nor was any provision made to regulate the amount. This unregulated dilution allowed the system to operate far below the design temperature of 450°F. It is believed that the fabric filter manufacturer was not aware of this poor temperature control system during the design phase.

Further measurement indicated that the cupola gas stream had a predictable temperature profile that resulted in the flue gases passing through the dewpoint each 20 min (Figure 1). The temperature increases as the cupola charge is consumed and then decreases sharply when a batch charge is added. The baghouse inlet temperature ranged between 130° and 230°F over this period. Each time the system dropped below the dewpoint, the limestone precoat on the bags would adsorb moisture; when the gas temperature increased, this precoat hardened to a cake that could not be removed easily without damaging the fabric (Figure 2). Due to the resulting high static pressure drop, cupola production capacity was limited.

Once the reason for the high pressure drop was identified, the plant reduced the use of limestone and limited the dilution air so as to maintain the temperature above 250°F. These changes reduced the static pressure drop of the system. Cleaning intensity also was reduced; however, the rate of bag failures continued to increase. Based on the assumption that the failures resulted from previous damage, a complete bag change was made, but the new bags continued to fail in unexpected numbers.

It must be noted that plant personnel were inexperienced in the care and installation of fiberglass bags. As a result, the bags were seriously abused during installation. Some were tied in knots to allow access to defective bags, some were dragged through the access doors, and others were walked on (Figure 3). Discussion with plant personnel indicated that

neither the filter manufacturer nor the bag supplier had provided instructions concerning the delicate handling required for fiberglass bags.

Mistreatment of the bags did not totally explain the high failure rate. The bags deteriorated in the lower 25 percent of their length and lost tensile strength. The failures did not appear to be associated with high temperature damage, but was more representative of chemical damage.

The slags contain trace amounts of fluorides, which are emitted as hydrogen fluoride under reducing conditions. These fluorides were eventually determined to be partially responsible for the failure of the fiberglass bags. The plant purchases slags from several sources, but does not have the option to limit purchases based on fluoride content. The obvious solution was to use a bag fabric resistant to fluorides. Because the fabrics available for high-temperature fluoride exposure were either expensive or subject to attack by the sulfur oxides in the gas stream, the plant eventually was forced to limit gas temperatures to a maximum of 350°F so that polyester bags could be used. These bags have provided good life under these conditions.

CUPOLA HYDROGEN SULFIDE EXPERIENCES

The maintenance of the fabric filter has been a burdensome and hazardous experience for the company because of the high levels of hydrogen sulfide present in the gas stream. This had not been anticipated by plant personnel. The system was equipped with isolatable compartments to allow on-line maintenance. Unfortunately, the butterfly dampers for compartment isolation did not seal and no compartment air-purge system was provided. Attempts to conduct on-line maintenance have on two occassions resulted in hospitalization of maintenance personnel.

Neighborhood complaints concerning odors forced the plant to determine the level of its hydrogen sulfide (H_2S) and SO_2 emissions. Six stack test runs using EPA Methods 11 and 6 indicated maximum H_2S emissions of 46.7 lb/h (500 ppm) and SO_2 emissions of 1.0 lb/h. The H_2S levels were highly variable and related to slag sulfur content. Individual test emission rates varied between 16.2 and 66.05 lb/h, and slag sulfur content varied between 1.84 and 3.02 percent. The State agency subsequently issued a notice of violation based on a boundry line H_2S concentration limit. Using worst case meteorological conditions, the agency calculated that the ambient concentration would be exceeded slightly at the maximum tested H_2S emission rate. The company was successful in overturning this citation since the regulation was vague regarding required emission limits.

The plant is now considering three options: 1) installation of positive sealing isolation dampers, 2) installation of a compartment air-purge system, and 3) use of air line respirators during internal maintenance.

SUMMARY

In retrospect, the unfortunate experiences described could have been avoided. Many of the operating problems were the direct result of design

deficiencies in the fabric filter itself or in its application to the process. The gas-temperature control system supplied by the plant did not provide adequate control of dilution air. The fabric filter manufacturer's isolation dampers operated poorly, and the filter medium was specified without regard for flue gas composition. Also, the manufacturer did not provide training or instruction in the installation or maintenance of the filter bags. Many of the bag failures were traced to improper installation.

The regulatory agency's permit review staff chose not to make a rigorous evaluation of the cupola fabric filter system which may have identified some of the problems. Furthermore, the agency's unbending enforcement posture distracted plant management personnel at the very times where efforts were being made to expeditiously resolve the technical problems.

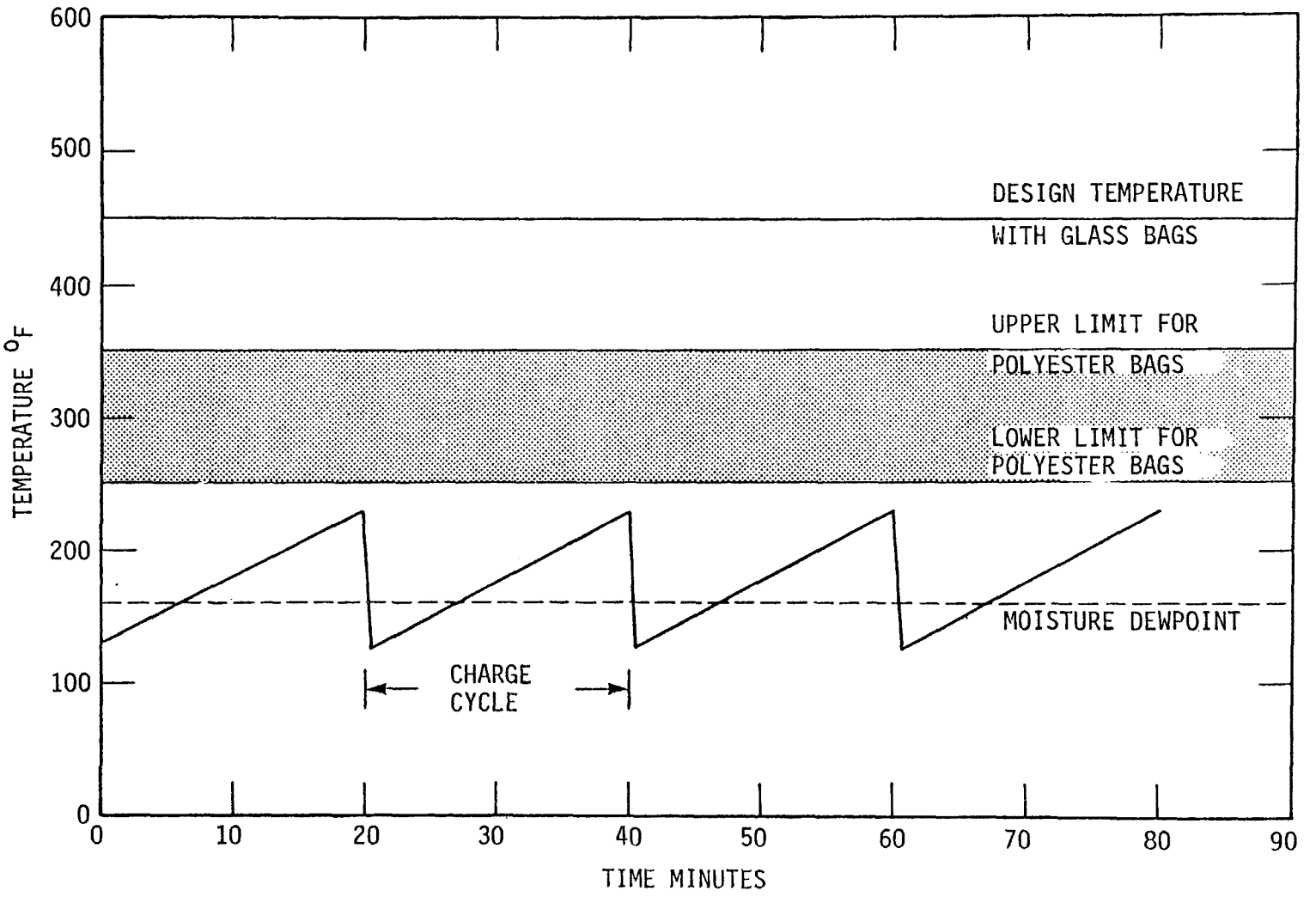

Figure 1. Temperature profile of cupola emissions entering fabric filter showing influence of charge cycle.

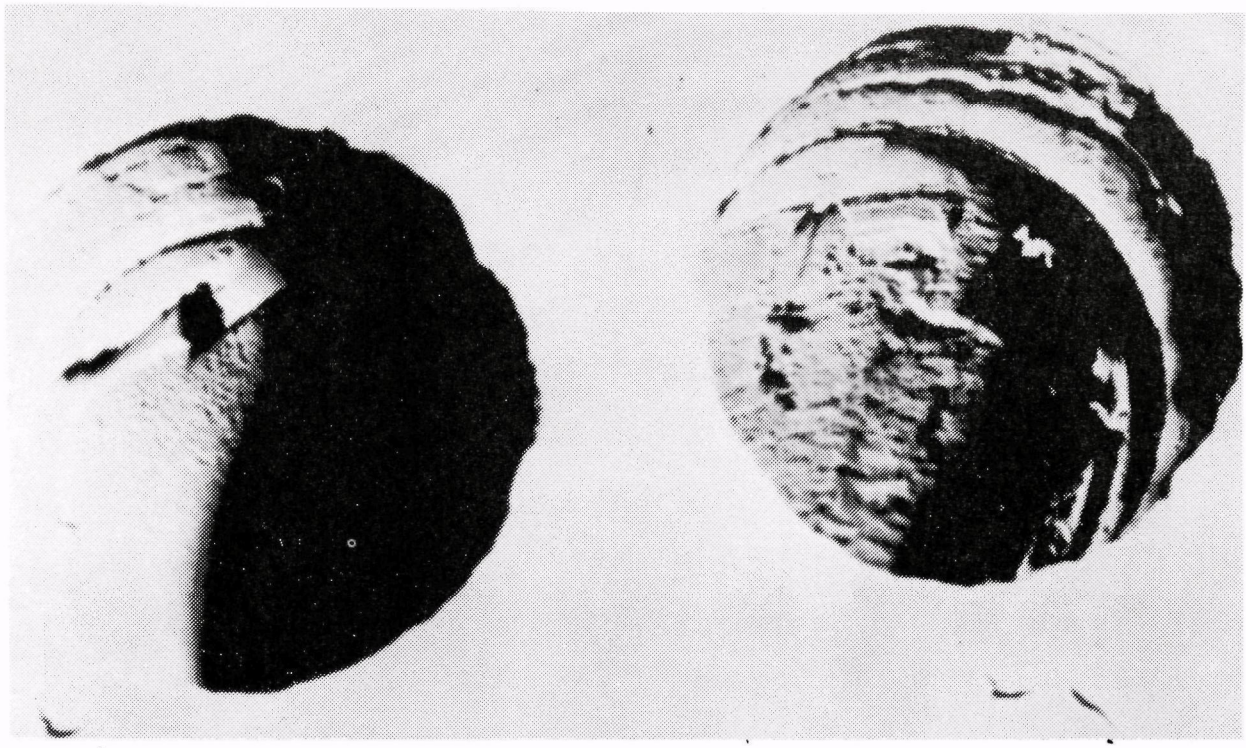

Figure 2. Photograph showing limestone precoat cake that could not be removed from the interior of fiberglass bags.

Figure 3. Photograph of typical treatment of fiberglass bags during installation.

ADVANCED FABRIC FILTER TECHNOLOGY FOR DIFFICULT PARTICULATE EMISSIONS

By: Heinz P. Beutner, Ph.D., President
Interel Corporation
7108 South Alton Way, Bldg.M
Englewood, Colorado 80112

ABSTRACT

The paper discusses fabric filter technology developed by H. Luhr of West Germany specifically for control of difficult submicron emissions, e.g., from metallurgical furnaces, electric arc furnaces, and glass and brick kilns.

The baghouse uses a dust conditioning drum, located in the hopper in place of a screw conveyor, to pretreat the gas entering the baghouse with dust returned from the bags. This approach increases the average particle size of the dust and reduces the required frequency of bag cleaning. The drum also can serve to hold additives in the baghouse for removal of gaseous components, such as HCl, HF, and SO3. The baghouse utilizes horizontally mounted, flat Twin-Bags and either low pressure reverse air or pulse jet cleaning.

Another element of the Luhr technology is an air-to-gas heat exchanger, which is designed to cool high temperature exhaust gases to the temperature acceptable in the baghouse. The gas cooler, which is equipped with an automatic cleaning mechanism, can be designed as an integral part of the baghouse and dust conditioning system.

INTRODUCTION

Luhr Staubtechnik of Germany has achieved international recognition in the pollution control field for the technology it pioneered and perfected in the filtration of submicron dust emissions. Many references on a variety of difficult dust applications testify to the success of this technology. Interel Corporation is the U.S. licensee of Luhr.

Submicron dust emissions, such as metallurgical fumes and emissions from glass furnaces, arc furnaces, incinerators, other high-temperature sources, have long been recognized as difficult control problems. Typical practice for fabric filtration of submicron fumes has been the application of a shaker-type baghouse with very low air-to-cloth ratios, such as 1:1 or 1.5:1. In many cases, precoating of the fabric after each cleaning was found to be necessary to prevent fabric blinding and to hold outlet dust loading within acceptable limits.

The Luhr technology utilizes several specialized approaches to the control of furnace emissions, including:

+ a fabric filter system with horizontally mounted flat bags (Twin-Bags) and either reverse air or pulse jet cleaning

+ dust conditioning and supplementary dust addition in a conditioning drum

+ gas cooling in a gas-to-air heat exchanger with heat recovery

As a result of application of the principle of dust conditioning, the Luhr baghouse can filter submicron furnace emissions at low pressure drop and air-to-cloth ratios ranging from 3:1 to 6:1, depending on the specific application. The high air-to-cloth ratio reduces the fabric area and size of the baghouse required for a given application; the lower fabric area reduces bag replacement cost. Combined with credits for heat recovery, substantial operating cost savings are often feasible.

Baghouse Design

The Luhr baghouse is based on dust collection on the outside surface of the bag, which is held by a support cage. The baghouse utilizes flat "Twin-Bags" up to 6.5 ft. long with fabric areas to 8.3 ft^2 each.

A unique aspect of the Luhr baghouse design is the horizontal arrangement of the Twin-Bags as shown conceptually in Fig. 1. This design allows for easy bag replacement from the front walkway through full-sized access doors to the clean air space. The design also permits easy visual detection of leaking bags. Also, it is easy to temporarily block the clean gas exit of a leaking bag.

The Twin-Bags are sealed to a perforated wall by means of a spring-loaded snap mechanism. The bag attachment is free of stress from the weight of the bag, bag cage, and dust compared with typical hanging systems. This design results in improved baglife. At the rear wall, the bag cage is held by a simple support.

The Twin-Bags are cleaned either by reverse air flow or by pulse jet. Reverse air is supplied by a traveling plenum, which is positioned in front of one vertical row of bags at a time while the clean air outlets of the two adjacent rows of bags are blocked off to prevent redeposition of the dust removed from the center row (type MWF filter). The flow of reverse air is 950 cfm at 20" WG for each 116 ft^2 of fabric area, equal to an air-to-cloth ratio of 8.2:1.

The pulse-jet design uses stationary air pipes with compressed air supplied to one or several vertical rows of bags at a time (type DF filter). The reverse air and the pulse-jet systems are also available with off-line cleaning.

Dust Conditioning

The dust conditioning drum, which has been developed by Luhr over a period of years, is an effective means of dust preconditioning. Installed

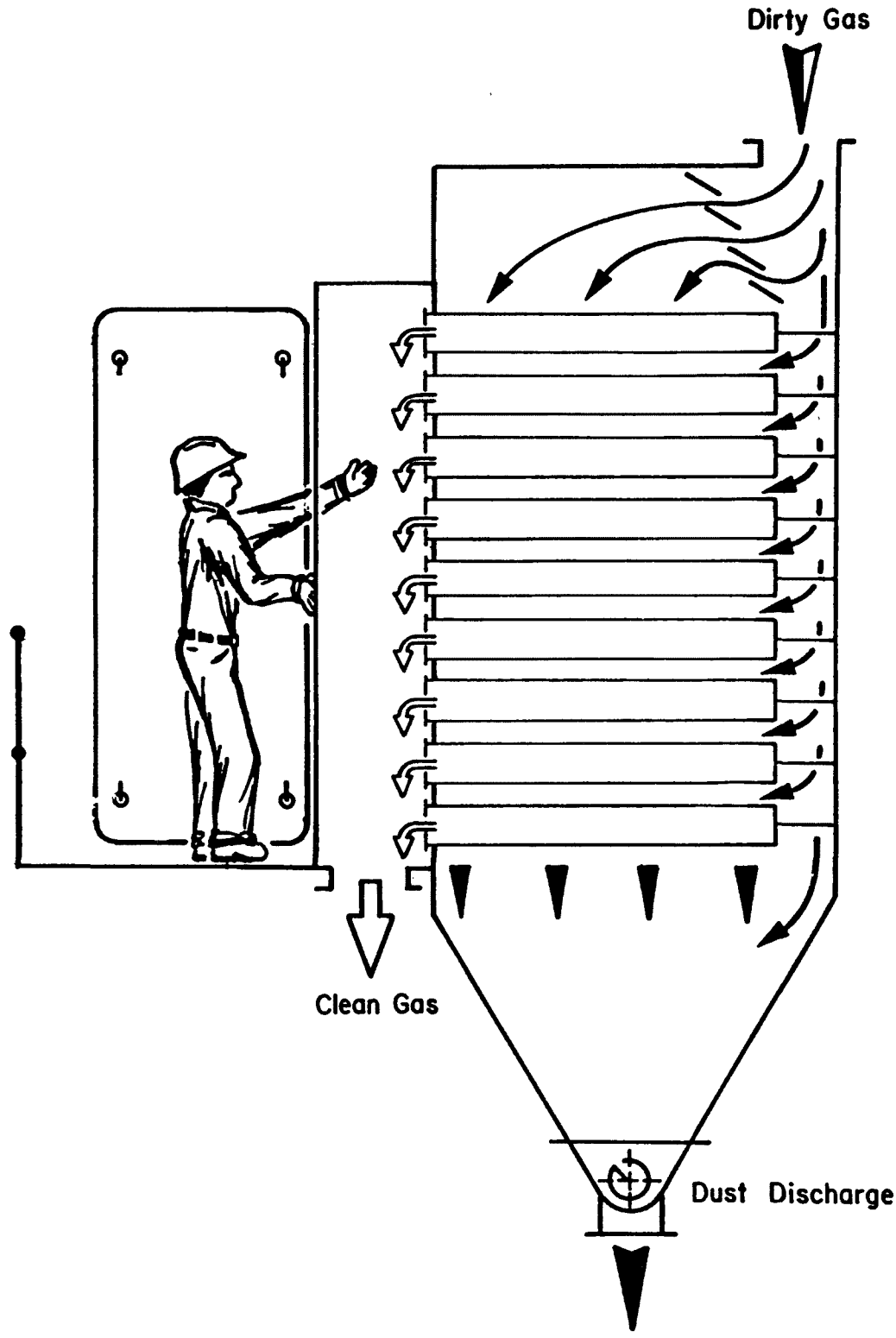

FIGURE 1
LUHR TWIN-BAG FABRIC FILTER -- GAS FLOW ENTERING FROM ABOVE AND BACK

generally in the gas inlet plenum, the drum is made of perforated metal and partially filled with ceramic balls (Fig. 2 & 4). In operation, the drum holds agglomerated dust returned from the bags while the entering gas is forced partially through and over this dust as in a fluidized bed. Fume particles in the gas stream adhere to larger particles in the bed, and this agglomerated dust is carried by the gas flow to the filter and returned to the bed upon cleaning of the bags. Excess dust flows in the slowly rotating drum toward the discharge valve. The pressure drop added by the drum is from 0.4 to 2 inches, depending on application.

In addition to promoting dust agglomeration, the drum serves as a buffer to prevent temporary condensates and other gas components from affecting the filter cloth. Such components as oils, acids, or water can be absorbed in the dust of the conditioning drum. Intermittent rotation of the drum breaks up any cake formation. The drum can be seen as a pretreatment of the gas by dust discharged from the filter.

The net effect of the use of a dust conditioning drum in a filter system is a larger particle size dust on the filter bags and longer intervals between required cleanings. The lower frequency of cleaning can substantially improve baglife. As an alternate, we can apply higher air-to-cloth ratios in many applications compared with operations without the dust conditioning drum.

The concept is extended in the use of the conditioning drum for holding additives in the gas stream, such as for removal of acid mist or reaction or absorption of HCl, HF, or SO_2 (dry scrubbing). The coarse additive material is continually milled in the drum and exposing new surface areas to the gas. This process improves the reactivity of the additive in addition to substantially increasing the residence time of the additive in the gas. The average residence time of an additive increases from 20 minutes to several hours with the use of the conditioning drum.

Another important benefit is the even flow distribution along the length of the filter (or cooler, see below) as a result of the pressure drop caused by the conditioning drum. The motion of the drum prevents localized deposits or caking and the constant pressure in the inlet plenum produces an even flow over the length of the drum into the lower pressure filter housing.

Gas Cooling

Submicron dust emissions are generally generated in high-temperature processes, such as metallurgical furnaces, glass furnaces, kilns, and combustion processes. An integral problem of any emission control process for these types of applications is the cooling of the exhaust gases to the temperature required for fabric filtration.

The design of the Luhr Flat-Tube air-to-process gas heat exchanger is based on cooling air passing through the inside of horizontally mounted flat tubes (Fig. 3). The process gas flows outside and between the tubes in the up or down direction, i.e., perpendicular to the cooling air flow. Swinging chains between the flat tubes prevent the buildup of deposits on the tube

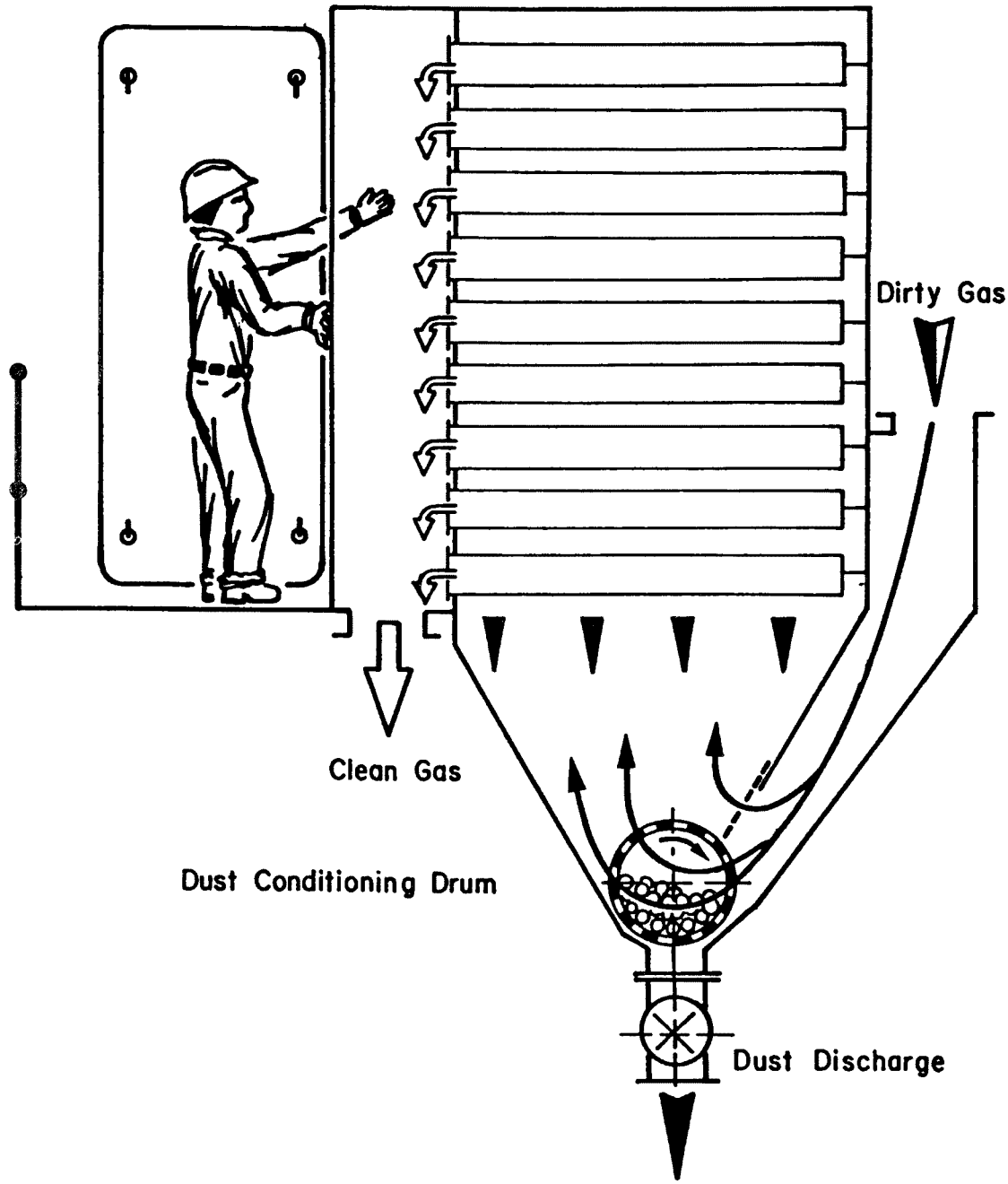

FIGURE 2
LUHR TWIN-BAG FABRIC FILTER
GAS FLOW ENTERING FROM BELOW THROUGH DUST CONDITIONING DRUM

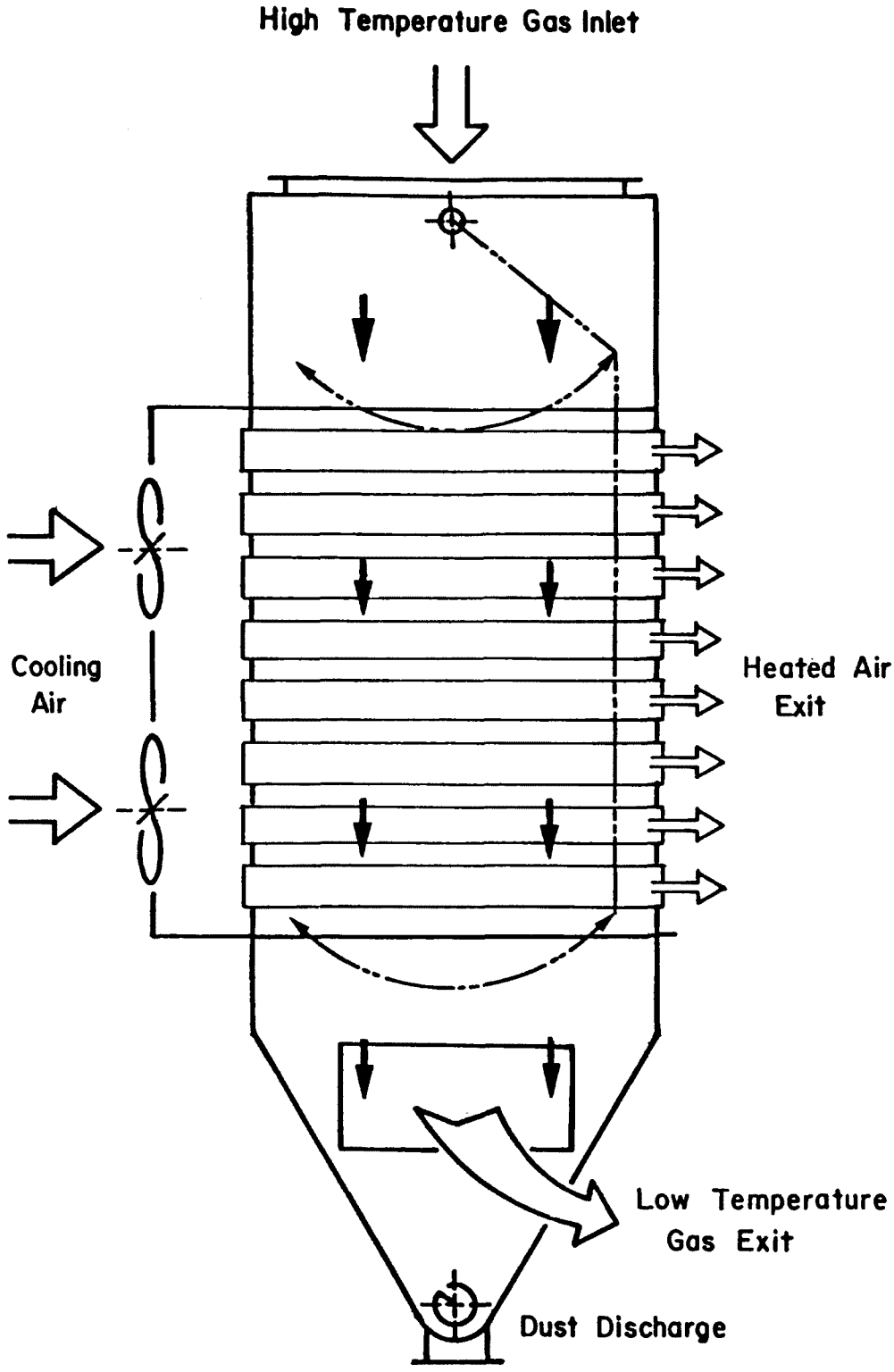

FIGURE 3
LUHR FLAT-TUBE GAS COOLER

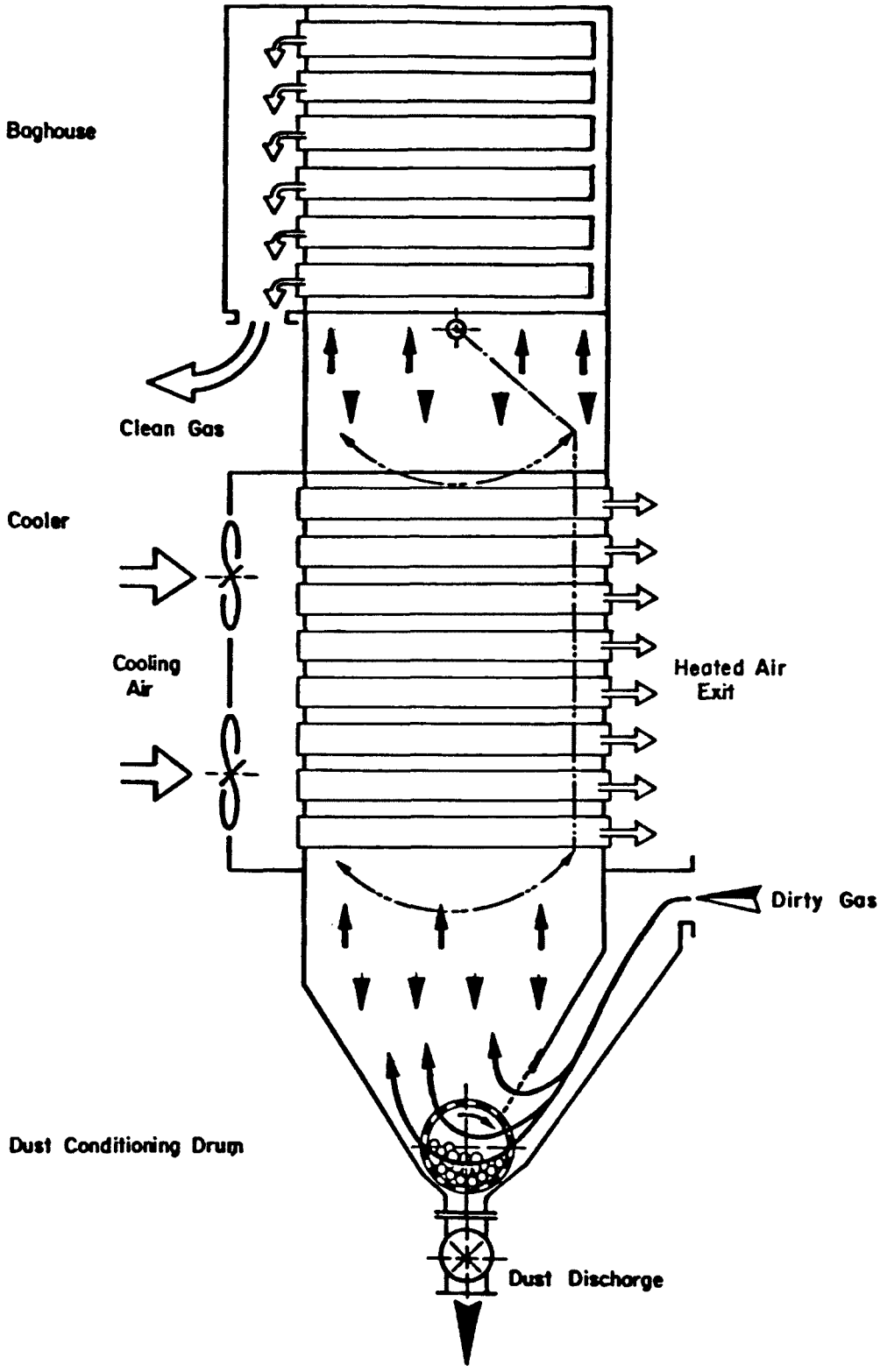

FIGURE 4
LUHR COOLER/BAGHOUSE COMBINATION
DIRTY GAS ENTERING FROM BELOW THROUGH DUST CONDITIONING DRUM AND COOLER

walls. The chains are attached to a shaft that is moved by a gear motor on the outside of the cooler.

Generally, the gas flow through the cooler unit is designed to maintain a low velocity of under 2400 ft/min. This approach holds the pressure drop through the unit in the range of 1-3 inches and causes larger dust particles to settle out. The cooler, therefore, performs the functions of a preseparator. In addition, the cooler assists agglomeration of submicron particulate matter. The low velocity also prevents abrasive wear on the cooling tubes.

A large excess of cooling air is normally supplied by axial fans, which keep the heat exchanger tubes at a relatively low temperature. The normal air flow is about 10 cfm/ft^2 heat exchange area.

The cooler is sized using heat exchange coefficients, which take into account the equilibrium coating of dust experienced in each type of application. Typical heat exchange values are between 2 and 4 Btu per hr. per ft^2 area and ^oF temperature differential.

The primary purpose of the Luhr cooler design is to cool hot process gas to the maximum safe operating temperature of the fabric selected for the baghouse. The cooler allows fine control over the gas exit temperature through on/off control of several groups of fans. The large mass of the cooler prevents sudden temperature changes in the exit gas.

The temperature control and the prevention of deposit buildup in the cooler are major advantages compared with simple U-tube duct cooling. Compared with water spray cooling, the indirect heat exchanger does not lower the dew point through addition of water vapor to the gas and, of course, eliminates the problems of spray nozzle maintenance, water droplet carryover to the baghouse, and consumption of cooling water.

Substantial space and cost savings are possible with a design that locates the filter housing on top of the cooler housing. The dust removed from the filter bags falls through the cooler into the common hopper. The system has one gas inlet plenum into the hopper and one gas outlet plenum from the filter clean air space (Fig. 4). This approach generally is feasible when the number of cooler and filter modules can be made equal.

Heat Recovery

In many typical applications of the cooler, the cooling gas flow is about 3 to 5 times the process gas flow. This means that the average temperature increase in the cooling air is about 1/3 to 1/5 of the temperature loss of the process gas. For a process temperature decrease from 100^oF to 250^oF, the average cooling gas temperature increase would be in the range of 150^oF to 300^oF.

The cooler can be modified to allow recovery of heated air in the 500^oF to 600^oF temperature range by multiple passes of the cooler air (Fig. 5). Because of the lower heat transfer efficiency, the cooler generally must be sized larger to allow the use of multiple pass/counter-current air flow.

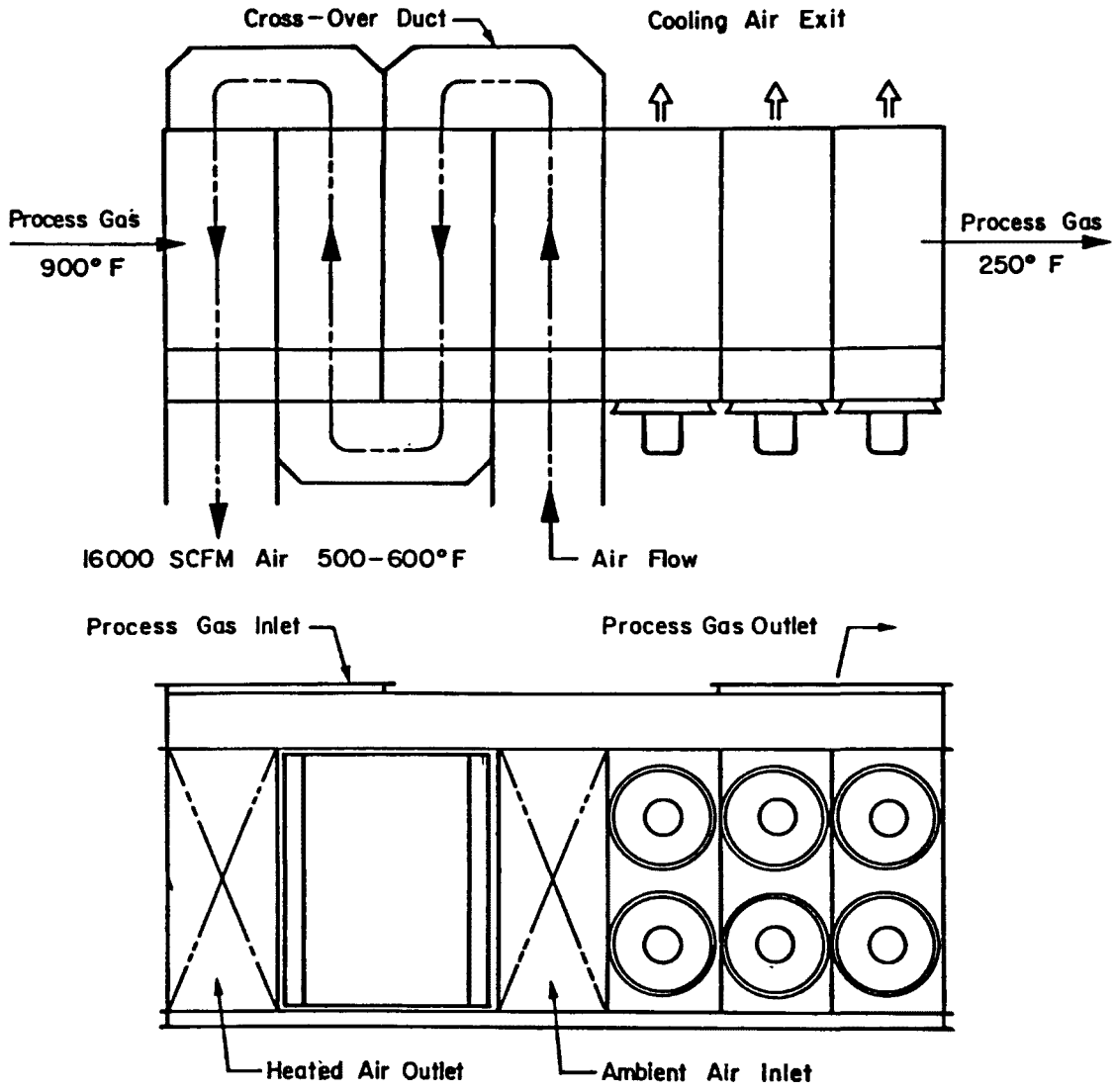

FIGURE 5
HIGH TEMPERATURE HEAT RECOVERY THROUGH
MULTIPLE PASSES OF COOLING AIR THROUGH COOLING TUBES

The air in the 500°F to 600°F range can be re-used as preheated combustion air in the burners of the furnace for a 10% to 12% fuel savings. Other uses of the heated air include drying of raw material and space heating during winter months. Many furnace applications draw substantial air from the plant area. In this case, the entire cooling air from the cooler can be used as heated make-up air for the plant during the winter months.

Cost Projections

The reverse air or the pulse-jet baghouse with dust conditioning drum is generally in the price range of $12 to $15 per square foot of fabric. Based on an air-to-cloth ratio of 5:1, the price is equal to $2.40 to $3.00 per cfm of gas processed (1980 prices; equipment only).

For many metallurgical or other types of submicron dust applications, the high-ratio baghouse competes in initial cost with the shaker-type baghouse applied at much lower air-to-cloth ratio. The high-ratio baghouse offers the advantage of substantially lower operating costs as a result of lower fabric area. Typically, the number of bags required and the cost of bag replacement is 1/2 to 1/3 that of a shaker baghouse.

In most furnace applications, the high-ratio Luhr baghouse can be combined with the gas-to-air heat exchanger. In this case, operating cost savings, compared with systems using air dilution or water spray cooling, can be substantial even before credits for heat recovery for low-temperature air. Any incremental investment required to achieve recovery of high-temperature air has a payout of under one year.

Installation Experience

Numerous installations of the Luhr baghouse with horizontal bags and dust conditioning drum are operating throughout Europe in the secondary metal industry on brass, copper, lead, aluminum furnaces, as well as on furnace emissions in the ferrous foundry industry and on glass furnaces. A number of systems are operating now on brick kilns for the purpose of hydrogen fluoride absorption by dry scrubbing with lime.

In North America, we presently have in operation a system on a lead rotary smelting furnace at Canada Metal Company in Calgary, Alberta, at an air-to-cloth ratio of 3.0:1; and a smaller baghouse unit on an aluminum induction furnace at H. O. Forgy & Sons in Jackson, TN, at an air-to-cloth ratio of 3.7:1. Both installations very successfully demonstrate the effectiveness of dust conditioning.

Gas cooler installations in the U.S. number some two dozen in a large variety of applications.

DEVELOPMENT OF GUIDELINES FOR OPTIMUM BAGHOUSE FLUID DYNAMIC SYSTEM DESIGN

By: David Eskinazi
Gerald B. Gilbert

Dynatech R/D Company
99 Erie Street
Cambridge, Massachusetts

Robert C. Carr
Electric Power Research Institute
Palo Alto, California

ABSTRACT

In recent years, the utility industry has turned to fabric filters as an alternative technology to electrostatic precipitators for particulate emission control from pulverized coal-fired utility boilers. One aspect of baghouse technology which appears to be of major importance in minimizing the size, cost, and operating pressure drop is the development of ductwork and compartment designs which achieve uniform gas and dust flow distribution. A recently com-pleted experimental modeling program focused on developing design guidelines for optimizing the fluid mechanic performance of baghouses. Tasks included evaluation of the current technology of baghouse systems, formulation of the appropriate modeling techniques for analysis of the flow of dust-laden gas through the collector system, and extensive experimental analysis of fabric filter duct system design. A matrix of geometric configurations and operating conditions was experimentally investigated to establish the characteristics of an optimum system, to identify the fluid mechanic integrity of current designs, and to validate the development of new ideas and designs. Experimental results indicate that the design of the inlet and outlet manifolds, hopper entrance, hopper region below the tubesheet, and the compartment outlet have not been given sufficient attention. Unsteady flow patterns, poor velocity profiles, recirculation zones, and excessive pressure losses may be associated with these regions. It is evident from the results presented here that the fluid mechanic design of fabric filter systems can be improved significantly.

INTRODUCTION

Increased emphasis by regulatory agencies on the application of high efficiency particulate control devices to coal-fired boilers has increased the popularity of fabric filter systems in the electric utility industry. In June 1980, 37 units, representing 3500 MW, were in operation. This increasing popularity and the tendency towards larger units have been the primary catalysts for the initiation of this program.

The focus of this program was to develop design guidelines and present technical information which will aid in the critical assessment of manifold and hopper designs in fabric filter systems. The necessity for this type of program manifests itself in the relatively severe penalty for high pressure losses in terms of the power requirements and boiler derating. Therefore, pressure loss reductions were strongly considered in this investigation, as were dust and flow balance among compartments and bags within a compartment.

This program has made substantial progress in developing guidelines and assessing the fluid dynamic performance of utility fabric filter systems. During the program, a state-of-the-art review of literature was completed, eight installations were visited, a system model and a single compartment model typical of utility fabric filter systems were constructed for experimentation, and the data collected from several configurations were analyzed. Emphasis has been directed toward providing information which can be used in the preparation of engineering specifications for baghouses. Of primary importance in this program was an increased knowledge of modeling field installations in a laboratory environment. Through design, construction, instrumentation, and experimentation, a procedure for modeling baghouse systems was developed and refined. In addition, the scaling laws for flyash trajectories were developed, and an appropriate model dust was selected.

DEVELOPMENT OF THE MODELING CRITERIA

Selection of Models

The experimental work conducted in this investigation was completed using models which are representative of the variety of configurations, geometries, and operating conditions currently employed in the field. Two separate models were used in the investigation of the fluid mechanic performance of fabric filter systems: 1) a system model, and 2) a single compartment model. Each model was selected and designed to be representative of all fabric filter systems rather than of a particular unit, although some inferences can be drawn regarding individual sites.

The system model (approximately 1/16 scale) was designed to investigate the performance of the inlet and outlet manifold systems. A plane of symmetry is assumed at the centerline of the baghouse along the manifold system such that a ten-compartment baghouse is simulated with a five-compartment model and a half-width manifold system (see Figure 1). The model has been designed with sufficient flexibility to allow most inlet and outlet manifold systems to be investigated.

The details of the performance criteria in an individual compartment are examined in the single compartment model (approximately 1/4 scale), which possesses the same flexibility as the system model. This apparatus is geometrically scaled from representative dimensions and included a hopper inlet, hopper, tubesheet, compartment region with 35 fiberglass bags, and a compartment outlet. Together these two models provide the opportunity to investigate a maximum number of configurations at a minimum cost. In this paper, only system model results are discussed.

Measurement and Analysis

During the experimental portion of the program a variety of measurements and analysis are required to document the performance of each configuration. These include flow visualization, velocity profiles at particular locations in the models, flow and dust balance among compartments, and pressure losses through the models. Whenever possible this data is normalized by average values. An analysis of pressure loss is one of the best assessments of the fluid mechanic performance of these particulate control devices. It is customary to report total pressure losses as non-dimensional loss coefficients. These loss coefficients are defined as the total pressure loss between two

locations divided by a representative velocity head in that region, usually the velocity head at the upstream location.

Four loss coefficients are discussed in this report. Losses described by these coefficients occur (1) from the inlet manifold just upstream of any take-off to just under the simulated tubesheet in that particular compartment; this coefficient is referred to as the hopper inlet loss coefficient (based on the average velocity head at the hopper inlet), (2) from the baghouse inlet flange to a station just upstream of the final take-off before the downstream end of the inlet manifold -- the inlet manifold loss coefficient (based on the average velocity head at the baghouse inlet flange), (3) from above the bag region in any one compartment to the outlet manifold just downstream of the corresponding outlet manifold entrance for that compartment -- the compartment outlet loss coefficient (based on the average velocity head through the com-partment outlet), and (4) from a point just downstream of the first (most upstream) outlet manifold entrance to the baghouse outlet flange -- the outlet manifold loss coefficient (based on the average velocity head at the baghouse outlet flange). The loss coefficients associated with typical hopper inlets and compartment outlets can be improved substantially by the addition of flow distribution devices.

RESULTS

Significant improvement can be made in the fluid mechanic performance of fabric filter systems. The objective of this type of analysis is to minimize duct pressure losses, improve dust and flow balance, and insure reasonable flow patterns throughout the system to avoid operating problems and improve flyash removal efficiency.

Optimizing the performance of baghouse systems includes evaluating the following performance criteria:

- the uniformity of ash loading and velocity profiles through the system,
- minimum manifold, control valve, and system pressure losses,
- even flow and dust balance among compartments and bags within a compartment,
- minimum dust accumulation in the inlet manifold,
- minimum turbulence levels in the hopper, and
- optimum transition designs for the geometry from 1) the inlet manifold to the hopper, and 2) the upper compartment to the outlet manifold.

Each of these objectives was examined, although the extent to which equipment modifications can be implemented depends on an economic analysis of suggested changes.

Description of Configurations

Two configurations have been examined using the system model (see Figure 2). System model experiments were useful in understanding the behavior of (1) the inlet and outlet manifolds in terms of general flow patterns and pressure losses, (2) inlet manifold-hopper inlet transitions and compartment outlet-outlet manifold transitions in terms of general flow patterns, hopper inlet velocity profiles and pressure losses, and (3) dust and flow balance among compartments. Each configuration was tested twice: once as base configuration without modifications and once with modifications. These modifi-

cations included either flow improvement devices, valving systems, or a combination of both. Flow improvement devices are uncommon in existing field manifold systems. The design velocity levels in the model were obtained from average field values at five critical locations in the fabric filter system. These levels are nominally (a) 60 ft/sec at the baghouse inlet and outlet flanges, (b) 5 ft/sec in the region just upstream of the simulated tubesheet, and (c) 40 ft/sec at the hopper inlet and compartment outlet.

Inlet Manifolds

The general flow patterns in the inlet manifold are uniform and steady. Figure 3 is a sketch of the flow patterns in the inlet manifolds of Configurations 1 and 2. A recirculation zone is observed at the end of the inlet manifold. This type of flow pattern is expected in designs which include an extension region beyond the last manifold take-off. Flyash accumulations are common in this region due to lower velocity levels and the horizontal deposition surface. As long as the structural integrity of this region to support flyash accumulations is considered in the design, no maintenance problems would be expected. Also, it is evident from the sketches and a fundamental knowledge of fluid mechanics that a separation region will be generated at the sharp edges as the flow passes into individual take-offs.

A more detailed comparison of the flow patterns in each configuration reveals that the character of the flow differs in the two geometries. In Configuration 1 the flow to each compartment is taken off in fairly well defined layers; that is, it is relatively easy to trace smoke introduced at a particular location at the model entrance to the compartment(s) it reaches. In contrast, due to increased mixing in the Configuration 2 inlet manifold, this same behavior is not observed.

The results of a pressure loss analysis indicate that the losses along the inlet manifold are minimal. The inlet manifold loss coefficient for each configuration is approximately 0.25.

Modifications to improve flow patterns or to examine the effects of valving systems were made for each configuration. These modifications were included to examine their effect on other regions in the fabric filter system; no effect was expected regarding the inlet manifold.

Inlet Manifold - Hopper Transitions

The design of the inlet manifold-hopper transition is important to the performance of fabric filter systems since it affects flow patterns in the hopper and the trajectories of flyash particles entering the bag region. Also, this region can be associated with abrupt changes in geometry and hence significant flow separations. These flow separations are strongly related to pressure losses. Three basic inlet manifold-hopper transitions are commonly used, although the classification system is dependent on the detail considered. They are:

- a 90° elbow from the bottom of the inlet manifold to the side of the hopper,
- an inclined or horizontal transition from the side of the inlet manifold to the side of the hopper, and
- a transition from the bottom of the inlet manifold directly to the upper corner of the hopper

Virtually all hopper inlet systems are some permutation of these classes. They can be circular or rectangular in cross-section, or offset on the side wall of the hopper. Four valving systems are commonly used: 1) poppet valves, 2) butterfly valves, 3) louver dampers, and 4) a more sophisticated butterfly-vane combination. The inlet manifold-hopper transition in Configurations 1 and 2 were selected to investigate experimentally the behavior of two these general classes.

Flow separation plays a significant role in the fluid mechanic behavior of this region. A penalty in the form of a pressure loss is incurred when the flow over a sharp corner separates. The separation zone is carried downstream, which reduces the effective cross-sectional area of the duct and increases local velocity levels above design values. These higher velocities (velocity heads) at the hopper inlet give rise to additional losses as the dust-laden gas enters the hopper. Due to the similarity of flow patterns in this region with the flow in an idealized sudden expansion, one inlet velocity head will be lost as the gas enters the hopper. Configuration 2 is a good example of this behavior. In Configuration 1 a similar event occurs; however, the two successive 90° bends in different planes lead to the generation of a vortex in the elbow. In addition to creating unfavorable flow patterns, the vortex is associated with additional pressure losses. This vortex, or swirling flow, rotates the separation region and skews the velocity vector at the hopper entrance. A velocity traverse at the hopper inlet quantifies the character of the flow in this region (see Figure 4). The separation zone is seen as a low (or zero) velocity region in the traverse. Also, velocity levels in non-separated regions are more than double their design values.

Each configuration was modified either to reduce the magnitude of flow separation, lessen the swirling, or examine the effect of a control valve on the flow patterns in this region (refer to Figure 3). In Configuration 1, the modifications to Compartments 1-4 (Compartment 1 is nearest the baghouse inlet flange) included the addition of a poppet valve, a poppet valve with a square grid just below the floor of the inlet manifold, a butterfly valve aligned parallel with the mainstream flow in the inlet manifold and skewed slightly towards the hopper, and a butterfly valve aligned normal to the mainstream flow in the inlet manifold with and without a vane at the upstream edge of the manifold take-off, respectively. The geometry of the hopper inlet region of Compartment 5 remained unchanged. The poppet valves in the first two compartments were located at a distance greater than 1.0D from the floor of the inlet manifold, (where D is the diameter of the poppet valve). Preliminary experiments indicate that as long as the poppet valve is at a distance greater than 1.0D, the flow in the manifold or the take-off is unaffected. This was observed in the modified configuration. The flow patterns in this type of inlet manifold-hopper transition are highly unsteady due to the flow separation and are associated with significant swirling due to the two successive 90° bends as described previously. The square grid in the second take-off reduced some of the swirling; however, the unsteadiness remained unchanged. The butterfly valve aligned with the mainstream flow again reduced the swirling by directing the flow through the take-off. The butterfly valve aligned normal to mainstream flow in the inlet manifold was most successful in reducing the swirling. The addition of a vane efficiently reduced the separated flow region, almost eliminating the unsteadiness. The hopper inlet velocity traverses for the compartments with (1) a poppet valve and a grid and (2) a butterfly valve aligned normal to the mainstream flow in the inlet manifold with a vane are shown in Figure 5. A comparison with the unmodified arrangement (Figure 4) indicates the improvement.

In Configuration 2 the modifications were intended to reduce the separation caused by the sharp corner (refer to Figure 3). These modifications for Compartments 1-5 included a single vane at the upstream sharp corner, a rounded corner with no vanes, a rounded corner with one vane, and a single vane with the sharp corner, respectively. Each modification reduced the flow separation by varying degrees. Clearly, an assessment of the best modification would require an associated economic analysis. However, it appears that a single vane or a rounded corner gives significant improvement for a minimum of modifications. The best hopper inlet velocity profiles are observed with two vanes or a rounded corner with a single vane. Two hopper inlet velocity profiles are included to quantify the improvement. These profiles are for a single vane with and without a rounded corner (see Figure 6). Again, a comparison can be made with the unmodified arrangement in Figure 4.

The analysis is not complete without quantitative pressure loss results since they can result in significant costs over the life of a power plant. A comparison of the hopper inlet loss coefficients for the two configurations with and without modifications is presented in Figure 7. The loss coefficients through similar inlet manifold-hopper transitions (basic configuration) decrease as the progression is made downstream along the inlet manifold. This decrease can be explained by (1) the component of the velocity vector directed into the take-off increases as the flow proceeds downstream along the inlet manifold; therefore, the severity of the separation region at the sharp corner is reduced, and (2) the velocity level further downstream along the inlet manifold decreases which also reduces the separation. Therefore, unmodified and modified transitions must be compared compartment by compartment. The losses in the basic arrangement for Configuration 2 are higher than these for Configuration 1 because of the severity of the separations. However, the losses in Configuration 2 with modifications are lower than those in Configuration 1 because a single 90° bend, which is rectangular in cross-section, is more easily adapted to vaning. Clearly, the pressure losses of these transitions can be improved significantly.

Compartment Outlet - Outlet Manifold Transitions

The compartment outlet-outlet manifold transition is another region in which pressure losses can be reduced through more careful designs. A reasonably uniform velocity profile is observed in the upper bag region due to the substantial pressure losses across the fabric. Two basic compartment outlet transitions are currently employed:

- a 90° elbow from the top of the compartment to the side of the outlet manifold,
- a side compartment outlet with a prechamber before the entrance to the outlet manifold (usually from the top).

The cross-section of outlet transitions may be rectangular or circular and in most cases are offset with respect to the centerline of the compartment. Three basic valving systems are used: 1) poppets, 2) louver dampers, and 3) flapper dampers. Configuration 2 is not considered typical of current field installations, but was selected because of its simplicity. Both of these configurations have side compartment outlets.

Again, the primary pressure losses are caused by turning the flow across sharp edges. The compartment outlet loss coefficients for Configurations 1 and 2 are 2.6 and 1.5 respectively, for the basic arrangements.

Non-uniform velocity profiles along the outlet manifold make accurate measurements of wall static pressure difficult to obtain. The compartment outlet loss coefficients for Configuration 1 are larger since this outlet geometry includes three consecutive 90° bends as compared with two bends for Configuration 2. Similar improvement can be made with the addition of vanes and/or rounded corners. In the current program, no attempt has been made to improve the compartment outlet loss coefficients.

Outlet Manifolds

The general flow patterns in the outlet manifolds of unmodified Configurations 1 and 2 are slightly unsteady and non-uniform. Again, a recirculation zone exists at the beginning of the outlet manifold. The characteristic of the flow in Configuration 1 is such that sequential jets layer the flow along the outlet manifold, but stronger flow is observed on the floor of the manifold. Configuration 2 flow patterns are characteristic of stronger mixing along the manifold. A convenient method of summarizing the outlet manifold flow patterns is to compare the fraction of points in a traverse at the baghouse outlet flange which fall between $\pm$ 10% of the average velocity. In Configuration 1, 24% of the points in the baghouse outlet flange traverse fall between $\pm$10% of the average velocity. In Configuration 2, 64% of the points meet this criterion.

To gain a better understanding of the pressure losses along the outlet manifold, a simple theoretical model based on the momentum equation was applied to the outlet manifold as a control volume. The results of this analysis indicate that significant losses along the outlet manifold are due to the effort required (loss in kinetic energy) for the mainstream flow, upstream of any incoming jet, to turn that jet coincident with the outlet manifold mainstream velocity vector. In both configurations each compartment produces a jet normal to the mainstream flow in the outlet manifold. This loss can be reduced by the addition of solid surfaces (vanes) to redirect the flow towards the baghouse outlet flange.

Modifications were made along the outlet manifolds of each of these configurations to examine this effect and improve the velocity profile at the baghouse outlet flange. A different set of vanes was designed and installed in each configuration. The vane geometry and a sketch of the general flow patterns are shown in Figure 8. A contoured vane is included at the beginning of the outlet manifold in each case. In Configuration 1 a different two vane set has been installed in Compartments 1-3. Each set directs the outlet flow to a corresponding portion of the baghouse outlet flange cross-section. No vanes were installed in the outlet manifold near the Compartment 4 exit. In Configuration 2 an identical two vane set was installed in Compartments 1-4. These vanes extend across the height of the outlet manifold entrance from each compartment but not the full height of the outlet manifold.

The results of experiments conducted with Configuration 1 showed a dramatic improvement. The outlet manifold loss coefficient for Configuration 1 without modifications is 1.6. This was reduced to 0.6 by the addition of the vanes described. Also, the uniformity of the velocity traverse at the baghouse outlet flange was greatly improved (all the points in the traverse fall between $\pm$10% of the average velocity). The outlet manifold loss coefficient for Configuration 2 without modification is 1.1. With the addition of vanes this value increased to 1.7. The uniformity of the baghouse outlet flange velocity traverse did not improve. At present, this is not fully

understood, and further experiments are needed. It is difficult to understand why the addition of vanes would increase the losses. The flow into the manifold in Configurations 1 and 2 is from the top and side of the outlet manifold, respectively. The nearer half-width manifold wall (imposed by the plane of symmetry assumption) may offer some turning effect for the normal jet without vanes. This plane of symmetry assumption may "over idealize" the impinging jet behavior with an outlet manifold side entrance geometry. Also, the character of the unvaned flow in Configuration 2 is to produce some swirling in the outlet manifold. This may limit the accuracy of the wall static pressure measurement by underestimating the outlet manifold loss coefficient. In summary, it appears as though the character of the flow has been changed by the addition of vanes. These results indicate that while flow improvement devices remain an effective means of reducing the pressure losses through improved flow patterns, a complete understanding of the fluid mechanic behavior of these systems in necessary in selecting appropriate designs.

Related Analysis

An understanding of the flow and dust balance among compartments is necessary to characterize fully the performance of these devices. Intuitively, a reasonable balance among compartments is required if the total fabric surface area is to be used effectively. Further work will be needed to quantify the limits of a reasonable balance.

The flow balance among compartments was measured for each unmodified configuration at a moderate fabric pressure drop simulation (2.7 inches of water, field). In addition, Configuration 1 was selected to document the effect of increasing fabric pressure drop (equal among all compartments) from 1.4 to 4.5 inches of water (field). Figure 9 summarizes the flow balance results for increasing fabric pressure drop simulation in Configuration 1. For a moderate fabric pressure loss (2.7 inches of water), the flow balance among compartments in Configuration 1 is $\pm$ 7.5% of the mean flow per compartment. At the same fabric pressure loss the flow balance among compartments in Configuration 2 is $\pm$ 3.5% of the mean flow per compartment (see Figure 10). It is evident from the graph in Figure 9 that as the fabric pressure loss per compartment (equal in all) increases, the flow balance improves. As we have seen from an analysis of loss coefficients along the inlet and outlet manifolds, the outlet manifold losses are significantly greater than the inlet manifold losses. Therefore, the flow balance is distributed according to the shortest path along the outlet manifold. That is, the flow balance adjusts itself such that the highest flow is observed in the compartment associated with the shortest outlet run. This is evident in Figure 10. This effect has been con-firmed by flipping the inlet manifold to simulate a baghouse with inlet and outlet flanges on opposite sides of the collector. This analysis is limited since in practice the fabric pressure loss does not increase uniformly across all compartments simultaneously. Additional work will be required with non-uniform fabric pressure losses to understand flow balance fully.

The dust balance among compartments is dependent, to some extent, on the flow balance. Figure 10 indicates that the dust balance among compartments is $\pm$ 11% and $\pm$ 24% of the mean dust loading per compartment for Configurations 1 and 2, respectively. This difference is not fully understood; however, the more uniform layering in the inlet manifold of Configuration 1 is undoubtedly part of the reason.

A critical evaluation of any flyash simulation experiments is mandatory, and caution must be applied in interpreting the results. Each set of results is valid for the particular flyash simulated through the scaling laws for flyash trajectory modeling. The variety of flyash characteristics makes it difficult to generalize these results. Clearly, particle size distributions which differ greatly from the simulated distribution will yield different results.

CONCLUSIONS

Experiments conducted in this program indicate that significant improvement in the fluid mechanic performance of fabric filter systems is possible. The primary objective of this effort is to upgrade the performance of baghouses through experimental modeling to improve existing designs and to begin to develop future designs.

It has been demonstrated that experimental modeling of these particulate control devices is a reasonable approach to optimizing the performance of fabric filter systems. Experimental modeling is particularly attractive since it offers flexibility, ease of geometrical modifications, and a partially controlled environment not available in field installations. The reduced size and minimal cost of experimental models offer more efficient troubleshooting and optimization of designs.

Although a complete set of design guidelines requires additional work, many significant results have been obtained furthering the development of improved designs. These improvements will primarily be reflected in a reduction in system pressure loss and perhaps fewer maintenance requirements, which translate into a reduction in operating costs.

The inlet and outlet manifold systems and compartment transitions are regions in which the greatest improvements can be made. Abrupt changes in geometry in the absence of flow improvement devices are common. The loss coefficients for typical inlet manifold-hopper inlet transitions are typically high. It has been demonstrated that these can be reduced with the addition of flow improvement devices and more careful design of each component in the system. Similar improvements can be made regarding the compartment outlet-outlet manifold transition loss coefficients. Reduction in pressure loss along the inlet manifold will be minimal since reasonably low values currently exist. However, improvements along the outlet manifold maybe possible by directing compartment outlet jets entering the outlet manifold towards the baghouse outlet flange.

Hopper inlet designs can be greatly improved by emphasizing lower hopper inlet velocities since the kinetic energy associated with the incoming flow to the hopper is essentially lost due to the sudden expansion. The addition of flow distribution devices will aid in controlling flow separations and will therefore reduce pressure losses. Careful monitoring of ash levels in the hopper can minimize the reentrainment of previously removed flyash. Additional work is necessary to understand the reentrainment process if the ash is allowed to accumulate in the hoppers.

NOTE: Many details have been omitted from the text due to space limitations. A more detailed version of this paper is available from the authors upon request.

Figure 1

SYSTEM MODEL GENERAL ARRANGEMENT
(ALSO CONFIGURATION 1)

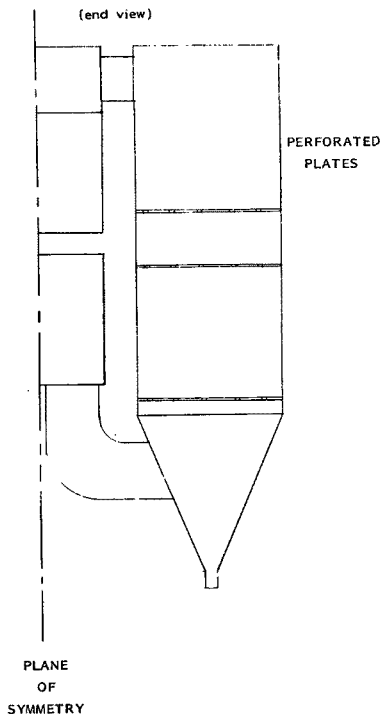

Figure 2

CONFIGURATION DESCRIPTION,
SYSTEM MODEL

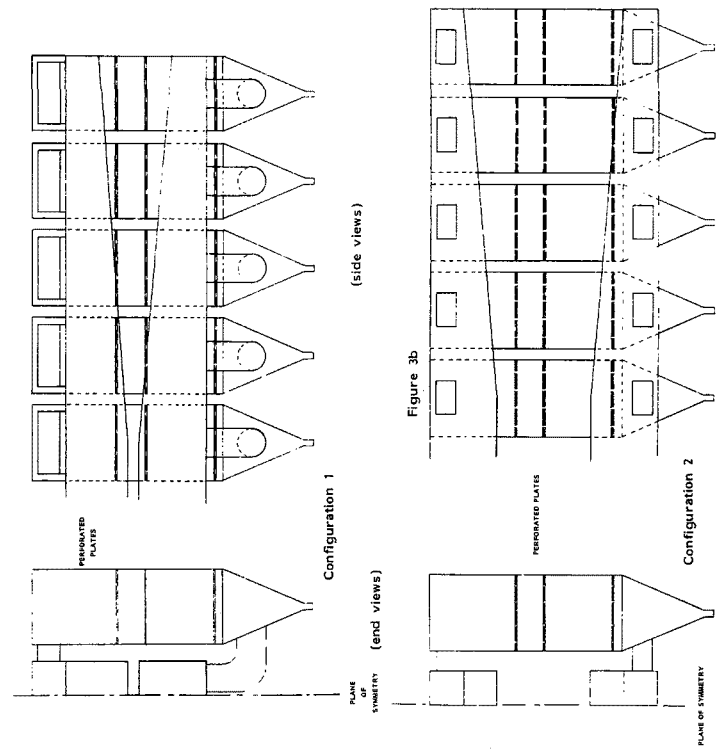

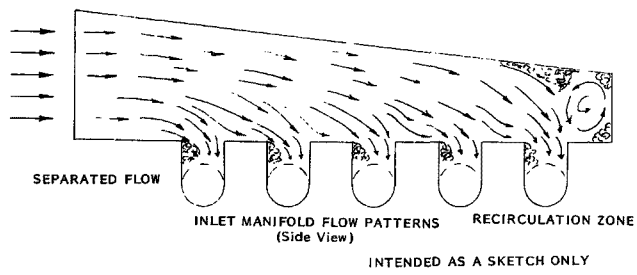

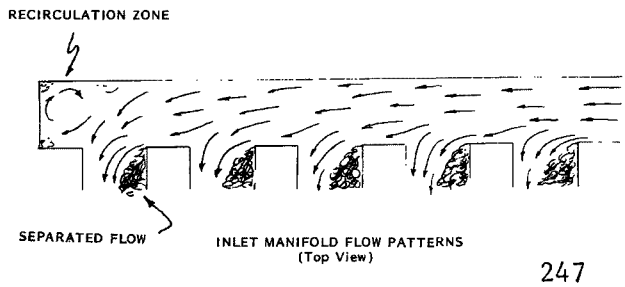

Figure 3

INLET MANIFOLD FLOW PATTERNS
(NO MODIFICATIONS)
(CONFIGURATIONS 1 & 2)

Figure 4

HOPPER INLET VELOCITY PROFILES
(NO MODIFICATIONS)
(VELOCITY/AVERAGE VELOCITY) -
AVERAGE DESIGN VELOCITY: 40 ft/sec

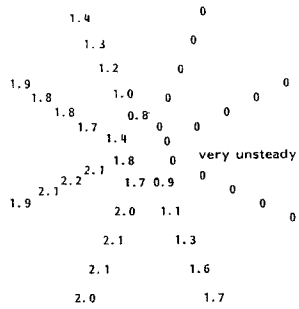

Configuration 1

0.3	0.3	0.3	1.3	1.4	2.5	2.5	2.5
0.2	0.2	0.2	1.3	2.0	2.5	2.5	2.5
0.2	0.2	0.3	1.4	2.5	2.5	2.5	2.5
0.2	0.3	0.3	1.7	2.5	2.5	2.5	2.5
0.2	0.3	0.3	1.3	2.0	2.5	2.5	2.5

very unsteady

Configuration 2

(mean flow into page)

Figure 5

HOPPER INLET VELOCITY PROFILES
(WITH MODIFICATION, CONFIGURATION 1)
(VELOCITY/AVERAGE VELOCITY) -
AVERAGE DESIGN VELOCITY: 40 ft/sec

POPPET VALVE
WITH A GRID

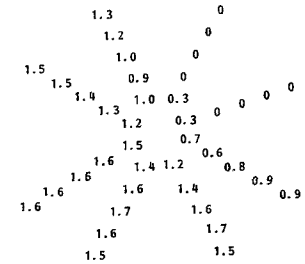

VANE AND
BUTTERFLY VALVE

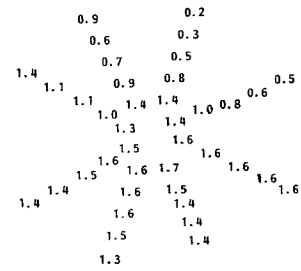

(mean flow into paper)

Figure 6

HOPPER INLET VELOCITY PROFILES
WITH MODIFICATIONS, CONFIGURATION 2

	0.3	1.7	0.5	0.2	0.2	0.0	1.1	1.2
	0.2	1.7	0.6	1.3	0.7	1.4	1.3	1.2
ONE VANE	0.2	1.5	1.1	1.6	1.5	1.4	1.3	1.2
	0.3	1.3	1.2	1.4	1.4	1.4	1.2	1.1
	0.5	1.4	1.0	0.5	0.5	1.0	1.2	1.1

Fraction of points which are ± 10% of the average: 0.15

	1.3	1.2	0.2	0.0	0.2	0.7	0.8	0.9
	1.4	1.3	0.6	0.2	0.6	1.0	1.0	1.0
ONE VANE AND ROUNDED CORNER	1.4	1.3	1.3	1.1	1.3	1.2	1.0	1.0
	1.4	1.3	1.1	1.3	1.2	1.2	1.1	1.0
	1.3	1.3	0.4	0.7	1.1	1.1	1.1	1.0

Fraction of points which are ± 10% of the average: 0.35

(mean flow into page)

Figure 7

HOPPER INLET LOSS COEFFICIENTS
CONFIGURATIONS 1 & 2 WITH AND WITHOUT
MODIFICATIONS

COMPARTMENT NUMBER	1	2	3	4	5
Configuration 1:					
Basic Arrangement	4.2	3.6	3.3	3.0	2.9
Modified Arrangement	5.2*	4.7*	4.3	3.6/2.4	2.8
Modification	poppet valve	poppet valve with a grid	butterfly valve aligned parallel with the inlet flow	butterfly valve aligned perpendicular to the inlet flow/with vane	none
Configuration 2:					
Basic Arrangement	5.2	4.6	5.1	3.8	2.9
Modified Arrangement	3.1	2.1	2.4	1.5	1.4
Modification	one vane	two vanes	rounded corner	rounded corner & one vane	one vane

(The first compartment is the one nearest the baghouse inlet flange.)

* questionable data point

Figure 8

OUTLET MANIFOLD FLOW PATTERNS
(WITH MODIFICATIONS)
(CONFIGURATIONS 1 & 2)

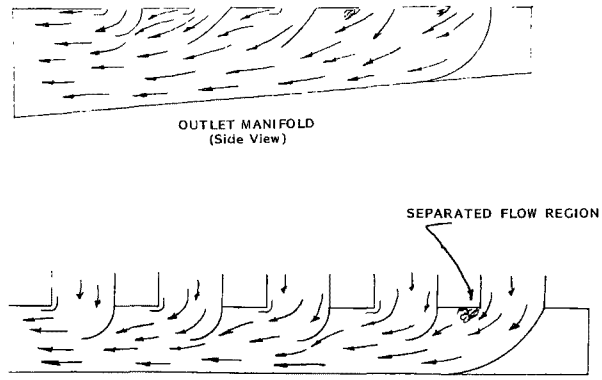

INTENDED AS A SKETCH ONLY

Figure 9

FLOW BALANCE AMONG COMPARTMENTS
(CONFIGURATION 1)

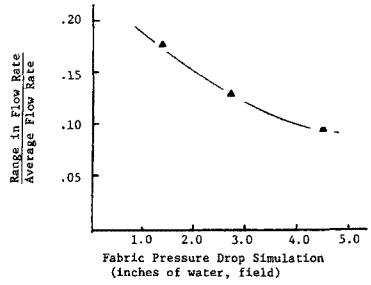

	Percent of Flow in Each Compartment				
COMPARTMENT NUMBER	1	2	3	4	5
Fabric Pressure Drop Simulation (field)					
4.5 inches of water	21.26	20.32	19.78	19.49	19.15
2.7 inches of water	21.50	20.51	20.05	19.43	18.51
1.4 inches of water	22.06	21.12	19.96	18.92	17.94

(The first compartment is the one nearest the baghouse inlet flange.)

Figure 10

DUST BALANCE AMONG COMPARTMENTS
(CONFIGURATIONS 1 & 2)

COMPARTMENT NUMBER	1	2	3	4	5
Configuration 1					
Percent of Dust in Each Compartment (by mass)	21.1	21.7	20.8	19.6	16.8
Percent of Flow in Each Compartment	22.2	21.1	20.0	18.9	17.9
Configuration 2					
Percent of Dust in Each Compartment (by mass)	24.9	21.7	19.5	18.5	15.4
Percent of Flow in Each Compartment	20.8	20.7	19.2	20.0	19.4

THEORETICAL ASPECTS OF PRESSURE DROP REDUCTION IN A FABRIC FILTER WITH CHARGED PARTICLES

By: Ta-Kuan Chiang, Eric A. Samuel, Kris E. Wolpert
Buell Emission Control Division
Envirotech Corporation
Lebanon, PA 17042

ABSTRACT

Various mechanisms have been presented in the past to explain the reduced pressure drop observed in a conventional fabric filter augmented with particle precharging. Such mechanisms involve dendrite formations, polarizations, and electric contact potentials. In this paper, yet another mechanism due to nonuniform dust profile is presented. Artificial step and bell-shape profiles are modeled to show the reduction of pressure drop without the assumption of a more porous cake. Laboratory experiments with metallic screens were used to verify the proposed mechanism.

INTRODUCTION

New concepts for fine particle control (1) were generated from time to time in the past. For fabric filtration, the concept was to enhance the fabric filtration with either charged particles (2), or noncharged particles in an electrostatic field (3). Reportedly, with electrostatic augmentation, the fabric filtration efficiency was increased considerably; and yet coincident with this improved filtration efficiency was an observed reduction of pressure drop. Improved filtration efficiency was easily understood due to an additional collection force introduced by the charged or noncharged particles in a nonuniform electrostatic field; whereas the experimentally observed reduction of pressure drop became a puzzle and a center of dispute. Various mechanisms were offered in the past to explain the reduced pressure drop. Notably, such mechanisms under investigations included dendrite formations (4), polarizations, and electric contact potentials (5,6); all of them lead to a more porous cake formation. In this paper, without the assumption of a more porous cake, another mechanism of nonuniform dust deposition caused by the fundamental behavior of charged particles in a combined flow field and electrostatic field is introduced.

MECHANISM OF REDUCED PRESSURE DROP

It is known that fundamentally the entrained particles in a flow system follow the air flow lines attaining same velocities as the air flow. Meanwhile, due to particle inertia, small particles follow the flow lines more readily than the large particles whenever there is a change of flow velocity. With this fundamental behavior of the particles, the nonuniform velocity distribution in a conventional bag filter, maximum at the entrance of the bag and zero at the other end, results in a particle size stratification. Since the resistance coefficient is sensitive to the porosity of dust deposits and the volume-to-surface ratio of the particles, size stratification will contribute

to changes in the resistance of the dust cake which in turn, due to the nature of air seeking the least resistance, redistributes the air velocity and particle size again. As this interaction between the flow and the dust goes on during the filtration, different filter velocities, amount of dust collected, and deposit structure occur at various locations on the filter surface. Since areas of low resistance will handle higher than average air volumes, and vice versa, consequently more dust is deposited on the low resistance areas, less on the areas of high resistance, and a self-balancing system exists. The result is a cake with a nonuniform porosity but a uniform areal density with actual filtration velocities much higher than the design velocity, and consequently a higher pressure drop.

When the particles are charged, an additional force of electrical origin is acting at the particles throughout the space via an externally applied electric field or a self-space-charge field of the charged particles. This additional force results in another particle drift velocity following the electric field lines in addition to the aforementioned velocity following the flow lines. When the charged drift velocity is much greater than the air velocity, for instance highly charged particles in a strong electric field, the particle trajectory is then completely governed by the electric field lines resulting in a field-controlled size stratification and deposition rate instead of a flow-influenced size stratification and a self-balancing deposition rate.

From the knowledge of electrostatic precipitation, the charged drift velocity for particles greater than 0.2 μm in diameter in the field charging regime is directly proportional to the particle size and approximately to the field square. Thus, the field-controlled size stratification in a conventional bag configuration will be more or less orderly along the axial direction starting with the largest particles at the entrance of the bag and ending with the finest particles at the other end. The field-controlled areal density will, however, be nonuniform. Unlike the self-balancing effect in a flow influenced system, this field-controlled size stratification and nonuniform areal density maintains the initial distribution of cake resistance invariant throughout the entire filtration cycle leading to an overall observed pressure drop reduction. Mathematical proofs using artificial deposition profiles appended with this paper further support this postulation. The cause of reduced pressure drop in a charged filtration system is thus believed, primarily because the charged particles follow preferentially the field lines. There is no need to assume the formation of a more porous cake caused by other phenomena.

Quantitatively, from the experience of electrostatic precipitation, the mean drift velocity experienced in an electrostatic precipitator is commonly quoted as 5 cm/s or approximately 10 ft/min transverses to a gas velocity of the order of 1.5 m/s (5 ft/s); and an appreciable precipitation is generally observed at the first meter of the first field. Relative to a conventional bag designed at a nominal air-to-cloth ratio of 1×10^{-2} m/s (2 ft/min), and an aspect ratio of 30, the maximum gas velocity at the entrance of the bag is 6×10^{-1} m/s (4 ft/s); filtration velocity at the bag surface is only 1×10^{-2} m/s (2 ft/min). It is seen that the radial drift velocity relative to the maximum entrance velocity is in line with the electrostatic precipitator

practice; and it is also approximately a factor of 5 larger than the mean nominal filtration velocity. It appears reasonable to assume that the particles if adequately charged would certainly follow the field lines rather than the flow lines, resulting in an electric field-controlled nonuniform areal density together with an electric field-controlled particle size stratification, both along the bag axis with the heaviest deposition and the largest particles at the entrance and decreasingly lighter and finer toward the other end.

LABORATORY EXPERIMENTS

Laboratory experiments were designed to verify the postulated mechanism. To eliminate possible effects of dendrite formation, polarization and contact potential, two metallic screens were used to simulate the fabric filtration. The first screen was a coarse mesh; the second screen was a fine mesh. Both screens were electrically grounded. D.C. corona discharge was used for particle charging. Two configurations, a patch and a cylindrical, were tested. Test conditions were all at high dust loadings of the order of 2×10^{-2} Kg/m^3 (10 grains/ft^3), and air-to-cloth ratios of 2.54×10^{-2} to 3.66×10^{-2} m/s (5 to 7 ft/min). Instantaneous pressure drop was continuously monitored and recorded.

Typical results obtained at room temperature are illustrated in Figures 1 and 2. Pressure drop reduction was observed for all tests and for all configurations. Exceptions were noted, however, when tests were conducted on high resistivity dusts. Due to a back corona problem, high resistivity particles were inadequately charged; consequently, the particles were controlled predominantly by the air flow lines instead of the electric field lines. On the other hand, when an appreciable reduction of pressure drop was observed for the patch configuration, a nonuniform deposition profile on the first screen as shown in Figure 3 was also visually observed. Dust deposition was concentrated opposite the corona wire and tapered off qualitatively according to the electric field distribution. Failure to show appreciable pressure drop reduction for high resistivity dusts, and a nonuniform deposition profile accompanied by an appreciable reduction of pressure drop were experimental evidences that were needed to support the postulated mechanism of pressure drop reduction.

DISCUSSIONS

Study of the fundamental interaction of charged particles in a combined flow field and electrostatic field indicates that qualitatively there exists a strong possibility of nonuniform dust deposition in an electrostatic augmented fabric filtration. Particle deposition, unlike a conventional fabric filtration, is predominantly controlled by the electric field lines instead of the flow lines. Consequently, fewer particles are brought to the least resistance areas where larger than average air volumes would pass. Thus, the least resistance areas would remain almost unchanged during the filtration, resulting in an overall reduction of pressure drop as reported. With this fundamental reasoning, it is thus concluded that the first order mechanism of pressure drop reduction in an electrostatic augmented fabric filtration is due to the electric field controlled dust deposition -- a nonuniform dust

profile; other mechanisms leading to a more porous cake formation are not needed. Due to the nature that the charged particle drift velocity is size dependent, there also exists an orderly stratified particle size distribution constituting the nonuniform dust deposition. It is further believed that this electric field-controlled particle size distribution enhances the effect of reduced pressure drop by maintaining an orderly distributed cake porosity throughout the filtration cycle.

To further confirm the postulated mechanism, laboratory experiments with metallic screens, thereby eliminating the possible phenomena of dendrite formation, polarizations and electric contact potentials, verified the existence of nonuniform dust profile coincident with the reduction of pressure drop. Also verified was an unobservable reduction of pressure drop when high resistivity dust particles, hence back corona and inadequately charged particles, were used as test particles.

Finally, the postulated mechanism is theoretically verified by modeling an artificial step and a bell-shape dust profile mathematically based on the fundamental laws of conservation of mass, conservation of volumetric flow rate, and equal pressure drop of parallel flow. Mathematical modeling indicate that there always exists pressure drop reduction relative to a uniform dust distribution; the relative magnitude of pressure drop reduction depends on the degree of nonuniformity.

SUMMARY

The observed pressure drop reduction in a conventional fabric filter augmented with particle precharging can be explained completely by a nonuniform dust profile without introducing the possible existence of a more porous cake. Fundamental reasoning of the behavior of charged particles in a combined flow and electric field, experience of electrostatic precipitation, laboratory experiments with metallic screens, and mathematical modeling of nonuniform dust profile all consistently support the nonuniform profile mechanism.

REFERENCES

1. Ariman, T. (Compiler). Proceedings - Symposium on New Concepts for Fine Particle Control. EPA-600/7-78-170 (NTIS PB-292 095), U.S. Environmental Protection Agency, Research Triangle Park, NC, August 1978.

2. Helfritch, D.J., and T. Ariman. Electrostatic Filtration and the Apitron - Design and Field Performance. In: Proceedings - Symposium on New Concepts for Fine Particle Control, Ariman, T. (Compiler). EPA-600/7-78-170 (NTIS PB-292 095), U.S. Environmental Protection Agency, Research Triangle Park, NC, August 1978. p. 286-304.

3. Lamb, G.E.R., P.A. Costanza, and D.J. O'Meara. Electrical Stimulation of Fabric Filtration, Part II: Mechanism of Particle Capture and Trials with a Laboratory Baghouse. Textile Research Journal, Textile Research

Institute, October 1978. p. 566-573.

4. Oak, M.J., and D.A. Saville. Dendrite Structures in Electrically Stimulated Filtration. (Presented at the Joint Symposium on Fibers, Electrostatics and Filtration, Princeton, NJ, November 14-15, 1979). p. 2.

5. Penney, G.W. Collection of Electrically Charged Particles in Filters. J.APCA. 26(1):58, January 1976.

6. Penney, G.W. Electrostatic Effects in Fabric Filtration: Volume 1. Fields, Fabrics, and Particles (Annotated Data). EPA-600/7-78-142a (NTIS PB-288 576), U.S. Environmental Protection Agency, Research Triangle Park, NC, September 1978.

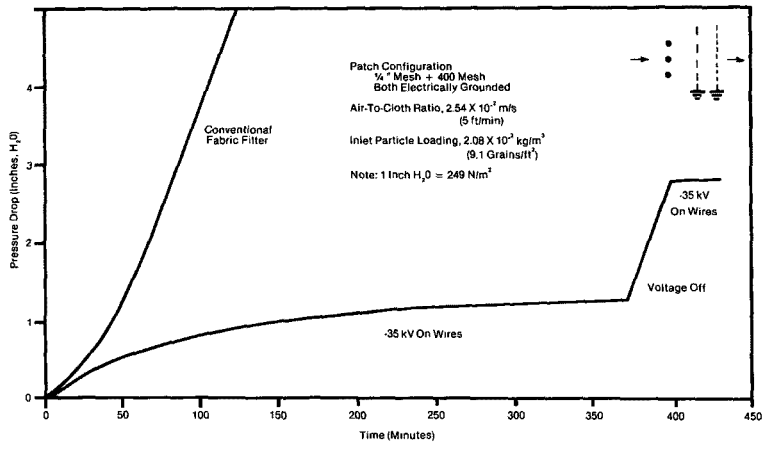

Figure 1. Laboratory Test Results - Patch Configuration

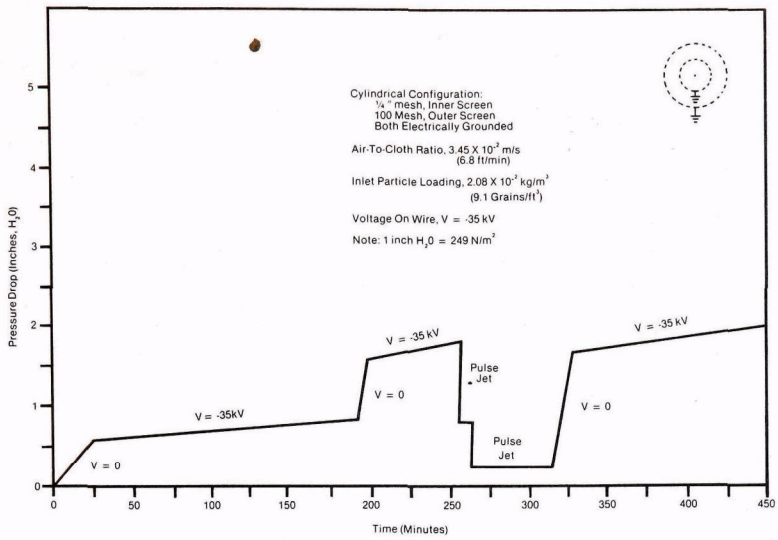

Figure 2. Laboratory Test Results - Cylindrical Configuration

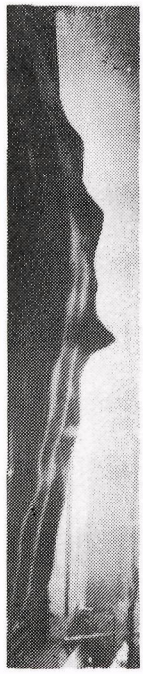

Figure 3. Nonuniform Dust Profile, Laboratory Test - Patch Configuration

APPENDIX

Mathematical Modeling of Nonuniform Dust Profile and Pressure Drop

Nomenclature

C, dust loading

U, mean filtration velocity, or air-to-cloth ratio

Δt, filtration time

A, fabric area

ΔP, pressure drop

ΔP_U, pressure drop of a uniform deposition profile

K_2, specific resistance coefficient

h, dust thickness

W, areal density

ℓ, linear dimension of filtration area

ρ, particle density

ε, cake porosity

Subscripts a and b denote parameters in deposition regions a and b respectively.

Step Profile

Let the dust profile be a discontinuous step as shown in Diagram A,

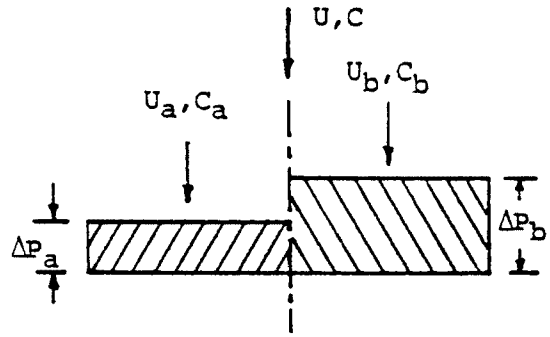

DIAGRAM A

From conservation of mass,

$$(C_a U_a \Delta t) A_a + (C_b U_b \Delta t) A_b = (CU\Delta t) A \tag{1}$$

From conservation of volumetric flow rate,

$$U_a A_a + U_b A_b = UA \tag{2}$$

From parallel-flow consideration,

$$\Delta P_a = \Delta P_b \tag{3}$$

From Carman-Kozeny equation, assuming the particle properties are the same in the two regions, i.e., $K_2 = K_2$, Equation (3) leads us,

$$C_a U_a^2 = C_b U_b^2 \tag{4}$$

Assuming the charged drift velocity results in different deposition rates, namely,

$$C_a U_a = (1/n)(C_b U_b)(A_b/A_a) \tag{5}$$

where $n > 1$ according to Diagram A.

Solving Equations (4) and (5), we have,

$$U_a = nU_b(A_a/A_b) \tag{6}$$

Solving Equations (1) and (5), we have,

$$(1+1/n) C_b U_b A_b = CUA \tag{7}$$

Let $A_a = A_b = A/2$, and from Equations (2) and (6),

$$U_b = 2U/(n+1) \tag{8}$$

From Equation (7),

$$C_b U_b = 2nCU/(n+1) \tag{9}$$

Substituting Equations (8) and (9) into Equation (3), we have,

$$\Delta P_b = 4nK_2CU^2\Delta t/(n+1)^2 \tag{10}$$

Let $\Delta P_U = K_2CU^2\Delta t$ be the pressure drop for a uniform dust profile, Equation (1) shows,

$$\Delta P_b = 4n\Delta P_U/(n+1)^2 \tag{11}$$

From Equations (11) and (5), for a uniform profile, n = 1, and thus, $\Delta P_b = \Delta P_U$. For n > 1, Table 1 illustrates that the pressure drop ratio, $\Delta P_b/\Delta P_U$, is always less than one.

TABLE 1. PRESSURE DROP REDUCTION DUE TO A STEP DUST PROFILE

n	$\Delta P_b/\Delta P_U$
2	0.889
3	0.750
4	0.640
5	0.556
6	0.490

Bell-Shape Profile

Let the dust height be h_o at center, and β be the weighted distribution. The bell-shape profile as illustrated in Diagram B can be presented by the expression,

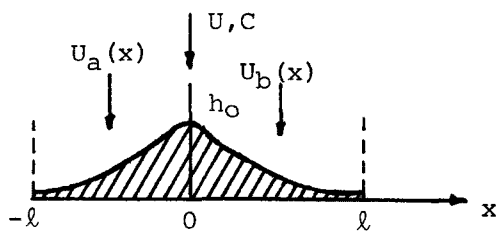

DIAGRAM B

$$h(x) = h_o\{1+(\beta x/\ell)^2\}^{-1}$$

Assuming the distribution is uniform in the Z-direction, from conservation of mass, we have,

$$2\int_o^{\ell} W(x)dx = 2(\ell/\beta)\int_o^{\ell} h_o\rho(1-\varepsilon)\{1+(\beta x/\ell)^2\}^{-1}d(\beta x/\ell)$$

$$= CU\Delta t(2\ell)$$

This normalization provides,

$$h_o = \beta CU\Delta t\{\rho(1-\varepsilon)\tan^{-1}\beta\}^{-1}$$

Therefore, the profile can now be represented by,

$$h(x) = \beta CU\Delta t\{\rho(1-\varepsilon)(1+(\beta x/\ell)^2)\tan^{-1}\beta\}^{-1} \qquad (12)$$

and the pressure drop $\Delta P_b(x)$ is,

$$\Delta P_b(x) = K_2 W(x) U_b(x)$$

$$= K_2\rho(1-\varepsilon)h(x)U_b(x)$$

Substitution of Equation (12), we have,

$$\Delta P_b(x) = \beta K_2 CU\Delta t \cdot U_b(x)\{(1+(\beta x/\ell)^2)\tan^{-1}\beta\}^{-1}$$

or,

$$U_b(x) = U\beta^{-1}\{1+(\beta x/\ell)^2\}(\tan^{-1}\beta)(\Delta P_b(x)/\Delta P_U)$$

From conservation of volumetric flow rate, and using the fact of parallel flow that $\Delta P_b(x)$'s are equal for all x's, we have,

$$2U\ell = 2\int_o^{\ell} U_b(x)dx$$

$$= \int_o^{\ell} U\beta^{-1}(\tan^{-1}\beta)(\Delta P_b/\Delta P_U)\{1+(\beta x/\ell)^2\}dx$$

Carrying out the above integration, and rearranging the terms, we have,

$$\Delta P_b/\Delta P_U = 3\beta\tan^{-1}\beta/(3+\beta^2) \qquad (13)$$

Table 2 illustrates how the pressure drop ratio varies with β.

TABLE 2. PRESSURE DROP REDUCTION DUE TO A BELL-SHAPE DUST PROFILE

β	$\Delta P_b / \Delta P_U$
1	0.955
2	0.774
3	0.600
4	0.476
5	0.390
6	0.198
Larger than 6	Approaches 0.190
0.4	0.998
0.3	0.999
Smaller than 0.3	Approaches 1.000, a uniform profile

EXPERIMENTAL CORRELATION OF DUST CAKE POROSITY, AIR-TO-CLOTH RATIO AND PARTICLE-SIZE DISTRIBUTIONS

By: Ta-Kuan Chiang
Buell Emission Control Division
Envirotech Corporation
Lebanon, PA 17042

Ronald L. Ostop
Department of Public Utilities
City of Colorado Springs
Colorado Springs, CO 80903

ABSTRACT

Experimental values of the mean specific resistance coefficients obtained from a full-scale utility baghouse and a slipstream Research and Development pilot baghouse were used to obtain the cake porosities using Carman-Kozeny equation. Log-log plot of the calculated mean porosity vs. the particle Reynolds number using volume-to-surface mean diameter indicated a functional dependence of minus two-thirds power to exist.

INTRODUCTION

Since the completion of the main baghouse and the "slipstream" pilot Research and Development (R&D) baghouse for Martin Drake Unit No. 6, the City of Colorado Springs, Colorado, an intensive R&D product optimization program was performed on site to evaluate and to advance the "State-of-the-Art" of fabric filtration for particulate and gaseous pollution control. This paper presents experimental correlation of dust cake porosity, air-to-cloth ratio and particle-size distribution found under the particulate control program.

Martin Drake Unit No. 6 is an 85-megawatt pulverized-coal-fired (PC) utility boiler with a flue gas volume of 189 actual cubic meters per second (400,000 ACFM) at full load. The main baghouse provided for the stack emission control is a conservative design using reverse air cleaning. Bag size is nominally 0.305 meters (12 inches) in diameter by 9.44 meters (30 feet) long with an effective cloth area of 8.454 square meters (91 square feet) per bag. The design air-to-cloth ratio is 9.398×10^{-3} meter per second (1.85 feet per minute) with all compartments in operation, and 1.128×10^{-2} meters per second (2.22 feet per minute) with two compartments out of service for maintenance or cleaning. The pilot R&D baghouse, provided for testing at higher air-to-cloth ratios without compromising the ability of the main baghouse to continue its basic stack emission control function, is a single compartment with a total of 16 full-size bags identical to the bags used in the main baghouse. A schematic flow diagram of the test setup is illustrated in Figure 1.

EXPERIMENTAL APPROACH

The test program was designed to determine the particle loading and particle size distribution simultaneously at the main baghouse and the slipstream

pilot R&D baghouse and to correlate their effect to the baghouse performances. After the establishment of the correlation of particle loading tests under identical operating conditions, extended range of tests, such as higher air-to-cloth ratio, would be performed at the pilot baghouse only. Analysis of the extended series of tests together with the simultaneous tests would then provide us data to develop a baghouse model that would be useful and practical in predicting filter operation throughout potential operation regimes, and to recommend the optimum operation regime for the main baghouse.

Since the important parameters which characterize a filter performance are the flow pattern, the dust particle properties, and the interactions between the flow pattern and the particle dynamics, test data obtained simultaneously at the main baghouse and the pilot R&D baghouse would be meaningful only if the condition of dynamical similarity between them was satisfied and maintained. In order to establish this dynamical similarity, the pilot R&D baghouse was thus purposely designed to accommodate full-size bags and bag spacings identical to the main baghouse. With this design, unlike laboratory bench scale or other small scale pilot tests, the flow Reynolds number in the pilot R&D baghouse and the main baghouse at the same air-to-cloth ratio would then be identical at the entrance of the bag, along the bag axis and at the bag surface leading to similar interactions between the flow pattern and the particle dynamics. Test data obtained from the pilot R&D baghouse of this program would thus be more representative, and can be scaled directly or generalized for a typical full-scale utility baghouse operation.

EXPERIMENTAL RESULTS

A total of 28 tests were conducted under this program. Among them, 13 tests were conducted simultaneously on the main baghouse and the slipstream pilot R&D baghouse. Air-to-cloth ratio covered a wide range from 7.620×10^{-3} to 2.235×10^{-2} meters per second (1.5 to 4.4 feet per minute).

As field testing proceeded and field data generated, it was found that the particle size distribution for the first eight tests was not log-normal and deviated from a normal utility PC boiler operation. Examination of cascade impactor results indicated that all the inlet samplers were flooded with more than 10 mg in the first few stages, and yet all the outlet samples were much less than 10 mg for reliable weighing. Inlet samples from absolute filter in accordance with EPA Method 5 for the remaining tests were then analyzed by laboratory sedimentation analyzers to establish the inlet particle size information. Further screening of test data based on the acceptable criteria of isokinetic sampling rate resulted in 10 valid tests as summarized in Table 1. The accustomed practical units were adopted to formulate Table 1. Conversion of practical units to MKS units are,

u,	air-to cloth ratio (A/C)	1 ft/min = 5.080×10^{-3} m/s
c,	dust concentration	1 grain/actual ft^3 (ACF) = 2.290×10^{-3} Kg/actual m^3 (ACM)
ΔP,	pressure drop	1 in. H_2O = 249 N/m^2

K_2,	specific resistance coefficient	1 in.-H_2O-min-ft/lb = $1x10^4$ N-S/Kg-m

From Table 1, although variations of particle loading and particle size distribution were found between the main baghouse and the pilot R&D baghouse, the ultimate results derived from this series of tests indeed characteristically demonstrated normal baghouse operations; namely, collection efficiencies of baghouses were both at 99.8 to 99.9 percent, nearly a constant for A/C of 1.6 to 2.4 for utility PC boilers without precollectors.

EXPERIMENTAL CORRELATION

By validating all the test results to within ±10 percent isokinetic sampling and by adapting laboratory particle size analyses, confidence was thus established for the key measurements which were needed for experimental correlations. These key measurements were:

- The air-to-cloth ratio,
- The inlet and outlet particle loading, and
- The inlet particle size distribution.

Using these key measurements together with bag pressure drop, ΔP, and time, t, strip chart recordings, the universally accepted Carman-Kozeny equation was then used to calculate the mean cake porosity. To avoid needless arguments on the validity of Carman-Kozeny equation, this calculated porosity was defined as ε_2, corresponding to K_2, which might or might not represent the real cake porosity if actual measurement was carried out. Table 2 listed the key parameters and their corresponding mean cake porosities, ε_2.

Following Carman-Kozeny equation, particle volume-to-surface mean diameter, d_{vs}, was used. Plotting of $\ell n\ \varepsilon_2$ vs. $\ell n\ d_{vs}$ as illustrated in Figure 2, apparently failed to show consistent functional relationship between ε_2 and d_{vs}. However, inspection of Table 2 indicated that the product of the air-to-cloth ratio, u, and d_{vs} might be a better choice. To generate a dimensionless plot, the product of ud_{vs} was normalized with gas density, ρ_g, and viscosity, μ, representing the particle Reynolds number Re_2. To generalize the plot representing baghouses at various aspect ratios (bag length/bag diameter), the air-to-cloth ratio, u, was further referred back to the air velocity, u_g, at the bag entrance. The final plot of $\ell n\varepsilon_2$ vs. $\ell n\ Re_2$ as shown in Figure 3 resulted in a straight line with a slope of minus two-thirds covering the ranges of experimental variation. Analytically, the experimental correlation found on the average was

$$\varepsilon_2 = 0.1945\ (Re_2)^{-2/3} \qquad (1)$$

Substituting Equation (1) into Carman-Kozeny equation, the mean specific resistance coefficient, K_2, was found,

$$K_2 = 2.448x10^4(\rho_g/\rho_p)\ (\rho_g u_g^2/\mu)\{1-0.1945(Re_2)^{-2/3}\} \qquad (2)$$

where ρ_p was the particle density and Kozeny constant of five was incorporated into the constant. Use of consistent units in Equation (2) provided us a tool to estimate K_2 either in practical engineering units or MKS units.

DISCUSSIONS

The physical significance of the particle Reynolds number can be interpreted the same way as the flow Reynolds number encountered in the fluid mechanics. In particular, the particle Reynolds number is a measure of the relative magnitude of the inertial forces of the gas flow and the particulate flow. The higher the particle Reynolds number indicates that particles would tend to follow the flow relatively readily. On the other hand, the opposite is true at lower particle Reynolds number. Consequently, at higher particle Reynolds number, particles follow readily with the flow seeking the least resistance resulting in a uniformly higher specific resistance coefficient; whereas at lower particle Reynolds number, particles are reluctant to follow the flow seeking the least resistance, leaving most particle collections to remain at the high resistance areas with least air velocity, and least particle collections to remain at the least resistance areas with the highest air velocity. Contrary to the flow and particle interaction at high particle Reynolds number, flow and particle interaction at low particle Reynolds number leads to, and more or less maintains, a nonuniform cake resulting in an overall lower mean specific resistance coefficient.

Understanding the physical significance of the particle Reynolds number, we have thus provided a sound physical foundation for the experimental correlations of Equations (1) and (2). Inspection of Equation (2) indicates that the upper limit of K_2 at high particle Reynolds number would be simply associated with the fluid acceleration. This is seen to be in agreement with the principle of fluid mechanics when the dust cake solidity, $(1-\varepsilon_2)$, approaches the limit of unity; it should be noted that, according to Carman-Kozeny equation, the limiting K_2 approaches infinity when the cake solidity approaches unity. On the other hand, the lower limit of K_2 approaches zero at low particle Reynolds numbers when the dust cake solidity approaches zero. Physically, zero dust cake solidity means strictly that there would not be any collection of particles on the fabric filter, and of course, the experimental correlations and the Carman-Kozeny equation would consequently break down at this extremely low particle Reynolds number. Therefore, the applicable criteria of Equations (1) and (2) for particle Reynolds number less than the experimental particle Reynolds number of 0.25 is dependent on the collection efficiency of fabric filtration. Furthermore, for particle Reynolds number less than 0.1, experimental correlations found here would be certainly invalid for the reason that a negative cake solidity, or a negative mean specific resistance coefficient, simply does not have any physical meaning. Apparently, for particle Reynolds number less than 0.1, or for fine particulate control, a different approach would certainly be needed.

SUMMARY

With the condition of dynamical similarity satisfied at a "slipstream" pilot R&D baghouse, and a utility baghouse, good correlation of baghouse performance was found between the two baghouses. After the verification of

baghouse performance between the two, testing proceeded at higher air-to-cloth ratios on the pilot R&D baghouse only. A total of 28 tests covering A/C of 1.5 to 4.4 were performed. Among them, 10 tests covering A/C of 1.6 to 2.4 were validated for experimental correlation of cake porosity, air-to-cloth ratio and particle size distribution. Using Carman-Kozeny equation and experimental K_2, mean cake porosities, ε_2, at various A/C and particle size distribution were then calculated. Log-log plot of the mean cake porosity and particle Reynolds number based on volume-to-surface mean diameter indicated that there existed functional dependence of minus two-thirds power. Physical significance of the particle Reynolds number was fully discussed to extend the applicable criteria of the finding outside its experimental range. Limiting value of K_2, according to the established experimental correlation, was found to be finite and proportional to the fluid kinetic energy, when the cake solidity, $1-\varepsilon_2$, approached the limit of one at high particle Reynolds number. Contrary to the Carman-Kozeny equation, the limiting K_2 approaches infinity when the cake solidity approaches one. With a finite limiting K_2, proportional to the fluid kinetic energy, it appears that the experimental correlation presented in this paper provides a better prediction of K_2 than the Carman-Kozeny equation.

At low particle Reynolds number, the experimental correlation indicated that there exists a critical particle size, or a critical air velocity, at the mean cake porosity of one, or K_2 of zero. To stay away from this physically meaningless regime from the viewpoint of cake filtration, the lower limit of particle Reynolds number was set at 0.1 with a caution that the filtration collection efficiency has to be high enough such that the inlet particle size distribution is a representative measure for the particles constituting the dust cake. It is further suggested that other approaches should be taken to extend the current finding for particle Reynolds number below 0.1.

By referring the particle Reynolds number to the bag entrance, we have generalized the experimental correlation to any aspect ratio. Thus, knowing particle size distribution, the experimental correlation presented here provides the confidence to predict baghouse performance for utility applications in particular, and other applications in general, provided that the particle shape is not much different from that of the fly ash.

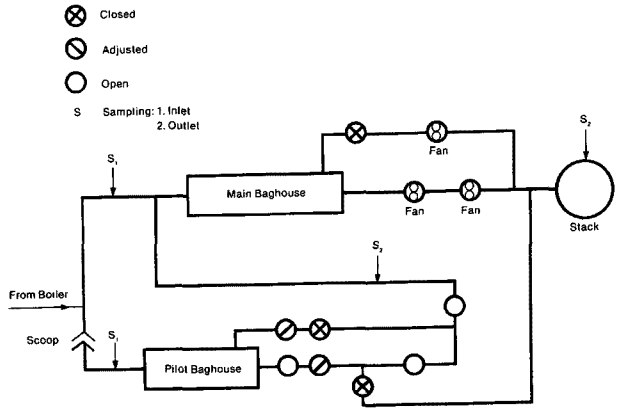

Figure 1. Test Setup

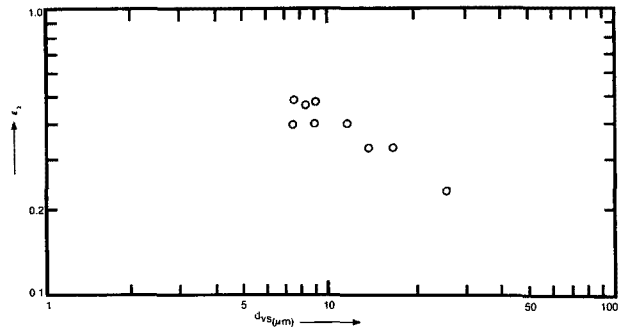

Figure 2. Mean Cake Porosity (ε_2) vs. Particle Volume-to-Surface Mean Diameter (d_{vs})

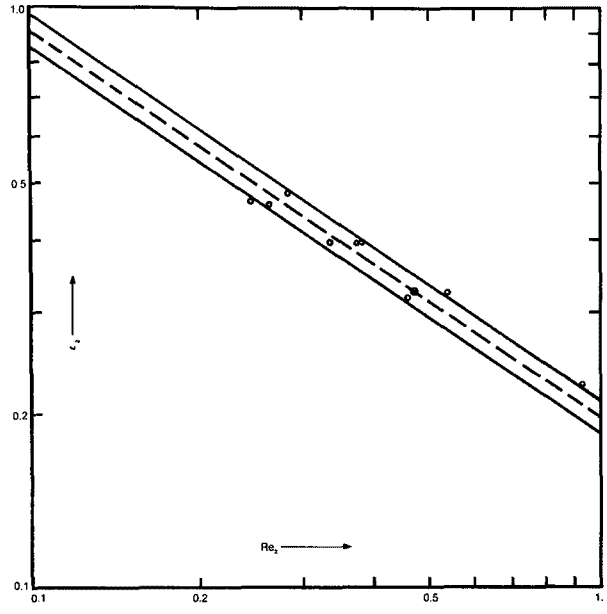

Figure 3. Mean Cake Porosity (ε_2) vs. Particle Reynolds Number (Re_2)

TABLE 1. VALIDATED TEST RESULTS

Test No.*	u	c	η	d_m +	σ +	d_{vs}	K_2 #
1P	1.613	1.8086	0.998	19.0	3.33	9.2	12.5
2M	1.691	2.1145	0.999	19.3	2.67	11.9	15.1
3P	1.554	1.9999	0.999	25.4	2.42	17.2	15.1
4M	1.616	1.8021	0.999	14.0	2.71	8.5	18.1
5M	1.683	1.5305	0.999	14.0	3.03	7.6	19.1
6M	1.637	1.7596	0.999	21.0	2.33	14.7	20.7
7P	1.731	1.5184	0.999	31.0	1.84	25.8	21.7
8M	1.651	1.9914	0.998	21.5	2.52	14.0	23.1
9P	1.801	1.4104	0.998	16.5	2.97	9.1	25.7
10P	2.437	1.4566	0.999	15.0	3.19	7.6	36.2

* Not in chronological order; P for pilot baghouse, M for main baghouse

+ d_m, mass median diameter, in μm; σ, standard deviation

K_2, in.-H_2O-min-ft/lb, derived from ΔP-t strip chart recordings and c, u in Table 1

TABLE 2. CALCULATED MEAN CAKE POROSITIES (ε_2)

Test No.	u	d_{vs}	ε_2	K_2	ρ_p *
1P	1.613	9.2	0.479	12.5	2.043
2M	1.691	11.9	0.392	15.1	2.157
3P	1.554	17.2	0.321	15.1	2.038
4M	1.616	8.5	0.458	18.1	1.958
5M	1.683	7.6	0.468	19.1	2.167
6M	1.637	14.7	0.318	20.7	2.064
7P	1.731	25.8	0.228	21.7	2.038
8M	1.651	14.0	0.316	23.1	2.170
9P	1.801	9.1	0.397	25.7	2.017
10P	2.437	7.6	0.391	36.2	2.137

* Particle density, in grams/cm^3

MODEL FOR DUST PENETRATION THROUGH A PULSE-JET FABRIC FILTER

By: D. Leith, M.J. Ellenbecker
Harvard School of Public Health
Department of Environmental Health Sciences
Boston, Massachusetts 02115

ABSTRACT

Presently, dust penetration through a pulse-jet filter cannot be interpreted or predicted well. This paper presents a model which considers penetration straight through the filter and penetration by seepage. Previous studies have considered penetration by the straight through process; however, a comparison of data from the literature with results from the present model shows that seepage and not straight through penetration accounts for virtually all penetrating dust. Although insufficient information is presently available to use the model to predict penetration, the model does show trends that should occur with changes in filter operating variables such as filtration velocity and pulse pressure, and suggests areas in which further research is necessary.

INTRODUCTION

Pulse-jet filters have captured a substantial portion of the fabric filter market[1] and the efficiency with which they operate is of strong interest to regulatory officials, to industrial users who must meet emission regulations, and to equipment manufacturers who supply these filters with a performance guarantee. In spite of many attempts to model penetration through fabric filters,[2-5] there is presently no satisfactory way to predict dust penetration through a pulse-jet cleaned fabric filter. This is not because of insufficient interest in the problem.

Performance characteristics which must be considered when modeling penetration include: (1) particle collection by clean fibers in a new fabric, (2) particle collection by the dust deposit accumulated on and in these fabrics, and (3) retention of this dust so it does not seep through the fabric during the rather violent cleaning cycle.

Penetration Straight Through a Clean Fabric

Particle collection by isolated, clean cylinders or fibers has been well studied, and adaptation of single fiber collection models into models for particle penetration through an array of clean fibers are well known.[6] Fraser and Foley[4] have made use of this work to describe penetration through a clean woven fabric and Hampl and Rimberg[2] have adapted clean fiber bed theory to a study of particle penetration through clean felt of the kind used in pulse-jet cleaned filters. The latter found that penetration of 0.35 to 1.1 μm particles through clean, new industrial felts ranged from 20 to 70% at typical pulse-jet filtration velocities, penetrations that are much higher than the 1% or less gererally found for intermittently

cleaned(7-9) industrial filters using fabrics well conditioned with dust. Although agreement is excellent between penetration theory and data for clean, new felt fabrics(2), the performance of new felt in the laboratory is clearly different from that of a well conditioned felt when used in an industrial pulse-jet filter.

Penetration Straight Through a Dust Deposit

The accumulation of dust in and on a fabric can affect dust collection in several ways. At low dust accumulation, before a continuous dust deposit forms on the fabric surface, dust particles collect on previously collected particles adhering to the fibers, as well as on the fibers themselves. Because of the greater collecting efficiency of the deposited dust particles for collecting additional particles, the apparent efficiency of individual fibers increases as dust collects upon them so that fabrics conditioned with dust have lower penetration than beds(6) or fabrics(3,4) composed of new, clean fibers. Fraser and Foley(4) modeled the effect of dust accumulating on woven fabrics by assuming the effect equivalent to a reduction of fiber diameter.

At high dust holdings, when the dust deposit is continuous and uniform on the fabric surface, the deposit acts as a filter cake and efficiency improves further. Cooper and Hampl(3) studied dust penetration straight through a well-developed dust deposit using an entirely theoretical model under the assumptions that impaction, interception(sieving), and diffusion are the important particle collection mechanisms. They determined that essentially no particles larger than 1 μm or so should pass through the dust deposit unless pinholes are present in it. Although models for penetration straight through a dust deposit are not as well developed as those for penetration straight through a clean fiber bed or a clean fabric, theory suggests that a continuous, unflawed deposit should collect virtually all particles from the aerosol passing through it. Theory predicts that penetration straight through a deposit should decrease with increasing particle diameter and increasing filtration velocity(3) for particle diameters larger than a few tenths micrometer.

Although penetration data must be carefully examined with reference to the conditions under which the tests were made, tests on new, clean felts by Hampl and Rimberg(2) show the decrease in penetration with increasing particle diameter and filtration velocity predicted by straight-through theory,and bench-scale experiments by Afify and Mohamed(10) and by Hall(11) show that penetration through an uncleaned felt becomes very low when a substantial dust deposit builds up on it. These conclusions generally confirm the Fraser-Foley(4) and Cooper-Hampl(3) theories that virtually no dust penetrates an established dust deposit. However, experiments on uncleaned fabrics are not relevant to the effects of seepage caused by filter cleaning.

Penetration by Seepage

Seepage penetration is defined as a process whereby collected particles later pass through the filter, i.e., seepage is a failure to retain collected

dust rather than a failure of collection. In pulse-jet cleaned filters, most seepage is thought to occur when the conditioned fabric strikes its supporting cage at the end of a cleaning pulse(12). Rapid deceleration of the residual dust deposit causes some particles or agglomerates to separate from the support (fabric fibers or other dust particles). As normal filtration flow resumes, some of these particles or agglomerates are swept through the fabric and into the cleaned gas stream.

Seepage penetration is likely to increase whenever the separation force between the collected dust and its substrate increases. For example, large particles or agglomerates with considerable inertia are likely to break loose more easily than small particles when the fabric strikes its supporting cage smartly at the end of a cleaning pulse. It is reasoned that high filtration velocity, which drives the fabric back on to its cage at a faster rate, causes it to hit with greater impact, and thereby aggravates seepage. In contrast, straight-through penetration theory predicts penetration should decrease with increasing particle size and with increasing filtration velocity(2-4) for particles larger than a few tenths micrometer in size. This is opposite to the trends expected from seepage.

PENETRATION MODEL

A reasonable model to describe dust penetration through a pulse-jet-cleaned filter should consider both straight-through penetration and seepage penetration. The rate at which dust passes through the filter can be expressed in terms of outlet mass flux, the mass of dust that penetrates per unit fabric area per unit time:

$$N = N_{st} + N_{se} \tag{1}$$

in which N represents the total outlet mass flux, N_{st} is the outlet flux due to straight-through penetration, and N_{se} is the flux due to seepage.

The total straight-through flux, for particles of all sizes, will depend on penetration for particles of each size in the inlet aerosol:

$$N_{st} = v\, c_i \int_0^1 P_{st}\, dG \tag{2}$$

in which v is superficial filtration velocity, c_i is the overall mass concentration for particles approaching the filter, P_{st} is the fraction of particles of a particular size that pass straight through the filter, and DG is the mass fraction of all incoming particles which are of that size.

If the relationship between particle diameter and straight-through flux is needed, then relationships among particle diameter, straight-through penetration, and inlet dust size distribution must be known. However, if an overall value for straight-through flux is sufficient, the overall mass fraction of the inlet dust that passes straight through the filter, $\overline{P_{st}}$, can be used in place of the integral in Equation 2.

As discussed above, dust that seeps through a pulse-jet-cleaned fabric may be comprised essentially of dust driven through the fabric when the fabric strikes its supporting cage as a cleaning pulse ends and filtration resumes. Deceleration of the dust held by the fabric as it strikes the cage may cause a separation force sufficient to free some dust which normal filtration air can then sweep through into the cleaned gas stream. If so, then seepage flux will be:

$$N_{se} = \frac{w}{t} \int_0^1 \varepsilon \, dH \tag{3}$$

in which w is the mass areal density of the total dust deposit on the fabric as it strikes its cage, t is the time interval between cleaning pulses, ε is the fraction of particles or agglomerates of a particular size in the dust deposit that are separated from the dust deposit as the fabric strikes the cage, and dH is the mass fraction of all particles or agglomerates in the dust deposit that are of that particular size.

If the relationship between particle diameter and outlet flux is required, the relationships among ε, dH, and particle or agglomerate size must be known. If an overall mass outlet flux is sufficient, an overall mass-weighted average for ε can be used, $\overline{\varepsilon}$, in place of the integral in Equation (3) Insufficient data are presently available to allow evaluation of the integral in Equation (3) and in the following discussion $\overline{\varepsilon}$ will be used.

The overall mass fraction of dust separated from a conditioned fabric, $\overline{\varepsilon}$, can be related(14) to the applied area-specific force causing the separation, F_s/A. The exact relationship between fraction of dust separated and separation force applied is not known, and is presently under investigation at this laboratory. Pending the outcome of this work, it will be assumed that these variables are proportional:

$$\overline{\varepsilon} = \frac{k^* F_s}{A} \tag{4}$$

Impulse-momentum considerations say that the area-specific separation force applied, F_s/A, times the time over which this force acts, t^*, will equal the momentum of the area-specific dust deposit as it begins deceleration upon striking the cage:

$$\frac{F_s t^*}{A} = w v \tag{5}$$

Substitution of Equations (4) and (5) into Equation (3) yields:

$$N_{se} = \frac{k^* w^2 v}{t^* t} = \frac{k w^2 v}{t} \tag{6}$$

in which the unknown proportionality constant, k*, and the time necessary to

stop the fabric as it strikes its cage, t^*, are combined in a new constant, k, which should depend on the dust separation and retention characteristics of the fabric and fabric elasticity.

Equations (2) and (6) can be substituted into Equation (1) to give an expression for overall outlet flux through the pulse-jet cleaned filter:

$$N = c_i v \overline{P_{st}} + k \frac{w^2 v}{t} \tag{7}$$

EXPECTED TRENDS IN OUTLET FLUX

Equation (7) predicts the effects of changes in filter operation on overall outlet flux, N. First, consider the case in which straight-through penetration is much more important than seepage; that is, the first term on the right side of Equation (7) is considerably larger than the second:

$$N \doteq c_i v \overline{P_{st}} \tag{8}$$

In this instance, Equation (8) shows that decreases in inlet dust concentration, c_i, should cause a decrease in outlet flux. However, Dennis(9) has determined from field and laboratory studies(7,15) that the mass emission rate or flux from a fabric filter is essentially constant despite changes in inlet concentration.

Straight-through theory predicts that factors which decrease overall penetration, $\overline{P_{st}}$, such as increasing diameter for particles larger than a few tenths micrometer, or increasing dust deposit areal density should also decrease outlet flux. However, Leith and First(8) determined that large particles penetrate a pulse-jet filter as readily as small particles, at variance with this prediction. Data(16,17) discussed later in this section of the report indicate that more dust penetrates if the dust deposit areal density increases, also at variance with this prediction.

The effect of increased filtration velocity on straight-through outlet flux is unclear. Equation (8) suggests that outlet flux should increase with velocity, v, if all else remains constant; however, increased velocity should also decrease penetration, $\overline{P_{st}}$, for particles collected by impaction so that the net effect of velocity changes on outlet flux is uncertain. In summary, straight-through penetration theory predicts trends generally at variance with those determined experimentally for changes in pulse-jet filter operating conditions such as inlet dust concentration, particle diameter, and areal density of the dust deposit.

Next, consider the case in which seepage is much more important than straight-through penetration, that is, the second term on the right side of Equation (7) is considerably larger than the first:

$$N \doteq k \frac{w^2 v}{t} \tag{9}$$

Equation (9) predicts that outlet flux should decrease with decreases in the areal density of the dust deposit, w, in marked contrast to straight-through theory, but in agreement with experimental data reported by Ellenbecker(16) and by Leith et al.(17). Equation (9) also indicates that decreases in filtration velocity should decrease outlet mass flux, in agreement with several experimental studies(8,18-20) using pilot scale and full scale pulse-jet filters. Dennis(9), Hall(11), and Löffler(13) have shown that outlet dust concentration from a pulse-jet cleaned filter increases substantially but momentarily, immediately after cleaning. Modifications to the cleaning pulse which ease the cleaned bag back to its supporting cage gently so that it hits with less impact have been shown to decrease penetration compared to that found with normal pulse-jet cleaning(21). These results are expected if seepage associated with pulse-jet cleaning causes penetration.

Leith and First(10) measured the relative amounts of straight-through flux and seepage flux for fly ash penetrating a pulse-jet filter using untreated but conditioned polyester bags at superficial filtration velocities from 50 to 150 mm/s. Outlet flux was very low for the straight-through mechanism under all conditions, but the seepage mechanism increased with increasing filtration velocity. In general, the conclusion was reached that seepage accounted for essentially all the dust that passed through the pulse-jet filter and was particularly important at high filtration velocities.

Although Equation (9) is presently inadequate to describe the dependence of outlet flux on particle diameter, this relationship can be incorporated into the equation when information adequate to allow integration of Equation (3) becomes available. It should be clear that penetration by particle size will be greatly influenced by filtration velocity, dust loading, pulse pressure, etc. In summary, penetration trends predicted by seepage theory seem generally to agree with trends observed in experiments conducted over a range of pulse-jet filter operating conditions. These trends require precise quantification to make possible a fully comprehensive mathematical model of a pulse-jet cleaned filter. These tests are presently under way at this laboratory.

COMPARISON OF MODEL WITH DATA

If seepage alone accounts for nearly all the dust penetration from a pulse-jet cleaned fabric filter, Equation (9) predicts that a log-log plot of outlet dust flux versus the group w^2v/t should yield a straight line with a slope of unity and air intercept at log(k). Data(16,17) adequate to check this prediction are summarized elsewhere(16,17). Bags made from untreated polyester felt and Gore-tex felt were tested in a three-bag pulse-jet filter at superficial filtration velocities from 50 to 150 mm/s. Outlet dust concentrations were measured and total outlet flux calculated. The areal density of the dust on the bags was measured by weighing the bags and subtracting the weight of the clean, new fabric. The interval between cleaning pulses was 60 s per bag in each test.

Figure (1) is a log-log plot of outlet dust flux, N, against w^2v/t. The data for both bag types scatter about lines with a unit slope as Equa-

tion (9) indicates will occur when outlet flux caused by straight-through penetration is negligible and seepage is caused by deceleration of the bag as it hits the supporting cage. A least squares fit for Equation (9) to the data shown in Figure (1) gives values of k = 0.0077 m·s/kg for untreated polyester fabric with coefficient of determination, r^2 = 0.92, and k = 0.034 m·s/kg for the Gore-tex fabric with r^2 = 0.96.

The higher value for constant k found for Gore-tex fabric should not necessarily be interpreted to mean that penetration in an operating filter will be higher using Gore-tex fabric, as this fabric retains less dust. Although Equation (9) shows that outlet flux increases with increasing k, it decreases with the square of areal dust density, w. Inter-fabric comparisons require knowledge of both factors.

DISCUSSION

To predict outlet mass flux using Equation (9) , values are needed for filtration velocity, v, time between cleaning pulses, t, constant, k, and areal density of the dust deposit, w. Although velocity and time between cleaning pulses are ordinarily known, the other two parameters might not be known. At present the only way to determine constant k is to evaluate data as done in Figure (1) . Our data to the present indicate that constant k depends on fabric type, although it is likely to depend as well on the characteristics of the dust collected, pulse pressure, filtration velocity, and other parameters.

The areal density of the dust deposit on the fabric is also likely to be unknown. The magnitude and distribution of the dust deposit on an operating nonwoven bag can be measured with difficulty(22). A procedure for calculating the areal density of the dust deposit on a pulse-jet cleaned filter has recently been developed as part of a theoretical model for pressure drop(14). This procedure, however, requires other information concerning the resistance of the fabric and the specific resistance of the dust deposit which may not be available. Regrettably, it is not presently possible to use Equation (9) to predict quantitatively the outlet flux from a pulse-jet-cleaned fabric filter; further work is necessary.

However, the model is useful to predict the direction of outlet flux to changes in pulse-jet filter operating variables. Equation (9) shows that outlet flux increases with increasing filtration velocity. Increased pulse pressure should decrease the areal dust density, w; if so, the outlet flux should also decrease although sufficient dust must remain on the filter to assure good collection of incoming dust. Equation (9) suggests that increasing t, the time between pulses to each bag, should decrease emissions, but this might also increase the areal density, w, of the dust deposit on the

bag. An increase in areal density should increase emissions so that the net effect of pulse interval on outlet flux is unclear. Changes to the size distribution of the dust, to the relative humidity or temperature of the gas stream, or to the electrostatic properties of the dust or fabric may all affect constant k; the relationships between these variables and this constant are presently unknown.

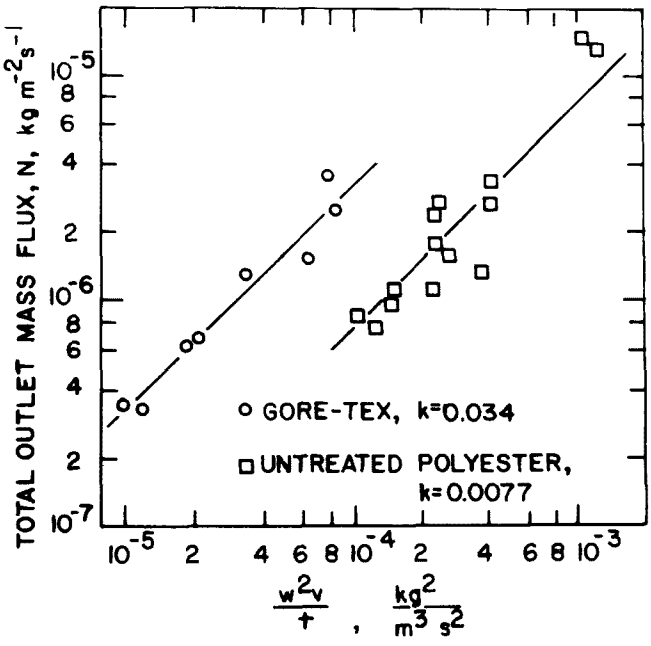

FIGURE 1. TOTAL OUTLET MASS FLUX, N, VERSUS w^2v/t, FOR BAGS MADE FROM GORE-TEX AND UNTREATED POLYESTER FELT

NOMENCLATURE

c_i	dust inlet concentration,	kg/m^3
dG	mass fraction of particles of a particular size in the inlet dust, dimensionless	
dH	mass fraction of particles or agglomerates of a particular size in the dust deposit, dimensionless	
F_s/A	area-specific force acting to separate the dust deposit from its substrate,	N/m^2
k	constant, see Equation (6)	m·s/kg
k*	constant, see Equation (4)	m^2/N
N	total outlet mass flux,	kg/m^2·s
N_{st}	outlet mass flux due to straight-through penetration,	kg/m^2·s
N_{se}	outlet mass flux due to seepage penetration,	kg/m^2·s
$\overline{P_{st}}$	mass fraction of a particular size that passes straight through the filter, dimensionless	

t time between cleaning pulses, s
t^* time during which dust deposit decelerates, s
v superficial filtration velocity, m/s
w areal density of dust deposit on and in the fabric, kg/m^2
ε fraction of particles or agglomerates of a particular size in the dust deposit that are separated from the dust deposit, dimensionless
$\overline{\varepsilon}$ mass fraction of the dust deposit that is separated from the dust deposit, dimensionless

REFERENCES

1. Frey, R.E. Types of Fabric Installations. J. Air Poll. Control Assoc. 24:1148, 1974.

2. Hampl, V. and D. Rimberg. Aerosol Penetration of Felt Filter Media. (Presented at Annual Conference of Gesellschaft für Aerosol-Forschung E.V. (Association for Aerosol Research), Bad Soden, Germany, Oct. 26, 1974).

3. Cooper, D.W. and V. Hampl. Fabric Filter Performance Model. In: Conference on Particulate Collection Problems in Converting to Low Sulfur Coals. Report EPA-600/7-76-016. NTIS, Springfield, Virginia, 1976. p. 149-185.

4. Fraser, M.D. and G.J. Foley. A Predictive Performance Model for Fabric Filter Systems. 1. Intermittently Cleaned Single Compartment Systems. (Paper 74-99 presented at 67th Annual Meeting of Air Poll. Control Assoc. Denver, Colorado, 1974).

5. Dennis, R., R.W. Cass, D.W. Cooper, R.K. Hall, V. Hampl, H.A. Klemm, J.E. Langley and R.W. Stern. Filtration Model for Coal Fly Ash with Glass Fabrics. Report EPA-600/7-77-084. NTIS, Springfield, Virginia, 1977.

6. Davies, C.N. Air Filtration. New York, Academic Press, 1973.

7. Dennis, R. and J. Wilder. Fabric Filter Cleaning Studies. Report EPA-650/2-75-009. NTIS, Springfield, Virginia, 1975.

8. Leith, D. and M.W. First. Performance of a Pulse-Jet Filter at High Filtration Velocity. 1. Particle Collection. J. Air Poll. Control Assoc. 27:534, 1977.

9. Dennis, R. Collection Efficiency as a Function of Particle Size, Shape, and Density: Theory and Experience. J. Air Poll. Control Assoc. 24: 1156, 1974.

10. Afify, E.M. and M.H. Mohamed. Collection of Efficiency and Pressure Drop of Needle Punched Filters. J. of Engineering for Industry. 98:675, 1976.

11. Hall, R.F. Getting the Best Results from Needlefelts in Dust Filtration. Filtr. and Sep. 14:350, 1977.

12. Leith, D. and M.W. First. Performance of a Pulse-Jet Filter at High Filtration Velocity III. Penetration by Fault Processes. J. Air Poll. Control Assoc. 27:754, 1977.

13. Löffler, F. Separation Efficiency and Pressure Loss of Filter Materials of Different Structure, at Differing Conditions. Staub, Reinhalt. Luft. 30(12):27, 1970.

14. Leith, D. and M.J. Ellenbecker. Theory for Pressure Drop in a Pulse-Jet Fabric Filter. Atmospheric Environment. 14:845, 1980.

15. Dennis, R., G.A. Johnson, M.W. First, and L. Silverman. How Dust Collectors Perform. Chem. Eng. 59:196, 1952.

16. Ellenbecker, M.J. Pressure Drop in a Pulse-Jet Fabric Filter. Sc.D. Thesis. Harvard School of Public Health, Boston, Massachusetts, 1979.

17. Leith, D., M.J. Ellenbecker, M.W. First, J.M. Price, A. Martin and D.W. Gibson. Performance of a High Velocity Pulse-Jet Filter II. EPA Publication 600/7-80-042. Research Triangle Park, North Carolina, 1980.

18. Billings, C.E., M.W. First, R. Dennis, and L. Silverman. Laboratory Performance of Fabric Dust and Fume Collectors. AEC Report No. NYO-1590 (revised), 1961.

19. McKenna, J.D., J.C. Mycock, and W.O. Lipscomb. Performance and Cost Comparisons Between Fabric Filters and Alternate Particulate Control Techniques. J. Air Poll. Control Assoc. 24:1144, 1974.

20. Mohamed, M.H., E.M. Afify and J.W. Vogler. Needle Punched Fabrics in Filtration. (Paper presented at Technical Symposium - Nonwoven Product Technology, International Nonwovens and Disposables Association, Washington, D.C., 1974).

21. Leith, D., M.W. First, and D.D. Gibson. Effect of Modified Cleaning Pulses on Pulse-Jet Filter Performance. Filtr. and Sep. 15:393, 1978.

22. Ellenbecker, M.J. and D. Leith. Dust Deposit Profiles in a High Velocity Pulse-Jet Fabric Filter. J. Air Poll. Control Assoc. 29:1236, 1979.

PERFORMANCES OF DUST LOADED AIR FILTERS

By: C. Kanaoka, H. Emi, M. Ohta
Department of Chemical Engineering
Kanazawa University
Kanazawa 920, Japan

ABSTRACT

It has been realized that dust load in an air filter enhances particle collection and pressure drop across the filter. However, it was almost imposible to predict its effects on both properties properly because of complexity in the structure of deposited particles.

In this study, growing process of particles on a fiber was simulated and it was utilized to the calculation of a collection efficiency of a dust loaded fiber. Experimentally particle agglomerates on a fiber, and collection efficiency and pressure drop of a filter were measured for various filtration conditions and times. Effects of loaded mass and filtration conditions on a single fiber collection efficiency and pressure drop were discussed through the comparison of those results. Finally estimation method for performances of dust loaded air filter has been proposed.

INTRODUCTION

Researches on the collection mechanisms inside a clean filter where no particles were captured on the filter, have been studied from various view points. These advances, however, have not yet reached the stages whereby the design and opertation of a fibrous air filter can be made on a rational basis, since mass of dust in a filter changes the performances of filters.

There are very few studies focused on these phenomena. Experimentally, two different kinds of approaches have been attempted, e.g., microscopic and macroscopic approaches. The former is the method to observe growing processes of dendrites on a fiber(1,2,3) and is suitable to the analysis of the growing process and the effect of collection mechanisms precisely.

While the latter is more practical method in obtaining the relations between collection efficiency and corresponding pressure drop and dust load in a filter as well as filtration time(4,5). Yoshioka et al. have obtained experimental correlation between collection efficiency of dust loaded fiber $\eta_{\alpha m}$ and accumulated mass of particles per unit filter volume m as,

$$\eta_{\alpha m}/\eta_{\alpha_0} = 1 + \lambda m \qquad (1)$$

where, λ is the collection efficiency raising factor and they have obtained 5 m^3/kg as the value of λ regardless of experimental conditions.

Theoretical approach is more difficult to describe the process because of the lack of knowledges on the phenomena. Recently, Payatakes and Tien(6) and Payatakes(7,8,9,10) have derives deterministic expressions for growing process of particle dendrites for several collection mechanisms using a set of successive differential equations. On the other hand, Wang et al.(11) and Kanaoka et al(12,13,14) have simulated growing process of dendrites on a fiber and a sphere in the case of interception and inertia.

In this paper, a very simple simulation method using Monte Carlo simula-

tion technique to estimate the process has been proposed. Then single fiber collection efficiency was evaluated using simulation results. Further it was utilized to predict performance of a fibrous filter. Obtained results were compared with experimental single fiber collection efficiency. Estimation method for pressure drop across a filter based on experimental observation was also proposed.

SIMULATION OF PARTICLE DENDRITES ON A CYLINDRICAL FIBER

The simulation has been performed in Kuwabara's cell shown in figure 1 by assuming that his equation in equation (2) holds even at dust loaded condition and dendrites have no effects on upcoming particles.

$$\psi = \frac{y}{2\kappa}\left[(1 - \frac{\alpha}{2})\frac{1}{x^2 + y^2} - (1 - \alpha) + \ln(x^2 + y^2) - \frac{\alpha}{2}(x^2 + y^2)\right] \qquad (2)^{15}$$

where κ is the hydrodynamic factor and is defined as

$$\kappa = -\frac{1}{2}\ln\alpha + \alpha - \frac{\alpha^2}{4} - \frac{3}{4} \qquad (3)$$

Thus, particle motion can be expressed by,

$$St\frac{dV}{dt} = U - V \qquad (4)$$

where U and V are dimensionless velocity vectors of fluid and particle, respectively.

In actual filtration, spatial distribution of aerosol particles is random at a microscopic level, even when time average concentration is kept constant. In other words, each particle passes through a plane, which is normal to mean flow direction, at an arbitrary time and position (y,z) of the plane as shown in figure 1.

Calculations were carried out by following procedures;

1) Construct three dimensional mesh network, dimensions of which were determined equal to particle diameter to be able to store one particle in it as shown in figure 2.

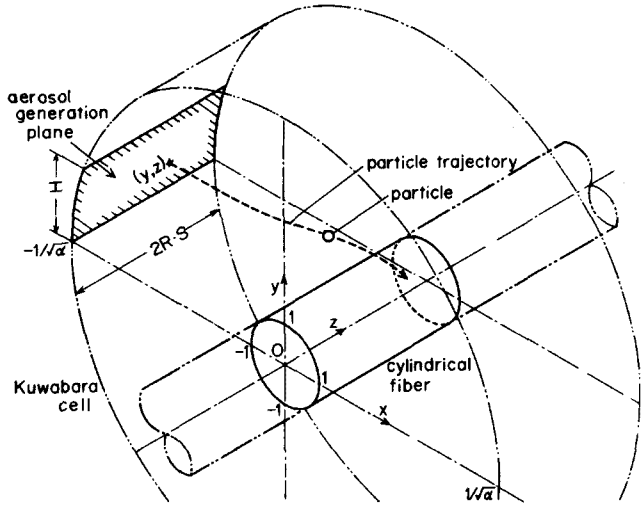

Figure 1 Schematic diagram of particle motion in Kuwabara's cell

2) Calculate all inlet heights of the trajectories which passes through nodal points in the network. They were used as the substitutes of nodal points.
3) Evaluate the particles trajectory by comparing the inlet height of the particle with those of nodal points until it collides with or passes through the fiber or dendrites.
4) Continue step 3 until one of dendrites reaches to the outmost layer of the network.
5) Repeat steps 3 and 4 several hundred times to obtain stochastically sufficient number of dendrites.

Simulations were carried out for various filtration conditions but packing density of the filter α and particle density ρ_p were fixed at α=0.03 and ρ_p= 1g/cm^3, respectively.

Simulation Results

Figure 2 is a typical simulation result. The numbers in each particle show the order of deposited particles. As seen from the figure, most of particles are captured on deposited particles rather than on the fiber surface and further their order is random. The shape of the particle dendrits simulated is similar to the observations shown in figure 3. Since growing process is random, number of stored particles in each mesh were counted and averaged and were plotted against circumferential angles. Calculated number distributions for R=0.1 were shown in figure 4. It is remarkable that maximum deposition appears at some certain angles and it increases as Stokes number decreases. Same tendency was observed in experiments as shown in figure 5.

Single fiber collection efficiency with M particles on a fiber of unit length η_{TIM} can be evaluated by equation (5) knowing the average imcoming particles during the collections of M-th and (M+1)st particles N_M, since mass of particles in unit volume of a filter is expressed by equation (6).

$$\eta_{TIM} = 1/N_M \tag{5}$$

$$m = \frac{4}{3} M\rho_p R^2 \tag{6}$$

Figure 6 shows the increases in calculated efficiency with deposited mass. As seen from the figure, it increases almost linearly with m which is the same as previously reported tendency(5) but value of slopes λ varies with filtration conditions. Table 1 shows the calculated values of λ. λ shows the highest at St=0 and lowest at St=∞ for any interception parameter R. This means that collection efficency increases rapidly with dust load m in small St region.

TABLE 1. COLLECTION EFFICIENCY RAISING FACTOR λ

R \ St	0.0	0.4	0.6	1.0	1.4	2.0	∞
0.05	56.1	-	45.1	16.4	0.873	0.238	0.0769
0.1	14.8	12.2	-	2.89	-	0.253	0.0696
0.2	3.09	-	1.82	0.783	-	0.144	0.0482

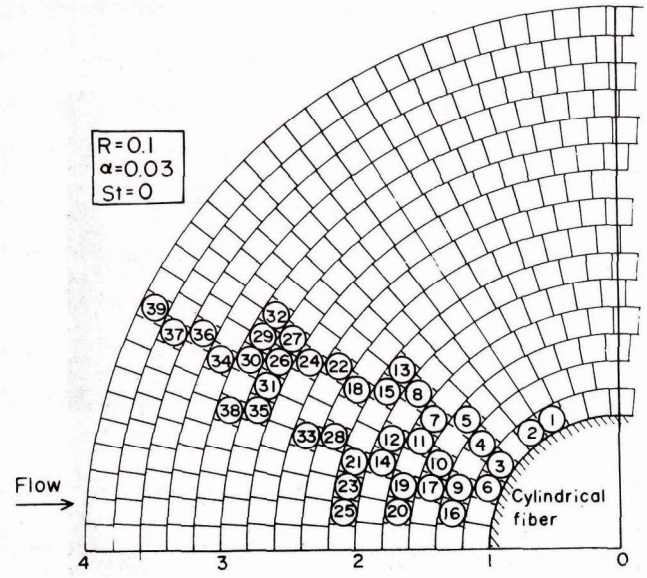

Figure 2 Cross sectional view of mesh network and a typical simulation result

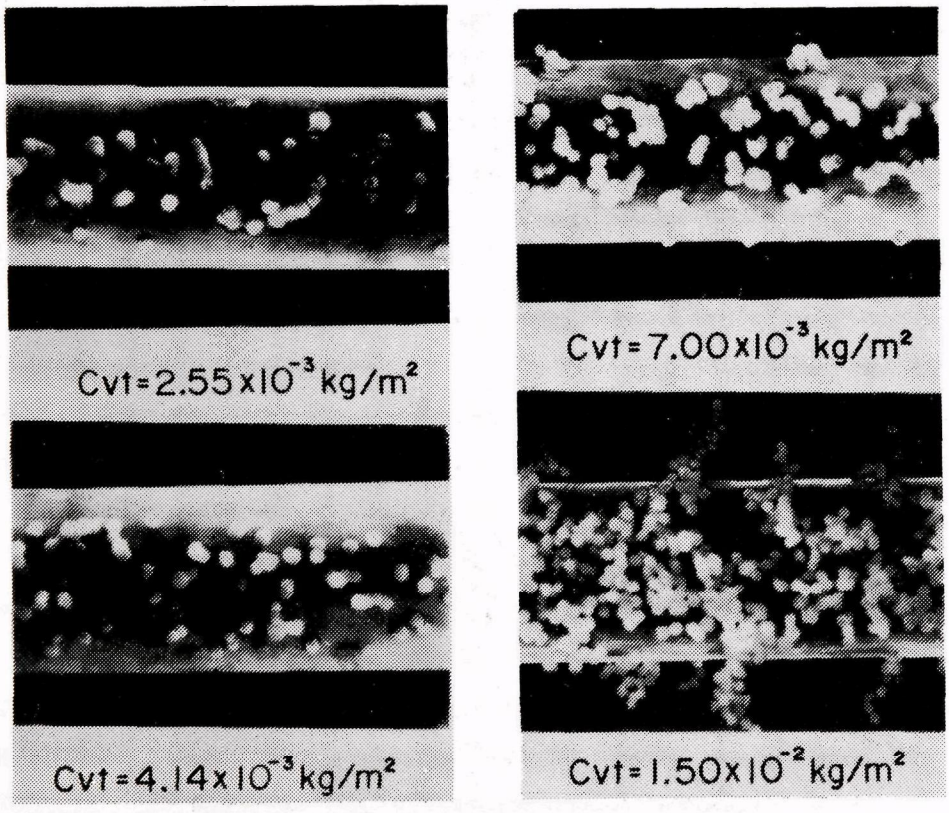

Figure 3 Front views of dust loaded fiber
experimental conditions:
methylene blue particles D_p=2.5 μm, stainless steel fiber D_f=30 μm, approaching velocity V=80 cm, Stokes number St=1.35, Interception parameter R=0.083

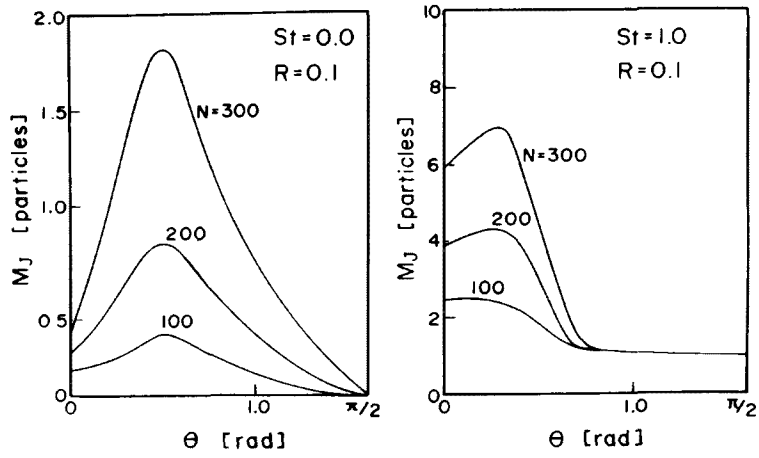

Figure 4 Change in average number of deposited particles on a fiber with time

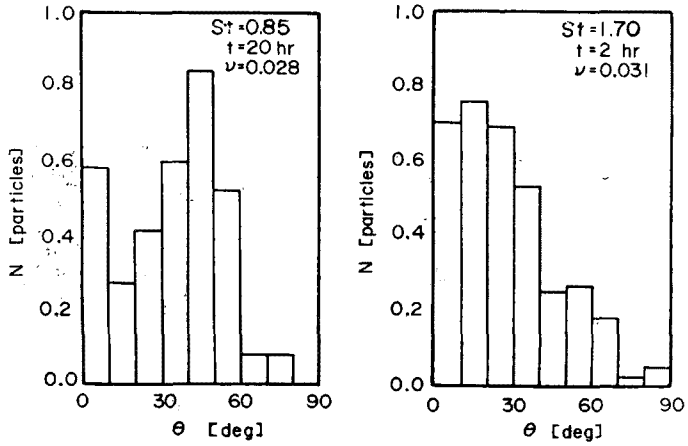

Figure 5 Experimental distribution of collected particles on a fiber

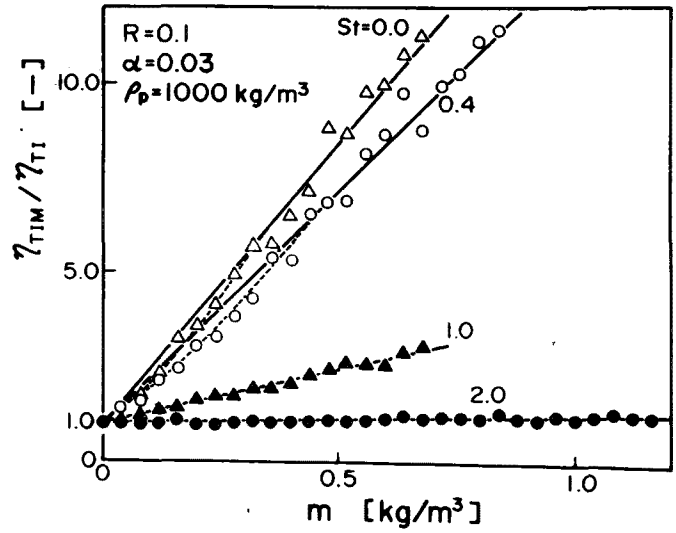

Figure 6 Collection efficiency of a single fiber with dust load

MEASUREMENT OF COLLECTION EFFICIENCY OF A DUST LOADED FILTER

Figure 7 is a diagram of the experimental apparatus used. Sodium chloride and methylene blue particles were used as test aerosols. They were generated by an ultrasonic nebulizer and a vibration orifice monodisperse aerosol generator(TSI Inc., Model 3050). Glass fiber mat, which is composed of three thin differential filters and fiber diameter of which is 11μm, was used as a test filter. After aerosol was deionized with radioactive isotope ^{241}Am, it was introduced to the test filter. Escaped aerosol particles from it were recovered with backup absolute filter. Pressure drop and aerosol concentration were monitored during the experiment. For given set of filtration conditions, experiments were carried out repeatedly but with different exposure times. Accumulated mass in each differential filter and backup filter were determined by colorimetric and titration methods.

Single Fiber Collection Efficiency

Figure 8 shows typical relations of m and CVt. Although values of m scatter in large CVt, m increases with CVt and filtration velocity V as a whole. Since collection efficiency of a differential filter is expressed by equation (7), E_m was obtained through graphical differentiation. Further single fiber collection efficiency was calculated from equation (8) assuming that it holds for a thin differential filter.

$$E_m = \frac{dm}{d(CVt)}\Delta X \tag{7}$$

$$\eta_{\alpha m} = -\frac{\pi}{4}\frac{(1-\alpha)}{\alpha}\frac{D_f}{\Delta X}\ln(1-E_m) \tag{8}$$

The calculated values of η_{TIm} from the above procedure was normalized by the experimental initial efficiency η_{TI} and it was plotted against m in figure 9. In the figure, η_{TIm}/η_{TI} increases almost linearly with m and slopes of these lines λ decreases with increasing filtration velocity V. These trends coincide with the simulation qualitatively but not quantitatively. This is probably because reentrainment of particles is not taken into account in the simulation.

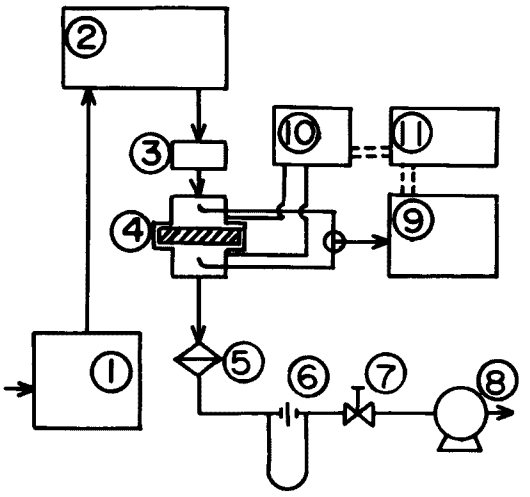

1. Aerosol generator
2. Plenum chamber
3. ^{241}Am
4. Test filter
5. Absolute filter
6. Orifice and manometer
7. Valve
8. Vacuum pump
9. Light scattering photometer
10. Pressure transducer
11. Recorder

Figure 7 Experimental apparatus

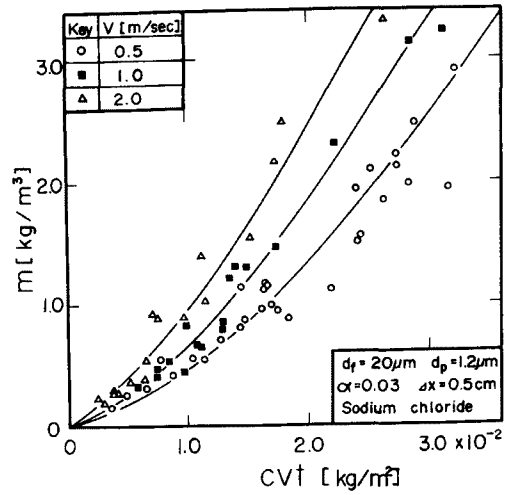

Figure 8 Experimental relation of dust load and total inlet mass of particles

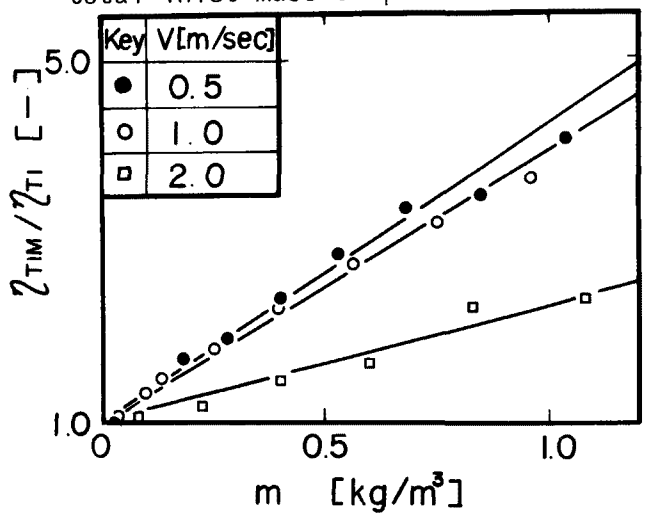

Figure 9 Experimental collection efficiency of a fiber

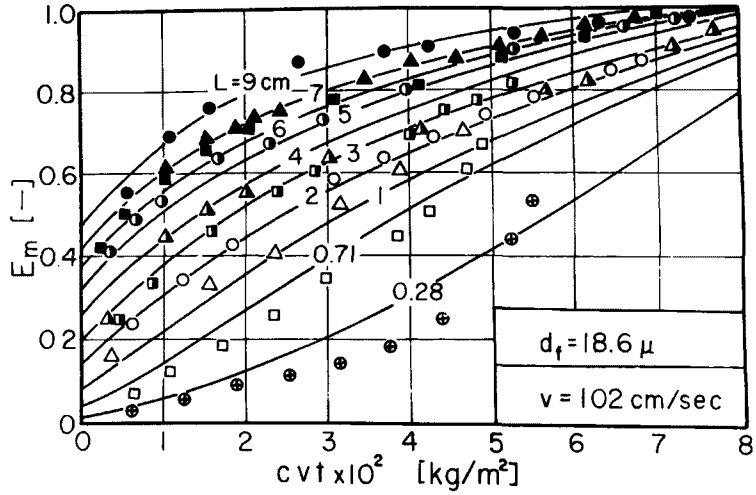

Figure 10 Comparison of experimental collection efficiency of dust loaded filter with predicted ones

Since it has become clear that single fiber collection efficiency is approximated with a linear function of m, time dependency of collection performance of dust loaded filter was estimated by following procedure.

When $\eta_{\alpha m}$ is a linear function of m, filter efficiency E_m is expressed analytically as

$$E_m = 1 - \frac{\exp(-\lambda ACVt)}{\exp(-\lambda ACVt) + \exp(AX) - 1} \qquad (9)$$

The estimated filter efficiency using the equation was compared with the experimental results with stearic acid particles in figure 10. Value of $6\,m^3/kg$ determined from experimental correlation, was used as λ in the calculation. As seen from the figure, predicted curves agree well with the experimental result at arbitrary total imcoming particles and filter depth.

ESTIMATION OF PRESSURE DROP OF A DUST LOADED FILTER

Drag theory, which is said suitable to the analysis of pressure of high porosity bed like a fibrous filter, was used in this study.

Based on the idea of the drag theory, pressure drop across a filter can be expressed by following equation.

$$\Delta P_m = \frac{4\alpha}{\pi D_f^2} \int_0^X F_m \, dx \qquad (10)$$

here, F_m denotes drag force of fiber of unit length and it is defined by,

$$F_m = C_{Dm} D_{fm} \frac{\rho_f V^2}{2} \qquad (11)$$

It is evident from the above equations that C_{Dm} and D_{fm} are the only terms that change with deposition of particles on a fiber. Consequently, they were investigated experimentally using model filters(D_f=30μm, 2h=190μm) and methylene blue particles(D_p=1μm). Figure 11 and 12 show experimental correlations of them with m. They increase smoothly with m and approximated by following equations.

$$D_{fm} = D_f(1 + 0.28m^{1.28}) \qquad (12)$$

$$C_{Dm} = C_D(1 + 0.064m) \qquad (13)$$

here, C_D is the drag coefficient of a clean fiber and following experimentally obtained correlation was used.

$$C_D = 24.8/Re \qquad (14)$$

Substituting equations (11)∿(14) to equation (10), pressure drop across a filter comprised of 44 model filter layers was calculated and was compared with experimental result in Figure 13. Predicted pressure drop agrees very well with the experiment. Although proposed method has been tested for the pressure drop of a model filter, this method could be applied to the estimation of real filter at arbitrary condition knowing changes in D_{fm} and C_{Dm} as a function of dust load m.

CONCLUSION

Collection process of particles and pressure drop of a dust loaded filter has been studied both theoretically and experimentally.

Growing process of particle dendrites on a fiber was simulated by Monte Carlo method. It was related to single fiber collection efficiency. As a result, it was expressed with a linear function of dust load and that of a clean fiber. Plausibility of the simulation was verified experimentally.

Further, estimation method based on drag theory has been proposed and

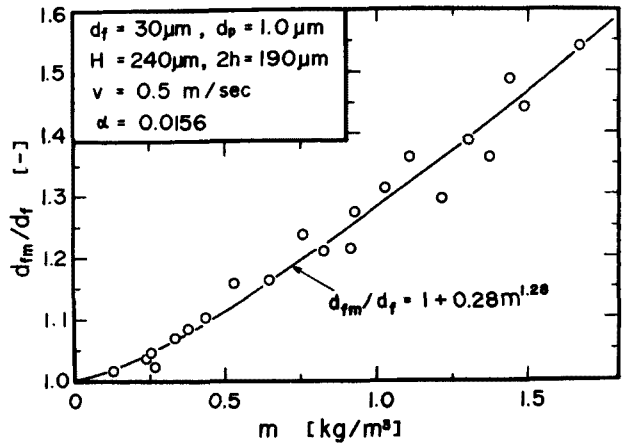

Figure 11 Experimental relationship between D_{fm}/Df and m

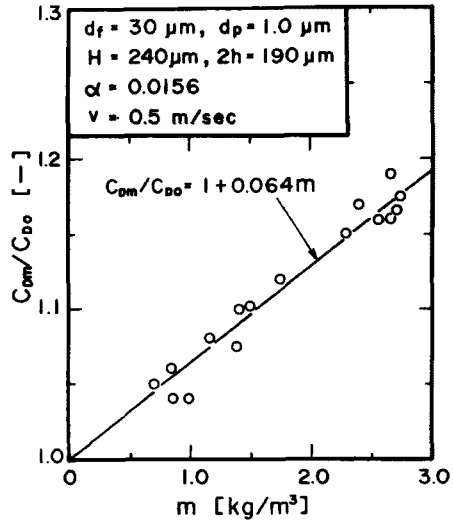

Figuer 12 Experimental relationship between C_{Dm}/C_D and m

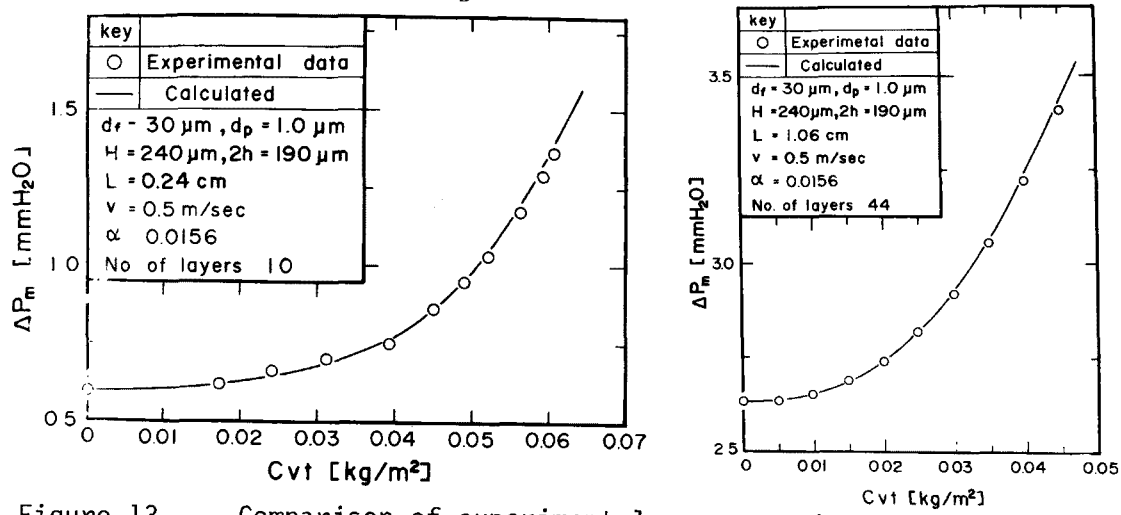

Figure 13 Comparison of experimental pressure drop of dust loaded filter with predicted ones

tested with experimental observations with a model filter. Evolution of filter efficiency and pressure were estimated using proposed methods.

NOMENCLATURE

A	constant used in equation (9)($=4\eta_{\alpha}\alpha/\{\pi D_f(1-\alpha)\}$)	[-]
C	particle concentration	[kg/m^3]
C_D	drag coefficient of a fiber	[dyne/m]
D	diameter	[μm]
F	drag force of a fiber of unit length	[dyne]
h	half distance of the center of two fibers in a model filter	[μm]
M,m	number and mass of collected particles in unit filter volume	[1/m^3][kg/m^3]
N_M	average generated particles during the collection of M-th and (M+1)st particles	[-]
ΔP	pressure drop	[dyne/cm^2]
R	interception parameter($=D_p/D_f$)	[-]
Re	Reynolds number($=D_f u\rho_f/\mu$)	[-]
St	Stokes number($=\rho_p D_p u/9\mu D_f$)	[-]
u,U,V	average and x, y directional fluid velocity	[m/sec]
t,x,y,z	time and Cartesian coordiantes	[sec][μm]
α	packing density of a filter	[-]
η	single fiber collection efficiency	[-]
κ	hydrodynamic factor	[-]
λ	collection efficiency raising factor	[m^3/kg]
ρ	density	[kg/m^3]
ψ	stream function	[-]

Subscripts

f	fiber
I	interception
M,m	M particles and dust loaded
p	particle
T	inertia

REFERENCES

1) Leers,R.: Staub, 50, 402(1957)
2) Billings, C.E.: Ph.D. dissertation, Calif. Inst. Technol. (1966)
3) Bhutra, S. and Payatakes, A.C.: J. Aerosol Sci., 10, 445(1979)
4) Kimura, N.and Iinoya, K.: Chem. Eng. Japan, 28, 729(1964)
5) Yoshioka, Y., Emi, H. and Sone, H.: Chem. Eng. Japan, 33, 1013(1969)
6) Payatakes, A.C. and Tien, C.: J. Aerosol Sci., 7, 85(1976)
7) Payatakes, A.C.: Filtration and Separation, 13, 602(1976)
8) idem: Powder Technol., 14, 267(1976)
9) idem: AIChE J., 23, 192(1977)
10) idem and Gradon, L.: Chem, Eng. Sci., 35, 1083(1980)
11) Wang. C.S., Beizaie, M. and Tien, C.: AIChE J. 23, 879(1977)
12) Kanaoka, C.,Emi, H. and Myojo, T.: Chem. Eng. Ronbunshu, 5, 535(1978)
13) idems: Chem. E. Symposium Series No. 59, 3:4/1(1980)
14) idems: J. Aerosol Sci., 11, 377(1980)
15) Kuwabara, S.: J. Phy. Soc. Japan, 14, 527(1959)

ELECTROSTATICALLY ENHANCED FABRIC FILTRATION OF PARTICULATES

by

Teoman Ariman[1]
and
Stuart T. McComas[2]

INTRODUCTION

Two main concerns are of importance in reducing the dust level in the gas leaving any process; the efficiency of collection and the energy cost in attaining a prescribed level of cleanliness in the exhaust gases. Both of these factors depend on the filtration system employed. The energy consumption of a fabric filter air pollution control system is a function of the pressure drop across the fabric-dust cake combination and the work required to remove collected dust from the fabric. Pulse jet systems, for example, consume about an equal amount of energy in cleaning as in over-coming pressure drop. The total cost may be on the order of 30¢/cfm-year.

Fabric filtration systems have been employed in industry for over a century with relatively few technological modifications [1,2]. Indeed, there have been in recent years only a few advances of note: development of pneumatic cleaning techniques, introduction of fabrics capable of withstanding higher temperatures, and the addition of microporous membrane on the collection side of a felt or fabric backing. For the most part, there was in the past little incentive for improvement--the collection of the systems was satisfactory and the units were inexpensive to purchase. However, with the recent substantial increase in energy costs attention should now be given to operating expenses (e.g., energy consumption) and also the possible recirculation of air for further energy conservation. As a result, the filtration systems of yesteryear may not be the best approach for future applications.

In examining the utility of employing electrostatics to fabric filtration systems, a literature review was conducted. The results of this review, which are presented below can be summarized as follows:

---

[1]Associate Dean and Director of Petroleum and Energy Research Institute, The University of Tulsa, Tulsa, Oklahoma 74104

[2]Professor of Mechanical Engineering Department of Aerospace and Mechanical Engineering, University of Notre Dame, Notre Dame, Indiana 46556

From both the theoretical and experimental standpoints, the application of electrostatics to fabric filtration systems tends to augment the already comparatively high value of collection efficiency (with the obvious exception of a case in which particles and fabric-dust cake are unipolarly charged). However, work is needed to advance the state-of-the-art in formulating and predicting pressure losses across the fabric-dust cake system for specific application. [2-8]

In general, a fabric filter is made up of a woven or felted textile in the shape of a cylindrical bag or flat supported envelope. The textile material is contained in a metal housing having inlet and outlet gas connections, a dust storage hopper, and means for cleaning the fabric periodically.

Woven fabrics consist of parallel rows of yarns in a square array. Open spaces between adjacent yarns are occupied by projecting fibers. Felted fabrics consist of close, randomly intertwined fibers compacted to provide fabric strength. In operation, dusty gas passes through the filter normal to the fabric and dust particles, and, at the start of filtration deposits on individual fibers and yarn surfaces. Particles are captured by such mechanisms as 1) direct interception, 2) inertial impaction, 3) diffusion, 4) electrostatic attraction, 5) gravitational settling, and 6) sieving.

Additional particles then deposit and accumulate on already deposited particles forming filamantous aggregate structures which project into the gas stream. As deposition and accumulation continue, openings between yarns and individual fibers become occupied by aggregates and reduced in size. If this process continues for a sufficient time, a more or less continuous dust cake forms. Particle collection then occurs by mechanisms normally associated with porous granular media. Thus the fabric filtration process may be considered to consist of at least three distinct phases: (a) initial or early deposition, when depositing particles land on individual fibers, fibrils or filaments of the yarns; (b) intermediate deposition when particles accumulate on previously depositied particles, (c) the continued deposition of particles on a matrix similar to a granular layer, leading to the formation of a filter cake.

The membrane covered fabric, trade name Gore-Tex, is purported to behave in a manner different than described above for plain fabric bags. The manufacturer states that this bag resists dust cake buildup because the filtration occurs on the surface of the membrane and that the release characteristics are superior. The result, as they state, is extended operation at a near clean bag condition.

When dealing analytically with the collection of dust from an air stream past a cylindrical fiber, inertia, interception, sedimentation and diffusion of particles are generally taken into consideration. Electrostatic effects are mostly neglected although they often occur and may play an important role. [8] However, for essentially isolated spheres and cylinders comparisons of the collection efficiency for electrical forces with that due to other mechanisms show that for low velocities, the electrical collection may be clearly dominant. Experimental confirmation of this prediction has been obtained [5]. Past results have shown filter efficiency to increase inversely with velocity and directly with fiber charge. An extensive review of the subject of the electrical behavior of aerosols is given by Whitby and Liu [9].

The present study was initiated to evaluate the performance of an electrostatically augmented bag filter system using dust samples from the foundries of the General Motors Corporation. A comparison of charged and uncharged

cases were made using a different air flow rate for each sample using dacron fabric filter bags. The performance of a Gore-Tex bag was also investigated with and without electrostatically charging the particles.

TEST APPARATUS AND PROCEDURES

All tests to evaluate the effect of electrostatic charge on bag filter operation and effectiveness were carried out using an electrostatically augmented single bag test unit supplied by the Apitron Division of American Precision Industries, Inc. This unit basically is a combination of a single unit cylindrical electrostatic precipitator and a single fabric filter bag in series. Several modifications to the apparatus were made by Notre Dame personnel including a continuous dust feeder system and sampling tubes and absolute filters located at the inlet and exit of the unit. Figure 1 is a schematic drawing of the apparatus as modified.

Inlet air to the test apparatus was infused with dust particles by means of a dust feeder shown in the lower left hand corner of the figure. Air at a regulated pressure of 12 to 18 psig was applied to a distribution tube located inside the chamber from which small jets of air impinged on the surface of the dust pile causing a dust storm to form. The number and diameter of the jets along with the supply air pressured governed the rate of dust delivery to the air in the upper portion of the dust feeder (storming chamber). In order to retain a relatively unpacked surface when dealing with sticky dust, a mechanical stirring device was added to this chamber. The pressure in the chamber was maintained at or near atmospheric by means of a cloth covered vent located on the top of the chamber.

The mixture of air and dust was drawn into the ionizing wire tube by means of an air jet vacuum pump and then through the one square foot area of fabric filter mounted on a metal cage. A calibrated orifice mounted just prior to the jet pump was used to determine the volumetric flow rate with an inclined water manometer being used to measure the pressure drop across this flow measuring device. The pressure drop across the fabric bag filter was measured by means of pressure taps located just prior to the lower metal cylinder and in the plexiglas outer shell. A U-tube water manometer was used to measure this pressure difference.

An aspirated sampler tube was placed in the inlet dirty air line. The air and dust sample passed through an absolute filter in order to measure the rate of dust flow. The volumetric air flow rate through the sampler and filter was monitored. A sampling tube and an absolute filter were placed in the exhaust line prior to the flow measurement orifice and jet vacuum pump in order to determine the amount of dust remaining in the air after filtration.

A small diameter tungsten wire located in the lower cylinder was used to create an electric corona and thus to charge the incoming dust particles. This wire was supported at the top of this cylinder by the teflon blow pipe thus insulating that end of the wire from the metal cylinder. The radial distance between the ionizing wire and the metal cylinder is approximately 2.8 centimeters. The lower end of the wire was connected to an electric terminal which passed through a ceramic insulator. This terminal was connected to an adjustable high voltage supply with the metal cylinder being grounded to that unit.

A high pressure air jet pulse was used to clean dust off the lower collector tube. Air was delivered to the blow pipe located at the top of this tube by means of a three way solenoid valve. When cleaning was in progress,

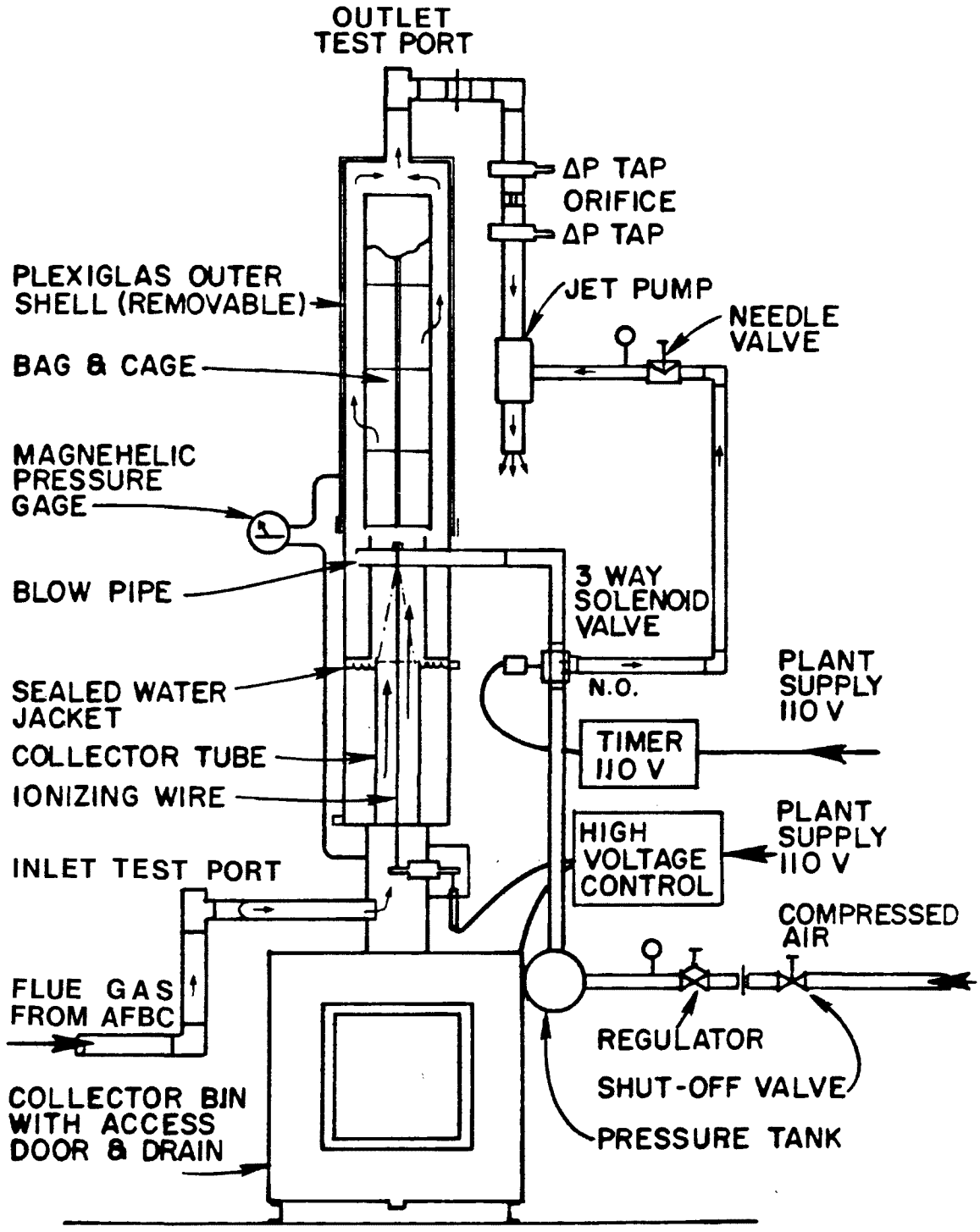

Figure 1. Test Apparatus - Modified Apitron Single Bag Test Unit

the air supply to the jet pump was interrupted and thus the through flow of dirty air to be filtered. At the same time, the solenoid valve located in the 6 psi pressure air line connected to the plexiglas outer shell was opened to ensure a reversal in pressure difference across the bag thus snapping the bag in order to remove collected dust from the bag. The cleaning time was preset by the timer at 0.18 seconds. The frequency of cleaning is controlled by varying the setting of the timer which actuated the two solenoid valves. The dust cleaned from the filter bag and lower cylinder were collected in a bin located at the bottom of the apparatus.

The plexiglas outer shell attaches to the lower portion by means of a bolted flange. In order to replace the fabric filter bag, this outer shell was removed and the old bag was detached from the metal frame which held it in place. A new bag was slid down over the frame and hose clamps were used to seal it to the frame at top and bottom.

At the start of each test run, the dust feeding chamber loaded with the appropriate dust was weighed. After one or two hours had ellapsed, the run was interrupted in order to reweigh the chamber to determine the amount of dust which has been delivered to the test unit. This procedure was repeated throughout the running of a test. A test was started by opening the valve which allowed pressurized air to be delivered to the jet vacuum pump and the air flow rate was set. The opening of the main compressed air line valve also applied pressure regulated air to the storming chamber and the tube connected to the top of the outer shell. The timer was actuated at the same time and if the particles were to be charged, the high voltage source was adjusted to the appropriate level.

During the test run the pressure drop across the bag filter was recorded every one-half hour on the average. In certain cases where this pressure drop was changing relatively rapidly, recordings were made more frequently. When it was determined that the bag fabric had been sufficiently seasoned, namely, that no appreciable increase in pressure drop took place thereafter, the inlet and outlet samplers were actuated and recordings of flow through each were recorded. For each of these two samplers, the absolute filter was weighed prior to its insertion into the holder. Upon completion of the sampling period the absolute filters were again weighted. Because of the relatively high dust loading, the inlet sampler was operated for about 10-15 minutes. The exit sampler was operated for one and one-half hours on the average due to the small rate of dust accumulation on that absolute filter. The amount of dust removed from the dust feeder chamber was also determined during the sampling period.

RESULTS

Tests were run with air containing no dust in order to determine the clean bag pressure drop of the dacron bag and the Gore-Tex bag. The results are indicated in Table 1. The flow rate area through each bag is one square foot.

As indicated from this data, the clean bag pressure drop for Dacron material is negligible for the flow rates used in the present investigation. On the contrary, the results for the Gore-Tex or microporous membrane coated bag are very significant.

Table 1. Clean bag ΔP

Air Flow Rate (CFM)	ΔP (inches water) Dacron	Gore-Tex
5	0.04	3.1
6	0.04	4.0
7	0.05	5.0
8	0.06	6.0
8.5		6.5

A summary of all the test runs are given in Table 2. Many preliminary runs had been made in order to establish the operating characteristics of the unit using a silica dust. An earlier attempt was made to connect the inlet pipe to the collector bin and place the air jets inside that bin to create a supply of dust laden air. This attempt was made in order to try to have a continuous supply of dirty air without the necessity of reloading a supply chamber. Because of the difficulties caused by the air pulse cleaning this method had to be abandoned and the storming chamber as previously described was fabricated.

Test runs number one through five were made with course dust supplied by GM. The source of this material is unknown. The characteristics are that there is some fine dust in this sample but much of it is very large particles. During test run one it was found that the pressure drop across the bag kept on increasing up to values on the order of 18 inches of water. Visual observation indicated insufficient snapping of the bag and thus a continuous build-up of a dust cake occurred. The frequency of bag snapping and the pressure of air delivered at the top of the unit during cleaning were varied in order to establish limits on these parameters in order to obtain proper cleaning of the bag. By this method, periods between cleanings of 30 seconds was established as the time to be used for all tests. Air at a pressure of 6 psig was established as being sufficient to properly snap the filter bag.

Test number two with course dust, an air flow rate of 4 CFM and no charge showed a very small pressure drop across the bag. For this reason no charge in case was run at this flow rate. At a flow rate of 8 CFM, test number three, and no charge the pressure drop was 3.1 inches of water and a collection efficiency of 99.22%. This test was run with the same bag as used at 4 CFM thus some seasoning of the bag had occurred. Test four repeated the conditions but with a new bag. The inlet dust loading was very much lower in this case and so was the pressure drop. The test was again repeated but with charging at 12 KV. The pressure drop was only one-tenth the value for the no charging test number 3 and the collection efficiency increased even though the inlet loading was somewhat higher. Because of the large size of some of the course particles, much of this dust may never have reached the bag. Instead, gravity effects may have prevented the large particles from being carried along with the air. This could contribute to the relatively low pressure drops measured using this particular dust.

Test runs numbered six through 11 were made using dust from the foundry cleaning room. This material contained quite a bit of metal particles and

TABLE 2

SUMMARY OF TEST DATA

MODIFIED APITRON SINGLE BAG UNIT

Test No.	Material	Air Flow Rate (CFM)	Charge (Kilovolts)	ΔP Across Bag (Inches Water)	Inlet Dust Load (gm/cu.ft.)	Collection Eff. (%)	Comments
1	C	8	0	1.8	0.23	-	Test Determined Required Snapping Time and Pressure
2	C	4	0	0.1	0.11	99.40	New D Bag
3	C	8	0	3.1	0.27	99.72	Same Bag as 2
4	C	8	0	0.5	0.05	99.22	New D Bag
5	C	8	12	0.3	0.37	99.96	New D Bag
6	CRD	5	0	5.0	0.68	99.95	New D Bag
7	CRD	8	0	10.4	0.21	99.98	Same Bag as 6
8	CRD	5	12	1.7	0.82	99.99	New D Bag
9	CRD	8	12	2.3	0.57	99.99	Same Bag as 8
10	CRD	8	0	10.5	0.18	-	Same Bag as 8 & 9
11	CRD	8	12	2.8	0.12	99.93	Same Bag as 8 → 10
12	AMD	5	0	2.4	0.02	-	New D Bag
13	AMD	10	0	4.4	0.02	-	Same Bag as 13
14	AMD	5	0	5.0	0.22	99.96	New D Bag
15	AMD	8	0	6.5	0.10	99.99	Same Bag as 15
16	AMD	5	12	0.2	0.17	99.99	New D Bag
17	AMD	8	12	2.5	0.08	99.99	Same Bag as 17
18	AMD	8	12	4.6	0.25	99.54	New D Bag
19	AMD	8	8.5	6.8	0.18	99.75	Same Bag as 24
20	AMD	8	0	10.8	0.22	99.33	Same Bag as 24 & 25
21	AMD	7.8	0	9.8	0.25	99.48	New G Bag
22	AMD	8	11	8.6	0.19	99.54	New G Bag

Notation:

Dust Material
C - Course
CRD - Cleaning Room
AMD - Arc Melt Furnace

Bag Material
D - Dacron
G - Gore-Tex

seemed to readily accept an electric charge. The flow rate was first set at 5 CFM without charge and the test completed. Then the flow rate was increased to 8 CFM using the same bag and a second test run. This procedure was repeated for the charge case at 5 and 8 CFM. At 5 CFM the charge reduced the pressure drop by a factor of 3 and at 8 CFM this value was reduced by a factor of over 4. The reduction in each of these cases occurred even though the inlet dust loading was larger for the charge case. The variation in pressure drop with time for these four tests are shown in Figure 2.

After running at 5 and 8 CFM with charge, the charge was removed and another test run. The pressure drop value increased and leveled off after 12 hours to a value near that of the previous no charge case with just a slightly smaller inlet loading. Reapplying the 12 KV charge at 8 CFM flow rate for the same bag reduced the pressure drop back down to 2.8 inches of water after 10 more hours of running. This is not quite as low as the previous charged case even though the inlet loading was much lower. Figure 3 indicates the pressure drop variation with time for these two tests. A difficulty arose in all charge runs with cleaning room dust in that dust would buildup on the lower ceramic insulator causing an electric short from the wire to the outer case. A deflector had to be placed above the insulator to reduce this buildup making it possible to run the previous cases. The collection efficiency for all test runs using this dust was extremely high and was better or the same when the particles were charged except when the charge was reapplied in test number 11.

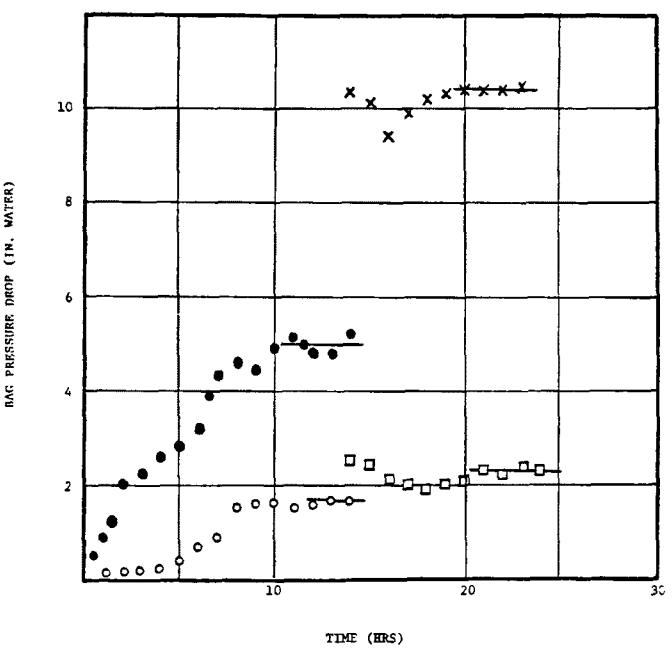

FIGURE 2. DACRON BAG CLEANING ROOM DUST

●	Test 6	5 CFM	No Charge	Inlet Load	0.66 gm/ft^3
X	Test 7	8 CFM	No Charge	Inlet Load	0.21 gm/ft^3
o	Test 8	5 CFM	12KV Charge	Inlet Load	0.62 gm/ft^3
□	Test 9	8 CFM	12KV Charge	Inlet Load	0.57 gm/ft^3

Test runs using arc melt furnace dust are number 12 through 20 using a dacron filter bag. This dust did not seem to accept a charge as readily as the cleaning room dust and it was extremely fine and stickly. A stirring mechanism was required in the dust feeder when this dust was used in order to keep the dust surface loose. Otherwise the air jets would dig a hole and compact the surface of the dust resulting in very little being entrained in the chamber air leading to extremely low inlet dust loading. In general, this dust tended to stick to everything. It would also buildup on the ledges of the frame holding the fabric filter bag and would not release when the bag was snapped. Any bag system using a frame requires a design which will prevent this from occurring otherwise excessive pressure drop will result. Tests 12 and 13 were run prior to addition of the mechanical stirrer. The low inlet loading thus obtained resulted in lower pressure drop then for the higher loadings of runs 15 and 16 also with no charge which were made after the addition of the mechanical stirrer. The addition of a 12 KV charge reduced the pressure drop very significantly for 5 CFM and by about 2 1/2 times at 8 CFM.

The collection efficiency was extremely high for all four runs and no effect of charge was noted. The pressure drop versus time for these four tests, numbers 14 to 17, are shown in Figure 4.

The strength of the electric field was varied in order to determine the resultant effect. A voltage of 12 KV was first applied, then 8.5 KV and next no charge. These are tests 18 through 20. The pressure drop did increase as voltage was decreased. The highest efficiency occurring at 8.5 KV is unexplained.

The last set of tests, number 21 and 22, were run using Gore-Tex bags made from material supplied by W.L. Gore and Associates, Inc. Without charge, the flow rate was first set at 8 CFM but had to be reduced to 7.8 CFM due to the inability of maintaining the higher flow rate was maintained at 8 CFM. The inlet load was about the same as used to test the dacron bags. A slight reduction in pressure drop was obtained for the charged case as compared to the uncharged case but the inlet loading was also slightly lower. The Gore-Tex bag did reach a constant pressure drop situation in a shorter time than did the dacron bag but at values near or above those for dacron bags. The pressure drop versus time for the Gore-Tex bag tests are shown in Figure 5. It should be noted that the clean bag pressure drop for the Gore-Tex bag was higher than for the seasoned dacron bag. The collection efficiency was approximately the same as those for dacron bags.

The effect of charge seems to be very much smaller for the Gore-Tex membrane surface bag as compared to the dacron bag. This is probably due to the dust being filtered at the membrane surface where only small pores exist. Under this surface condition the effect of charge cannot change the dust cake buildup characteristics as is the situation with a fabric filter without this special coating.

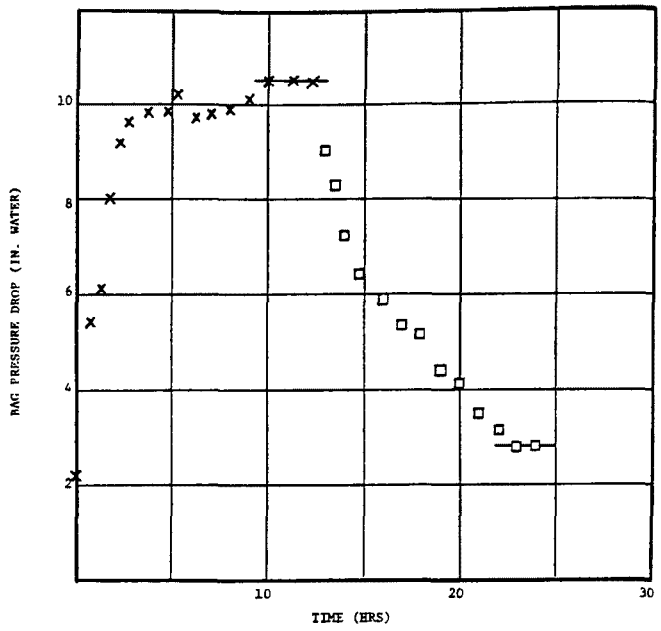

Figure 3. DACRON BAG - CLEANING ROOM DUST
BAG SEASON IN TEST 8 & 9

X	Test 10	8 CFM	No Charge	Inlet Load	0.18 gm/ft^3
□	Test 11	8 CFM	12KV Charge	Inlet Load	0.12 gm/ft^3

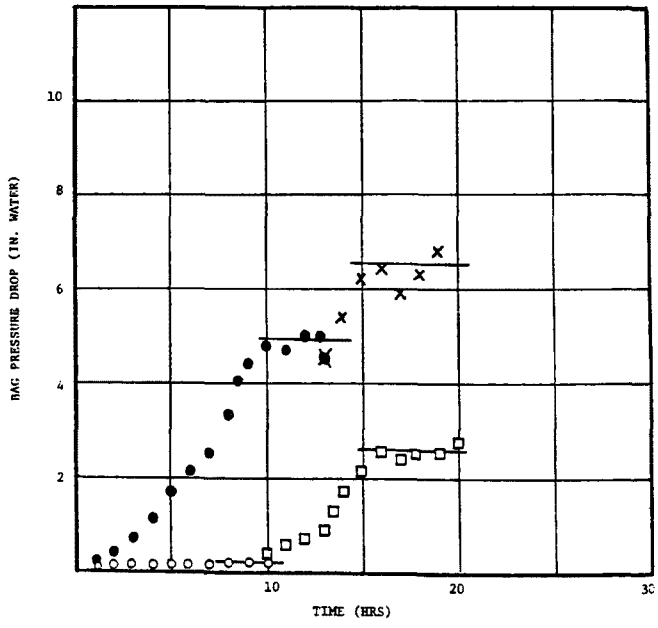

FIGURE 4. DACRON BAG - ARC MELT FURNACE DUST

●	Test 14	5 CFM	No Charge	Inlet Load	0.22 gm/ft^3
X	Test 15	8 CFM	No Charge	Inlet Load	0.10 gm/ft^3
○	Test 16	5 CFM	12KV Charge	Inlet Load	0.17 gm/ft^3
□	Test 17	8 CFM	12KV Charge	Inlet Load	0.08 gm/ft^3

CONCLUSIONS

A test program carried out on the Apitron single bag test unit using three different dust samples supplied from General Motors Corporation foundries indicate that electrostatically charging the particles decreases the pressure drop across the fabric filter bag as compared to the uncharged case. Tests run to study the effect of variation of voltage applied to the ionizing wire indicate that pressure drop across a dacron fabric filter bag decreases with increased voltage. The collection efficiency was high for the fabrics used and for this test unit and the charging of particles, in almost all cases, caused an increase in collection efficiency.

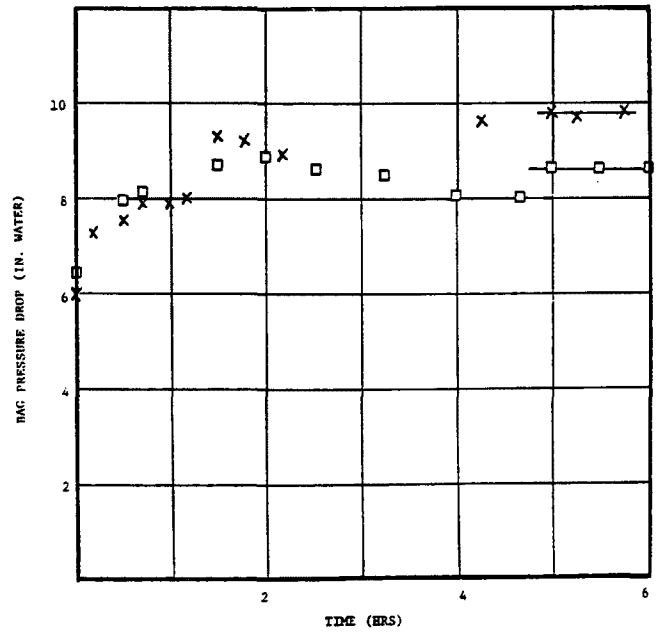

FIGURE 5. GORE-TEX BAG - ARC MELT FURNACE DUST

X Test 21 8 CFM No Charge Inlet Load 0.25 gm/ft^3
□ Test 22 8 CFM 12 KV Charge Inlet Load 0.19 gm/ft^3

The pressure drop decrease when particles were charged prior to filtration through a dacron bag was significant. However, only a slight effect was found for the arc melt furnace dust when using the Gore-Tex material. Also, the clean bag pressure drop for the Gore-Tex bag was quite high when compared to that for dacron bags. There did not seem to be any advantage, and possibly a disadvantage, in using the Gore-Tex material.

A buildup of dust material was found to occur on the insulators holding the ionizing wire. If the dust particles are highly electrical conducting this caused an electrical short across the insulator and a subsequent overload on the high voltage supply. A final design for operational size bag house filter incorporating electrostatic charging of the particles must take into account this problem. Dust deposits on the insulator from the inflowing stream of air and dust and when the air pulse cleaning blows dust down past these insulators. Locating the lower insulator below the incoming air stream would help. Also, both insulators should be protected by means of some type of deflector.

REFERENCES

1. Billings, C.E. and Wilder, J., Handbook of Fabric Filter Technology, Volumes I-IV, GCA-TR-70-17-G, prepared for NAPCA (EPA) (1970.

2. Butterworth, E., Manufacturing Chemist, 65, Feb. (1964).

3. Helfritch, D.J. and Ariman, T., "Electrostatic Filtration and the Apitron Design and Field Performance," Novel Concepts, Methods and Advanced Technology in Particulate/Gas Separation, Teoman Ariman, Editor, University of Notre Dame, 1979.

4. Ariman, T., Rao, K.S., Yang, K.T. and Hosbein, R.L., "Collection of Dust by Fabric Filtration in an Electrostatic Field," Proceedings of the Second Annual Environmental Engineering and Science Conference, p. 555 (1973).

5. Ariman, T. and Helfritch, D.J., "Pressure Drop in Electrostatic Fabric Filtration," Proceedings of the Second Symposium on the Transfer and Utilization of Particulate Control Technology, volume III, Particulate Control Devices EPA-600/9-80-039c, (1980).

6. Ariman, T., "Electrostatic Fabric Filtration in Industrial Dust Control - A Review," UND-DOE-EFF, TR. No. 1, April (1979).

7. McComas, S.T. and Ariman, T., "Collection Efficiency and Pressure Drop in Dust Collection by Fabric Filters in an Electrostatic Field," University of Notre Dame, Final Report for General Motors Corporation, Notre Dame, Indiana, November (1979).

8. Davies, C.N., Air Filtration, Academic Press, New York (1973).

9. Whitby, K.T. and Liu, B.Y.H., Aerosol Science, Academic Press (1966).

A STAGGERED ARRAY MODEL OF A FIBROUS FILTER WITH ELECTRICAL ENHANCEMENT

By: Frank Henry
Department of Mechanical Engineering
Brunel University
Kingston Lane
Uxbridge, Middlesex UB8 3PH United Kingdom

Teoman Ariman
Associate Dean
College of Engineering and Physical Sciences
The University of Tulsa
Tulsa, OK 74104

ABSTRACT

The staggered array of parallel circular cylinders (fibers) is proposed as a model for a fibrous filter. The electrical enhancement of the model is accounted for by the method of images. Stokes' approximation is utilized in the analysis of viscous flow around fibers. The predicted pressure drops and collection efficiencies are compared to experimental data. The model is shown to over predict the pressure drop but give reasonable predictions of collection efficiencies in certain cases.

INTRODUCTION

The theory of fibrous filtration is essentially concerned with the prediction of two important parameters. These are: the filter collection efficiency, and the resistance experienced by the gas stream as it passes through the filter. Theoretically, if the flow field within a fibrous filter could be mathematically described such parameters could be precisely calculated. This is assuming that all other transport mechanisms, such as gravity, inertia, diffusion, and electrical forces, could be described with equal precision. However, the random distribution of the fibers within a filter makes it impossible to analytically describe the flow field within a real filter.

Various simplified models of fibrous filters have been proposed. An account of the history of filter modelling is provided by Davies (1). The most common model consists of an isolated cylinder in an otherwise undisturbed flow. Neglecting the influence of the surrounding fibers can only be justified, however, for especially designed excessively porous filters. An unsolved theoretical problem with this model is the lack of a closed form solution to the viscous flow around an isolated cylinder. While the isolated cylinder model has been quite useful in illustrating the importance of the various transport mechanisms present in a filter, it has not been possible to relate the results to real filters without the use of empirical constants.

Kuwabara (2) developed a cell model of Stoke's flow over an array of parallel circular cylinders. This model has been used by several researchers (3,4,5) as a fibrous filter model. It has the advantage over the isolated

cylinder model of addressing the problem of the influence of the surrounding fibers. However, the Kuwabara model has been shown to have significant shortcomings (6). Another model of flow over parallel cylinders proposed by Happel (7) has similar deficiencies. Yeh (5) constructed a numerical model of flow over a staggered array of cylinders to investigate Kuwabara's model. He provided results for a particular array configuration and for a packing density of 0.1. Hence, it appears that the use of a staggered array of parallel cylinders as a model for a fibrous filter has not been fully investigated. This paper attempts to address this problem by solving for the flow over various configurations of parallel cylinders arrays. The effect of an external electrical field is also considered in the analysis. The predicted pressure drop and collection efficiency of the model are compared with experimental data.

THE NUMERICAL MODEL

The finite difference technique was used to solve Stokes' flow over an array of parallel cylinders shown in Figure (1). Polar coordinates were used in the two regions close to the cylinders and Cartesian coordinates were utilized in the connecting outer region.

The biharmonic Stokes' equation was split into two Poisson equations, i.e.

$$\nabla^2\psi = -\omega \tag{1}$$

and

$$\nabla^2\omega = 0 \tag{2}$$

where ψ = stream function, and ω = vorticity. The finite difference analogues of equations (1) and (2) were solved using the Gauss-Seidel iterative technique. For any interior node, (i,j), and Cartesian coordinates, this can be given as

$$\psi_{i,j}^{k+1} = \frac{1}{A_{i,j}} \left[\omega_{i,j} + B_{i,j}\psi_{i+1.j}^{k} + C_{i,j}\psi_{i-1,j}^{k+1} + D_{i,j}\psi_{i,j+1}^{k} + E_{i,j}\psi_{i,j-1}^{k+1}\right] \tag{3}$$

where the superscript k denotes the iteration step and

$$A_{i,j} = 2\left[\frac{1}{\Delta x_i \Delta x_{i-1}} + \frac{1}{\Delta y_j \Delta y_{j-1}}\right] \tag{4}$$

$$B_{i,j} = 2/[\Delta x_i(\Delta x_i + \Delta x_{i-1})] \tag{5}$$

$$C_{i,j} = 2/[\Delta x_{i-1}(\Delta x_i + \Delta x_{i-1})] \tag{6}$$

$$D_{i,j} = 2/[\Delta y_j(\Delta y_j + \Delta y_{j-1})] \tag{7}$$

and

$$E_{i,j} = 2/[\Delta y_{j-1}(\Delta y_j + \Delta y_{j-1})] \tag{8}$$

Similar expressions can be given for equation (2) and for equations (1) and (2) in polar coordinates.

The symmetry of the array requires the top and bottom boundaries of the solution domain to be both streamlines and lines of zero vorticity. The values of the vorticity and streamfunction on the vertical boundaries were calculated by employing the periodicity of the solution. The streamfunction was also known on the cylinders' surface as they are streamlines. However, on these surfaces the vorticity had to be calculated using an approximate formula, i.e.

$$\omega_{s,n} = 2(\psi_{s+1,n} - \psi_{s,n})/\Delta r_s^2 \tag{9}$$

where, n is the nodal index in the angular direction and s denotes the cylinder surface.

It was found that the numerical solution was insensitive to any reasonable initial condition. However, the pressure drop, through the vorticity, was found to be sensitive to the nodal density. A more detailed description of the numerical model can be found in Henry and Ariman (6).

ELECTRICAL ENHANCEMENT

The collection efficiency of a fibrous filter can be substantially increased by applying a high voltage (usually of the order of 10 kv/cm) across the filter. The electric field is usually aligned with the flow direction. See, for example, the experimental work of Bergman et al (8). Using the method of images, Henry and Ariman (9) investigated the influence of the neighboring fibers on the electric field of an enhanced filter. As the strength of successive images quickly decreases it is only necessary to consider first-order-images.

For the configuration of thirteen cylinders shown in Figure (2) the complex potential, W, can be approximated by,

$$W(Z) = \phi_e + i\psi_e = - E_o Z + \alpha r_f^2 E_o \sum_{i=1}^{13} \left(\frac{1}{Z-Z_i} - r_f^2 \sum_{j=1}^{12} \frac{1}{d_j(Z-Z'_{ij})} \right) \tag{10}$$

where

ϕ_e = electric potential

ψ_e = electric streamfunction

E_o = electric field intensity

α = $(\varepsilon_f - 1)/(\varepsilon_f + 1)$

ε_f = dielectric constant of fiber

Z_i = position of the ith cylinder

r_f = cylinder radius

d_j = $|Z_i|^2$

Z'_{ij} = position of first-order image of cylinder 'j' in cylinder 'i'.

A charged dielectric particle entering an electric field such as that given by equation (10) will experience two distinct forces. The first, known as electrophoresis, is due to the interaction between the particle charge and the electric field. The second, known as dielectrophoresis, is due to the interaction between the particles' polarizability and the divergence of the field. Note that electrophoresis will be present even if the dielectric constant of the fiber is unity i.e., the lines of electric force are parallel, whereas, in this case, dielectrophoresis will not occur. Also, as dielectrophoresis is proportional to the cube of the particle radius it is less important for smaller particles. Because of the above and the fact that a streamfunction for the dielectrophoresis force does not exist, it was decided to include only electrophoresis as a first approximation to an enhanced fibrous filter.

The streamfunction for the electrophoresis force ψ_c can be shown to be,

$$\psi_c = q\ \gamma\ \mathrm{Im}[W] \tag{11}$$

where q = particle charge, γ = mechanical mobility of particle

and $\mathrm{Im}[W]$ = imaginary part of equation (10).

Hence, the streamfunction for the trajectory of an inertialess particle ψ_t neglecting gravity, diffusion, fluid inertia, hydraulic interaction, dielectrophoresis and the image effect of the particle charge and the cylinder, can be given by superposition as,

$$\psi_t = \psi_c + \psi \tag{12}$$

where ψ and ψ_c are given by equations (1) and (11), respectively.

RESULTS

Pressure Drop

For Stokes' flow, the pressure p is given by,

$$\nabla p = - \mu \nabla \times \omega \tag{13}$$

where μ is the fluid viscosity.

The pressure drop over the solution domain, Δp_c, shown in Figure (1) was calculated from the predicted vorticity field using Simpson's rule (6). The total pressure drop, Δp_t, over an array of finite thickness, h, could then be estimated by

$$\Delta p_t = M \Delta p_c \tag{14}$$

where, M = number of cells = $h/2b \cos\phi$

Davies (1) defined a dimensionless pressure drop coefficient, f(c), for fibrous filters which is only a function of the packing density. This can be written as,

$$f(c) = \frac{\Delta p_t r_f^2}{\mu U_o h} \tag{15}$$

through the use of dimensional analysis and experimental data for pressure drops over real filters, Davies found f(c) to be given by

$$f(c) = 16c^{1.5}(1 + 56c^3) \tag{16}$$

Curves of f(c) predicted by the numerical model and equation (16) are shown in Figure (4). Experimental results derived from the works of Yeh (5) and Whitby (10) are also included. The pressure drop over the array of cylinders predicted by the numerical model is considerably higher than the experimental measurements. Davies' equation (16) can be seen to be mid-way between the experimental results and the numerical prediction. It appears that a change in the relative orientation of the cylinders, i.e. a change in ϕ, has a negligible effect on the predicted pressure drop.

A possible explanation for the difference between the numerical and experimental values of pressure drop is that real filters do not have equi-spaced fibers. The work of Yano and Kieda (11) shows that the drag created by two parallel cylinders decrease as the distance between the cylinders' centers decreases. Hence, if the fibers in a real filter are grouped in bundles the pressure drop can be expected to be lower than if the fibers were equi-spaced. As the packing density is only a measure of the volume of the fibers relative to the volume of the filter it unfortunately, does not give any indication of how the fibers are distributed.

Collection of Inertialess Particles

If it can be assumed that the particles follow the streamlines described by equation (12), the amount of particles that are intercepted by a cylinder (fiber) can be estimated. For a specific particle size there will be a critical trajectory or streamline that just grazes the cylinder. Below this line all particles will deposit on the cylinder, but particles travelling on higher streamlines will miss the cylinder. This is schematically illustrated in Figure (5). Assuming the particles are homogeneously distributed within the array, the amount of particles entering the solution domain or cell shown in Figure (5) will be proportional to the cell height, $2b\sin\phi$. The amount of particles captured by the cylinder will be proportional to the height of the critical trajectory as it enters the cell, y^*_c. Hence, the cell penetration, P_c, can be estimated by,

$$P_c = \frac{2b\sin\phi - y^*_c}{2b\sin\phi} = 1 - \frac{y^*_c}{2b\sin\phi} \tag{17}$$

The total filter efficiency, E, can be given as,

$$E = 1 - P \simeq 1 - P_c^M \tag{18}$$

where, P is the total penetration, and M is the number of cells in the filler thickness, h, i.e.

$$M = h/2b\cos\phi \tag{19}$$

Equation (18) can be rearranged to give,

$$E = 1 - e^{h\Phi} \tag{20}$$

where, the penetration function, Φ is given by

$$\Phi = \frac{\log(P_c)}{2b\cos\phi} \tag{21}$$

Figure (6) shows the dependence of Φ on the electric-flow velocity ratio, G, where $G = q\gamma E_o/E_o$. From these curves and equation (20), an estimate of the collection efficiency of an enhanced fibrous filter can be made.

Figure (7) shows the influence of the angular orientation on the collection efficiency of the model. Two experimental points due to Whitby (10) for a commercially available paper filter [c = .096] were also plotted. Whitby's filters were not electrically enhanced but it is possible that, due to natural charges, electrostatic attraction between particles and fibers was present. Also, it appears that, in some cases, the particle sizes and velocities used in his experiments were such that inertial effects were significant. Hence, it would be expected that the model prediction would be lower than

those given by Whitby. This would suggest that the 60 degree model overpredicts the collection efficiency of a real filter. Figure (7) also shows the substantial increase in collection efficiency that can be expected if a filter is electrically enhanced.

Figure (8) compares the predicted efficiency using the 45 degree model and the experimental results of Yeh (5). Yeh's measurements are of particular interest because the filter used was specially manufactured using dacron fibers of uniform diameter. However, the fiber distribution was random. The experimental results show the influence of diffusion, which is not included in the model. The smaller particles are more subject to random Brownian motion and can be expected to deviate from the predicted streamline pattern. Yeh's particles were made electrically neutral and hence, there were no electrical effects present. In contrast the work of Bergman et al (8) shown in Figure (9) is for naturally charged particles collected by a fibrous filter polarized with an electric field of 10 kv/cm. In the numerical model the average particle charge, $\bar{q}$, was estimated by employing a formula given by Nelson et al (12) i.e.

$$\bar{q} = 6(d_p/C_s^{1/3})^{1/2} \tag{22}$$

where, d_p is the particle diameter and C_s is the concentration (1%) of the sodium chloride solution from which the particles were created. It can be seen that the model underpredicts the efficiency for the larger particles. This is probably due to the neglect of dielectrophoresis in the model.

CONCLUSIONS

The staggered array model has been shown to overpredict the pressure drop of real fibrous filters. It is thought that the discrepancy is largely due to the nonuniform distribution of fibers within a real filter. Particle deposition on individual fibers has been shown to be a function of the angular orientation of the surrounding fibers. While the 30 and 45 degree arrays predict comparable collection efficiencies the 60 degree array gives much higher values. The experimental data of Whitby (10) appears to suggest that the 60 degree array model overpredicts the collection efficiency of real filters.

It must be remembered that the staggered array model is a two-dimensional approximation of a complex three-dimensional flow field and that only a limited number of transport mechanism were considered. Hence, it can not be expected that the model will give results that agree precisely with experimental measurements on real filters. The model should be viewed as the next step on from the isolated cylinder models. This model can describe the dependence of the collection efficiency on fiber orientation which is an important feature and can not be achieved by the cell models of neither Kuwabara (2) nor Happel (7).

ACKNOWLEDGEMENTS

This paper is a partial outcome of the research program supported by the National Science Foundation under Grant No. ENG-77-0938. The second author acknowledges the continuous interest and advice of Dr. M. S. Ojalvo, Director of the Particulate and Multiphase Processes Program of the NSF.

ENDNOTES

1. Davies, C.N. Air Filtration. Academic Press, 1973.

2. Kuwabara, S. J. Phys. Soc. Japan. 14:527, 1959.

3. Henry, F., and T. Ariman. A Cell Model of Aerosol Filtration by Fibrous Filters in an Electrostatic Field. Technical Report, UND-AFEF TR No. 3, University of Notre Dame, 1979.

4. Pich, J. Aerosol Science. Davies, C.N. (ed.). Academic Press, 244, 1966.

5. Yeh, H.C. Fundamental Study of Aerosol Filtration by Fibrous Filters. Ph.D. Dissertation, University of Minnesota, 1972.

6. Henry, F., and T. Ariman. A Numerical Study of the Kuwabara Model. Technical Report, UND-AFEF TR No. 5, University of Notre Dame, 1980.

7. Happel, J. Am. Inst. Chem. Eng. J. 5:174-177, 1959.

8. Bergman, W., H. Hebard, R. Taylor, and R. Lum. Electrostatic Filters Generated by Electric Fields. UCKL-81926, 1979, presented at the Second World Filtration Congress, London, England, September, 1979.

9. Henry, F., and T. Ariman. The Effect of Neighboring Fibers on the Electric Field in a Fibrous Filter. Technical Report, UND-AFEF TR No. 4, University of Notre Dame, 1980.

10. Whitby, K.T. Am. Soc. Heating, Refrig. Air Cond. Engrs. J. Sept. 56-65, 1965.

11. Yano, H., and A. Kieda. J. Fluid Mech. 97:157-179, 1980.

12. Nelson, G.O., W. Bergman, H. Miller, C.P. Richards, and A.H. Bierman. Enhanced Filtration. UCID-16949-76-3, 1977.

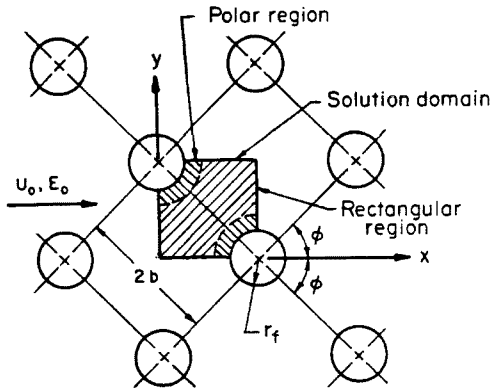

Figure 1 Cylindrical Fiber Array and Solution Domain

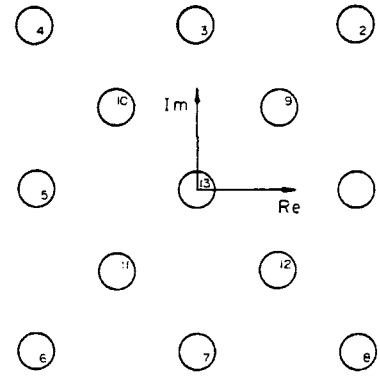

Figure 2 Thirteen Fibers Array for Electrical Field

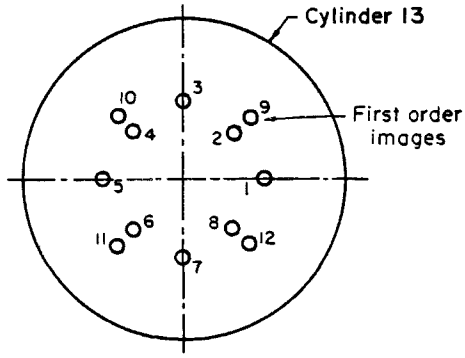

Figure 3 First-Order Images

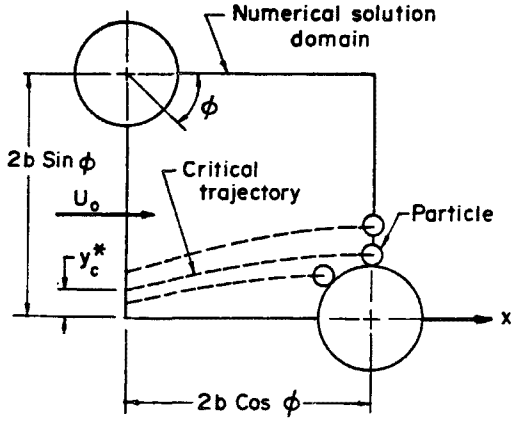

Figure 5 Numerical Solution Domain and Critical Trajectory

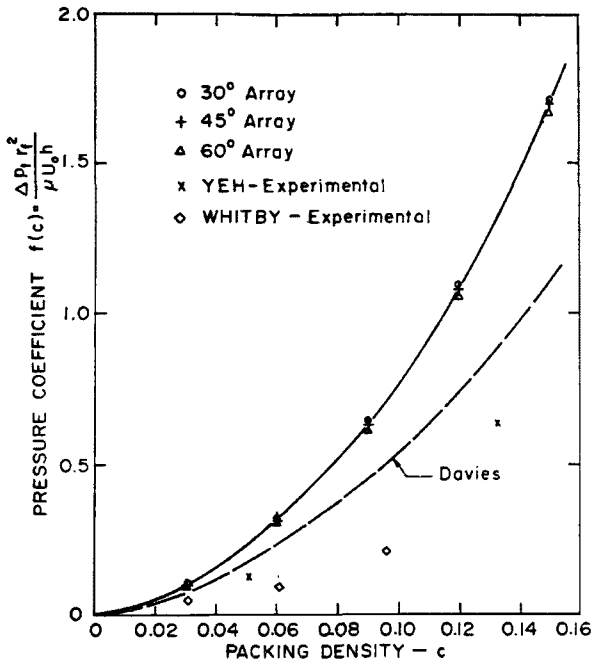

Figure 4 Dependence of Pressure Coefficient on Fibrous Filter Packing Density and Comparison With Related Experimental Work

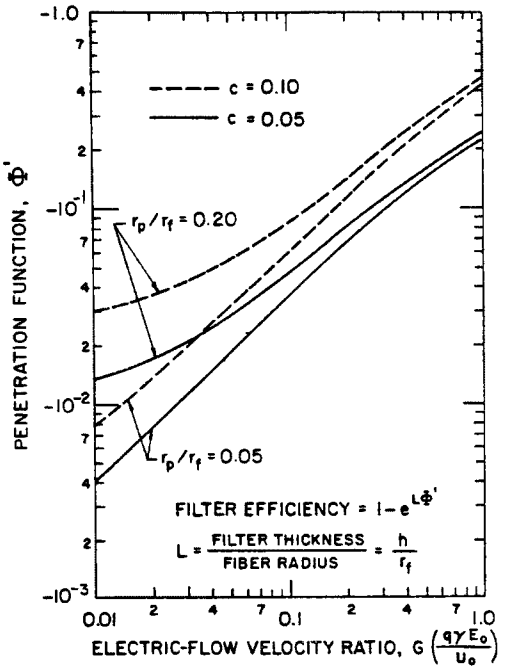

Figure 6 Dependence of Penetration Function on Electric-Flow Velocity Ratio

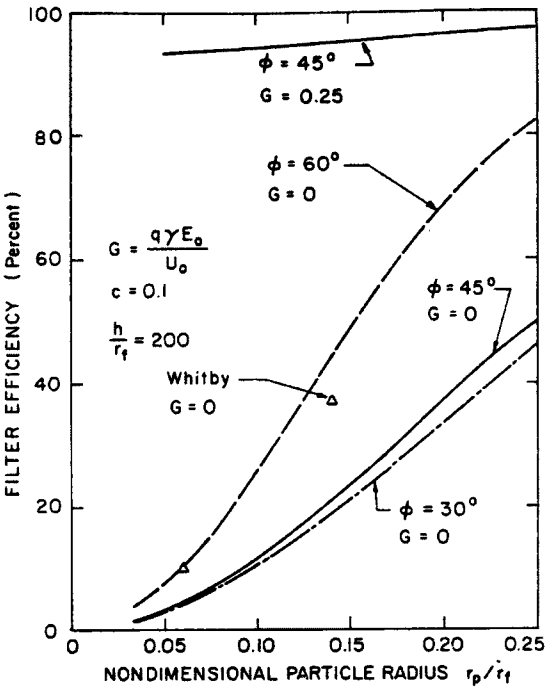

Figure 7 The Effect of Angular Orientation of Fibers on Collection Efficiency

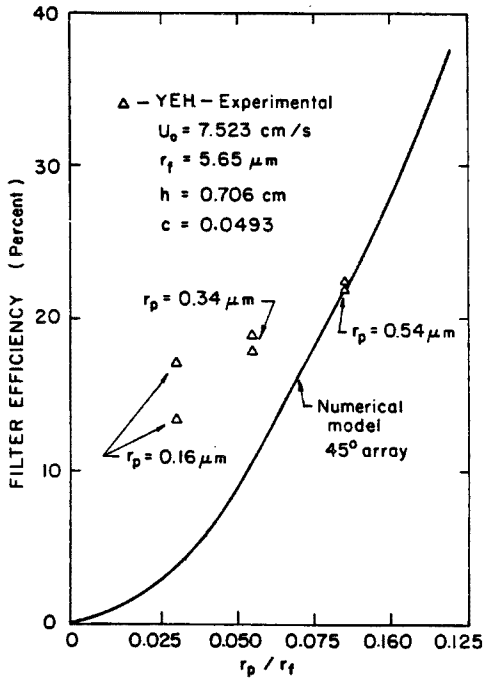

Figure 8 Comparison of the Predicted Filter Efficiencies with the Experimental Results of Yeh (5)

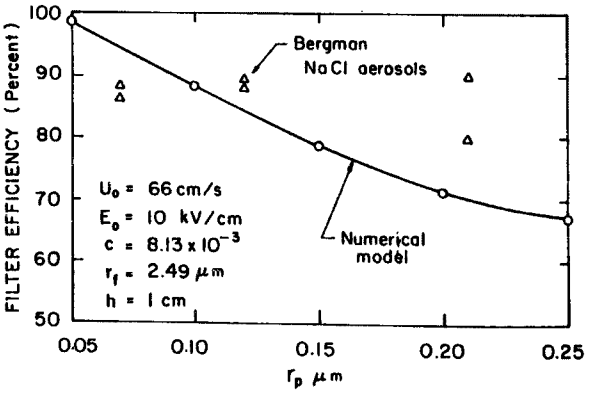

Figure 9 Comparison of the Predicted Filter Efficiency with the Experimental Results by Bergman et al (8)

AEROSOL FILTRATION BY A COCURRENT MOVING GRANULAR BED: PENETRATION THEORY

By

Thomas W. Kalinowski and David Leith

Department of Environmental Health Sciences
Harvard School of Public Health
Boston, MA 02115

ABSTRACT

A penetration model for aerosol filtration by a cocurrent moving bed of granules has been developed. The model incorporates straight-through penetration and reentrainment of previously collected dust due to granule motion, both mechanisms having been found significant in experiments. The model, an extension of classical clean granular bed theory, utilizes the familiar concept of a single granular coefficient for collection and proposes a similar coefficient for reentrainment.

Reentrainment was found in experiments to be a function of particle size and other factors such as gas velocity, granule velocity and the extent of intergranular dust deposit. The single granule reentrainment coefficient for moving granules, η_R, was found to depend upon the product of intergranular dust deposit and the square root of particle diameter ($K\sqrt{d_p}$) for particle diameters between 0.16 and 5.5 μm.

INTRODUCTION

Granular bed filters are of interest for collection of particles from hot gas streams. A recent review of granular bed filtration theory and experiments is provided by Yung et al. (1). A common feature of practical granular bed filters is bed motion for granule cleaning and recharge. Most previous experiments and theory concerned stationary clean beds. These studies are useful to explain results from clean-bed experiments but have not been extended to more practical, loaded-bed cases.

Recent theoretical studies to model loaded granular beds consider enhanced particle collection by previously captured particles as well as reentrainment of collected particles (2, 3). Hydrodynamic factors affecting particle collection by already-deposited particles or by dendrites near the surface of a granule are complex. Factors affecting reentrainment are also poorly understood. However, reentrainment in moving granular bed filtration experiments significantly affects overall bed efficiency (4, 5). A penetration model for a moving granular bed filter must account for reentrainment related to granular motion.

PENETRATION MODEL

A previous study of Cocurrent Moving Granular Bed Filter (CMGBF) performance showed that some dust penetrates straight through, and some captured

dust is reentrained due to granule motion (5). Penetrating dust from these two sources had different size distributions. This paper considers these two separate penetration mechanisms and discusses a model that is an extension of the classical clean granular bed filtration model, to which it reduces when reentrainment is negligible.

Mass Balance on the Aerosol

In the CMGBF, clean granules and dusty gas are added continuously at the bed top, then pass downward cocurrently and exit at the bed bottom. A unique feature of the CMGBF is the controlled formation of an intergranular dust deposit to enhance filtration of submicron particles. A mass balance on the aerosol in the differential volume AdZ is:

$$\text{Rate In} = \text{Rate Out} + \text{Accumulation}$$

$$Q_g C = Q_g (C + dC) + E - R \tag{1}$$

Solution of equation 1 requires expressions for the collection rate, E, and reentrainment rate, R.

Particle Collection Rate

Consider particle collection analogous to classical clean bed theory except that the single granule collection coefficient, η_G, accounts for the effect of dust adhering to the granule as well as for the granule itself.

The collection rate, E, can be expressed as the product of the cross-sectional area swept clean by these collectors and the particle flux through the differential volume:

$$E = [Adz(1 - \varepsilon_o)\ (\frac{\pi d_G^{\,2}/4}{\pi d_G^{\,3}/6})\eta_G][C\frac{V_g}{\varepsilon}] \tag{2}$$

The porosity, ε, in the flux expression is the effective porosity accounting for reduced voidage due to the intergranular dust deposit. The effective porosity can be estimated by

$$\varepsilon = \varepsilon_o - K\ (\rho_{bG}/\rho_{bp}) \tag{3}$$

Particle Reentrainment Rate

Consider a particle reentrainment rate, R, based on removal of dust already collected and adhering to the granule surface. The mass of collected dust in the differential volume is:

$$(1 - \varepsilon_o)A\ dZ\ \rho_G\ K \tag{4}$$

Next define a gas parcel as the gas volume equivalent to the volume of a single granule. The number of gas parcels per second passing each granule is:

$$\frac{(\pi d_G^2/4)}{(\pi d_G^3/6)} \frac{V_g}{\varepsilon} \tag{5}$$

A dimensionless single granule reentrainment coefficient, η_R, will now be defined as the fraction of all dust adhering to a single granule that is reentrained from that granule by a single gas parcel passing it. The reentrainment rate in the differential volume is the product of equations 4, 5, and the single granule reentrainment coefficient:

$$R = \frac{3}{2} \frac{(1 - \varepsilon_o)}{\varepsilon} \frac{V_g}{d_G} \rho_G K \eta_R A \, dZ \tag{6}$$

Substituting equations 2 and 6 into equation 1 gives an expression for the mass balance on the aerosol:

$$dC = - \frac{3}{2} \frac{(1 - \varepsilon_o)}{\varepsilon} \frac{(\eta_G C - \eta_R \rho_G K)}{d_G} \, dZ \tag{7}$$

Before equation 7 can be integrated across the depth, Z, of the bed, an expression for K in terms of dust concentration, C, is required.

Equilibrium Mass Balance

The CMGBF is designed for continuous operation, and at equilibrium all dust which enters the bed must leave in the aerosol stream or on the granules. Assuming dust entering on the granules is negligible, an equilibrium mass balance on total dust in the aerosol and on the granules yields:

$$Q_g C_i = Q_g C + Q_G \rho_G K \tag{8}$$

Solving equation 8 for K produces:

$$K = (Q_g [C_i - C])/(Q_G \rho_G) \tag{9}$$

Substituting equation 9 into equation 7 produces:

$$dC = - \frac{3}{2} \frac{(1 - \varepsilon_o)}{\varepsilon \, d_G} [C(\eta_G + \eta_R \frac{Q_g}{Q_G}) - \eta_R C_i \frac{Q_g}{Q_G}] dZ \tag{10}$$

If porosity, ε, is independent of bed depth, equation 10 can be integrated readily. This approximation is valid when the equilibrium dust deposit is established near the bed surface so that it does not vary appreciably through the bed depth. Pressure drop data indicate that a stable deposit is formed within two or three centimeters of the bed surface (6).

Integration of equation 10 yields:

$$Pt = \frac{C_o}{C_i} = \frac{\eta_R \frac{Q_g}{Q_G} + \eta_G \exp\left[-\frac{3}{2}\frac{(1-\varepsilon_o)}{\varepsilon}\frac{Z}{d_G}\left(\eta_G + \eta_R \frac{Q_g}{Q_G}\right)\right]}{\eta_G + \eta_R \frac{Q_g}{Q_G}} \qquad (11)$$

This is the theoretical expression for particle collection and reentrainment in a cocurrent moving granular bed filter. Equation 11 is for steady state operation with a continuous dust feed at constant concentration.

If no reentrainment occurs ($\eta_R \to 0$) equation 11 reduces to the classical granular bed penetration expression (7):

$$Pt_{\eta_R \to o} = \exp\left[-\frac{3}{2}\frac{(1-\varepsilon_o)}{\varepsilon}\frac{Z}{d_G}\eta_G\right] \qquad (12)$$

To demonstrate the effect of reentrainment on bed performance, consider the situation when the bed is very deep, $z \to \infty$; in this case:

$$Pt_{z\to\infty} = \left(\frac{\eta_R}{\eta_G}\frac{Q_g}{Q_G}\right) \Big/ \left(1 + \frac{\eta_R}{\eta_G}\frac{Q_g}{Q_G}\right) \qquad (13)$$

Even if particles are collected efficiently, $\eta_G \to 1$, significant penetration may occur if reentrainment is important, $\eta_R > 0$.

Discussion of Theory

Although many theories are available to describe clean granule efficiency, no adequate theories are presently available to predict the single dirty granule efficiency, η_G, or to predict the single granule reentrainment coefficient, η_R. As a first approximation, a lower bound for efficiency of the conditioned granule, η_G, might be calculated from theory for clean, unconditioned granules. Reentrainment should depend upon the ratio of separation forces to adhesion forces for particle-to-granule and particle-to-particle interactions. Adhesion forces include van der Waals, electrostatic, and surface tension capillary forces. Separation forces should be related to air drag and mechanical shear due to granule slippage. A review of the literature suggests that these forces, for other than the most simple configurations, are poorly understood and cannot be predicted accurately (6).

EXPERIMENTS

Experiments were performed to quantify the coefficients η_G and η_R in equation 11 and to investigate the functional relationship of factors affecting reentrainment. The CMGBF experimental apparatus consisted of a 203-mm diameter column, granule control mechanism, circumferential gas exit screen and simultaneous upstream and downstream isokinetic samplers, as described elsewhere (5). Samples for particle size analysis were collected on 0.2 μm pore diameter Nuclepore filters. Photomicrographs were obtained by scanning electron microscope (SEM), and particles were sized and counted with a Zeiss-MOP image analyzer.

High density (ρ_G = 3250 Kg/m^3) alumina granules with a diameter of average mass of 2.1 mm were used for all runs. The test aerosol was electrostatically precipitated fly ash from a utility boiler fired with pulverized coal and had a count median diameter of 0.3 μm.

Twenty runs with the CMGBF were conducted at ambient temperature and pressure in a "central composite design" experiment for three control variables: V_g, superficial gas velocity; V_G, granule velocity; and K, the ratio of collected dust mass to granule mass within the conditioned bed at steady state (8). Nominal factor levels are shown in Table 1. All experiments described here were conducted at constant bed depth and granule size; effects of these factors were reported elsewhere (5).

TABLE 1. EXPERIMENTAL CONDITIONS

Block I				Block II				Block III			
Run No.	K*	V_G+	V_g§	Run No.	K*	V_G+	V_g§	Run No.	K*	V_G+	V_g§
18	1.3	0.026	261	13	1.3	0.026	139	4	0.5	0.037	200
17	3.7	0.026	139	12	3.7	0.026	261	6	4.5	0.037	200
16	1.3	0.049	139	9	1.3	0.049	261	3	2.5	0.019	200
20	3.7	0.049	261	11	3.7	0.049	139	7	2.5	0.056	200
15	2.5	0.037	200	14	2.5	0.037	200	2	2.5	0.037	100
19	2.5	0.037	200	10	2.5	0.037	200	1	2.5	0.037	300
								5	2.5	0.037	200
								8	2.5	0.037	200

* K = intergranular dust deposit ratio (% by weight)
\+ V_G = granule velocity (mm/sec)
§ V_g = superficial gas velocity (mm/sec)
(Bed depth = 130 mm and granule diameter = 2.1 mm for all runs)

Mass penetration and pressure drop data for all runs shown in Table 1 are reported elsewhere (6).

Penetration data by count in particle size categories between 0.08 μm and 7.3 μm were obtained for the eight runs in Block III of Table 1 and the third run of Block II. Fractional penetration data were obtained for these nine runs for the conditions of (1) an initial clean moving bed when dust

feed began, (2) a normal cocurrent steady state bed at the end of at least two bed volume replacements and (3) straight through penetration of the stationary loaded bed. Particle size distributions were also obtained for the particles reentrained from the moving bed when dust feed had stopped.

RESULTS

Fractional Penetration

Average fractional penetration data for Runs 1 through 9 are shown in Figure 1 for the moving and stationary loaded bed cases. Penetration in the submicron range was approximately the same whether the loaded bed was moving or not; however, penetration in the larger particle sizes was clearly greater when the loaded bed was moving. The relatively greater variability in the penetration data for the normal moving bed is due to the influence of control variables, other than particle size, not separated in this crude average but discussed below. Straight through penetration was influenced much less by these factors as indicated by reduced variability in the lower curve in Figure 1.

Particle size data from the photomicrographs clearly showed that the reentrained particles were larger than the particles penetrating straight through the stationary loaded bed. Very small particles (approximately less than 0.3 μm) were not found on the photomicrographs of reentrained particles, suggesting that small particles were not reentrained. Although agglomerates were present in the reentrained particles as observed on SEM photomicrographs, the proportion of agglomerates in any size category was not significantly different from the proportion of agglomerates in the same size category either upstream of the CMGBF or in the particles penetrating straight through. The fly ash was well-combusted and consisted of glassy spheres which normally do not agglomerate appreciably. Thus, it appears that most particles penetrated or were reentrained without significant additional agglomeration.

Single Granule Reentrainment Coefficient

Reentrainment due to granular motion is exemplified by the difference between penetration when the bed is operating normally and straight through penetration immediately after the bed is stopped. The increased penetration due to reentrainment in larger particle sizes can be seen in Figure 1.

Equation 11 with $\eta_R = 0$ was used to calculate the single dirty granule collection coefficient, η_G, from the straight through penetration data in different particle size categories. The empirical collection coefficient, η_G, calculated in this fashion may contain the effects of simple air scouring, bounce and reentrainment of particles unrelated to granular motion. On an overall mass penetration basis, simple air scouring of particles from the loaded, stationary bed was generally found to be negligible at the deposition velocity (5).

With values of η_G, ε and bed geometry, the single granule reentrainment coefficient, η_R, was obtained from equation 11 using penetration data for the

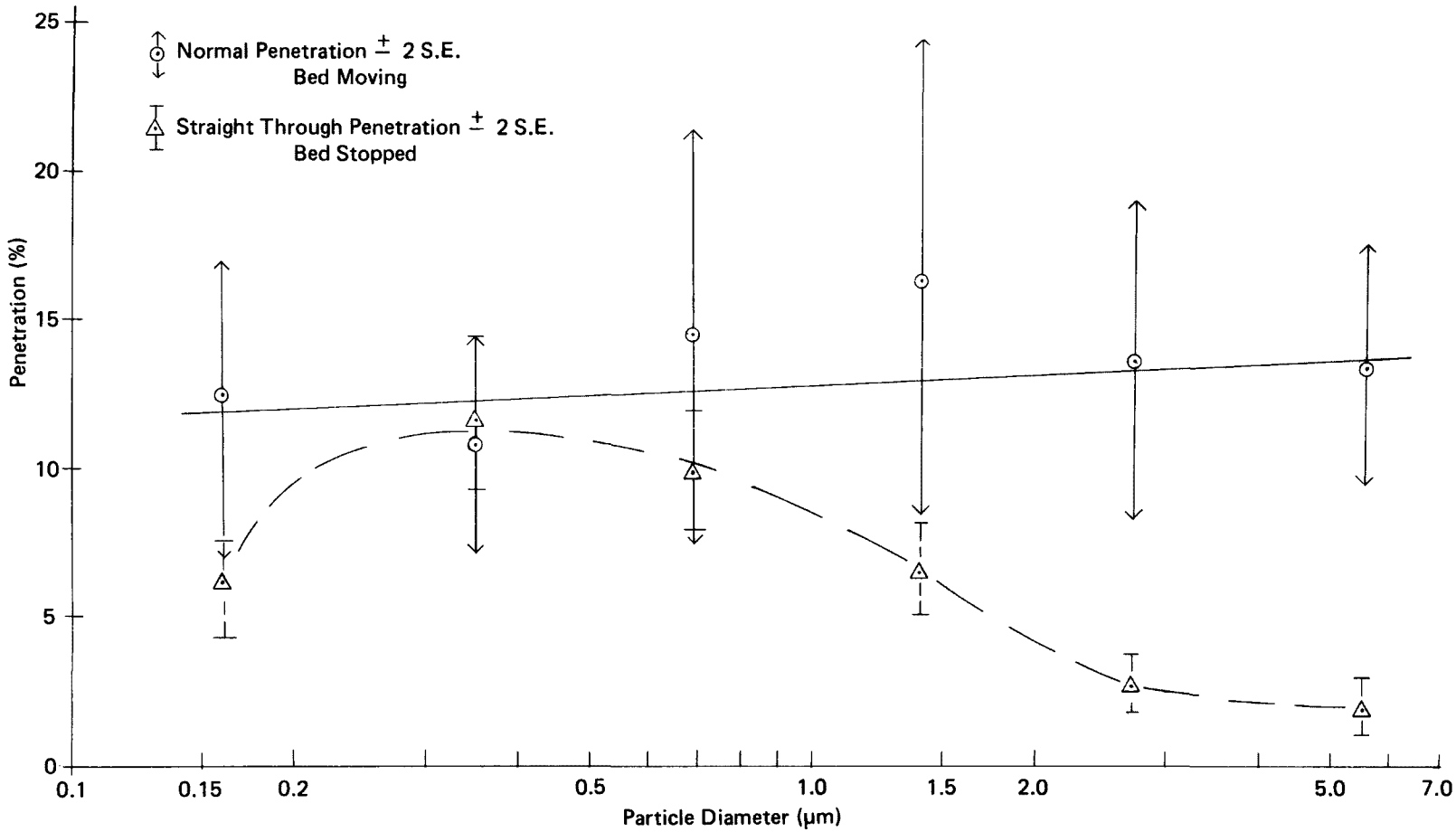

Figure 1. Average Penetration versus Particle Size for Run Nos. 1 through 9.

bed under normal operating conditions. Calculated values of η_R for the nine runs with alumina granules are presented in Table 2. A negative value of η_R results when the penetration straight through the stationary loaded bed exceeds the penetration in the moving bed case and occurs where measurement error for the two penetration measurements overlap.

TABLE 2. CALCULATED SINGLE GRANULE REENTRAINMENT COEFFICIENT, η_R*

	Particle Diameter, μm					
Run No.	0.16	0.35	0.69	1.4	2.7	5.5
1	1.31	-13.4	-2.50	3.64	1.46	11.4
2	9.61	-7.99	-21.3	2.63	30.7	(58.3)+
3	14.9	-8.01	9.73	28.7	24.7	(91.6)+
4	5.61	2.47	2.18	-8.46	18.8	19.5
6	47.3	3.97	80.9	88.3	82.9	37.9
7	49.1	22.0	18.6	82.1	49.0	45.8
9	0.0	-3.42	9.71	13.6	33.3	64.0
5	2.15	-6.57	-4.56	3.66	19.9	52.7
8	22.3	15.5	8.73	40.9	58.0	20.7
Average	16.9	0.51	11.3	28.3	35.4	36.0

Conditions: ε_o = 0.4; ε from eq. (3); ρ_{bG} = 1.95 g/cm^3; ρ_{bp} = 0.90 g/cm^3; Z = 130 mm; d_{8G} = 2.1 mm (alumina)

* listed values are $\eta_R \times 10^8$.

+ Pt straight through = 0 ∴ η_R estimated and not included in regression.

The anomalously high values of η_R in the smallest particle size category in Table 2 suggest that particles 0.16 μm in diameter were reentrained, but this appears to be an artifact of the calculation procedure which assumes the difference between normal penetration and straight through penetration is due solely to reentrainment. Photomicrographs of particles reentrained from moving loaded beds, after dust feed had ceased, show a complete absence of very small particles approximately less than 0.3 μm.

The effects on η_R of particle size, d_p (μm); intergranular dust deposit, K (% by weight); gas velocity, V_g (mm/sec); and granule velocity, V_G (mm/sec), were investigated by multiple regression. The resulting equation for prediction of η_R for moving alumina granules over the range of variables in Table 1 is:

$$\eta_R = (-23.2 + 6.56\ K\ \sqrt{d_p} - 1.22\ [(\frac{V_g}{100})^2 - 4]^2 + 849\ V_G) \times 10^{-8} \quad (15)$$

The multiple correlation coefficient, R^2, for equation 15 is 49% and all coefficients except the intercept are highly significant ($P < 0.01$). Standardized residuals were approximately normally distributed.

The most significant term in equation 15 with respect to percent of variance explained is the product $K\sqrt{d_p}$, indicating a positive interaction between K and $\sqrt{d_p}$. The second term in equation 15 indicates a parabolic function for superficial gas velocity with reentrainment first increasing with gas velocity but then decreasing at the highest gas velocity, which may be explained by greater removal of reentrained particles by subsequent impaction on other collectors. Finally, granule velocity is seen to have a positive effect on reentrainment in the form of an incremental increase in η_R in the various particle sizes.

As defined here, reentrainment depends on granule motion. For a CMGBF with circumferential screen gas outlet, factors affecting intergranule shear at the wall should also strongly affect reentrainment; for example, increases in bed depth, granular bulk density, column diameter and fluid pressure drop should all increase reentrainment. However, variations in these factors were not examined in the present study. A previous study demonstrated increased reentrainment with increased bed depth (5). Equation 15 considers the effect of variables perhaps more closely related to resuspension of dust freed from granules by wall shear, rather than freeing of the dust from the granules in the first place.

These results show that reentrainment of collected dust strongly affects penetration in a CMGBF with a circumferential screen gas outlet as tested here. Alternate gas outlet designs, such as that used by Rudnick and First (9) or a sheath of clean granules at the gas exit, which minimize intergranular shear and granule-wall shear at the gas outlet should minimize reentrainment and reduce overall penetration appreciably.

ACKNOWLEDGEMENT

This work was supported by the National Science Foundation, grant ENG77-26975. Alumina granules were supplied by Electrorefractories and Abrasives Division of Ferro Corp., East Liverpool, Ohio.

NOMENCLATURE

A = cross-sectional bed area perpendicular to gas and granule flow, cm^2
C = particle concentration in gas stream, g/cm^3
C_i = particle concentration in gas stream inlet, g/cm^3
C_o = particle concentration in gas stream outlet, g/cm^3
D = bed diameter, cm
K = mass ratio of dust in bed, g dust/g granules
Pt = (C_o/C_i), penetration fraction
Q_g = gas volumetric flowrate, cm^3/s
Q_G = granule volumetric flowrate, cm^3/s

V_g = superficial gas velocity, cm/s
V_G = granule velocity, cm/s
Z = bed depth, cm
dZ = differential bed depth, cm
d_G = granule diameter, cm
d_p = particle diameter, cm
ε_o = clean bed porosity, fraction
ε = loaded bed intergranular porosity, fraction
ρ_G = granule density, g/cm^3
ρ_{bG} = loose bulk density of granules, g/cm^3
ρ_{bp} = loose bulk density of dust, g/cm^3
η_G = single dirty granule collection coefficient, dimensionless
η_R = single dirty granule reentrainment coefficient, dimensionless

ENDNOTES

1. Yung, S. L., R. Patterson, R. Parker and S. Calvert. Evaluation of Granular Bed Filters for High Temperature High Pressure Particulate Control (prepared by Air Pollution Technology, Inc., San Diego, Ca.) U.S. Environmental Protection Agency Report No. 600/7-79-020, January 1979.

2. Payatakes, A. C. Advances in Dendritic Deposition of Aerosols by Inertial Impaction and/or Interception. Proceedings of the 2nd World Filtration Congress, London, September 18-20, 1979.

3. Goren, S. L. Appendix B: A Mathematical Model for the Moving Granular Bed Filter. In: Granular Bed Filter Development Program, Theoretical Analysis of Granular Bed Filtration Principles and Performance Prediction (prepared by Combustion Power Corporation, Menlo Park, Ca.). U.S. Department of Energy, Report No. FE-2579-18, January 1978.

4. Wade, G., H. Wigton, J. Guillory, G. Goldback and K. Phillips. Granular Bed Filter Development Program Final Report (prepared by Combustion Power Corporation, Menlo Park, Ca.). U.S. Department of Energy Report No. FE-2579-19, April 1978.

5. Kalinowski, T. W. and D. Leith. Aerosol Filtration by a Cocurrent Moving Granular Bed: Penetration Mechanisms. Proceedings of 73rd Annual Meeting of the Air Pollution Control Association, Montreal, June 22-27, 1980.

6. Kalinowski, T. W. Aerosol Filtration by a Cocurrent Moving Granular Bed. Sc.D. Thesis, Harvard University, 1981.

7. Tardos, G. I., N. Abuaf and C. Gutfinger. Dust Deposition in Granular Bed Filters: Theories and Experiments. J. Air Poll. Control Assoc. 28:354-363, April 1978.

8. Cochran, W. G. and G. M. Cox. Experimental Designs. Wiley, New York, 1957.

9. Rudnick, S. and M. W. First. High-Efficiency Filtration in Cocurrent Moving Granular Bed. Proceedings of the 73rd Annual Meeting of the Air Pollution Control Association, Montreal, June 22-27, 1980.

FUNDAMENTAL EXPERIMENTS ON A GRANULAR BED FILTER

By: K. Iinoya and Y. Mori
Department of Chemical Engineering
Kyoto University, Kyoto, 606 Japan

ABSTRACT

The filtration performance of granular packed beds has been studied experimentally. The filter media are silica sand and glass beads of various sizes, ranging from 1 to 5 mm. The test dust is calcium carbonate, and the filtration velocity is 20, 30 and 40 cm/s.

The additional pressure loss due to the collected dust load does not depend on the filtration velocity, because of pin-hole formation at higher velocities. The collection efficiency is improved at higher velocities and for heavier dust loads collected in the beds. The dust distributions in the filter media are also measured by use of a chemical analysis.

INTRODUCTION

A granular bed filter is a particulate control device to remove dusts from hot gas streams. Most previous studies have been concerned with clean packed beds [1-4]. The fundamental performance of packed beds must be studied for dust loaded conditions, while moving granular bed filters of various configurations are investigated for particle collection.

This paper presents the results of fundamental experiments on a granular packed bed filter, the granules of which are retained by a stainless steel screen. It describes the effects of filtration velocity and the diameter of granules on the filtration performance as well as the dust distributions collected in the bed.

EXPERIMENTAL APPARATUS

A schematic diagram of the experimental apparatus is shown in Figure 1. The test dust, calcium carbonate, is uniformly fed into a mixer type disperser by use of a table feeder (Micro Feeder, Sankyo Dengyo Co., Tokyo), and is suspended in the air flow.

The packed bed consists of a 150 mm square acrylic column, and is horizontally retained between stainless steel screens having 0.8 mm openings. The total thickness of the packed bed is 128 mm. The bed is divided into five sections perpendicular to the gas stream. The length of the divided bed section just above the inlet screen is 0.3-0.35 cm, and the lengths of the other four sections are about 25 mm, respectively.

The air with suspended dust flows upwards in the packed bed, and the dust penetrated through the packed bed is collected on a high efficiency glass fiber filter (GB 100R, Toyo Roshi Co., Tokyo). The gas flow rate is measured by an orifice meter, and the pressure loss across the packed bed is

continuously recorded on a chart.

EXPERIMENTAL PROCEDURES

Experimental studies on the packed bed have been conducted in order to investigate the effects of filtration velocity and granule size on the pressure loss across the packed bed and on the collection efficiency. The properties of the granules used in the test are given in Table 1. The used granules are washed with water and dried before the next test. The intergranular void of clean beds is 0.366 through all test runs. The effect of the thickness of the packed bed is investigated by measuring the dust weight collected in each divided bed section after filtration, instead of by changing of bed thickness.

The particle size distribution of the test dust is measured by a cascade impactor (226 type, Sierra Co.) just in front of the packed bed. It is expressed approximately as a log-normal distribution with the mass median diameter of 3.5 μm and the geometric standard deviation of 3.5.

The dust weight penetrated through the packed bed is determined from the weight of the dust collected on a high efficiency back-up filter. The method for measuring the dust weight collected in each sections of the packed bed is different for glass beads from that for slica sand. When the filter media are silica sand, after a test run the packed bed is divided into two sections, one of which is about 0.35 cm thick section with the inlet screen. The weight of the collected dust is determined by subtracting W_o from W_f, where W_f is granules plus dust weight in each section after a run, and W_o is the granule weight in each section after cleaning.

When the filter media are glass beads, after a test run the packed bed is divided into five sections. Calcium carbonate collected in each section is dissolved into hydrochloric acid. The weight of the dissolved dust is determined from the concentration of the calcium ion in the solution by a titration method using EDTA (ethylene diamine tetraacetic acid).

RESULTS AND DISCUSSION

Pressure Loss

Figure 2 shows the effect of the thickness of the packed bed on pressure loss through the clean packed bed of glass beads of 1.1 mm diameter. Pressure loss is proportional to the thickness of the packed bed.

Figures 3 and 4 are the relationships of pressure loss per unit bed thickness and unit filtration velocity against filtration velocity, when the bed is clean. The broken lines in Figures 3 and 4 are calculated by use of the following Ergun equation [5],

$$\frac{\Delta P_o}{L} = \frac{150}{36}\mu S_c^2 \frac{(1-\varepsilon_o)^2}{\varepsilon_o^3} u + \frac{1.75}{6}\rho S_c \frac{(1-\varepsilon_o)}{\varepsilon_o^3} u^2 \qquad (1)$$

where the granules are assumed to be spherical, the diameters of which are uniform and equal to the mean diameter of the granules. The solid lines in Figures 3 and 4 are calculated by using the equation obtained by Macdonald et. al. [6], which has the modified experimental constants of 180 instead of 150 as its in the right hand first term of Equation 1, and of 1.8 instead of 1.75 in the second term. Our experimental results appear to agree with the equation obtained by Macdonald et. al..

The additional pressure loss is defined as the value of subtracting the pressure loss of the clean bed from the one of the dust loaded bed. Figures 5 and 6 show relationships between the additional pressure loss and the dust load. The dust load is defined as the dust weight collected in the packed bed divided by the filter area. The additional pressure loss is proportional to the 1.7th power of the dust load, and is not affected by the filtration velocity. The latter phenomena shows that the drag of the dust layer deposited into the bed decreases as the filtration velocity increases. The following experiment has been tried in order to confirm the above phenomena. Figure 7 shows the relationship between the additional pressure loss and the filtration velocity at a dust load in the packed bed. Point 1 in Figure 7 expresses the additional pressure loss for 0.84 kg/m^2 dust load at 20 cm/s filtration velocity. Then the filtration velocity is increased without dust feed. Points 2, 3 and 4 in the same figure are the additional pressure losses at the velocities of 30, 40 and 45cm/s, respectively. When the velocity decreases from 45 to 20 cm/s, the pressure losses decrease from the former values at the same velocities. That is, points 5, 6 and 7 are the pressure losses at 40, 30 and 20 cm/s, respectively. Finally, when the filtration velocity increases from 20 to 45 cm/s, the pressure losses have the same values as before from points 7 to 4. Therefore, the constant pressure losses at points 1 to 4 indicate the formation of pin-holes in the dust layer.

Collection Efficiency

Figures 8 and 9 show the relationships between the cumulative penetration through the packed bed and the dust loads. The filter media in Figure 8 are glass beads, and that in Figure 9 is silica sand. The cumulative collection efficiency becomes higher as the filtration velocity increases, and the instantaneous penetration becomes promptly lower as the dust load increases.

The cumulative penetrations for various granule sizes becomes lower with smaller glanules, and the higher dust load in the bed improves the collection efficiency remarkably, as shown in Figure 10. Figure 11 shows the relationship between the cumulative penetrations and the granule size at a dust load of 0.2 kg/m^2. The penetration with silica sand seems to be slightly lower than that with glass beads. This improvement may be due to the irregular shape of granules.

Figure 12 shows the dust distribution collected in the filter media, that is the effect of the thickness of the packed bed on the penetration. Most of dusts are collected within the several layers of granules from the inlet screen of the packed bed. The penetration decreases almost exponentially after the thin inlet layers as the bed thickness increases. Figure 13

shows relationships between the cumulative penetration and the dust load for various bed thicknesses, which are calculated by use of the dust distributions collected in the filter media. The penetrations of the 0.3 cm thick bed, i.e. about one layer of the granules, has a minimum value because of reentrainment. On the other hand, the collection efficiency becomes higher as the dust load increases when the bed thickness is more than 2.8 cm.

Figure 14 shows the effect of the granule size on the penetration for two kinds of the thickness. Reentrainment becomes dominant at higher dust load for the thin bed of 2.9 or 5.2 mm glass beads. However, penetration becomes lower even at higher dust load for the 0.3 cm thick bed of 1.1 mm diameter granules. All penetrations becomes lower at higher dust load for the 5.3 cm thick bed, independent of the granule size.

Figure 15 shows the effect of the filtration velocity on the collection performance for two thicknesses. The penetrations do not depend on the filtration velocity for the 0.3 cm thick bed. Considering no effect of the filtration velocity on the additional pressure loss as mentioned before, it may be concluded that the pin-hole formation in the dust layer does not increase the penetration at higher velocity for the thin packed bed. On the other hand, the filtration velocity has an effect on the penetrations for the 5.3 cm thick bed. Figure 16 shows the relationship between the cumulative penetration and the dust load in the 0.35 cm thick bed with silica sand. The penetrations also do not depend on the filtration velocity.

CONCLUSIONS

The filtration performance of granular packed beds has been studied experimentally, and the following results are obtained:

1) The equation by Macdonald et.al. or the Ergun equation can be used to predict the pressure loss through the packed beds with clean granules.
2) The additional pressure loss due to the collected dust load does not depend on the filtration velocity. The reason may be pin-hole formation in the dust layer deposited in the bed at higher filtration velocities.
3) The collection efficiency is improved at higher filtration velocities, for heavier dust loads collected in the beds and with smaller size of granules.
4) When the thickness of the packed bed becomes comparative to the granule size, the cumulative penetration has the minimum value and does not depend on the filtration velocity for both filter media.
5) The cumulative penetration decreases almost exponentially as the bed thickness increases over a few cm. This means that the log-penetration law is valid.

NOMENCLATURE

D_c	= diameter of granule of packed bed	[cm]
D_p	= diameter of dust particle	[cm]
E	= collection efficiency	[-]
L	= thickness of packed bed	[cm]
m	= dust load collected in packed bed	[g/m^2]
Δp	= pressure loss through dust loaded packed bed	[Pa]

Δp_o	= pressure loss through clean packed bed	[Pa]
S_c	= surface area per unit volume of granules, $=6/D_c$, if granules are uniform size spheres	[cm^2/cm^3]
u	= filtration velocity	[cm/s]
ε_o	= intergranular void of clean bed	[-]
μ	= coefficient of air viscosity	[g/cm·s]
ρ	= air density	[g/cm^3]
ρ_p	= dust particle density	[g/cm^3]

ENDNOTES

1. Miyamoto, S. and H.L.Bohn. Filtration of Airborne Particulates by Gravel Filters. J. Air Poll. Control Assoc. 24:1051-1054, November 1974.
2. Schmidt, E.W., J.A.Gieseke, P.Gelfand, T.W.Lugar, and D.A. Furlong. Filtration Theory for Granular Beds. J. Air Poll. Control Assoc. 28: 143-146, February 1978.
3. Gutfinger, C. and G.I.Tardos. Theoretical and Experimental Investigation on Granular Bed Dust Filter. Atmos. Env. 13:853-867, June 1978.
4. Lee, K.W. and J.A. Gieseke. Collection of Aerosol Particles by Packed Beds. Env. Sci. Tech. 13:466-470, April 1979.
5. Ergun, S. Fluid Flow through Packed Columns. Chem. Eng. Prog. 48: 89-94, February 1952.
6. Macdonald, I.F., M.S.El-Sayed, K.Mow, and F.A.L.Dullien. Flow through Porous Media - the Ergun Equation Revised, Ind. Eng. Chem. Fundam. 18:199-208, March 1979.

Table 1. GRANULE CHARACTERISTICS

	Glass Beads			Silica Sand
Mean Diameter D_{p50} [mm]	1.1	2.9	5.2	2.2
Size Range D_p [mm]	1.0-1.2	2.3-3.4	5.0-5.6	2.0-2.4
Density ρ_p [g/cm^3]	2.45	2.49	2.50	2.52

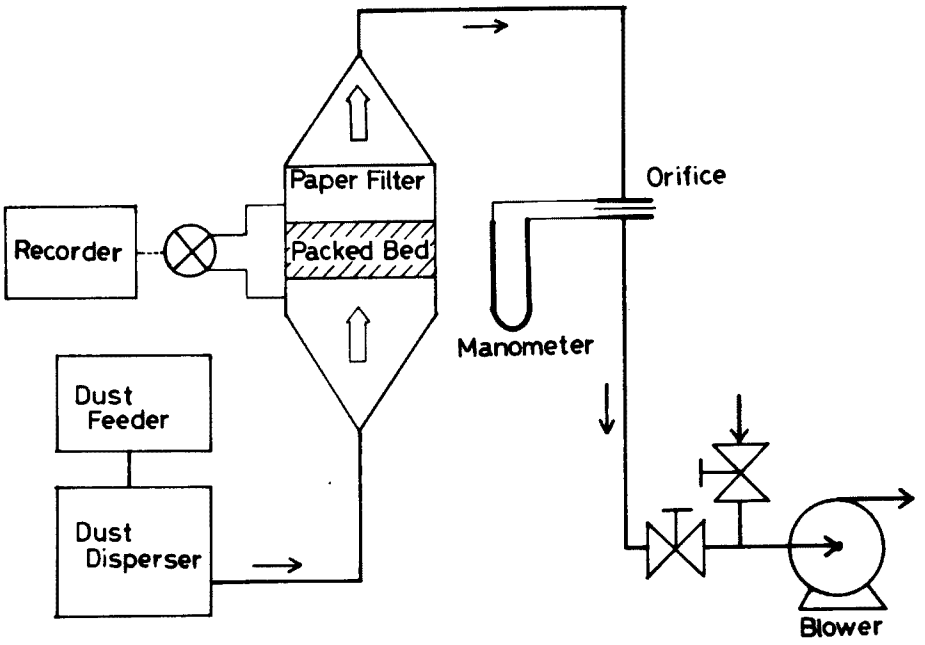

Figure 1. Experimental apparatus of packed granular bed filter.

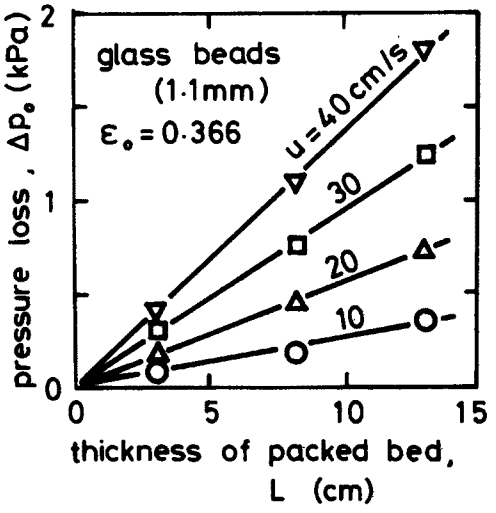

Figure 2. Effect of thickness of packed bed on pressure loss through packed bed of glass beads.

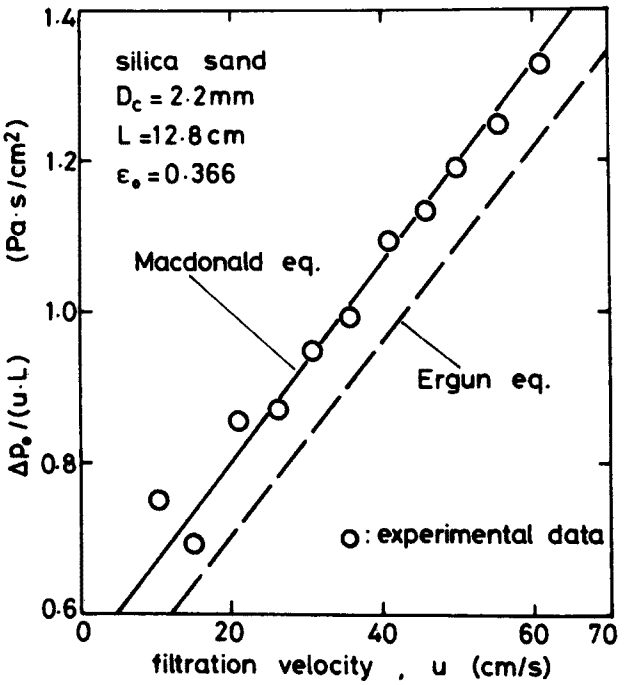

Figure 3. Relationships between pressure loss and filtration velocity (silica sand).

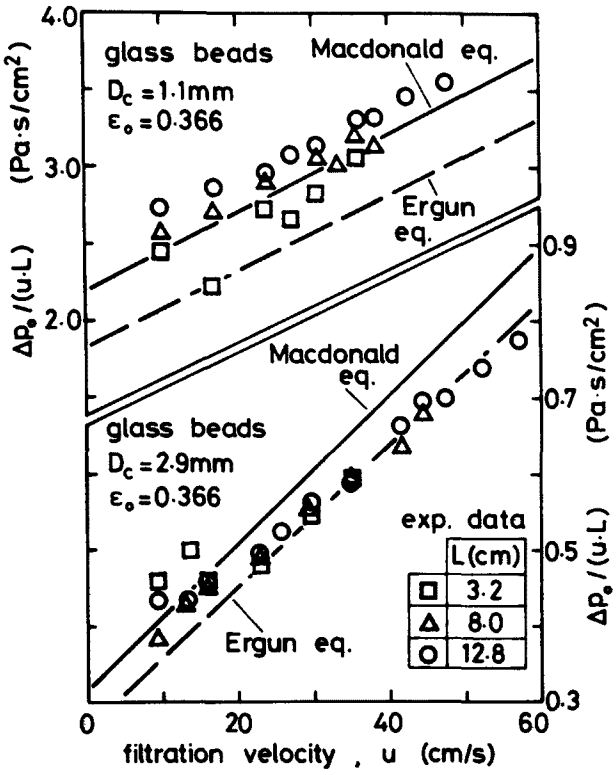

Figure 4. Relationships between pressure loss and filtration velocity (glass beads).

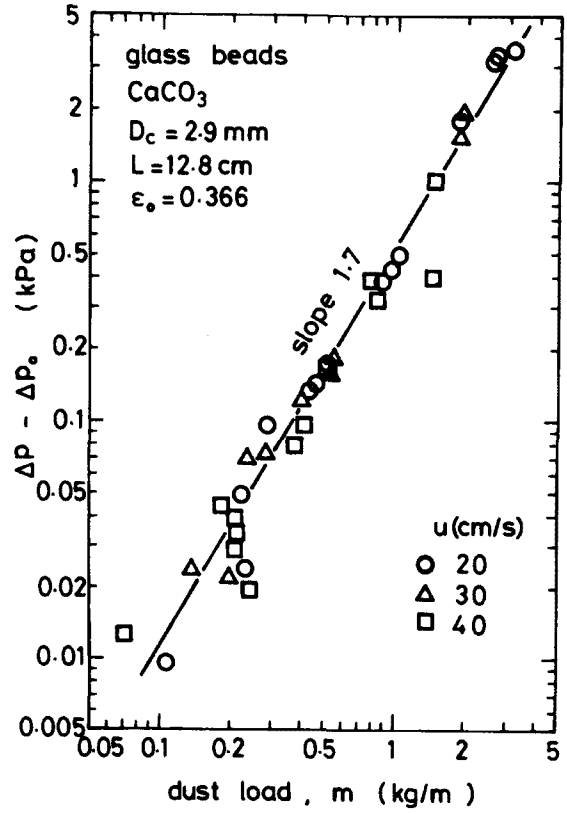

Figure 5. Relationship between additional pressure loss and dust load (glass beads).

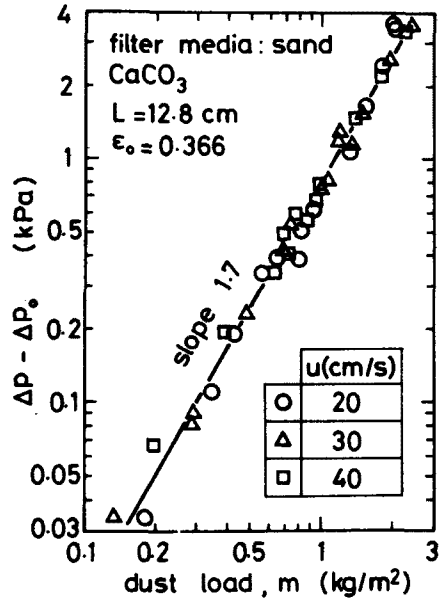

Figure 6. Relationship between additional pressure loss and dust load (silica sand).

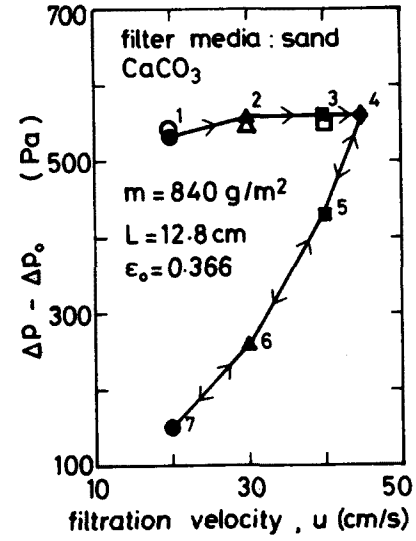

Figure 7. Relationship between additional pressure loss and filtration velocity at 840 g/m² dust load in packed bed.

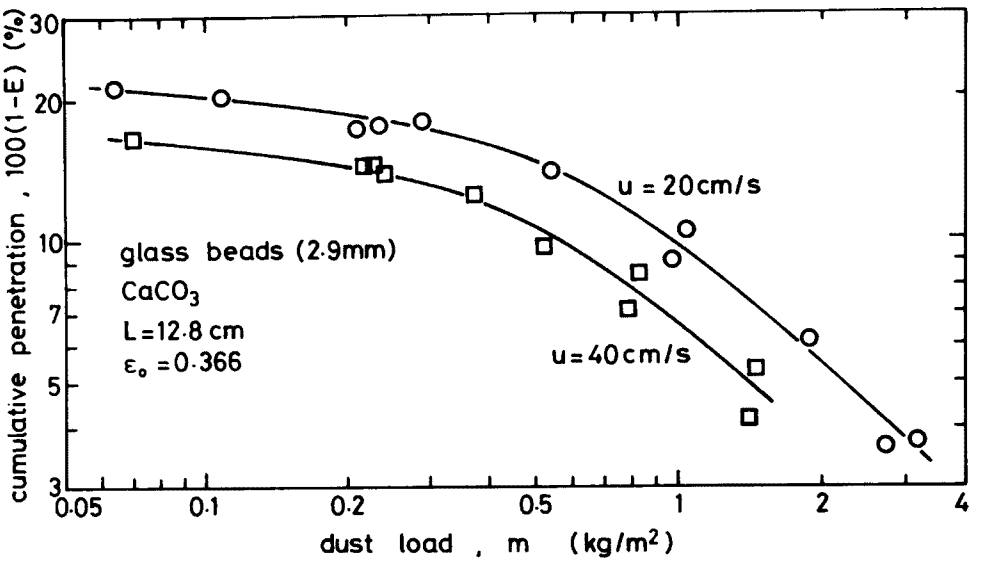

Figure 8. Relationship between cumulative penetration and dust load (glass beads).

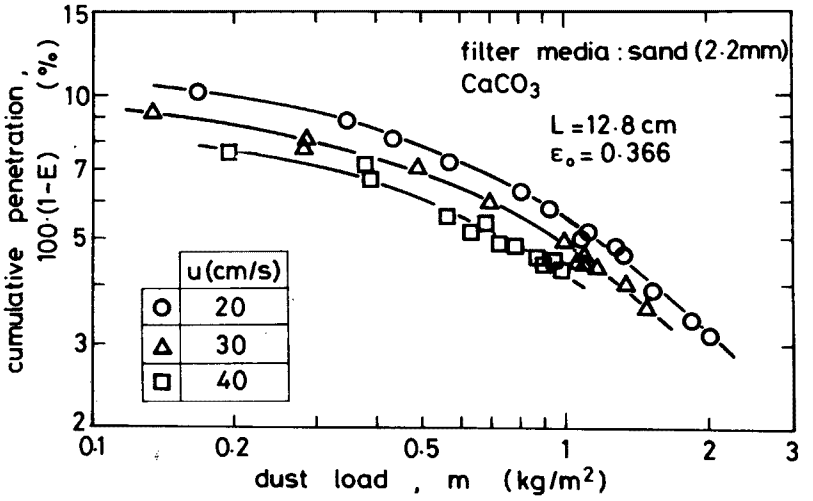

Figure 9. Relationships between cumulative penetration and dust load (silica sand).

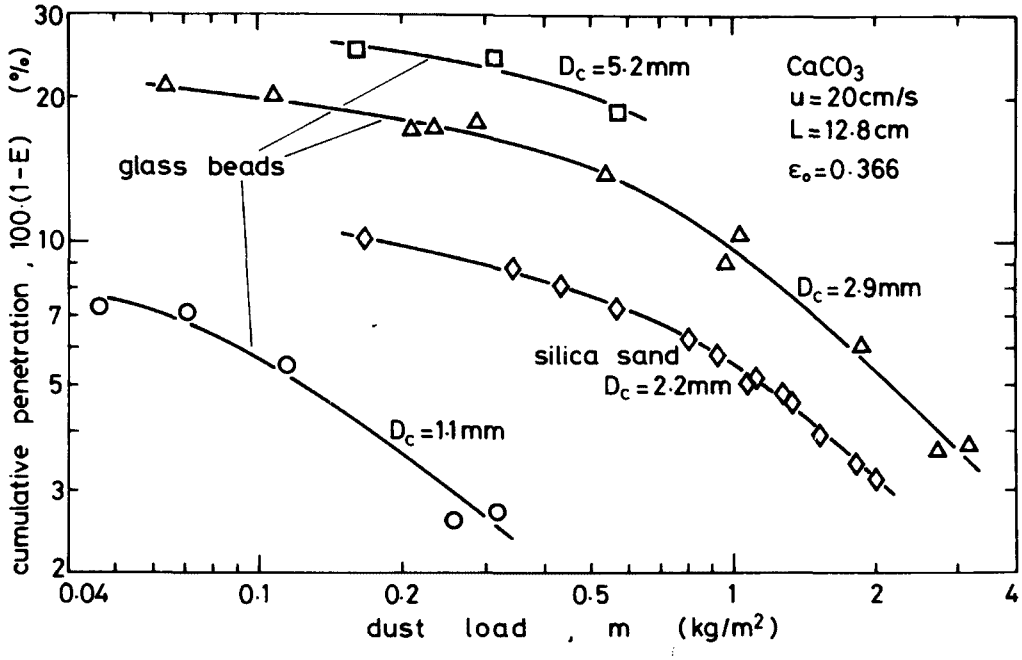

Figure 10. Cumulative penetration for packed bed of various granule sizes.

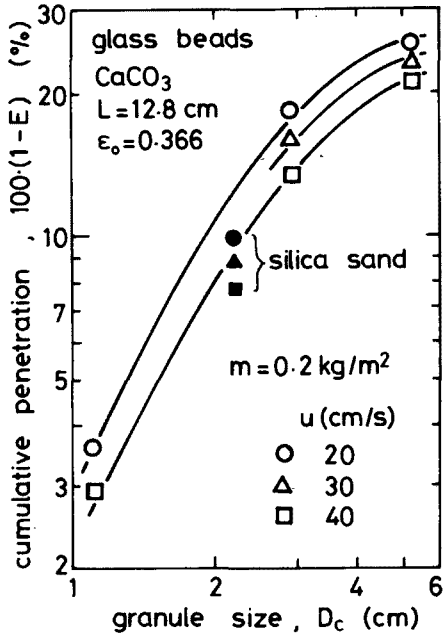

Figure 11. Relationships between cumulative penetration and granule size at dust load of 0.2 kg/m^2.

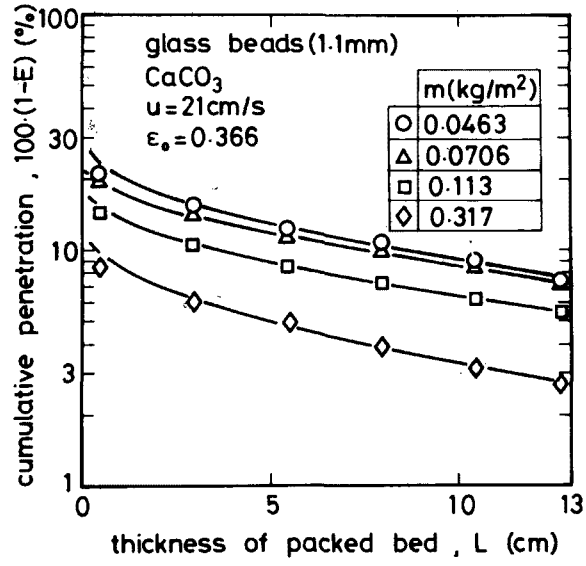

Figure 12. Effect of thickness of packed bed on cumulative penetration.

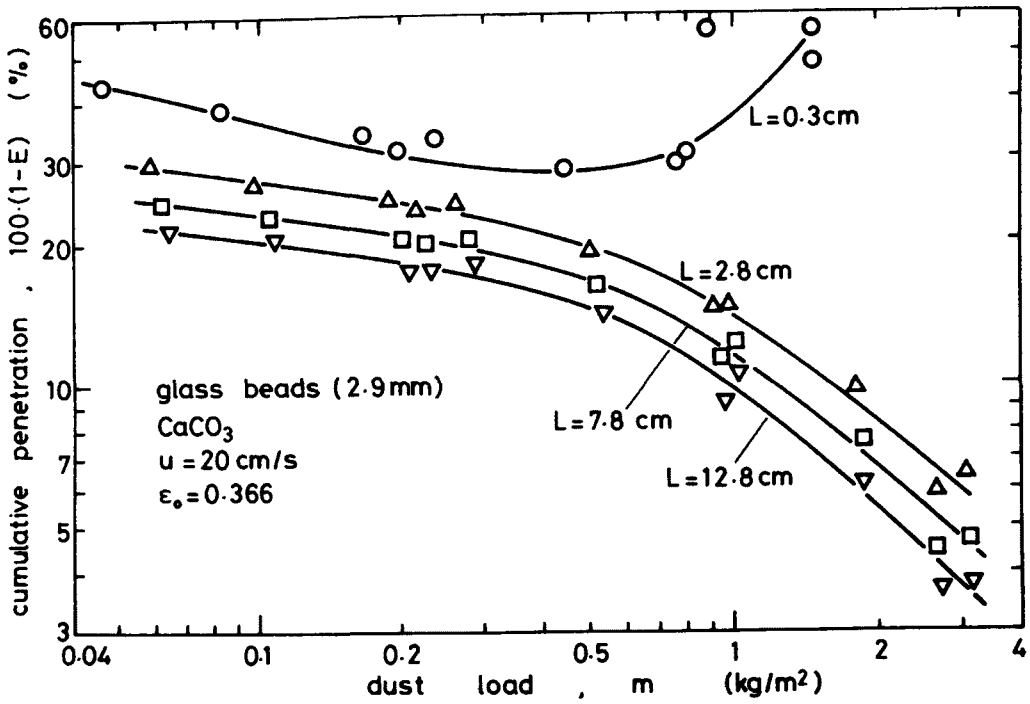

Figure 13. Cumulative penetration of packed beds for various thicknesses.

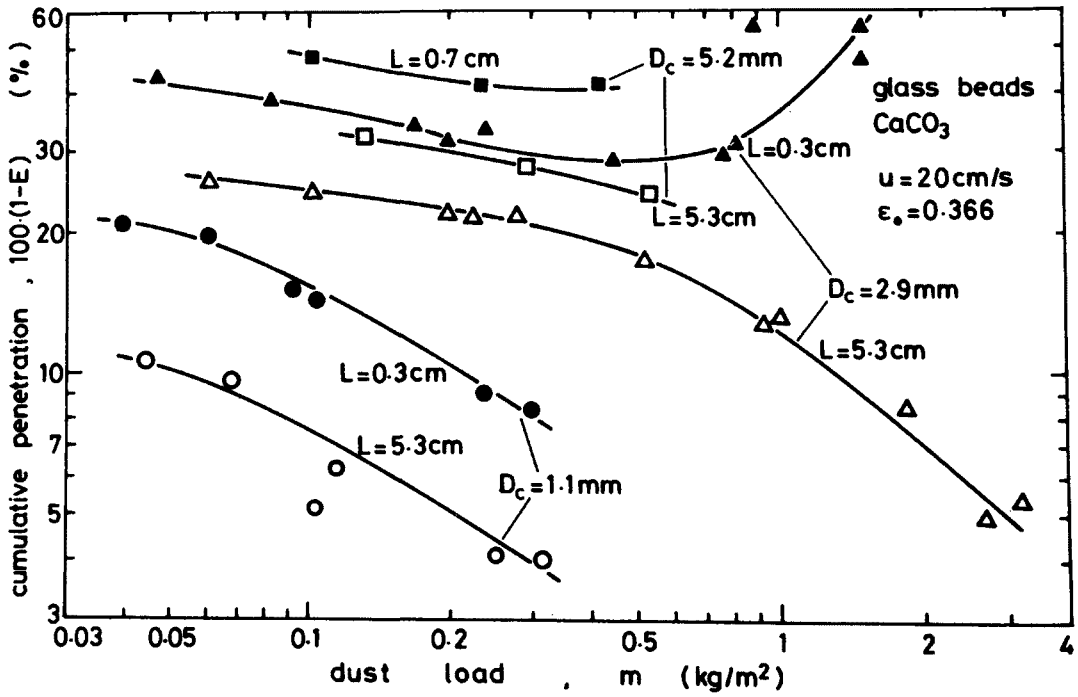

Figure 14. Effects of granule size on cumulative penetration of packed beds for two thicknesses.

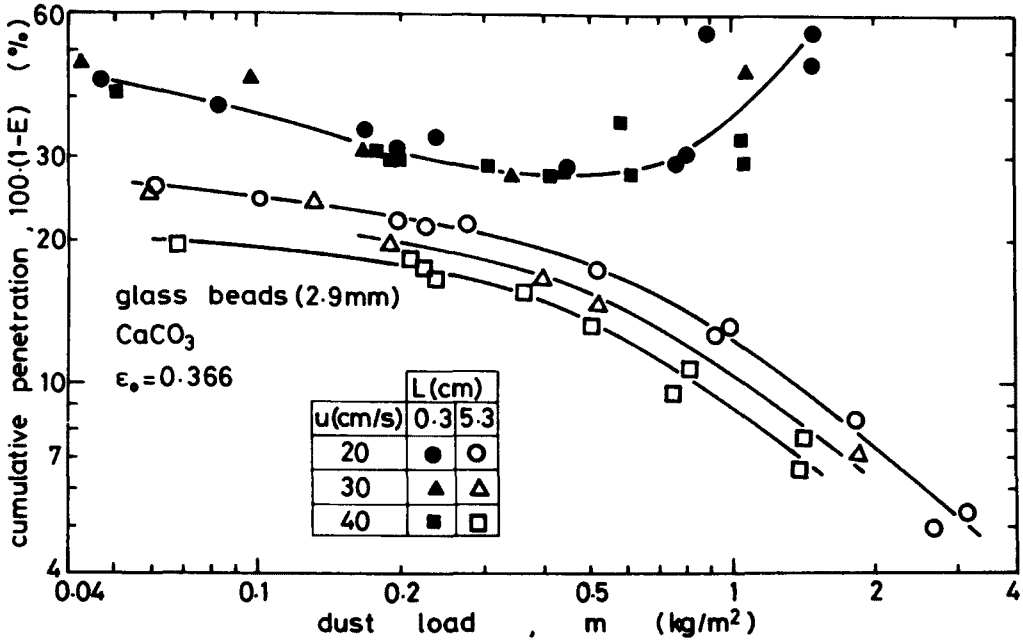

Figure 15. Effect of filtration velocity on cumulative penetration of packed beds for two thicknesses.

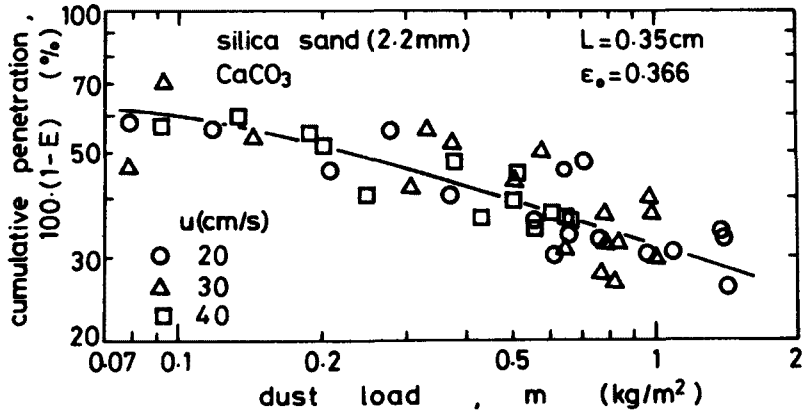

Figure 16. Relationship between cumulative penetration and dust load for 0.35 cm thick bed with silica sand.

DRY DUST COLLECTION OF BLAST FURNACE EXHAUST GAS BY MOVING GRANULAR BED FILTER

By : A. Wakabayashi, T. Sugawara, S. Watanabe
Kobe Steel, Ltd.
Kobe, Japan

ABSTRACT

For the purpose of attaining more effective power recovery of blast furnace top gas energy by dry dust collection, a pilot plant of one module of a plant of commercial size was installed to ensure performance and reliability in the field operation, where it proved to have sufficient applicability in various operating conditions.

This report is to succeed the first report of the small scale fundamental test which was published at the first symposium on the Transfer and Utilization of Particulate Control Technology held in Denver, July 24 - 28, 1978.

INTRODUCTION

As for the dust collection device for blast furnace top gas, it is essential to ensure stable performance and reliability in long time operation. Therefore, we installed the pilot plant device having the same size and construction as one module of the full size plant which consists of multiple modules of cylindrical vessels to treat the whole volume of gas from a blast furnace and to contain the high pressure gas.

The pilot plant test was performed in two stages in the field of our KAKOGAWA steel making plant. The first stage test entered into operation in March, 1979 by inducing the top gas from No.1 blast furnace, and continued until January, 1980. The test was carried out for the filteration velocity across the inside of the filters of 0.2 to 0.37 m/sec. By reviewing the result of the first stage test, we concluded that :

1) The filteration velocity can be increased up to 0.4 m/sec or more, to make an equipment smaller and attain a smaller installation space and a more reasonable cost in commercial use.
2) Longer operating duration should be preferable to prove the reliability of the equipment.

Then, the second stage test started in July, 1980 by inducing the top gas from No.2 blast furnace to attain the above mentioned objects and continued until January, 1981. The test result showed the acceptable performance for particle collection efficiency on the increased filteration velocity of 0.4 m/sec and justified the reliability of the device.

Specifications of Pilot Plant

Specifications of the pilot plant are shown in Table 1. In the first

stage test, the ranges of the operating factors such as gas velocity across the filter, dust load in the media, and media size were decided according to the result of the preceding fundamental test, and in the second stage test, those factors were decided based on the test results in the first stage test.

TABLE 1. SPECIFICATION OF TEST FACILITIES

	First Stage Test	Second Stage Test
Gas induced to Test Device	No.1 Blast Furnace Top Gas	No.2 Blast Furnace Top Gas
Gas Capacity	40000 to 60000 Nm^3/h	40000 to 80000 Nm^3/h
Gas Pressure	1.7 kg/cm^2g	2.1 kg/cm^2g
Gas Temperature	average 140°C	average 120°C
Filteration Velocity Inside Filter/Outside Filter	0.2 ~ 0.37/ 0.12 ~ 0.23 m/sec	0.4 ~ 0.6/ 0.3 ~ 0.45 m/sec
Layer Thickness Inside Filter/Outside Filter	200/200 mm	200/400 mm
Media Size Inside Filter/Outside Filter	1.2 ~ 2.5/ 1.2 ~ 2.5 mm	1.2 ~ 2.5/ 1.2 ~ 2.5 mm

Description of Pilot Plant

The view of the pilot plant is shown in Figure 1; and Figures 2 and 3 show the gas flow and the layout of the plant.

Gas Flow

Figure 2 shows the gas flow from the blast furnace to the pilot plant. The dust-laden top gas from which large particles are collected previously by the dust catcher is supplied to the pilot plant by-passing the venturi scrubber. As shown in Figure 3, the gas from the dust catcher first enters the multi-cyclone in which coarse particles are removed from the gas stream, and flow into the vessel of the granular bed filter device, and then flow through the inner and the outer granular bed filters arranged in the cylindrical vessel. The particulate in the gas stream is captured in the granular media, and the cleaned gas exists from the vessel.

Gas flow capacity is controlled by the flow control valve to balance the flow rate of the main line and the by-pass line.

Shut-down valves are provided at the inlet and the outlet of the device to shut down the gas stream from the device at any time. In the case of shut-down, the top gas in the device is replaced with nitrogen gas to avoid

water vapor condensation in the gas. The nitrogen gas in the device is replaced with air at the time of inspection inside of the device. For the use of the replacement of the gas in the device, the breather valves (V_1 to V_7) and the inlet ports of air and nitrogen gas are provided at the suitable positions in the device.

Moving of Granular Media

Figure 3 shows the layout of the pilot plant. The two staged moving granular bed filters are located in equi-central multi-angular double rows, and the granular media in the filters moves slowly and continuously downward by gravity, controlled by table feeders. The setting of the table feeders can be regulated independently to control the speed of the media movement in the inner and the outer filter. The granular media in the outer filter moves more slowly than that in the inner filter to capture the finer particles.

The gas seal valve assemblies are provided at the top and the bottom of the vessel so that the granular media is fed to and discharged from the vessel without gas flowing out from the vessel.

The dust-laden granular media is discharged from the bottom of the gas seal valve, and conveyed to the vibrating screen by the belt feeder and the bucket elevator to remove the dust from the media. The cleaned media is stored in the granule storage tank and conveyed to the top of the vessel by the bucket elevator and the vibrating feeder, and then recycled back to the top of the filter through the gas seal valve.

Test Results

In filteration of granular bed filter, filteration velocity and dust load in the media make the strongest effect on the performance such as collection efficiency and pressure drop across the filter. Therefore, the test was performed on the various conditions of filteration velocity and moving speed of the media.

Filteration Performance

Figures 4 and 5 show the effect of the filteration velocity on the dust concentration at the outlet of the granular bed filter in the first stage test and the second stage test. In the first stage test, 200 mm - thick filters were applied for both the inner and the outer filter, and in the second stage test, 200 mm - thick filter was applied for the inner filter and 400 mm - thick filter was applied for the outer filter. The data obtained from both tests demonstrate a considerable decrease in the dust concentration at the outlet of the granular bed filters in the second stage test. The second stage test data indicates that the specified dust concentration of 5 mg/Nm^3 or less at the outlet of the granular bed filters is attained at the filteration velocity of 0.4 m/sec at the inside of the filters. The range of the dust concentration at the inlet of the multi-cyclone and of the granular bed filters were 2 to 5 g/Nm^3 and 0.2 to 0.5 g/Nm^3 in both tests. The data in both tests indicate that the dust concentrations at the outlet of the granular bed filters are not affected by the inlet values.

In filteration of granular bed filters, collection efficiency and pressure drop across the filter are affected by dust load in the media, therefore, we kept in each test the optimum moving speed of the media, which was obtained in the beginning.

Figure 6 shows the particle size distribution at a few points in the system by dust sampling in the second stage test, and Figure 7 shows the average collection efficiency in the granular bed filters in each particle size. The data indicates that particles over 10μ m are almost perfectly captured and even finer particles than 10μ m are collected efficiently by the two-staged granular bed filters.

In both tests, the relationship between the pressure drop across the filters and the collection efficiency was not observed.

Gas Temperature

Figure 8 shows the photograph of a record of the gas temperatures. As shown in the record, the gas temperature at the inlet of the granular bed filters fluctuates widely according to the operation of the feeding system at the top of the blast furnace, but the fluctuation of the gas temperature at the outlet of the granular bed filters is moderated by the heat capacity of the granular media. This phenomenon benefits the energy recovery system of the top gas in commercial use in the field, because the temperature fluctuation of the gas into the energy recovery turbine is moderated and the stable load is obtaineded from the turbine.

Reliability of Device

During the test period of two years, the device has been confirmed to endure for long-time operation.

Conclusion

For dry dust collection of blast furnace top gas by a pilot plant, the granular bed filter proved acceptable applicability in spite of wide fluctuation of gas volume, gas temperature, and dust load in gas stream.

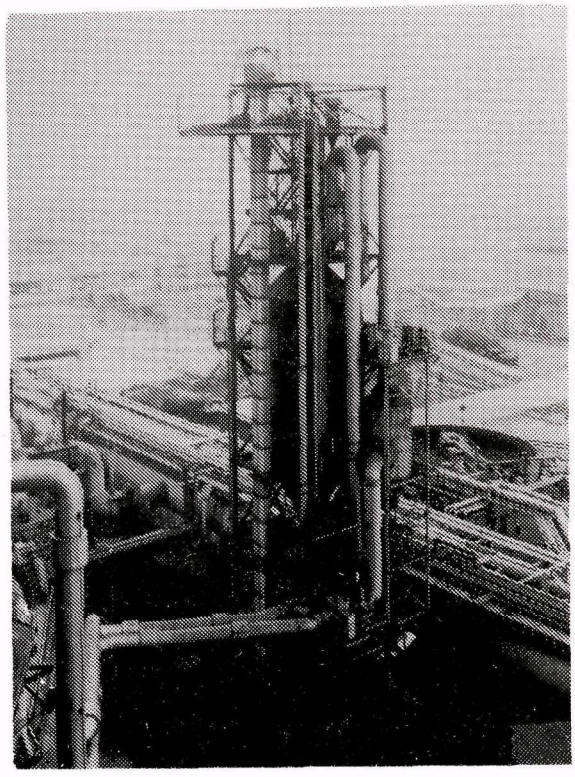

Figure 1 View of Pilot Plant

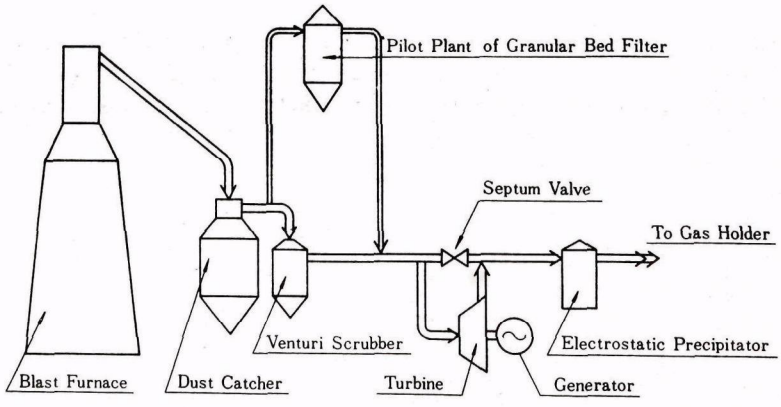

Figure 2 Gas Flow to Pilot Plant

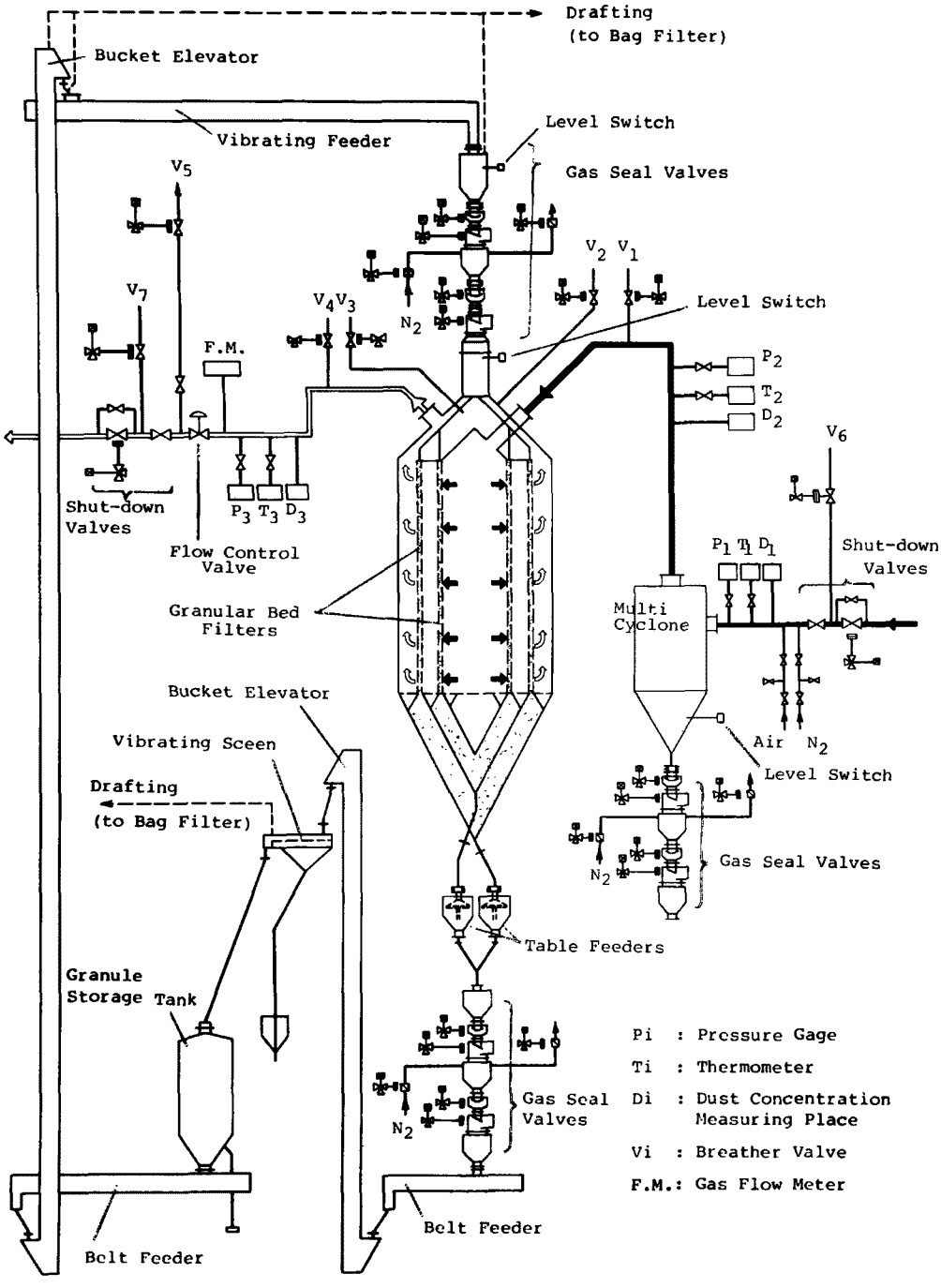

Figure 3 Layout of Pilot Plant

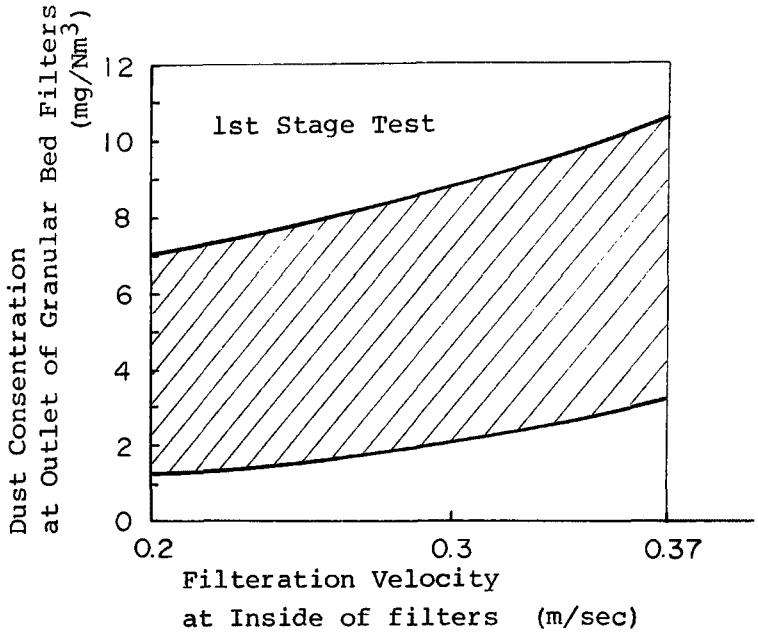

Figure 4 Effect of Filteration Velocity on Dust Consentration at Outlet of Granular Bed Filters

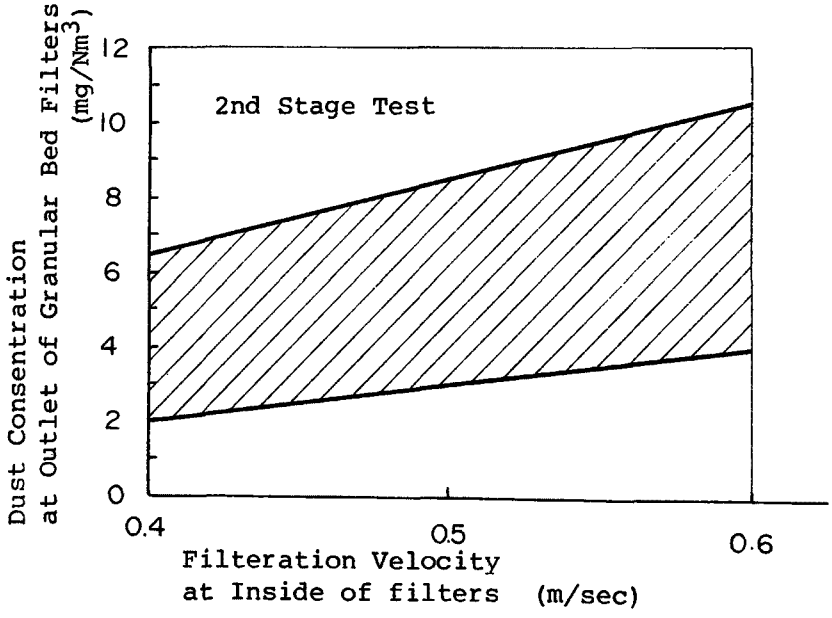

Figure 5 Effect of Filteration Velocity on Dust Consentration at Outlet of Granular Bed Filters

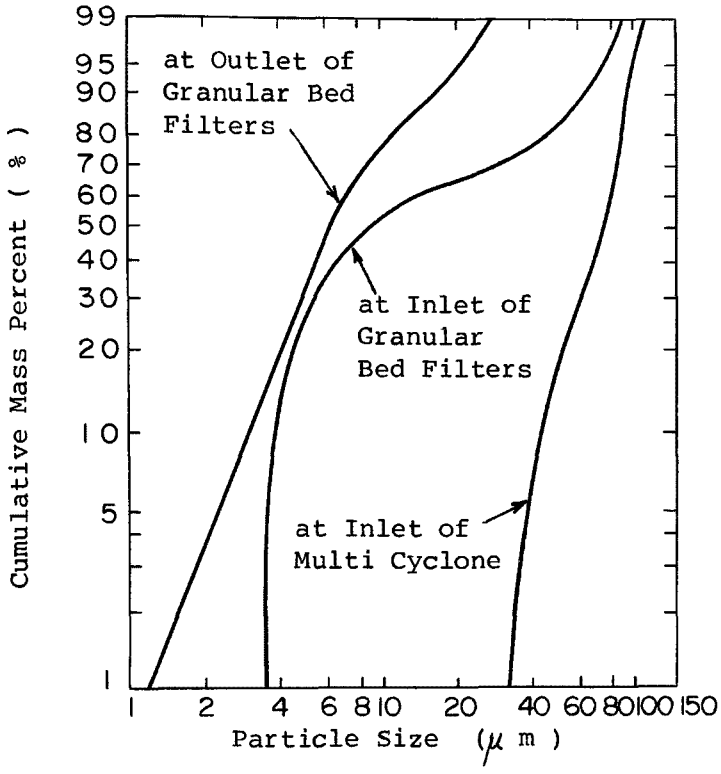

Figure 6 Particle Size Distribution at Each Place of System

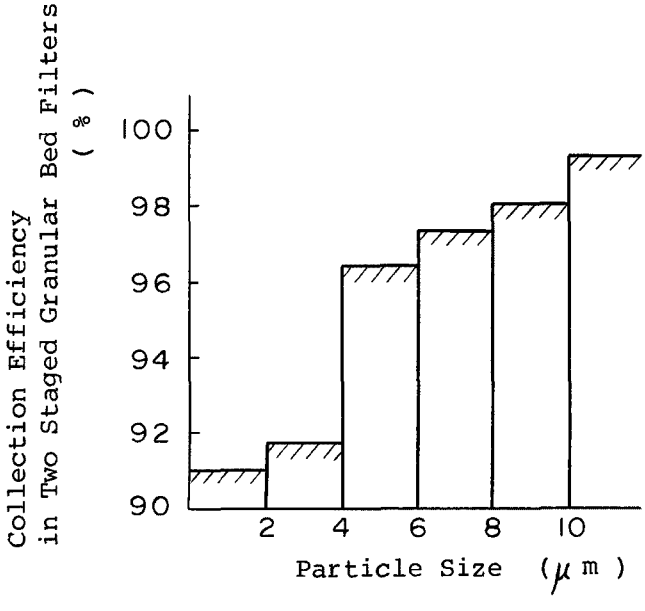

Figure 7 Collection Efficiency in Two Stage Granular Bed Filters in Each Particle Size

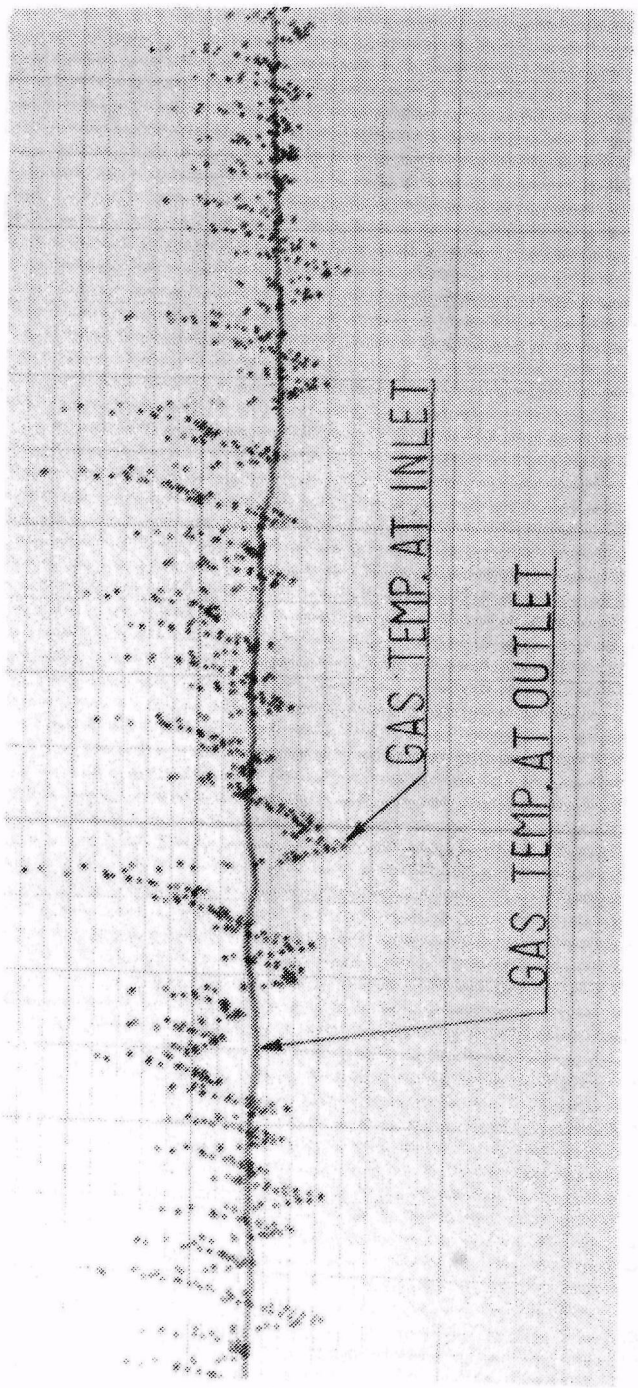

Figure 8 Fluctuation of Temperature at Inlet and at Outlet of Granular Bed Filters

IRON AND STEEL AIR POLLUTION CONTROL USING MAGNETIC SEPARATION

By: D. C. Drehmel
Industrial Environmental Research Laboratory
U.S. Environmental Protection Agency
Research Triangle Park, NC 27711

C.E. Ball
Research Triangle Institute
Research Triangle Park, NC 27709

C.H. Gooding
Clemson University
Clemson, SC 29631

Introduction

The separation of process streams according to magnetic susceptibility has been an area of expanding research and development. During the last decade well over 100 patents, reports, and technical papers have been published throughout the world. Some of the application areas are mineral beneficiation (1,2); taconite beneficiation (3); coal de-ashing and desulfurization (4-10); wastewater treatment (11,12); steel mill wastewater treatment (13,14); municipal wastewater treatment (15,16); blood component separation (17); and catalyst recovery (18). While application of magnetic separation to water pollution problems has received extensive investigation, application to air pollution problems is a recent development. Among the major industrial groups with significant air pollution problems, the iron and steel industry has sources which are difficult to control by conventional devices and which have particulate emissions with high specific magnetizations. Specific sources which would be most favorable for magnetic separation are the basic oxygen furnace, open hearth furnace, and the scarfing machine. Other possible sources for application are the blast furnace, electric arc furnace, and the sinter machine. The results reported in this paper are for a field test using a side stream of the exhaust from the sinter windbox.

Application of magnetic separation to air pollution control could take many forms. Possible variations include:

a) Permanent vs electromagnet.
b) Dipole vs quadrapole magnet.
c) Collection by filtration vs diversion to a secondary collector.

d) Gas flow parallel or perpendicular to magnetic field lines.
e) If the collection is by filtration, collection by fibers vs collection by granules.
f) On-line vs off-line cleaning of the collector.

With so many possible combinations, it will take extensive research and development to fully assess the applicability of magnetic separation to air pollution control. The subject of this paper is a stainless-steel deep-bed fiber filter enhanced by a magnetic field from a dipole electromagnet. The filter is cleaned by off-line reverse air flow. Theoretical considerations and general applicability of this type of system have been discussed in detail in previous papers (19,20). For the sinter plant field tests, the magnetic separation equipment was installed on a 13 m trailer and trucked to the plant. In order to provide continuous operation during periods of off-line filter cleaning, this mobile pilot plant actually consisted of two sets of magnetic separation equipment as described below.

Apparatus

The mobile pilot plant was designed for a nominal flow capacity of 5100 m^3/hr (3000 CFM) based on the previous experimental work. The dirty gas enters the trailer via a 0.317 m ID, 316 stainless steel pipe (12 in., Schedule 5) and passes by test ports through which samples can be drawn to determine the size distribution and concentration of the inlet dust. The gas is then directed to one of two functionally identical magnetic separation devices. One magnet was constructed by Magnetic Corporation of America (MCA), Waltham, MA, and the second magnet was originally constructed by Sala Magnetics, Inc., Cambridge, MA, for use in the laboratory pilot plant. This second magnet was later modified by the addition of new pole pieces and a stand purchased from MCA. Each of the magnetic filters consists of an iron-bound solenoid surrounding a canister that measures 0.432 m ID by 0.305 m long. The canisters are filled with an appropriate amount of magnetic stainless steel wool as dictated by the test program. Each of the magnets can be energized to provide an applied field of up to 0.5 tesla throughout the canister volume. The magnets are energized by DC modular power supplies manufactured by Controlled Power Company (Troy, MI) and purchased from MCA.

After passing through the filter, the cleaned gas travels past another set of test ports and exits the trailer. The exterior pipe size is reduced to 0.266 m ID (10 in., Schedule 5). The gas passes through an orifice and an induced draft blower and is then exhausted to the atmosphere through an 11 m high stack.

The filters are cleaned by backflushing with compressed air provided by a Worthington Model 7-1/2 EDBR two-stage compressor (Worthington Compressors, Inc., Holyoke, MA) that is mounted to the underside of the trailer. The compressed air tank associated with each filter has a volume of approximately 0.28 m^3. To pulse the filter, the compressed air is released through an 8 in. (nominal pipe size) Galigher Delta valve (Galigher Company, Salt Lake City, UT). The Galigher valves are

pneumatically actuated pinch valves with an equivalent throat diameter of approximately 20 cm and a fully open C_v rating of 1300. Each valve consists of a pair of identical elastomeric diaphragms contained within a cast aluminum, split housing. The diaphragms are closed by introducing compressed actuator air into the chamber between the housing and the diaphragms. The valve can then be opened very rapidly by exhausting the actuator air through two large ports provided in the housing. The actuator air was controlled to a pressure approximately 140 kPa (20 psi) higher than the cleaning air and was released through 1-1/2 in. (nominal) Model 168S poppet valves manufactured by Kay Pneumatics (Commack, NY). Dynamic flow calculations conducted during the design phase indicated that the Galigher valves should be able to achieve the required C_v of 750 within 0.05 seconds of the initial diaphragm separation and thus release the cleaning air in a pulse sufficient to clean the filters.

The agglomerated dust that is flushed off the filter is removed from the cleaning air by a Kirk and Blum Size 6, Type C7 cyclone (Kirk and Blum Manufacturing Company, Cincinnati, OH). The exhaust from the top of the cyclone is routed back to the dirty gas stream and into the operating filter. Dust can be removed from the cyclone during operation through the double seal formed by two 6 in. (nominal) Norris butterfly valves (Dover Corporation/Norris Division, Tulsa, OK) that are mounted in line at the bottom of the cyclone hopper. Pneumatic vibrators are mounted on the walls of the dust hopper to aid in dust discharge.

Results

The test program was conducted to give results on the effects of suspected parameters and on reliability during long term testing. Parameters which were directly varied include filter density and depth, applied magnetic field strength, and gas velocity. Resultant observed values include temperature, pressure drop, outlet concentration, total collection efficiency, and collection efficiency by particle size. By statistical analysis of the data it was determined that outlet concentration and collection efficiency were significantly correlated to pressure drop but not to magnetic field strength or velocity. Magnetic field strengths tested were 0.25 and 0.50 tesla and velocities ranged from 3.0 to 8.8 m/s. Failure to obtain a significant correlation does not imply that these variables do not affect the performance but only that this approach was not conclusive. The next step was to average data taken with varying field strength and velocity in order to determine the effect of other parameters. In particular, one may note the change of average pressure drop and outlet concentration with changing filtration media. The stainless steel wool filter bed was either 0.2 or 0.3m long and was packed into the canister described above with a void fraction of 0.990 or 0.986. For the shorter length of bed, lowering the void fraction quadrupled the pressure drop and halved the outlet concentration. Similarly for the larger void fraction, increasing the bed length more than quadrupled the pressure drop and more than halved the outlet concentration. It is possible to further interpret the relationship between outlet concentration and pressure drop by curve fitting the individual data points. The

apparent relationship is:

$$c = k\ (p)^{-0.5} \qquad (1)$$

where: c is the outlet concentration,

k is a constant, and

p is the pressure drop.

Although large changes in pressure drop are associated with bed characteristics, a significant range of pressure drops can be found for a given bed and the same general relationship between outlet concentration and pressure drop can be found.

A complete listing of the results of the performance characterization is shown in Table 1. Two levels each of the parameters filter length, filter density, and applied field provide the basic eight experimental conditions which were tested at varying superficial velocities. The resultant pressure drops ranged from 9 to 114 cm W.C. and the collection efficiency from 46.6 to 94.5%. As expected the short low-density filter gave the low pressure drops and low collection efficiencies while the highest collection efficiency was found with the long high-density filter. Not all collection efficiencies with this latter filter were high because the efficiency tended to decrease with increasing gas velocity. This is the opposite trend seen with the short low-density filter. Other filter combinations did not show clear trends with velocity. It is proposed that, as the filter becomes more efficient, the role of velocity shifts from promoting collection with increased impaction to degrading collection with increased reentrainment of collected material.

Discussion of Results

In the preceding section it was noted that the results were correlated with pressure drop. Pressure drop is more usually a dependent variable and is a function of filter density, F; filter length, L; and superficial gas velocity, V. In the case of these data it was found that pressure drop was significantly correlated to the product of F, L, and V^2. To further define the relationship between the results and filter properties, the experimental results were compared to a model developed by Gooding (21). The equation for this model is:

$$E = 1 - \exp\left(-\frac{4FL\ Y_c\ P}{\Pi^2\ S\ (1-F)}\right) \qquad (2)$$

where: E is the collection efficiency,

Y_c is the collision radius,

P is the probability of particle retention, and

S is the radius of the collecting wire.

Table 1. RESULTS OF PERFORMANCE CHARACTERIZATION

Filter Length (m)	Filter Density (metal fraction)	Applied Field (tesla)	Superficial Velocity m/s	Filter Pressure Drop cm W.C.	Collection Efficiency %
short	low	low	3.6	9	56.6
(0.2)	(0.010)	(0.25)	4.4	11	51.9
		high	3.8	9	48.7
		(0.50)	3.9	11	46.6
			4.9	17	51.1
			7.9	32	66.1
	high	low	3.7	18	85.6
	(0.014)		5.8	41	83.9
			7.4	66	86.2
		high	4.0	25	86.7
			5.8	64	79.6
			7.9	76	74.4
long	low	low	3.8	38	78.2
(0.3)			5.9	44	90.5
			7.7	79	91.2
		high	3.9	31	81.5
			6.0	72	87.2
			6.9	114	87.7
	high	low	3.0	89	94.5
			6.4	102	83.4
			8.8	109	75.7
		high	6.5	76	76.1

The collision radius, Y_c, is a dimensionless value derived from solution to a trajectory model for magnetic filtration. In this trajectory model four parameters--A, G, K, and W-- describe the behavior of the particle. Parameter A accounts for the relative magnitudes of the magnetic field induced in the ferromagnetic wire and the applied field. After magnetic saturation of the steel wool filter, increased applied field would cause A to decrease from unity. However, for these experiments, the steel wool was at or below saturation where A may be taken as constant at unity.

Parameter G accounts for the effect of gravity, which is small for these experiments. The calculated value for G was less than 2×10^{-5} and G was taken as zero.

The parameters W and K account for the effects of magnetic field and inertia on collection and are defined as:

$$W = \frac{\mu_o \chi^* H_a^2}{\rho_p V_o^2} \tag{3}$$

$$K = \frac{2b^2 \rho_p V_o}{9S\eta} \tag{4}$$

where: μ_o is the magnetic permeability of a vacuum,

χ^* is the effective magnetic susceptibility of the particle,

H_a is the magnetic field,

ρ_p is the density of the particle,

V_o is the fluid velocity upstream of the wire,

b is the particle radius, and

η is the fluid viscosity.

With G taken as zero and A as unity, the effect of W and K on the collision radius, Y_c, is shown in Figure 1 as contours of constant values for Y_c for varying W and K. As the magnetic field decreases, W decreases and the value of Y_c is identical to conventional inertial impaction in potential flow. As the magnetic field increases, the value Y_c can be significantly increased by as much as an order of magnitude. The physical significance of this is that the individual collection fiber may collect particles that would have bypassed the fiber without the magnetic field. In fact the fiber may cover a radius as great as many times its physical radius.

Given the collection efficiency of the individual fiber, the model assumes a randomly packed filter which gives an active projected area of $2/\pi$ times the fiber area given as $2hS\,Y_c$ where h is the wire length and S is the wire radius. By integrating over the entire length of the

filter and using a plug-flow reactor mass balance, Equation (2) is obtained except for the P. The factor P was developed after analysis of in-house pilot scale data as shown in Figure 2. The physical significance of P is that it removes the assumption that all particles which reach the fiber are permanently collected. The model without P predicts well for small particle sizes but overpredicts collection efficiency at larger particle sizes. The loss of efficiency at larger sizes may be attributed to reentrainment of agglomerates or lack of retention of impacting large particles. This latter case was analyzed by computing the energy needed to cause particle bounce. A theoretical critical impaction angle was fitted to pilot data by adjusting parameters within certain bounds. The model with bounce correction agreed with some data as shown in Figure 2 but in general underpredicted efficiency at high gas velocity or large particle size.

An alternative approach was to assume that reentrainment and bounce would be some function of W and K. Analysis of the in-house pilot scale data showed that P was directly related to W and inversely to K. The field test data were also analyzed by this approach and the best fit was obtained when P was described as follows:

$$P = 2 \left(10 W^2 + \frac{0.1}{K} \right) \qquad (5)$$

Using Equation (5) for P, the comparison between the model and experimental data is shown in Figure 3. Agreement is good but some collection efficiencies are over or under predicted by as much as 30% (the dashed lines give boundaries of 30% over and under prediction).

With regard to ultimate application of magnetic filtration, these tests are not conclusive. Although three tests had efficiencies in excess of 90%, the lowest pressure drop for these was 44 cm W.C. The high pressure drop needed for good collection is an ultimate consequence of the low iron content and poor magnetic properties of the sinter plant particulate matter. Values of W ranged from 0.0077 to 0.083 with K values in the range from 0.16 to 0.46. Figure 1 shows that W has no impact on Y_c over much of the experimental range. Only when W is large and K is small is Y_c significantly different from that predicted for impaction only. As described in Equation (3), W is related directly to magnetic susceptibility and magnetic field. Although the magnetic field could be increased, the cost could outweigh the savings in pressure drop. However, magnetic susceptibility could be increased 20 to 30 times by applying magnetic filtration to particulate from an electric arc furnace or basic oxygen furnace instead of that from a sintering machine. The corresponding increase in W of 20 to 30 times yields an increase in Y_c of approximately 4 to 10 times. Using Equations (1) and (2), the ultimate result is that the pressure drop could be decreased by a factor of approximately 20 and still maintain 90% collection. In other words a less-dense shorter filter could be used to give a collection efficiency greater than 90% and a pressure drop less than 5 cm W.C. By similar calculations a 99% collection efficiency should be achievable with a pressure drop less than 20 cm W.C. This hypothesis will be tested in

a pilot demonstration on an electric arc furnace.

The pilot demonstration on an electric arc furnace will take place at the Georgetown Steel Corporation plant in Georgetown, SC. The waste gas stream to be treated is collected from three EAFs with direct shell evacuation and canopy hoods above. A slipstream of gas will be taken from a duct upstream of the fabric filter serving the EAFs.

The mobile pilot plant is a continuous HGMF system which is designed for a nominal flow capacity of 3,060 m^3/hr (1,800 cfm). The pilot plant contains a SALA-HGMS® Carousel Model 120-05-00 (Sala Magnetics, Inc., Cambridge, MA), which is a continuous device that incorporates a magnet head and a cleaning station mounted 180° apart on a rotating carousel. The magnet coils are split into a mirrored-saddle configuration to allow the carousel to be rotated through the magnetized zone by a variable speed drive. The carousel contains 48 removable cassettes which can be loaded with filter material to a depth of 0.47 m (5.8 in.). The magnet head encloses an active face area of 0.085 m^2 (133 $in.^2$) in the direction of fluid flow. The magnet head is designed to provide an applied field from 0.0 to 0.5 tesla. The cleaning station is designed to provide a pulse of air to clean the collected particles from the filter material once it has left the magnetized zone.

The agglomerated dust cleaned from the filter material with the cleaning air pulse is sent to a Kirk & Blum size 4, Type C5 cyclone. (Kirk & Blum Manufacturing Company, Cincinnati, OH). Exhaust from the top of the cyclone is then recycled into the dirty gas stream.

The test program is designed to test the effects of four parameters on collection efficiency, and the reliability of the equipment during long term operation. The four parameters which will be varied are filter packing density, filter type (steel wool, expanded metal), applied field, and gas velocity.

After the performance characterization tests are completed, long term testing will be started. During this test, the pilot plant will be operated continuously for 500 hours. The pilot plant tests are now scheduled to run from June to December 1981.

Conclusions

Pilot scale field tests of magnetic filtration were conducted at a sintering plant. The 5,100 m^3/hr magnetic filter was examined under varying conditions of an extensive test matrix and in a long term (450 hour) test. No fundamental difficulties were encountered either during long term testing or at high gas velocities up to 8.8 m/s. High collection efficiencies (greater than 90%) were achievable but generally at the expense of high pressure drop (greater than 44 cm W.C.). It is felt that magnetic filtration would not be cost effective at high pressure drop even though the high superficial velocity is attractive for compactness of the control device. Analysis with a theoretical model predicts that the

pressure drop could be reduced by at least an order of magnitude while maintaining high collection efficiency if the specific magnetization of the dust were more than an order of magnitude higher. Previous in-house pilot plant work has shown that both basic oxygen furnace (BOF) and electric arc furnace (EAF) dust provide the high specific magnetization indicated as necessary by analysis in this study and both BOF and EAF dust have been collected with 99% efficiency in in-house work. It is concluded that magnetic filtration would be cost effective for application to BOF and EAF control even though it is not cost effective for sinter plants. To test this conclusion, a pilot demonstration of magnetic filtration on an EAF is being planned for the near future.

References

1. Kelland, D. R., "High Gradient Magnetic Separation Applied to Mineral Beneficiation," IEEE Trans. Magn., Mag-9, 307 (1973).

2. Murray, H. H., "Beneficiation of Selected Industrial Minerals and Coal by High Intensity Magnetic Separation," IEEE Trans. Magn., Mag-12, 498 (1976).

3. Kelland, R. R., and E. Maxwell, "Oxidized Taconite Beneficiation by Continuous High Gradient Magnetic Separation," IEEE Trans. Magn., Mag-11, 1582 (1975).

4. Ergun, S., and E. H. Bean, "Magnetic Separation of Pyrite from Coals," Report of Investigation No. 2718, U. S. Bureau of Mines, Pittsburgh, PA (1968).

5. Trindale, S. C., and H. H. Kolm, "Magnetic Desulfurization of Coal," IEEE Trans. Magn., Mag-9, 310 (1973).

6. Vives, D. L., L. J. Hirth, and W. H. Summerlin, "Direct Reduction and Magnetic Beneficiation of Alabama Brown Ore with Lignite," IEEE Trans. Magn., Mag-12, 490 (1976).

7. Maxwell, E., I. S. Jacobs, and L. M. Levinson, Magnetic Separation of Mineral Matter from Coal Liquids, EPRI AF-508, Electric Power Research Institute, Palo Alto, CA (1977).

8. Maxwell, E., and D. R. Kelland, "High Gradient Magnetic Separation in Coal Desulfurization," IEEE Trans. Magn., Mag-14, 482 (1978).

9. Maxwell, E., D. R. Kelland, and I. Y. Akoto, "High Gradient Magnetic Separation of Mineral Particulates from Solvent Refined Coal," IEEE Trans. Magn., Mag-12, 507 (1976).

10. Liu, Y. A., G. E. Crow, C. J. Lin, and D. L. Vives, "A Pilot-Scale Study of High Gradient Magnetic Desulfurization of Solvent Refined Coal (SRC)," IEEE Trans. Magn., Mag-14, (1978).

11. Mitchell, R., G. Bitton, and J. A. Oberteuffer, "High Gradient Magnetic Filtration of Magnetic and Non-Magnetic Contaminants from Water," Separation and Purification Methods, 4, 267 (1975).

12. Petrakis, L., and P. F. Ahner, "High Gradient Magnetic Separations in Water Effluents," IEEE Trans. Magn., Mag-14, 491 (1978).

13. Oberteuffer, J. A., I. Wechsler, P. G. Marston, and M. J. McNallan, "High Gradient Magnetic Filtration of Steel Mill Process and Waste Waters," IEEE Trans. Magn., Mag-11, 1591 (1975).

14. Harland, J. R., L. Nilsson, and M. Wallin, "Pilot-Scale High Gradient Magnetic Filtration of Steel Mill Wastewater," IEEE Trans. Magn., Mag-12, 904 (1976).

15. DeLatour, C., and H. H. Kolm, "Magnetic Separation in Water Pollution Control-II," IEEE Trans. Magn., Mag-11, 1570 (1975).

16. Yadidia, R., A. Abeliovich, and G. Belfort, "Algae Removal by High Gradient Magnetic Filtration," Envr. Sci. and Tech., 11, 913 (1977).

17. Melville, D., F. Paul, and S. Roath, "High Gradient Magnetic Separation of Red Cells from Whole Blood," IEEE Trans. Magn., Mag-11, 1701 (1975).

18. Whitesides, G. M., C. L. Hill, and J. Brunie, "Magnetic Filtration of Small Heterogeneous Catalyst Particles. Preparation of Ferrimagnetic Catalyst Supports," Ind. Eng. Chem., Process Des. Dev., 15, 226 (1976).

19. Drehmel, D. C., and Gooding, G. H., "High Gradient Magnetic Particle Collection," AIChE Symposium Series 74 (175) (1978).

20. Gooding, G. H., and Drehmel, D. C., "Application of High Gradient Magnetic Separation to Fine Particle Control," JAPCA, 29 (5) (May 1979).

21. Gooding, C. H., "High Gradient Magnetic Filtration of Fine Particles from a Gas Stream," Ph.D. Thesis, North Carolina State University, Raleigh, N. C. (1979).

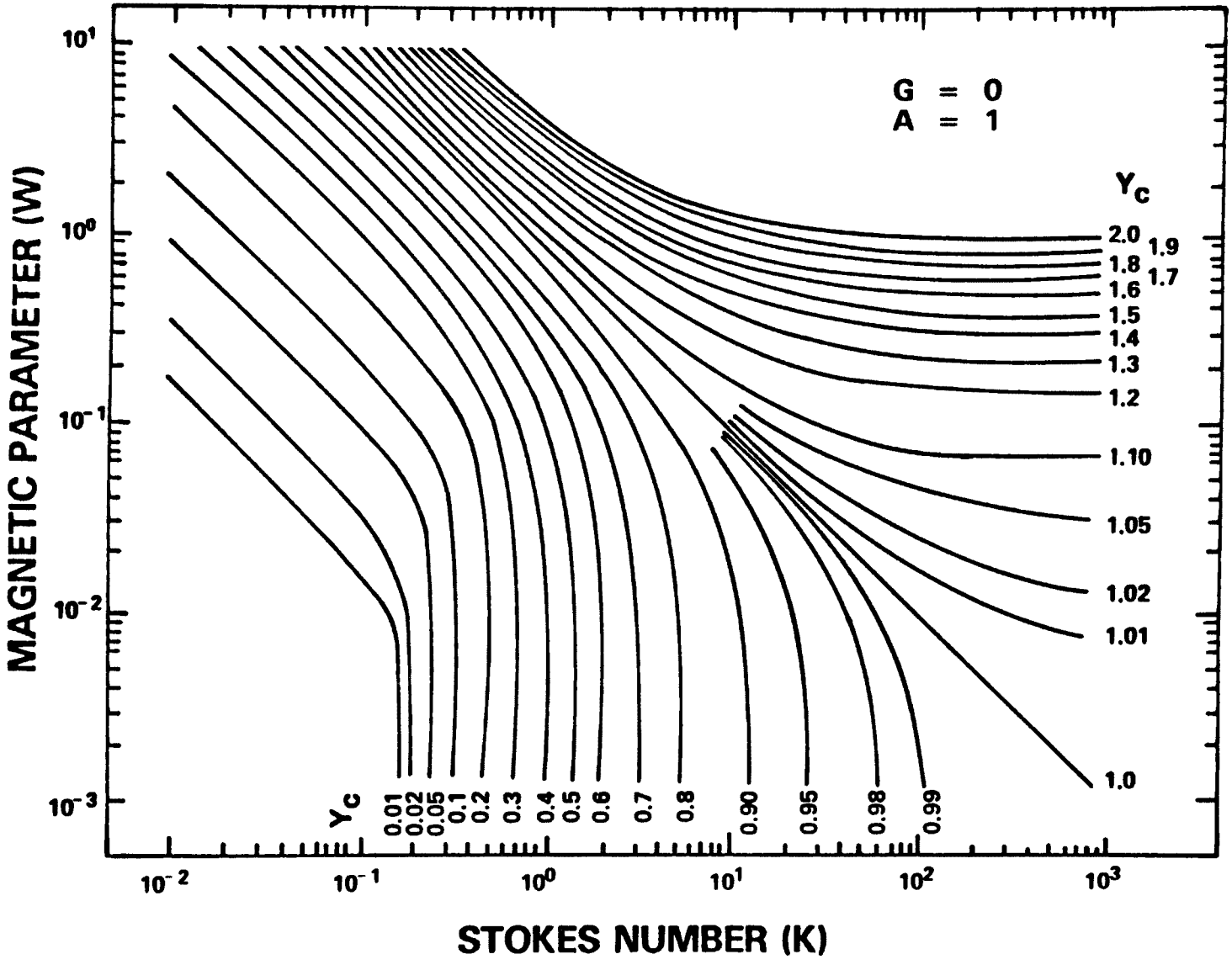

Figure 1. Contour map of collision radius, Y_c.

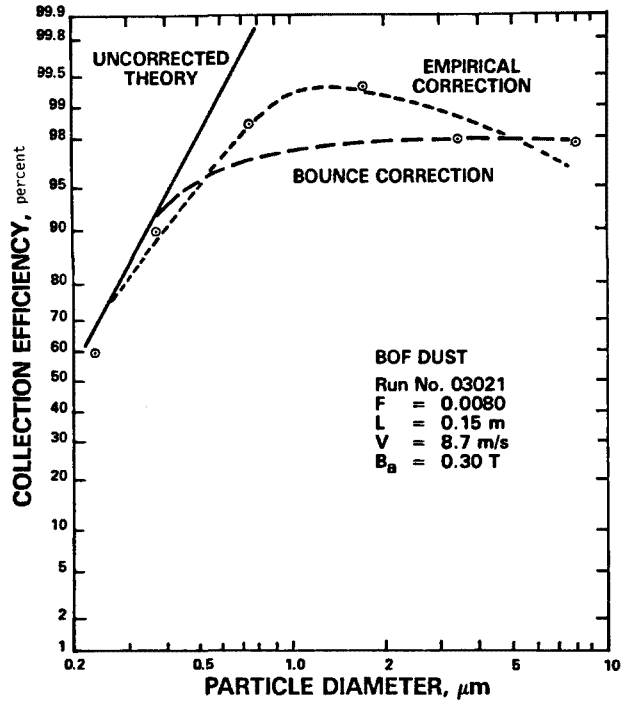

Figure 2. Comparison of models for magnetic filtration.

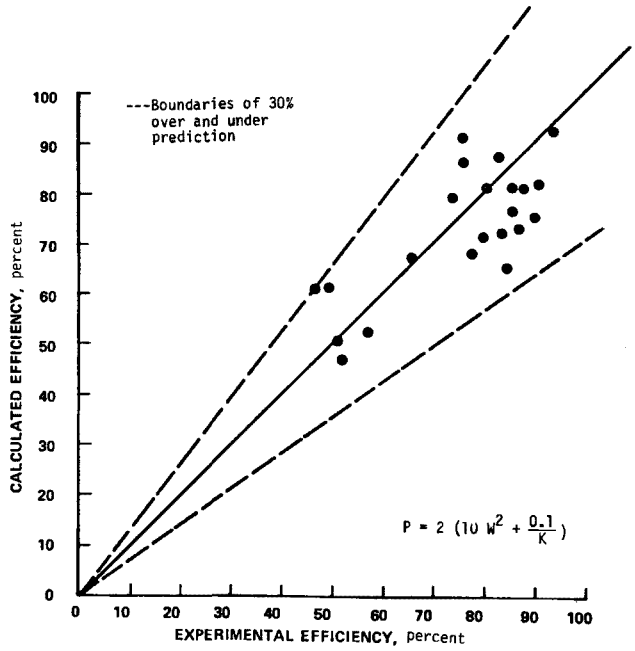

Figure 3. Comparison of data and model.

TECHNICAL AND ECONOMIC EVALUATION OF TWO NOVEL PARTICULATE CONTROL DEVICES

By: R.R. Boericke, J.T. Kuo, K.R. Murphy
General Electric Company
Energy Systems Programs Department
1 River Road
Schenectady, NY 12345

ABSTRACT

A system-level comparison study is made for two novel particulate removal devices, based on both technical and economic considerations. The two novel devices are an acoustic agglomerator and an electrocyclone. These devices are considered in combination with conventional cyclones, electrostatic precipitators, and a baghouse.

Analytical models for the electrocyclone and the acoustic agglomerator have been used to establish preferred geometries and operating parameters, and to predict the performance of these devices in two specific applications: a 663 MWe Pressurized Fluidized Bed (PFBC) power plant and a 475 MWe conventional Pulverized Coal (PC) power plant. It is shown that both the electrocyclone and the acoustic agglomerator appear economically attractive for PFB power plants, but are not competitive with electrostatic precipitators for conventional pulverized coal burning plants.

INTRODUCTION

Two novel methods for dust removal are the electrostatically enhanced cyclone (or electrocyclone), and acoustic agglomeration. The electrocyclone combines electrostatic and inertial forces to achieve improved performance and larger (more reliable and economical) unit size compared to conventional cyclones. The acoustic agglomerator uses the oscillating flow of an acoustic field to cause particle collision and agglomeration. The resulting large particles are then more readily separable by conventional methods.

The application of these novel devices to pressurized fluidized bed combustion (PFBC) is of special interest. PFBC is an advanced method for direct combustion of coal in an environmentally acceptable manner and is particularly suited to central station power generation. The major technology issues in the development of PFB combined cycle power plants are associated with the combustor/gas turbine interface. The hot combustion gas contains significant amounts of fine dust composed of coal ash and attrited sorbent bed materials. This dust, impacting on the turbine blades at high velocity, can rapidly erode the metal and cause premature failure.

Figure 1 shows the dust load and size distribution leaving the combustor exit, as well as current estimates of the dust load required to protect the turbine (1). Also shown on Figure 1 is the maximum dust load of 0.03 $lb/10^6$ Btu allowable under the EPA New Source Performance Standard. Note that if

the dust is sufficiently free of coarse particles, the turbine can tolerate total dust loadings of several hundred parts per million, well in excess of the 22 ppm required to meet the EPA limit.

The fact that the gas turbine can tolerate dust loads in excess of the EPA limit suggests that a relatively simple cleanup device (such as a cyclone or electrocyclone) could be used for turbine protection, together with conventional (low-temperature, low-pressure) cleanup equipment (e.g., baghouse) downstream of the turbine to remove the fine dust particles. An important economic and technical issue is whether the electrocyclone can also, with appropriate design, provide good removal efficiency in the respirable dust range, and thus eliminate the need for supplementary stack gas cleanup. Similarly, the acoustic agglomerator may enable a HTHP cleanup device suitable for turbine protection to also meet the EPA limit by agglomerating the fine respirable dust particles into coarser ones which can then be removed upstream of the turbine.

EQUIPMENT DESCRIPTION

Electrocyclone Concept

The electrocyclone concept is a synthesis of two significant improvements to conventional cyclones which offer promise of meeting the cleanup requirements in a PFB combined cycle system. These two features, the air shield and electrostatic augmentation have been combined to yield a new cyclone concept, the electrocyclone, with significantly enhanced performance.

The General Electric electrocyclone concept is illustrated in Figure 2. The electrocyclone incorporates a clean air shield adjacent to the exhaust duct which prevents short circuiting of dust into the outlet. The clean air is provided by an axial flow separator/electrostatic charger device positioned in the exhaust duct of an upstream cyclone. This axial flow component uses a high voltage corona electrode to charge the dust particles and improve the separation efficiency. The vortex field in the axial flow component is provided by the swirling motion naturally present in the exhaust of a conventional reverse flow cyclone. Within the electrocyclone the separation of dust is strongly augmented by another high-voltage field applied with an electrode along the axis of the cyclone.

A principal advantage of the electrocyclone concept is that a large diameter unit can be built to give the same efficiency as a small conventional cyclone. The large unit is possible because the electrostatic separative force is independent of the cyclone diameter in contrast to the centrifugal force which decreases as the cyclone is made larger.

The physics of operation of the electrocyclone based on studies with a two-dimensional electrovortex apparatus (3), have been incorporated into a mathematical cyclone model, developed previously by GE (4). This original three-region cyclone model was modified to accommodate electrostatic effects and the air-shield feature of the GE electrocyclone concept. This was

achieved by adding two new regions, resulting in a five-region model (2, 5, 6). Complete turbulent mixing is assumed within each region, and analytical expressions for the cyclone collection efficiency are developed from the resulting differential equations. The new model also includes improvements for molecular slip and corona charging of small (respirable) particles.

Acoustic Agglomeration Concept

Acoustic agglomeration (AA) has been used successfully in the past as an aerosol preconditioner. Most of the past experiments on AA were summarized in an excellent work of Mednikov (7). More recently, the subject was reviewed by Shaw (8). AA can be applied effectively for the removal of airborne dust particles when it is used as a preconditioner in series with more conventional devices such as cyclones and filters. The dust laden gas (or aerosol) first enters the AA chamber. As it passes through the chamber, the gas is subjected to the action of the sound waves radiated by the sound generator, which can be a mechanically vibrating piston, a siren, or a whistle. In the AA chamber, smaller particles (diameter $<10\mu m$) agglomerate into larger ones which can be effectively removed by conventional cyclones.

A model for predicting the performance of acoustic agglomerators has been developed independently by Prof. David T. Shaw at SUNY-Buffalo, who served as consultant to GE in performing the present study. This model incorporates Shaw's most recent findings on the dramatic improvement in agglomeration at sound levels above 160dB due to the onset of acoustic turbulence, and is documented in Reference 2.

APPLICATION TO POWER GENERATION SYSTEMS

Application to PFB Combustion System

The design of a 663 MWe PFB combined cycle reference plant has been established by General Electric in considerable detail (9). The plant consists of three PFB/gas turbine modules which generate a total of 154 MW and a single steam turbine generating 530 MW. The net plant output is 663 MW. Table I summarizes the gas cleanup requirements. The cleanup equipment must operate at 1650°F and 10 atmospheres and be capable of handling 155,000 acfm gas flow in each of the three gas turbine modules. The dust load leaving the combustor is about 19,000 ppm and consists of virtually all the coal ash and about a third of the dolomite in the form of fine solids worn from the larger fluidized bed particles by abrasion. The gas cleanup systems for the PFB application are designed to meet both the gas turbine protection requirement and the EPA particulate emission standard of 0.03 $lb/10^6$ Btu, as shown previously in Figure 1.

The electrocyclone design selected for the PFB system was based on parametric studies carried out with the five-region performance model. The unit is 12 feet diameter, and the design details are shown in Figure 3. The size of the electrocyclone was chosen such that the total flow of a PFB module can be handled by four electrocyclones. The design flow rate for each electrocyclone is 38750 acfm.

TABLE I. CLEANUP SYSTEM REQUIREMENTS (PER PFB/GAS TURBINE MODULE)

Gas Flow	1.81×10^6 lb/hr (503 lb/sec)
	1650°F
	10 atm
	155,000 acfm
Dust Load	
Coal Ash (100%) (9.6%) (515,300 lb/hr)/3	16,500 lb/hr
Dolomite (32.5%) (173,000 lb/hr)/3	18,700 lb/hr
Total Dust	32,200 lb/hr
Concentration	19,000 ppm

The individual acoustic agglomerator designed for the PFB system is an 18-inch diamter, 33 feet long cylindrical chamber. Each acoustic agglomerator is designed to handle 4080 acfm of gas flow. Nineteen acoustic agglomerators are packed into one unit, and two units are required per PFB/gas turbine module. Figure 4 shows the configuration of the assembly and the packing arrangement of the acoustic agglomerators. Gas flows into the acoustic agglomerators from the bottom through the flow distribution plate and exits from the top. The sound generators are air horns installed at the top of each agglomerator chamber. The sound frequency is 900 Hz and the sound level is 160dB. The length of the acoustic agglomerator is designed for one second of residence time. The 900 Hz frequency was chosen to avoid exciting lower resonant frequencies in the ductwork or structure of the power plant. These natural frequencies are generally on the order of 300 Hz. The sound intensity of 160dB ($1w/cm^2$) was chosen such that the particle agglomeration processes would be dominated by turbulent interactions.

Analysis of the grade efficiency obtainable with an electrocylcone based on the analytical model studies reveals that it is impractical to design an electrocyclone system to meet the EPA particulate limit. Instead, a three-stage configuration is employed to satisfy the gas turbine requirement, together with a baghouse downstream of the turbine to reduce the particulate emission to the EPA limit.

A combination of acoustic agglomerators and electrocyclones gives very high collection efficiency in collecting particles of all sizes, readily meeting the EPA limit as shown in Figure 5. In this application, acoustic agglomerators increase the collection efficiency of the 3-stage electrocyclone system from 98% to 99.92%. Figure 6 shows a typical layout of the gas cleanup system including the acoustic agglomerator units and electrocyclones.

Application To Pulverized Coal System

The gas cleanup systems for the pulverized coal system are designed to operate at 310°F and 1 atm. The reference plant is a 475 MW unit patterned after TVA's Bull Run Plant (10) and has a total flue gas flow of about 1.46×10^6 acfm. The estimated dust concentration is approximately 2.6 gr/scf (4700 ppm).

The electrocyclone for the PC system is a 12-foot size design with a nominal gas flow of 9.12×10^4 acfm. Sixteen parallel units in each of three stages are needed to handle the total gas flow. The internals and geometrical proportionality of the electrocyclone are similar to the one shown in Figure 3 except that the refractory and stainless steel liners are not required. Since the operating temperature is relatively low, electrical insulation for the high voltage electrodes will be less of a problem.

The acoustic agglomerator designed for the PC system is a 12-inch diameter tube 58 feet long. The length of the tube was designed for 1 second residence time. The design acoustic frequency is 860 Hz at a sound level of 160dB. The sound frequency and intensity are chosen for the same reasons as given for the AA design for the PFB system. Figure 7 shows the acoustic agglomerator system configuration and the tube arrangement.

Several particulate removal systems including combinations of acoustic agglomerators, conventional cyclones or electrocyclone and electrostatic precipitators were considered for the PC systems. Currently, most PC plants are built with electrostatic precipitators to control the plant particulate emission. Predictions based on the Deutch equation showed that with acoustic agglomerators, about 67% less plate area is required to meet the EPA emission standard. If conventional cyclones are used with acoustic agglomerators, a system consisting of a large (4 foot) size first stage cyclone followed by one stage of 10-inch multiclones could meet the EPA limit. The estimated particulate collection efficiency for this system is 99.45%. With electrocyclones alone, performance calculations showed that the number of stages (about 8 in series) required to meet the EPA requirement is impractical. With the acoustic agglomerators, only 3 stages of 12 foot electrocyclones (per path) are necessary to meet the EPA standard. The calculated performance for the three alternate systems (acoustic agglomeration plus electrostatic precipitation, conventional cyclones, or electrocyclone) is shown in Figure 8.

SYSTEM COST ESTIMATES

Component Costing

The cost estimates given here were developed by first estimating the cost of major components and then combining these elements into a complete system. Whenever possible, component costs were obtained from established vendors. In some cases (e.g., acoustic horns, D.C. power supplies) a cost allowance was added to upgrade an existing commercial unit to the desired specifications. Where no vendor cost data was available (i.e., electrocyclone, multiclone, and agglomerators) a design drawing was prepared. From that design drawing the quantities of various materials were computed. Unit costs for these materials

(i.e., carbon steel at $1.00 per lb), were used to develop the cost for that entire item. For conventional cleanup equipment, historical cost data published by EPA has been employed (11).

System Costing

Accurate estimates of installed cost for air pollution control equipment require either detailed engineering drawings or an extensive data base. The advanced designs under consideration in this study afford neither; thus, an alternate approach was taken. This was to assume that installation costs for particulate control parallel those for SO_2 scrubbers. The Tennessee Valley Authority has done extensive cost estimates for these SO_2 cleanup systems. In a recent presentation (12), they showed that the total capital investment could be ratioed to the equipment costs by a factor of 4.38. Using this method, costs for the capital investment of the various particulate cleanup options have been developed and are discussed in the following paragraphs.

Table II summarizes the installed costs for two particulate cleanup systems. System A comprises three stages of electrocyclones at high pressure and temperature, coupled with a conventional baghouse located downstream of the turbine as a final cleanup device. System B considers acoustic agglomerators to shift the particle size distribution so that electrocyclones can remove sufficient particles to meet the EPA NSPS. This option offers a saving of $9 Million installed cost, and considerable reduction in space required since the agglomerator is much smaller than the bag filter system.

TABLE II. 663 MWe PFB PARTICULATE CLEANUP SYSTEM COSTS

CLEANUP SYSTEM	ITEM	EQUIPMENT COST	INSTALLED COST
A. Electrocyclone/Baghouse	Electrocyclones	$12,700,000	$56,000,000
	Baghouse		29,000,000
	TOTAL		$85,000,000
B. Acoustic Agglomerator/ Electrocyclone	Agglomerator	4,600,000	$20,000,000
	Electrocyclones	12,700,000	56,000,000
	TOTAL		$76,000,000

Table III summarizes system costs for a 475 MWe pulverized coal plant. System A, the baseline cleanup system, is either an electrostatic precipitator or a bag filter system. For comparison, System B comprises an acoustic agglomerator coupled with a smaller ESP. The costs shown in Table IV show that the reduction in precipitator size and cost is not sufficient to offset the capital cost of the acoustic agglomerator. The cost of an electrocyclone system has not been shown in Table III as it offers no advantages for a pulverized coal application relative to a baghouse or precipitator.

TABLE III. 475 MWe PULVERIZED COAL PARTICULATE CLEANUP SYSTEM COST

CLEANUP SYSTEM	ITEM	EQUIPMENT COST	INSTALLED COST
A. Precipitator	ESP		$15,700,000
OR			
Baghouse	Baghouse		24,700,000
B. Acoustic Agglomerator/ Precipitator	Agglomerator	$5,100,000	$22,100,000
	ESP		8,100,000
	TOTAL		$30,200,000

SUMMARY AND CONCLUSIONS

The application of an electrostatically agumented cyclone to both a PFB and a conventional pulverized coal power plant has been investigated. This investigation revealed that three stages of electrocyclones would reduce the concentration of particles larger than 5μm to levels sufficient to protect the gas turbine from erosion in the PFB case. However, the NSPS limit on particulates could not be met in either the PFB or the PC cases with realistic assumptions regarding size, configuration or number of electrocyclones in series.

System cost studies show that the electrocyclone continues to offer an attractive cleanup system for the PFB application even if a baghouse must be added downstream of the gas turbine in order to meet the NSPS limit. The inability of the electrocyclone, as presently conceived, to effectively remove particles in the respirable range effectively eliminates it from consideration for pulverized coal power plant flue gas cleanup.

Studies of acoustic agglomeration have shown that at sound levels above 160dB (in the acoustic turbulence regime) a gas residence time of one second in the agglomerator chamber is sufficient to effectively agglomerate the respirable aerosol particles in either the PFB or PC cases. An agglomerator chamber coupled to either a conventional cyclone system (roughing cyclone plus two stages of 10" multiclones) or to 3 stages of 12-foot diameter electrocyclones could effectively meet the NSPS particulate limit. Alternatively, the acoustic agglomerator could reduce the plate area required in an electrostatic precipitator by 67%.

Cost studies of acoustic agglomeration applied to the PFB power plant indicate a potential cleanup system cost saving of 13% through elimination of the baghouse otherwise required with the electrocyclone base case. The potential cost saving with acoustic agglomeration is contingent on the development of a suitable low-cost acoustic driver, as no suitable commercial equipment presently exists.

Cost studies of the PC power plant indicate that acoustic agglomeration with cyclones, electrocyclones or ESP is non-competitive with a conventional

electrostatic precipitator or with a baghouse. This finding is consistent with the earlier study by Hegarty and Channon (13), despite a reduction in gas residence time made possible by the higher acoustic intensity.

ACKNOWLEDGEMENT

This work was supported by the Environmental and Safety Engineering Division of the U.S Department of Energy under Contract DE-AC02-79EV10143, Dr. Fred E. Witmer was the Project Technical Manager.

REFERENCES

1. Boericke, R.R., Hantman, R., and Kuo, J. "Assessment of Gas Turbine Erosion by PFB Combustion Products," proceedings 6th International Conference on Fluidized Bed Combustion, Atlanta, GA, April 9-11, 1980.

2. "Novel Methods for Respirable Dust Removal," Final Report, Contract DE-AC02-79EV10143, General Electric Co., Schenectady, NY, Sept., 1980.

3. Dietz, P.W. "Electrostatically Augmented Collection in Vortical Flows," (see this conference proceedings).

4. Dietz, P.W. "Collection Efficiency of Cyclone Separators," Report No. 79CRD244, Dec., 1979, General Electric Co., Schenectady, NY.

5. "Advanced Cleanup Device Performance Design Report (Task 4.3, Volume A - Cyclone Theory and Data Correlation," Report FE-2357-70, Contract DE-AC21-76ET10377, Oct., 1980, General Electric Co., Schenectady, NY.

6. Boericke, R.R. "Electrocyclone for High Temperature High Pressure Dust Removal," paper 81-0393, AIAA 19th Aerosapce Sciences, Jan. 12-15, 1981, St. Louis, MO.

7. Mednikov, E.P. Acoustic Coagulation and Precipitation of Aerosols, transl. from Russian by C.V. Larrick, Consultants Bureau, New York, 1965.

8. Shaw, D.T. Recent Development of Aerosol Science, Wiley-Interscience, 1978, Chap. 13, pp. 279-319.

9. "CFCC Development Program, Commerical Plant Design Definition," General Electric Co., Energy Systems Programs Department Report FE-2357-28, March, 1978 (Contract EX-76-C-01-2357).

10. "Bull Run Steam Plant," Tennessee Valley Authority No. 38, pp. 27-152, 1967.

11. "Particulate and SO_2 Emission Control Costs for Large Coal Fired Boiler," EPA-450/2-78-007, Feb., 1978.

12. Stephenson, C.D., and Torstrick, R.L. "The Shawnee Lime-Limestone Computer Program" presented at EPA's 5th Industry Briefing, Dec., 1979.

13. Hegarty, R., and Shannon, L.J. "Evaluation of Sonics for Fine Particulate Control," EPA 600/2-76-001, Jan., 1976.

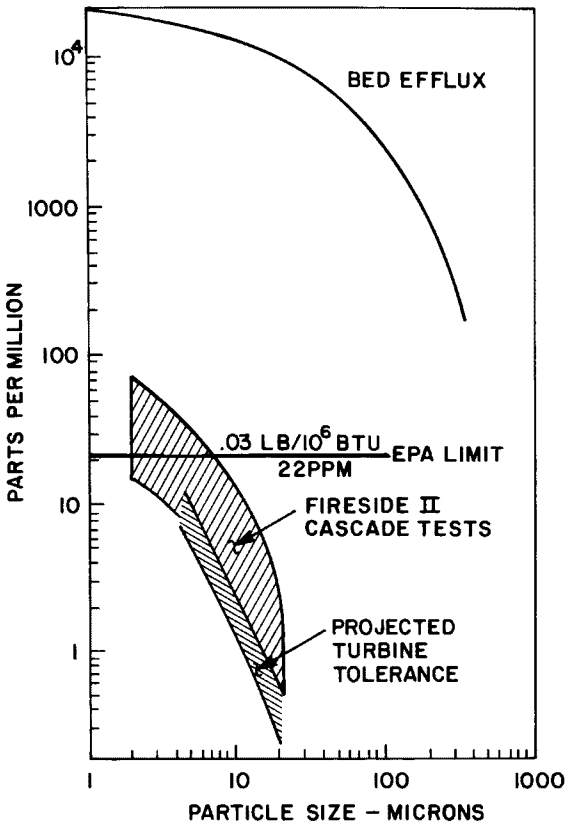

Figure 1. Allowable Dust Load to Prevent Turbine Erosion and to Meet EPA New Source Performance Standard

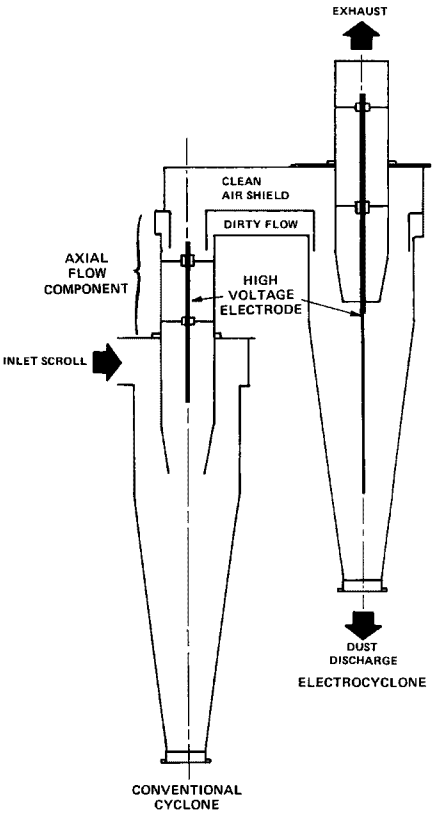

Figure 2. Electrocyclone Configuration

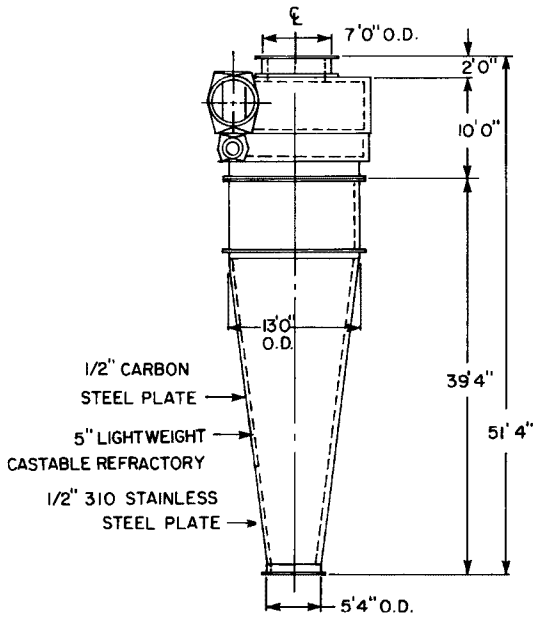

Figure 3. Electrocyclone Design for PFB Application

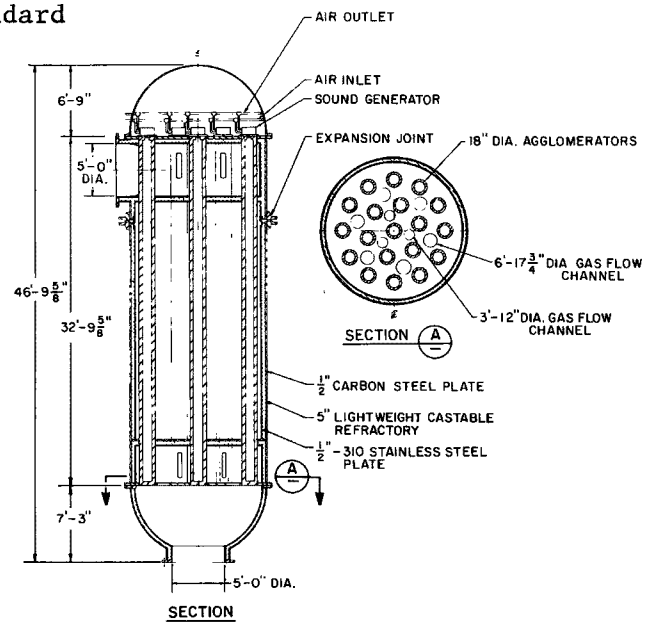

Figure 4. Acoustic Agglomerator Configuration for PFB Application

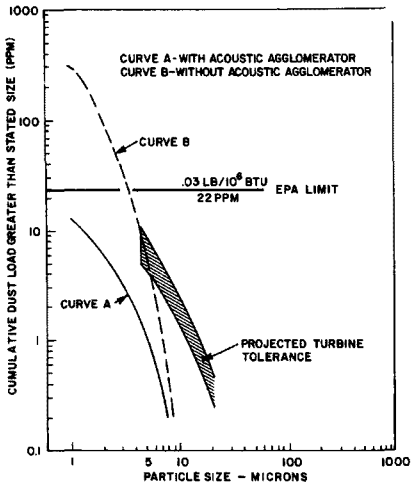

Figure 5. Three-Stage Electrocyclone System Performance

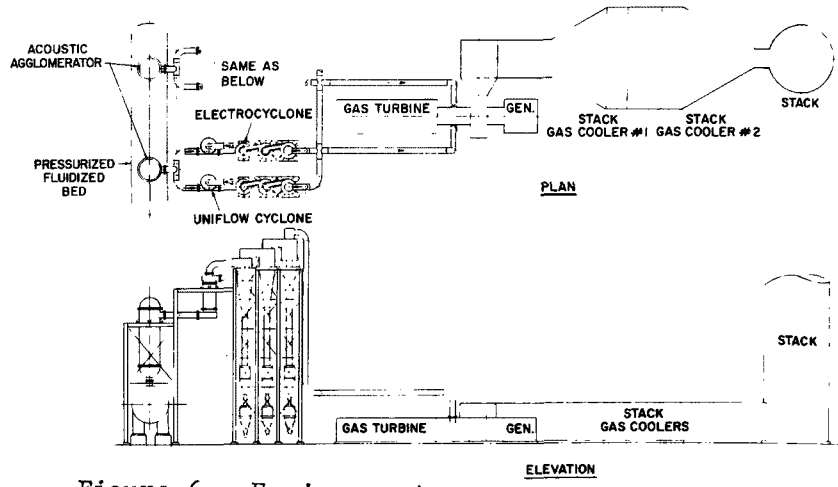

Figure 6. Equipment Arrangement For PFB System With Acoustic Agglomerator and Electrocyclone

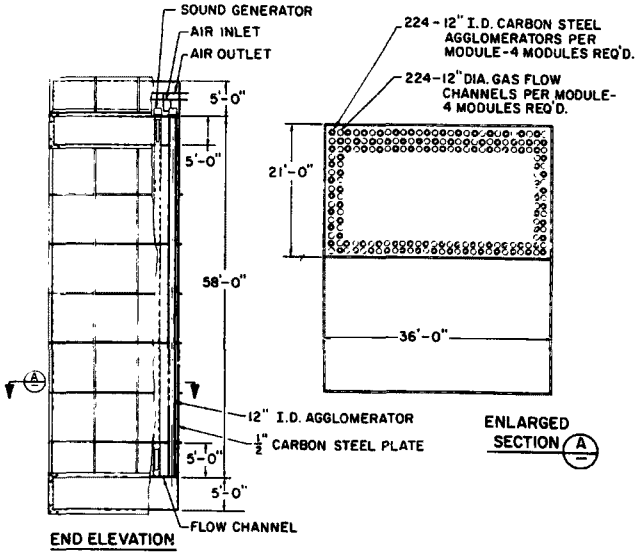

Figure 7. Acoustic Agglomerator Configuration for Pulverized Coal Application

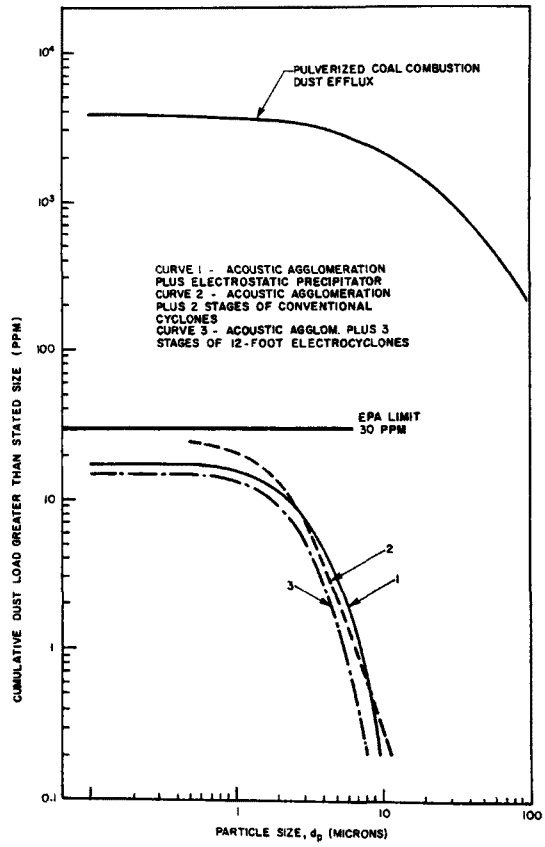

Figure 8. Particulate Removal Performance for PC Plant Using Acoustic Agglomeration with ESP, Cyclones, or Electrocyclones

THE ELECTROSCRUBBER* FILTER
APPLICATIONS AND PARTICULATE COLLECTION PERFORMANCE

By: David Parquet
Combustion Power Company, Inc.
A Weyerhaeuser Company
Menlo Park, California

ABSTRACT

The Electroscrubber Filter, used to remove particulate in dry form from gas streams, is a simple but dramatic improvement to Combustion Power Company's DRY SCRUBBER. Achieving "the best of both worlds" of the DRY SCRUBBER granular filter and electrostatic collection, the ELECTROSCRUBBER Filter utilizes a moving bed of filtering media and a pneumatic media recirculation and dust collection system, allowing self cleaning operation on a continuous basis. The concept development and principle of operation is discussed along with emission test data from selected applications.

INTRODUCTION

In 1974, Combustion Power Company started up on a small wood fired boiler its first DRY SCRUBBER. Since that first unit, CPC has installed collectors on numerous other applications. More significantly, as it pertains to the ever more stringent particulate emissions codes, a second generation filter was developed that retained the good points of the DRY SCRUBBER while much improving particulate collection performance, replacing the maintenance prone mechanical equipment of the former unit with a simple air blower, and reducing the cost of the unit as well. This new filter has only a single moving part and includes an electrostatic grid to augment the basic collection phenomena of the granular filter. The ELECTROSCRUBBER Filter can accept higher inlet loadings than the DRY SCRUBBER and will provide outlet loadings lower than New Source Performance Standard levels. High collection efficiencies are attainable on fine, submicron particulate.

ELECTROSCRUBBER FILTER PRINCIPLE OF OPERATION

Conceptually, as shown in Figure 1, the ELECTROSCRUBBER Filter consists of a cylindrical vessel containing two concentric louvered cylindrical tubes. The annular space between the tubes is filled with pea-sized gravel media. The particulate-laden exhaust gas enters the filter through appropriate breeching and is distributed to the filter face by the plenum section formed by the inner louver cylinder. Dirty gas is passed through the filter media at velocities ranging from 100 to 150 feet per minute and the particulate is removed from the gas stream by impaction with the media. Clean gases exit to downstream breeching or directly to the atmosphere through a free-standing exhaust stack that can be added to the top of the ELECTROSCRUBBER Filter unit.

* Registered U.S. Patent & Trademark Office

To prevent a filter cake from forming on the face of the filter, and the resulting potential plugging problems and high pressure drop, the filtering media is continuously, but slowly (six to ten feet per hour), moved downward in plug or mass flow. The resulting churning action across each louver opening prevents a filter cake from forming. To provide complete cleaning of the louver face, the louvers are designed so that some of the media is pushed through each louver opening thus preventing any bridging or buildup of particulate material.

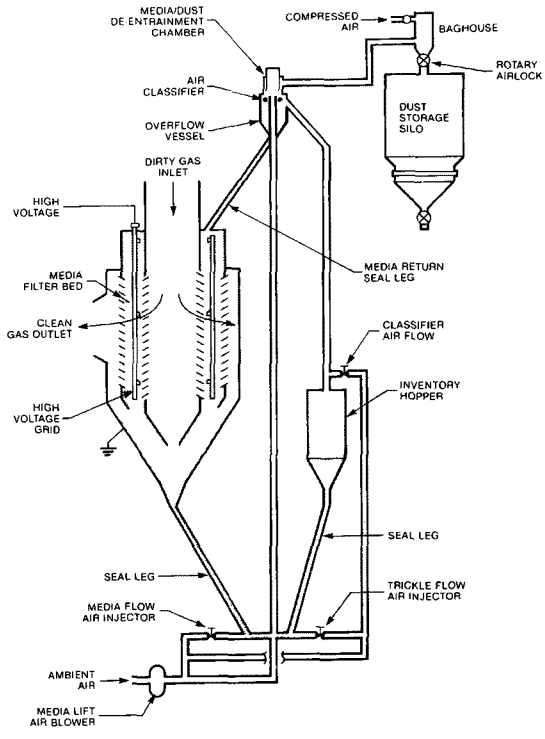

Figure 1 ELECTROSCRUBBER Filter Flow Schematic

The particulate-laden media is continuously removed at the bottom of the ELECTROSCRUBBER Filter where it is transported by a pneumatic conveying system to the media/particulate de-entrainment section of the system. The action of the media being transported vertically in the pneumatic lift pipe separates the particulate from the media so that the particulate can be pneumatically removed from the de-entrainment section for pneumatic transport to a particulate separation and storage silo. The clean media then drains by gravity from the de-entrainment section and is returned to the top of the ELECTROSCRUBBER Filter unit for recycling.

The ELECTROSCRUBBER Filter module is designed to operate full of media at all times. To accomplish this, the media overflow vessel, as shown in Figure 1, is used to assure that the freeboard section of the ELECTROSCRUBBER Filter module remains full and to eliminate any differential media flow down to the two media return pipes. Excess media is returned from the media level control section by the media overflow pipe to the media inventory hopper. Media from this hopper is continuously "trickle" fed back into the media lift pipe to provide an oversupply of media to the media overflow vessel to assure that the ELECTROSCRUBBER Filter module is always completely full of media. Air is piped from the media lift air blower into the lower portion of the media overflow pipe to provide purge air up this pipe which prevents any residual dust from re-entering the top of the ELECTROSCRUBBER Filter.

An electrical conductor, configured in the form of a cage, is positioned within the media bed of the ELECTROSCRUBBER Filter as shown in Figure 2. A high voltage is applied to this conductor and the electrical field generated between the conductor and the inlet and outlet louvers enhances the collection of the particulate in the gas stream, greatly increasing the efficiency of

the basic granular filter system. (See Figure 3). This enhancement phenomenon relies on the fact that industrial processes produce particulate with slight positive or negative charges. Put simply, the electrical field greatly increases the probability that the particulate will impact with a piece of media in its long, tortuous path through the filter. As also seen in Figure 3, electrostatic augmentation of particulate collection is especially pronounced on the fine, submicron particulate.

The ELECTROSCRUBBER Filter provides extremely high collection efficiency with very low pressure drop, collects particulate in a dry form and, because of the large heat sink provided by the filtering media, the propagation of an explosion or fire is eliminated under all conditions within the ELECTROSCRUBBER Filter. And, because it is not required that the charge of the particulate be changed to allow collection (as in an electrostatic precipitator), the ELECTROSCRUBBER Filter is insensitive to such particulate characteristics as resistivity. Power requirements for the electrostatic grid are typically only 10 to 20 watts per 1000 acfm.

APPLICATIONS HISTORY

As of March, 1981, DRY SCRUBBERS and ELECTROSCRUBBER Filters have had experience on five separate applications including boilers burning wood, salt-laden wood, coal, or combination fuels; lime kilns; coke calciners; municipal solid waste incinerators; and steel sinter machines. As shown in Table 1, a total of 117 separate filters have been or are being installed at 25 sites for a total of over 8 million acfm.

In the Application Summaries (AS) that follow, selected test data has been presented with the intention of

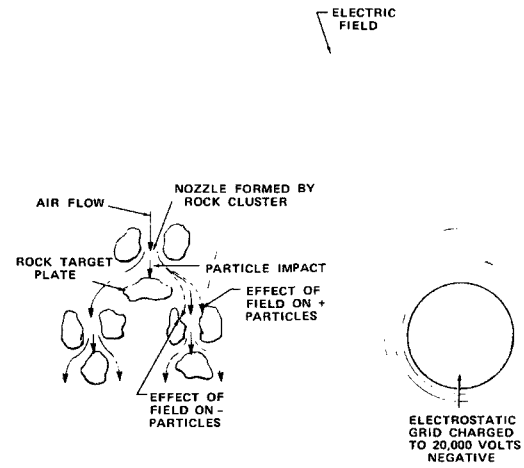

Mechanical Impaction Mechanism of Particulate Collection in a Granular Filter Augmented by Electrostatic Field

Figure 2 ELECTROSCRUBBER Filter High Voltage Particulate Collection Concept

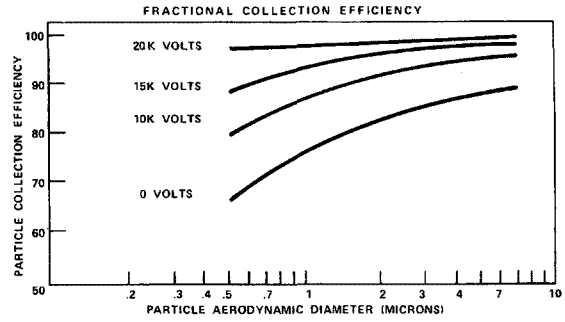

Figure 3 Typical Effect of Voltage on Fractional Efficiency of Particulate Collection. (Example is from a Wood Boiler ELECTROSCRUBBER Filter

TABLE 1. DRY SCRUBBER & ELECTROSCRUBBER FILTER INSTALLATION SUMMARY

Application	Quantities Sites/ Filters	Total Gas Flows (acfm) In Operation	In Startup	In Construction	Total
Boilers					
Wood	13/48	2,040,000	443,000	546,000	3,029,000
Wood (salt)	2/6	300,000		223,000	523,000
Coal	2/4	346,000			346,000
Coal/wood	2/28			960,000	960,000
Lime Kilns	2/3	262,000			262,000
Coke Calciners					
Cooler	2/2	40,000	95,000		135,000
Kiln Gas	1/2			220,000	220,000
MSW Incinerator	1/2		90,000		90,000
Steel Sinter Plant	3/22	781,000		1,740,000	2,521,000
	28/117	3,769,000	628,000	3,689,000	8,086,000

presenting the reader with a cross-section of ELECTROSCRUBBER Filter capabilities. Note that when the term "DRY SCRUBBER" is used, it refers to the filter schematically shown in A.S. No. 1. The granular filter section is identical to that already described. The DRY SCRUBBER, however, the predecessor of the ELECTROSCRUBBER Filter, utilized a vibrating screen-type dust removal system and a bucket elevator to transport the media back to the top of the module filter area.

A.S. No. 1 is a DRY SCRUBBER which had an electrostatic grid retrofitted into the media cavity on a wood fired boiler application. A.S. No. 2 depicts full scale pneumatic ELECTROSCRUBBER Filter performance on the same application. A.S. No. 3 and No. 4 show ELECTROSCRUBBER Filter fine particulate performance as demonstrated with a mobile 500 acfm test unit and with a stationary 7000 acfm test unit, respectively, on two diversely different applications. A.S. No. 5 compares the performance of a DRY SCRUBBER with a grid retrofit operating on a pulverized coal boiler to the performance of the ELECTROSCRUBBER Filter 7000 acfm test unit. A.S. No. 6 provides a similar comparison for a lime kiln application. These summaries clearly portray the ELECTROSCRUBBER Filter as a versatile, high performing system fully capable of meeting the difficult requirements of diverse applications.

APPLICATION SUMMARY NO. 1

APPLICATION: WOOD FIRED BOILER
MAXIMUM DESIGN GAS FLOW: 50,000 acfm
DUST COLLECTOR: 1 DS400 DRY SCRUBBER RETROFITTED WITH ELECTROSTATIC GRID IN SEPTEMBER 1978

The DRY SCRUBBER granular filter was invented in 1973 and was installed on this wood boiler application in 1974. At that time, lenient pollution codes did not require the stringent outlet loadings of today's requirements. During the last seven years, however, the ever more difficult requirements caused CPC to re-evaluate and improve its technology. After extensive lab tests the first improvement, the electrostatic grid, was developed and retrofitted into this first DRY SCRUBBER unit in order to demonstrate its capability on an operating system. (The second improvement, the pneumatic media recirculation and ash collection system, was not retrofitted into this unit). As shown below, the performance of the grid was marked: outlet loading reduced by a factor of five to 0.01 gr/dscf and outlet opacity reduced by a factor of eight to clear stack opacity. Grid power consumption was typically only 400 to 1000 watts.

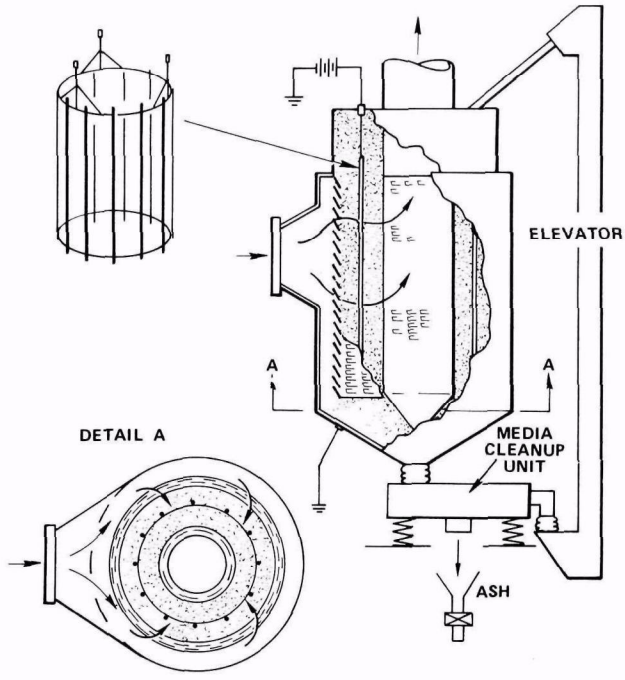

Retrofit of Electrostatic Grid into DRY SCRUBBER with Mechanical Media Recirculation of Ash Collection System

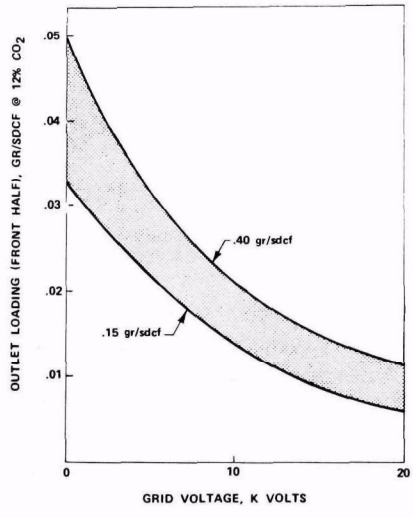

Outlet Loading vs. Grid Voltage and Inlet Loading

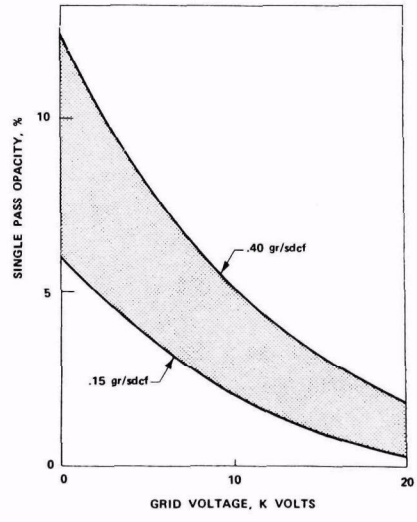

Single Pass Opacity vs. Grid Voltage and Inlet Loading

APPLICATION SUMMARY NO. 2

APPLICATION:	WOOD FIRED POWER BOILER
CAPACITY:	550,000 pph @ 30% MOISTURE HOGGED FUEL
MAXIMUM DESIGN GAS FLOW:	420,000 acfm @ 345 F
DUST COLLECTOR:	3 ES250-4 ELECTROSCRUBBER FILTERS
STARTUP:	SEPTEMBER 1979

After an extensive economic tradeoff analysis against alternative particulate collection technologies and a test and demonstration program that included the grid retrofit program discussed in A.S. No. 1, this ELECTROSCRUBBER Filter system was designed for and installed on the (then) largest 100% wood waste fired boiler in the world. These filters included the pneumatic media recirculation and ash collection system that had been in development in CPC's test labs since 1974. After startup in 1979, the filter system has NEVER caused the boiler to go down in over a year and a half of operation. Performance is shown below for good fuel (normal wetness, summer quality) and for poor fuel (reclaimed, high moisture). The results show trends not typical of other particulate collectors, that is, outlet loading remains constant even though steaming rate and inlet loading are increasing. The emissions from this ELECTROSCRUBBER Filter system have been tested both by the user and the EPA with similar results.

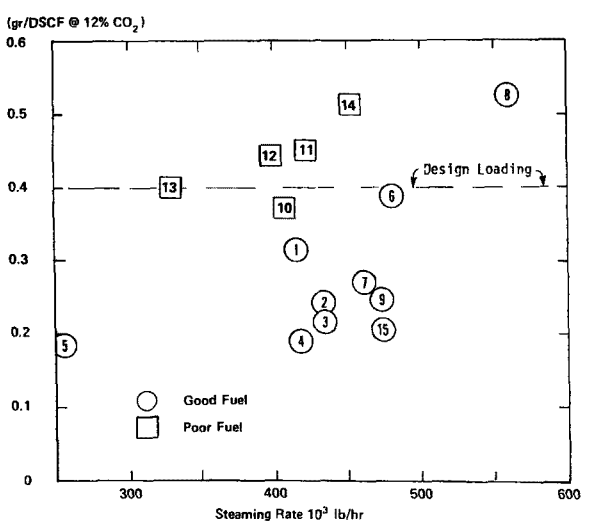

1980 Test Data: Inlet Loading vs. Steaming Rate

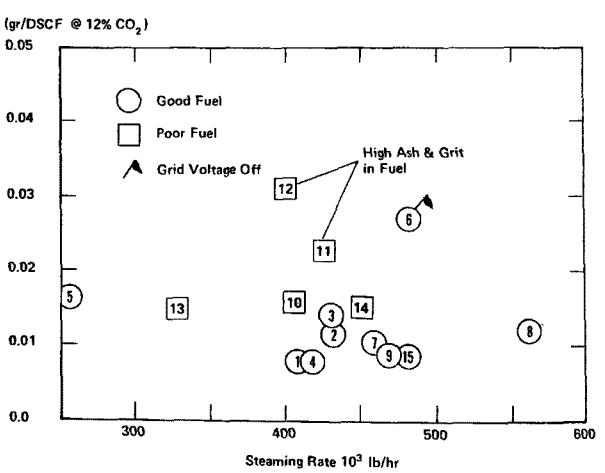

1980 Test Data: Outlet Loading vs. Steaming Rate

APPLICATION SUMMARY NO. 3

APPLICATION: SALT LADEN WOOD FIRED BOILER TEST PROGRAM
FINE PARTICULATE COLLECTION (50% $< 1.6\ \mu$)
TEST DATE: MARCH 1980

In March 1980, CPC sent its 500 acfm ELECTROSCRUBBER Filter mobile test unit for demonstration testing on a wood boiler fired with hogged bark from logs floated in sea water. The application is a particularly difficult one in that the particulate is primarily salt (60±% salt, 40±% ash) and has a very high proportion of submicron material. As has been reported elsewhere, the salt-laden ash was a troublesome material for the DRY SCRUBBER. First, simply stated, the vibrating screen used on those filters did not thoroughly remove collected particulate from the media, thus recycling it back into the filter area and causing buildup. Second, the large portion of submicron material was difficult for the filter to capture, resulting in rather high outlet opacities. The curves and table below demonstrate the effectiveness of the improvements made to the ELECTROSCRUBBER Filter. Since a large portion of the particulate was submicron, the effectiveness of the electrostatic grid was particularly evident.

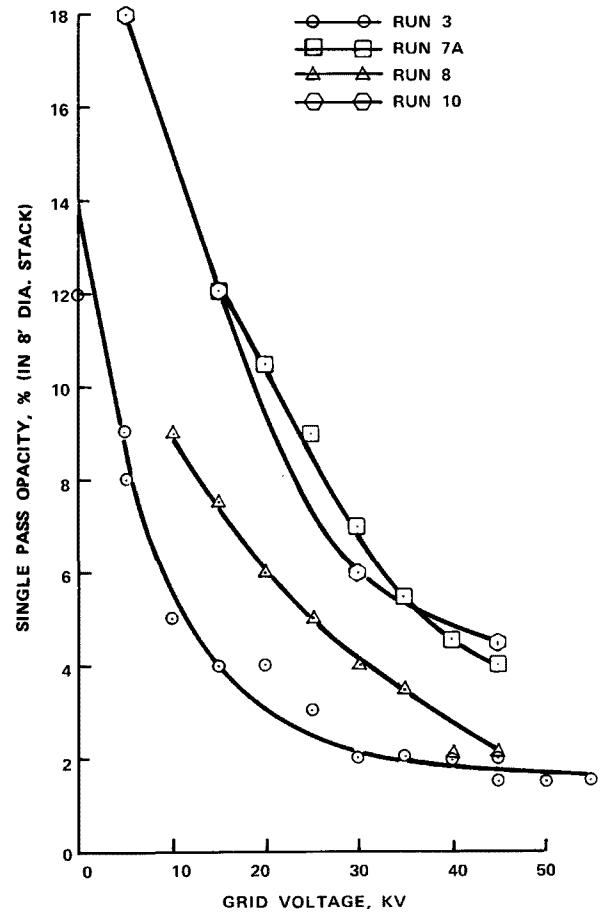

Outlet Opacity vs. Grid Voltage

SUMMARY OF PARTICULATE EMISSIONS TEST

Run No.	Gas Flow (acfm)	Grid Voltage (kV)	Inlet Dust Loading (gr/dscf @ 12% CO_2)	Outlet Dust Loading (gr/dscf @ 12% CO_2)	Efficiency (%)	Single Pass Opacity (%)
1	570	45	0.283	0.010	97	--
2	570	45	0.271	0.015	94	--
3	560	45	0.399	0.024	94	2
4	560	45	0.325	0.011	97	2
5	520	45	0.357	0.020	94	3
6	530	0	0.329	0.088	73	10-30*
7	560	45	0.412	0.027	93	2
7A	~800	45	--	--	--	4
8†	--	--	--	--	--	--
9	540	45	0.513	0.013	98	3
10δ	570	45	0.855	0.012	99	5
11†	--	--	--	--	--	--

* Actual value uncertain but significantly higher than other runs.
† Particulate sizing only.
δ Blowing soot during entire run.

PROCESS CONDITIONS: Gas temperature: 400 F; Mean particle size tests 1-8: $1.6\ \mu$; Mean particle size tests 9-11: $5\ \mu$; Average NaCl content in fuel: 0.32%; Average moisture in fuel: 44%.

APPLICATION SUMMARY NO. 4

APPLICATION: STEEL SINTERING MACHINE TEST PROGRAM
FINE PARTICULATE COLLECTION (80% < 1 μ)
TEST DATE: MAY 1980

For this application, the application's process parameters were very closely duplicated on a 7000 acfm ELECTROSCRUBBER Filter stationary test unit at CPC's test labs. In the actual sintering process, the customer had developed a method of adding calcium chloride to the sinter mix to reduce the alkali content of the sinter material for the blast furnace. The process is successful, but the particulate released is almost entirely submicron potassium chloride (KCl). As shown, a KCl fume generator produced particulate as high as 90% in the submicron range with inlet loadings averaging 0.26 gr/acf. Two of the data sets presented below clearly demonstrate the effect of the electrostatic grid. It is interesting to note that the highest power required for the grid occurred during the 75 kV test and was less than 8 watts/1000 acfm.

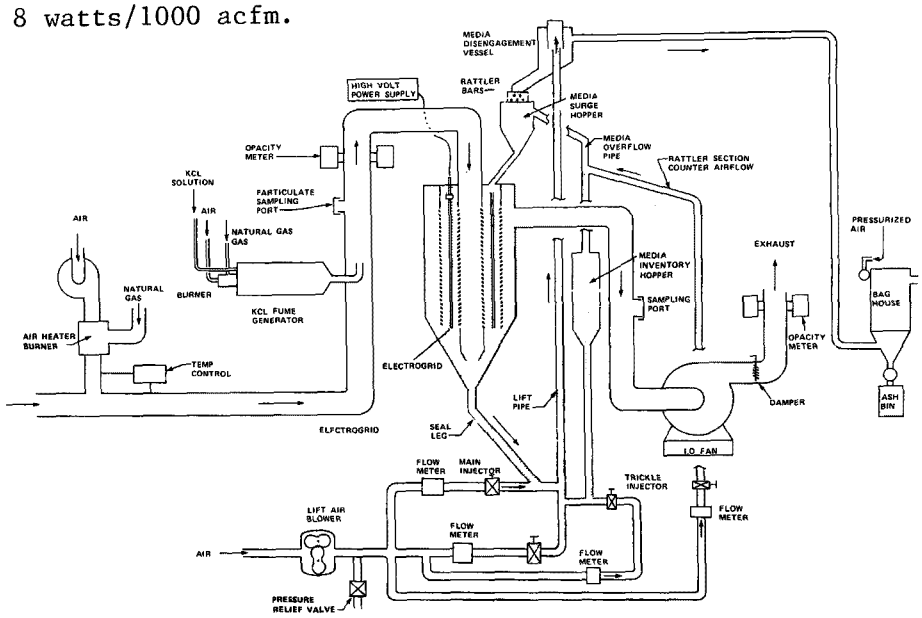

Schematic of 7000 acfm ELECTROSCRUBBER Filter Stationary Test Unit

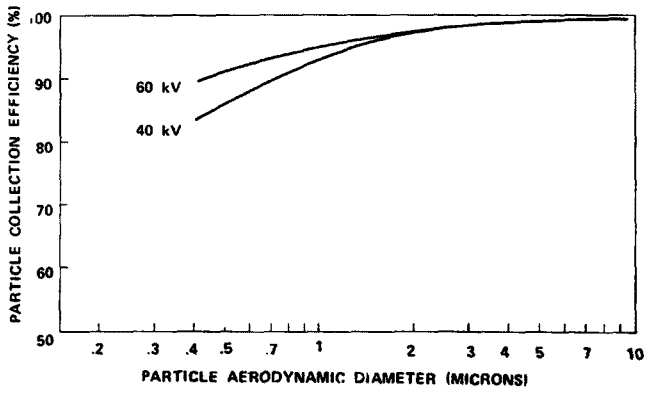

Fractional Particulate Collection Efficiency vs. Grid Voltage.

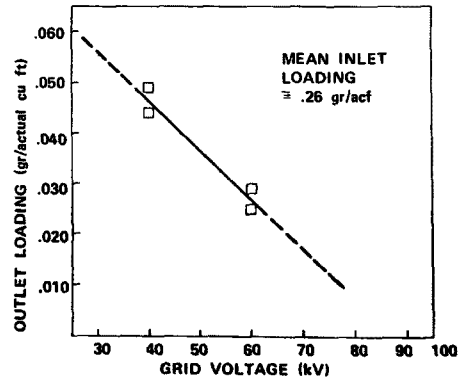

Outlet Loading vs. Grid Voltage

APPLICATION SUMMARY NO. 5

APPLICATION: PULVERIZED COAL FIRED BOILER

In 1977, two DRY SCRUBBER filter units were installed on a pulverized coal fired boiler. After startup, it was determined that the filter panel area many times had inlet loadings higher than expected causing the filter to "saturate" or to run with characteristics detrimental to the health of the unit. A resultant effect was an outlet loading higher than allowable. Similar to A.S. No. 1, electrostatic grids were retrofitted into these units with the results as shown in the first table below. When the inlet loading to the filter panel is below an allowable level, the filter provides below-code performance.

The second table below presents the performance of the improved ELECTROSCRUBBER Filter as demonstrated on the 7000 acfm stationay test unit described in A.S. No. 4. As has been suggested, there are many other features in the ELECTROSCRUBBER in addition to the electrostatic grid and the pneumatic media cleanup system which result in reduced outlet loading for greatly increased inlet loadings.

SUMMARY OF PARTICULATE EMISSIONS TESTS ON 2 DS600C DRY SCRUBBERS STARTED UP IN NOVEMBER 1977 AND RETROFITTED WITH ELECTROSTATIC GRID IN AUGUST 1979

2 DS600C DRY SCRUBBERS	DRY SCRUBBERS before Grid Installation	DRY SCRUBBERS after Grid Installation
Gas Flow	134,000 acfm	124,000 acfm
Gas Temperature	425 F	425 F
Scrubber ΔP	6-7 in. H_2O	6 in. H_2O
Inlet loading	0.45 gr/acf	0.46 gr/acf
Grid voltage	0	20,000 volts
Actual outlet loading	0.134 gr/acf	0.023 gr/acf
Allowable outlet loading	0.067 gr/acf	0.067 gr/acf
Collection efficiency	70%	95%

SUMMARY OF PARTICULATE EMISSIONS TESTS ON PULVERIZED COAL FIRED DUST WHEN TESTED IN 7000 ACFM ELECTROSCRUBBER FILTER STATIONARY TEST UNIT

Gas Flow (acfm)	Temp (F)	Grid Voltage (kV)	Grid Current (ma)	Inlet Loading (gr/acf)	Outlet Loading (gr/acf)	Efficiency (%)	Outlet Opacity Double Pass (%)
6450	290	20	0.4	0.530	0.008	98.5	3.7
6670	290	20	0.4	1.864	0.012	99.4	3.0
6600	300	20	0.4	3.387	0.024	99.3	3.5

APPLICATION SUMMARY NO. 6

APPLICATION: LIME KILN

In 1977, a DRY SCRUBBER unit was started up on a small 200 ton per day lime kiln. Although the unit regularly collected between 800 and 1000 pounds per hour of particulate, the outlet loading was not consistently below regulatory requirements. After making some other modifications, an electrostatic grid was installed in the unit and activated in 1979. As shown in the first table below, the performance improved dramatically. Since the retrofit, the unit continues to consistently provide below-code outlet loadings at power levels of less than 10 watts per 1000 acfm.

The second table below presents the performance of the improved ELECTROSCRUBBER Filter as demonstrated on the 7000 acfm stationary test unit described in A.S. No. 4. As has been suggested there are many other features in the ELECTROSCRUBBER Filter in addition to the electrostatic grid and pneumatic media cleanup system which produce very low outlet loadings at high inlet loadings. Note that for lime dust, voltages much in excess of 30 kV could be used which would result in even lower outlet loadings.

SUMMARY OF PARTICULATE EMISSIONS TESTS ON 1DS400C DRY SCRUBBER STARTED UP IN NOVEMBER 1977 AND RETROFITTED WITH ELECTROSTATIC GRID IN NOVEMBER 1979

1 DS400C DRY SCRUBBER	DRY SCRUBBER (before Grid Installation)	DRY SCRUBBER (after Grid Installation)†		
Grid voltage (kV)	N/A	10 kV	20 kV	30kV$^{\delta}$
Gas flow (acfm)	36,000	37,792	41,182	37,724
Gas Temperature (F)	375	375*	375*	375*
DRY SCRUBBER ΔP (in. H_2O)	7.5	7.6*	7.7*	7.6*
Inlet loading (gr/acf)	2.6	3.26	3.04	3.18
Actual outlet loading (gr/acf)	.08	.030	.026	.022
Allowable outlet loading (gr/acf)	.10	.090	.092	.090
DRY SCRUBBER collection efficiency (%)	96.9	99.08	99.15	99.31

* Estimated

† Grid current drain less than 10 ma in all cases

$^{\delta}$ Higher voltages possible

SUMMARY OF PARTICULATE EMISSIONS TESTS ON LIME DUST WHEN TESTED IN 7000 ACFM ELECTROSCRUBBER FILTER STATIONARY TEST UNIT

Gas Flow (acfm)	Grid Voltage (Kv)	Inlet Dust Loading (gr/acf)	Outlet Dust Loading (gr/acf)	Efficiency (%)	Opacity (%)
6900	0	0.7	0.02	97.7	8
6400	20	0.7	0.004	99.3	1
6000	0	6.6	-	-	19
6000	20	6.6	-	-	2
6000	30	6.6	-	-	<1

HIGH EFFICIENCY PARTICULATE REMOVAL WITH SINTERED METAL FILTERS*

By: B. E. Kirstein, W. J. Paplawsky and D. T. Pence
Science Applications, Inc.
4030 Sorrento Valley Boulevard
San Diego, California 92121

T. G. Hedahl
EG&G Idaho, Inc.
P.O. Box 1625
Idaho Falls, Idaho 83415

ABSTRACT

Because of their particle removal efficiencies and durability, sintered metal filters have been chosen for high efficiency particulate air (HEPA) filter protection in the off-gas treatment system for the proposed Idaho National Engineering Laboratory Transuranic Waste Treatment Facility. Process evaluation of sintered metal filters indicated a lack of sufficient process design data to ensure trouble-free operation. Subsequence pilot scale testing was performed with flyash as the test particulate. The test results showed that the sintered metal filters can have an efficiency greater than 0.9999999 for the specific test conditions used. Stable pressure drop characteristics were observed in pulsed and reversed flow blowback modes of operation. Over 4900 hours of operation were obtained with operating conditions ranging up to approximately 90°C and 24 vol% water vapor in the gas stream.

INTRODUCTION

Transuranic Waste Treatment Facility

During the past 26 years, thousands of tons of nuclear waste contaminated with transuranic (TRU) elements have been stored or buried at the Idaho National Engineering Laboratory (INEL). This waste, composed of both combustible and noncombustible materials, may be retrieved, processed, and shipped to a federal repository for permanent disposal. An attractive method for processing this waste is to convert it by means of a high temperature slagging pyrolysis incinerator (SPI) process into an inert, basalt-like solid that encapsulates the TRU elements. The SPI has been selected as a processing method to be incorporated into the INEL Transuranic Waste Treatment Facility (TWTF) (1).

---

*Work performed under USDOE Contract EY-76-C-07-1570

The major process operations in the TWTF will be waste receiving, waste preparation, incineration, slag handling, and off-gas treatment. The Waste Processing Building will incorporate the latest available technology in waste handling, fissile material assaying, criticality control, instrumentation, off-gas cleanup, remote operation/maintenance, and decontamination. Process equipment generally will be operated remotely using both local and central controls.

A key to ensuring safety and environmental acceptability for the TWTF is an efficient off-gas treatment system. The off-gas treatment system for the TWTF must establish effective control of radioactive and other potentially harmful airborne materials. Various off-gas treatment technologies were evaluated with respect to fine particle recovery for use in the TWTF. A detailed evaluation of the material balance of the incinerator off-gas stream indicated that high efficiency particulate air (HEPA) filters alone would become overloaded and plug after approximately 1/2 hour of operation. Therefore, some type of continuous particulate recovery equipment would be required in the off-gas treatment system.

The removal efficiencies of venturi scrubbers fall off rapidly for particles with aerodynamic diameters below about 1 μm, which makes their use impractical for this application. Electrostatic precipitators (ESP) also do not appear to have sufficient fine particulate removal efficiencies, and the design of an ESP requires far more information about the incinerator particulate than is available. Bag filters do not have a sufficiently fine particulate recovery efficiency for this application, and further, pose other safety problems for a secure radioactive materials off-gas treatment system. A dry off-gas treatment system using sintered metal filters (SMFs) was selected for development and design, based on SMFs high particulate removal efficiency, reduced maintenance (possibly in a remote environment), and absence of any secondary contaminated liquid waste. However, the lack of adequate design information for SMF's necessitated a pilot scale test program to verify the reported fine particulate recovery efficiencies and operating conditions. The description of this program is presented in the sections that follow.

Background of Sintered Metal Filters

The use of SMFs to remove particulate from a gas stream has been practiced for over 25 years (2). Yet, in this time, quantitative design equations have not been developed nor has a satisfactory explanation been given of how the filters operate without plugging over long operating times. These filters have been used in a variety of nuclear applications that are only partially documented with respect to operating conditions and particulate characterization. Industrial experience with SMFs is virtually nonexistent in the literature. While it is known that there are industrial users, limited contact with these users reveals their desire not to advertise certain aspects of their manufacturing processes. In the presentation that follows, experimental results are provided describing the operation of SMFs to remove flyash from a gas (air) stream where the primary objective was to obtain stable operation with respect to pressure drop and to obtain high particle removal efficiencies. These results were then used in the conceptual design of an off-gas treatment system for a radioactive processing facility that uses a SPI as described earlier.

EXPERIMENTAL PROGRAM TO TEST SINTERED METAL FILTERS

Purpose

The primary objective of the SMF test program was to verify the applicability of the filters in the INEL TWTF off-gas treatment system. Two criteria that were considered necessary for applying SMFs were particulate removal efficiency and stable pressure drop. The particulate size distribution used in the tests had to match or be finer than that expected from the SPI. The pressure drop requirements were stable operation at as low a pressure drop as practicable. A further objective was to test both blowback methods to determine any advantage of one over the other with respect to obtaining these primary objectives.

Basic System Description

The pilot plant apparatus used for evaluating the performance of the SMFs is shown in Figure 1. The major design considerations in the use of SMFs involve controlling the gas flow through the filter and providing blowback to clean the filter. A blower supplies air to the apparatus in which flyash is redispersed by an air ejector. The air/flyash mixture flowrate is measured and controlled prior to the filter vessel. Six cylindrical SMFs were installed in the vessel, with filter exhausts manifolded to provide a single off-gas stream for sampling. Total collection filters, or in-line filters, were used to quantitatively collect all entrained particles for SMF efficiency measurements.

An auger feeder gradually adds flyash to the ejector apparatus, which is supplied by an external pressurized 310 kPa air supply. The ejector consists of a stainless steel tube inserted in a tee to provide the aspirating action necessary to finely disperse the flyash into the gas stream. Gas flow measurements were accomplished using venturi and pitot tubes. The gas flow rate was maintained at an essentially constant value of 1.25 normal cubic metres per minute (Nm^3/min).

The main air supply is provided by a regenerative blower. The total flow from the blower is split into two streams: a main flow to the filters and a vent flow used to control the main flow rate. As filter pressure drop increases with time for a specified flowrate, the vent valve position provides the control variable necessary to maintain the desired flow.

The tested SMFs were cylinders 0.91 m long by 6.8 cm OD with a 0.15-cm wall thickness. The porosity of the filters was 0.5 absolute. One end of each filter element is capped, and the other end is connected to exit gas piping. Six filters were installed in a vessel 34.5 cm in diameter by 1.03 m long. A 60-degree cone was welded to the bottom for particulate collection following blowbacks.

The most important operating variable for an SMF appears to be the superficial velocity. The recommended superficial velocity determined by experience is usually 1.2 to 2.1 m/min, or sometimes even less, even though pressure drop versus superficial velocity for clean filters is advertised at considerably greater velocities (3,4).

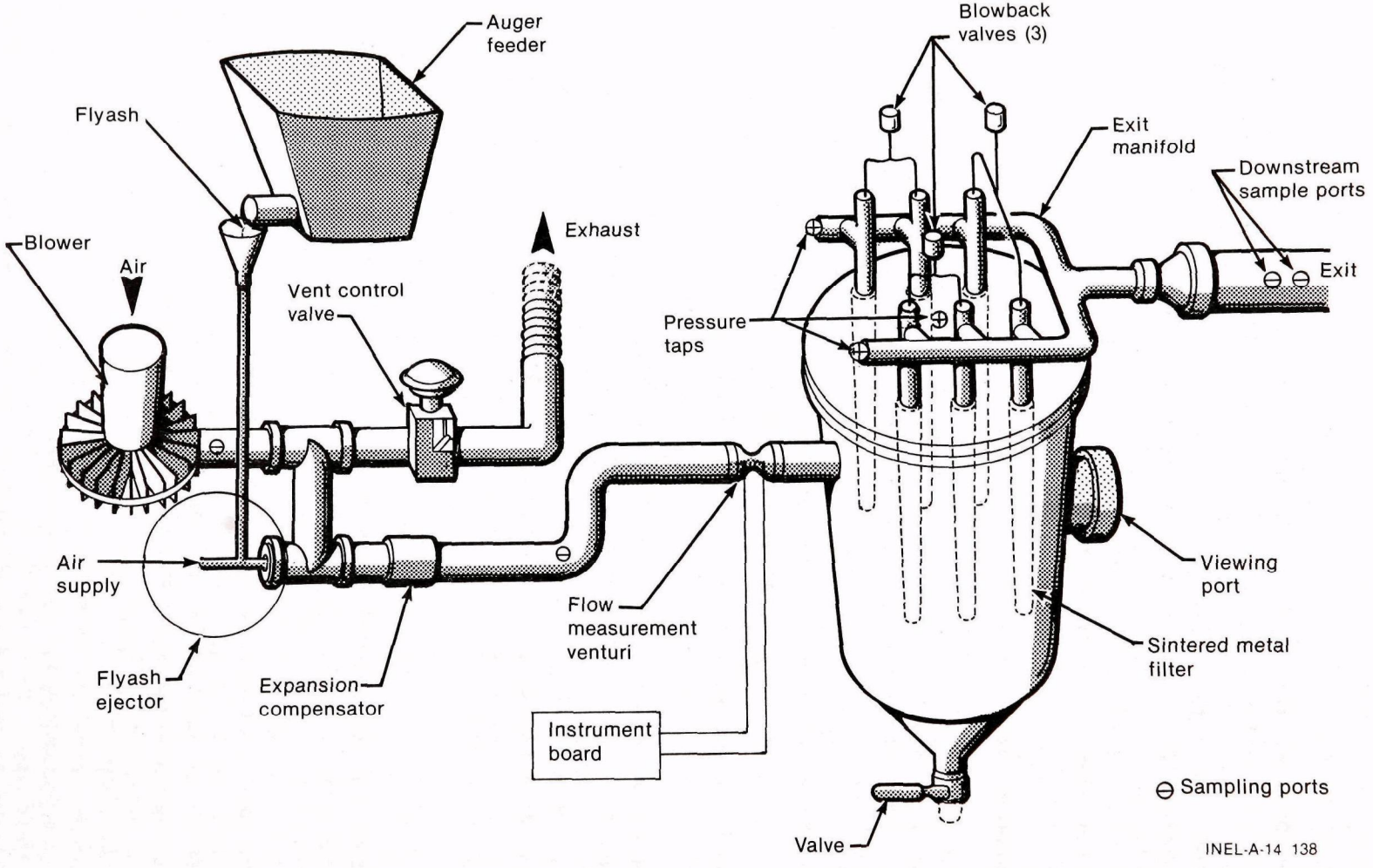

Figure 1. General Schematic of Pilot-plant apparatus for testing sintered metal filters.

During operation of the pilot plant system, the gas and particles enter the filter vessel such that the inlet stream does not impinge directly on a filter surface. A baffle was installed to distribute the gas and particles into the vessel. The gas and particles flow to the surface of the filter where the particles are collected, and the gas flows through the filter element. A pressure drop results due to the gas flow resistance of the porous metal and filter cake. The pressure drop increases with time due to the increasing cake thickness. When the pressure drop reaches a prescribed value (depending on the test), blowback is initiated.

Two blowback techniques were tested and evaluated based on literature (5,6) and vendor information: pulsed and reverse flow. In the pulsed blowback method, a tube or nozzle is directed to the filter exit. During blowback, a pulse of approximately 414 kPa air was delivered to a pair of filters for a fraction of a second through the blowback valves. Two filters were blown at a time with a 20-sec pauses between pulses until all filters were cleaned. During the series of SMF tests, the effect of blowback nozzle tube diameter was also investigated.

The reverse flow method uses a secondary air system (1.4 m^3/min regenerative blower) which operates continuously. During SMF loading, exhaust valves remain open and the reverse flow air is vented; the blowback air supply valves remain closed. When blowback is initiated (pressure drop controlled) the exhaust valves close and the blowback valves are opened, thus diverting the reverse flow blowback air through the filter set and into the vessel. This flow configuration is applied to two SMFs at a time for approximately 3 sec. The other pairs of filters are then sequentially blown back at 30-sec intervals.

Test Program (7,8)

Particulate Size Distribution and Loading

The particulate size distribution and loading of the redispersed flyash reaching the SMFs were measured by sampling after the filter vessel when no filters were installed. The reason for obtaining these measurements in this manner was that the filter vessel had an efficiency for particulate removal of about 60% for the flyash used. The filter efficiencies reported here are based on these downstream measurements to ensure that artificially high results are not reported.

The particulate size distribution expected from the SPI system is characterized by 100 wt% less than 32 μm in aerodynamic diameter, 50 wt% less than 10 μm, and 0.1 wt% less than 1 μm. The redispersed flyash that reached the SMFs in the laboratory system was finer than the incinerator par- ticles below 10 μm as measured by a cascade impactor. The particulate loadings to the filters were in the range of 3 g/Nm^3 with an initial flyash injection rate of 10 g/min into a gas flowrate of 1.25 Nm^3/min.

During the final stages of SMF testing, 5 wt% red iron oxide paint pigment in the flyash was used as the test particulate. The iron oxide was added to increase the percentage of fines, and cascade impactor measurements indicated that the iron oxide increased the submicron fraction by approximately 80%.

Sintered Metal Filter Efficiencies

The SMF filter efficiencies for both sets of filters were determined in a total of 15 tests. Two of these tests in the pulsed blowback mode lasted over 280 hours and yielded the highest estimates of particulate removal efficiency (greater than 99.99999% for flyash removal on a mass basis). In each long-term test, no mass change was observed on the filters. Since no mass change could be observed on these filters, a mass of 0.1 mg collected was assumed. The value of 0.1 mg was based on numerous experiments in the laboratory on filter handling procedures and repeated mass determinations. In other tests with reverse flow blowback, some discoloration of the filter was observed, but the mass gain was not measurable. This discoloration was determined to be due to the unfiltered blowback air. In the tests with iron oxide plus flyash, no red discoloration of the sampling filters was observed.

The conditions of the two tests conducted for over 200 hours were a superficial velocity of 1.16 m/min with a pulsed blowback initiation pressure drop of 6.25 kPa. The gas was air at ambient temperature and humidity and the temperature in the filter vessel was approximately 40°C. These conditions are referred to as the base condition.

Thirteen additional SMF tests at other conditions were made with gas particulate sampling times less than 200 hours. Since no mass gain on the sampling filters was observed, with one exception, the 0.1 mg gain was assumed. These tests yield efficiencies on the order of 99.999%. The one exception, where a mass change was observed on the filter, was attributed to the downstream piping being contaminated with flyash due to previous cascade impactor measurements. Subsequent recleaning of the piping resulted in no mass increase of the sampling filters. Pressure indications also showed that no gross loading of particulate was occurring on the in-line filters.

It must be noted that a determination of the absolute particulate removal efficiency of the SMFs was not possible with the hardware and techniques used. Only bounded estimates could be obtained for the particulate source used.

Pressure Drop Characteristics

The porous SMF pressure drop immediately after blowback is called the recovery pressure drop. For stable operation, this pressure drop must remain well below the blowback initiation pressure drop. The recovery pressure drop after every blowback in the tests described here was recorded. In the pulsed blowback mode, the initiation pressure drop was 6.25 kPa. The recovery pressure drop appears to stabilize at 3.75 to 4.25 kPa.

Over 100 blowback cycles were required to attain apparently stable operation. These test results do not indicate infinitely stable pressure drop characteristics; however, the data for over 400 cycles on two different sets of SMFs did not indicate an increasing trend in the recovery pressure drop.

Reverse flow blowback tests were conducted at the base condition. Initially, the reverse flow superficial velocity was one-half the forward velocity and resulted in a recovery pressure drop only slightly below the

initiation pressure drop. Increasing the reverse flow superficial velocity to 1.2 m/min resulted in a recovery pressure drop of 4.5 kPa for over 250 cycles.

Other tests conducted on pressure drop characterizations include variation of the blowback initiation pressure drop, increased superficial velocity, particulate size distribution change, and temperature and humidity changes of the process air stream. Changing the pulse blowback initiation pressure drop had no observable effect on the recovery pressure drop at the base condition. However, increasing the superficial velocity did result in an increase in the recovery pressure drop. Returning to the base condition after increasing the superficial velocity did not result in the prior recovery pressure drop. It appears that the porosity and/or thickness of the permanent cake on the filter are determined by the highest superficial velocity. Changing the particulate size distribution with iron oxide, as previously noted, had no effect on the recovery pressure drop compared to the base condition.

Probably the most significant tests with respect to pressure drop characteristics were performed with conditions of high humidity and temperature. By injecting steam into the air process stream, a gas composition containing approximately 24 vol% water vapor was obtained. The process stream was heated to approximately 90°C to maintain a dry system. These conditions resulted in a rapid increase in the recovery pressure drop from 4.5 kPa at the base condition to greater than 5.2 kPa. Temperature alone was the variable that affected the recovery pressure drop. This was determined by allowing the system to stabilize with steam injection, then stopping the steam injection, and finally shutting down the process heater. There was no change in the recovery pressure drop when the steam was stopped, but the recovery pressure drop decreased to 3.9 kPa as the air stream cooled down after the process heater was shut down. Repeated applications and removal of heat appeared to indicate that the change in pressure drop is reversible. This pressure drop change with respect to temperature appears to be due to a change in porosity and viscosity, and has been quantified for a clean SMF.

CONCLUSIONS

Particulate Removal Efficiencies

The SMF particulate removal efficiencies reported here were obtained from a specific experiment. The efficiency of the SMFs are absolute in the sense that no measurable particulates were ever collected downstream from the filter vessel. The estimated efficiencies are on the order of 99.99999%, based on the minimum assumed mass gain of downstream collection filters. This estimate is limited by the efficiency of the collection filters themselves, which were HEPA filters. Other detection methods for particulate passing through the SMFs could very well yield a different result, but the detection method used in these experiments is similar to the intended application of HEPA filter protection. The efficiencies reported here are only for the particulate size distribution used and should not be interpreted or applied in any other sense.

Pressure Drop Characteristics

The pressure drop across the SMFs appeared to stabilize after an initial startup period. The pressure drop of interest is the recovery pressure drop that occurs immediately after blowback. It is not possible to demonstrate a nonplugging operation in an absolute sense, but only over the time frame of an actual test. The pressure drop characteristics reported here are only for the specific conditions and flyash tested. Over 4900 hours of operation with over 5100 blowbacks were conducted on SMFs with no apparent plugging observed.

Other Applications of SMFs

A process design engineer is reluctant to use a unit operation that is not well understood. In the case of SMFs, there are very few large applications of thousands of square feet of SMFs not only because of the cost, but also because of the lack of design equations. On the other hand, there are numerous applications involving hundreds of square feet of SMFs, where the relative size involved presents a smaller risk to the user. At the present, it appears that data and design information are emerging that will make rigid barrier filters usable in such systems as incinerator flue gas filtration, extreme temperature environments, and where extremely high particulate removal efficiencies are required on a continuous use basis.

ENDNOTES

1. Ralph M. Parsons Company, Conceptual Design Report: Design Description for the Slagging Pyrolysis Incinerator Project, 5942-SPI-05, May 1980 (Prepared for U.S. Department of Energy, Idaho Operations Office).

2. Pall, D.B., Filtration of Fluid Catalyst Fines from Effluent Gases, Ind. & E.C., 45, 6, p. 1197-1202, June 1953.

3. Mott Metallurgical Corporation, Farmington, Conn., Introduction to Engineering Controlled Porosity Products, Catalog No. 1000.

4. Pall Trinity Micro Corporation, Cortland, New York, The Pall Porous Metals Filter Guide, PSS-700a, September 1978.

5. Bjorklund, W.J., Development and Use of Sintered Metal Filters with Fluidized Bed and Spray Calcination of Simulated High-Level Waste, BNWL-2074, Battelle Pacific Northwest Laboratories, Richland, Washington, July 1976.

6. Carls, E.L., and N.M. Levitz, Blowback of Sintered Metal Filters: A Review of Tests and Operating Experience, ANL-7392, Argonne National Laboratory, January 1968.

7. Kirstein, B.E., et al., R&D for an Off-Gas Treatment System for a Slagging Pyrolysis Radioactive Waste Incinerator, Final Report for Phase III, prepared for EG&G Idaho, Inc., Idaho Falls, Idaho, by Science Applications, Inc., San Diego, California, June 1979.

8. Kirstein, B.E., et al., R&D for an Off-Gas Treatment System for a Slagging Pyrolysis Radioactive Waste Incinerator, Final Report for Phase IV, prepared for EG&G Idaho, Inc., Idaho Falls, Idaho, by Science Applications, Inc., San Diego, California, February 1980.

APPLICATION OF ELECTROSTATIC TECHNIQUES TO THE REMOVAL OF DUST AND FUME FROM THE INDUSTRIAL ENVIRONMENT

By: Stuart A. Hoenig, Professor
Department of Electrical Engineering
University of Arizona
Tucson, Arizona 85721

ABSTRACT

In earlier reports we discussed the application of charged fog to the control of fugitive dust. Fogging units are now sold commercially but there are many areas where it is impractical to use any water whatsoever.

For one application of this type we have designed and tested an electrostatic dust rejector that removes dust from the air being drawn into the turret of a military vehicle. Another system of this type is used to clean air before it is drawn through the air filter of an internal combustion engine. In both of these situations the dust is not "collected" but rather simply rejected back to the environment thereby simplifying the overall system.

Dust rejection can also be used to collect dust from air that is to be passed from a source to a cyclone or baghouse. This reduces the load on the regular control facilities while at the same time improving the overall system operation by taking out the small (under 10 micrometer) particulates.

Other systems for control of water droplets have been developed and will be discussed.

INTRODUCTION

In earlier publications [1,2] we reported on the development of charged fog systems for control of fugitive dust. These units are now sold worldwide by the Ritten Corporation of Ardmore, Pennsylvania, and there is every indication that charged fog can be used to solve pollution problems in a number of industrial areas. One study, under Environmental Protection Agency (EPA) sponsorship, indicated that for a smelter application the cost reduction with charged fog versus conventional techniques was a factor of 28 while the energy costs for operation were reduced by a factor of 13.3 [3]. Other fog gun data, developed by a private organization also under EPA support, indicated significant reductions in fugitive dust at a rock quarry with the charged fog guns during rock crushing [4].

SPINNING CUP FOG THROWERS

Conventional fog generators with nozzles are prone to clogging because of dirt or dissolved salts that deposit when the units are turned off. In theory, filters and/or treated water can be used but we suggest that it is more appropriate to design equipment that can withstand exposure to contaminated water.

Spinning cup fog generators break up the water into fine drops by means of a rotating element and an associated peripheral airflow that provides a shearing effect [5]. Typical applications include throwing of limestone slurries and drying of milk suggesting that clogging is not a problem. We have developed a small 2 inch diameter spinning cup system with a blower to provide the shearing airflow. A very satisfactory fog is produced; charging is accomplished by holding the cup at high (10 kV) voltage while isolating it from the water line with a proprietary droplet generation system. In Figure 1, we show a photograph of the unit in operation. Further development to produce a "field useable" system is planned for the next calendar year.

PERMISSIBLE FOG GUNS FOR EXPLOSIVE ENVIRONMENTS

At present the fog guns are not approved for use in flammable areas or for underground operation in coal mining. There have been a number of tests that indicated the foggers were very effective on coal dust, cotton linters, and wood flour, suggesting that development of a permissible unit would be appropriate. The problem here involves controlling the maximum energy release in a way that precludes ignition of gas or dust/air mixtures. It is worth noting that the problem involves not only controlling the amount of energy released, but the time or rate of release is important. A recent study [6] has indicated that hot sparks of the type that might be produced by a momentary short circuit in a fog gun are not nearly as effective for ignition as a long term, lower temperature, heat source where a stuck roller on a conveyor belt might be considered a typical example.

We have begun a study of the problems associated with meeting the "permissible standard" and hope to have an operational unit under test by the fall of 1981.

ELECTROSTATIC DUST CONTROL TECHNOLOGY

There are many areas where it is not practical or possible to make use of charged fog and we have been investigating the use of unconventional dust collectors. One such system involves a sticky cloth collector material that can be held at a positive voltage by a metallic backing material which is driven by a small power supply. The cloth itself has a high resistance so that there is no danger of shock on contact but the electrostatic field is large enough to pull in dust in the vicinity of the cloth. The effect is enhanced if the dust in the room is charged with a small negative ion generator. Figure 2 shows a system of this type in the off and on condition; in one case, the dust simply "drifts" about while in the other, the dust is drawn in and held on the cloth collector. We anticipate that devices of this type will be used in

clean rooms or observatories where float dust is a severe problem.

We have developed a version of this device for use on an astronomical telescope where falling dust can obscure the image from the primary mirror. The system is shown schematically in Figure 3. In Figure 4, we show photographs taken on a model system some 24 inches in diameter. In one case, the field was off and the dust simply floated about; in the other case, the unit was "on" and the dust was drawn to the central collector. Calculations indicate that systems of this type would be effective on mirrors with a diameter as large as 2032 inches (8.0 meters) in an orbital telescope.

Another area of application for electrostatics in dust control relates to the use of repulsion systems that can either "push" the dust, smoke, or fume in a particular direction for collection or actually "hold back" the dust while allowing clean air to move through the repulsion unit. The technology is based on the system shown in Figure 5, where an array of needles is mounted adjacent to a grounded mesh screen. When the needle array is driven at a high (usually negative) voltage, with respect to the screen, the intense corona discharge produces a significant electric wind (velocities as large as 200 m/min has been reported). At the same time there is a flow of oxygen O_2^- ions that transfer their charge to any dust particles that they come in contact with. These charged dust particles are then repelled by the electrostatic field of the needle array. (It is important to appreciate that the electrostatic field from the needle array can penetrate the grounded screen thereby providing a significant repulsion effect.)

In Figure 6, we show one of the dust repulsion systems in and out of action; the smoke (ammonium chloride) was easily repelled when the system is "on." It is worth noting that the design of these systems is not a simple thing. Typical variables include needle to needle spacing, needle to grounded screen spacing and screen opening. Figure 7 shows the results of one test where only the needle to screen distance was changed; it is clear that this distance is critical if best operation is to be achieved. We have found that it is possible to optimize the electrostatic wind velocity or the current in the space ahead of the screen but not both at the same time. This allows the user to choose between a repulsion system that emphasizes the wind effects versus one where the electrostatic effects dominate.

As an application of the pushing system, we show, in Figure 8, a diagram of a system designed to remove the smoke and particulates from the chimney of a home furnace burning wood or coal. (Reference 7 suggests that smoke from wood combustion is a major source of air pollution in many parts of the United States.) The moving belt system is part of the technology for removing the collected material from the unit while at the same time allowing the chimney to be cleaned by conventional sweeping techniques. (A proposal suggesting further work in this area has been submitted to the Department of Energy.)

In Figures 9 and 10, we show the movement of smoke in a full scale model of the dust-smoke collection system. In this case, the smoke was ammonium chloride moving at 3 m/min and with the system on collection was quite effective. Similar results have been obtained with oil smoke but that material is more difficult to photograph. In Figure 11, the same system is shown

in action on particulates (AC Fine) dropped through the system. Again, collection was very effective and we see this as the prototype of a unit that might be a significant step toward the improvement of urban environments even with large scale combustion of fossil fuels for home heating.

Another version of the repulsion system has been developed for the turret blower on the U.S. Army's M60-A1 Main Battle Tank. The blower is designed to provide ventilation air at up to 1100 CFM and under normal conditions any dust in the ambient is brought in with the air. Figure 12 is a schematic drawing of a system designed to repel the dust before it can enter the blower while at the same time providing the necessary ballistic characteristics to preclude damage by light weapons in a combat environment. Figure 13 shows some of the data with a system of this type; even at the high airflows significant repulsion of dust (AC Fine) occurred. The unit is even more effective at lower airflows that might be used under nuclear, biological or chemical attack conditions and some of these data are shown in Figure 14.

Another point of interest relates to the performance in "heavy dust" that might be observed during desert operations. It is worth noting that here "heavy dust" is a level far above that normally observed in industry. Typical levels of military importance may range as high as 883 mg/cu m or even 8900 mg/cu (8.9 g/cu m). These conditions are far above 100% obscurity; you cannot see your hand in front of your face. Typical results with a small scale repulsion system are shown in Figure 15. It is clear that at dust levels that might occur in industry there was very significant rejection. We see systems of this type being applied in industry where it is important to keep dust from escaping or entering a closed area while at the same time allowing the passage of "clean air."

One very obvious application of this technology is in air cleaners for internal combustion engines. Some modifications are necessary to permit effective operation in the confined area of an engine housing but in Figure 16, we show a full scale unit designed for the air filter on a D-10 Caterpillar Tractor. There was effective repulsion of the dust and some of the results are shown in Figure 17. We see this as the first of a whole series of applications where the electrostatic technology is used to alleviate dust problems without the complexities associated with conventional filters and collection systems.

Another example of applied electrostatics exists in lead fume collection. Lead fume is typically 0.1 micrometer in diameter and is therefore difficult to collect with conventional systems. In many cases the fume source is a smelting pot where crane movements preclude the use of conventional hoods. At the same time the product (lead) is of some commercial value and it would be advantageous to have a collection system that would allow the lead to be recycled. In Figure 18, we show a schematic drawing of a lead collection unit installed above a smelting pot. The system is designed to swing out of the way when the crane is in operation and to collect the lead fume on lead wool that can be returned to the smelting pot after collection is complete. Figure 19 is a photograph of a prototype lead fume collector off and on. The lead fume is drawn in by the lower electrostatic needle array that charges the fume and forces it to deposit on the lead wool. We noted earlier that lead fume is

difficult to charge and have therefore arranged for a second needle array to charge and push any uncharged fume back toward the lead wool. If the two needle arrays are properly arranged there will be a flow of "clean air" through the system while the lead fume is collected on the lead wool. We see this as the prototype of a system that might be used in a number of industrial areas.

Large scale electrostatic wind arrays can be used to charge and push dust from one area to another. One application of this type is shown in Figure 20, where the objective was keeping dust out of an electrostatic precipitator insulation box. At 30 kV and some 10 mA, the wind velocity, at a distance of 1.53 meters, was some 54.9 m/min.

One last application concerns the collection of diesel exhaust particulates by a modified tube and wire electrostatic precipitator (ESP). ESP units are well known to be effective on the fine (0.1 micrometer) carbon flakes produced by a diesel engine but the problem has been removal of the collected material and protection against insulator contamination by the conductive carbon flakes. We have solved the cleaning problem by means of a rotating liner and scraper-worm system that carries the collected material out of the system. The insulators are protected by a small flow of clean air that keeps the carbon from depositing. Some data taken with the cleaner on a 45 Hp engine supplied by the John Deere Company is shown in Figure 21. We anticipate developing a cleaner-muffler unit that will combine both functions into a single unit. This should allow the system to operate on a wide variety of diesel powered systems.

CONCLUSIONS

We have discussed a number of applications for electrostatic technology in the reduction of dust and fume. We see electrostatics as playing an important part in low cost, low energy, pollution control systems.

ENDNOTES

1. Hoenig, S.A. Fugitive and Fine Particle Control Using Electrostatically Charged Fog. EPA-600 7-79-078, March 1979. Available from NTIS, Springfield, Virginia 22161.

2. Hoenig, S.A. New Applications of Electrostatic Technology to Control of Dust, Fumes, Smokes and Aerosols. IAS Conference Record. CH1575-0/80/000-1032, September 1980. p. 1032-1037.

3. Daugherty, D.P., D.W. Coy. Assessment of the Use of Fugitive Emission Control Devices. EPA-600/7-79-045, February 1979. Available from NTIS, Springfield, Virginia 22161.

4. Brookman, E.T. Demonstration of the Use of Charged Fog in Controlling Fugitive Dust from Large-Scale Industrial Sources. (Presented at the 1980 Symposium on Iron and Steel Abatement Technology, Philadelphia, Pennsylvania, November 18-19, 1980.)

5. Hinze, J.O., H. Milborn. Atomization of Liquids by Means of a Rotating Cup. Jnl. Appl. Mech. 17:145, 1950.

6. Eckhoff, R.K. Towards Absolute Minimum Ignition Energies for Dust Clouds. Comb. and Flame. 24: 53-64, 1975.

7. Cooper, J.A. Environmental Impact of Residential Wood Combustion Emissions and Its Implications. Jnl. Air Poll. Cont. Assoc. 30:855, August 1980.

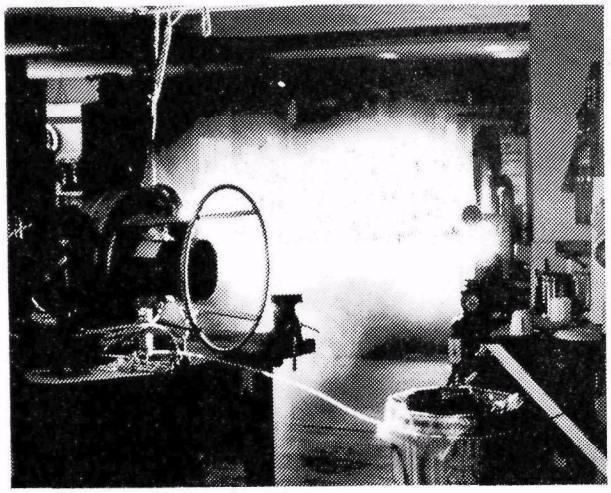

Figure 1. Spinning Cup Fog Thrower In Action.

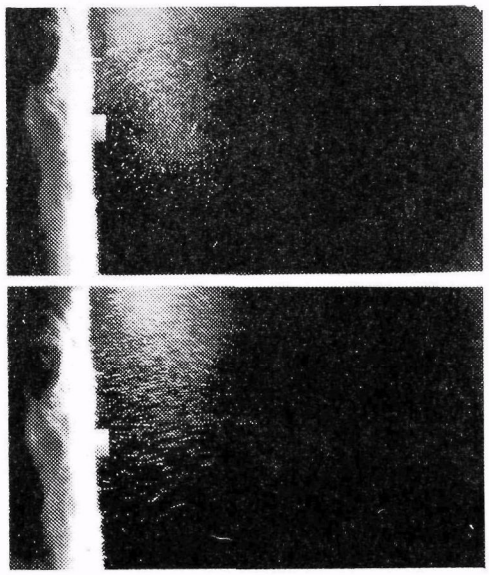

Figure 2. Electrostatic Dust Collector "Off" and "On."

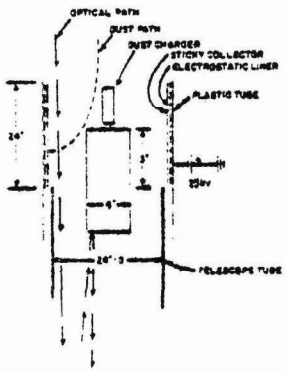

Figure 3. Schematic Diagram Electrostatic Dust Collector for 24" Astronomical Telescope

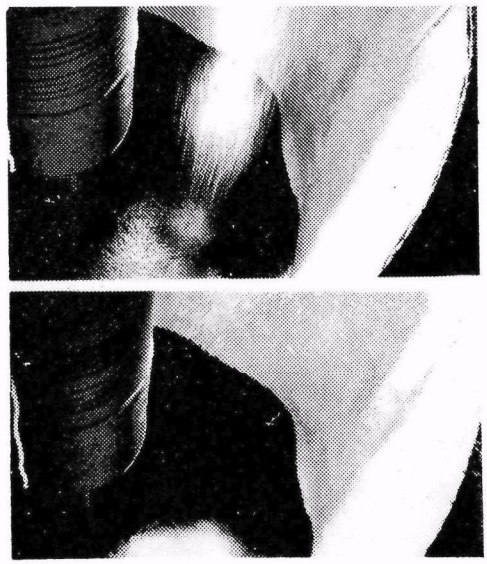

Figure 4. Electrostatic Dust Collector "Off" and "On."

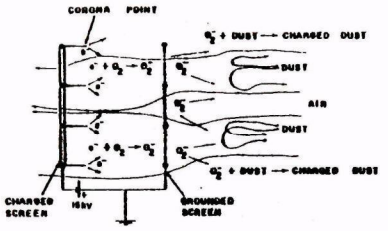

Figure 5. Schematic Diagram of Electrostatic Fence to Reject Dust and Admit Air.

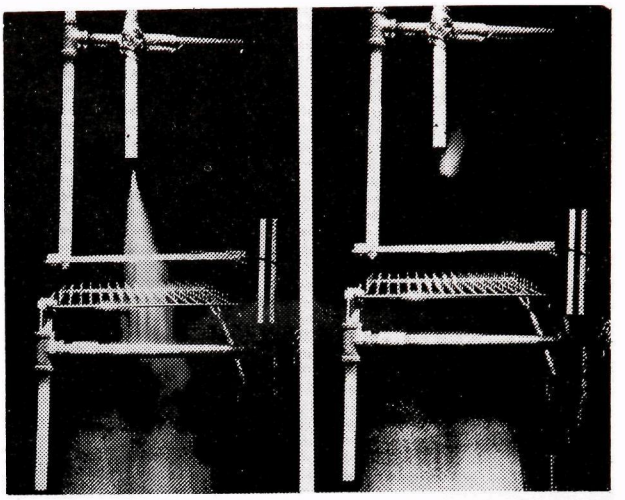

Figure 6. Electrostatic Dust Repulsion System "Off" and "On".

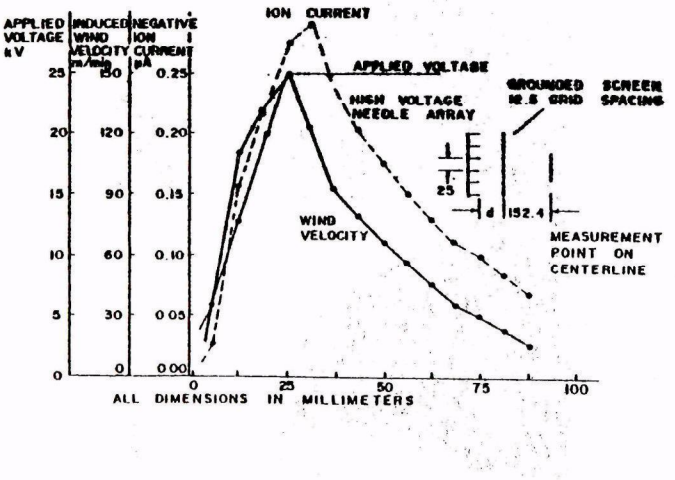

Figure 7. Effect of "d" Needle to Screen Distance on Electrostatic Wind Parameters.

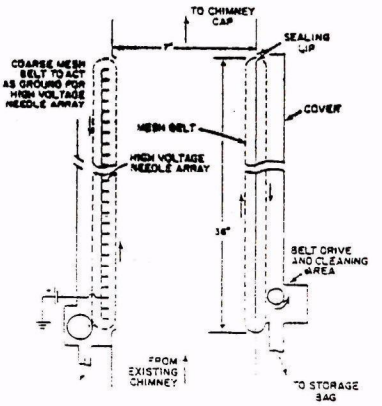

Figure 8. Schematic Drawing Cleaning System for Wood Burning Stoves.

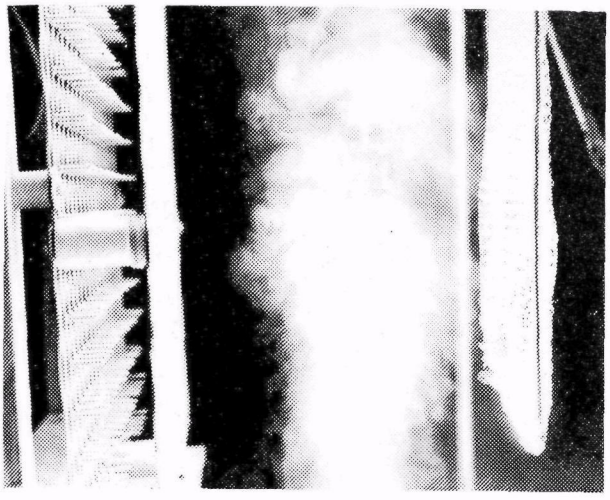

Figure 9. Electrostatic Smoke Collector "Off."

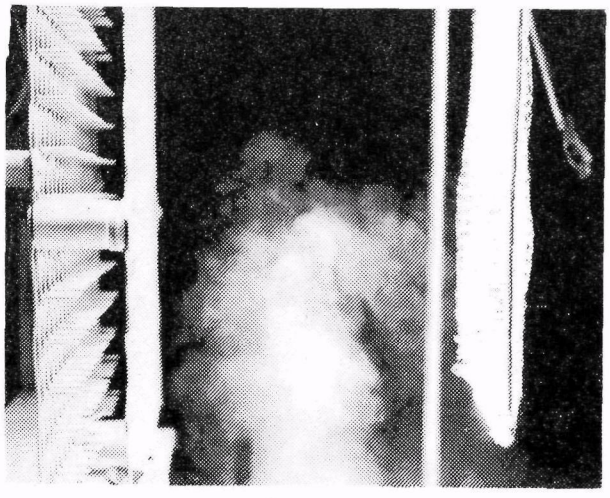

Figure 10. Electrostatic Smoke Collector "On."

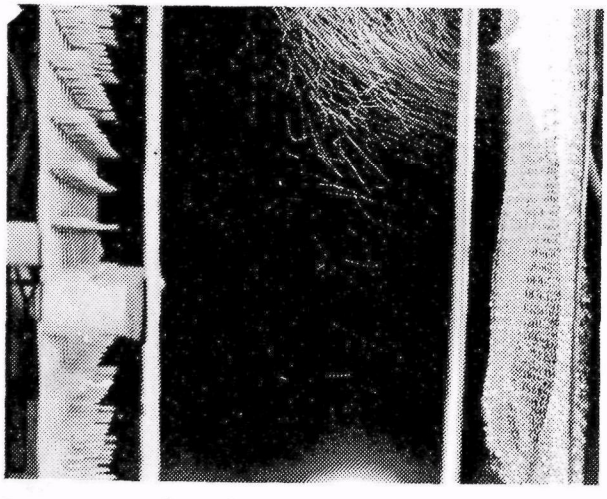

Figure 11. Electrostatic Dust Collector "On."

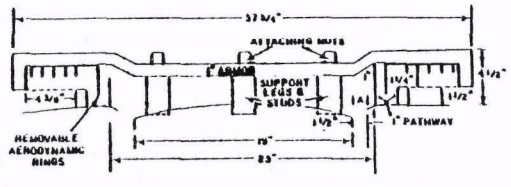

Figure 12. Schematic Drawing Inverted Dust Rejection System for M60-A1 Tank.

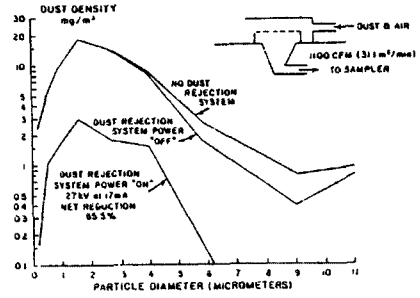

Figure 13. Experimental Results Electrostatic Dust Rejection System.

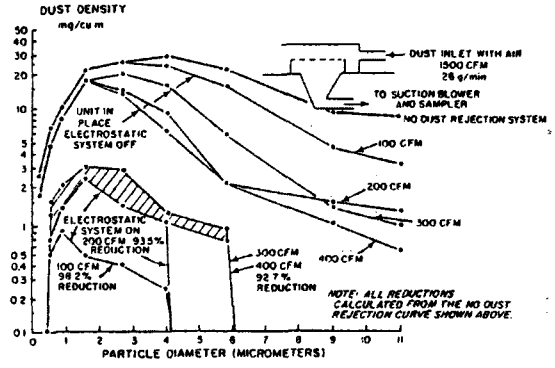

Figure 14. Experimental Results Electrostatic Dust Repulsion System.

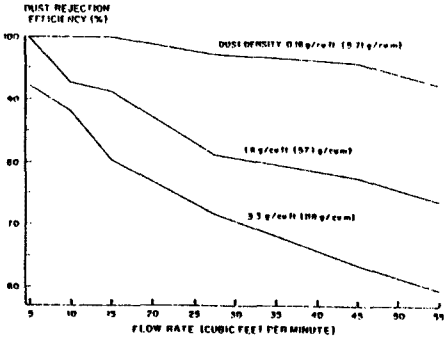

Figure 15. Laboratory Data Electrostatic Dust Repulsion With the Bypass Flow System.

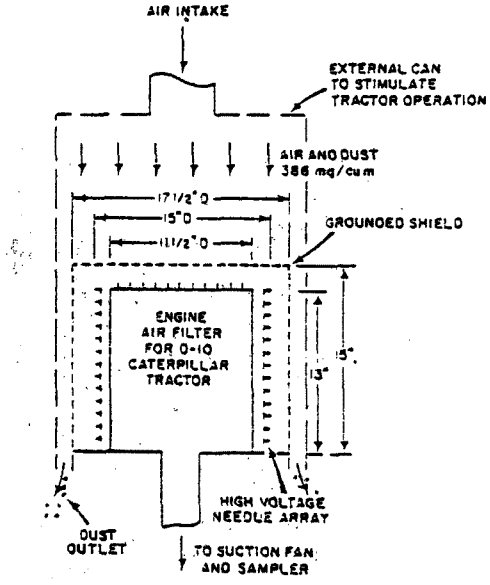

Figure 16. Schematic Drawing Electrostatic Test System for Engine Air Filter.

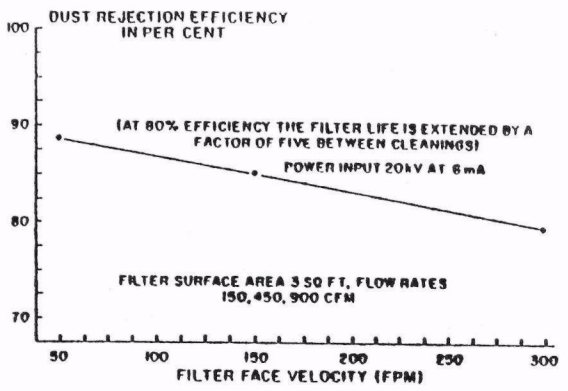

Figure 17. Laboratory Results Tests of Electrostatic System for Dust Repulsion on Engine Air Filter.

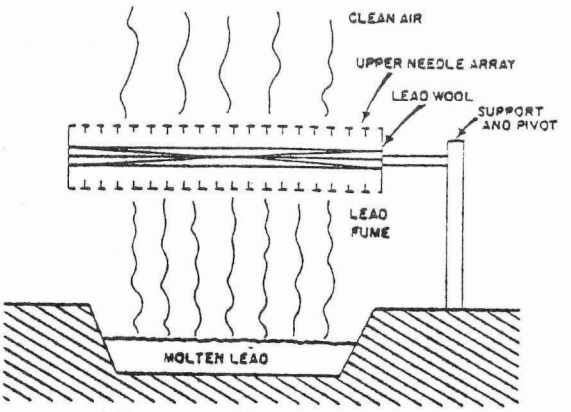

Figure 18. Schematic Drawing Electrostatic Lead Fume Collection System.

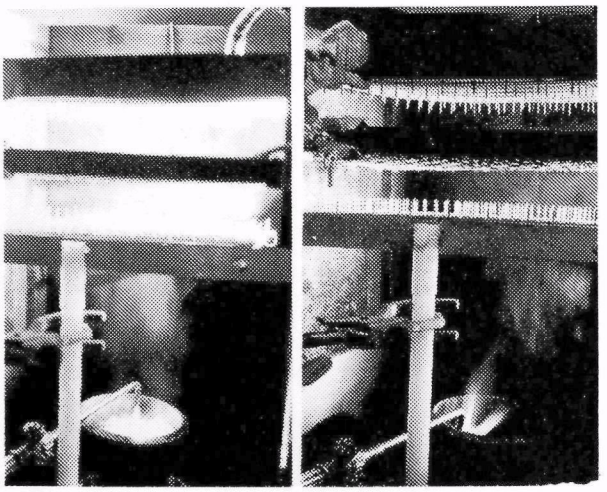

Figure 19. Electrostatic Lead Fume Collector "Off" and "On."

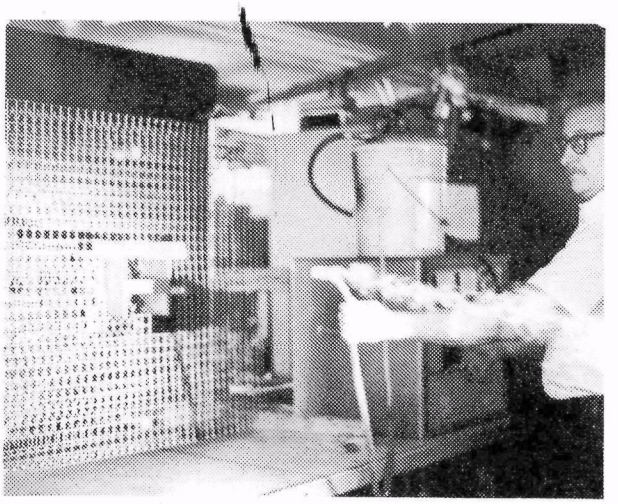

Figure 20. Large Scale Dust Pusher.

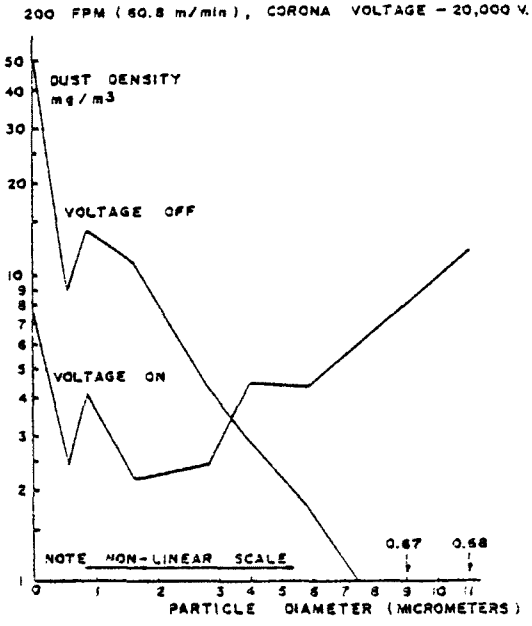

Figure 21. Laboratory Experiments Control of Diesel Exhaust Particulates by Means of Electrostatic Techniques

THE DRY VENTURI

BY: A.J. Teller, D.R.J. Roy

Teller Environmental Systems, Inc.
415 Boston Turnpike
Shrewsbury, Massachusetts 01545

ABSTRACT

The major problem in particulate emission recovery is the reliability of collection of submicron particles. The use of electrostatic precipitators has often resulted in time degradation of performance and that of baghouses in blinding or low bag life. A dust agglomeration and capture process (dry venturi) with a pressure drop of 0.2 KPa, providing removal of the submicron particulates in the duct prior to the final collector results in the increased effectiveness and reliability in the operation of the final collector. The system has been successfully operated in the fiberglass, municipal incineration, combustion, secondary aluminum, and fertilizer industries.

INTRODUCTION

A process has been developed to effect reliable capture of submicron particulates with low energy consumption. The mechanism of capture is inertial impact in a "dry environment."

Inertial impact, an established method for collection of particulates suspended in a gas stream, is normally conducted with the capture targets as fixed members placed in the gas stream or liquid droplets dispersed in the gas stream. The efficiency of capture has been modeled by Ranz and Wong (1) and Langmuir and Blodgett (2).

The models both indicate that the efficiency of particle capture is a function of equivalent particle size, target size and shape, and relative velocity of the particle and target for a given fluid environment.

Simplistically, therefore for a given particle to be captured,

$$\text{Efficiency of capture} = f\left(\frac{V_R\ Dp}{Dt}\right) = f\ (N_S)$$

The conventional inertial impact capture device, the wet venturi, creates its own targets. The gas is accelerated to a high velocity and impacted on liquid. The velocity energy is transferred to shearing action thus creating the targets. The target droplets, formed at zero velocity, have a relative velocity to the gas stream, equal to the gas velocity. The drop size of the target is approximately inversely proportional to the gas velocity [Nukiyama-Tanasawa] (3). Thus to achieve high efficiency, significant energy must be expended to create the small droplet target.

Typical anticipated behavior of a wet venturi based on established relationships is as follows (provided an adequate number of targets is available).

TABLE I

WET VENTURI CHARACTERISTICS

Particle Size (μ) Capture	Gas Vel Venturi m/s	Target Droplet Size (μ)	ΔP Venturi mm H_2O	Power Consumption Gas KW/1000 CMH	Ns	Eff. %
1	52	140	280	1.10	0.37	97
0.5	52	140	280	1.10	0.18	90
0.3	52	140	280	1.10	0.11	80
1	91	75	635	2.50	1.21	99
0.5	91	75	635	2.50	0.61	96
0.3	91	75	635	2.50	0.36	92

The excessive power consumption prohibits the use of the venturi for removal of submicron particulate when handling large volumes of gas.

The new system, dry venturi (fig. 1), circumvents the limitation of high energy consumption. The target material is supplied to the system as a dry powder, in a crystalline form. Thus, the gas velocity can be reduced significantly.

For the same anticipated efficiency as a 635 mm H_2O ΔP venturi, the relative velocity in a dry venturi need be only 18 m/s, normal duct conveying velocity, if a 15μ target is used.

Thus, the use of small solid targets, in the 5-25μ range permits the achievement of high capture at duct velocities and with an energy consumption approximately 4% of that required in a high energy liquid venturi,

Although dry powdered solids have in the past been introduced into a duct (for various reasons), there has been little or no particulate capture reported as a result. The reason is that solids have been introduced into the gas stream in the conveying duct as a dense agglomerate. By the time the powder was dispersed, a condition essential for capture, the powder had attained the velocity of the gas since the dispersion occurred due to the conveying capacity of the gas stream.

The dry venturi is designed to introduce the target material in a dispersed state, at the maximum desired relative velocity to the gas stream at minimal power consumption. The dry venturi permits the optimization of capture efficiency by selecting the target size, the target population density, and velocities for a specific application. Typical of presently operating systems the separation number function, Ns, obtained for a 0.5 micron capture with a 20 micron target is 1.2.

FIGURE 1

DRY VENTURI

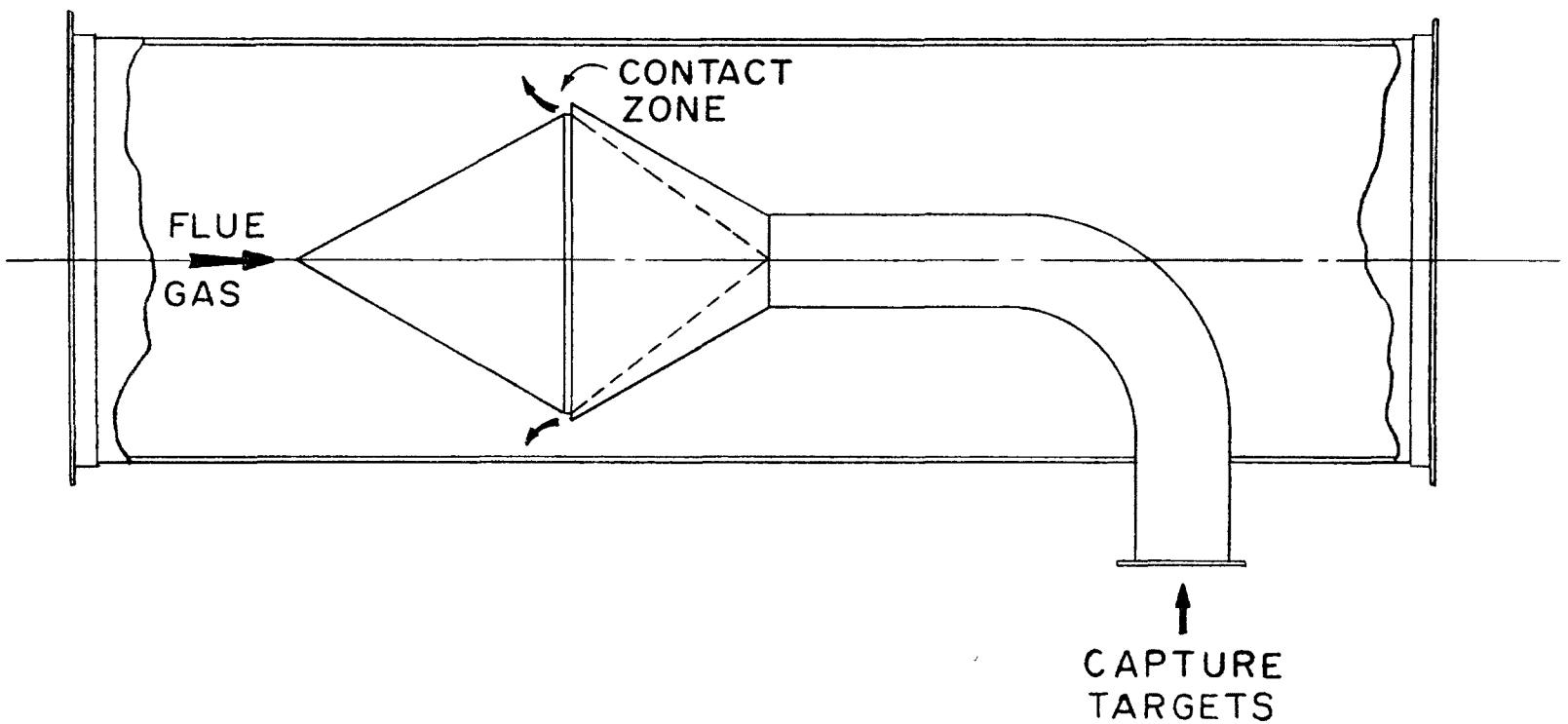

The power required to effect this capture is 0.08 KW per 1000 cubic meter per hour of gas treated, only 3-5% of that required in a conventional wet venturi. It is noted, however, that the power input for the capture of the submicron particulate must be combined with that required to make the final separation of captured particulates from the gas stream. Experience with commercial systems has shown that collection equipment in conjunction with the dry venturi have demonstrated power consumption in the order of 0.35 to 0.5 KW per 1000 cubic meter per hour of gas treated.

The dry venturi is operational in six industries and has been piloted in the US, UK, and Japan. The final collectors have been the electrostatic precipitator and the baghouse.

The effectiveness of the combined utilization of the dry venturi and a baghouse final collector is unique.

Primarily, it permits application of the baghouse to collection of deliquescent, cohesive, adhesive submicron, and combustible particulates where its use was previously restricted. It functions well with submicron particulates and hydrophilic or cohesive particulates without blinding or high pressure drop. It functions safely with combusting feed particulate.

But more significantly, the capture of the submicron particulates in the duct by crystalline targets results in exceedingly low pressure drop buildup in the baghouse. As a result, the shake cycle has been extended from the normally anticipated 5 min. to 30 min. to 4 hrs. to 36 hrs. Two characteristics are affected.

Bag life is extended because of the decrease in shaking requirement, and the lack of permeation of submicron particulates into the interstices in the cloth.

Lower and more constant pressure drop is obtained when the baghouse is operated in conjunction with the dry venturi.

Residence time of the cake on the cloth is increased by a factor of approximately 30. As a result, where the system provides the dual service of particulate and acid gas collection, residual unreacted reagent is accumulated and in residence on the bag surface. Thus "polishing" of acid gases occurs in the long residence reaction time on the bag surface. The advantage of this phenomenon becomes more significant when the acid gas content is a variable.

Particulate emissions from the baghouse are lower than obtained in conventional filtration.

No corrosion is evident after 5 years in acid gas service.

The performance of the dry venturi - baghouse system is indicated in Table II.

TABLE II

PERFORMANCE CHARACTERISTICS OF THE
DRY VENTURI - BAGHOUSE SYSTEM

INDUSTRIAL APPLICATION	ΔP MM H_2O DRY VENTURI	ΔP MM H_2O BAGHOUSE	SHAKE CYCLE HRS	PART EMISSION GR/DSCF	ACID GASES COLLECTED
Fiberglass	25	80	24	0.002-0.004	HF, SO_x
Glass	30	100	16	0.004-0.008	SO_x
Municipal Incinerator	20	90	8	0.003-0.006	HCℓ,HF,SO_x
Coke Calciner	25	125	8	0.004-0.006	SO_x
Secondary Aluminum	20	150	INT ~48	0.001-0.003	HCℓ, HF

The dry venturi has operated commercially as an effective particulate collector with an energy requirement of less than 5% of an equivalent performance wet venturi.

Because of removal of submicron particulates prior to the final collector, the effectiveness of the final collector is enhanced.

Specifically, when used in conjunction with a baghouse, it permits lower particulate emissions, decreases baghouse pressure drop, increases the cycle interlude, extends bag life, and extends the reliable application of the baghouse to recovery of materials previously considered incompatible with baghouse collection.

ENDNOTES

(1) Ranz & Wong IEC, 44, 1371-1381, (1952)
(2) Langmuir & Blodgett U.S. Army Tech. Report 5418, (1946)
(3) Nuikyama & Tanasawa, Trans. Soc. Mech. Eng. (Japan) 5, 18, 68-75, (1939)

FIBER BED FILTER SYSTEM CONTROL OF WELDING PARTICULATES

By: Judith Ann Bamberger and W. Kevin Winegardner
Battelle Memorial Institute
The Pacific Northwest Laboratories

ABSTRACT

The Electrostatic Fiber Bed Filter (EFBF), patented and developed at the Pacific Northwest Laboratories of Battelle Memorial Institute, is a highly efficient method for removal of submicron particles from gas streams. This paper describes the EFBF system and the results of a parametric study to evaluate the EFBF's ability to control the fine particulates generated during welding operations. The results of the parametric analysis show the dependence of collection efficiency on electric field, face velocity, fiber bed depth, and welding fume concentration.

System collection efficiencies above 95% were routinely measured at velocities from 200 to 400 ft/min. For welding fume concentrations of 1 to 2 mg/m^3 collection efficiencies were consistently 99.9%. Pressure drop across the fiber bed was extremely low, ranging from 0.07 to 0.82 in. H_2O.

INTRODUCTION

This report describes the investigation of the use of the Electrostatic Fiber Bed Filter (EFBF) to reduce ambient concentrations of welding fume fine particulates. Literature review suggests that exposure to the gases and particulates generated during welding operations is not a health hazard provided adequate ventilation is maintained (1). However, welding fumes contain fine or submicron particulates that can be inhaled deep into the lung. A growing awareness of potential health effects is focusing attention on the need to assure control of fume constituents below specified limits.

The EFBF is a patented, highly efficient system for removing fine, highly resistive particles from gas streams (2). In addition to their small size, welding fume particulates are electrically resistive. These two characteristics make the EFBF an especially attractive particulate control device. The parametric investigations discussed in this paper are part of a license agreement with The Bahnson Company for application of the EFBF in the field of building air cleaning.

THE ELECTROSTATIC FIBER BED FILTER

Basic components of the EFBF include a corona chamber and a highly porous bed of dielectric fibers. Particles are first given an electrical charge in the corona chamber and then collected in the downstream fiber bed.

Corona Chamber

A primary requirement of the particle removal process is the generation of large quantities of gas ions for charging the particles of the aerosol. Ion generation is accomplished in a stable, self-maintaining discharge

between two electrodes, termed a corona discharge. High voltage is applied to one of the electrodes, a wire or other geometry with sharp radius. The other electrode, usually adjacent parallel plates or a concentric cylinder, is grounded. Such an electrode arrangement results in a highly non-uniform electric field and ionization near the wire. The particles acquire an electric charge by passing through the dense, unipolar cloud of ions that fills most of the space between the electrodes.

Fiber Bed

Highly efficient particulate removal in the fiber bed is attributed to diversion of the charged particles from normal flow paths by the force of an electric field. The field is believed to be the result of volumetric charge buildup within the bed produced by particle deposition on the dielectric fibers. Collection enhancement by the field is almost instantaneous. The fact that particle collection is enhanced by a bed charged with the same sign as incident particles is perhaps initially surprising. However, development of an analytical model has revealed that the electric field resulting from the deposited charges is significantly larger near a fiber than local Coulomb repulsion and dramatically increases the capture cross section.

The fibers occupy only 5% to 8% of the total bed volume. The high fiber bed void fraction and the inherently open corona chamber geometry result in low pressure drop and energy requirements for routing an aerosol through the system. The bed can be cleaned by liquid sprays, air jets or other methods, depending upon the specific application.

EXPERIMENTAL APPARATUS

The modular EFBF bench-scale system used in the parametric study is shown in Figure 1. A 3-ft-long diffuser section was provided upstream of the approximately 10-ft-long, 10-in. x 10-in. main lucite duct. A wire-plate electrode arrangement was used in the corona chamber. Plate-to-plate and wire-to-plate spacings of 2 in. and 1 in., respectively, were used. One

FIGURE 1. SCHEMETIC DRAWING OF EFBF EXPERIMENTAL APPARATUS

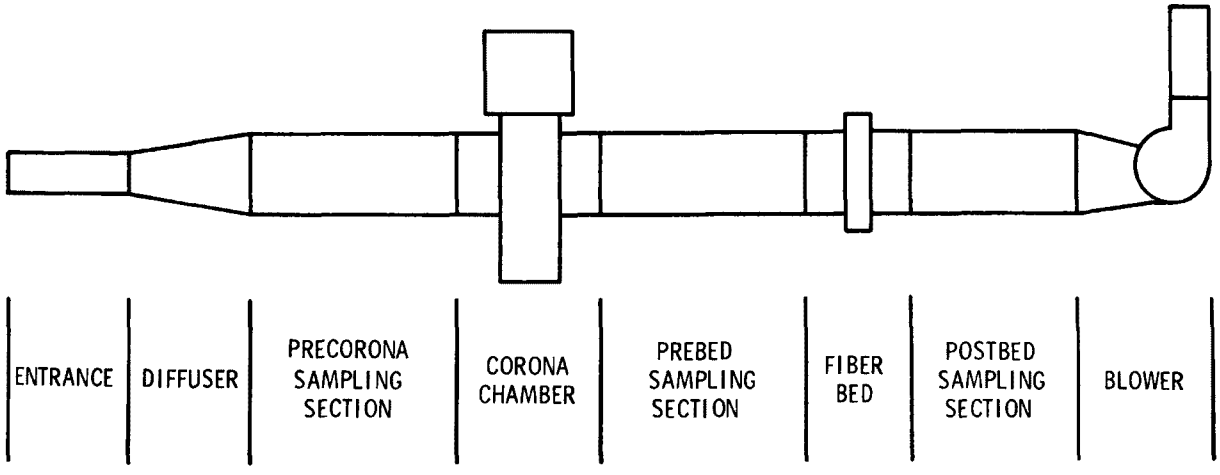

10-mil-diameter tungsten wire discharge electrode was centered between each pair of the 1.5-in.-deep grounded aluminum plates.

The fiber bed, installed downstream from the corona chamber, consisted of layers of uniformly packed polypropylene knit material. Particle leakage around the bed edges was minimized by providing a small diversion baffle (normal to the direction of flow) around the interior perimeter of the bed holder. Sampling locations were provided upstream of the corona chamber and fiber bed, and downstream of the fiber bed, permitting gravimetric determination of total system, fiber bed, and corona chamber particulate collection efficiencies.

EXPERIMENTAL PARAMETERS/TECHNIQUES

The range of parameters used in the investigation is summarized in Table 1. The fiber bed void fraction, the fraction of the bed not occupied by fibers, was calculated from the weight of fiber per unit length, fiber diameter, and the weight and volume of the bed. Fumes were generated by shielded metal-arc welding.

TABLE 1. SYSTEM TEST PARAMETERS

Air Velocity	200, 300, 400 ft/min (0.51, 0.76, 1.0 m/s)
Welding Fume	
Electrode	E7024
Concentration	1-35 mg/m^3 (0.0004-0.015 gr/ft^3)
Corona Chamber	
Particle Residence Time	0.019-0.038 s
Applied Voltage	0, -15, -18, -21 kV
Fiber Bed	
Material	Polypropylene
Fiber Diameter	0.008, 0.012 in. (0.020, 0.030 cm)
Bed Depth	1, 3 in. (2.5, 7.6 cm)
Void Fraction	0.93

Total system, bed, and corona chamber particulate collection efficiencies were determined gravimetrically from samples collected isokinetically on fiber glass filters. As previously indicated, three sampling locations were used. Further, the square, 10-in. x 10-in. duct was divided into quadrants for sampling. Samples were taken from each quadrant at each of the three locations. Aerosol concentrations were determined from the quantities collected on the filters, sampling times, and volumetric sampling flow rates.

Evaluation of a selected parameter, termed a test, consisted of a series of efficiency measurements. Insofar as possible, variables were held constant throughout the test. No attempt was made to clean the system until the

test was complete. Results from a typical test, consisting of 11 efficiency measurements, are shown in Figure 2.

FIGURE 2. COMPARISON OF SYSTEM, FIBER BED AND CORONA CHAMBER COLLECTION EFFICIENCY (200 ft/min velocity, 35 mg/m^3 average concentration, 3 in. thick fiber bed)

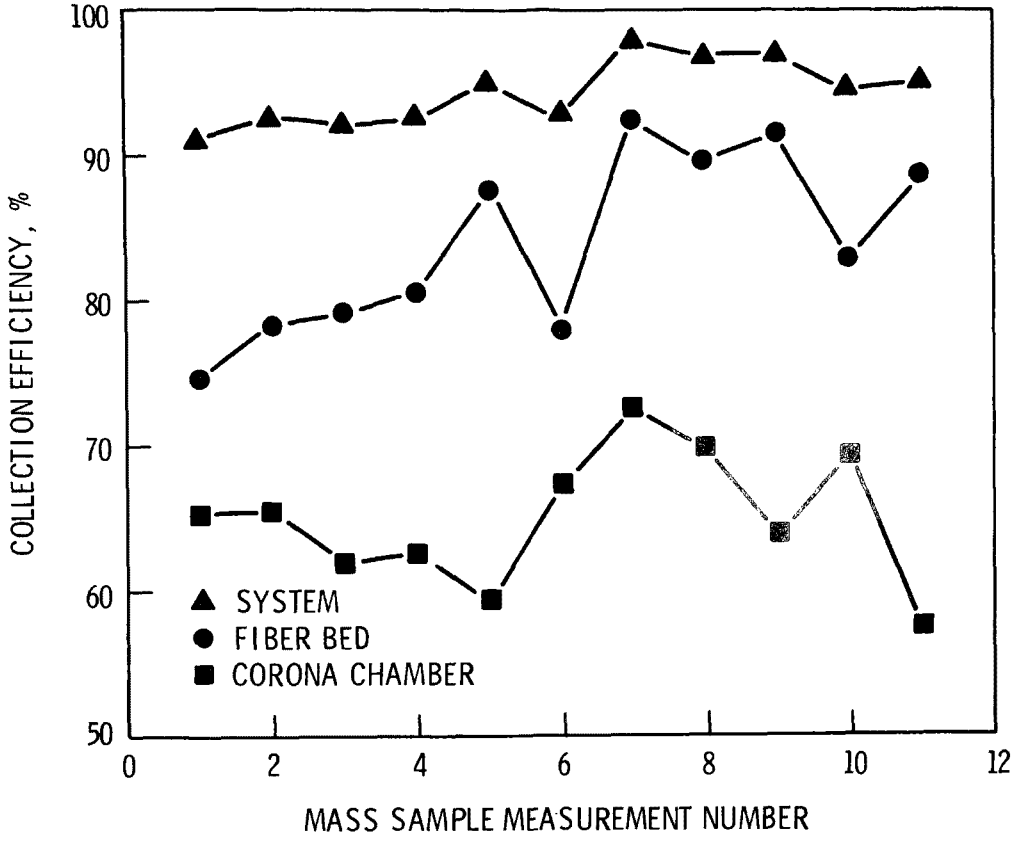

TEST RESULTS

Effect of Particle Charging

To confirm that the EFBF system is highly efficient only when the particles are electrically charged, efficiency measurements were made with and without corona chamber applied voltage. Results in Figure 3 show that system collection efficiencies of 88 to 99% were obtained with corona enhancement. With particle collection only by the conventional mechanisms of impaction, interception, and diffusion, system collection efficiencies dropped to 18 to 35%.

Concentration

Welding fume concentration ranged from 1 to 35 mg/m^3 during the tests (Table 1). The effect of concentration on system performance as a function

FIGURE 3. EFFECT OF PARTICLE CHARGING ON EFBF SYSTEM, FIBER BED AND CORONA CHAMBER PERFORMANCE (300 ft/min velocity, 12 mg/m^3 average concentration, 3 in. thick fiber bed)

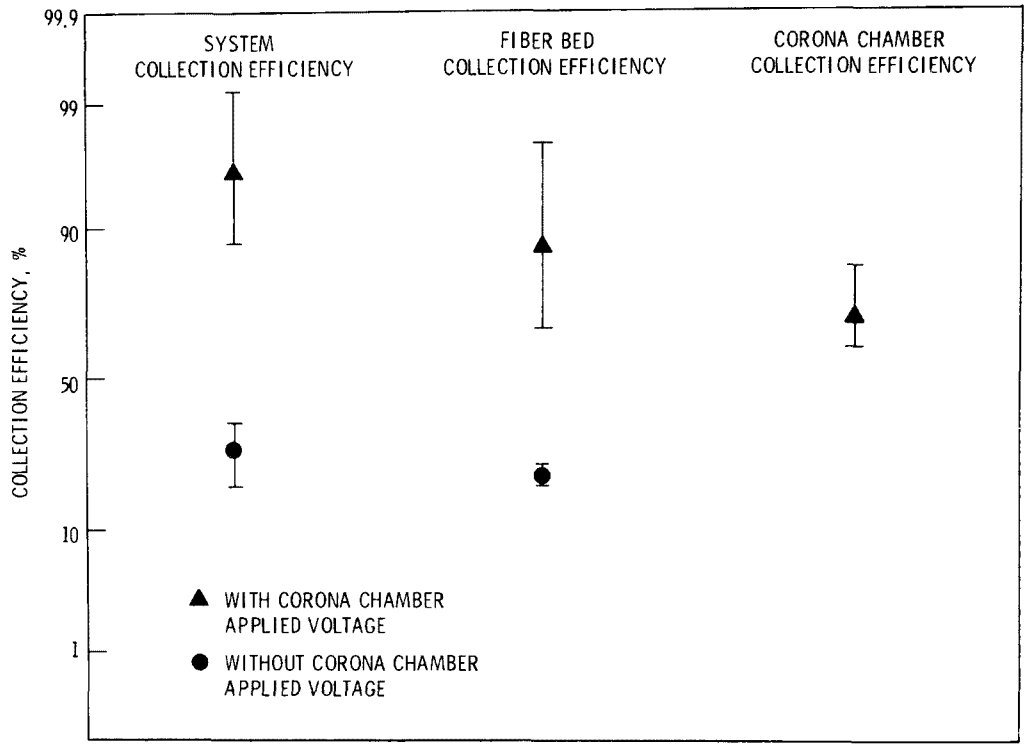

FIGURE 4. THE EFFECT OF CONCENTRATION ON SYSTEM PERFORMANCE (3 in. thick fiber bed, 0.008 in. fiber diameter)

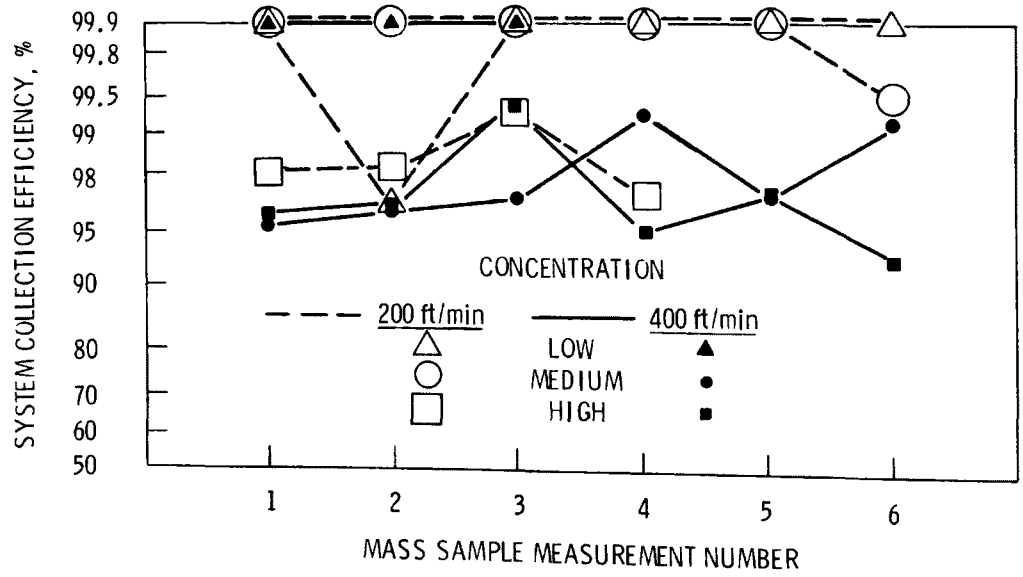

of velocity is shown in Figure 4. At low concentration (1-2 mg/m^3) velocity did not affect system performance (99.9%). At medium concentration (5-10 mg/m^3) system performance at 200 ft/min remained 99.9%, but dropped to 96% at 400 ft/min. At high concentration (15-25 mg/m^3) system performance varied from 96 to 98% at both velocities.

Bed Thickness

System performance of 1-in.-thick and 3-in.-thick fiber beds, both having the same void fraction and fiber diameter, was investigated as a function of velocity. Results presented in Figure 5 show that the average collection efficiency of the 3-in. bed was 6% higher than the average collection efficiency of the 1-in. bed.

FIGURE 5. EFFECT OF BED THICKNESS ON SYSTEM COLLECTION EFFICIENCY

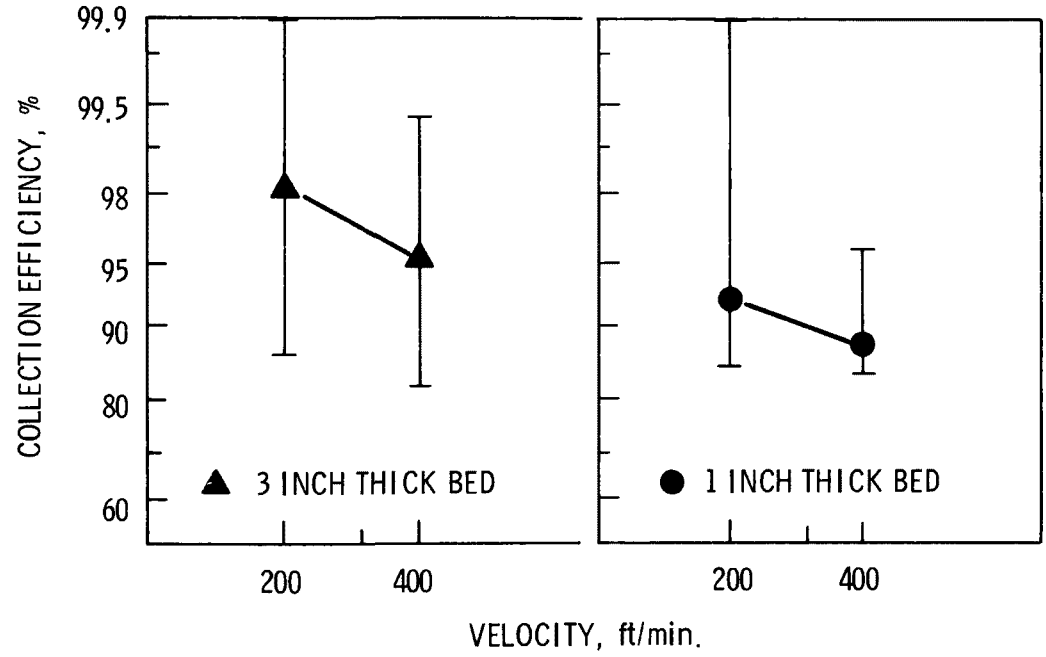

Fiber Diameter

Fiber beds of 0.008- and 0.012-in.-diameter polypropylene knit, with identical void fraction and bed thickness, were tested at 200, 300, and 400 ft/min. Data presented in Figure 6 show the average performance of the 0.008-in.-diameter fiber to be 15% higher than the performance of the 0.012-in.-diameter fiber.

FIGURE 6. EFFECT OF FIBER DIAMETER ON EFBF COLLECTION EFFICIENCY

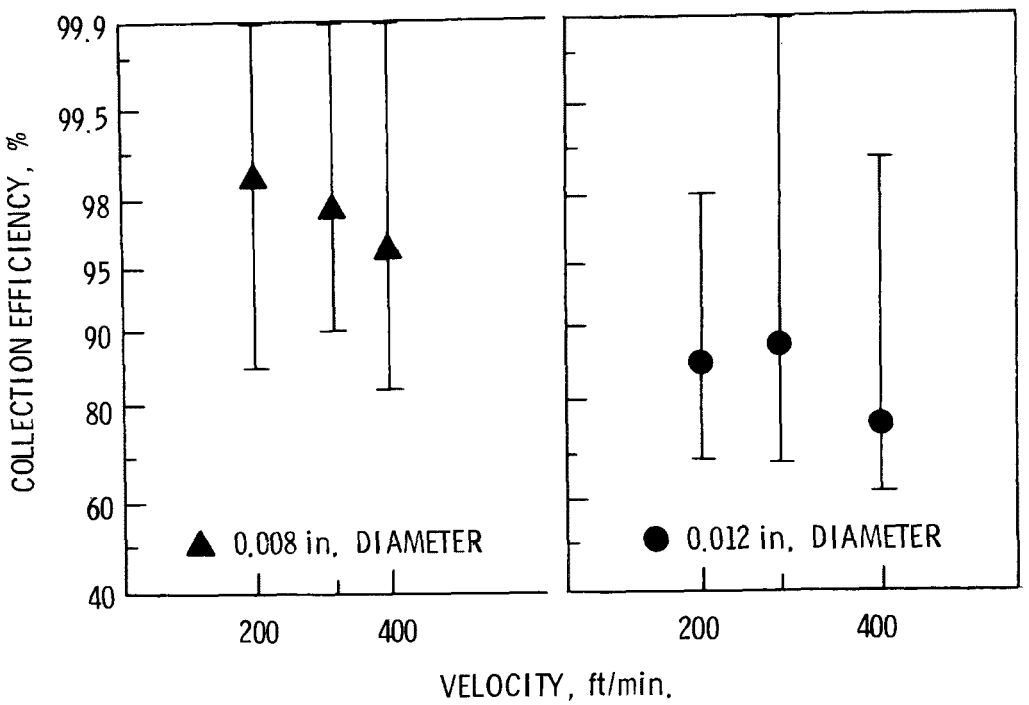

Pressure Drop

Pressure drop data for each fiber bed as a function of velocity are presented in Figure 7. The clean bed pressure drops ranged from 0.068 in. H_2O for the 1-in.-thick bed at 200 ft/min to 0.540 in. H_2O for the 3-in.-thick bed, 0.008-in.-fiber diameter, at 400 ft/min. During operation, pressure drop increases of 0.010 and 0.360 in. H_2O were measured for the 1-in. and 3 in. beds, respectively. Clean bed pressure drop as a function of velocity appears to be linear up to 300 ft/min bed face velocity.

The pressure drop across the 1-in. bed was one-third that of the 3-in. bed with the same diameter fiber. Pressure drop across the 3-in. bed with 0.008-in.-diameter fiber was consistently greater than that across the 3-in. bed with 0.012-in.-diameter fiber.

FIGURE 7. COMPARISON OF PRESSURE DROP ACROSS CLEAN BED AS A FUNCTION OF BED FACE VELOCITY FOR THREE FIBER BEDS

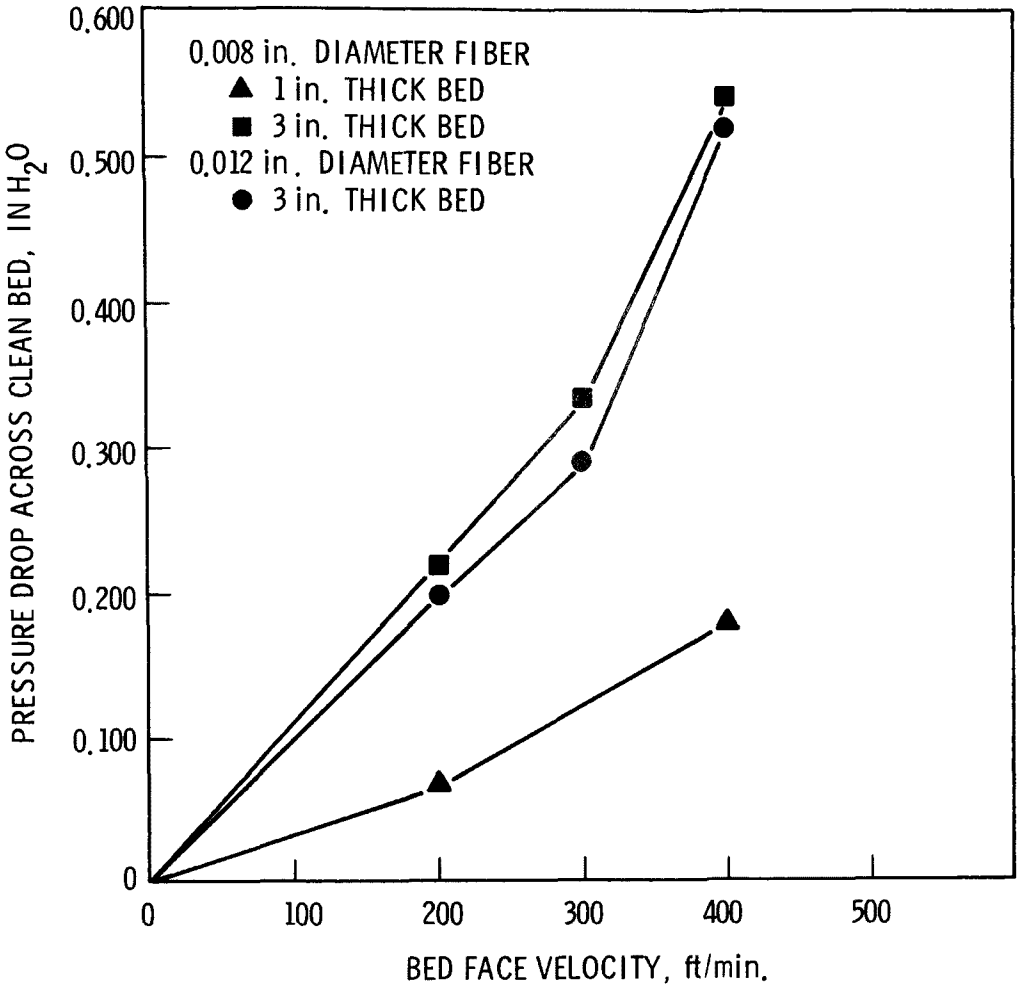

SUMMARY

Electrostatic Fiber Bed Filter System collection efficiencies of 95% or greater were routinely obtained over the velocity range of this study, 200 to 400 ft/min. For welding fume concentrations of 1 to 2 mg/m^3 collection efficiencies were consistently 99.9%. System pressure drop was extremely low, ranging from 0.07 to 0.82 in. H_2O.

ENDNOTES

1. The Welding Environment. American Welding Society, Miami, 1973.

2. Reid, Donald L. Electrostatic Capture of Fine Particles in Fiber Beds. In: Novel Concepts, Methods and Advanced Technology in Particulate-Gas Separation, Ariman, Teoman (ed.). Univ. of Notre Dame, 1978. p. 305-316.

THE USE OF GLASS CAPILLARY FILTERS TO CLASSIFY ACTINOLITE FIBERS

By: J. W. Gentry
Institute for Physical Science & Technology
University of Maryland
College Park, Maryland 20742

T. C. Chen, S. W. Lin, P. Y. Yu
Department of Chemical Engineering
University of Maryland
College Park, Maryland 20742

ABSTRACT

Described in this paper are recent results in the development of a GCAF (glass capillary array filter) inertial impactor. This instrument was designed to separate mixtures of fibers and isometric particles and to classify fibers according to their aerodynamic diameters.

Experimental evidence, suggesting that the more abundant particles are removed by the GCAF while fibers penetrate, is discussed. However, the principal thrust of the paper is the description of developments in simulating instrument performance. The simulations were designed to resolve two questions: 1) why do the GCAF stages preferentially remove isometric particles of relatively small aerodynamic diameters; and 2) how can penetration measurements be used to obtain unambiguous estimates of fiber length and diameter?

Because an exact simulation of the collection of particles by the GCAF would require the solution of the non-linear Navier-Stokes equations in three dimensions, analytical solutions are not possible. However, analytical solutions are possible for related problems which illustrate the collection mechanisms and elucidate our experiments. These solutions are discussed.

A computer code showed that fiber length as well as diameter could be characterized. The ideas developed here demonstrate that the physical dimensions of the fibers could be determined from penetration measurements if the fibers have a preferential alignment, indicate the sensitivity of such measurements, and indicate qualitatively the effect of polydispersity on the measurements.

TEXT

The aerodynamic separation or classification of fibers poses a number of interesting and, presently, unresolved problems. In a recent paper, Spurny (1) suggested that an aerosol of asbestos or actinolite fibers with a narrow size range could be prepared

by first grinding a mineral sample and then producing an aerosol with a vibrating bed generator. The fibers are then collected and size classified by selective sedimentation in aqueous solutions. This process is quite tedious requiring several months to prepare a sample. A method based on either aerodynamic and/or electrostatic classification of a fibrous aerosol presents the possibility of rapid size classification.

In measuring fibers either in remote rural areas or in the work place, a major difficulty is separating the more abundant isometric particles from the fibers. Typically, the fiber to isometric particle ratio is 1:3000 (2). Recently, we have developed a GCAF (glass capillary array filter) inertial impactor which shows promise both in preferentially removing isometric particles and in classifying fibers according to their size.

The GCAF inertial impactor has been described previously (3-5). The principal properties of the instrument are as follows:

1. The impactor consists of six two-section stages.

2. The first section of each stage is a glass capillary array filter (Galileo Electro-Optics Corporation) which hopefully will remove the isometric particles while allowing the fibers to pass through.

3. The second section of each stage is a Mercer type impactor (6).

4. The GCAF consist of uniform, equally spaced pores with diameters of 10, 25, or 50 μm. Their porosity is 50%, and their pore length is 0.055 cm.

In this paper, results are presented which suggest that the fibers preferentially penetrate the GCAF while the isometric particles collect in the interstitial areas between pores. However, the bulk of this paper deals with the simulation of the GCAF. Specifically, we consider the questions: 1) why are isometric particles collected in the interstitial areas between pores; and 2) if the GCAF are mounted horizontally (the axial flow is perpendicular to the gravitational field), can one determine fiber lengths as well as diameters?

Although in this paper there is insufficient space to describe the experimental measurements in detail, it is important to indicate the key results. These are as follows:

1. Several investigators (7, 8) have shown that when polystyrene latex aerosols deposit on nuclepore filters, the deposition on the narrow bridges between pores is significantly greater than around isolated pores.

2. In our laboratory, the fractional penetrations of polystyrene latex aerosols as a function of flow rate through the GCAF were measured (9). Typical results are shown in Figure 1. The efficiency is plotted as a function of the Stokes number (based on the jet diameter of the Mercer impactor) with the solid and open symbols representing the absence and presence of the impaction plate.

Several points are significant about these results. First, there is little difference with or without the impaction plate indicating that collection is on the GCAF. Secondly, the efficiency is near its maximum value of 50% (the GCAF porosity). In Figure 1, these experimental results were compared with the Pich model for collection on capillary filters. Agreement is good for the lower velocities. As the velocity (i.e. Stokes number) increases, the collection efficiency decreases. This result is typical of what would be expected if there were significant "bounce" and reentrainment. What is surprising is that this apparent reentrainment occurs at velocities much lower than predicted by theory (10).

In addition, there is qualitative evidence pointing to a different mechanism than that suggested by Pich. From this theory, one would expect that the particles would be collected at the rims of the pores; whereas from scanning electron micrographs the heaviest particle depositions were in the center of the narrow regions between pores.

3. In our laboratories, the GCAF have been used to remove agglomerates from test aerosols of actinolite. SEM micrographs of crocidolite fibers passing through a 25 μm GCAF are shown in Figure 2. What is significant from these micrographs is that the fibers penetrate but that most of the small isometric fragments of fibers were removed. These results are especially significant in view of recent theoretical and model simulations of fibers penetrating through orifices (11).

Based on these experimental results, a prima facie case exists for believing that the GCAF could be used to increase the fraction of fibers.

The principal objective of the simulations was to determine whether a filter with irregularly spaced pores would have the same collection efficiency as a filter with regularly spaced pores and the same porosity. As mentioned above, experiments with nuclepore filters and with the GCAF showed a heavier deposit in the interstitial areas. If the GCAF impactor is to operate effectively, there must be significant collection of isometric particles in the interstitial areas. Furthermore, there must be relatively sharp velocity gradients in the vicinity of the pores in order to impose a preferential alignment of the fibers. It should be stressed that the goal of the simulation is to deter-

mine how the fluid velocity and its gradients are altered as the distance between pores decreases. This differs significantly from the objective of previous investigators (12-14) who, in their simulation of collection by nuclepore filters, have focused on the collection efficiency of a centered pore within equally spaced cells.

In general, this simulation, because of the lack of angular symmetry, would require a solution of the Navier-Stokes equation including the inertial terms in three dimensions. Moreover, an analytical solution is precluded because the Navier-Stokes equation is non-linear, and one needs to reduce the dimensionality to two in order to define a stream function ψ. In previous numerical simulations, the dimensionality was two (the coordinates were the radial distance from the center of the pore R and the down stream distance Z) with the velocity field determined from a finite difference algorithm.

Our approach was as follows:

1. The velocity field was determined analytically for two related problems: the flow through a filter consisting of identical cells, each cell containing two parallel slits; and the flow through a filter consisting of identical cells, each cell having a centered central pore surrounded by an annulus.

2. The filter was divided into equally spaced cells assuming that laminar flow was established within the slit, pore or annulus. By shrinking the distance between the slits (or the pore and annulus), the closing of two pores together could be approximated.

3. Since there is angular symmetry, a stream function can be defined. Neglecting the inertial terms and eliminating the pressure from the Navier-Stokes equations results in

$$\frac{\partial \omega}{\partial t} = \frac{1}{Re} \nabla^4 \psi \qquad (1)$$

where ω is the vorticity and ψ is the stream function.

4. For the "slit" model, the solution of the stream function is a Fourier series; while for the "pore and annulus" model, the solution is an infinite series of Bessel functions. Manton (15) has applied this method to simulate a "cell" model with a single centered pore.

5. The three dimensional Navier-Stokes equation will be solved with a self-adjusting finite element method (16) with the analytical solutions providing a check on the accuracy of the numerical solution.

6. Finally, the particle trajectories are determined by numerical solutions for the particle trajectories ($\vec{V}$)

$$\frac{d\vec{V}}{d\bar{t}} = \frac{1}{Stk} (\vec{U} - \vec{V}) + \vec{F} \qquad (2)$$

where $\vec{U}$ is the dimensionless fluid velocity, $\vec{F}$ is external forces acting on the particle, and Stk is the Stokes number. In the simulations below, the fluid velocity $\vec{U}$ was determined from the analytical solution for the slit model.

As pointed out by Manton, neglecting the inertial terms is reasonable for nuclepore filters where the Reynolds number (Re)<0.005. For the GCAF filters used in this study, Re~0.1-1.0, and the physical basis for neglecting the inertial terms is less sound. Therefore, simulations for the analytical flow field can best be regarded as asymptotic approximations. A "cell" with two identical pores is simulated by requiring the flow through the pore and annulus to be equal.

An important feature of these simulations is that very accurate estimates of the velocity are required. If the velocity field is to be used to determine the trajectory of fibers, not only the velocity but the gradients and vorticity must be specified. It is for this reason that a finite element rather than a finite difference algorithm was deemed more useful.

For these simulations, the porosity was 0.10. The "cell" was characterized by two dimensions: a coordinate perpendicular to the slits and parallel to the face of the filter (Y), and a coordinate perpendicular to the face of the filter (Z). The slits were symmetrical around the centerline of the cell (Y=0) with midpoints occurring at $Y=\pm Y_o$). The boundaries of the cell were located at $Y=\pm 1$ and were characterized by $V_y \equiv 0$ and $\partial V_z/\partial Y \equiv 0$. The slits were assumed to be of sufficient length that end effects could be neglected.

With these assumptions, the stream function could be expressed by:

$$\psi = - Y + \sum_{j=1}^{\infty} a_{1j} (1 + \lambda_j Z) e^{-\lambda_j Z} \sin \lambda_j Y \quad \text{with} \qquad (3)$$

$$a_{1j} = \frac{12}{\lambda_j^4 (b-a)^3} [2 (\sin \lambda_j a - \sin \lambda_j b) + \lambda_j (b-a) (\cos \lambda_j a + \cos \lambda_j b)] \qquad (4)$$

From the stream function, the velocity components and vorticity

can be expressed by:

$$V_y = \frac{\partial \psi}{\partial Z} \qquad V_z = \frac{-\partial \Psi}{\partial Y} \tag{5}$$

$$\omega = \frac{\partial^2 \psi}{\partial Y^2} + \frac{\partial^2 \psi}{\partial Z^2} \tag{6}$$

For a porosity of 0.1, the width of the slit is 0.1 with its midpoint at Y_o. Even though the net flow through the slits is not altered by the location Y_o, the collection efficiency changes significantly as $Y_o \rightarrow 0.05$. In Figure 3, the collection efficiency for a Stokes number of 0.1 is plotted as a function of Y_o. The upper curve represents the total collection efficiency, and the dashed curve corresponds to the fractional collection efficiency in the narrow region between the slits. The relative deposition between the slits becomes much heavier as the distance between the pores shrinks, and the overall collection efficiency increases dramatically as the slits approach one another. This result suggests an explanation as to why heavier depositions are observed in the bridge between pores in nuclepore filters, and it is a possible explanation as to why the experimental collection efficiency with nuclepore filters of very small particles is larger than expected from theory (17).

In Figures 4 and 5, a comparison is made of the trajectories for a particle initially at a location of Y_o-0.025 with the Stokes number as a parameter. When Y_o is equal to 0.15, the gas stream lines (solid curve) are strongly distorted. The smaller particles (small Stokes number) tend to follow the gas stream lines and, consequently, are not collected. The particles of very large size do not deviate significantly from the vertical stream lines upstream from the filter. Intermediate particles are collected as they follow the initial distortion of the stream lines, but are unable to follow the sharp reverse bend near the filter surface. Consequently, one has the interesting result that for conditions where inertial impaction is the principal collection mechanism and where there is no reentrainment or bounce-off, the collection efficiency first increases and then decreases as the particle size (or as the upstream velocity) increases. This provides an explanation for the surprisingly experimental results shown in Figure 1. When the slits are more equally spaced (a value of Y_o=0.5 would correspond to uniform spacing), one does not have the distortion of the stream lines, and this effect is not observed.

In considering particle collection by the glass capillary array filters, account must be taken of several mechanisms: 1) diffusional collection within the pores; 2) gravitational settling within the pores; and 3) inertial impaction on the interstitial areas between pores at the filter face. Here the collection of fibers within the GCAF is simulated. Specifically,

we wish to examine whether it is possible to determine both length and diameter from penetration measurements, and what effect polydispersity of the fibers will have on the penetration. The simulations were carried out using a computer code developed in our laboratory and discussed elsewhere (18). The principal features of the code were:

1. Actinolite fibers were represented by prolate spheroids of diameter D_p and mean aspect ratio B_o. The aspect ratio B was distributed log normally with a standard deviation σ.

2. The fibers were aligned with their major axis parallel to the direction of flow (an option of randomly distributed fibers was provided).

3. The mechanical properties of the glass capillary filters were completely determined by a porosity (ε), a flow rate (Q), a pore diameter (D_f) and length (L_f), a cross-sectional area (D_o) and an angle of inclination (θ).

4. The penetration where only gravitational settling was a mechanism for particle removal was given by the expression of Pich where the settling velocity was given by the expressions of Oberbeck for spheroids.

5. When Brownian diffusion was predominant, the Gormley-Kennedy expression was applied.

We first considered whether the length and diameter could be determined independently. Experimental conditions were chosen where diffusion could be neglected. The standard deviation σ was chosen as 0.1 corresponding to a distribution of almost constant diameters and lengths. In Figure 6, the ratio of the apparent aerodynamic diameter at an angle θ to the apparent diameter at 0° is plotted as a function of angle θ. The aerodynamic diameter is the diameter of a hypothetical sphere of unit density that has the same settling velocity as the fiber.

An "apparent" diameter corresponds to the diameter of a monodisperse particle distribution having the same penetration as the distribution. For $\sigma \leq 0.1$, the "apparent" aerodynamic diameter is simply the aerodynamic diameter.

For spheres or randomly aligned fibers of a monodisperse distribution, the aerodynamic diameter does not vary with angle. This follows because the penetration Pt is a function of a variable χ where:

$$\chi \sim \frac{V_s}{Q} \cos \theta \qquad (7)$$

with V_s the settling velocity. If the particle were spherical

or if it were randomly aligned, V_s could be constant. On the other hand, if the fibers have a preferential orientation, the values of V_s (and the aerodynamic diameters) would vary with orientation. In Figure 6, the ratio is plotted as a function of angle for different values of mean aspect ratio. For B_o=1 (spheres), as expected, it is observed that the aerodynamic diameter remains constant, whereas for values of B= 10 and B= 100 the aerodynamic diameter decreases with respect to B. This would suggest that it is feasible to distinguish between aerodynamic diameters and hence fiber length depending on the angle of orientation.

However, if the method is to be useful, one must be able to detect meaningful differences in the experimental penetration at different orientations. In Figure 7, the penetration is plotted as a function of Q/cos θ for two different aspect ratios. For each value of mean aspect ratio, three angles of orientation are used: 0°, 45°, and 60°. Since the penetration varies by more than 5 %, greater than the uncertainty in measurements, penetration measurements have the capability of discriminating between fibers of different lengths when the fibers align with the flow field.

In this paper, it was demonstrated that one could determine fiber length from fractional penetration measurements if the angle of the elutriator or settling chamber were varied and if the fibers acquire a preferential alignment. These results suggest a method for classifying fibers according to their length as well as diameter.

Numerical simulations indicate why much heavier depositions are observed in the interstitial areas between pores. These results and preliminary experimental measurements suggest that the GCAF may be used to remove isometric particles and to concentrate fibers.

ACKNOWLEDGEMENT

This research was partially supported by the Environmental Protection Agency (Grant # R 8065 180 1) and by the National Science Foundation (Grant # CPE 80 11269).

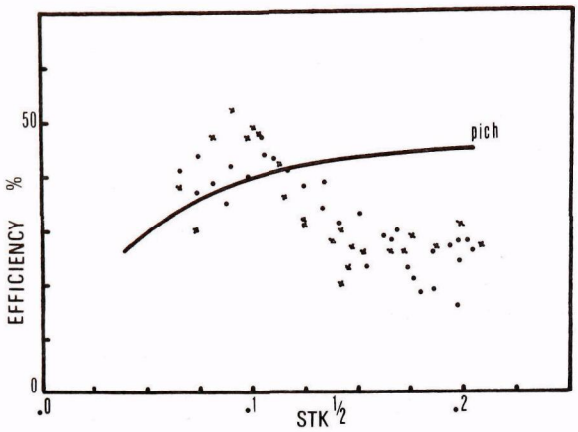

Fig. 1 Collection Efficiency for 0.62 μm PSL Aerosols (25 μm GCAF)

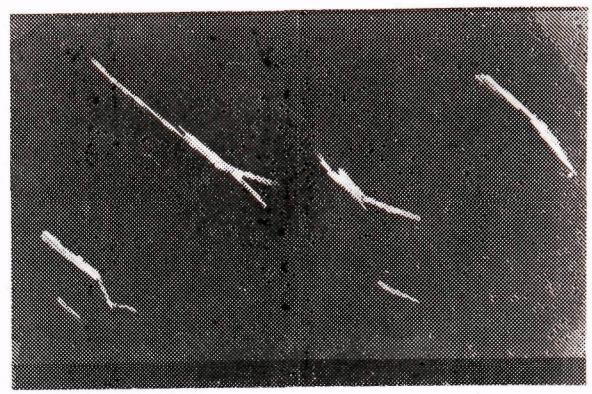

Fig. 2 Chrysotile Fibers After a 50 μm GCAF

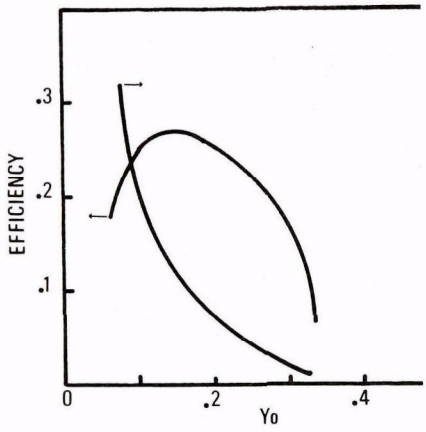

Fig. 3 Collection Efficiency at Stk=0.1 for "Slit" Model as Function of Slit Location

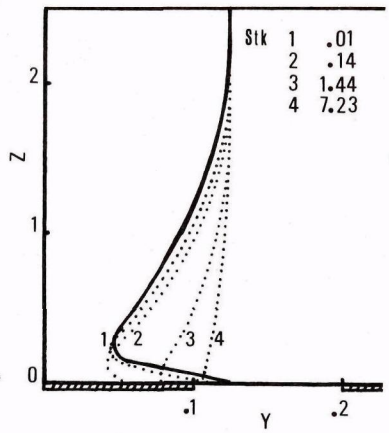

Fig. 4 Particle Trajectory as a Function of Location and Stokes Number

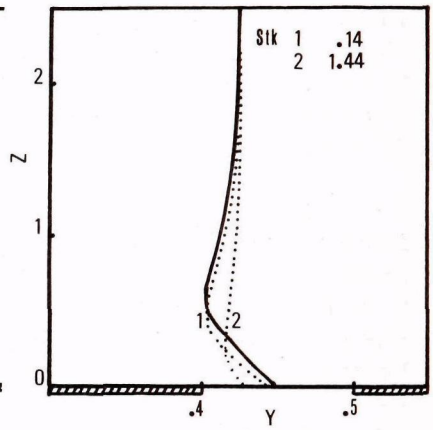

Fig. 5 Particle Trajectories as a Function of Location and Stokes Number

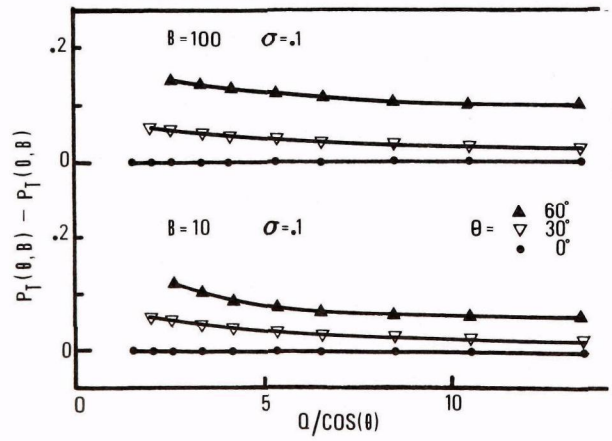

Fig. 6

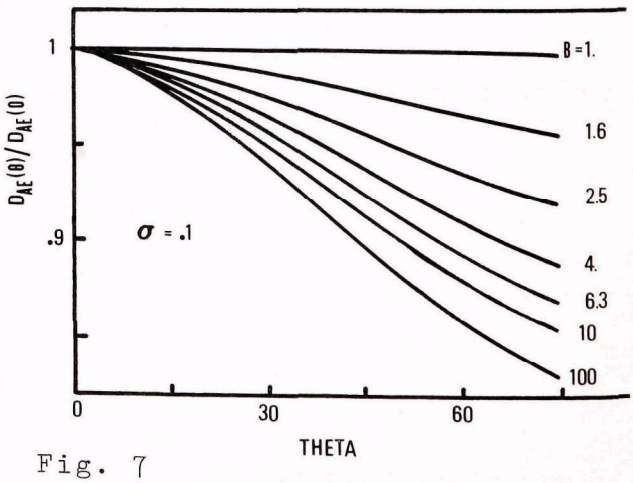

Fig. 7

ENDNOTES

1. Spurny, K., W. Stöber, H. Opiela, and G. Weiss. Am. Ind. Hyg. Assoc. J. 4: 198-203, March 1980.

2. Spurny, K., J. Gentry, and W. Stöber. In: Fundamentals of Aerosol Science, Shaw, D. (ed.). New York, John Wiley & Sons, Inc., 1978. p. 257-324.

3. Kellert, R., R. Preston, C. Johnson, D. Safferman, M. Shapiro, and J. Gentry. I&EC Prod. Res. and Develop. 19: 502-506, December 1980.

4. Lin, S., L. Colcord, M. Triantafillou, C. Field, and J. Gentry. (Presented at the Fine Particle Society Meeting, College Park, Md., Sept. 16-18, 1980).

5. Lin, S., R. Preston, and J. Gentry. In: Atmospheric Pollution, Benarie, M. (ed.). Amsterdam, Elsevier Scientific Publishing Company, 1980.

6. Mercer, T., and R. Stafford. Ann. of Occup. Hyg. 12: 41-48, 1969.

7. Fan, K., C. Leaseburge, Y. Hyun, and J. Gentry. Atmospheric Environment. 12: 1797-1802, No. 8, 1978.

8. John W., G. Reischl, D. Bettencourt, S. Goren, and D.Plotkin. (Presented at the 10th Aerosol Technology Meeting, N.M., 1977).

9. Lin, S. M.Sc. Paper, University of Maryland, 1980.

10. Dahneke, B. J. of Coll. & Inter. Sci., 51: 58-65, April, 1975.

11. Cohen, A., J. Gallily, A. Schiby, W. Holländer, P. Mause, D. Schiless, and W. Stöber. (Presented at the GAeF Conference, Schmallenberg, West Germany, 1980).

12. Smith, T., C. Phillips, and O. Melo. Environ. Sci. Technol. 10: 274-277, March, 1976.

13. Parker, R. Ph.D. Diss. Duke University, N.C. 1975.

14. Parker, R., and G. Buzzard, J. Aerosol Sci. 9: 7-16, No. 1, 1978.

15. Manton, M. Atm. Environ. 12: 1669-1675, 1978.

16. Babuska, I. In: The Mathematics of Finite Elements and Applications, Whiteman, J. R. (ed.). London and New York, Academic Press, 1976. p. 125-142.

17. Gentry, J., K. Spurny, and J. Schoermann. (To be published in Atm. Environ. 1981).

18. Colcord, L., Y. Park, P. Anderson, and J. Gentry. (Presented at the GAeF Conference, Schmallenberg, W. Germany, 1980).

ULTRA-HIGH EFFICIENCY FILTRATION SYSTEMS (AIR RECIRCULATION)

Robert W. Potokar
Staff Development Engineer
General Motors Corporation
Manufacturing Staff
Warren, Michigan

ABSTRACT

The metal casting industry is becoming increasingly aware of the role energy availability and its efficient use has on productivity and profitability. One of the major uses of energy in a foundry is for heating and distributing make-up air. Efficient filtration and recirculation of presently exhausted air could be a viable technique for energy conservation in some cases. This paper will review new hardware and test data from pilot testing sponsored by the American Foundrymen's Society (AFS) which indicates that particulate removal efficiencies in excess of 99.96% are feasible from casting cleaning operations. In addition, guidelines for a complete system design will be presented.

TEXT

One of the major uses of energy by all foundries is for heating and distributing make-up air. On a yearly basis, heating, ventilation, and air conditioning (HVAC) energy usage averages over 15% of the total energy used by an iron foundry. During a winter month, this percentage may rise significantly. The amount of energy going to HVAC has accelerated in recent years because of increasing pressure from OSHA, unions, and employes to meet contaminant standards and improve worker comfort. The recirculation of exhaust air can provide for significant reductions in consumption of energy for tempering make-up air. Filtered and cleaned exhaust air can help improve the in-plant environment by allowing the ventilation engineer to use more air volume to capture air contaminants without overtaxing make-up air systems and disrupting the static pressure balance within the plant.

Why air recirculation as an energy conservation means? The majority of the air exhausted from foundries is near ambient temperature. The volume may be in the order of 10 million ft^3/minute in some of the large automotive casting facilities. The magnitude of the air handling problem is exemplified by the fact that some iron foundries use up to 40 air changes per hour resulting in 112 tons of air being handled per one ton of iron poured. The fact that we are dealing with large air volumes at relatively low temperatures makes the cost effectiveness of heat recovery marginal. Also, heat recovery equipment (heat wheels, heat pipes, air-to-air heat exchangers, etc.) only offer a 40% to 70% BTU recovery potential, whereby air recirculation approaches 100% recovery of the energy in an air stream.

Present day foundry process exhaust systems have, as an integral part of particulate removal systems, baghouses, electrostatic precipitators, or wet scrubbers. However, the efficiencies to meet EPA emission requirements do not approach the efficiencies needed to meet recirculation guidelines. What we find in many foundries is the make-up air system inlet near an exhaust duct resulting in the worst system possible. The heat is lost from the exhaust, but the contaminants are partially recirculated. Some states do have prescribed limits for the type and concentration of contaminants allowed in recirculated air, but many do not. A general rule is that the recirculated air should contain no contaminant in excess of 10% of the permissible exposure levels (PEL) for each substance. These PEL are set by OSHA.

To help coordinate the metal casting industry's efforts on air recirculation and stimulate supplier R&D, the American Foundrymen's Society organized the Air Recirculation for Energy Conservation Committee in 1977. The Committee has focused its efforts on filtration and reintroduction of exhaust air into the work space to conserve energy. Not considered is the utilization of dirty exhaust in other processes or the use of unheated make-up air around ventilation hoods to provide the needed draft and exhaust volume. These types of conservation techniques are best handled on an individual plant basis. Also, because of the poor efficiency of heat recovery and the fact that suppliers, engineers and engineering societies are addressing indirect heat recovery, these areas would not be considered.

From the Committee's inception up to today, significant progress has been made where filtration hardware is available which we believe can meet the requirements for ultra-high filtration efficiencies on heavily loaded particulate streams such as casting cleaning process exhaust. Before a detailed review of where the technology stands today, a brief outline of the Recirculation Committee's activities to date is warranted.

Foundries, as all complex multi-process facilities, have numerous exhaust streams, all with different temperatures and contaminants. Exhaust emanates from the mold room, core room, shakeout, sand handling systems, cleaning room, and other processes. To obtain a background on present recirculation installations and past attempts, a questionnaire was sent to 3500 industry executives. Based on this survey, and on the fact that the exhaust from the cleaning room should have no products of combustion, it was decided that the first process to be fully investigated for recirculation would be the cleaning room. The cleaning room operations are a conglomerate of processes such as grinding and debugging. They employ the largest percentage of people and run production during periods when other heat-producing operations of the foundry would not be able to supply heat necessitating the use of outside energy or make-up to replenish exhaust. Generally, the cleaning room exhaust volume is about 20% of the total foundry exhaust. This may add up to 1,500,000 cfm or more in a large automotive facility.

From the survey, we found no installation that represented the best engineering practices, which includes properly specified air filtration equipment followed by a return air monitoring system and a bypass to atmosphere in case of failure or efficiency problems. Some of the newer recirculation installations from blast cleaning in the cleaning room are using opacity meters to monitor the cleanliness of the exhaust before return to the work space. However, the sensitivity of opacity meters is quite limited. It would require a path length of 10 feet between the light source and sensor to enable a 1% opacity change to relate to a rise in particulate concentration from 1 mg/m^3 to 2 mg/m^3. Because opacity is an optical measurement, it is dependent on particle size distribution and reflectivity characteristics of the particulates in the gas stream. So, to use an opacity meter, the instrument has to be calibrated versus in-stack mass measurements and the particle characteristics must remain constant over all conditions.

Getting back to the results of the survey, it was found that some foundries have attempted to recirculate from different operations without success. In one case, the recirculation was in operation for a year before it was discovered that the concentration of free silica in the breathing zone was too high due to the recirculation. From this background, it was decided that a demonstration recirculation system be installed on the cleaning room exhaust following these steps: (1) emission characterization, (2) filtration equipment specification, (3) monitoring equipment specification, (4) integration of a complete system, (5) build and installation, and (6) performance testing.

To determine the type of filtration required to recirculate cleaning room process exhaust emissions, characterizations were done on a select blast cleaning process at five different foundries. AFS research funds were used to accomplish this task, and the five participating facilities provided the required test ports, access scaffolding, and site coordination. The five facilities ranged from the highly automated automotive casting plants to small batch operations, all with a variety of ventilation and collection systems. The tests were conducted in the following manner. The data will not be identified as to the source to insure confidentiality.

Simultaneous inlet and outlet process emission samples from a cleaning room shot blast exhaust stack and existing collector discharge were performed in duplicate at each of the five foundries. Each emission characterization included all the parameters listed in Table I and was conducted in the prescribed manner.

Both inlet and outlet from existing collectors is important in the development of design criteria for either a complete new process filtration system or for an add-on polishing filtration system.

For uniformity in having equipment suppliers bid on systems to meet recirculation requirements, a "typical exhaust" was formulated in Table II. The particle size distribution of the inlet and outlet

mass is shown in Figures 1 and 2, respectively. Because of the large amount of submicron material, with the inlet having approximately 700 mg/m^3 of particulate < 4μ, fabric filtration is a good candidate treatment system type.

Using these data, over 50 equipment vendors were requested to specify a 5000 cfm collection system to act as either a process collector or a finishing collector on top of the existing collector. Manufacturers of all generic types of air pollution control equipment were included on the bid list. Of the over 50 suppliers contacted, four generic types appeared, on paper, to have the potential for high efficiency and reasonable maintenance.

All four systems were tested at the Central Foundry Division of General Motors Corporation, Pontiac plant. The pilot units were tested on a slip stream of direct process exhaust from an iron casting blast cleaning cabinet. The unit's performance was tested using the same sampling procedures previously described. All of these filtration systems are now commercially available. The four systems included an electrostatically augmented baghouse, a two-stage baghouse system, a single baghouse using polyester felt bags with a teflon lamination, and a two-stage cartridge filtration system.

The operation of the electrostatically augmented baghouse uses an ionizing section directly upstream from a baghouse. As particulate matter passes through, it is charged to saturation. The charged particles create a polarization effect between the particles and the fabric surface. Our pilot testing confirmed that significantly higher filtration efficiencies occur with the use of the high voltage charge. Also, a reduced pressure drop was witnessed when the electrostatic charging section was used. With the charge, the particulate removal efficiencies were in excess of 99.98%. During the course of over two months of on-stream running, it was determined that if the electrostatic section was turned off, the pressure drop across the system would build up six times faster. This is due to the polarized particles which form a "fluffier" dust cake on the fabric and to precipitation within the ionization section on the cylinder walls supporting the corona wires.

The unit tested had the ionizing hardware integrated into the baghouse system where the reverse jet air was also used to purge dust from the corona wires, grounded tubes, and supports. Preliminary investigations have been made by the supplier to determine if a separate ionization section could be used to achieve the same effects. It is envisioned that the ionizer could be located in ductwork upstream from an existing baghouse, thus enabling retrofit of conventional equipment now in the field. A drawback of this approach is that the ionized particles tend to precipitate out on the grounded duct between the ionizer and the entrance to the baghouse. Also, compressed air or another cleaning mechanism is required in two locations to remove dust build up in the corona section and in the baghouse.

Before I discuss the remaining work, I want to point out that the AFS and Committee policy is not to mention suppliers by name, but merely refer to generic system type.

The second pilot system tested was a two-stage baghouse. The first stage was a reverse jet system with a 7:1 air-to-cloth ratio using dacron felt bags. The second stage was a shaker-type unit with a 6:1 air-to-cloth ratio, with cotton bags and a cellulose pre-coat filter aid. The filter aid effectively forms a high efficiency filter in place. The first stage is designed to reduce dust loading from the approximately 1000 mg/m^3 down to approximately 20 mg/m^3. The second stage, ultra-filtration step, reduces dust loading to less than 0.3 mg/m^3. The test data shows that upon start up, the system efficiency was 99.96-99.97% and after one month of continuous on-stream operation, the efficiency rose slightly to 99.98%. Before concluding all tests with this system, a breakdown in the first stage baghouse was stimulated. Two of the 36 bags in the first stage were intentionally torn. The subsequent emission tests documented that the efficiency was still in excess of 99.96%. A second stage baghouse using a pre-coat filter aid can be used to retrofit an existing system presently exhausting to increase efficiency for possible recirculation. However, the efficiency in the first stage must be adequate; that is, the outlet from the first stage should be in the magnitude of 20 mg/m^3 to avoid overload of the second stage.

The third pilot system tested utilized only the first stage baghouse from the aforementioned system. The dacron felt bags were replaced with a new type of bag. The new bags have a microporous teflon membrane laminated to a felt filter media. The manufacturer claims that unlike typical fabric or felt filter media, which depends upon particle build up or a pre-coat for filtration, the filtration takes place both on the surface of the membrane and on the collected particles. Thus, a steady high efficiency can be achieved without the need for a pre-coat. Our tests with these membraned bags resulted in a particulte removal efficiency of 99.59% on the blast cabinet exhaust. Only limited testing was done with these bags due to time restraints. No estimate can be made on bag life or if the efficiency would increase or decrease with use. The emission testing was done the same day the new bags were installed. Only 45 minutes of on-stream running occurred before emission testing commenced. The efficiency of the pilot one-stage system with conventional bags was 98.6%, which means a significant increase in efficiency did occur. The penetration of particles decreased with the new bags from 1.4% to 0.41% which is over a three-fold decrease in penetration.

The final pilot filtration system evaluated was an aspirated cartridge dust collector with a second stage filter for monitoring the entire air stream. The primary pleated cartridges instead of bags are used for particulate collection and compressed air is used to back flush the cartridges for cleaning. The cartridges are made of a non-woven, synthetic and cellulose material, and the back-up monitoring filter is also of cellulose. During the first tests on the unit, the total

particulate load was dropped from a 925 mg/m^3 inlet to 0.20 mg/m^3 on the outlet. After this test, a team from the manufacturer checked the system for leaks and one cartridge was changed because of a suspected leak. This leak may have occurred in shipment or during manufacture. Another test was performed and during this test, the efficiency increased to 99.997%. The inlet concentration was 1248 mg/m^3 and the outlet 0.033 mg/m^3. This system was on-stream for four months with no apparent problems.

The particulate removal efficiencies quoted and summarized in Table III are based on total gross particulate load. A complete breakdown of composition of particulates and gases will be made part of our committee report due for publication this year, if our committee completes the laborious task of writing in a timely manner.

Our goal as an American Foundrymen's Society committee was not to certify or test every piece of filtration equipment, but to stimulate suppliers to develop equipment to meet the needs of high efficiency filtration and the unique needs of our industry. We feel this goal has been met. The pilot demonstration and test program also showed that this type of equipment can operate in a foundry environment without oberburdening maintenance.

Before any of these or any other system should be considered for an application, a complete specification should be developed. The criteria of loading, particle size, particulate and gas composition, along with all the other parameters outlined in Table I, must be measured. The data should include the extremes that the exhaust stream may vary to. Any control system must be able to not only meet the normal conditions, but also perform under the abnormal conditions.

The allowable contamination in the recirculated air is not a definitive value. Some states and foreign countries use the value of 1/10 the TLV for any contaminant in the recirculated air. NIOSH, the National Institute for Occupational Safety and Health, has published "A Recommended Approach to Recirculation of Exhaust Air" in an attempt to address this question. This 184 page document presents complex mathematical means for back calculating the effect of recirculated air on the air that workers will breathe. The AFS Committee on Exhaust Recirculation has taken the stance that (1) the recirculated air should not contain any contaminate in excess of four times the Primary Ambient Air Standard. (If a particular contaminant is not covered under the Ambient Air Standard, the value 1/10 the established PEL should be used.)

The quality of the recirculated air should be monitored on a regular basis. The definition of regular is subject to a great variance in interpretation. As a committee, we recommend that a method be used to continuously monitor the recirculated air return and a bypass to atmosphere in case of filter failure be tied into the system. Also, periodic measurements should be taken, at least upon system installation and at a minimum of once a year thereafter in workers breathing

zones, to determine the effect of the recirculation system. There are a variety of methods which can be used to continuously on-line monitor the particulate content in recirculated air. It must be re-emphasized that our efforts to date have centered on air streams which do not contain toxic or detrimental gaseous constituents. If gaseous contaminants are to be continuously monitored, the specific component may be determined by infrared or another method. A number of such continuous readout monitors are on the market today.

For a determination of available equipment for particulate monitors at the low concentration levels required, we as a committee sent a survey to over 40 suppliers in the particulate sampling and monitoring business. Again, this effort was not only to determine the present state of the art, but also to stimulate effort for this market. The response has been gratifying. There are various light scattering instruments, both side scattering and forward scattering instruments, which are now coming on the commercial market. We are now working on a plan to evaluate a group of these instruments. All of these instruments cost between $2500-5000 per sensor point, and the sensitivity is approximately $\pm$ 0.005 mg/m^3 in the 0-0.5 mg/m^3 range.

Another method to continuously monitor the particulate level in recirculated air is by an after filter. This filter can either be for the entire air stream or for part of the air stream. The pressure drop across the after filter is sensed, and if the pressure drop exceeds a pre-determined level or rate of rise, an alarm can be activated along with a bypass to atmosphere. We plan to continue to gather data and information on feasible monitoring methods. This information will be made available through the American Foundrymen's Society.

The economics involved with air recirculation are continually changing. Today in the geographic climate area of Chicago or Detroit, the energy cost to heat and distribute one cfm of make-up air is about 50¢/year. The direct heat energy dollar value is not the only dollar savings. Other factors should be included such as the filter and maintenance cost for an existing conventional make-up air system and exhaust cleaning system. With a properly operating air recirculation system, both jobs can be done in one unit. Other benefits include: (1) tendency to neglect dust collectors is minimized because recirculation systems can substantially reduce the plant's energy bill; consequently, the equipment gets the inspection and maintenance it requires; (2) heat added by the dust collector fan (approximately 1°F for every two in. w.g.) is distributed along with the recirculated air; (3) tendency to starve dust collector fans because of inadequate make-up air is minimized; (4) a plant can afford to handle larger air volumes, increasing the capture efficiency of hoods, since make-up air heating costs are not a consideration.

As more plants become air tempered or conditioned for summer, the dollar savings for energy will approximately double. In addition, if a facility is in a non-attainment region and there is a need for a particulate emission reduction or tradeoff, high efficiency particulate removal systems may be dictated. If so, it would make good sense to consider recirculation. The estimated cost of a nominal 40,000 cfm process filtration system for a typical casting cleaning room exhaust capable of recirculation is in the range of $2-4 per cfm (not installed).

In the decade of the 1980's, the metal casting industry, as all American industry, will have difficulty in meeting the demands of increasing productivity and profitability while still meeting ever tighter government regulations and employe expectations. The AFS is committed to coordinating increased information and stimulating research, development, idea and experience exchange to help meet this challenge. On the subject of air recirculation, the AFS 10H Committee needs to continue to receive your comments and cooperation.

As I said before, a detailed report on this subject will be available soon. However, feel free to contact the AFS or me if we can be of service.

TABLE I

TEST METHODS

Parameter	Method
Total particulate concentration and stack conditions, temperature, velocity, etc.	EPA Methods 1-5
Particle size distribution	In-stack cascade impaction
Carbon monoxide	Wet chemistry
Phenols	Wet impingement, distillation and gas chromatography
Formaldehyde	Wet chemistry
Particulate chemical analysis on fraction ≥5μ and <5μ	
a. Free silica	X-ray diffraction
b. Cristobalite	"
c. Quartz	"
d. Tridymite	"
e. Cu	Atomic absorption spectrophotometry
f. Zn	"
g. Fe	"
h. Organics	Hexane extraction
i. Total inorganics	Difference

TABLE II

TYPICAL EXHAUST

	Inlet	Outlet
Emission particulates, mg/m^3	3500	60
Size distribution		
D_{p50}, microns	3.0	1.7
σ_g	4.3	3.0
Temperature, °F	70°	70°
Moisture content, %	4.0	4.0
Particulate breakdown		
Fe total, mg/m^3	595	9
Fe <5μ, mg/m^3	525	9
Ni total, mg/m^3	4.2	0.0
Ni <5μ, mg/m^3	2.8	0.0
SiO_2 total, mg/m^3	805	10.2
SiO_2 <5μ, mg/m^3	630	7.2
Benzene extractable total, mg/m^3	56	1.1
Benzene extractable <5μ, mg/m^3	46	0.8

TABLE III

SYSTEM EFFICIENCIES
(TOTAL PARTICULATE)

UNIT TYPE	TEST #	INLET (mg/m^3)	OUTLET (mg/m^3)	EFFICIENCY (%)
Electrostatic Baghouse	1	1054	0.19	99.982
	2	743	0.11	99.985
Two-Stage Baghouse	1	1040	0.26	99.975
	2	848	0.29	99.966
Two-Stage Baghouse (after 1 month)	1	656	0.13	99.980
Two-Stage Baghouse (2 bag failures first stage)	1	860	0.29	99.966
Single-Stage Baghouse (conventional bags)	1	1804	25.17	98.605
Single-Stage Baghouse (membrane lined bags)	1	1300	5.37	99.586
Cartridge Filter	1	925	0.20	99.978
	2	1248	0.033	99.997

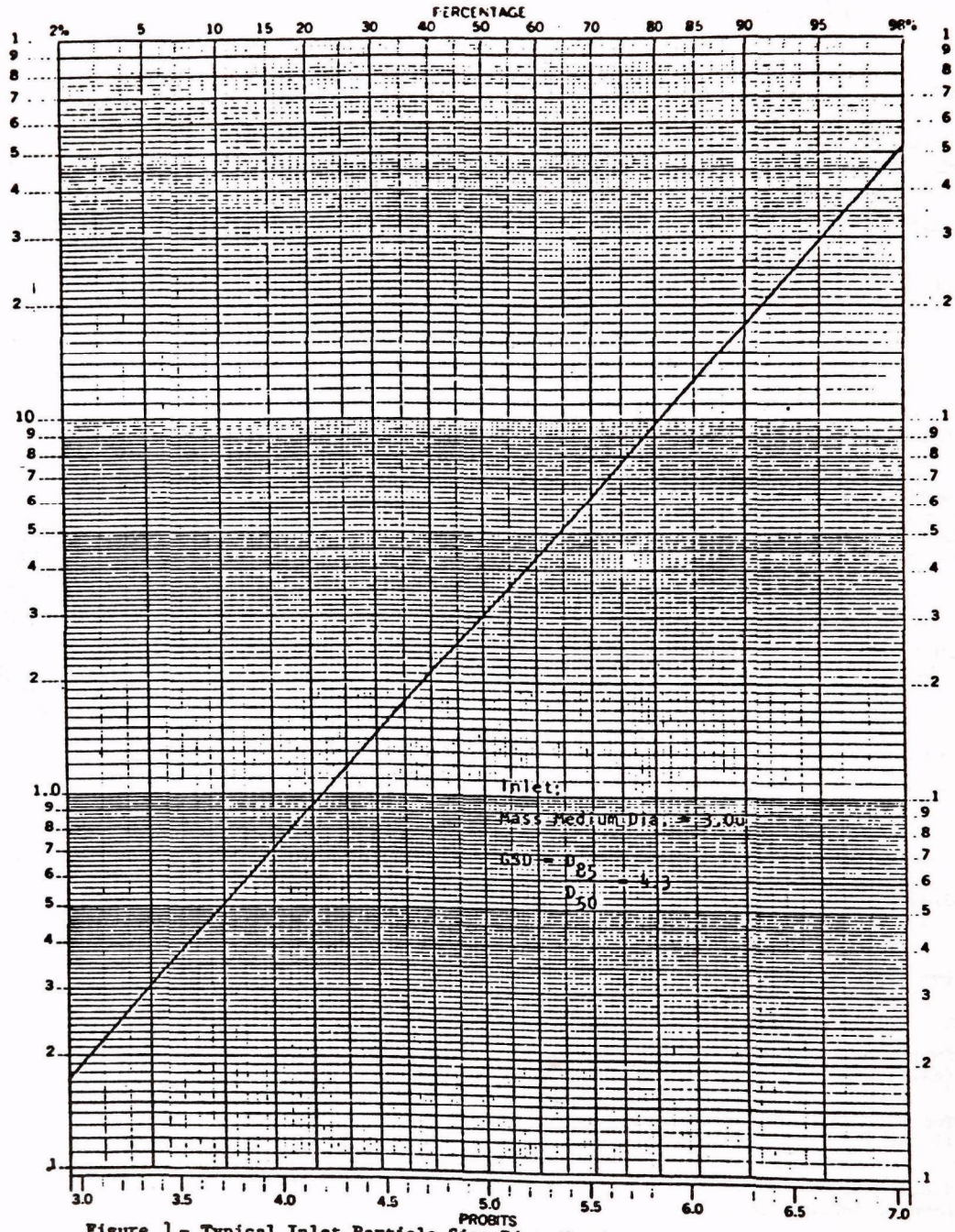

Figure 1 - Typical Inlet Particle Size Distribution

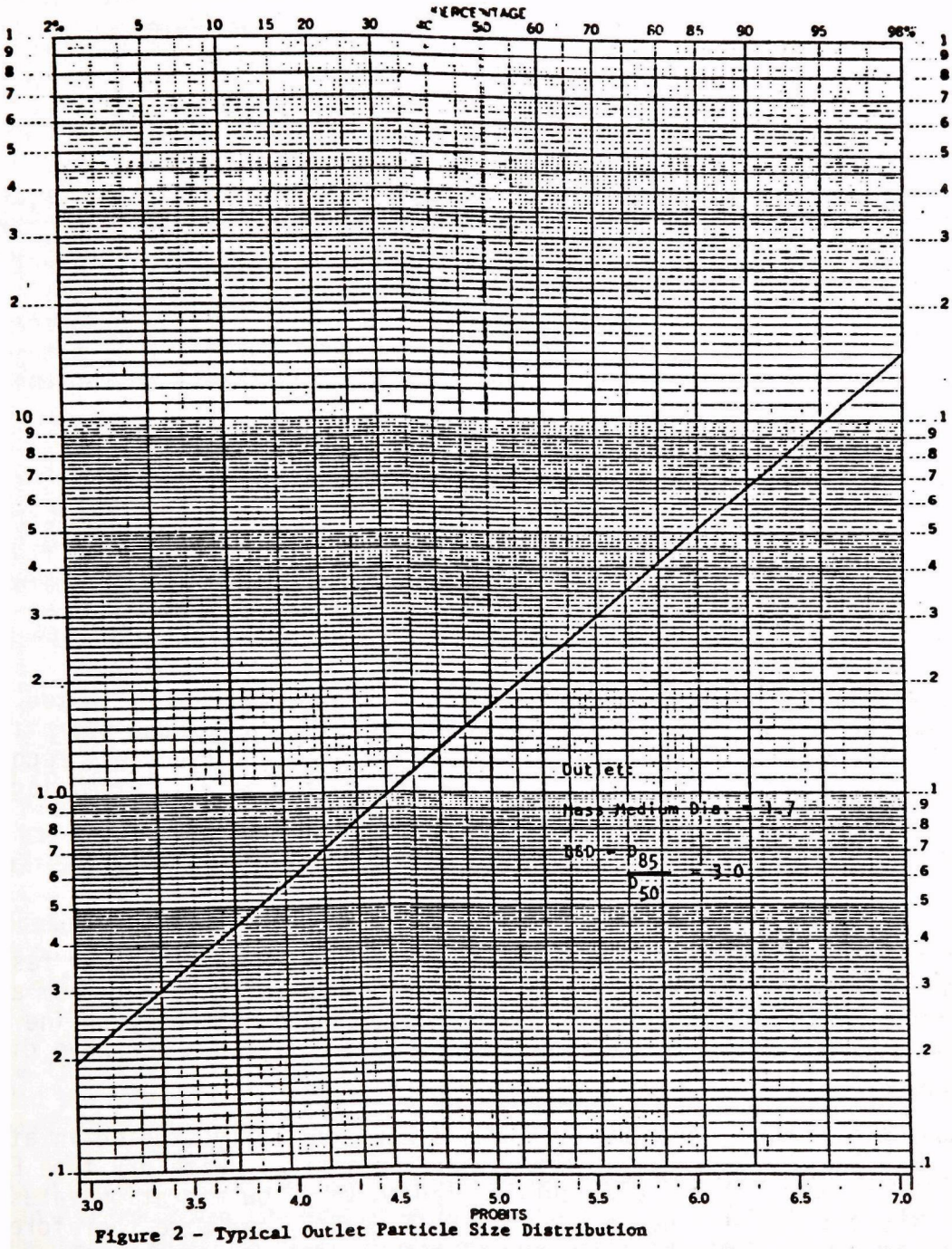

Figure 2 - Typical Outlet Particle Size Distribution

THE WET WALL ELECTROSTATIC PRECIPITATOR

By: Dr.-Ing. J. Starke
Phys. Forschungsinstitut (AP)
Bayer AG
Leverkusen, W. Germany

Dipl.-Ing. J. Kautz, Ober.-Ing. K-R. Hegemann
Gottfried Bischoff GmbH & Co., KG
Essen, W. Germany

ABSTRACT

The operating principles of electrostatic precipitators, particularly those of conventional wet electrostatic precipitators, are well known. The incentive to develop a new variation of the wet ESP - the wet wall electrostatic precipitator (WWP) - derived from investigations on the removal of particulates from waste gas from a plant designed to incinerate organically loaded wastewaters having high salt contents. Conventional ESP's, both wet and dry, as well as venturi scrubbers and fabric filters were tested and found to be uneconomical.

The most efficient and economical solution proved to be a wet ESP of new design with vertical, water-cooled ground electrodes. The water film resulting from vapor condensation on the cool electrodes instantaneously dissolves the soluble particulates and suspends the insoluble dusts, flushing both from the discharge zone. Thus the efficiency of such a precipitator remains constant since it is free of dust deposits and uninterrupted by flushing cycles.

The wet wall electrostatic precipitator has been thoroughly tested. It has a simple structural design permitting reasonable capital and operating costs. In the laboratory typical separation efficiency curves were recorded. Of several different applications tested in the field the most promising were those dealing with submicron particulates and aggressive gases.

INTRODUCTION

The development of this new wet-type electrostatic precipitator resulted from experiments on the precipitation of particulates originating from a plant for the incineration of organically contaminated, strongly saline effluent. These particulates form during cooling of the flue gas and have diameters in the order of 0.1 µm.

Conventional dust collection processes were initially studied in attempts to deal with particulates having these characteristics. With dry type ESP's the extreme fineness of the particulates led to very low migration rates. In addition the particulates had a very low bulk density and were therefore difficult to remove from the collector plates by rapping.

The acidic pollutants present in the flue gas and the latters high dew point dictated that only fabric filters such as glass, with working temperatures above 250°C, were applicable. It is known that it is difficult to remove sub-micron particulates from fabrics without damaging the fabric and lessening the service life. Reasonable service lives could only be obtained by setting specific loading per unit of surface area at uneconomical levels.

A conventional low pressure scrubber was tested at an efficiency of only 50%. By extrapolation, a venturi scrubber capable of adequate removal efficiency would require a pressure differential of 2,000 mm W.G. and unacceptable energy costs.

Experiments with vertical tubular ESP's of the wet type were more encouraging. There were; however, two remaining disadvantages. In wet ESP's designed for corrosion protection the collecting electrodes are fabricated from non conductive plastics. Plastics formulated to be conductive are not sufficiently resistant to damp corrosive flue gases. The surface of plastics which are used becomes conductive through deposition of moisture from the water separated; however, these electrodes become progressively drier and less conductive in the cleaned gas direction. Thus the contribution of this section of the ESP to cleaning is minimal.

The second disadvantage is that the electrodes must be rinsed down at regular intervals. During this period the collection efficiency drops considerably, a characteristic which is overcome in actual operating practice by providing more expensive dual zone precipitators.

Design and Operating Principle of the Wet Wall Precipitator

The Wet Wall Electrostatic Precipitator (WWP) was designed to incorporate the useful features of conventional wet type ESP's and overcome the disadvantages referred to above. As seen in Figure 1, the novel feature is the cooled collecting electrode design which facilitates the condensation of water vapor from the gas being treated. The condensed water film then provides the desired surface conductivity and rinsing characteristic. The thermal conductivity of the plastic tubes is an important consideration.

These concepts were initially tested in a wet wall ESP which was retrofitted to permit collector electrode cooling. A steady flow of cooling water caused water to condense on the collecting surface at a dew point of 60°C in the gas being cleaned. The resulting thin film of water was sufficient to dissolve and constantly flush away the saline deposits. It was possible to operate the precipitator continuously at high collection efficiency for extended periods of time with gas velocities of about 1 m/s and particulate concentrations of 20 g/m^3.

As a result of these encouraging findings the full scale installation shown in Figure 2 was designed and built. The most important component is the tubesheet, which is made entirely of plastic and enclosed in a rubber-lined steel casing. To compensate for the differences in thermal expansion of steel and plastic, special packing was provided between the respective

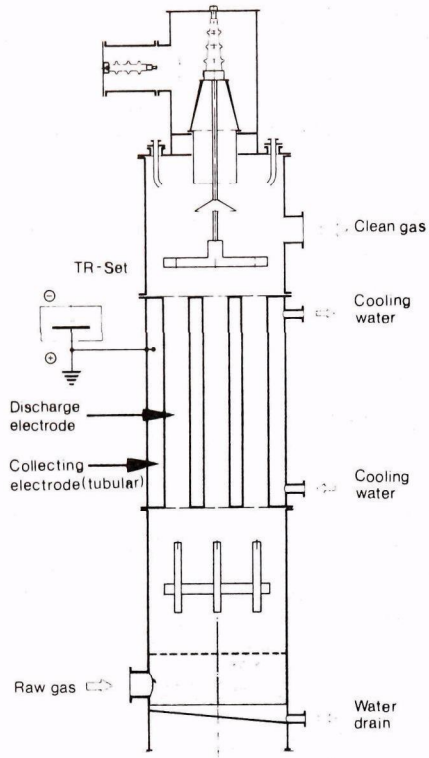

Figure 1.
Bischoff Wet Wall Electrostatic Precipitator With Indirectly Cooled Collecting Electrodes

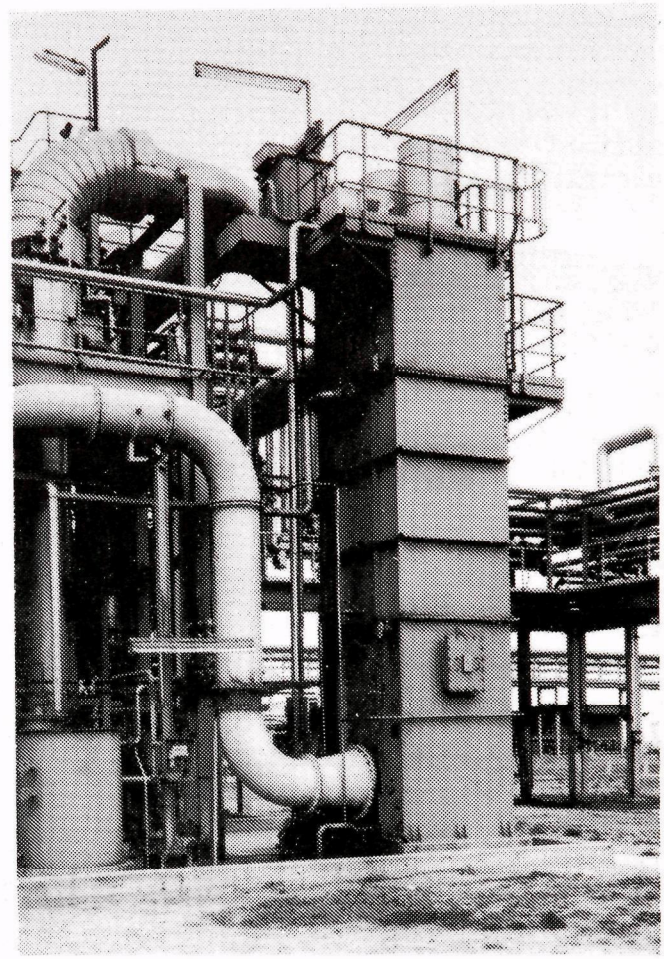

Figure 2. Precipitation of Extremely Fine Salt Aerosols from an Effluent Incinerator

The water inlet and outlet were carefully designed to ensure their structural rigidity and to provide uniform cooling. In other respects the design does not deviate markedly from that of conventional vertical, wet type electrostatic precipitators.

Nozzles for spraying the collecting surfaces were provided but were only used to develop surface conductivity during static (non-operational) tests. No provisions were made for periodic flushing.

The success of this small commercial unit in treating flue gas from saline liquor incineration led to a decision to investigate the concept further, both in the laboratory and in the field.

The program consisted of:

* Laboratory comparison tests with standard particulates in which test runs would be compared with results already known for high performance scrubbers.

* Application oriented field tests with small experimental WWP's.
* Analysis of experience gained from operating commercial units.

Experimental Program

Laboratory Experiments

Initial tests demonstrated that even dusts insoluble in water were easily flushed off. Experimental conditions could therefore be selected which were identical to those used during experiments previously carried out with wet type precipitators.

The pilot unit was designed for a throughput of 1,500 m^3/h. The test setup is shown in Figure 3.

The raw gas was saturated with water and raised to the desired temperature by injecting steam into the input air. Measurements have shown that this technique has no influence on the precipitator's collecting efficiency. Particulates were fed into this gas stream using a compressed air injector and a manually controlled vibrating chute. All raw gas ducts were insulated and heated. Upstream from the particulate feed there is a mist eliminator to prevent any agglomeration of dust due to carryover of drops of condensate.

The pilot precipitator is of vertical tubular design. The precipitation unit consists of nine internally rubber lined steel tubes of 200 mm diameter. Tube clusters varying in length from 1 to 3 meters were evaluated. Cooling water flows continuously around the outside of the tubes. The remaining elements of the equipment are of conventional design.

On the clean gas side the residual dust content is measured in a long straight section of the tube by the standard method of isokinetic partial flow aspiration (1,2). In addition, the gas velocities, pressures, and temperatures are measured at various locations in the experimental setup, cf. Figure 3.

In the experiments to date the following parameters have been varied within the indicated limits:

* Length of the precipitation unit (1 to 3m)
* Raw gas temperature, T (50° or 80°C)
* Gas velocity in the precipitation tube, v (1 to 2.5 m/s)
* Raw gas particulate loading, δ, (1 to 5 g/m)
* Electrode voltage, u_e (30 to 70 kV)
* Type of particulate (grain diameter, electrical resistance, wettability)

Data evaluation in respect to the total collection efficiency, η, and the size fraction collection efficiency, η_f, is made in accordance with the details given by Holzer (2).

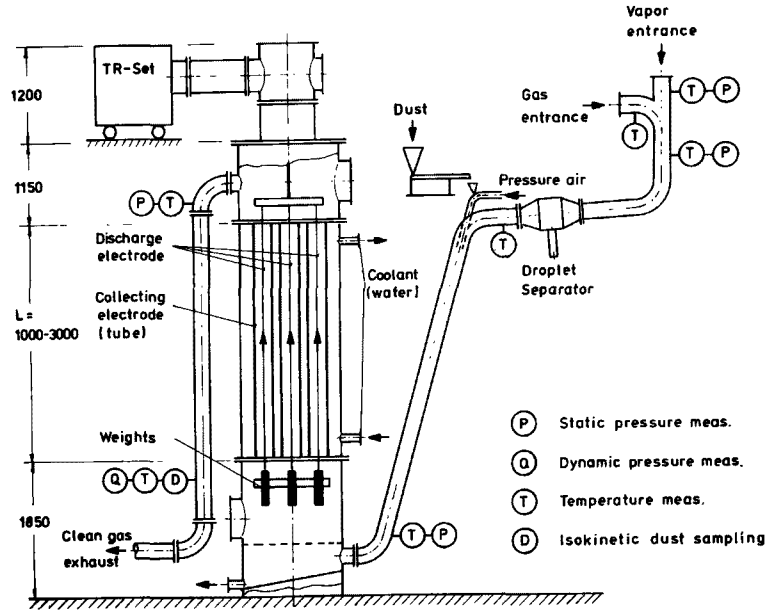

Figure 3. Experimental Apparatus

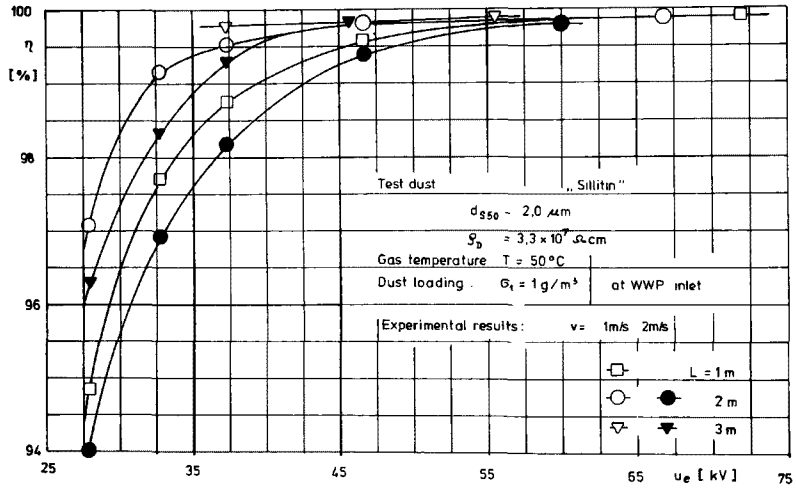

Figure 4. Collecting Efficiency η of the Test WWP as a Function of Electrode Voltage, U_e

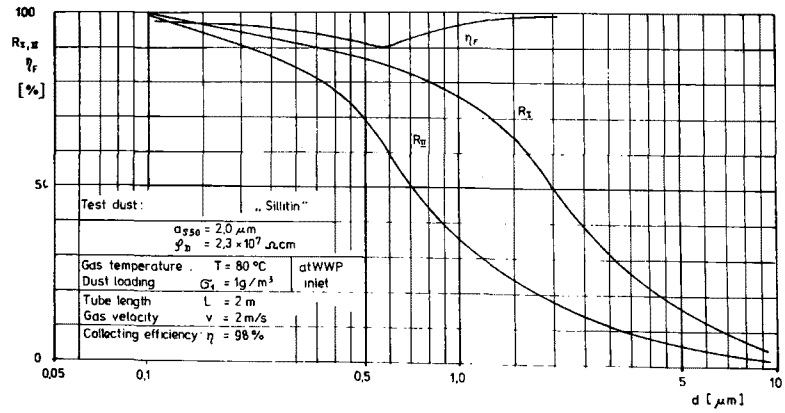

Figure 5. Retained Fraction Curves, R_I and R_{II}, and Fractional Collecting Efficiency, η_F.

Some typical results from the experimental program are given in Figure 4, where total collection efficiency, η, is plotted as a function of electrode voltage, u_e. Parameters varied included the length of the collection tubes and the velocity of the gas in the tube. The experiments were carried out using "Sillitin", a fine quartz powder, as the test particulate at a raw gas loading of 1 g/m^3 and a temperature of 50°C.

When the length of collection tubes and gas velocity were varied the plots relating collection efficiency to electrode voltage are seen to be a family of similar curves. With increasing voltage these curves rise sharply at first, then progressively more gradually, and finally coincide. At constant voltage, lengthening the tube and reducing the gas velocity produced, as expected, an improvement in collection efficiency.

It is noteworthy that with a collection tube length L=1m and a gas velocity of v=1m/s better collection efficiency values are achieved at all voltages then when L=2m and v=2m/s. The generally accepted correlation between collection efficiency and specific area of precipitation A/Q (with a constant tube radius A/Q is identical to the retention period) does not yield conclusive results in this instance, cf also (3). Clarification of this matter is still under study.

The migration velocities are about 25 cm/s, a normal rate for experimental precipitators. For practical applications these discrepancies are of less importance.

The most important result, which can be seen in Figure 4, is that starting from a relatively low voltage, i.e. about 50 kV, the length of the collection tube, the gas velocity, and the voltage itself no longer are controlling factors and that a collection efficiency of 99.9% is attained. Experiments at higher gas temperatures and other particulate loadings also did not provide data significantly different from that plotted in Figure 4.

Figure 5 shows the size fraction collection efficiency, ηF, of the condensation electrostatic precipitator as a function of the grain diameter, d. The size fraction collection efficiency is calculated from the residue curves R_I and R_{II} for raw and cleaned gas respectively (2).

Unlike the case with wet scrubbers, a minimum is noted at a grain diameter of about 0.6 µm. Overall, the curve is close to the total collection efficiency of 98% (see also (3), where similar curves are shown from both theoretical and experimental research). The minimum is typical of electrostatic precipitators since with grain sizes in the range of 0.5 µm charging of the particle is less intense because of ion deposition and without ion diffusion (3,4).

The evaluation of the size fraction collection efficiency could not be carried out for grain diameters below 0.1 µm since the grain analysis method used (centrifugal sedimentation) does not yield reliable results in this range. The limiting grain diameter as normally defined cannot therefore be determined for the condensation precipitator from the available data. It can only be concluded that the limiting grain diameter is less than 0.1 µm.

Further research is in progress to determine the extent to which the principle of wet wall condensation contributes to the level of collection efficiency.

Field Tests

Glass Trough

The condensation precipitator concept was tested on waste gas from a molten glass trough. The gas contained a mixture of solid dust particles and P_2O_5 mist.

At the time of these tests the plant had a venturi scrubber installation which did not meet the collection efficiency required under the latest emission control regulations - approximately 20 mg/m^3 NTP.

A pilot WWP with one pipe, but retaining the original geometry of the precipitation field, was installed in parallel with the scrubber plant. The waste gas was cooled from about 150°C by spraying with water in a pipe immediately upstream of the filter, passed through the precipitator, and fed into the gas line again upstream of the existing blower.

The following residual contents were achieved at gas flow rates of 1.2 - 1.3 m/s:

P_2O_5	approx.	1 mg/m^3 NTP
As_2O_3		0.1 mg/m^3 NTP
Total Collection Efficiency		>99.8%

Commercial Units

The condensation precipitator concept has been employed with great success in the full scale plants built to date, particularly where full corrosion protection has been employed. Two of the plants already built provide for the precipitation of pigments from flue gas and the precipitation of sulfuric acid mists, mixed with particulates, from an acid waste incinerator.

Comparison of Costs and Performance

Performance Compared With Wet Scrubbers

In Figure 6 the power consumption of various types of scrubbers is plotted against the limiting particle size of the test dust, i.e., against the particle diameter at which just 50% is cleaned. Below the typical curves drawn for each scrubber type is a lower boundary line below which no scrubber dropped.

The performance characteristic of the WWP is designated by a cross-hatched area rather than a linear plot. There are two reasons for this. As discussed above, the limiting particle size for the condensation precipitator cannot be defined since it lies beyond the range of available metrological equipment. The lack of precision in particle size data also contributes to a lack

of precision in power consumption figures. The performance band given for the WWP in Figure 6 does; however, clearly show that power consumption lays one or two powers to ten below the level for conventional scrubbers and the particle diameters which can be handled lie outside the range that scrubbers can normally cope with. In other words, the condensation precipitator can operate beyond the capability of scrubbers.

As part of the energy consumption study, the power required for ionization, that for producing the small pressure drop across the electrostatic precipitator, and that for insulator heating, was considered.

The low water consumption is also worthy of note. During the series of tests it was not necessary to spray additional water into the precipitator inlet beyond that needed for gas saturation. The condensate produced was more than enough for satisfactory operation. Pollutants were separated in optimal concentrations of 25 g/l.

Comparable results can only be obtained from scrubbers by multiple recycling which is generally not possible in practice because of difficulties such as increased wear on pumps and nozzles.

Costs and Performance Comparison With Conventional Precipitators

Cost comparisons between conventional electrostatic precipitators and the wet wall electrostatic precipitator were developed on a percentage basis with assumptions set out below.

The WWP operates with essentially constant collection efficiency and can therefore, other conditions permitting, be safetly operated with just one collection zone.

By contrast, two zones must be provided in a conventional wet electrostatic precipitator since the collection efficiency drops appreciably as the solid precipitated particles are rinsed away. It was assumed for the purposes of this comparison that the migration velocity would be 50% of the normal value when rinsing was being carried out in one of the two zones. This means that if the precipitation area of the WWP is taken as 100%, that of the conventional precipitator will have to be 133%.

The wet wall precipitator involves more structural expense due to the cooled tubes and the dead space for water cooling. The precipitator shell must also be larger. In the conventional precipitator; however, the required significant amount of dead space was included in the second zone. Two spray zones and rectifier systems were allowed for the conventional precipitator, reduced size not playing a significant role here.

The relationships can be seen in Figure 7 which shows diagramatically a wet wall precipitator and its functionally equivalent conventional precipitator. Costs for the five major elements of the WWP are given the value 1.0; corresponding costs for the same elements in the two stage conventional electrostatic precipitator are assigned proportional values.

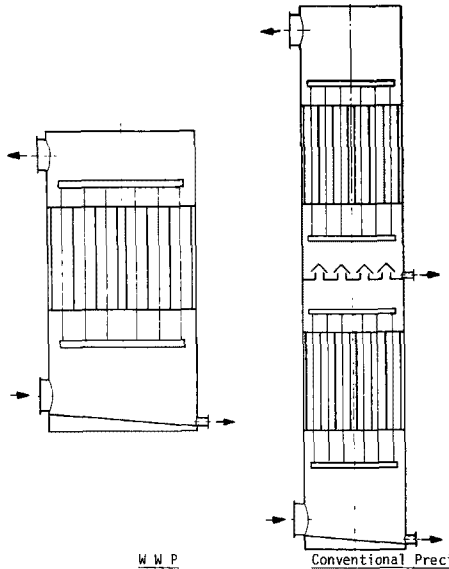

	WWP			Conventional Precipitator		
	Size	Costs	Ratio	Size	Costs	Ratio
Casing	1.0	1.0	0.375	1.26	1.35	0.51
Collecting electrode	1.0	1.0	0.375	1.33	0.95	0.36
Discharge electrode	1.0	1.0	0.12	2x 0.67	1.8	0.22
TR-Set	1.0	1.0	0.10	2x 0.67	1.8	0.18
Flushing system	0.5	1.0	0.03	2x 0.67	2.0	0.06
Total			1.0			1.33

Figure 7. Size and Cost Comparisions Wet Wall Precipitator and Conventional Wet Precipitator

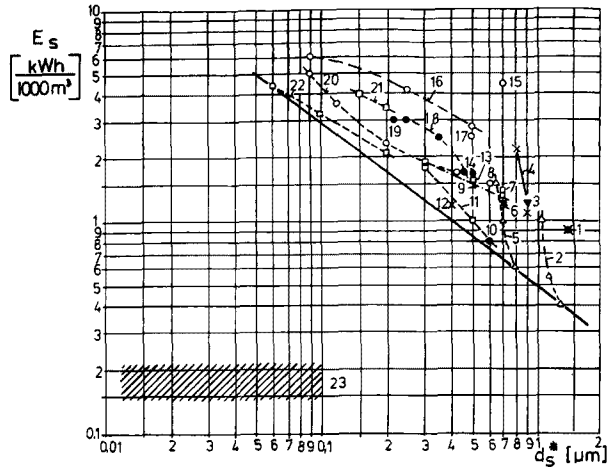

Nr.	type	mark	gas volume	pressure drop m bar	water consumption ltr/m³
1	wet cyclon	⊠ BVT	450	19	0,2 - 0,8
2	washing tower	△ HY	250	6 – 20	0,5 – 1
3	vortex	▼ AS	3000	20	
4	jet-scrubber	× KO	500	(+2)	3 – 10
5	washing tower	△ GLK	1000	6 – 18	0,5 – 1
6	vortex	▼ CR	2500	15 – 22	
7	LP-Venturi	□ HS	2000	15 – 20	
8	rotation scrubb	○ CS	17500	10	2 – 3
9	LP-Venturi	□ BC	3000	15 – 40	
10	impinger	● PB	1000	18	0,5
11	LP-vent+imp.	□ PB	1000	22 – 37	0,5 – 1
12	wet cyclonette	⊠ BT	500	18	0,6 – 1
13	LP-Venturi	□ KV	3500	20	
14	Mixer-type	● VO	1000	20	
15	} rotation scrubber	○ ST	300	8	
16		○ PZ	600	18 – 70	0,5 – 2
17		○ CN	2000	(+15)	0,1 – 0,4
18	} Mixer type	● PD	600	20 – 50	0,5
19		● RD	2000	(+15)	0,5 – 0,8
20	rotation scrubber	○ KN	2800	8 – 10	1 – 2
21	} HP Venturi	□ LR	1500	25 – 100	0,8
22		□ BG	500	40 – 100	1 – 3
23	WWP	////	1500	2	0,04 *

Figure 6. Power Consumption Versus Diameter For Various Wet Gas Cleaning Installations

The actual calculations were too involved to be fully described in this paper. The size of the precipitator shell was worked out on the basis of surface area; costs were for realistic designs. The actual or equivalent cost of electricity required to overcome the head loss can also be expected to involved extra operating costs of about 35%.

These figures demonstrate that it is worth considering the installation of a wet wall precipitator for all possible applications.

Summary - Applications - Future Work

The first precipitators using the wet wall principle have all been designed for the wet separation of corrosive waste gases and were therefore fully protected against corrosion. Despite these expensive provisions for corrosion protection the plants offered overall savings as compared to the costs for simple wet precipitation.

The condensation precipitator principle permits the use of highly insulating, corrosion-resistant plastics as electrodes and collecting surfaces.

In addition to the special applications described above it is believed that the basic principle has application for all waste gases containing fine particulates and for which a given water vapor dew point can be maintained. In addition to low inital costs, the virtual absence of maintenance expense is especially notable.

Further investigations are needed before more definitive application predictions can be made. The correlation between gas dust content and amount of condensate must be studied. Dust characteristics must be investigated to learn why materials such as soot resist washdown.

Random observations suggest that condensation effects significantly promote precipitation. More detailed study of the influence of condensation near the precipitator walls on the precipitation process is being made.

References

1. VDI - Richtlinie 2066. Leistungsmessungen an Entstaubern.

2. Holzer, K. Nassabscheidung von Feinstaeuben und Aerosolen. VDI-Berichte Nr. 349, 1979. p. 102-109.

3. Maartmann, S. Moeglichkeiten zur Feinstaubabscheidung mit trockenarbeitenden Electroentstaubern. Staub-Reinhaltung Luft 34 Nr 10, 1974. p. 353-380.

4. White, H. I. Industrial Electrostatic Precipitation. Reading, Mass. Addison - Wesley Publishing, Inc. 1963.

TROUBLESHOOTING MULTIPLE CYCLONES ON FUEL-OIL-FIRED BOILERS

By: F. Crowson and R. L. Gibbs
Naval Surface Weapons Center
Dahlgren, Virginia 22448

ABSTRACT

The body of information presented in this paper is directed to the particulate control of boilers fired with No. 6 fuel, a problem when stringent standards must be met. The success of meeting regulatory standards is highly dependent on the availability of data for emission characterization, as well as the availability of space and funds for control equipment. Early efforts toward controlling emissions from boilers fired by No. 6 fuel at two Navy shore facilities resulted in the selection of multiple cyclone collectors. Since their installation, both facilities have failed to meet compliance with local standards. A study was made to troubleshoot the boilers and their associated pollution control equipment. The problems associated with the multiple cyclone collector design, installation, and operation are examined.

INTRODUCTION

The U. S. Navy is required by executive order to assume the initiative in complying with state and federal regulations governing discharge of emissions from stationary sources (1). Initial efforts to meet the requirements were directed toward providing the quickest, least-cost, and best control technology available to meet existing regulations. In the mid-1970's, heavy-fuel-fired boilers at two Navy installations were equipped with multiple cyclone collectors to meet the emission regulations for the District of Columbia and the state of Maryland. Initially, these boilers were fired with No. 6 fuel, and dust collector design was based upon this factor. Unfortunately, limited funds precluded obtaining particle sizing data and flue gas characteristics to allow the evaluation of other control devices. The major factors governing the selection of cyclones were space availability, design simplicity, and cost.

Since the multiple cyclones were installed, emissions from the units under full-load operation at both facilities have not met the requirements set by the regulating districts. Source emission tests (SETs) were performed at various boiler settings in an attempt to verify at what loads compliance could be achieved. These tests attempted to confirm acceptable operation until modifications or necessary design changes could be made to ensure a more efficient system. To date, no systematic study has been conducted to determine emission characteristics at various loads and to quantify necessary design parameters. The lack of stack gas data and incomplete operation records further complicated effecting a ready solution. The purpose of this investigation was to troubleshoot the boilers with the present multiple cyclone collectors and to provide an engineering assessment for further action based on existing information.

PROCESS EVALUATION

Certain criteria were used for evaluating each process at both facilities. The factors for the evaluation of the boilers and burners included (1) installation, (2) maintenance, (3) internal deterioration (corrosion/erosion), (4) flame impingement, (5) flame pattern and length, (6) stack outlet conditions, (7) fuel flow, temperature, and pressure, (8) fuel analysis, and (9) instrumentation for boiler operation and stack gas analysis. Assessment of the pollution control equipment included surveying (1) design, installation, and maintenance, (2) dimensional parameters, (3) wall roughness of the cyclone tubes, (4) plugging and bridging in vanes, cones, or hoppers, (5) leaks or infiltration at gaskets and valves, (6) erosion and corrosion, (7) hopper loading, (8) pressure drop and inlet flow distribution, (9) insulation, (10) auxiliary equipment such as fans and expansion joints, and (11) instruments for opacity measurement.

Washington DC Facility

The Washington DC Facility consists of twin, No. 6 fuel boilers each rated at 100 million British thermal units (MBTUs) and utilized for heating buildings. Each boiler is fired by a steam-atomized burner capable of a maximum flow rate of 700 gallons per hour (GPH). The average firing rate for these boilers is 84 MBTUs. An evaluation was first made of the boilers and burners. Historical data were obtained by reviewing previous operation and maintenance records, Orsat analyses, SETs, and installation drawings. A visual inspection was then made of the equipment and boiler room areas.

Minimum deposits on the boiler tubes confirmed that the boiler internals had received proper lancing during the scheduled weekly maintenance period. No corrosion was evident in either of the units. Surface temperatures were low and no hot spots could be found indicating that the boilers were properly insulated. Flame patterns were observed to fill the firebox with only minor impingement occurring in one boiler. Boiler controls appeared to be adequate and properly calibrated. The fuel oil being used during the survey was reported to be a blend of No. 6 and No. 4 which was necessary to lower the sulfur content to an acceptable value. During the initial inspection, the fuel oil pressure was maintained at 157 psi for a flow rate of 240 GPH. The fuel oil temperature was 130°F which appeared to be low for the blend of oil reported. No viscosity measurement could be made during the allotted survey time to verify the temperature required for good combustion.

Next, the multiple cyclone collectors were evaluated. Each collector consists of 128 high-efficiency cyclones each having a 6-in. inside diameter and a 33-in. total length. The vanes for turning the gas flow within the cyclone are mounted on the 4-in.-diameter exit tube external of the cyclone body. This arrangement allows the stack gas to enter the cyclone radially, as well as axially. Exit angles of the vanes are approximately 45°. The cyclones were designed for a total gas flow rate of 35,000 actual cubic feet per minute (ACFM) at a maximum pressure drop of 4.5 in. H_2O across the entire collector. A design efficiency of 80% at these conditions is based on a particle size distribution with a mass median diameter less than 13μ.

The first efforts in evaluating the dust collectors were to measure dimensions for the individual cyclones and to monitor pressure drops across the collector. With the data obtained and SET report results, a relative evaluation could be made of the adequacy of design for these units to meet the required emission levels. This approach was taken in an attempt to estimate cyclone performance prior to making a decision to conduct extensive emission tests.

The first problem encountered in design verification was the unavailability of particle size distribution data for these particular boilers. A brief search was made of air pollution literature to locate particle sizing for similar boiler operations. Figure 1 shows the particle sizing data for No. 6 steam-atomized burners together with data on the outlet emissions of a multiple cyclone installed on a similar No. 6 fuel boiler (2,3). The mass median particle size can be seen to decrease from about 13.0μ to a value of 0.38μ. The data presented for No. 2 fuel oil shows the particle sizes are similar to those emitted from an efficient multiple cyclone.

Using the data in Figure 1 and the dimensions obtained during the field inspection, calculations for vane-axial cyclones were made to confirm the reported fractional efficiencies and the total mass efficiencies. Entering the data of the upper curve into vane-axial cyclone design equations, overall mass efficiency was calculated to be 69% which is low compared with the specified efficiency of 80%. If the efficiency of the collector can be increased to the 80% design value, a mass emission rate of 0.050 lb/MBTU could be achieved, which is well below the DC standard of 0.061 lb/MBTU.

Observations made during the field visits uncovered more significant problems with the dust collectors. Initial installation of the collector at the Washington DC Facility resulted in a poor flow distribution to the inlet of the multiple cyclone. The contractor installed a series of flow distribution vanes, and adjustments were made based on pressure measurements before the vanes were permanently fixed in position. The overall pressure drop was measured as 0.4 in. H_2O maximum instead of the 4.5 in. H_2O design value. Inspection of the interior of this collector showed a hardened buildup on the cyclone tubes and bridging of material between the cyclone turning vanes. The material that was impacted in certain areas appeared to be collected as agglomerates of soot. All of these factors suggest low gas flows and periods of operation below the dew point of the flue gas constituents. However, no severe corrosion or erosion was observed. Since no dust was being collected, the hopper and its method of emptying were inspected. The dust could be emptied through a rotary valve into a 10-ft length of 10-in. diameter duct. The duct can then be emptied into a 32-gal container through a slide gate valve. The rotary valve had never been checked for wear on the rotor blades and maintenance had been limited to lubrication of the electric motor bearings. When the slide gate was opened, dust particles were observed to fall from the outlet and then to be pulled back up into the duct work. Additionally, inleakage could be felt around the slide gate flange. Gaskets on the hopper access doors were inspected and found to be in good condition. No inleakage could be determined at any of the hopper flanges.

Upon completion of the survey, the following observations and recommendations were made using the process evaluation criteria discussed earlier. The boilers appeared to be installed and maintained properly resulting in minimal or no internal deterioration. The method of operation apparently contributed very little to the emissions. The burner flame exhibited minor impingement, but flame pattern and length was good in general. Measurements taken at the outlet stack conditions showed moderate to high boiler efficiencies. The fuel oil temperature appeared to be low; however, a viscosity measurement would be required to confirm an optimum temperature setting. The boiler instrumentation appeared adequate and properly calibrated. An opacity monitor was in use, but its location prevented representative sampling of a sufficient path length. A camera was being used to visually monitor smoke from the stack.

The individual cyclones within the collector were determined to be correctly designed for the assumed particle sizes; however, the low pressure drops measured across the collector indicated the total unit was oversized for the particular system. Additionally, the original installation and current operation and maintenance of the pollution control equipment contributed to the pollution problem. This conclusion was based on the following observations: (1) scale was evident on the cyclone walls, (2) some bridging of the inlet turning vanes was obvious, (3) inleakage was occurring through improperly maintained valves and airlocks, and (4) the exhaust gas was being diluted through deteriorated expansion joints at the induced draft fan inlet.

Since some problem areas would require additional time to correct, minor burner adjustments (primarily nozzle replacement) and increased fuel oil temperatures were tried to optimize combustion and minimize emissions. A private contractor was used to refurbish the the burners and to conduct stack sampling. Fuel oil temperatures were increased to 180°F. All efforts to meet standards using this approach have been unsuccessful because optimized boiler operations did not significantly reduce emission levels. To comply with the District of Columbia regulations, the boilers are being operated at a maximum load of 80%. Further work on the multiple cyclone collectors has been postponed until installation of preheaters (for energy conservation purposes) is completed. The suggested method for blocking the individual cyclones is presented in Figure 2. Blocking the gas flow consists of capping the cyclone outlet tube and the cyclone discharge tube using a threaded rod to hold tension at both ends. This method is preferred for this particular collector primarily because of access to individual cyclones.

Maryland Facility

The Maryland Facility has four boilers that are used for general heating and intermittently for operating a steam injector at a research area. Three of these were originally rated at 40 MBTU and the fourth at 20 MBTU. The exhaust for the small unit is common with the exhaust of one of the larger boilers. The other two boilers have separate exhausts. All units are fired by pressure-atomized burners at flow rates of 260 GPH and 120 GPH respectively. The boilers and burners were evaluated using the same approach and techniques discussed earlier in this section.

Review of previous SETs and boiler plant records produced a list of several problems with the entire system. The boilers, which are 1945 vintage, had operated fairly efficiently until the dust collectors were installed in 1977. Routine Orsat analyses had been discontinued after oxygen analyzers were installed at the same time as the collectors. Unfortunately, the oxygen analyzers had never operated properly and no plant records of analyses were available regarding combustion efficiencies. SETs conducted immediately after the collector installation and at two-year intervals reported excess air values in the stack greater than 150%. Efficiencies ranged from 78% to 82% for boiler loads through 30 MBTU. These low efficiencies apparently contributed to the emission levels measured during the SETs.

Review of records prior to the current effort revealed the following facts leading to the existing conditions, all of which affect the variables to be evaluated in order to eliminate the pollution problem. The induced draft fans were original equipment. After installation of the cyclone collectors, the 10-hp blower motors had to be replaced with 30-hp motors and the blower speeds had to be increased to overcome the pressure drop of the collectors. The increased speed resulted in excessive noise from the stack which required installation of mufflers and a reduction in the speed to attain acceptable noise levels. This loss in induced draft fan capacity lowered the maximum firing rate to 30 MBTU for the larger boilers. After carefully reviewing the existing data and taking the above facts into consideration, an on-site inspection was made of the boiler plant using the criteria listed initially under PROCESS EVALUATION.

Inspection of the interior of each boiler confirmed that the brickwork and refractory were in good condition. Further inspection of the exteriors revealed areas of severe inleakage. Inleakage was attributed to missing or deteriorated gaskets and packing around inspection and cleanout ports, blowout doors, steam drums, and the outlet steam manifolds due to poor maintenance. In some instances, leakage was determined by locating cold spots on the boiler casing. Accumulation of extraneous material was observed on the forced draft fan blades and a considerable amount of rubbish was removed from the tunnel supplying forced draft air to one boiler allowing higher flows to be attained. Flame patterns were pulsating and smoke and sparks were often observed. Impingement was observed on both walls. Orsat analyses were made for one boiler operating at 60% boiler load. Excess air was about 190% and the combustion efficiency was determined to be about 80%. Fuel temperatures were between 145°F and 150°F which was considered low for the No. 6 fuel being used. The instrumentation used for boiler control was outdated and in need of calibration. Oxygen analyzers, opacity monitors, and the viscosity monitor were all inoperative.

The pollution control equipment at the Maryland Facility consists of four multiple cyclone units. The collectors for the three large boilers contain 36 high-efficiency cyclones and the collector for the small boiler has 18 cyclones. The cyclones have an inside diameter of 9-in. and are 56- to 80-in. in length. The turning vanes are of the vane-axial type with exit angles of approximately 45°. The cyclones were designed for a total gas flow of 22,000 ACFM at a pressure drop of 3-in. H_2O across the total collector. The design efficiency

at these conditions was reported to be 50% for mass median particle sizes less than 10-μ; however, particle size/efficiency design data could not be located for this particular installation.

During the initial survey, the following observations were made regarding the collectors. Internal inspection showed few deposits, no bridging or scaling, and no corrosion or erosion. Impacted material was white and very little soot was observed. The hopper was emptied by two slide gate valves into a sealed 55-gal barrel. No evidence of inleakage through the hopper was observed. Calculations for overall mass efficiencies using the No. 6 fuel particle size data in Figure 1 resulted in a predicted collection efficiency of 50% at existing flow conditions.

Since several problem areas required addressing, a full analysis of the Maryland Facility was undertaken. The objective of the analysis was to reduce emissions by modification or adaptation of existing equipment as a short term solution. To prevent interference with plant operations, one boiler was taken off line for modifications. The approach used included the following steps: (1) repair monitoring equipment, (2) seal the boiler, (3) calibrate the boiler controls, (4) modify the burners, and (5) optimize the collector efficiency. Steps (1) and (2) were accomplished by refurbishing all instruments and installing new gasket materials around all leak areas. In order to calibrate the viscosity monitor, a fuel viscosity determination was made. To improve burner operation, several modifications were made to the existing burners. These included installing new burner tips, tightening the air register for better adjustments, and modifying the diffusers. The boiler controls manufacturer was contracted to optimize the boiler control instrumentation. A check was made of the collector pressure drop. A pressure drop of 1.8 in. H_2O was measured at 22,000 ACFM instead of the 3.0 in H_2O design value. This confirmed that the collector was oversized and that the required pressure drop would be achieved only by blocking off a certain number of the individual cyclones. The method used for blocking individual cyclones for this specific design is shown in Figure 3. Custom made collars were made for the cyclone inlets. The cyclone discharge tube was capped by merely fitting a flat plate into the existing ring. Blocking the cyclone tubes increased the collector pressure drop significantly enough to further reduce the capacity of the induced draft fan resulting in even lower firing rates. The compromise was to seal only the number of tubes required to achieve the design pressure drops and velocities while maintaining an adequate boiler firing rate. Twelve of the thirty-six tubes were blocked and preliminary testing was conducted at a new firing rate of 23 MBTU. A pressure drop of 2.4 in. H_2O was obtained at a flow rate of 15,000 ACFM which is near the design values predicted for the specific cyclones. Higher flow rates were unattainable due to the limitation of the induced draft fan.

Improvements in combustion during initial tests were attributed to lower fuel viscosities, improved flame patterns, lower excess air values, and higher combustion efficiencies. Some flame impingement occurred during optimization tests; however, excess air was reduced to 33% at the boiler outlet and efficiencies were on the order of 86%. Preliminary SET data indicated that emissions are near or below the 0.03 gr/dscf requirement. Preliminary particle

size data indicate that inlet and outlet sizes are approximately 1.0μ mass median diameters and collector efficiencies are very low because of these small particles. If the preliminary particle size distribution data is correct, low efficiencies would be expected. However, since mass loadings are near the applicable standard, only small increases in efficiency would be required. Installation of an induced draft fan having sufficient capacity to return the firing rate to 37 MBTU would increase the velocity in the cyclone to its design value and provide a small efficiency increase.

CONCLUSIONS AND RECOMMENDATIONS

Selection of air pollution control equipment requires a good knowledge of the process gas stream to be controlled as well as a basic awareness of how the control device operates. When an off-the-shelf device is chosen, care must be taken to ensure that the collector is compatible with the process and can effectively remove the pollutant. After installation, the collector should be thoroughly inspected for proper flows, pressures, temperature limitations, construction, and maintenance required. Guarantees for the level of emissions should be obtained and tests should be required to confirm the collector's efficiency prior to acceptance of the device. Care and logic should be used in selecting the types and location of the instrumentation for monitoring outlet stack conditions.

In view of future decisions to install economizers and possibly replace the existing control devices, two approaches were recommended as intermediate actions to improve the collection efficiencies for the two cases discussed in this paper. For the Washington DC Facility, inleakage through the collector should be stopped by ensuring that valves and fittings are adequately maintained and sealed. Velocities through the cyclones should be increased by decreasing the number of cyclones. This decrease can be achieved by blocking the inlets and outlets of certain cyclones in a manner that will not affect the flow distribution through the overall device that could result in channeling through adjacent cyclones. The collector should be preheated and remain heated during startup and lancing operations to prevent scale buildup. Additionally, the induced draft fan size should be increased commensurate with the increased collector pressure drop. Efforts to reduce pollution at the Maryland Facility will require increasing the velocity through the collector to its design value. Additional induced draft fan capacity is required to accomplish this end and to return the firing rate to its original value of 37 MBTU.

In summary, the evaluation of multiple cyclone collectors for heavy-fuel-oil boilers should consider the following recommendations. The collector design and installation should be commensurate with the boiler loads encountered in routine operation. Maintenance of particulate collectors is often neglected and adequate procedures, such as maintaining temperatures during downtimes to prevent scaling, are required. Prior to acceptance of a mechanical collector, dimensional parameters should be double-checked to ensure proper sizing for a given process. After installation and initial operation, collectors should be inspected for erosion, plugging, and bridging of internal components. Inspection for inleakage should be routine and procedures should

be exercised to prevent excessive inleakage. Low hopper loadings are a sure indication of inleakage through the collector. Pressure drops across the collector should be routinely monitored to provide first indications of collector deterioration. The inlet flow distribution to any mechanical collector should be consistent to prevent irregular velocity patterns and inefficient collector operation. Finally, ancillary items such as collector insulation, instrumentation and stsck gas monitoring equipment should be properly installed and operated to insure that the collector operation is adequate at all times.

ENDNOTES

1. Executive Order 12088, Federal Compliance with Pollution Control Standards, 13 October 1978.

2. McGarry, F. J. and C. J. Gregory. A Comparison of the Size Distribution of Particulates Emitted from Air, Mechanical, and Steam-Atomized Oil Fired Burners. J. Air Poll. Control Assoc. 22:636, 1972.

3. Cheng, R. J. et. al. Characterization of Particulates from Power Plants. J. Air Poll. Control Assoc. 26:787, 1976.

4. Navy Environmental Support Office. Source Emission Tests of Boilers Alpha and Beta at the Naval Training Center Great Lakes, Illinois. NESO Document No. 2-093. Port Hueneme, California, July 1978.

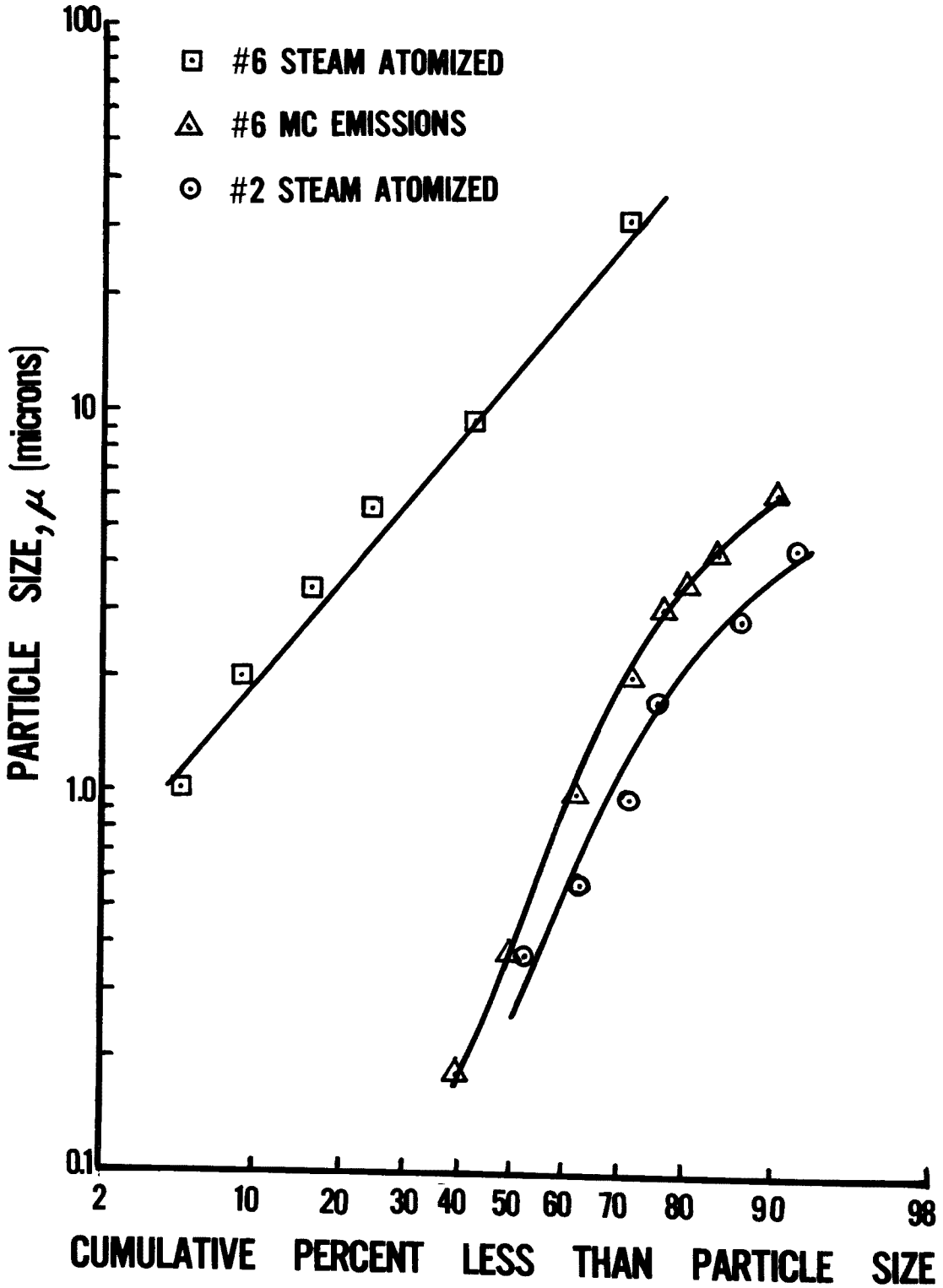

Figure 1. Particle Size Distributions

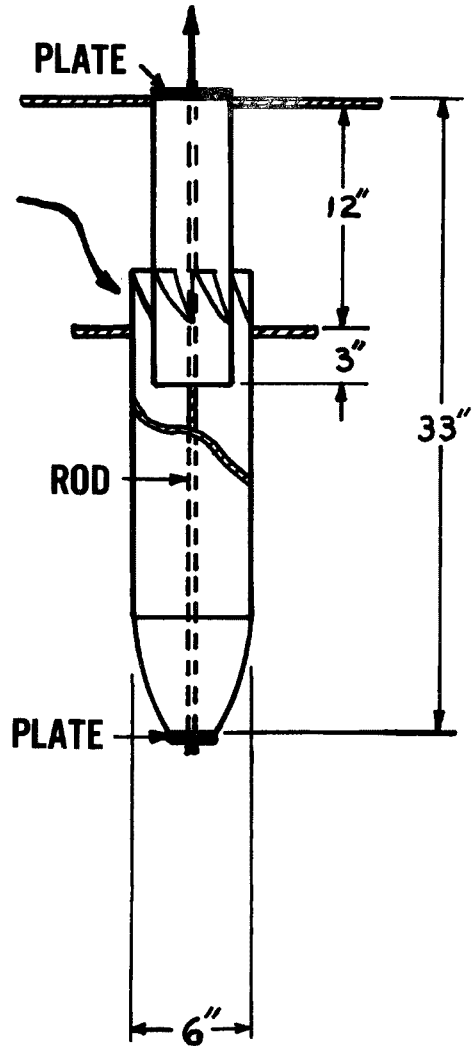

Figure 2. Proposed Cyclone Sealing Method at the Washington DC Facility

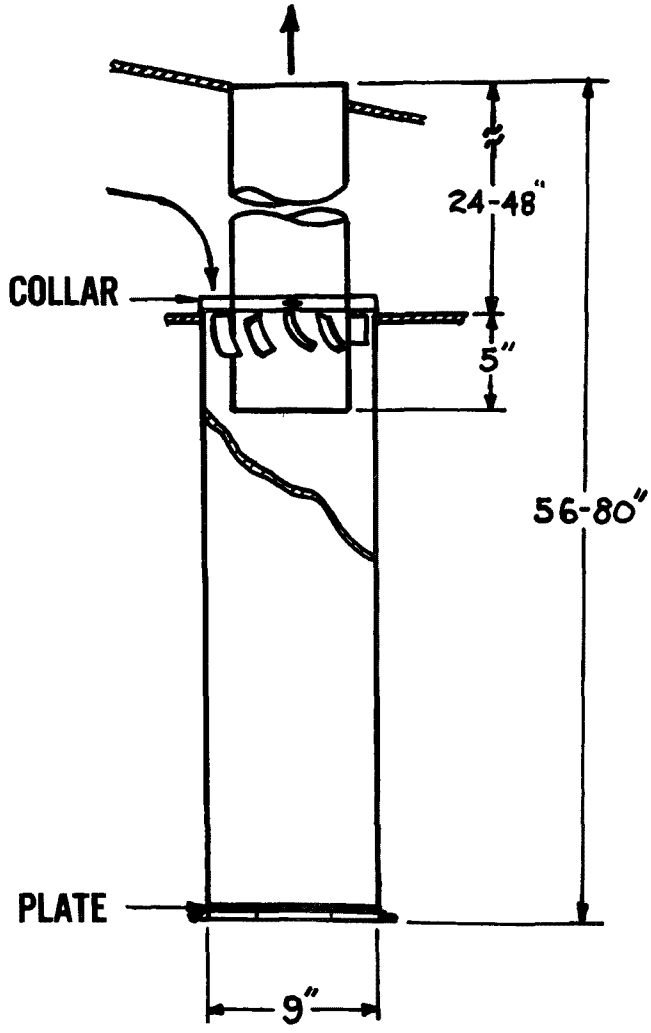

Figure 3. Cyclone Sealing Method Used at the Maryland Facility

COLLECTION EFFICIENCIES OF CYCLONE SEPARATORS

By: P.W. Dietz
General Electric Company
Corporate Research & Development
Schenectady, New York 12301

ABSTRACT

An improved model for particle collection in cyclone separators is presented. The model is predicated on the identification of three distinct regions: the inlet region, the downflow region, and the core region. In each of the three regions, turbulent mixing is assumed to result in a uniform radial concentration profile. The effects of cyclone geometry on the gas flow pattern are included so that the model incorporates the distribution of gas residence times.

Experimental results from several sources are compared to the model predictions and favorable agreement is obtained.

INTRODUCTION

With the growing concern for the environmental effects of particulate pollution, it is becoming increasingly important to be able to design optimized pollution control devices. Unfortunately, existing models for many control devices are inadequate for this task. For example, although measurements of the fractional efficiency of cyclone separators can be used to predict the performance of a given design in new applications, the efficiency of new cyclone designs cannot be predicted based on current theories. In an effort to address this situation, an improved cyclone model has been developed! In the present paper, an overview of this new cyclone model is presented and a preliminary qualification of this new design tool is achieved through a comparison of the model with the measured efficiencies of cyclones tested at the Exxon Pressurized Fluidized Bed (PFB) miniplant and at the National Coal Board's (NCB's) PFB facility.

Historically, cyclones were characterized by a cut size (d_{pc}) which was defined to be the particle size for which the cyclone efficiency was 50 percent. This cut size can be approximately computed by equating the centrifugal force on a particle (due to its angular velocity) to the drag on the particle due to the radial gas velocity.(2,3) Unfortunately, this procedure does not allow prediction of the shape of the grade-efficiency curve. Nonetheless, this simple approach can be used to scale experimental data for geometrically similar cyclone.(3,4) Deviations from this model have been attributed to reentrainment, particle bounce, and gas by-passing (sneakage). Unfortunately, new cyclone designs must be tested before this technique can be employed.

Recent papers by Leith and Licht (5) and Dietz (1) have proposed improved models which recognize the turbulent nature of the flows within cyclones. Consequently, both models, which incorporate turbulent back-mixing of the suspended particles, provide reasonable agreement with data. The Dietz model is preferred for two reasons. First, it incorporates the distribution in gas

residence times. Consequently, the model describes the particle by-pass caused by short gas residence times. Second, the Dietz model more accurately describes conventional reverse-flow cyclones because it includes the exchange of particles between the core and annular regions. Consequently, particles which enter the core region can be collected.

Theory

An analytic model (1) has been developed for predicting the collection efficiency of a conventional, reverse-flow cyclone (see Figure 1). This model is predicated on the identification of three distinct flow regions: the entrance region, the downflow (or annular) region, and the upflow (or core) region. Within each region, turbulent mixing is assumed to be effective at maintaining uniform radial concentration profiles. In addition, both particle- and gas-exchange are allowed along the entire interface between the annular and core regions. Consequently, the model includes the effects of particle by-pass due to short gas-residence times.

In developing the model, certain assumptions were incorporated with the goal of simplifying the analysis while retaining the critical elements of the cyclone system. These assumptions are as follows:

- the effective engagement length of the cyclone, D, is equal to the actual engagement length minus half of the axial extent of the inlet,

$$D = S - a/2$$

- the effective length of the cyclone, ℓ, is the length of the cyclone below the outlet duct,

$$\ell = H - S$$

Of course, if the length is greater than the natural turning length of the vortex, (6) then

$$\ell = 7.3\, R_t \left(\frac{R_c^2}{ab}\right)^{1/3}$$

- the radial velocity does not vary axially
- the tangential velocity does not vary axially
- the radial dependence of the tangental velocity is given by a modified form of the equation for a free vortex in an inviscid fluid

$$U_t(r) = U_{tw}\left(\frac{R_c}{r}\right)^m$$

where m is between 0.5 and 1.0 and is typically taken as 0.7.

- particles which impact the cyclone wall are collected (consequently, re-entrainment, particle bounce, and base pick-up are neglected).
- the radius of the boundary between the core region and the annular region is equal to the radius of the exit tube. Thus

$$R_v = R_t$$

(This boundary can also be taken as the location of the maximum separative force (2) with little effect on the predictions of the model.)

- the drag on the particles is given by Stokes' drag (the result can be easily modified to incorporate other drag laws).

From this model, a set of coupled, nonconstant-coefficient, ordinary differential equations is obtained for the particle concentration. An analytic solution to these equations has been developed and an expression for the fractional efficiency of the cyclone is obtained (the symbols are defined in the nomenclature and in Figure 1).

$$\eta = 1 - \left[K_o - \left\{K_1^2 + K_2\right\}1/2\right] \exp\left[\frac{-2\ R_c U_{pw} D}{Q_{vo}}\right]$$

where

$$K_o = \frac{R_c U_{pw} + R_v U_r + R_v U_{pv}}{2R_v U_{pv}}$$

$$K_1 = \frac{R_v U_{pv} - R_v U_r - R_c U_{pw}}{2R_v U_{pv}}$$

and

$$K_2 = \left(\frac{R_v}{R_c}\right)^{2m}$$

where

$$U_{pw} = \frac{2\rho_p R_P^2 U_{tw}^2}{9\mu R_c}$$

$$U_{pv} = U_{pw}\left(\frac{R_c}{R_v}\right)^{1+2m}$$

and

$$U_r = \frac{Q_{vo}}{2\pi R_v \ell}$$

The tangential velocity at the cyclone wall, U_{tw}, is obtained by matching the angular momentum of the flow in the inlet to the angular momentum of the flow in the entrance region. Because many inlet geometries are employed, this balance will be illustrated for a scroll inlet (see Figure 2).

$$a\int_{R_c}^{R_1} U_o^2\, r\,dr = 2\pi\int_{R_t}^{R_c} U_{tw}\left(\frac{R_c}{r}\right)^m \left[\frac{Q_{vo}}{\pi(R_c^2 - R_t^2)}\right] r^2 dr$$

where $U_o = \dfrac{Q_{vo}}{a(R_1 - R_c)}$

Thus,

$$U_{tw} = \frac{(3-m)Q_{vo}}{4aR_c} \frac{(R_1 + R_c)}{(R_1 - R_c)} \left[\frac{1 - \left(\frac{R_t}{R_c}\right)^2}{1 - \left(\frac{R_t}{R_c}\right)} \right]^{3-m}$$

(For tangential inlets, the tangential velocity at the outer wall is approximately the same as the inlet velocity for many cyclones.)

Comparison With Experiment

Particulate captive efficiencies have been reported for various cyclones operating on the Exxon Miniplant PFB Combustor and on the Natural Coal Board's Coal Utilization Research Laboratory PFB Combustor. The dimensions of these cyclones are reported in Table 1. The data are plotted in Figures 3 through 7 and the theoretical efficiencies are presented in the same Figures. During the testing, the Exxon facility was operated over a range of conditions. However, since the range was small, the data from all of the runs are presented on the same Figures. The data have been scaled to an assumed operating condition through the conventional, dimensionless scaling parameter

$$\psi = \frac{\rho_p U d_p^2}{2\mu R_c}$$

The use of this scaling factor affect the data only slightly since over three quarters of the data was corrected by 5% or less.

Discussion

In the present paper, the three-region model for cyclone performance has been compared with cyclone efficiencies from PFB applications at the Exxon miniplant and the NCB/CURL facility. Based on the excellent agreement between the predictions of the model and the experimental data, a preliminary qualification of this new design tool has been achieved for cyclones in which the assumptions outlined in this paper are applicable.

Notation

a	axial extent of inlet (inlet length)
A,C	intermediate variables for computing β
b	radial extent of inlet (inlet width)
D	effective engagement length
K_o, K_1, K_2	intermediate variables in computing efficiency
ℓ	effective cyclone length
m	vortex strength ($0.5 < m < 1.0$)
n	number density
Q_v	volume flow rate

R_c radius of cyclone

R_p particle radius

R_t radius of exit tube

R_v radius of vortex

S engagement length of cyclone

U_t tangential gas velocity (U_{tw}, wall; U_{tv}, vortex)

U_p particle velocity (U_{pw}, wall; U_{pv}, vortex)

β exponent in solution

η cyclone efficiency

ρ_p particle mass density

μ gas viscosity

Γ particle flux

ψ dimensionless cyclone scaling parameter

Acknowledgment

This work was performed under DOE Contract No. EX-76-01-2357 to the General Electric Energy Systems Programs Department by Corporate Research and Development. Data analysis were performed by Dr. J.T. Kuo.

References

1. P.W. Dietz. Collection Efficiency of Cyclone Separators. Accepted AIChE J., 1981.

2. C.J. Stairmand. The Design and Performance of Cyclone Separators. Trans. Inst. Chem. Engrs, 29, 1951. p. 356.

3. A.C. Stern, K.J. Caplan and P.D. Bush. Cyclone Dust Collectors. Am. Petrol Inst., New York, 1955.

4. C.E. Lapple. Process Uses Many Collector Types. Chem. Eng., 58, 144, 1951.

5. D. Leith and W. Licht. The Collection Efficiency of Cyclone Type Particle Collectors - A New Theoretical Approach. AIChE Symp. Series. Series, No. 126, Vol. 68, 1972. p. 196.

6. R. Mck. Alexander. Fundamentals of Cyclone Design and Operation. Proc. Aust. Inst. Mining and Met., 152-153, 1949. p. 203.

7. Advanced Cleanup Device Performance Design Report (Task 4.3), Volume A - Cyclone Theory and Data Correlation. General Electric Co., Schenectady, NY, Report No. FE-2357-70, DOE Contract DE-AC21-76ET10377, October 1980.

Exxon 1200-1540 °F
900 KPA

TABLE 1. CYCLONE DIMENSIONS AND OPERATING PARAMETERS

	NCB/CURL Cyclones			Exxon Cyclones	
	Primary Stream 1	Secondary Stream 1	Secondary Stream 2	Cyclone B	Cyclone C
Diameter (2R)	50.8	39.1	25.4	17.8	17.8
Length (H)	193	148	102	68.0	71.2
Barrel Length (h)	66.5	51.6	50.8	23.5	26.7
Engagement Length (S)	---+	---+	19.1	7.62	7.62
Inlet Height (a)	23.4	18.0	12.7	8.18	8.18
Inlet Width (b)	10.7	8.2	6.4	3.66	3.66
Exit Tube Diameter ($2P_t$)	15.2	7.4	12.7	5.25	3.51
Inlet Type	Scroll	Scroll	Tangential	Scroll	Scroll
Inlet Velocity	18.6_m/sec	31.4_m/sec	30.5_m/sec	45.7_m/sec*	
Pressure	600-620kPa			920kPa*	
Temperature	840 °C			840 °C	

All lengths in centimeters

*Typical

+Van Tongern proprietary

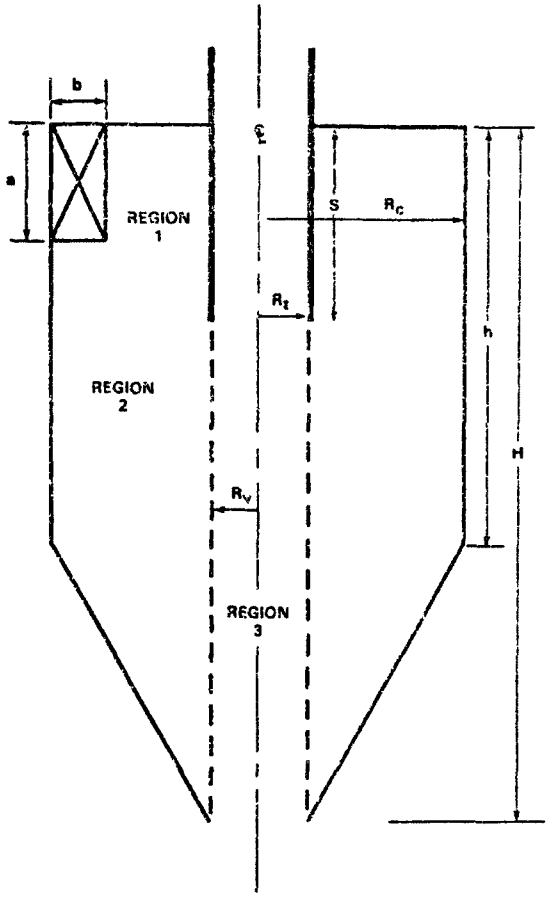

Figure 1. Conventional Reverse-Flow Cyclone

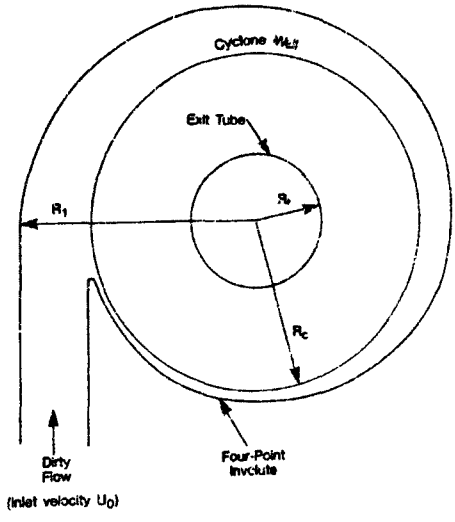

Figure 2. Top View of Typical Scroll Inlet

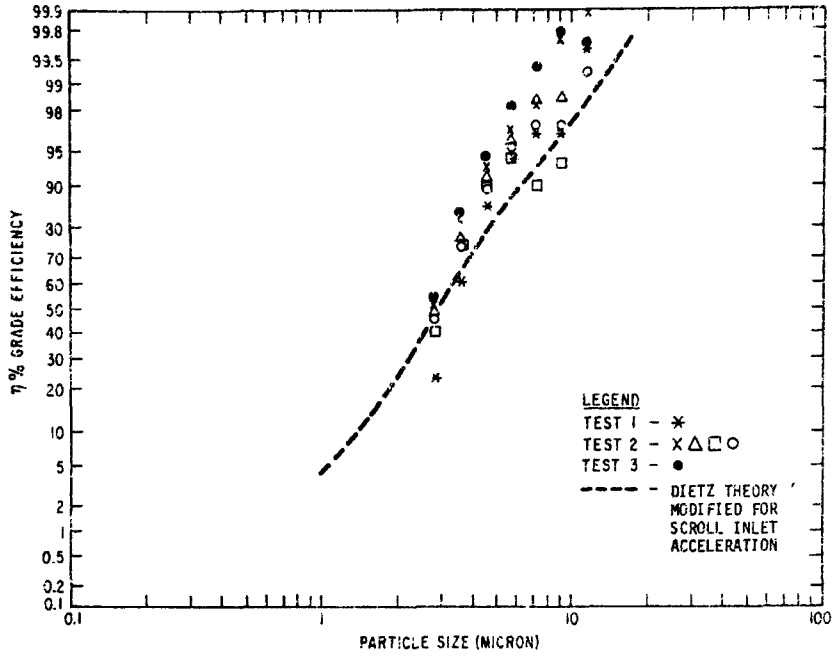

Figure 3. Fractional Efficiency of the Primary Cyclone on Curl Stream 1

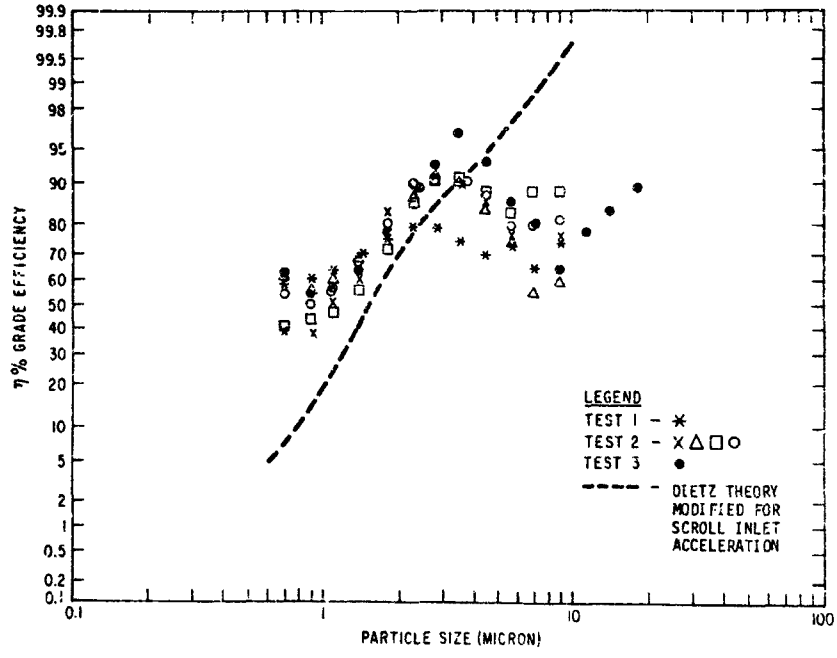

Figure 4. Fractional Efficiency of the Secondary Cyclone on Curl Stream 1

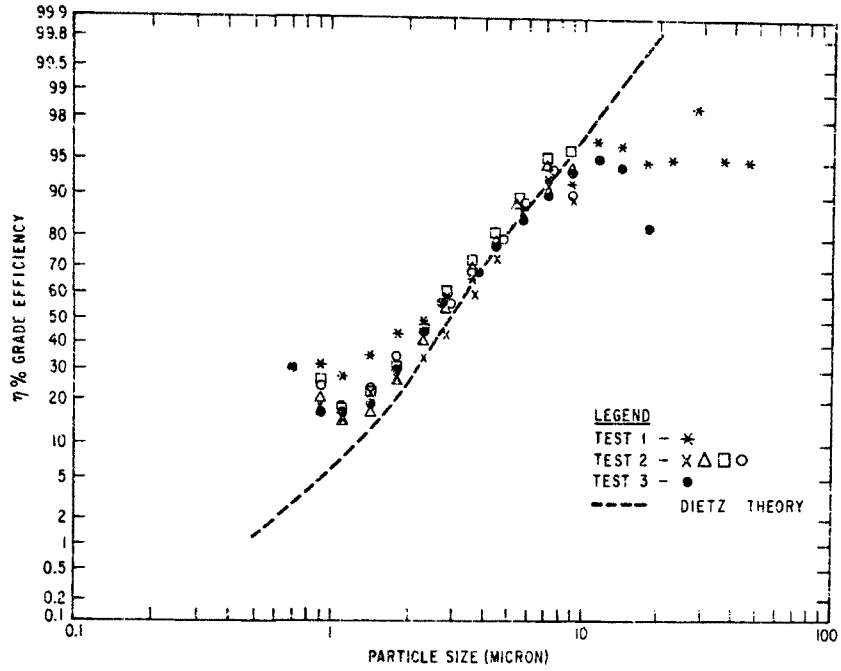

Figure 5. Fractional Efficiency of the Secondary Cyclone on Curl Stream 2

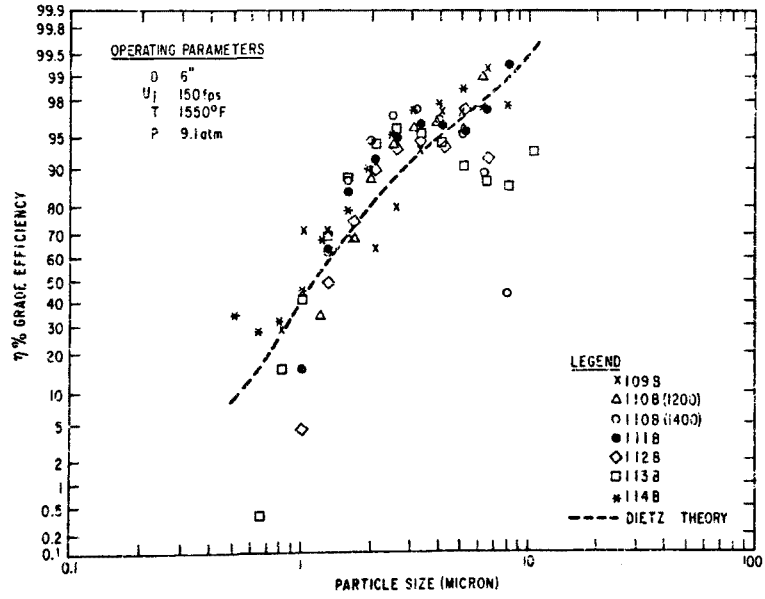

Figure 6. Fractional Efficiency of the Exxon Cyclone B

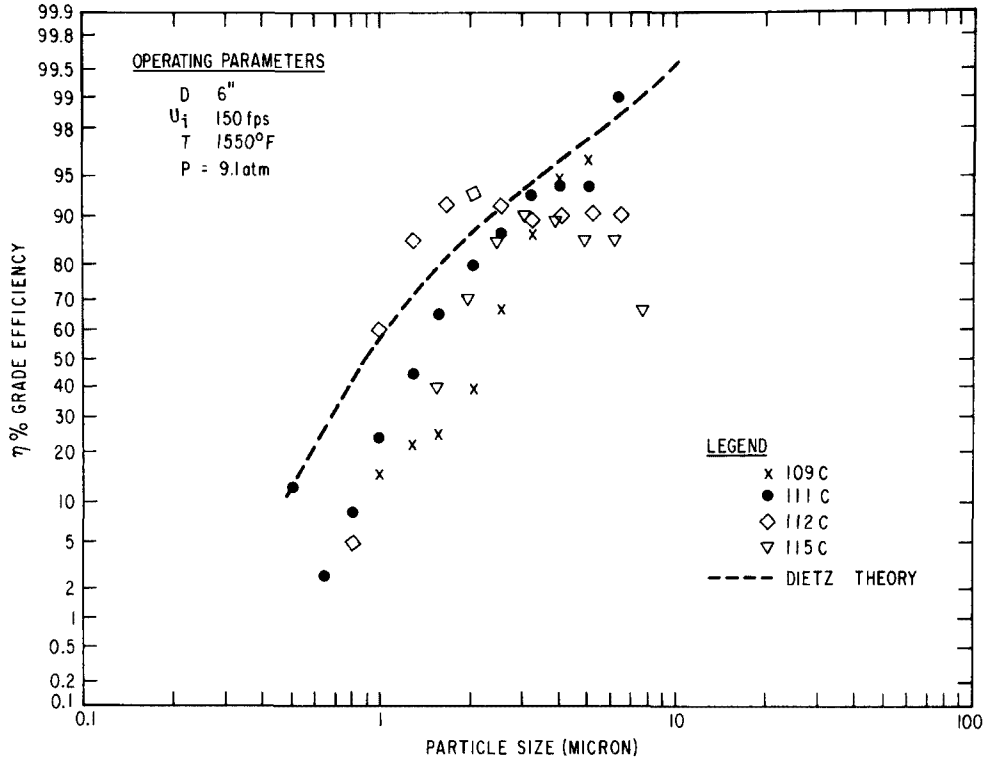

Figure 7. Fractional Efficiency of the Exxon Cyclone C

ELECTROSTATICALLY AUGMENTED COLLECTION IN VORTICAL FLOWS

By: P.W. Dietz
General Electric Company
Corporate Research & Development
Schenectady, New York 12301

ABSTRACT

Electrostatic forces have been demonstrated to provide significant enhancement in the efficiency of cyclone separators. To study these effects, experiments have been performed in a two-dimensional vortical flow. In these experiments, the effect of an applied electric field on collection efficiencies has been measured for a range of flow rates for 2.02 μm particles. These measured efficiencies are compared with an analytic model and excellent agreement is demonstrated.

INTRODUCTION

Electrostatic augmentation of the inertial forces in conventional cyclones has been proposed as a means for improving cyclone efficiencies. Historically, various methods for electrostatically augmenting axial and reverse-flow cyclones have been investigated by Molyneux, (1) Petroll and Langhammer, (2) Reif (3–5) and Giles.(6) Although encouraging results have been claimed for these "electrocyclones," this enhancement technique has yet to find significant application. However, as specific applications are identified which are not amenable to conventional cyclone technology, the potential of electrostatic augmentation will be investigated. To this end, recent work (7–9) has again demonstrated that cyclone efficiencies can be significantly enhanced through the application of an electric field within the cyclone. This work has also demonstrated potential advantages of the electrocyclone – including improved filtration during flow transients and turn-down capability. Theoretical models (10,11) have been developed which indicate that electrocyclones may have radically different scaling laws than conventional cyclones. In particular, large electrocyclones can be as efficient as small ones!

The ability to significantly enhance the collection efficiency of cyclone separators may have an additional benefit: it may be possible to enhance the collection of particles in the respirable size range. Because these particles are preferentially deposited in the lungs, particles between 0.3 and 3.0 μm (the respirable size range) are of special concern. Since potentially toxic and/or carcinogenic compounds may be concentrated in these fine particles, significant accumulations of these particles in the respiratory tract can have a detrimental effect on human health.

To develop an advanced cyclone which employs these electrostatic effects, a research program has been established under DOE funding. The program has two immediate goals: to demonstrate significant electrostatic enhancement in reverse flow cyclones and to develop an understanding of the physical phenomena which lead to the enhancement. The first goal has been achieved (7–9) and work is proceeding to develop a practical electrocyclone for use in the high-temperature, high-pressure environment prior to the gas turbine in a coal fired combined cycle power plant.

To address the second task, a simplified cyclone geometry is developed (see Figure 1). The flow within a cyclone is modeled in a two-dimensional geometry. The resulting vortical flow retains the essential features of both the inertial and electrostatic forces on the particles without the complications of the three-dimensional flow patterns. As this system lends itself to analysis, a collection model has been developed.(7) Thus, what is reported here is the data from the vortex system and a comparison between the theory and experiment.

Experimental Apparatus and Results

To study the combination of electrostatic and inertial forces in vortical flows, a simple two-dimensional test cell was designed (see Figure 1). Particle laden gas is introduced tangentially into a cylindrical test volume defined by two coaxial cylinders. The outer cylinder contains eight tangential slots for introducing the gas. The inner cylinder is constructed of sintered metal to provide sufficient pressure drop that axial velocity components can be neglected. The end pieces are fabricated from clear plastic so that a potential difference can be applied between the two cylinders.

Sampling/instrumentation ports on the end piece are provided. Measurements with a hot-wire anemometer indicate that the flow is two-dimensional. In addition, the flow measurements indicate that the tangential velocity is described by

$$U_t = U_{to} \left(\frac{R_c}{r}\right)^m \qquad (1)$$

where U_{to} is the tangential velocity at the cyclone wall, R_c is the radius of the cyclone and the power $m = 0.7$.

A Climet Particle Generator is used to disperse 2.02 μm Dow microspheres into the inlet gas stream (see Figure 2). These particles can be electrically charged prior to introduction into the electrovortex inlet plenum with the main gas flow. Particle concentrations within the electrovortex are measured with a Climet Particle Counter.

Sampling probes are designed to be nearly isokinetic. Measurements of particle concentration indicate that 2.02 μm particles do not require isokinetic sampling. Similarly, the sampling of charged particles is only slightly affected by probe voltage (provided the probe is not isolated).(12) Nonetheless, sampling conditions were maintained nearly isokinetic and "iso-electric."

Particle charging is accomplished by a corona charger. The mobility analyzer (11) indicates that the electrical charge acquired by the particles is quite uniform. In particular, for the charger parameters employed here the electrical charge is

$$q = 9.6 \times 10^{-17} \text{ coul} \qquad (2)$$

Because the particle generator displayed a slight drift in its output concentration, the order in which the data was taken is also reported.

Theory

In the laminar, two-dimensional flow of the electrovortex, the collection efficiency is characterized by a single cut-size, d_{pc}, above which all particles are collected. This cut-size can be computed from a force balance on the particle at the position of maximum separative force, (10) R_i.

$$bE_o + \frac{\beta U_{to}^2}{R_i}\left(\frac{R_c}{R_i}\right)^{2m-1} = U_o \qquad (3)$$

where b is the electrical mobility of the particle in an electric field at the wall E_o, β is an inertial parameter $\left(\beta = \frac{d_p^2 \rho_p}{18\mu}\right)$, and U_o is the radial gas velocity at $r = R_i$. For typical corona chargers.

$$b = \frac{\epsilon_o d_p E_c}{\mu} \qquad (4)$$

where $\epsilon_o = 8.854 \times 10^{-12}$ F/m is the permittivity of free space, d_p is the particle diameter, E_c is the charging field, and μ is the gas viscosity.

For the particle sizes considered here, the inertial force is negligible compared to the electrostatic force, In this case, an explicit expression for the cut-size can be developed.

$$d_{pc} = \frac{\mu U_o}{\epsilon_o E_o E_c} \qquad (5)$$

Below this cut-size, additional collection results from the inlet flow. Because this gas is introduced over a finite thickness (see Figure 7), the radial velocity of the gas goes to zero at the outer wall. Consequently, even extremely fine particles which enter near the wall can be collected. Integration over this entrance layer (10) gives (again assuming negligible inertial effects):

$$\eta = 1 - \frac{n}{n_o} = \frac{bE_o}{U_o} \quad \text{for } d \leq d_{pc} \qquad (6)$$

This theoretical result is presented as the solid lines shown in Figures 3 to 6. (The zero voltage intercept is taken to be the average of the data.)

Discussion

The theoretical model developed by Dietz (10) predicts that electrostatically enhanced cyclones can be substantially more efficient than conventional cyclones. In addition, the model anticipates two important features of electrocyclone performance for PFB CFCC applications. First, a large electrocyclone can be as efficient as several smaller cyclones. Consequently, a single, large electrocyclone may be able to replace many smaller cyclones (multiclone) and eliminate the associated problems of gas distribution and

dipleg plugging. And second, the efficiency of an electrocyclone does not necessarily degrade with flow reductions. Consequently, cyclone efficiency will not be lost during power plant turndown.

In the present article, experimental data has been presented for electrostatically enhanced collection of 2-micron particles in a vortical flow. Complete collection of these fine (respirable) particles has been demonstrated at moderate applied voltages. Comparison of the results with the theoretical model yields satisfactory agreement, and this agreement is viewed as a preliminary validation of the model. Consequently, the unique scaling of the electrocyclone is substantiated.

Acknowledgment

This work was supported by DOE (Dr. Fred E. Witmer of the Environmental and Safety Engineering Division) under Contract DE-AC02-79-EV10143.

References

1. F. Molyneux. Electrostatic Cyclone Separator. Chem and Process Eng., 517, 1963.

2. J. Petroll and K. Langhammer. Vergleichsversuche an Zyklonabscheidern. Freiberger Forschunsheft A-220, 175, 1962.

3. R.B. Reif et al. Final Report on Highly Efficient Dust Filtration System for Use in Cotton Textile Mills. USDA Contract 12-14-7001-365, 1977.

4. D.P. Thibodeaux, A. Baril and R.B. Reif. A Wet-Wall Electroinertial Precipitator: A Highly Efficient Air Cleaner for Cotton Dust. Annual Meeting IEEE Ind. Appl. Soc., 1976. p. 333-339.

5. R.B. Reif. Electro-Inertial Air Cleaner. US Patent No. 4,010,011, 1977.

6. W.B. Giles. Electrostatic Separation in Cyclones. Proc. of the First Symposium on the Transfer and Utilization of Particulate Control Technology, Vol. 3, 1978. p. 291.

7. W.B. Giles. Submitted for the Third Symposium on the Transfer and Utilization of Particulate Control Technology, Orlando, Florida, 1981.

8. R.R. Boericke, J.T. Kuo, P.W. Dietz and W.B. Giles. Electrocyclone for High-Temperature, High-Pressure Dust Removal. AIAA 19th Aerospace Sciences Meeting, St. Louis, Missouri, January 1981. p. 12-15.

9. Novel Methods for Respirable Dust Control. General Electric Company Report No. EV-01043-1, DOE Contract DE-AC02-79EV10143, September 1980.

10. P.W. Dietz. Electrostatic Effects in Vortical Flows. Session Q1, Second Symposium on the Transfer and Utilization of Particulate Control Technology, Denver, July 1979.

11. P.W. Dietz. Electrostatically Enhanced Cyclone Separators. Submitted Powder Technology, 1980.

12. W.B. Giles and P.W. Dietz. Electrostatic Effects on Sampling Through Ungrounded Probes. Second Symposium on the Transfer and Utilization of Particulate Control Technology. Volume IV Special Applications for Air Pollution Measurement and Control, EPA-600/9-80-039d, September 1980.

13. J.R. Melcher and K.S. Sachar. Charged Droplet Scrubbing of Submicron Particulate. Environmental Protection Technology Series, No. EPA-650/2-07, 1974.

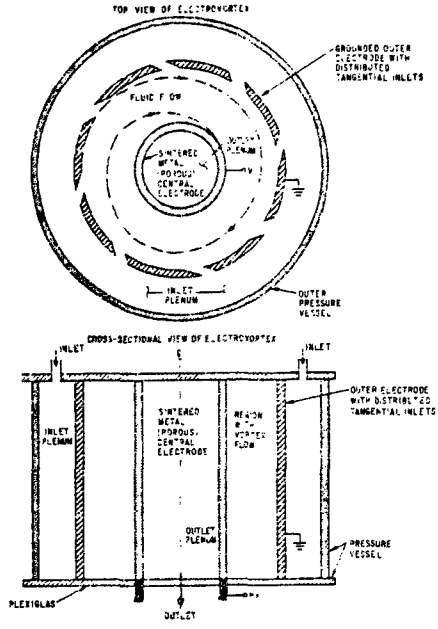

Figure 1 Electrovortex Apparatus (Top and Side Views)

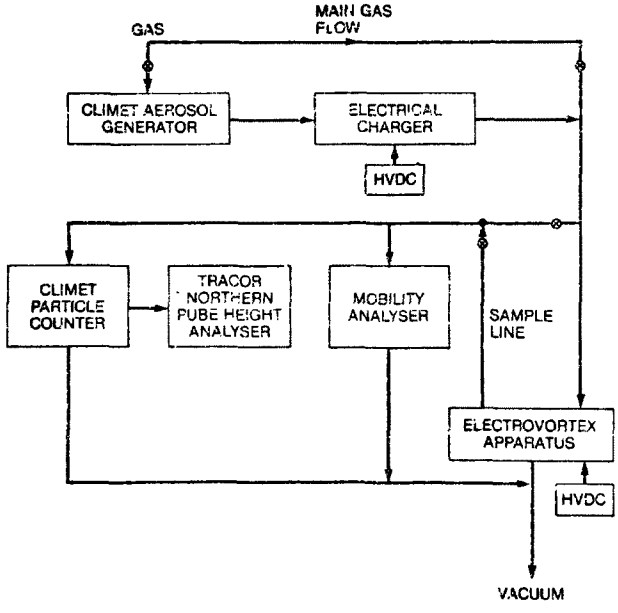

Figure 2 Schematic of Experimental System

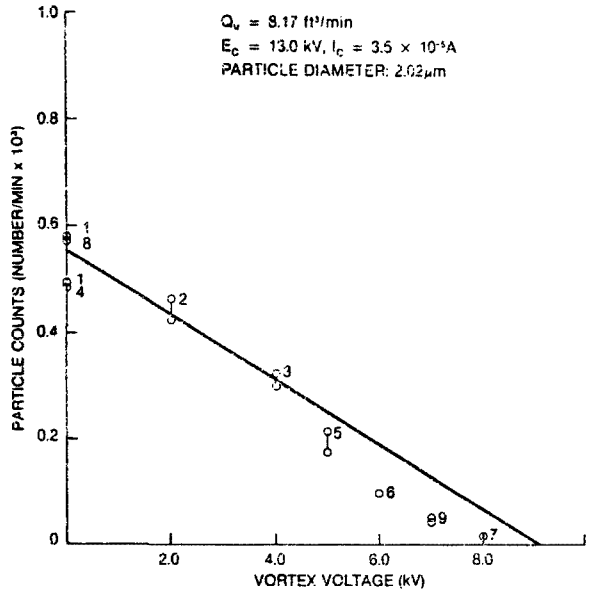

Figure 3 Particle Concentration in Electrovortex (8.17 ft^3/min)

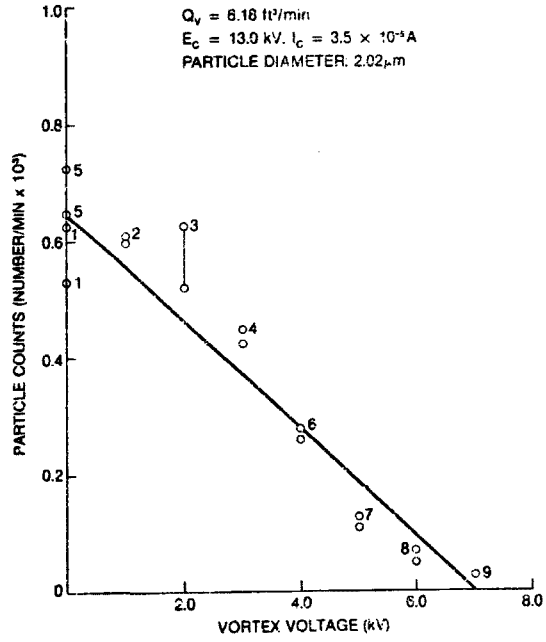

Figure 4 Particle Concentration in Electrovortex (6.18 ft^3/min)

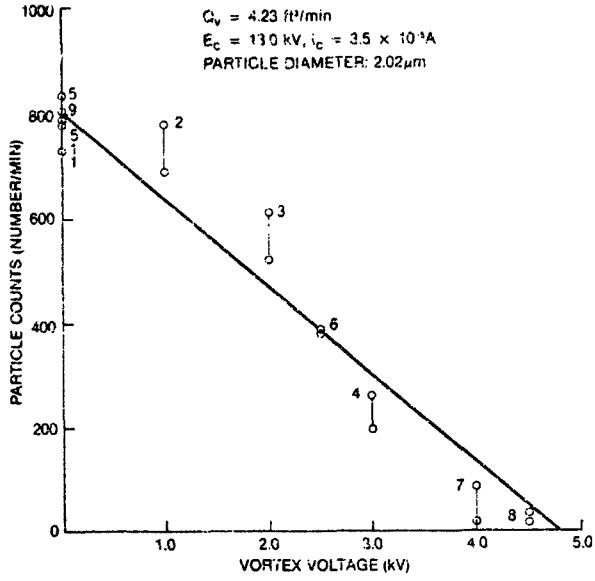

Figure 5 Particle Concentration in Electrovortex (4.23 ft^3/min)

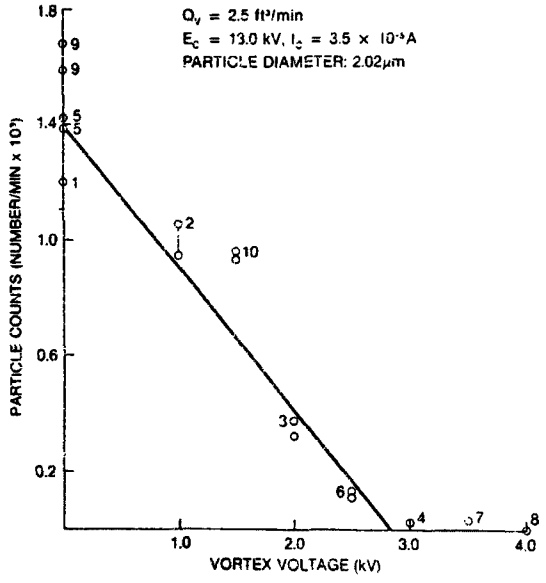

Figure 6 Particle Concentration in Electrovortex (2.5 ft^3/min)

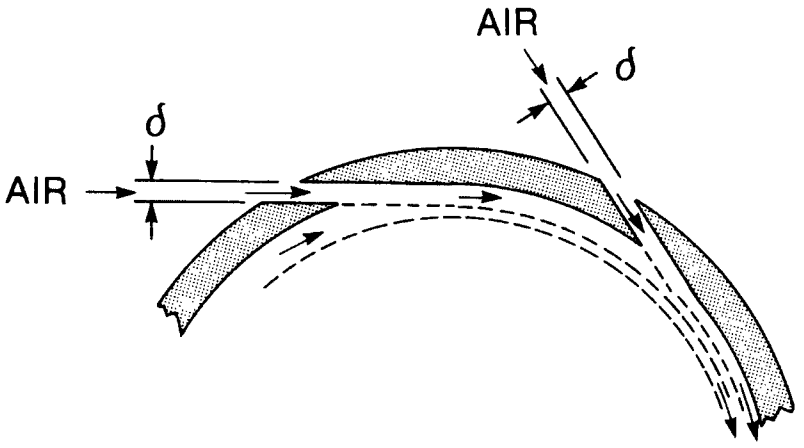

Figure 7 Close-up View of Distributed, Tangential Inlets

HIGH PERFORMANCE CYCLONE DEVELOPMENT

By W.B. Giles
Corporate Research and Development
General Electric Company
Schenectady, New York

Abstract

The results of cold flow experiments at atmospheric conditions of an air-shielded 18 inch diameter electrocyclone with a central cusped electrode are reported using fine test dusts of both fly-ash and nickel powder. These results are found to confirm expectations of enhanced performance, similar to earlier work on a 12 inch diameter model.

An analysis of the combined inertial-electrostatic force field is also presented which identifies general design goals and scaling laws. From this, it is found that electrostatic enhancement will be particularly beneficial for fine dusts in large cyclones.

Recommendations for further improvement in cyclone collection efficiency are proposed.

Introduction

Earlier experiments found (1) a marked influence of natural electrostatic forces in enhancing cyclone collection efficiencies, particularly at low velocities. This naturally-occurring phenomena, if present, is evident as a relatively constant collection efficiency with throughput. Evidence of this anomolous behavior is present in the literature (2,3,4,5,6) without explanation. Also Siemens' experience found weak influence due to both velocity and cyclone size (7). Experiments using a Faraday cage to sense air-borne particle charge levels show that triboelectric charges are induced by particle-wall collisions. Certain dusts are found to have a much higher propensity for this charge generation than others. For example, Exxon flyash have been observed to generate levels of 100 fold greater than CURL flyash. Within the cyclone, these charged particles are mutually repulsive and the resultant space charge augments inertial separation. In the present work, applied electrostatics are used to enhance performance. Similar effort is found in the literature (8,9,10). One study (2), in fact, concludes that the benefit does not justify the complication. However, for hot gas cleaning in coal-fired power generation systems large cyclones offer an economically attractive option. Small, multicyclones pose a substantial risk of fouling, whereas large conventional cyclones have poor performance for fine particle collection. Thus, the objective is to attempt to obtain, in large cyclones, the equivalent performance of small, inertial cyclones through the application of

electrostatics. In addition, the cyclonic action provides a mechanism of dust removal from the collecting electrode surface that precludes the problem of dust conductivity at high temperature which inhibits collection with conventional electrostatic precipitators.

Preliminary Experiment

The general characteristics of using applied electrostatics are shown in Figure 1. Here, a central cusped electrode was supported within the exhaust duct to protrude down into the cyclone body. When charged, this electrode provides an electric field from the electrode to the grounded cyclone body with a corona source at the four cusped edges of the electrode. The data indicates that the application of a charge results in a significant improvement in collection at the lower test velocities.

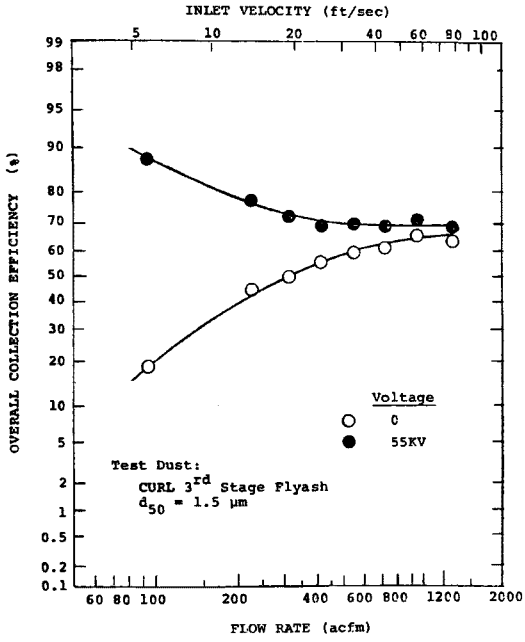

FIGURE 1 12-INCH AIR SHIELD MODEL WITH CUSPED ELECTRODE

General Theory

In a reverse flow cyclone, a swirl flow is induced, and the flow moves radially inward to the exhaust. A centrifugal, or inertia force, F_i, is produced on the air-borne particles acting against the inward drag force, F_d. Additionally, with charged particles in an electric field, an electrostatic force, F_e, aids the centrifugal force to promote particle separation.

The separative efficiency of cyclone, η, is functionally dependent on the separative parameter, S, which can be determined empirically. The general collection characteristics may be studied by considering the combined inertial-electrostatic separative parameter, S, where

$$S = \frac{F_i}{F_d}\left(1 + \frac{F_e}{F_i}\right) = S_i\left(1 + \frac{F_e}{F_i}\right) \qquad (1)$$

in which,

$$F_i = \rho_p \frac{\pi}{6} d_p^3 \frac{V_t^2}{r}, F_d = 3\pi\mu d_p U_r, F_e = q_p E(r)$$

and,

$$q_p = 3\pi\varepsilon_o d_p^2 E_c, \text{ with } E_c \approx E(r) \approx \frac{V_o}{r \ln(D/Del)}$$

The maximum g-field occurs* at the edge of the core flow region which is assumed here as equal to the exit duct radius or $r=D_e/2$. The maximum E-field, however, is greater at smaller radius, e.g. particles convected to smaller radius can become electrostatically dominated. For present purpose, the E-field will be evaluated also at $r=D_e/2$.

Since the radial inflow velocity is approximately uniform,

$$\pi D_e L\, U_r = \left(\frac{A_i}{D^2}\right) D^2 V_i = Q, \text{ where } A_i = 2\left(\frac{x}{D}\right)^2 D^2$$

The spin-up, via conservation of angular momentum, is

$$(1+2x')D\, V_i = D_e V_t, \quad x' = x/D$$

Then equation 1 becomes

$$S = k_1 \frac{V_i}{D_e}\left[1 + \frac{k_2}{(V_i/D_e)^2}\right] \tag{2}$$

where,

$$k_1 = \frac{\pi \rho_p d_p^2}{18\mu}\left(\frac{1+2x'}{x'}\right)^2 \frac{L}{D_e}$$

$$k_2 = \frac{\varepsilon_o}{\rho_p d_p D_e^3}\left(\frac{D_e}{D}\right)^2\left(\frac{1}{1+2x'}\right)^2\left(\frac{6\ V_o}{\ln\ D/Del}\right)^2$$

Equation 2 indicates a minimum exists when $V_i/D_e = \sqrt{k_2}$, and this minimum separative parameter is

$$S_{min} = \frac{\pi}{1.5\mu}\sqrt{\frac{\rho_p d_p^3 \varepsilon_o}{D_e^3}}\ \frac{L}{D}\left(\frac{1+2x'}{x'^2}\right)\frac{V_o}{\ln\ D/Del} \tag{3}$$

The design of the electrocyclone should be such as to make S_{min} as large as possible. This indicates that the desired features are:

1. Long cyclone length, L/D, consistent with vortex stability
2. Small inlet area, x', consistent with good inlet flow swirl turning, e.g. flow acceleration into the annular passage
3. Small exit diameter, D_e
4. High applied voltage, V_o, consistent with arc-over constraints, and
5. Large electrode diameter, Del, consistent with the internal corona production.

In addition, cyclone operation should be at maximum allowable velocity (subject to constraints of erosion, pressure loss and particle bouncing). This allows minimized cyclone size, D_e, to maximize performance.

*Some independent evidence suggests that in the presence of a strong corona source the E-field may be relatively constant.

The influence of electrostatic augmentation, relative to pure inertial separation, S_o, is indicated by the ratio,

$$S/S_o = 1 + \frac{\varepsilon_o D}{\rho_p d_p V_i^2}\left(\frac{D_e}{D}\right)\left(\frac{1}{1+2x'}\right)\left(\frac{6\ V_o/D}{\ln\ D/De1}\right) \qquad (4)$$

thus, there is a greater enhancement with large electrostatic cyclones, than with small cyclones.

Test Model Design

The general design configuration was derived from Stairmand's High Efficiency design with major modifications. An outline of the design is shown in Figure 2. Similarity is found in the cylindrical, conical and exhaust length-to-diameter ratios, plus use of a small inlet area ($A_i=0.1D^2$). In addition, the air shield feature (12) is employed using a double scroll inlet with the clean air inlet sized for 80% of the total flow, and a conical section added to the exhaust inlet to increase gas spin-up.

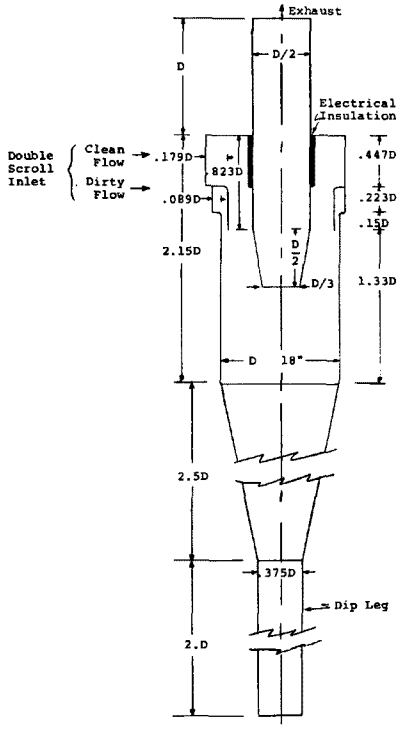

FIGURE 2: 18" D ELECTROCYCLONE MODEL

The electrostatic features included the electrical isolation of the lower end of the exhaust duct with high voltage supplied to a central electrode. The original configuration, shown in Figure 3, consisted of bundled wire and is similar to the electrode Petroll and Langhammer (2). It was found to result in excessive vibration, singing, and poor cyclone performance. The next design used a central cusped electrode supported by crossed non-conductive rod. Figure 4 shows the original installation in the 12-inch diameter air shield cyclone as used in the experiment in Figure 1. This electrode was then incorporated in the 18-inch diameter electrocyclone testing program.

The completed cold flow electrocyclone installation is shown in Figure 5.

General Experimental Technique

The experimental procedure consisted of supplying metered clean and dirty flows (80% and 20% respectively) to the two cyclone inlets. Both flows were provided by a blower using filtered air at the input to the blower. A small fluid bed dust generator, operating on shop air, provided a known particulate contaminant to the dirty air cyclone inlet line.

Particle measurement was provided by two optic techniques. One measured the overall dust concentration at both the inlet

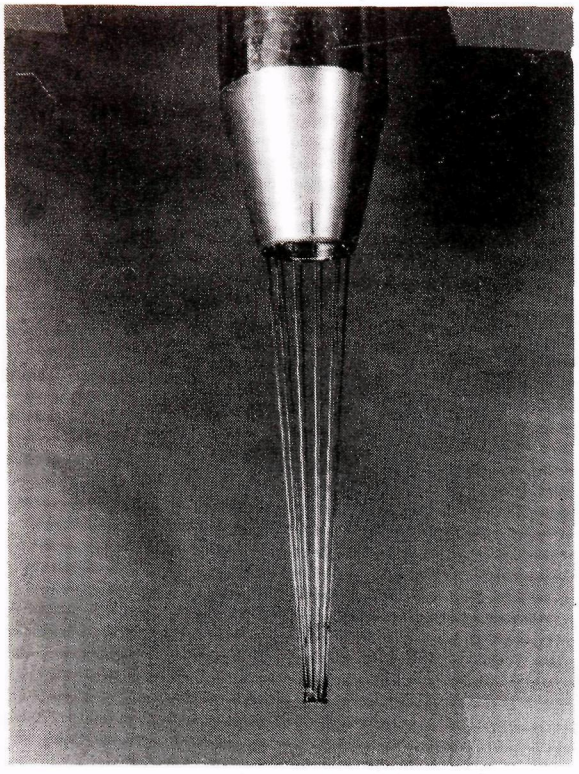

FIGURE 3: BUNDLED WIRE ELECTRODE

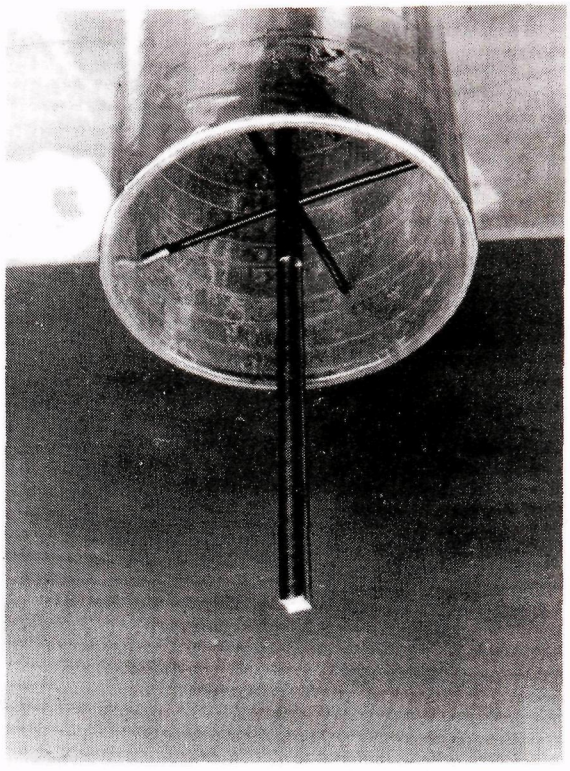

FIGURE 4: CENTRAL CUSPED ELECTRODE IN AIR SHIELD EXHAUST

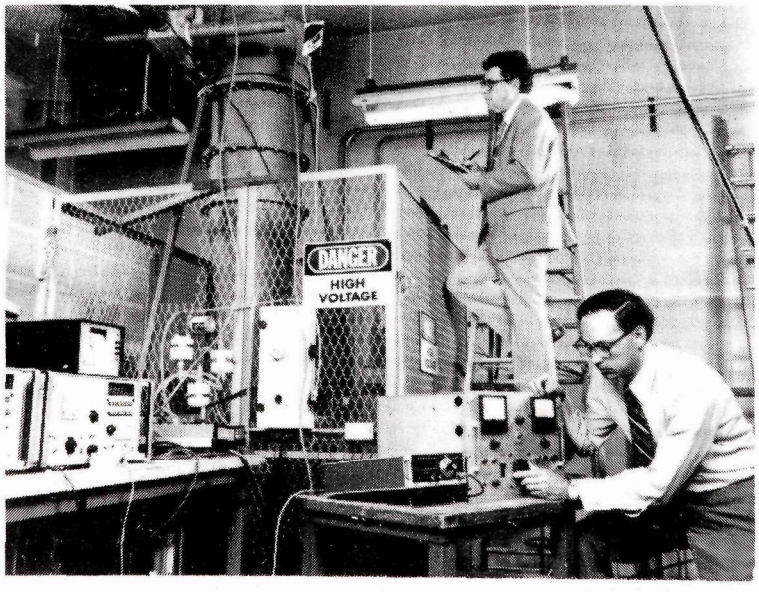

FIGURE 5: EIGHTEEN INCH DIAMETER ELECTROCYCLONE TEST INSTALLATION

and outlet using two PILLS V Mass Concentration Monitors. The other measured size distribution at both inlet and outlet using two Royco Airborne Particle Counter Systems. The latter used isokinetic probe sampling, followed by dilution to avoid coincidence errors.

Results and Discussion

Pressure Loss

The flow impedance of the cyclone was determined by measuring pressure loss, Δp, versus input volume flow. The correlation based on inlet kinetic heads to give

$$\Delta p / \frac{1}{2}\rho V_i^2 = 8.2 \text{ for } D_e/D = \frac{1}{3}$$

This may be compared to the reported (11) High Efficiency Stairmand design giving a value

$$\Delta p / \frac{1}{2}\rho V_i^2 = 6.0 \text{ for } D_e/D = \frac{1}{2}$$

Scoping Experiments

Preliminary experiments were first tried with an external corona particle charger, and separately, with an internal voltage field. Neither were found to yield significant enhancement. However, tests with an internal corona source to produce both particle charging and an applied voltage field did show promise as found in Figure 1. The results of a series of scoping tests using the 18 in. diameter electrocyclone are summarized in Figure 6. These results indicated that an upstream corona source was not significant and a positive corona was slightly beneficial at atmospheric conditions, relative to a negative corona source. The data shown is plotted in terms of the overall efficiency vs. volumetric flow times the square of input mass mean particle size as an indicator of the inertial similarity parameter. CURL flyash is used as the test dust and the exhaust duct is insulated from ground.

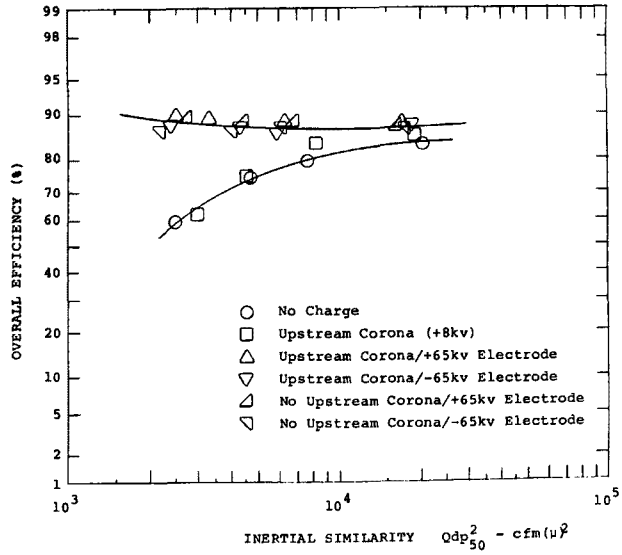

FIGURE 6: SCOPING EXPERIMENTS WITH 18" D ELECTROCYCLONE MODEL

Inertial Performance with Flyash and Nickel

Figure 7 shows the experimentally determined fractional efficiency of the electrocyclone operated in an uncharged state with flyash; and, with nickel shown in Figure 8.

Correlation with the inertial separative parameter is found to be excellant for the case of flyash. Good repeatability is noted with replicated runs. Also overall efficiency versus mass average separative parameter (solid symbols) is in good agreement with fractional efficiency data.

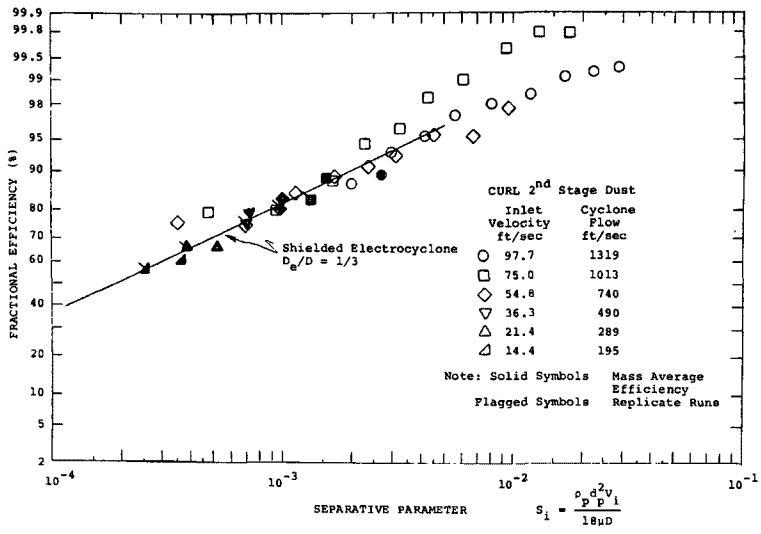

FIGURE 7: UNCHARGED ELECTROCYCLONE (18"D)

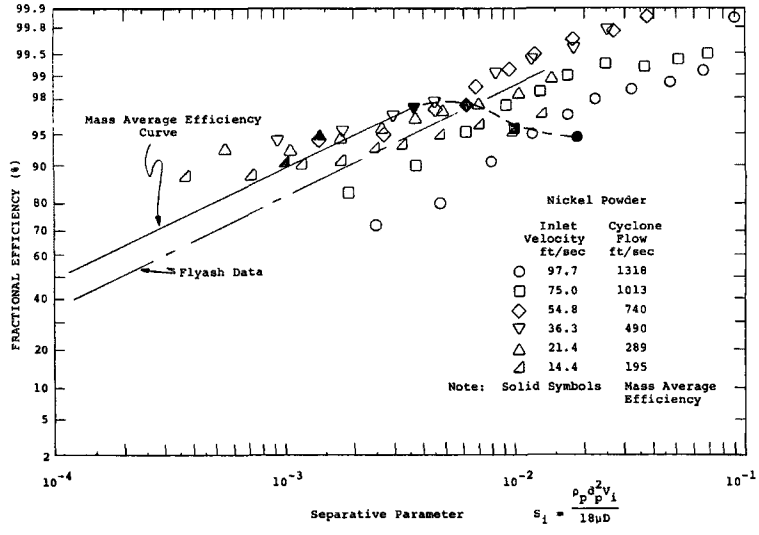

FIGURE 8: UNCHARGED ELECTROCYCLONE (18"D)

The data using nickel, in Figure 8, (with particle density taken as 8, versus 2 for flyash) shows the same approximate agreement, particularly for data in the range of 21 to 75 ft/sec inlet velocity. The mass average efficiency curve, however, is at significant variance from the fractional efficiency curves. The behavior of the former is suggestive of "coarse particle bouncing." The data suggests that this effect is primarily dependent on particle kinetics, $\rho_p V_i^2$, rather than particle size, d_p, since the effect is not evident in the fractional efficiency data. This is taken to infer that performance degradation might become important for flyash at velocities greater than 100 ft/sec; however, material differences may be expected to play an important role.

The inferred fractional efficiency is found to fit the approximate empirical expression;

$$\ln(1-\eta_f) = -1.75 \left[\frac{\rho_p d_p^2 V_i}{18\mu D} 10^3 \right]^{1/2} \qquad (5)$$

Electrostatic Performance

Figure 9 shows the relative influence on overall cyclone efficiency with a charged central cusped electrode. The exhaust duct

was electrically insulated from ground and hence, could float at some intermediate voltage level. Typical current flux was measured at 0.35 ma. It is noted that performance is substantially independent of cyclone inlet velocity and significantly superior to inertial operation. Figure 10 shows the same data after minor correction for particle size errors, associated with the PILLS sensor versus the mass average separative parameter. Also shown are typical measurements of inlet and outlet flyash size distributions. The very close similarity of these distributions can lead to experimental errors in deducing fractional efficiency. Figure 11 shows the deduced fractional efficiency with a charged central electrode. Generally, it is found that efficiency is substantially independent of inlet velocity.

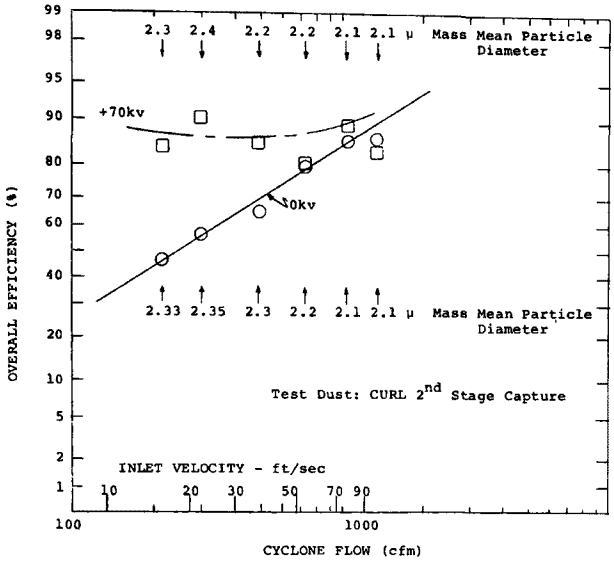

FIGURE 9: OVERALL EFFICIENCY AT 18" D ELECTROCYCLONE WITH CENTRAL CUSPED ELECTRODE AND FLOATING EXHAUST

Using nickel as a test dust, as shown in Figure 12, there is a more distinct difference between inlet and outlet dust distributions, and thus markedly less ambiguity in measuring fractional efficiency. Again, there appears to be a pronounced performance degradation due to particle kinetic energy. This is clearly evident in Figure 13 which shows the overall efficiency as measured by the PILLS instrumentation versus cyclone velocity.

Theoretical Correlation

The performance data with a charge and using flyash may be achieved by replacing the inertial term in equation 5 with the complete separative parameter, or

$$\ln(1-\eta_f) = -1.75 \left[k_1' \frac{V_i}{D_e} \left(1+\frac{k_2 D_e^2}{V_i^2}\right) 10^3 \right]^{0.5} \qquad (6)$$

where

$$k_1 = \frac{\rho_p d_p^2}{18\mu} \frac{D_e}{D}$$

An analytic fit may be taken from the experimental data at a median velocity of 40 ft/sec using η_f=0.83 at d_p=2μ and η_f = 0.935 at d_p = 4μ to give,

$$\left[\frac{\ln(1-\eta_f)}{-1.75}\right]^2 = 1.18 \times 10^{-3} \; d_p^2 \; V_i \left(1+\frac{14245.}{d_p V_i^2}\right) \qquad (7)$$

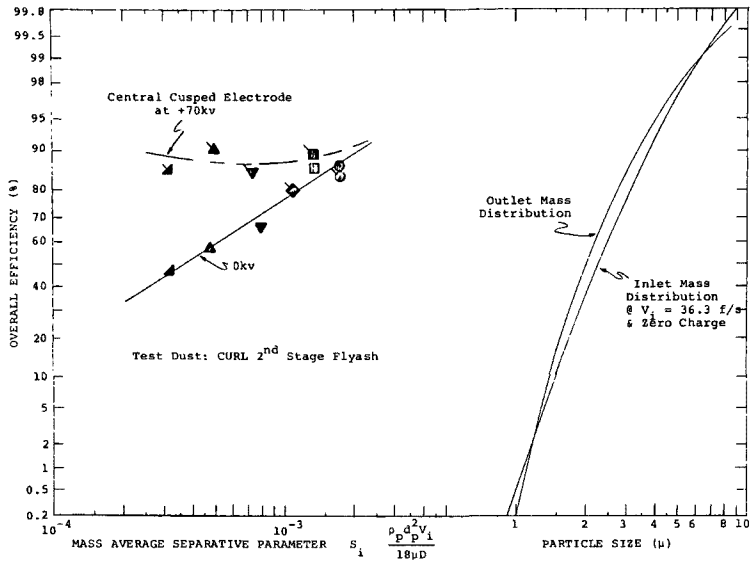

FIGURE 10: OVERALL EFFICIENCY & SAMPLE DISTRIBUTION AT 18"D ELECTROCYCLONE TEST

wherein the particle size is in microns and the cyclone inlet velocity is in ft/sec.

The trends of this theoretical correlation are shown in Figure 14 over the general range of experimentation. It is noted that a loss of performance is anticipated at increased velocity due to a weakening of the relative influence of electrostatics and the predicted performance increases with particle size. Equation 7, however, predicts a higher performance level for coarse particles than found experimentally.

The indicated enhancement for electrostatic enhancement is

$$\frac{\ln(1-\eta_f)}{\ln(1-\eta_{f_o})} = 1 + \frac{14245.}{d_p V_i^2} \approx 1 + \frac{\varepsilon_o D}{\rho_p d_p V_i^2} \frac{D_e}{D} \frac{1}{1+2x'} 2 \frac{6\ V_o/D_e}{\ln D/De1}^2 \quad (8)$$

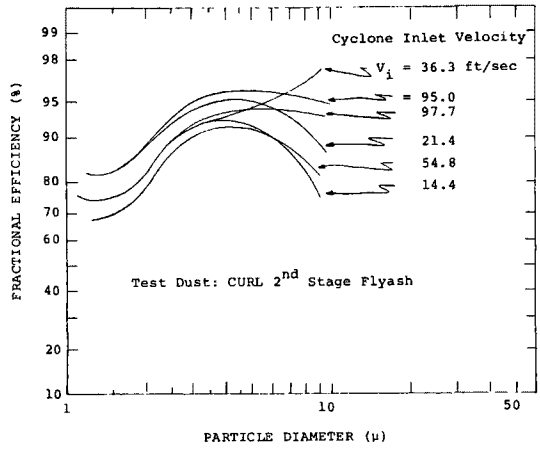

FIGURE 11: FRACTIONALLY EFFICIENCY OF ELECTROCYCLONE WITH CENTRAL CUSPED ELECTRODE AT +70kv (0.35 ma)

Thus, for a fixed voltage gradient, geometric similarity, and fixed inlet velocity, performance is improved with electrostatic augmentation at increased cyclone scale.

For application in the PFB-CFCC system, special interest is directed to controlling erosive particles of the order of 5 microns and larger. Assuming cyclone inlet velocities of the order of 100 ft/sec, the indicated enhancement in separative effectiveness (from equation 8) is increased by 28% for an 18 inch diameter cyclone, or by 112% for a 6 ft dia. cyclone. This empirically-deduced theoretical correlation finds that electrostatic augmentation should be highly desirable for turbine erosion control using large cyclones. However, the apparent variation of coarse particles is critically important.

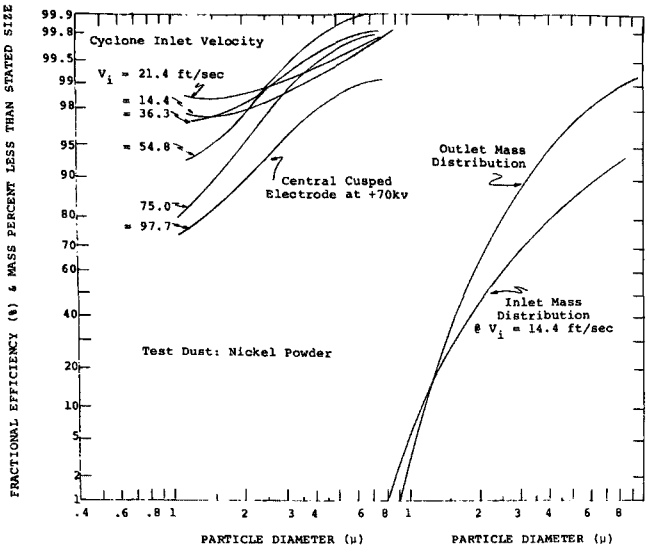

FIGURE 12: FRACTIONAL EFFICIENCY & SAMPLE DISTRIBUTION AT 18"D ELECTROCYCLONE TEST

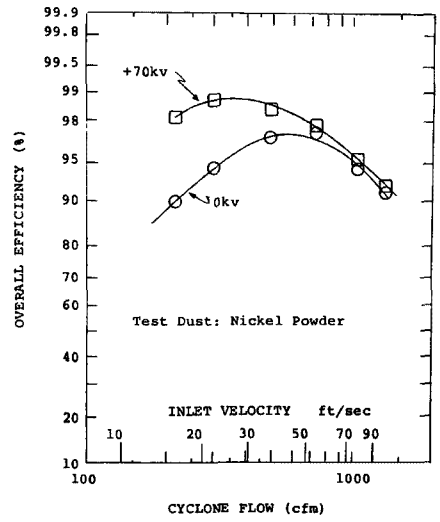

FIGURE 13: OVERALL EFFICIENCY OF ELECTROCYCLONE WITH CENTRAL CUSPED ELECTRODE & FLOATING EXHAUST

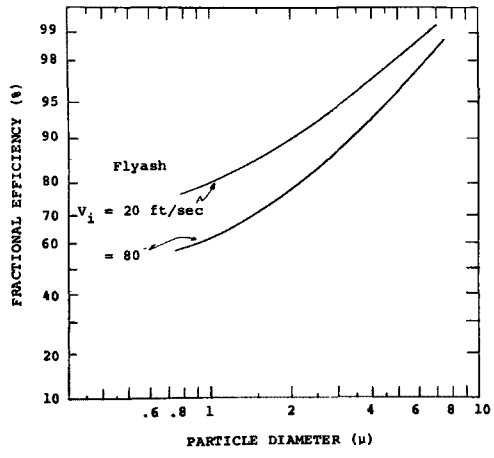

FIGURE 14: THEORETICAL CORRELATION OF ELECTROSTATIC AUGMENTATION WITH FLYASH

Comparative Performance

Figure 15 compares the test results of the present work with previous work. All data is without electrostatic augmentation. As previously noted, the 18 in. diameter electrocyclone model is a derivative of the Stairmand High Efficiency design (with low flow handling capacity, $Q = 0.1D^2V_i$)while the earlier 12 in. diameter air shield model is a derivative of the Stairmand High Flow design ($Q=0.281D^2V_i$). Hence, the reported data is shown for reference. The reported data for the high flow design appears to be unduly pessimistic. Tests of an approximate model were found to yield much higher efficiency of collection (13). The earlier air shield cyclone, both with and without the clean air shielding feature, was found to embody design features significantly superior to the basic Stairmand design. These are presumed to include a longer engagement length (between the exhaust and the cyclone body)and a smaller exhaust diameter (increased spin-up). The present model data in this comparison is found to provide only a slight additional improvement in spite of the much higher spin-up provided by the smaller exhaust. It is concluded that an additional design feature is penalizing the present design.

Table 1 summarizes the basic design features of different cyclones, exclusive of the air shielding feature.

Particular attention may be drawn to the ratio of flow area at the cyclone annulus versus inlet. It is noted that excessive flow diffusion exists with the High Efficiency configuration. This would be expected to result in excessive flow separation and turbulent mixing at the cyclone inlet. This situation is also evident in the High Flow design, but to a much lesser extent. A preferred design would provide for an accelerating inlet flow turn (or the use of axial swirl vanes) as indicated for a recommended design shown in Figure 16. The ideal design is intended to suggest preferred trends.

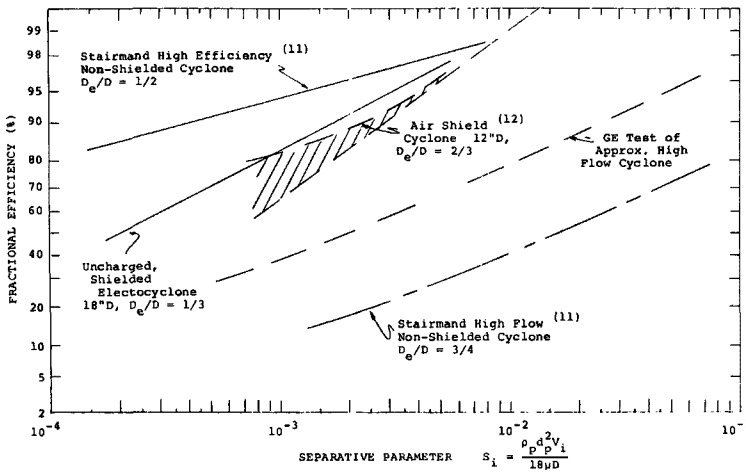

FIGURE 15: COMPARATIVE CYCLONE PERFORMANCE DATA

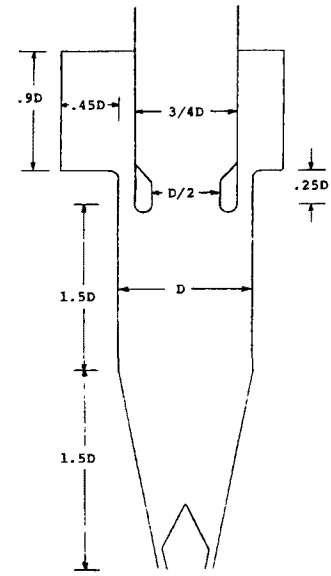

FIGURE 16: BASIC RECOMMENDED DESIGN

Summary

These cold flow investigations show an electrostatic enhancement particularly for fine dusts which are projected to be especially beneficial for large cyclones. Present data suggests, however, that performance is inhibited for dense dusts and at high velocity. It is hypothesized that the main problem is due to an inlet flow maldistribution associated with the use of small inlets, typical of high performance cyclones.

Acknowledgement

This work was performed under sponsorship of the U.S. Department of Energy, Contract No. DE-AC01-80ET17091.

References

1. Giles,W.B. "Electrostatic Separation in Cyclones" Symposium on the Transfer and Utilization of Particulate Control Technology, Vol. III, Sect. B., p. 291-302, Feb., 1979.

TABLE 1
BASIC CYCLONE DESIGN PARAMETER COMPARISON
(Body Diameter = D)

	Stairmand High Efficiency	Stairmand High Flow	Basic Air Shield	Recommended	R&D Ideal
Inlet Type	Tangential	Scroll	Scroll	Scroll	Annular Turn
Inlet, x/D	0.5 x 0.2	0.75 x 0.375	0.75 x 0.375	0.9 x 0.45	0.9 x 0.45
Overall Length, L/D	4	4	3	4.15	≈ 6
Dust Exit, D_e/D	3/8, Dump	3/8, Dump	3/8, V.S.*	3/8, V.S.*	3/8, V.S.*
Inlet Area/D^2	0.10	0.2813	0.2813	0.405	0.405
Annulus Area/D^2	0.589	0.3434	0.3434	0.3434	<0.3434
Outlet, D_e/D	0.5	0.75	0.67	0.5(Dif.)**	<0.5(Dif.)**
Outlet Area/D^2	0.1963	0.4416	0.3489	0.1963	<0.1963
Inlet Vol./D^3	0.2944	0.783	0.783	0.663	>0.663
Body Vol./D^3	1.776	1.482	1.085	1.772	≈3.225
Spin-up Ratio	2.8	2.33	2.63	3.90	>3.90
Engagement Length/D***	0	1/8	1/8	1/4	>1/4

* Vortex Shield

** Diffuser

*** Axial Length Between Inlet and Exhaust

2. Petroll, J. & Langhammer, K., "Comparative Tests on Cyclone Precipitators," Breiberger Forschungsheft, Vol. A220, pp. 175-196, 1962.
3. Ludewig, H., "Cyclone Model Experiments Regarding the Effect of the Dip Pipe Depth on Separating Efficiency and Pressure Drop," Vol. 7, No. 8, pp. 416-421, 1958,Maschinenbautechnik.
4. ter Linden, A.J., "Investigations in Cyclone Separators," VDI Seminar, Vol. 3, 1954, VDI Verlag.
5. Berth, W. & Trunzk, "Model Test with Water Stream Cyclone Separator for Predetermining Removal Efficiency," Z.F. Angew , Mat and Mech., Vol. 30, 1950, No. 8/9.
6. Rammler, E. and Breitling, K., "Comparative Tests with Centrifugal Separators," Freiberger Forschungsheft, A56, 1957.
7. Verbal communication with Weber and Klein of Siemens Kraftwork Union.
8. Reif, R., U.S. Patent 4,010,011, March 1, 1977.
9. Hodson, P., U.S. Patent 2,748,880, June 5, 1956.
10. Rommel, W.R., U.S. Patent 2,594,805, June 26, 1945.
11. Stairmand, C.J. "Design and Performance of Cyclone Separators" Trans. Instn. Chem. Engr's., Vol. 29, 1951, p. 356-383.
12. Anomy. "PBG-CFCC Development Program-Adv. Cleanup Device Performance Design Report (Task 4.3) Vol. B-Air Shield Cyclone Evaluation", Prep. for U.S. DoE Contract No. EX-76-C-01-2357, Dist. Category UC-90e, FE-2357-70.
13. Bekofske, K.L."Air Shield Cyclone in Non-Shielded Configuration", Letter report dated 1/24/80.

Nomenclature

A_i = cyclone inlet area
d_p = particle diameter
D = cyclone diameter
D_e = exhaust diameter
D_{el} = electrode diameter
E = electric field
F_d = drag force
F_e = electrostatic force
F_i = inertial force
L = length
Δp = differential pressure
p = penetration = $1-\eta_f$
Q = cyclone flow
q_p = particle charge
r = radius
S = separative parameter
S_i = inertial separating parameter
U_r = radial velocity at r
V_i = cyclone inlet velocity
V_t = cyclone tangential velocity
V_o = voltage differential
x = inlet scroll width

Greek

η = overall cyclone efficiency
η_f = fractional efficiency
ρ = gas density
ρ_r = particle density
μ = absolute gas viscosity
ε = permittivity of air

AUTHOR INDEX

AUTHOR NAME	PAGE
Albrecht, P.R.	IV-116
Anderson, M.H.	II-334
Arce-Medina, E.	II-76
Ariman, T.	III-290
Armstrong, J.A.	IV-188, IV-252
Bakke, E.	I-236
Balfour, W.D.	III-119
Bamberger, J.A.	III-398
Bergmann, L.	I-323
Berlant, M.J.	II-218
Bernstein, S.	II-405
Beutner, H.P.	III-71, III-228
Bickelhaupt, R.E.	I-165
Boericke, R.R.	III-353
Bohn, R.	IV-344
Borenstein, M.	III-90
Brookman, E.T.	IV-125
Bump, R.L.	II-425
Bush, P.V.	I-157
Calvert, S.	III-1, III-10, IV-156
Carnes, D.	IV-135
Carr, R.C.	I-118
Chamberlain, H.L.	IV-406

AUTHOR INDEX (cont.)

AUTHOR NAME	PAGE
Chambers, R.	I-45
Chiang, T.	III-250, III-261
Chou, K.H.	IV-73
Cowen, S.J.	IV-264
Crippen, L.K.	I-148
Crowson, F.	III-438
Crynack, R.R.	II-242
Czuchra, P.A.	IV-55
Dalmon, J.	II-390
Demski, R.J.	I-341
Dennis, R.	I-1, III-140
Dietz, P.W.	III-449, III-459
Donovan, R.P.	I-11
Drehmel, D.C.	III-341, IV-210
DuBard, J.L.	IV-383
Durham, M.	II-54, IV-285
Ensor, D.S.	I-176, IV-242
Eskinazi, D.	III-238
Faulkner, M.G.	II-199, IV-395
Feldman, P.L.	IV-3
Ferrigan III, J.J.	I-197
Finney, W.C.	II-358
Fjeld, R.A.	II-179
Fortune, O.F.	I-82

AUTHOR INDEX (cont.)

AUTHOR NAME	PAGE
Frazier, W.F.	III-171
Gardner, R.P.	III-128
Gaunt, R.H.	I-216
Gehri, D.C.	I-333
Gentry, J.W.	III-406
Giles, W.B.	III-468
Hardison, L.C.	III-33
Harmon, D.L.	IV-317
Hawks, R.L.	III-221
Helfritch, D.	I-75
Henry, F.	III-301
Henry, R.F.	IV-63
Hesketh, H.E.	IV-222
Hoenig, S.A.	III-382
Hovis, L.S.	I-23
Hyde, R.C.	I-129
Iionya, K.	III-181, III-321
Jaworowski, R.J.	I-185
Jensen, R.M.	I-138
Joergensen, H.J.	II-370
Johnson, C.A.	I-352
Kalinowski, T.W.	III-311
Kanaoka, C.	III-280
Kirstein, B.E.	III-373

AUTHOR INDEX (cont.)

AUTHOR NAME	PAGE
Kolnsberg, H.J.	IV-179
Krishnamurthy, N.	IV-232
Ladd, K.	I-55, I-65
Lagarias, J.S.	I-272
Landham, Jr., E.C.	I-237
Langan, W.T.	III-211
Lawless, P.A.	II-25, II-35, II-44
Leith, D.	III-270
Leonard, G.L.	II-120
Maartmann, S.	II-130
Mahoney, D.F.	I-206
Mappes, T.E.	III-150
Martin, D.	IV-145
Masuda, S.	II-189, II-380
Mathai, C.V.	IV-200
Mazumder, M.K.	II-160, II-169
McCrillis, R.C.	IV-306
McElroy, M.W.	I-94
McLean, K.J.	I-265, II-304
Menegozzi, L.	II-404
Menoher, C.	III-111
Mitchner, M.	II-97
Moore, W.E.	IV-105
Mormile, D.	IV-363

AUTHOR INDEX (cont.)

AUTHOR NAME	PAGE
Moslehi, G.B.	II-109
Mosley, R.B.	II-1, II-13
Musgrove, J.G.	III-193, III-201
Noonan, F.M.	IV-326
Oglesby, H.S.	III-80
Ostop, R.L.	I-107
Parker, R.	III-51, IV-2
Parquet, D.	III-363
Parsons, Jr., E.L.	I-303
Patton, J.D.	III-160
Pearson, G.L.	I-120
Pedersen, G.C.	III-60
Petersen, H.H.	I-291
Piulle, W.	I-253
Potokar, R.W.	III-417
Prem, A.	III-21
Presser, A.M.	IV-26
Pyle, B.E.	II-66
Raemhild, G.A.	II-349
Reardon, F.X.	III-102
Rimberg, D.B.	II-262
Rinaldi, G.M.	IV-95
Rinard, G.	II-283, II-295
Rubow, L.N.	IV-83

AUTHOR INDEX (cont.)

AUTHOR NAME	PAGE
Rugg, D.	II-273
Samuel, E.A.	II-149
Schliesser, S.P.	II-252
Semrau, K.T.	III-43
Shilling, N.Z.	II-230
Smith, W.B.	I-96
Snaddon, R.W.L.	IV-74
Sparks, L.E.	II-314, II-326
Spawn, P.D.	IV-335
Starke, J.	III-428
Stevens, N.J.	I-313
Sullivan, K.M.	II-141
Tatsch, C.E.	IV-353
Teller, A.J.	III-393
Thompson, C.R.	II-415
Urone, P.	IV-275
VanOsdell, D.W.	I-35
Viner, A.S.	IV-168
Wakabayashi, A.	III-332
Wang, H.H.	IV-36
Wang, J.C.F.	IV-373
Wegrzyn, J.	IV-46
Weyers, L.L.	I-226
Wilks, W.H.	IV-15

AUTHOR INDEX (cont.)

AUTHOR NAME	PAGE
Williamson, A.D.	IV-297
Yamamoto, T.	II-87
Yung, S.	IV-1, IV-155
Zarfoss, J.R.	II-208

☆USGPO: 1982 — 559-092/0431